FLORIDA INTERNATIONAL UNIVERSITY

Miami, Florida

FUNCTIONAL STRATEGIES OF TREE FINE-ROOTS IN RELATION TO THE SOIL ENVIRONMENT AND MICROBIOME: VARIATION IN ROOT MORPHOLOGY, TISSUE CHEMISTRY AND PHYSIOLOGY

A dissertation submitted in partial fulfillment of

the requirements for the degree of

DOCTOR OF PHILOSOPHY

in

BIOLOGY

by

James Aaron Hogan

2021

To: Dean Michael R. Heithaus
College of Arts, Sciences and Education

This dissertation, written by James Aaron Hogan, and entitled Functional Strategies of Tree Fine-Roots in Relation to the Soil Environment and Microbiome: Variation in Root Morphology, Tissue Chemistry and Physiology, having been approved in respect to style and intellectual content, is referred to you for judgment.

We have read this dissertation and recommend that it be approved.

_____
Steven F. Oberbauer

_____
Michael S. Ross

_____
Diego Salazar Amoretti

_____
Kenneth J. Feeley

_____
Christopher Baraloto, Major Professor

Date of Defense: November 5, 2021

The dissertation of James Aaron Hogan is approved.

_____
Dean Michael R. Heithaus
College of Arts, Sciences and Education

_____
Andrés G. Gil
Vice President for Research and Economic Development
and Dean of the University Graduate School

Florida International University, 2021

DEDICATION

I dedicate this dissertation to the late Dr. Roper – one of the many educators, mentors, and friends I have had along my academic journey. You were always a supporter and an inspiration. You showed me that it is possible to surmount obstacles with dignity and grace and you always carried yourself with an upright sense of belonging and security, which I deeply admired. You were a good man, friend, and confidant. May you rest in peace.

ACKNOWLEDGMENTS

I am supremely thankful to my parents for their unwavering and continued love and care over the many years. I am deeply indebted to the nurturing support of my family and many friends, who helped me navigate this journey. Moreover, many institutions and individuals have aided along the way.

Funding was received from the Department of Biology at Florida International University (FIU), the Smithsonian Forest-GEO program, the FIU Tropics program, the Garden Club of America, the United States Department of Energy, and many individual donors who graciously donated to help fund laboratory analyses of soils for the first field work campaign in Hainan Island, China.

Facilities at the Chinese Academy of Forestry, the Jianfengling Field Station in Hainan, China, the Chinese Academy of Sciences, the Xishuangbanna Tropical Botanical Garden, the Matthew Smith Lab at the Department of Plant Pathology of the University of Florida, the Soil Testing and Plant Analysis Laboratory at Louisiana State University, and Oak Ridge National Lab were made available and utilized. This dissertation could not have been possible without the use of these world class facilitates.

The following colleagues were very helpful, patient and advised projects: Oscar Valverde-Barrantes, Xu Han, Ding Qiong, Xiaoyang Song, Jie Yang, Min Cao, Yuehua He, Michelle Jusino, Matthew Smith, Adriana Corrales, Jeffrey Warren, David Weston, Cari Ficken, Jesse Labbé, and Jennifer Franklin.

Laboratory sample analyses were provided by: Liyuan Chen at the China Xinhua Agricultural Technical Development Limited Company, Michael D. Breithaupt at the Plant Analysis Laboratory at Louisiana State University, Sarah Wilson and Jim

Fourqurean at the Seagrass Lab at FIU, and Will Cook at the Duke Environmental Analysis Lab.

I am grateful to the following individuals, who helped collect data: Shaojun Ling, Yaxin Xie, Jaming Wang, Siqi Yang, Tang Wuenguang, Shitaing Ma, Qiqi Zhang, and Jiazhu Shi, Iwan Guan, Run Shen, Yuan Zi, and Xiao (Lilly) Taiyang, and Dong-Hai Yang, Lionel Collazo Perez. David MacLennan, Deanne Brice, Joanne Childs, Jana Philips, Mindy Clark, Yvonne Hitchcock, Kevin Hoyt, Zach Ziegler, and Kieth Van Schiack.

Lastly, I am thankful to Ken Feeley, Mike Ross, Diego Salazar and Steve Oberbauer for their service as the members of the dissertation committee. I reserve the deepest appreciation for my major professor, Christopher Baraloto, who was exceptionally instrumental in this work via his guidance, advice, and care for me during my doctoral studies.

I cannot begin to express the sense of gratitude I have to all of the institutions and individuals listed above. The ability practice the biological sciences is an honor and a privilege, and these institutions and individuals have made it a pleasure.

ABSTRACT OF THE DISSERTATION

FUNCTIONAL STRATEGIES OF TREE FINE-ROOTS IN RELATION TO THE SOIL ENVIRONMENT AND MICROBIOME: VARIATION IN ROOT MORPHOLOGY, TISSUE CHEMISTRY, AND PHYSIOLOGY

by

James Aaron Hogan

Florida International University, 2021

Miami, Florida

Professor Christopher Baraloto, Major Professor

Tree root systems have evolved multidimensional functioning, specializing in water and nutrient acquisition via different strategies. Root functional strategies vary among tree species and are adapted to the abiotic and biotic soil environment. This dissertation explores how three facets of root system functional strategies – morphology and chemistry, biotic associations with fungi, and respiration rates – vary within and among tree species along environmental gradients. Chapter one examines how root system morphology varies with forest succession and soil environment in a tropical forest of Hainan, China, finding that root systems had larger diameters and fewer root tips in the younger forest, and that soil phosphorus and base saturation affected intraspecific root trait variation. Chapter two compares root and leaf tissue chemistry within the same forest, finding that root systems function to maintain tree elemental homeostasis despite variation in morphology and soil environment. Chapter three links morphological variation of roots and leaves from chapter one to forest compositional turnover at the landscape-scale using existing plot data, finding that trait variation negatively co-varied

with species turnover to influence community-weighted mean trait estimates. Chapter four assesses how root-associated fungal communities are structured by the soil environment and root traits in three tropical forest plots of varying age and soil fertility in Xishuangbanna, China. Variation in the soil environment strongly influenced root-associated fungal communities, outweighing the effects of root morphological traits, although root system architecture and root calcium were important secondary determinants. Chapter five explores how root functional strategies shape the contribution of root system respiration to soil respiration among eight temperate tree species. Root system tissue respiration rates were greater with root system length and root tissue nitrogen concentrations. The root-associated fraction of soil respiration increased with specific root length, tip abundance, but decreased with root tissue density. Lastly, chapter six chronicles a warming experiment with the model tree, *Populus trichocarpa*, finding that acclimation of root respiration was less than leaf respiration and was mediated by soil nitrogen availability. Interspecific differences in root functional strategies evidence evolved trade-offs in nutrient and water uptake strategies among species; however, the environment exerts considerable influence on root morphology, chemistry, physiology, and root-soil interactions.

TABLE OF CONTENTS

LIST OF TABLES

TABLE PAGE

LIST OF FIGURES

FIGURE PAGE

LIST OF ABBREVIATED TERMS

Abbreviated terms are listed in order of appearance for each chapter, except for chapter 5, where they are listed alphabetically.

Chapter 1: Morphological variation of fine root systems and leaves in primary and secondary tropical forest of Hainan Island, China

Abbreviation	Complete Term	Definition	Units
SLA	specific leaf area	The ratio of the leaf area to leaf dry mass. The inverse of leaf mass per area. Our measurements of SLA include the leaf petiole and were done using complete leaves (i.e., included the petiole and all leaflets for compound leaves).	$m^2\ kg^{-1}$
SRL	specific root length	The ratio of total linear length of root system to the root system dry mass.	$m\ kg^{-1}$
SRA	specific root surface area	The ratio of the entire root system area to its dry mass.	$m^2\ kg^{-1}$
SRTA	specific root tip abundance	The ratio of the number or terminal, first-order root tips to roots system dry mass.	$tips\ g^{-1}$
RBI	root branching intensity	The ratio of the number or terminal, first-order root tips to the total root system length.	$tips\ cm^{-1}$
RTD	root tissue density	The root system dry mass divided by the total root system volume. RTD calculation assumes circularity of roots, WinRHIZO estimates root system volume from diameter.	$g\ cm^{-3}$
BS	soil base saturation	The percentage of soil cation exchange capacity occupied by base cations – calculated as the ratio of total exchangeable bases (*100) to the soil total exchangeable bases (both of which were measured using in the lab using the ammonium acetate exchange-flame atomic absorption method).	%

Chapter 2: Intraspecific trait variation and species functional turnover in successional tropical forests: assessing gap-filling for community-weighted means

Abbreviation	Complete Term	Definition	Units
AWM	assemblage-weighted mean	A partial community functional trait metric. The same as a community weighted mean, but for an assemblage (i.e., incomplete sample) of species from within that community, weighted by relative abundance.	—
CWM	community-weighted mean	Aggregate community functional trait metric. It is weighted by the basal area of species in the community of forest inventory plots.	—
ITV	intraspecific trait variation	trait variation that is the result of a genotype expressing various phenotypes in each environment; it's a combination of genetic (i.e., evolution) and environmental variation reflected in the trait variability within species or populations.	—
JFL	Jjianfengling	The forest in Hainan Island, China where the study sites are located.	—
pGLM	phylogenetic generalized linear model	—	—
RRTA	specific root tip abundance	The ratio of the number or terminal, first-order root tips to roots system dry mass. N	tips g^{-1}
RBI	root branching intensity	see Chapter 1	tips cm^{-1}
RTD	root tissue density	see Chapter 1	g cm^{-3}
SLA	specific leaf area	see Chapter 1	m^2 kg^{-1}
SRL	specific root length	see Chapter 1	g m^{-1}
WD	wood density	The oven-dried mass of a wood sample divided by its green mass.	g cm^{-3}

Chapter 3: Evidence of elemental homeostasis in fine root and leaf tissue of saplings across a fertility gradient in tropical montane forest in Hainan, China

Abbreviation	Complete Term	Units
N	Nitrogen	%
P	Phosphorus	ppm
C	Carbon	%
Al	Aluminium	ppm
B	Boron	ppm
Ca	Calcium	ppm
Cu	Copper	ppm
Fe	Iron	ppm
Mg	Magnesium	%
Mn	Manganese	%
Mo	Molybdenum	ppm
Na	Sodium	ppm
K	Potassium	ppm
S	Sulphur	ppm
Zn	Zinc	ppm
soil BS	soil base saturation	%
soil N	total soil nitrogen content	$g\ kg^{-1}$
soil P	Total soil phosphorus content	$g\ kg^{-1}$
LMM(s)	Linear mixed effects model(s)	—

Chapter 4: Root associated fungi are structured more by soil environment than by plant-host functional traits in a Chinese tropical forest

Abbreviation	Complete Term	Definition	Units

MRM	multiple regression of distance matrices	linear regression framework that vectorizes distance matrices prior to regression on a multivariate response	—
ECM	ectomycorrhizal	Plant fungal association type where root fungal hyphae encase the exterior of root tissues	—
AM	arbuscular mycorrhizal	Plant fungal association type where root fungal hyphae penetrate the cells of cortical root tissues, oftentimes creating arbuscules.	—
RTD	root tissue density	see Chapter 1	$g\ cm^{-3}$
CERN	Chinese Ecological Research Network	—	—
XTBG	Xishuangbanna Tropical Botanical Garden	—	—
PCA	principal components analysis	—	—
RDMC	root dry matter content	The ratio of root system dry mass to root system fresh mass	$mg\ g^{-1}$
RTMF	root tip mass fraction	The ratio of the fresh mass of root tips to the total root system fresh mass	%
SRL	specific root length	see Chapter 1	$cm\ g^{-1}$
SRA	specific root surface area	see Chapter 1, note that units are different from chapters 1 and 3	$cm^2\ g^{-1}$
SRTA	specific root tip abundance	see Chapter 1	$tips\ g^{-1}$
RBI	root branching intensity	see Chapter 1	$tips\ cm^{-1}$
CTAB	cetyl trimethyl	—	—

	ammonium bromide buffer		
Al	Aluminium	—	ppm
B	Boron	—	ppm
Ca	Calcium	—	ppm
C	Carbom	—	%
Cu	Copper	—	ppm
Fe	Iron	—	%
Mg	Magnesium	—	%
Mn	Manganese	—	ppm
Mo	Molybdenum	—	ppm
N	Nitrogen	—	%
Na	Sodium	—	ppm
P	Phosphorus	—	%
K	Potassium	—	ppm
S	Sulphur	—	ppm
Zn	Zinc	—	ppm
ITS2	Fungal nuclear ribosomal internal transcribed spacer 2	The genetic marker of fungal nuclear ribosomal DNA (about 200 bases in length, on average). This marker has been shown to adequately differentiate fungal taxa.	—
PCR	Polymerase chain reaction	The biochemical reaction used to replicate (i.e., amplify) DNA sequences.	—
OTU	operational taxonomic unit	the basic bioinformatic unit for species classification from gene sequence	—

		similarity.	
SynMock	synthetic mock community	a non-biological community of fungal ITS gene-sequences used to identify index-bleed in next-generation sequencing.	—
FUNGuild	functional guild	Fungal functional guild from the Nguyen et al. FUNGuild database.	—
H`	Shannon's diversity	Shannon's index to summarize the diversity of species within a community, calculated as: $H = \sum_{i=1}^{s} p_i \ln p_i$, where p is proportion of individuals of a species (i.e., OTU reads) in a community, and s is species richness.	—
J`	Pielou's species evenness	Pielou's index to describe the relative abundance of species within a community, cacluated as $J = {H'}/{\ln s}$, where H` is Shannon diversity and s is species richness.	—
db-RDA	distance-based Redundancy Analysis	A method of constrained ordination using a community dissimilarity as the response variable	—
GAM	generalized additive model	a gereralized linear model method where the response variable depends on a linear and smooth term(s).	—
SIMPER	similarity percentage analysis	a statistical test which calculates the average relative contribution of individual species to the dissimilarity in community composition among sites.	—
PD	Phylogenetic distance	A pairwise metric that quantifies the relatedness among species using phylogenetic tree branch lengths.	—

Chapter 5: The physiological acclimation and growth response of Populus trichocarpa to warming

Abbreviation	Complete Term	Units
A	net photosynthetic rate	μmol m^{-2} s^{-1}
A_{max}	the maximum rate of light-saturated photosynthesis	μmol m^{-2} s^{-1}
$A_{net,29}$	the net photosynthetic rate at 29°C	μmol m^{-2} s^{-1}
A_{opt}	the rate of net photosynthesis at the thermal optimum of photosynthesis	μmol m^{-2} s^{-1}
C	Carbon	—
CO_2	carbon dioxide	—
ETR_{PSII}	electron transport rate of photosystem II	μmol m^{-2} s^{-1}
g_{sw}	stomatal conductance to water vapor	mol m^{-2} s^{-1}
IRGA	infrared laser gas analyser	—
$J_{max,\ 25}$	the maximum rate or electron transport at 25°C	μmol m^{-2} s^{-1}
N	Nitrogen	—
Φ	The apparent quantum yield of photosynthesis	unitless
Φ_{CO_2}	the quantum yield of CO_2 assimilation corrected for dark respiration	unitless
Φ_{PSII}	the quantum efficiency of photosystem II	unitless
PPFD	photosynthetic photon flux density	μmol m^{-2} s^{-1}
R_{BG}	belowground (i.e., soil and soil + root) respiration (see methods)	μmol m^{-2} s^{-1}
$R_{d,29}$	leaf dark respiration rate at 29°C	μmol m^{-2} s^{-1}
R_r	root respiration rate (mass-based)	μmol g^{-1} s^{-1}
$R_{r,\ opt}$	the mass-based root respiration rate at the temperature optimum of root respiration	μmol g^{-1} s^{-1}
$R_{r,29}$	the mass-based root respiration rate at 29°C	μmol g^{-1} s^{-1}

$R_{r\text{-}N}$	N-mass based root respiration rate	nmol g N^{-1} s^{-1}
$R_{r\text{-}N,\ opt}$	the N-mass based root respiration rate at the temperature optimum of root respiration	nmol g N^{-1} s^{-1}
$R_{r\text{-}N,29}$	the N-mass-based root respiration rate at 29°C	nmol g N^{-1} s^{-1}
R_s	rate of soil CO_2 efflux	µmol m^{-2} s^{-1}
R_{s+r}	rate of soil plus plant root CO_2 efflux	µmol m^{-2} s^{-1}
$R_{s+r} - R_s$	the difference between the rate of soil only CO_2 efflux and the rate of soil plus plant root CO_2 efflux	µmol m^{-2} s^{-1}
T	Temperature	°C
T_{leaf}	leaf temperature	°C
T_{opt}	thermal optimum of photosynthesis	°C
T_{opt} R_r	the thermal optimum of root respiration	°C
Q_{10}	the temperature sensitivity of leaf respiration	unitless
Q_{10} $R_{r,29}$	temperature sensitivity of root respiration at 29°C	unitless
RuBP	ribulose bisphosphate	—
$V_{cmax,25}$	the maximum rate of carboxylation at 25°C	µmol m^{-2} s^{-1}
VPD	vapor pressure deficit	kPa

Chapter 6: Functional variability in specific root respiration translates to slight differences in belowground CO_2 efflux in a temperate deciduous forest in Oak Ridge, Tennessee.

Abbreviation	Complete Term	Definition	Units
CO_2	carbon dioxide	—	—
R_S	belowground respiration	Soil CO_2 release	nmol s^{-}

	(including autotrophic and heterotrophic components)		[1]
C	carbon	—	—
R_a	autotrophic (i.e., root) respiration	Belowground CO_2 release in soil from root tissues only	mg g^{-1}
N_{root}	root nitrogen concentration	the amount of nitrogen in root tissue	mg g^{-1}
R_r	root tissue specific respiration rate (mass-based)	The rate of CO_2 release per gram of root tissue	nmol g^{-1} s^{-1}
RTD	root tissue density	See Chapter 1	g cm^{-3}
AM	Arbuscular mycorrhizal	see Chapter 4	—
ECM	Ectomycorrhizal	see Chapter 4	—
MANE	Mycorrhizal absorption nutrient economies hypothesis	Hypothesis where arbuscular mycorrhizal associations facilitate inorganic nutrient economies (i.e., mineralization), while ectomycorrhizal associations facilitate organic nutrient economies (i.e., plant-derived).	—
R_a / R_S	the contribution of root respiration to total belowground respiration	—	unitless
C_{root}	Root carbon concentration	the amount of carbon in root tissue	mg g^{-1}
SRL	specific root length	see Chapter 1	g m^{-1}
SRA	specific leaf area	see Chapter 1	m^2 kg^{-1}
N	nitrogen	—	—
TC	total soil carbon	—	mg L^{-1}

DOC	dissolved organic soil carbon	—	$\mu g\ g^{-1}$
MBC	microbial soil carbon	—	$\mu g\ g^{-1}$
TN	total soil nitrogen	—	$mg\ L^{-1}$
DN	dissolved soil nitrogen	—	$\mu g\ g^{-1}$
MBN	microbial soil nitrogen	—	$\mu g\ g^{-1}$
ANOVA	analysis of variance	—	—
HSD	Tukey's post-hoc test for honest significant difference	—	—
PCA	principal components analysis	—	—
SRTA	specific root tip abundance	see Chapter 1	$tips\ g^{-1}$

INTRODUCTION TO THE DISSERTATION

Background

Plant roots have evolved concurrently with and have led to the diversification of land plant lineages (Kenrick and Strullu-Derrien 2014). The evolutionary evidence points to the evolution of the first root systems of land plants during the early Devonian period about 410-395 million years (Raven and Edwards 2001). The specialization of plant tissues, including meristematic elongation, played a principal role in root system origins (Harrison 2017). The first plant root systems were primitive collections of bifurcating shoot-like projections (called rhizomorphs) with spirally attached rootlets and root hairs (Raven and Edwards 2001, Kenrick and Strullu-Derrien 2014). Since their evolution, tree roots have become intimately specialized to their environment, developing distinct functional strategies (Weemstra et al. 2016, Laliberté 2017, McCormack and Iversen 2019, Bergmann et al. 2020).

A comparative functional approach is used to understand the dimensions of root functional strategies among tree species. Because of the varied morphologies of roots has this evolutionary context, we must explicitly account for plant phylogenetic-relatedness when assessing root function (Valverde-Barrantes et al. 2017, Wang et al. 2018). We know that across taxa, there are general patterns, with gymnosperms and lesser evolved angiosperms (e.g., Magnoliids) having thicker, less dense, shorter roots, with fewer fine root tips (i.e., low specific root length: SRL) (Kong et al. 2014, Valverde-Barrantes et al. 2016, Ma et al. 2018); thus they probably relying more on mycorrhizal associations for nutrient acquisition (Guo et al. 2008, Eissenstat et al. 2015, Chen et al. 2016, Valverde-Barrantes et al. 2016). Evidence of this reliance is a greater percentage of cortical tissue,

which may have evolved to promote fungal colonization and nutrient exchange (Bonfante and Genre 2010, Chen et al. 2011, Kong et al. 2014, Eissenstat et al. 2015, Valverde-Barrantes et al. 2016, Maherali 2017, Valverde-Barrantes et al. 2017), however competing hypotheses exist on the evolution of root morphology (i.e., root stele diameter to total diameter ratio variability among species in reference to an ancestral state) (Kong et al. 2017).

Variation in root traits has immense ramifications for species ecologies; conservative root trait values (low SRL, low nutrient uptake capacity, low root respiration, large diameter, high C:N ratio, high tissue density, and long root lifespan) should correspond to a slow-growth, long-lived plant strategy, and vice versa (Grime 1977, Reich 2014) The dimensions of variation in root functional traits may not perfectly interrelate, because of the myriad of strategies for nutrients and water uptake that roots can employ (Ma et al. 2018, Kong et al. 2019, McCormack and Iversen 2019, Bergmann et al. 2020, Weemstra et al. 2020). For example, SRL, a proxy for the root absorptive potential and nutrient uptake area at a given biomass cost, is independent of root diameter and root tissue density (Kramer-Walter et al. 2016). SRL is positively correlated with plant performance (e.g., relative growth rate) (Comas and Eissenstat 2009, Kramer-Walter et al. 2016), supporting the idea that acquisitive, fast-growing species potentially produce inexpensive roots with minimal carbon investment, low root tissue densities, and short lifespans. This tradeoff logically corresponds to our knowledge about tradeoffs between acquisitive and conservative leaf functional traits (Shipley et al. 2006) and plant strategies along a fast-slow spectrum (Shipley 1995, Wright et al. 2010, Reich 2014). Tradeoffs in root system morphology represent abiotic

root system adjustment among species or concerning the environment, which is the first axis of functional variation of root systems addressed in this dissertation. It is incorporated within chapters one, two, four, and five.

Differences in root morphology among species have evolved because of a divergent gradient of strategies for nutrient uptake (Eissenstat et al. 2015, Lu and Hedin 2019). A single tree can have hundreds of kilometers of roots with hundreds to thousands of root tips, potentially millions of microbiological interactions with fungi and bacteria in the rhizosphere (Eshel and Beeckman 2013). Much of tree root length is devoted to the transport of water and nutrients to the stem and leaves of the plan, with the fine roots (those <2mm in diameter) being most responsible for water and nutrient uptake through interactions with the biotic and abiotic environment (Fitter 1991, McCormack et al. 2015). Thus, variation in fine root length, surface area, and tip abundance are inherently key to tree biological functioning because they provide the interface for biochemical reactions that sustain plant life. The current paradigm of the biotic dimension of root function variation is that roots either invest resources (mainly C) in nutrient foraging via root biomass and enzyme production or allocate them to mycorrhiza in exchange for other nutrients (Roumet et al. 2016, Faucon et al. 2017, Bergmann et al. 2020). This is supported by a wide range of nutrient foraging strategies, including nonmycorrhizal roots, and the observation that evolutionary-stable differences in root morphology can arise among arbuscular mycorrhizal (AM) vs. ectomycorrhizal (ECM) hosts (Lu and Hedin 2019). Thus, the root system fungal (and bacterial) communities reflect their function (i.e., strategy for obtaining water and nutrients) within a multidimensional soil environment that includes complex abiotic (i.e., biochemical) and biotic (i.e., bacterial,

and fungal) interactions within the rhizosphere (Laliberté 2017). The soil environment's interactions with fungi and bacteria represent the second (i.e., biotic) dimension of root functional variation evaluated. This dimension is investigated in chapters four and five.

This dissertation's main idea on tree root morphology and functioning is the hypothesis of an acquired abiotic and biotic tradeoff (Bergmann et al. 2020), which directly relates to tree nutrient acquisition strategy, root morphology, and its expression within environments. Together, these and other characteristics like root tissue elemental (e.g., nitrogen: N) collective, make up the root-functional strategy (Fig. 1). Furthermore, recent research has shown that the root functional strategy of trees is highly dimensional (Weemstra et al. 2016, Laliberté 2017) for two main reasons: 1) that roots are 3-dimensional structures, and 2) that root function is related to the foraging for many nutrients, which is coupled with the diffuse flow of water through the soil matrix and into the root (a nonlinear process) (Fitter 1991, Warren et al. 2015).

We hypothesize that a critical tradeoff axis exists with respect to abiotic vs. biotic nutrient foraging strategies of tropical trees (Fig. 1). On one side of the continuum, nonmycorrhizal (or less-mycorrhizal) associated species invest more in developing fine roots with higher enzymatic activity (Cabugao et al. 2017, Lugli et al. 2020, Cabugao et al. 2021); on the other, mycorrhizal species have evolved symbiotically with their fungi (Valverde-Barrantes et al. 2017), but at what cost? and with what consequences for plant and soil communities and ecosystem functioning? The carbon investment costs in either biomass production or mycorrhizal association is a process that likely varies by species and across root order but is seemingly relatively unaffected by soil fertility (Burton et al. 2002, Hendricks et al. 2006). However, root morphology-soil nutrient relationships must

exist due to the heterogeneity of the soil matrix and the wide variety of root morphologies found in forests (Powers et al. 2005).

Furthermore, within the above-outlined tradeoff in carbon investment, little is known about associated differences in root biological functioning and morphology, how environmental influences may affect them, or how they relate to the higher-order community or ecosystem processes (Bardgett et al. 2014, Freschet et al. 2021). In the abiotic dimension, acquisitive roots have higher specific root length, area, and more developed branching morphologies (i.e., high specific root tip abundance). Conservative fine roots have more carbon investment, greater average diameter, and higher tissue densities. Biotic interactions with mycorrhizae slightly favor acquisitive root strategies but are ubiquitous. Understanding how these processes scale up in space (i.e., along an environmental gradient) and with time (i.e., forest succession) is an important theme addressed in this dissertation.

Focus

This dissertation focuses on the fine root systems of a diverse group of woody tree species and their variation in form and function in an environmental context. Most measurements are done at the individual root system level, containing 3-4 orders of physiologically active fine roots (<2mm diameter) (McCormack and Iversen 2019). Other measurements are made at the tissue level (e.g., elemental analyses or sequencing work), limited to the finest first-order roots. I also address patterns in leaf functional traits within a similar context. Although this is not an explicit focus of this dissertation, it helps frame our understanding of root functional variation because leaves are studied

much more heavily, and collecting leaves is little additional work when collecting entire root systems.

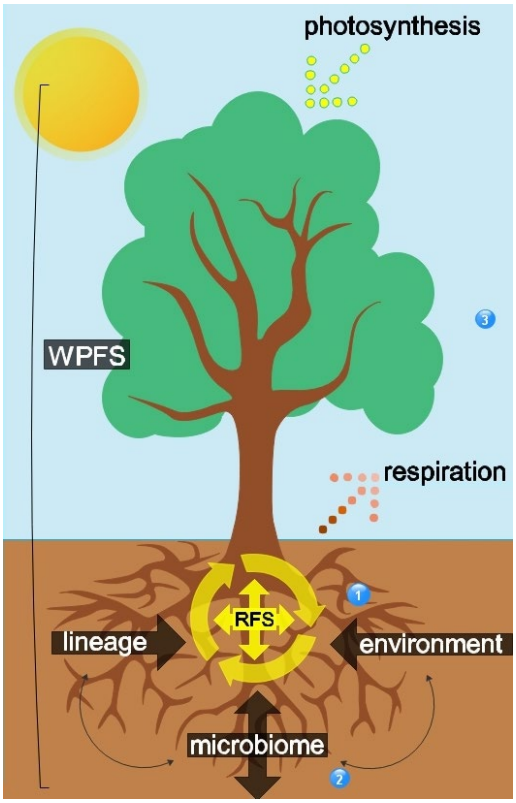

Fig. 1: Tree root functional strategy (RFS) is defined by plant lineage, the biotic dimension of the root microbiome within the soil and the soil environment itself (the abiotic dimension). We assess evaluate this framework in the context of whole plant functional strategy (WPFS, which incorporates leaf and stem economics and species life history). Part one of the dissertation evaluates how environment and lineage shape tree RFS. Parts 2 and 3 investigates how the microbiome interacts with RFS. Part 3 looks at whole plant physiology and root respiration to link RFS to the environment in a greater ecosystem context.

Value

The value of this work arises from the linkage of the functional perspective to physiological measurements and across ecological scales (roots, individual trees, species, and communities) within an environmental context. I incorporate intraspecific trait variation in the designs where root traits were measured and where other biological or physiological measurements were taken; they were measured on individual root systems. I also try to scale measurements where appropriate to try to compare or inform on community or ecosystem processes. Significant value also lies in the exhaustive exploration of the dimensions of root functional strategies. I measure a wide variety of root characteristics, which vary in their difficulty to assess and their degree of study. The

incorporation of root chemistry, physiology, and genetic sequencing add value to the morphological measurements of root systems.

Research Objectives

In part one of this work, I address how root functional strategies vary among species and along a soil gradient in tropical forest successional status. I link variation in root functional form to plant performance in terms of species turnover with the environment at the community level and in terms of how whole-plant element status varies with the soil environment. In part two, I similarly evaluate how the soil environment affects root functional strategy with tropical forest succession; however, in this part, I focus on the biotic dimension of root-inhabiting fungi. Lastly, in part three, I address the effect of root functional strategy on soil respiration, a directly emergent ecosystem response. I explore vital dimensions that control root respiration rates, like temperature, root nitrogen content, and the microbiome. Taken in concert, the three parts of this dissertation seek to build a comprehensive discourse on the functioning of tree roots, which links aspects of plant functional and physiological ecology to community and ecosystem ecology.

References

Bardgett, R. D., L. Mommer, and F. T. De Vries. 2014. Going underground: root traits as drivers of ecosystem processes. Trends in Ecology & Evolution **29**:692-699.

Bergmann, J., A. Weigelt, F. van der Plas, D. C. Laughlin, T. W. Kuyper, N. Guerrero-Ramirez, O. J. Valverde-Barrantes, H. Bruelheide, G. T. Freschet, C. M. Iversen, J. Kattge, M. L. McCormack, I. C. Meier, M. C. Rillig, C. Roumet, M. Semchenko, C. J. Sweeney, J. van Ruijven, L. M. York, and L. Mommer. 2020. The fungal collaboration gradient dominates the root economics space in plants. Science Advances **6**:eaba3756.

Bonfante, P., and A. Genre. 2010. Mechanisms underlying beneficial plant–fungus interactions in mycorrhizal symbiosis. Nature Communications **1**:48.

Burton, A., K. Pregitzer, R. Ruess, R. Hendrick, and M. Allen. 2002. Root respiration in North American forests: effects of nitrogen concentration and temperature across biomes. Oecologia **131**:559-568.

Cabugao, K. G., C. M. Timm, A. A. Carrell, J. Childs, T.-Y. S. Lu, D. A. Pelletier, D. J. Weston, and R. J. Norby. 2017. Root and rhizosphere bacterial phosphatase activity varies with tree species and soil phosphorus availability in Puerto Rico tropical forest. Frontiers in plant science **8**:1834.

Cabugao, K. G., D. Yaffar, N. Stenson, J. Childs, J. Phillips, M. A. Mayes, X. Yang, D. J. Weston, and R. J. Norby. 2021. Bringing function to structure: Root–soil interactions shaping phosphatase activity throughout a soil profile in Puerto Rico. Ecology and Evolution **11**:1150-1164.

Chen, I.-C., J. K. Hill, R. Ohlemüller, D. B. Roy, and C. D. Thomas. 2011. Rapid range shifts of species associated with high levels of climate warming. Science **333**:1024-1026.

Chen, W., R. T. Koide, T. S. Adams, J. L. DeForest, L. Cheng, and D. M. Eissenstat. 2016. Root morphology and mycorrhizal symbioses together shape nutrient foraging strategies of temperate trees. Proceedings of the National Academy of Sciences **113**:8741-8746.

Comas, L., and D. Eissenstat. 2009. Patterns in root trait variation among 25 co-existing North American forest species. New Phytologist **182**:919-928.

Eissenstat, D. M., J. M. Kucharski, M. Zadworny, T. S. Adams, and R. T. Koide. 2015. Linking root traits to nutrient foraging in arbuscular mycorrhizal trees in a temperate forest. New Phytologist **208**:114-124.

Eshel, A., and T. Beeckman. 2013. Plant roots: the hidden half. CRC press.

Faucon, M.-P., D. Houben, and H. Lambers. 2017. Plant functional traits: soil and ecosystem services. Trends in plant science **22**:385-394.

Fitter, A. 1991. Characteristics and functions of root systems. Plant roots: the hidden half **2**:1-29.

Freschet, G. T., C. Roumet, L. H. Comas, M. Weemstra, A. G. Bengough, B. Rewald, R. D. Bardgett, G. B. De Deyn, D. Johnson, J. Klimešová, M. Lukac, M. L. McCormack, I. C. Meier, L. Pagès, H. Poorter, I. Prieto, N. Wurzburger, M. Zadworny, A. Bagniewska-Zadworna, E. B. Blancaflor, I. Brunner, A. Gessler, S. E. Hobbie, C. M. Iversen, L. Mommer, C. Picon-Cochard, J. A. Postma, L. Rose, P. Ryser, M. Scherer-Lorenzen, N. A. Soudzilovskaia, T. Sun, O. J. Valverde-Barrantes, A. Weigelt, L. M. York, and A. Stokes. 2021. Root traits as drivers of plant and ecosystem functioning: current understanding, pitfalls and future research needs. New Phytologist doi: 10.1111/nph.17072.

Grime, J. P. 1977. Evidence for the existence of three primary strategies in plants and its relevance to ecological and evolutionary theory. The american naturalist **111**:1169-1194.

Guo, D., M. Xia, X. Wei, W. Chang, Y. Liu, and Z. Wang. 2008. Anatomical traits associated with absorption and mycorrhizal colonization are linked to root branch order in twenty-three Chinese temperate tree species. New Phytologist **180**:673-683.

Harrison, J. C. 2017. Development and genetics in the evolution of land plant body plans. Philosophical Transactions of the Royal Society B: Biological Sciences **372**:20150490.

Hendricks, J. J., R. L. Hendrick, C. A. Wilson, R. J. Mitchell, S. D. Pecot, and D. Guo. 2006. Assessing the patterns and controls of fine root dynamics: an empirical test and methodological review. Journal of Ecology **94**:40-57.

Kenrick, P., and C. Strullu-Derrien. 2014. The Origin and Early Evolution of Roots. Plant Physiology **166**:570-580.

Kong, D., C. Ma, Q. Zhang, L. Li, X. Chen, H. Zeng, and D. Guo. 2014. Leading dimensions in absorptive root trait variation across 96 subtropical forest species. New Phytologist **203**:863-872.

Kong, D., J. Wang, H. Wu, O. J. Valverde-Barrantes, R. Wang, H. Zeng, P. Kardol, H. Zhang, and Y. Feng. 2019. Nonlinearity of root trait relationships and the root economics spectrum. Nature Communications **10**:2203.

Kong, D., J. Wang, H. Zeng, M. Liu, Y. Miao, H. Wu, and P. Kardol. 2017. The nutrient absorption–transportation hypothesis: optimizing structural traits in absorptive roots. New Phytologist **213**:1569-1572.

Kramer-Walter, K. R., P. J. Bellingham, T. R. Millar, R. D. Smissen, S. J. Richardson, and D. C. Laughlin. 2016. Root traits are multidimensional: specific root length is independent from root tissue density and the plant economic spectrum. Journal of Ecology **104**:1299-1310.

Kramer-Walter, K. R., P. J. Bellingham, T. R. Millar, R. D. Smissen, S. J. Richardson, and D. C. Laughlin. 2016. Root traits are multidimensional: specific root length is independent from root tissue density and the plant economic spectrum. Journal of Ecology **104**:1299-1310.

Laliberté, E. 2017. Below-ground frontiers in trait-based plant ecology. New Phytologist **213**:1597-1603.

Lu, M., and L. O. Hedin. 2019. Global plant–symbiont organization and emergence of biogeochemical cycles resolved by evolution-based trait modelling. Nature Ecology & Evolution **3**:239-250.

Lugli, L. F., K. M. Andersen, L. E. Aragão, A. L. Cordeiro, H. F. Cunha, L. Fuchslueger, P. Meir, L. M. Mercado, E. Oblitas, and C. A. Quesada. 2020. Multiple phosphorus acquisition strategies adopted by fine roots in low-fertility soils in Central Amazonia. Plant and Soil **450**:49-63.

Ma, Z., D. Guo, X. Xu, M. Lu, R. D. Bardgett, D. M. Eissenstat, M. L. McCormack, and L. O. Hedin. 2018. Evolutionary history resolves global organization of root functional traits. Nature **555**:94-97.

Maherali, H. 2017. The evolutionary ecology of roots. New Phytologist **215**:1295-1297.

McCormack, M. L., I. A. Dickie, D. M. Eissenstat, T. J. Fahey, C. W. Fernandez, D. Guo, H. S. Helmisaari, E. A. Hobbie, C. M. Iversen, and R. B. Jackson. 2015. Redefining fine roots improves understanding of below-ground contributions to terrestrial biosphere processes. New Phytologist **207**:505-518.

McCormack, M. L., and C. M. Iversen. 2019. Physical and Functional Constraints on Viable Belowground Acquisition Strategies. Frontiers in Plant Science **10**.

Powers, J. S., K. K. Treseder, and M. T. Lerdau. 2005. Fine roots, arbuscular mycorrhizal hyphae and soil nutrients in four neotropical rain forests: patterns across large geographic distances. New Phytologist **165**:913-921.

Raven, J. A., and D. Edwards. 2001. Roots: evolutionary origins and biogeochemical significance. Journal of experimental botany **52**:381-401.

Reich, P. B. 2014. The world-wide 'fast–slow'plant economics spectrum: a traits manifesto. Journal of Ecology **102**:275-301.

Roumet, C., M. Birouste, C. Picon-Cochard, M. Ghestem, N. Osman, S. Vrignon-Brenas, K. f. Cao, and A. Stokes. 2016. Root structure–function relationships in 74 species: evidence of a root economics spectrum related to carbon economy. New Phytologist **210**:815-826.

Shipley, B. 1995. Structured interspecific determinants of specific leaf area in 34 species of herbaceous angiosperms. Functional Ecology:312-319.

Shipley, B., M. J. Lechowicz, I. Wright, and P. B. Reich. 2006. Fundamental tradeoffs generating the worldwide leaf economics spectrum. Ecology **87**:535-541.

Valverde-Barrantes, O. J., A. L. Horning, K. A. Smemo, and C. B. Blackwood. 2016. Phylogenetically structured traits in root systems influence arbuscular mycorrhizal colonization in woody angiosperms. Plant and Soil **404**:1-12.

Valverde-Barrantes, O. J., G. T. Freschet, C. Roumet, and C. B. Blackwood. 2017. A worldview of root traits: the influence of ancestry, growth form, climate and mycorrhizal association on the functional trait variation of fine-root tissues in seed plants. New Phytologist **215**:1562-1573.

Wang, R., Q. Wang, N. Zhao, Z. Xu, X. Zhu, C. Jiao, G. Yu, and N. He. 2018. Different phylogenetic and environmental controls of first-order root morphological and nutrient traits: Evidence of multidimensional root traits. Functional ecology **32**:29-39.

Warren, J. M., P. J. Hanson, C. M. Iversen, J. Kumar, A. P. Walker, and S. D. Wullschleger. 2015. Root structural and functional dynamics in terrestrial biosphere models – evaluation and recommendations. New Phytologist **205**:59-78.

Weemstra, M., L. Mommer, E. J. Visser, J. Ruijven, T. W. Kuyper, G. M. Mohren, and F. J. Sterck. 2016. Towards a multidimensional root trait framework: a tree root review. New Phytologist **211**:1159-1169.

Weemstra, M., K. G. Peay, S. J. Davies, M. Mohamad, A. Itoh, S. Tan, and S. E. Russo. 2020. Lithological constraints on resource economies shape the mycorrhizal composition of a Bornean rain forest. New Phytologist **228**:253-268.

Wright, S. J., K. Kitajima, N. J. Kraft, P. B. Reich, I. J. Wright, D. E. Bunker, R. Condit, J. W. Dalling, S. J. Davies, and S. Díaz. 2010. Functional traits and the growth-mortality tradeoff in tropical trees. Ecology **91**:3664-3674.

PART 1: Within and among species variability in root and leaf functional traits

CHAPTER 1: Morphological variation of fine root systems and leaves in primary and secondary tropical forest of Hainan Island, China

This chapter has been published in *Annals of Forest Science*:

Hogan JA, Valverde-Barrantes OJ, Ding Q, Xu H & Baraloto C. Morphological variation of fine root systems and leaves in primary and secondary tropical forest of Hainan Island, China. *Annals of Forest Science* 77:79. doi: 10.1007/s13595-020-00977-7. It is reproduced, here, with permission from Springer Nature.

Key message

In older, unlogged rainforest of Hainan Island, China, leaves of saplings were larger, and fine root systems of saplings were thicker with fewer root tips than in historically logged areas. These results were consistent among 15 Angiosperm lineages, even though families differed widely in their leaf and root traits.

Abstract

How plant organ morphologies vary with environment is key for inferring plant functional strategies. We were interested in quantifying any changes in fine root and leaf morphology of saplings with local-scale environmental variation in tropical forest, and if any variation in organ morphologies differed with plant lineage. We measured functional traits of fine root systems and leaves of saplings from 15 families in historically logged and unlogged Chinese tropical forest, where soil fertility and texture slightly decreased with greater forest age. Root morphological traits were more conservative, while leaf morphologies were more acquisitive in primary forest than in secondary forest. From secondary to primary forest, mean root system diameter increased 0.4 mm, mean specific root length decreased 0.35 m g^{-1}, and mean root system branching intensity decreased by 0.3 tips cm^{-1}. Similarly, from secondary to primary forest, average leaf area increased 7 cm^2 and specific leaf area decreased 0.8 $m^2 kg^{-1}$. Leaf thickness and root tissue density were not different. Among the selected plant families, root and leaf morphological differences between forest types were consistent. Within lineage (i.e., intraspecific) root and leaf morphological variation showed contrasting patterns. Local-scale variation in

soil phosphorus and base saturation affected intraspecific variation in root diameter and SRL.

Keywords: plant functional traits, trait variation, root morphology, leaf morphology, tropical forest, Jianfengling, Hainan Island.

Introduction

Comparative ecology with plant traits has been a popular approach to understand trade-offs in plant form, physiology, and biological functioning, which generally scale with variation in plant ecological life-history (Keddy 1992; Weiher et al. 1999; Westoby and Wright 2006; Shipley et al. 2016; Körner 2018). Functional traits, such as specific leaf area (SLA, Garnier et al. 2001), or wood density (Chave et al. 2009) inform about resource allocation within the plant in relation to a fast or slow growth strategy (Wright et al. 2010; Reich 2014), total photosynthetic potential (Shipley 1995), or other measures of the relative performance across plant species (Weiher et al. 1999; Ackerly et al. 2002; Díaz et al. 2016). Interspecific tradeoffs in resource allocation concerning the most-commonly measured functional traits have been observed along at least two orthogonal axes of variation (Díaz et al. 2016): one encompassing stem economics (Baraloto et al. 2010) related to whole plant size (King 1996), and another related to the leaf economics spectrum (Wright et al. 2004).

Functional trait measurement of fine roots is a relatively recent development in plant functional ecology (Bardgett et al. 2014; Laliberté 2017; Iversen et al. 2017). The emerging hypothesis for variation in root functional traits among plant species is that low specific root length (SRL), thick root diameter, high C:N ratios in tissues, and high root tissue density should relate to low nutrient uptake capacities, low rates of root respiration, and long root lifespans, and are thus, considered conservative root traits (Fig. 1). By extending plant economics theory (Bloom et al 1985; Reich 2014) to roots, such conservative root traits should reflect a slow-growth plant strategy (Reich 2014; Weemstra et al. 2016), although a consensus is currently lacking. In contrast, thin root diameters, high SRL, high root tissue N content, and low root tissue densities should relate to higher rates of root respiration, fast rates of root turnover, and should be acquisitive traits indicative of a fast-growth plant strategy (Fig. 1). Root tissue density

and diameter are positively related to root lifespan and drought-resistance, but negatively related to nutrient uptake potential (Kramer-Walter et al. 2016; Valverde-Barrantes and Blackwood 2016). Accordingly, root diameter and tissue density should increase among species with a fast-growth to a slower-growth strategy, while SRL, root area, and root tip abundance should decrease (Weemstra et al. 2016; McCormack et al. 2012; Fig. 1).

Plant evolutionary history strongly constrains root morphologies. Across taxa, the general pattern is that gymnosperms and basal angiosperms (e.g., Magnoliids) have thicker, less-dense, shorter roots, with fewer fine root tips than more derived angiosperms (Kong et al. 2014; Valverde-Barrantes et al. 2016; Wang et al. 2019). This may signify a greater reliance on mycorrhizal associations for nutrient acquisition (Eissenstat et al. 2015; Chen et al. 2016; Valverde-Barrantes et al. 2016; Kong et al. 2017), or it may be a result of divergent evolutionary processes that have created a high degree of phylogenetic conservatism in Angiosperm root diameter (Ma et al. 2018; Lu and Hedin 2019). Thus, because of the systematic variation in root diameter, studies investigating intraspecific variation in root morphologies in relation to the environment should account for plant lineage. Demonstratively, using family-level data from 581 species from 22 plant orders (Valverde-Barrantes et al. 2017), Maherali (2017) showed that the standard deviation of root diameter increased with the average root diameter. Yet, there was substantial variation among families, and therefore it remains uncertain how intraspecific variation in root morphology due to environment scales with root diameter, plant lineage, or plant strategy. A large proportion of the variation in root morphologies can be explained by continental-scale climate variation (Jackson et al. 1996; Freschet et al. 2017; Wang et al. 2019), yet some variation remains unaccounted for (Freschet and Roumet 2017; Valverde-Barrantes et al. 2017). For example, specific root length and root tissue density of Gymnosperm roots decrease with increasing latitude in boreal forests; that is, roots show an intraspecific conservative shift with decreasing temperature and increasing soil fertility (Zadworny et al. 2016; Defrenne et al. 2019). In addition, a more-general community shift in root acquisitiveness occurs toward the tropics as Angiosperms dominate over Gymnosperms (Wang et al. 2018; Wang et al. 2019).

Root morphology also varies with the local soil environment. At the individual plant scale, variation in root traits can be large; for example, interspecific variation in root diameter, specific root length (SRL), and link length within a community can be twenty-fold (Comas and Eissenstat 2009; Guo et al. 2008). Such variation has potentially large ramifications for the ecologies of plant species (Schenk and Jackson 2002; Craine et al. 2001; Comas and Eissenstat 2009; Van Kleunen et al. 2010; Bardgett et al. 2014; Wang et al. 2018), including nutrient acquisition and use strategies (Warren et al. 2015)and how species respond to selection pressures (e.g., altered soil fertility, land-use change, or forest recovery). Despite interspecific differences in root diameter, plants have been shown to modulate root architecture in response to cues in the soil environment (i.e., soil moisture and fertility; Fitter and Stickland 1991; López-Bucio et al. 2003; Hodge et al. 2009). Nutrient deficiencies in the soil usually lead to the lengthening and architectural development of root systems, for example, a more pronounced herringbone topology, with more root branching and longer lengths originating from a single main root (Fitter and Stickland 1991; López-Bucio et al. 2003; Giehl et al. 2013). Thus, understanding interspecific and intraspecific variation in root morphologies with soil conditions, may help quantify the relative role of belowground specialization versus local adaptation among plant lineages.

Leaf morphologies of plants are as less phylogenetically constrained than those of roots (Kembell and Cahill Jr. 2011; Flores et al. 2014), indicating an independence in drivers of among and within species variation in leaf versus root functional traits (Wang et al. 2017). Like roots, climate strongly influences leaf morphology at the continental scale (Wright et al. 2017). At the local-scale, light availably is the primary driver of leaf morphology, with leaves tending to become more acquisitive in more shaded environments. For example, leaves of the same species increase in SLA as light becomes increasingly limited (Liu et al. 2016). The increase in SLA is mainly driven by an increase in leaf area, in response to increasing forest canopy coverage and competition for light (Givnish 1984; Rijkers et al. 2000; Keenan and Niinemets 2017). Yet, despite the relatively subtle shifts in leaf morphologies that occur in response to the light environment, large interspecific differences in leaf morphologies exist among taxa

(Wright et al. 2004; Wright et al. 2010; Wright et al. 2017). Thus, understanding how interspecific and intraspecific variation in leaf morphology interacts with the understory forest light environment (i.e., forest structure and successional status) is important to interpret how environments shape functional trait-environment relationships of plants. Additionally, some evidence shows that among species leaf and root morphologies are related (i.e., SRL increases with increasing SLA, Valverde-Barrantes et al. 2017), however the degree to which intraspecific variation in root systems coordinates with variation in leaves, and how variation relates to the soil environment is not completely understood. Notably, one study found that among Neotropical trees, coarse woody root traits were more aligned with stem than leaf functional traits and that relationships were consistent across different soil habitats present in the Amazon (Fortunel et al. 2012).

Generally, root biomass and competition for soil nutrients increase with forest succession, which drives shifts in the amount and form of available nutrient pools in the soil (Christiansen and Peet 1984; Hertel et al. 2003; Craine; 2006). One might hypothesize that roots of the same species should become more acquisitive (i.e., an intraspecific shift toward acquisitive root functional traits like and increase in root length, see Fig 1), as soil fertility changes with succession (e.g., shifts from nitrate to ammonium dominated nitrogen cycling and cation and base saturation decreases, Werner 1984). However, several studies have documented intraspecific conservative shifts in root morphologies as soil fertility decreases (Eissenstat et al. 2000; Holdaway et al. 2011; Li et al. 2018). Only a few studies have examined how root morphologies vary with forest age in tropical forest (see Hopkins et al. 2006; Hertel et al. 2003; Leuschner et al. 2008; Zangaro et al. 2012; Powers and Peréz- Aviles 2013). Those that have focused on root morphologies in tropical forest have found that root biomass increases, root turnover decreases and generally roots become less acquisitive (e.g., decrease in root length and number of root tips) with increasing successional status (Hertel et al. 2003; Leuschner et al. 2008). However, differences in methodology exist because all of these studies use soil coring methods, which limits their ability to directly assess intraspecific variation in root morphologies. Additionally, competition for light generally increases with forest succession. Morphological plasticity in leaf morphologies in response to light

availability illustrates intraspecific trait variation with environment. Plant root systems must simultaneously forage for 14 mineral elements from the soil in addition to absorbing water (Lynch 2005; Warren et al. 2015), whereas leaves principally respond to light availability. Thus, it is not unreasonable to hypothesize that morphological plasticity of root systems could be more pronounced and multidimensional than that of leaves, due to the more complex nature of soil resource acquisition compared to light interception (Fitter 1991; Weemstra et al. 2016; Maherali 2017; Laliberté 2017)

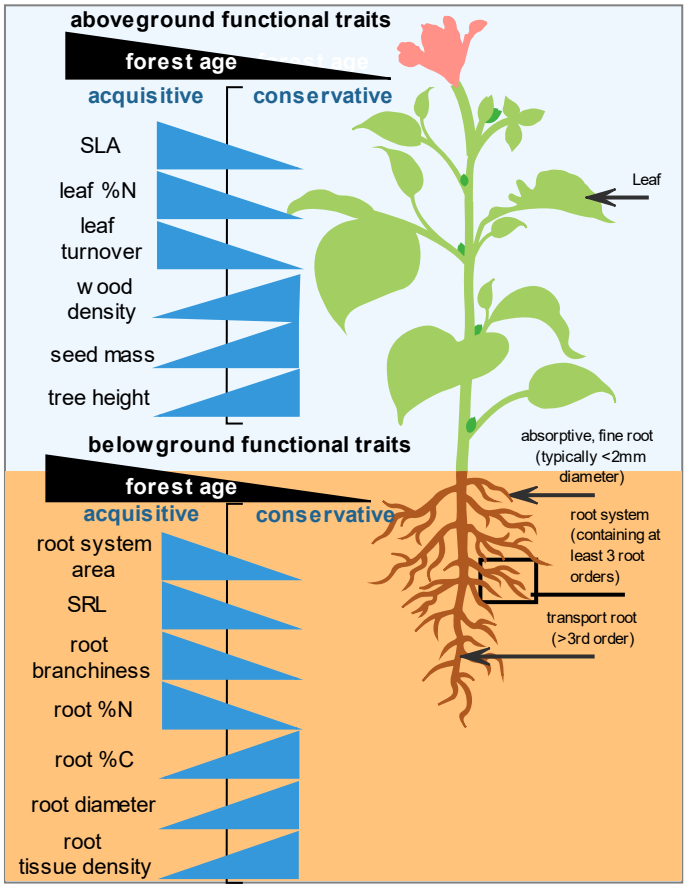

Fig. 1: Conceptual diagram of commonly measured aboveground and belowground functional traits along an acquisitive-conservative life-history continuum (i.e., fast-slow plant spectrum, Reich 2014). Hypotheses for how within-species (i.e. intraspecific) variation in root and leaf morphologies should relate to increasing forest age (i.e. forest succession) are shown in black (see research question 1).

In that context, our two research questions and accompanying hypotheses were:

1. How does functional trait variation in leaves and fine root systems relate to local-scale environmental variation in soil fertility and texture attributable to topical montane forest successional status? *We hypothesized that intraspecific morphologies in understory leaves should become more acquisitive (e.g., increase SLA) as light availability decreases from secondary to primary forest. We hypothesized that roots of the same species would also become more acquisitive (e.g., increase in SRL, diameter)*

from secondary to primary forest. Incorporated in these two independent hypotheses is the idea that individual plants coordinate leaf and root traits to become more acquisitive with increasing forest age (Fig 1).

2. Is morphological variation in root and leaf morphologies consistent across plant lineages? *The testable null hypothesis, here, is that plant organ morphology-environment relationships do vary across lineages, so we hypothesized that intraspecific trait variation with environment would be consistent across taxa.*

To test these hypotheses, we employed a paired sampling design that measured root and leaf morphological traits and soil chemistry within fifteen families, along a 6.6-km transect in a tropical forest in southern China.

Materials and methods

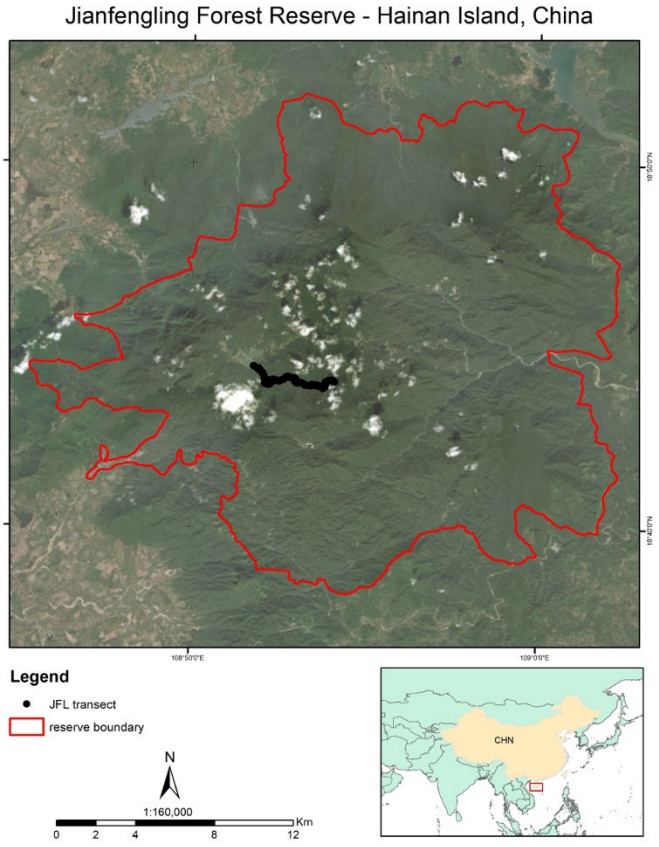

Fig. 2: The study site: the Jianfengling Forest Reserve (JFL) of Hainan Island, China. Hainan Island is a small continental island off the south-eastern coast of China, shown in the red box of the inset map. The 47,200 ha JFL boundary is shown in red. The 6.6 km transect of where functional traits of saplings were sampled is shown in black (see Fig 5. for a topographic map and an elevational profile of the transect). The first half of the transect is in secondary forest with a history of logging with and estimated forest age of about 50 years, and the second half of the transect is in unlogged, primary forest.

Study site: Jianfengling, Hainan Island, China

The Jianfengling forest reserve (JFL), of south-western Hainan Island, China (18°23'–18°15'N & 108°36'–109°05'E, Fig. 2, Fig. 6) is a 47,200-ha area of

mountainous tropical forest with a history of logging and forest resource extraction. Beginning in 1957, about two-thirds of the area was either clear-cut or selectively logged, meaning 30-40% of large timber-valuable trees were extracted (Zhou 1995; Xu et al. 2015). All logging ceased in 1994 under a state-wide (Hainan Island only) logging ban, followed by a Chinese national logging ban in 1998 (Zhou 1995; Wenhua 2004). The reserve encompasses several ecological life zones of vegetation, from tropical semi-deciduous monsoon forest at the lower elevations to mossy high elevation forest, with evergreen-monsoon forest dominated by Podocarpaceae intermixed throughout at elevations < 1000 m (Huang et al. 1995). The most common vegetation life zone is tropical montane rain forest, which occurs at elevations between 600 and 1100 m. This forest is characterized by a mix of palms (principally *Livistona saribus* (Lour.) Merr. ex A. Chev.) and broadleaf evergreen trees that reach an average canopy of height of 18 m (Jin et al. 2013).

The forest has a tropical monsoon climate with seasonal rainfall, where most of the rainfall occurs between May and October (Zeng 1995). From 1965 to 1995, the average annual rainfall in the montane rain forest of JFL averaged about 2700 mm (Wu 1995). The soils are classified as lateritic and humic yellow soils, being derived from porphyritic granite (Wu 1995). Such soils are characterized by surface accumulation of organic matter, slower rates of mineral and organic matter cycling than other tropical soils (e.g., latisols), intermediate rates of mineral leaching, some accumulation of Aluminum, and exchangeable base content of about 30 mL kg^{-1} of soil (Wu 1995).

Field methods

During the summer (May 4 to June 30) of 2017, roots and leaves of juvenile trees (individuals >1m in height but <10 cm diameter at breast height, hereafter saplings) of fifteen families were sampled along a 6.6 km transect within the JFL reserve (Fig. 2, Fig.5, Hogan et al. 2019). The transect was positioned to cover the transition from secondary to primary forest. The secondary forest area of the transect was extensively logged or cut over between 1964 and 1970, making the forest about 50 years old. The primary forest area has no recorded logging history or other anthropogenic land use and included areas of the Jianfengling permanent forest dynamics plot. Forest basal area in

primary and secondary forest is roughly equal, averaging 40.5 (±0.2, standard error) m^2 ha^{-1} in primary forest and 42.7 (±0.2) m^2 ha^{-1} for secondary forest (Xu et al. 2015). A total of 423 individuals (198 in primary and 225 in secondary forest) of 72 species from the 15 focal families (Table 6) were collected in a paired approach, that sought to collect three individuals of each species in each half of the transect.

Lateral fine roots from the top 10 cm of soil were traced out from an identified individual and gently excavated. Excavation of living root systems from saplings was done carefully to preserve root networks to finest first-order roots, using hand trowels. Following root collection, ca. 1 kg of surface soil was collected from the excavated area where roots were collected. Healthy, entire leaves were manually cleaved off the plant at the base of petiole and collected. Leaves and roots were transported back to the lab in plastic bags for processing. Measurements of leaf morphologies were done immediately, and roots were placed in a refrigerator for storage until they could be processed.

Functional trait measurements

For three leaves of each sapling, leaf thickness was measured using a Vernier micrometer (Mitutoyo USA) precise to a thousandth of a millimeter. Leaves, including petioles, were scanned (single-sided scans) for leaf morphological measurements.

Prior to scanning, roots were washed thoroughly. For each individual, three to five root systems, containing at least the first 3 root orders (*sensu* McCormack et al. 2015) were selected from the excavated material. Roots were placed in an acrylic root scanning tray with a cover glass, submerged in water and scanned at high resolution (1200 dpi) in black and white using a double-sided optical scanner (Epson Perfection V800, Epson America, Inc.). Following scanning, leaves and roots were dried in an oven at 70°C for at least 48 hours, before recording their dry mass.

Scanned images of leaves and roots were respectively analyzed using WinFolia (2007b version, Regent Instruments, Quebec, Canada) and WinRhizo (2016 version, Regent Instruments, Quebec, Canada) software. WinFolia measures leaf area, height, width, perimeter, and aspect ratio. Specific leaf area (SLA) was calculated as the ratio of the surface area to the dry mass. WinRhizo measures root length, area, average diameter, volume, and architecture (i.e., the number of root tips and forks) for each root system.

Specific root length (SRL), specific root surface area (SRA), and specific root tip abundance (SRTA) were calculated by dividing root length, root area, and the number of root tips for each root system, respectively, by its dry mass. Root branching intensity (RBI) was calculated by dividing the number of root tips by the root system dry mass. Finally, root tissue density (RTD) was estimated by dividing root system volume by its dry mass.

Soil laboratory analyses

Soils were analyzed for 300 of the 423 individuals collected (150 per forest type of 50 species, see Table 6). Collected soil samples were air dried and sieved using at 2mm mesh sieve. For each sample, about 300 g of soil was analyzed for soil texture and nutrient content. Soil pH was measured using a glass electrode in a 2.5:1 water to soil dilution. The high temperature, external-heat, potassium dichromate oxidation volumetric method was used to measure soil organic matter. The Kelvin-distillation titration method was used to measure soil total nitrogen (N). Total phosphorus (P), available potassium (K), and exchangeable sodium, calcium and magnesium were all measured using an ammonium-acetate extraction, followed by flame atomic absorption spectrophotometry. Total soil K was measured using sodium-hydroxide melting-flame atomic absorption spectrophotometry. Available (i.e., alkali-hydrolysable) soil N was measuring using the alkali-solution diffusion method. Soil available P was measured using by the hydrochloric acid–ammonium fluoride extraction and the molybdenum antimony anti-coloring method. Lastly, soil base saturation (BS) and cation exchange capacity were measured with the ammonium acetate methods.

Data analysis

Principal components analyses (PCA) were carried out on root and leaf functional trait matrices to help reduce dataset dimensionality and identify relationships between leaf and root functional traits (see Figs. 7 & 8). This was done separately for root and leaves, and in our case, we were interested in them separately. The traits used in the PCA for leaves were leaf area, leaf perimeter, leaf width, leaf height, leaf mass, SLA and leaf thickness (see Table 4). The traits used in the root PCA were root length, SRL, SRA, average diameter, RTD, RBI, and SRTA (see Table 5). PCAs were successful in

reducing the dimensionality of morphological trait data, with the first two axes of each PCA explaining 67% of the variability in the leaf trait data (Fig. 7), and 72% of the variability in the root trait data (Fig. 8). Leaf morphological traits were summarized by two main axes of variation (Table 4): mass-based variation (SLA, dimension 2 in Fig. 7) and area-based variation (leaf area, dimension 1 in Fig. 7). Root morphological traits were not as orthogonally organized as leaf traits (Fig. 8, Table 5). Therefore, based on trait correlation with PCA-axes (Tables 4 and 5), three leaf traits: leaf area, SLA, and leaf thickness, and four root traits: Root system average diameter (hereafter root diameter), RTD, SRL, and RBI were chosen for subsequent analyses. We used traits values, instead of PCA axis loadings in analyses to make our results easier to generalize with other studies.

Two-way, univariate analyses of variance (ANOVA) were conducted separately with each of the seven selected functional traits as the response variable. Functional trait values were $\log_{10}$ transformed as necessary to improve their normality, as was the case for leaf area, SRL, root area, and RBI. The two-way ANOVA models were fit in the form of: trait ~ lineage × forest type. Forest type was represented in each model as two-level factor (i.e., primary vs secondary), and plant lineage was represented as species nested within plant family, which allowed us to assess intraspecific trait variation.

Stepwise ANOVA model selection was performed using all possible combinations of species lineage and forest type as factors. In all cases, the best-fitting models included the interaction between lineage and forest type. Those models were then used to predict the least-squared (i.e., marginal) mean trait values with respect to lineage and forest type (i.e., β coefficients were used to estimate mean trait values and their confidence intervals for each lineage in both forest types). Analyses were carried out in R v.3.5.0 (R Core Team 2018) and made use of the 'emmeans' package (Lenth 2018) for predicting the least square mean values. Effect sizes for predictors were calculated using the ω^2 estimator via the 'sjstats' package (Lüdecke 2019). We chose to use the ω^2 effect size estimator, opposed to the η^2 (eta-squared) or η_p^2 (partial eta-squared) estimators, because when predictor variable has many groups levels, η^2 and η_p^2 can be biased, where ω^2 is corrected for this bias (Lüdecke 2019). For interpretation of effect sizes, ω^2 values near

0.01 are considered small, near 0.06 are considered medium and near 0.14 are considered large.

In order to directly assess how variation in soils related to any variation in root traits because of forest type, we conducted analyses of covariance (ANCOVA). One-way ANCOVA models were conducted to determine if statistical differences existed between root functional traits and soil variables controlling for forest type. We used average root trait values for each individual (i.e., for the three to five root systems measured for each sapling), and soils data from the 300 individuals of 50 species where we measured soil properties. ANCOVAs were done using the four root traits from the previous analyses: root diameter, RTD, SRL and RBI and four soil variables of interest: soil base saturation, total nitrogen (N), total phosphorus (P), and total potassium (K). ANCOVA models were constructed similarly to the ANOVA models in the form: trait ~ soil variable * forest type × lineage, where like before, forest type was a two-level factor (i.e., primary vs secondary) and lineage was species nested within family. This is akin to conducting ordinary least-squares regression between soil variables and root trait values by forest type, which we did to graphically assess the direct influence of soil variation on root trait variation relationships.

Results

Soil properties along the transect

Soils in primary forest area of the transect were significantly more acidic and of coarser texture than soils from the secondary portion of the transect (Table 1). The range of soil nutrient contents was greater in secondary than in primary forest. Soils in the secondary forest portion of the transect were more fertile than those of the primary forest area, in that they measured significantly higher in total Phosphorus, total Potassium, available Potassium, total exchangeable bases, effective cation exchange capacity, and base saturation. Soil organic matter, total Nitrogen available Nitrogen, available Phosphorus did not differ along the transect by forest type.

Table 1: Mean and standard error for 14 soil variables from rhizosphere soil in the soil A horizon (0-10 cm depth) for 300 soil samples (150 per forest type) collected during root excavation in the Jianfengling Forest Reserve, Hainan Island, China during summer 2017. Abbreviations are TEB: total exchangeable bases, ECEC: effective cation exchange capacity, and BS: base saturation. Soil grain sizes are 0.5-2 mm, (0.002-0.5mm), and < 0.002 mm for sand, silt and clay, respectively.

Transect area	Soil quality		Total soil nutrients			Available soil nutrients			Soil cations			Soil texture		
	pH (in water)	Organic matter (g kg^{-1})	N (g kg^{-1})	P (g kg^{-1})	K (g kg^{-1})	N (mg kg^{-1})	P (mg kg^{-1})	K (cmol kg^{-1})	TEB (cmol kg^{-1})	ECEC (cmol kg^{-1})	BS (%)	% sand	% silt	% clay
Primary forest (n=150)	4.27 ±0.02	36.80 ±1.45	1.39 ±0.04	0.11 ±<0.01	15.40 ±0.70	186.56 ±5.71	1.32 ±0.08	0.19 ±0.01	0.64 ±0.03	8.60 ±0.27	8.31 ±0.41	73.01 ±0.50	20.65 ±0.38	6.34 ±0.19
Secon-dary forest (n=150)	4.39 ±0.02	36.56 ±1.28	1.42 ±0.04	0.13 ±<0.01	19.89 ±0.98	176.38 ±4.12	1.58 ±0.19	0.26 ±0.01	1.28 ±0.10	9.78 ±0.21	13.94 ±1.12	67.06 ±0.55	24.63 ±0.38	8.31 ±0.25

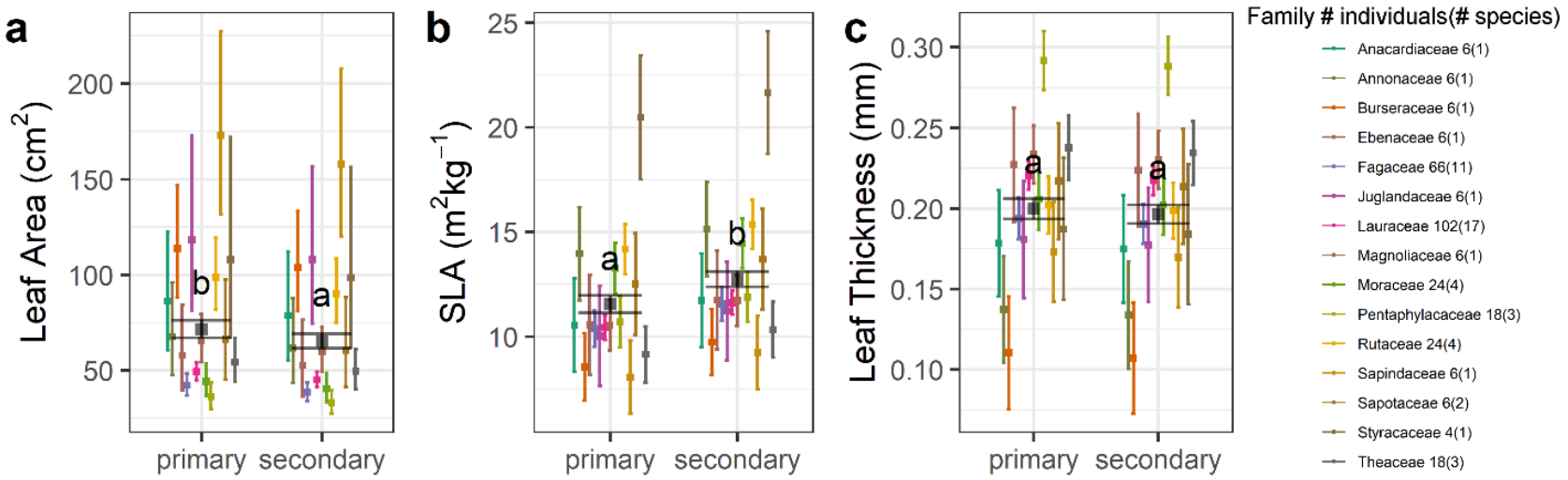

Fig. 3: Least-squared mean (points) with 95% confidence intervals (vertical bars) for three morphological leaf traits. Leaf area (a), specific leaf area (SLA) (b), and leaf thickness (c) by forest type and plant family using data from 423 individuals from 72 species sampled along a 6.6 km transect from secondary to primary forest. Values were predicted from linear models fit to field data in the form of trait ~ forest type * species|family. Colored bars are predicted values by family and the black bars are predicted values with respect to forest type. Count data for the number of individuals and species (in parenthesis) per family along the transect are shown in the legend. Letters denote the statistical groupings by forest type of a post-hoc Tukey HSD test.

Table 2: Analysis of variance table for linear models in the form: Trait ~ Species|Family × Forest type. Prior to model fitting, traits were $\log_{10}$ transformed in the case of leaf area, root diameter, SRL, root tissue density, and root branching intensity to improve data normality. *df* = degrees of freedom, MS = Mean squares, Effect size = ω^2, **p* < .05, ***p* < .01, ****p* < .001, *n.s.* = non-significant. Effect size (ω^2) values near 0.01 are considered small, near 0.06 are considered medium and near 0.14 are considered large.

Trait (units)	Source	*df*	*F*	*p*	ω^2
Leaf Area (cm^2)	Species	71	24.19	***	0.531
	Forest type	1	10.51	**	0.003
	Species × Forest type	58	3.21	***	0.041
	Residuals	1184	—	—	—
Specific Leaf Area ($m^2\ kg^{-1}$)	Species	71	19.38	***	0.451
	Forest type	1	47.36	***	0.016
	Species × Forest type	58	4.96	***	0.079
	Residuals	1183	—	—	—
Leaf Thickness (mm)	Species	69	22.54	***	0.500
	Forest type	1	1.69	*n.s.*	0.000
	Species × Forest type	57	5.73	***	0.091
	Residuals	1090	—	—	—
Root Diameter (mm)	Species	71	21.15	***	0.404
	Forest type	1	15.58	***	0.004
	Species × Forest type	58	3.56	***	0.042
	Residuals	1818	—	—	—
Specific Root Length ($m\ g^{-1}$)	Species	71	10.19	***	0.237
	Forest type	1	7.64	**	0.002
	Species × Forest type	58	3.58	***	0.054
	Residuals	1818	—	—	—
Root Tissue Density ($g\ cm^{-3}$)	Species	71	19.96	***	0.397
	Forest type	1	0.97	*n.s.*	0.000
	Species × Forest type	58	2.69	***	0.029
	Residuals	1818	—	—	—
Root Branching intensity ($tips\ cm^{-1}$)	Species	71	9.76	***	0.213
	Forest type	1	81.66	***	0.028
	Species × Forest type	58	5.72	***	0.094
	Residuals	1818	—	—	—

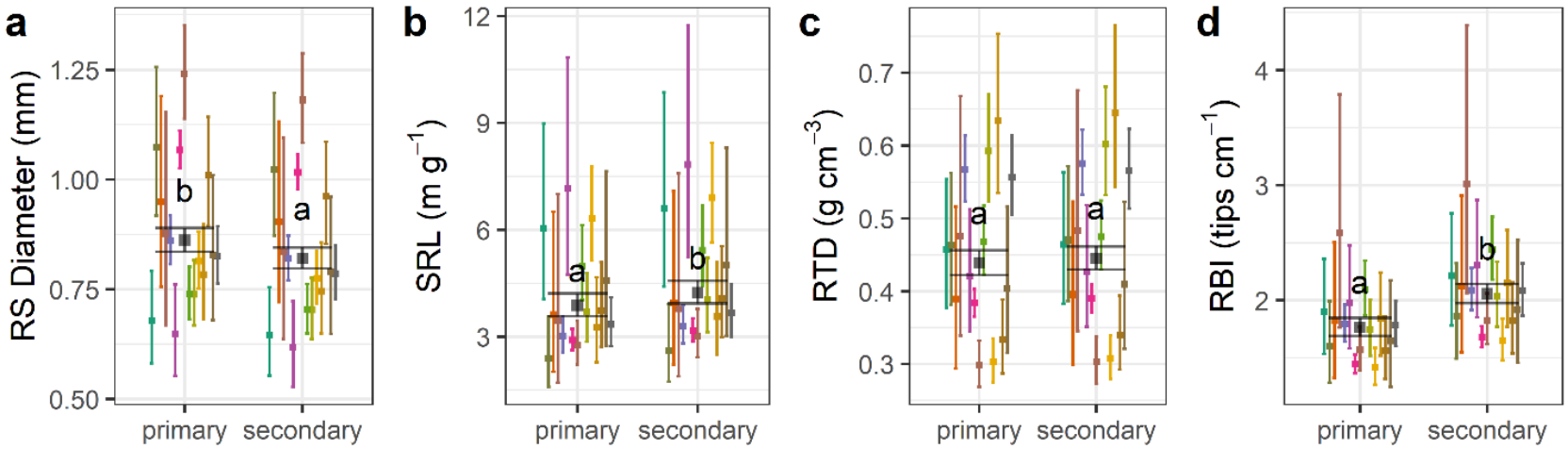

Fig. 4: Least-squared means (points) and 95% confidence intervals (vertical bars) for four morphological root traits. Average root-system diameter (a), specific root length (SRL) (b), root tissue density (RTD) (c), and root branching intensity (RBI) (d) by forest type and plant family using data from 423 individuals from 72 species sampled along a 6.6 km gradient from secondary to primary forest. Colored bars are predicted values by family (refer to legend of figure 3) and the black bars are predicted values with respect to forest type. Letters denote the statistical groupings by forest type of a post-hoc Tukey HSD tests

Variation in leaf morphology along the transect

Analysis of 1315 leaves and 1949 root systems from 423 individual saplings from 72 species showed significant interspecific trait variation. For example, predicted marginal-mean SLA values varied from 8.1 (± 0.6, standard error) to 20.5 (± 0.9) $m^2 kg^{-1}$ for Sapindaceae and Sytracaceae, respectively (Fig. 3b). In the secondary forest portion of the transect, predicted marginal-mean SLA values for those two families increased to 9.3 (± 0.3) and 21.7 (± 1.0) $m^2 kg^{-1}$. Differences in SLA by forest type were consistent with plant lineage, with SLA being on average 1.18 $m^2 kg^{-1}$ greater in secondary than in primary forest (Fig. 3b). Results were similar but inverse in directionality for leaf area (Fig. 3a), with predicted marginal-mean leaf area being 68.0 (±1.0) cm^2 in secondary and 74.5 (±1.0) cm^2 in primary forest, a difference of about 6.5 cm^2 that was largely consistent across plant families (Fig. 3b). No differences in leaf thickness were measured with respect to forest age (Fig. 3c, Table 2)

Variation in fine root system morphology along the transect

Root diameters for all root systems measured ranged from 0.3 to 3.3 mm and incorporated fine roots of the first three root orders. Root systems ranged in total root length from 9.4 to 415.67 cm, averaging 97.5 (± 1.4) cm. Regarding root morphology, the predicted-marginal mean difference in SRL was on average about 0.35 m g-1 greater in secondary than in primary forest (Fig. 4b). For example, in the secondary forest, values ranged from 2.60 (± 0.06) m g−1 for species in the Annonaceae to 7.83 (± 0.06) m g−1 for the Juglandaceae. In the primary forest, values ranged from 2.36 (± 0.06) m g−1 for species in the Annonaceae to 7.17 (± 0.06) m g−1 for the Juglandaceae (Fig. 4b). Like the SLA, leaf area- relationship, root-system diameter had an opposite relationship to SRL, being generally 0.04 (±1.01) mm narrow in secondary than in primary forest (Fig 4a). That trend was statistically significant (Table 2: $F = 15.58$, $p < .001$, $\omega^2 = 0.004$) and consistent across species (Table 2). No difference in RTD with respect to forest type was detected, although there was substantial interfamilial variation (Fig. 4c). For example, of the 15 families sampled, RTD was lowest for Sapotaceae, measuring 0.33 (±0.02) g cm-3 in both secondary and primary forest, and was greatest for Sapindaceae, measuring 0.64 (±0.02) g cm-3 in both secondary and primary forest. Across all plant lineages, root

branching intensity averaged 1.7 (±1.0) tips cm-1 in secondary and 2.0 (±1.0) tips cm-1 in primary forest (Fig 4d). For measured Lauraceae saplings, least-squared mean root branching intensity was 1.7 (±1.0) tips cm-1 in the secondary forest and 1.5 (±1.0) tips cm-1 in the primary forest. For species in the Fagaceae, values were 2.1 (±1.0) tip cm-1 in the secondary forest and 1.8 (±1.0) tip cm-1. Those differences may seem small, but when root system length is accounted for, averaging 94 cm for species in the Fagaceae family, and 95 cm for those in the Lauraceae, the 0.3 tips per cm difference in root topology equals 23 to 24 root tips per root system.

The effect of forest type on organ morphology along the transect

Two leaf traits – leaf area and SLA, and three root traits – root diameter, SRL, and RBI, showed morphological differences between primary and historically-logged tropical forest (Table 2). Effects sizes for forest type on leaf traits were small, being 0.003 for leaf area and 0.016 for SLA. For root traits, forest type effect sizes were 0.004 for root system diameter, 0.002 for SRL, and 0.028 for branching intensity. Interspecific variation in traits was always significant with very large effect sizes, which spanned from 0.213 for root branching intensity to 0.531 for leaf area. Interactive effects between species and forest type were small to medium, and statistically significant in all cases, even when the effect forest type alone was non-significant, as was the case for leaf thickness and root tissue density.

We related root traits to the soil environment for 300 individuals of 50 species (3 per forest type of each species, Table 6). The analyses of covariance (ANCOVA) models showed that forest type interacted with forest type to significantly affected root morphologies in 3 of 16 cases. Interactive effects of soil N and K with forest type on root morphology were insignificant in all the cases (i.e., for all four traits), therefore we limit the results to soil base saturation and total P. After controlling for species differences, soil base saturation had a significant interactive effect on SRL ($F^1_{247} = 5.26$, $p < .05$). Soil total P interacted with forest type to significantly affect SRL ($F^1_{247} = 4.45$, $p < .05$) and RTD ($F^1_{247} = 5.26$, $p < .05$) (Table 3). We fit individual regressions for the four root functional traits in relation to soil BS and total P. No relationships were found with respect to RTD or RBI (Fig. 5 c and d, Table 3). Regressions were statistically

significant for soil BS on root diameter in both primary and secondary forest (Fig. 5a, Table 3), and for SRL in primary forest (Fig. 5b, Table 3). Soil total P was negatively related to root diameter and positively related to SRL in primary forest only (Fig, 5, Table 3).

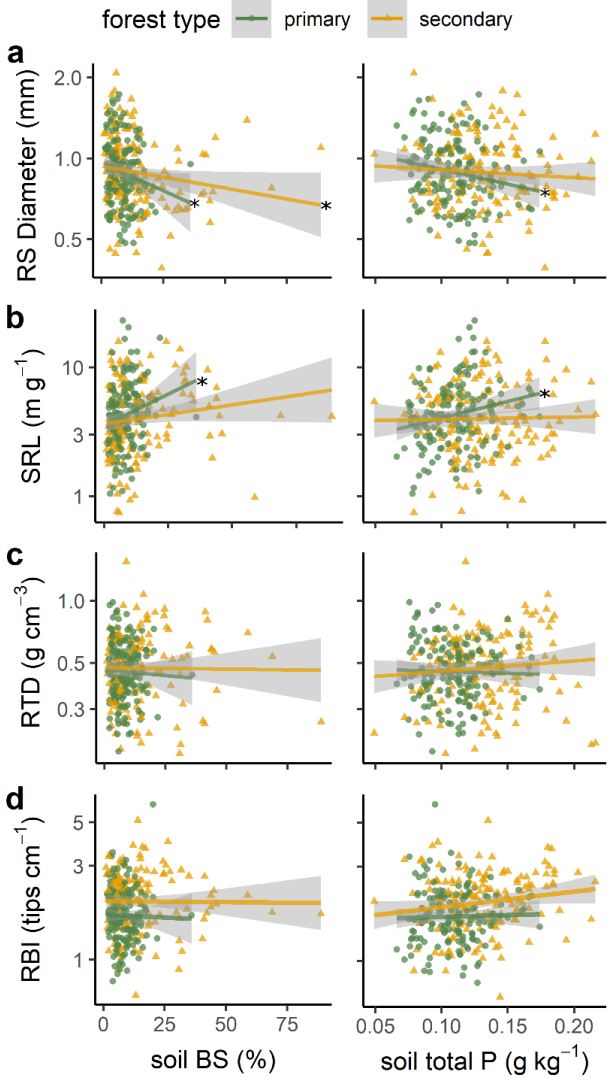

Fig. 5: Relationships between root functional traits (average root system diameter, RS Diameter, specific root length, SRL, root tissue density, RTD, and root branching intensity, RBI) and soil variables (base saturation, BS and phosphorus, P). Points show average individual trait values for 3-5 root systems (y-axis) and soil percent base saturation and phosphorus content of 1 kg of soil collected from where root systems were excavated (x-axis) for 300 individuals of 50 species. Lines represent ordinary least-squares regression, with 95% confidence intervals (shading) in the form of trait~soil variable. Models were fit separately by forest type (see Table 4). Asterix show statistically significant regression slopes ($\alpha = 0.05$).

Discussion

We confirm widely reported plasticity in plant leaf area with light environment (Fig. 3), specifically the shaded environmental conditions of saplings in older growth forest (Givnish 1984; Rijkers et al. 2000; Keenan & Niinemets 2016; Liu et al. 2016). In our study, shade-inhabiting saplings in primary forest had larger leaves than those in secondary forest (on average 6.5 cm^2 greater in area, Fig 3a). Variation in leaf morphologies was consistent across families, with a wide range in leaf morphological traits (Fig 3). On average, SLA was 1.2 m^2 kg^{-1} greater in secondary than primary forest, so area-based variation in leaf morphology accounted for most of the variation is SLA with forest type (Fig. 3). Our results are inconsistent with those of Rijkers et al. (2000), who found that SLA of four tropical forest tree species in French Guiana halved from to 25 to 12.5 m^2 kg^{-1} as canopy openness increased from 0 to 25%. In 2008, leaf area index in the secondary forest portion of the transect measured about 5, whereas leaf area index in the primary forest portion of the transect measured approximately 6.5 (Qui 2008), so we the canopy openness gradient between primary and secondary forest was not as steep as that of Rijkers et al., with negligible apparent differences.

Generally, root traits varied more than leaf traits across forest type, with root diameter and root tissue density varying less than that of SRL and root topology (i.e., RBI). These results suggest that there exist two or more axes of root morphological variation (Weemstra et al. 2016; Kramer-Walter et al. 2016). The first axis encompasses root diameter and root tissue density, which we found to be less-plastic across soil conditions and more-constrained by plant lineage (i.e., the evolved root strategy of the species), whether that be one of thicker or thinner roots (Valverde-Barrantes et al. 2017; Maherali 2017). The second, associated with SRL and root topology, was more variable with soil-fertility and texture. This second axis seeks to optimize root structural investment into a topology that is most efficient for nutrient foraging, with some potential trade-off between purely abiotic and abiotically-assisted ways in doing so, (e.g., associations with mycorrhizae, chemical alterations of the rhizosphere, etc.; Fitter 1991; Lynch et al. 2005; Craine 2006; McCormack & Iversen 2019).

SRL, or the distance a root can travel for a given amount of structural investment, trades off with the production of absorptive fine-root tips (i.e., branching intensity), and thus species seek to optimize nutrient foraging with root architecture in a wide variety of morphologies. For example, the Fagaceae species in this study have a highly dichotomously-branched root system with a network of fine root tips that form an absorptive mat just under the leaf litter layer, while the Lauraceae have a much more herringbone architecture with a long slender transportive root that supports many short lateral roots, which occupy the mineral soil layer several inches below the soil surface. Root system stratification within the soil profile is common in temperate forest systems where few species compete for soil resources (Parrish and Bazzaz 1976). In the tropical forests of southern China, where temperate and tropical taxa have mixed to a large degree (Zhu 2017), such separation via complimentary resource acquisition strategies within the soil profile may promote species coexistence (Guo et al. 2008, Ma et al. 2018, Lu and Hedin 2019).

Tropical forest saplings modulate the root length-branching intensity trade-off in root architecture with local-scale variation in the soil environment. In soil where nutrients are more abundant, root systems prioritize acquisitive architectures (e.g., higher SRLs and RBIs, Fig 4), yet where competition for soil nutrients is high (i.e., in primary forest), root systems had more-conservative morphologies, such as slight increases root diameter, and likely seek to maximize root lifespan to hold on to soil space (Craine 2006). Other studies have found highly variable root system morphologies with the soil environment. Generally, N-depleted soils lead to increased lateral root elongation, while P-depleted soils cause more branched root systems (López-Bucio et al. 2003; Giehl et al. 2013). Notably, along very-strong Phosphorus (P) gradients, plant species have been shown to modulate root morphologies and nutrient acquisition strategies in relation to how they partition soil P, with more enzymatic activity and more-architecturally advanced roots in P-improvised soils (Lambers et al. 2006; Niu et al. 2013; Zemunik et al. 2015; Lambers et al. 2017). In a meta-analysis of the factors affecting tropical forest root morphologies, Addo-Danso et al. (2019) reported that SRL was positively related (albeit weakly) to soil P and base saturation.

P-poor, highly-weathered, leached tropical soils, such as the yellow soils of JFL, are also thought to have the ability to support a high diversity of plant species because of the way they allow plants to diversify and partition nutrient-use strategies in many ways within the soil environment (Laliberté et al. 2015; Turner 2008; Turner et al. 2018). Soil N, P, and base saturation all decrease along the gradient from secondary to primary forest in JFL (Table 1).

Increasing soil base saturation led to a slight decrease in root system diameter in both primary and secondary forest, with the decreases in primary forest being slightly greater than those in secondary forest, despite the soils occupying a smaller range of soil base saturation values (Fig. 5a, Table 3). Increasing soil total P had a negative relationship on root diameter, but only in primary forest (Fig. 5a, Table3). Similarly, soil base saturation and total P were positively related to SRL, but only in primary forest (Fig. 5b, Table 3). Regressions included very high variance, similar to those reported in other studies (i.e., with low coefficients of determination, see Addo-Danso et al. 2019), because at the local scale of the analysis, we have a relatively low range in soil nutrients when compared to the range of variation throughout the tropics (Addo-Danso et al. 2019), and because we controlled for taxonomic identity across the gradient, potentially limiting any environmental-filtering effects (Table 6). These results support that root morphologies of the tropical saplings studied here employ many root functional trait strategies to inhabit similar soil environments in both primary and secondary forest (Mommer and Weemstra 2012; Bardgett et al. 2014; Weemstra et al. 2016; Laliberté 20107).

Table 3: Regression results from least-squared linear models in the form of Trait ~ Variable. Table to accompany figure 5. Models were fit separately by forest type. Model coefficient estimates (β), standard errors (*se*), and associated probabilities (p) are given for each variable by forest type (intercept terms are not shown). Probabilities are denoted as follows: *p <.05, **p < .01, ***p < .001, *n.s.* = non-significant. Regression F-statistics (F) and coefficients of determination (R^2) and root mean squared error (*RMSE*) are given for each model. Note: the $F_{(1,148)}$ critical value at $\alpha = 0.05$ is 3.905. Bolded model coefficients show significant ANCOVA interaction terms between forest type and soil variable ($p < 0.05$).

Trait (units)	Forest type	Variable (units)	β	*se*	p	$F(1,148)$	R^2	*RMSE*
Root Diameter (mm)	secondary	Soil BS (%)	-0.004	0.002	*	4.39	0.03	0.29
	primary		-0.010	0.004	*	4.96	0.03	0.65
	secondary	Soil P (g kg^{-1})	-0.703	0.792	*n.s.*	0.79	<0.01	0.29
	primary		-2.350	1.002	*	5.50	0.04	0.26
Specific Root Length (m g^{-1})	secondary	Soil BS (%)	**0.262**	0.188	*n.s.*	1.94	0.01	3.11
	primary		**1.117**	0.055	*	4.53	0.03	3.38
	secondary	Soil P (g kg^{-1})	**23.42**	8.48	*n.s.*	0.08	<0.01	3.13
	primary		**32.41**	12.43	*	6.38	0.04	3.36
Root Tissue Density (g cm^{-3})	secondary	Soil BS (%)	0.001	0.001	*n.s*	0.07	<0.01	0.20
	primary		-0.002	0.003	*n.s*	0.73	<0.01	0.16
	secondary	Soil P (g kg^{-1})	**0.837**	0.540	*n.s.*	2.40	0.02	0.20
	primary		**-0.523**	0.613	*n.s.*	0.73	<0.01	0.16
Root Branching intensity (tips cm^{-1})	secondary	Soil BS (%)	-0.001	0.004	*n.s*	0.02	<0.01	0.72
	primary		0.002	0.011	*n.s*	0.02	<0.01	0.65
	secondary	Soil P (g kg^{-1})	3.188	1.922	*n.s*	2.75	0.02	0.65
	primary		-0.48	1.922	*n.s*	2.75	0.02	0.72

We are unable to assess if investment in root tissues (i.e., allocation to root biomass) is greater in primary than secondary forest, although some research has shown that root biomass increases with forest age (Jackson et al. 1996; Leuschner et al. 2008). Using root coring sampling methods, Hertel et al. (2003) found that fine root biomass increased with increasing forest age, but also found more root tips per unit area in the mineral soil of early and mid-successional than in primary wet forest in Costa Rica, estimating 560,000 tips m^{-2} in the former and 260,000 tips m^{-2} in the latter. In tropical forests, as fine root biomass increases with succession (Hopkins et al. 1996; Powers and Peréz-Aviles 2013), intraspecific shifts toward a more-conservative strategy that maximizes root lifespan would seem advantageous, because competition for soil space is greater in late-successional forest relative to secondary forest (Jackson et al. 1996, Craine 2006). Because of differences in soil space availability, root morphologies in primary forest may favor the production of thicker roots with more root tips over the elongation of roots, whereas roots in secondary forest may favor the opposite.

These morphological differences are likely very subtle, evidenced by relatively weak effect sizes of forest type in the ANOVA models (Table 2). Some previous work supports that claim; indeed, Zangaro et al. (2012) reported increased root diameters, but no difference in SRL or root length for mature relative to secondary forests in *Araucaria* forests of the southern Brazilian Pantanal. Hopkins et al. (1996) reported that SRL in secondary forest was twice that of primary forests in *Acacia*-dominated wet forests of northern Australia. Several previous studies have also demonstrated that SRL increases with soil fertility (Ostonen et al. 2007; Kong et al. 2014). We found that difference in root diameter by forest type were highly conserved and consistent across the 15 Angiosperm families we measured (Fig. 4, Comas and Eissenstat 2009; Kong et al. 2014; Valverde-Barrantes et al. 2017). In the ANOVA models (Table 2), interaction effects between plant lineage and forest type were statistically significant, meaning that there was some difference in the magnitude of the response of each species to forest type, even though all plant lineages responded similarly in terms of direction (Figs. 3 & 4). Examining comparable root systems across individuals, we provide evidence for juvenile tropical trees, that intraspecific variation in root diameter in relation to the soil

environment is ubiquitous and potentially consistent, albeit small in magnitude. Our results suggest that variation in root diameter trades off with investment of structural resources in root length (SRL) or tips (RBI).

Conclusion

With increasing forest age, plasticity in leaf morphologies showed an acquisitive shift, but variation in root morphologies and architectures showed conservative shifts, which was contrary to our hypothesis where we predicted acquisitive morphological shifts for both leaves and roots with increasing forest age. Variation in leaf and root morphologies were consistent across plant lineages, although large interspecific differences in leaf and root trait measurements were observed. Leaves were larger in primary forest than in secondary forest. Root-system diameter increased, and root systems were less architecturally developed (i.e., had fewer root tips per unit length) in primary than in secondary forest (Figs. 3 & 4). These results exemplify how the soil environment can control root morphology in an abiotic context (Powers and Peréz-Aviles 2013; Freschet et al. 2017; Addo-Danso et al. 2019).

Intraspecific morphological shifts were observed along functional axes toward more-conservative root strategies, however one major limitation of this study lies in its inability to investigate if such shifts are accompanied with any compensation via biotic methods of acquiring nutrients (i.e., more association with mycorrhizal symbionts, increases in root enzymatic activity or shits in chemical partitioning of soil nutrients; McCormack & Iversen 2019) among primary and secondary forest areas. Some research has shown root diameter to be correlated to mycorrhizal colonization; and it would make sense that thicker roots, in later-successional forest, are likely more-biotically reliant on mycorrhizae for in their nutrient-acquisition strategy (Phillips et al. 2013; Rosling et al. 2016; Kong et al. 2017; McCormack & Iversen 2019). Additionally, in older forests where the leaf litter layer is thicker and of greater quality (i.e., higher C:N ratio), ectomycorrhizal roots, such as those of many of the Fagaceae species in this study, forage nutrients more-directly from leaf detritus via fungal hyphae to a greater degree than in forests where leaf layers are thinner or of lower quality (Phillips et al. 2013). Although we demonstrate morphological plasticity of root morphologies with local, variation in the

soil environment (i.e., soil total P and base saturation, Fig. 5, Table 3), further data are needed to determine differences in root function (Warren et al 2015).

By comparing fine root systems and leaves of the same individuals, we illustrate a decoupling of intraspecific variation in leaf and root morphologies. Although leaves became increasingly acquisitive from secondary to primary forest – increasing leaf area, and decreasing SLA, root systems showed conservative intraspecific shifts – increasing root diameter and decreasing SRL and RBI. This could be indicative of the relative strength of aboveground-belowground plant competition, in that from secondary to primary forest, sapling competition for light tends to increase, potentially changing the aboveground-belowground competition balance. We show this competitive balance operates consistently across the roots systems and leaves of 15 Angiosperm families, potentially helping predict how plant organ morphologies vary with local scale variation in tropical forest environment and age.

References

Ackerly D, Knight C, Weiss S, Barton K & Starmer K (2002) Leaf size specific leaf area and microhabitat distribution of chaparral woody plants: contrasting patterns in species level and community level analyses. Oecologia 130:449-457.

Addo-Danso SD, Defrenne CE, McCormack ML, Ostonen IV, Addo-Danso A, Foli EG, Borden KA, Isaac ME & Prescott CE (2019) Fine-root morphological trait variation in tropical forest ecosystems: an evidence synthesis. Plant Ecol 221:1-13

Bardgett RD, Mommer L & De Vries FT (2014) Going underground: root traits as drivers of ecosystem processes. Trends Ecol Evol 29:692-699.

Baraloto C, Paine CET, Poorter L, Beauchene J, Bonal D, Domenach A-M, Hérault B, Patiño S, Roggy J-C & Chave J. Decoupled leaf and stem economics in rain forest trees. Ecol Lett 13:1338-1347.

Chave J, Coomes D, Jansen S, Lewis SL, Swenson NG & Zanne AE. (2009) Towards a worldwide wood economics spectrum. Ecol Lett 12:351-366.

Christensen, N. L. & Peet, R. K. (1984) Convergence during secondary forest succession. J Ecol 72, 25-36.

Chen W, Koide RT, Adams TS, DeForest JL, Cheng L & Eissenstat DM. (2016) Root morphology and mycorrhizal symbioses together shape nutrient foraging strategies of temperate trees. P Natl Acad Sci USA 113 8741-8746.

Comas L & Eissenstat D. (2009) Patterns in root trait variation among 25 co-existing North American forest species. New Phytol 182:919-928.

Craine JM. (2006) Competition for nutrients and optimal root allocation. Plant Soil 285: 171-185.

Craine JM, Froehle J, Tilman D, Wedin D & Chapin FS. (2001) The relationships among root and leaf traits of 76 grassland species and relative abundance along fertility and disturbance gradients. Oikos 93:274-285.

Defrenne CE, McCormack ML, Roach WJ, Addo-Danso SD & Simard SW. (2019) Intraspecific Fine-Root Trait-Environment Relationships across Interior Douglas-Fir Forests of Western Canada. Plants 8:199.

Díaz S, Kattge J, Cornelissen JH, Wright IJ, Lavorel S, Dray S, Reu B, Kleyer M, Wirth C & Prentice IC. (2016) The global spectrum of plant form and function. Nature 529:167.

Eissenstat D, Wells C, Yanai R & Whitbeck J. (2000) Building roots in a changing environment: implications for root longevity. New Phytol 147:33-42

Eissenstat DM, Kucharski JM, Zadworny M, Adams TS & Koide RT. (2015) Linking root traits to nutrient foraging in arbuscular mycorrhizal trees in a temperate forest. New Phytol 208:114-124.

Fortunel C, Fine PVA & Baraloto C. 2012. Leaf, stem and root tissue strategies across 758 Neotropical tree species. Funct Ecol 26:1153-1161.

Fortunel C, Ruelle J, Beauchêne J, Fine PVA & Baraloto C. 2014. Wood specific gravity and anatomy of branches and roots in 113 Amazonian rainforst tree species across environmental gradients. New Phytol 202:79-94.

Fitter A. (1991) Characteristics and functions of root systems. In: Y. Waisel A. Eschel T. Beeckman U. Kafkafi (eds.) Plant roots: the hidden half 3rd edition pp. 49-78 Marcel Decker Inc. New York.

Fitter A & Stickland T. (1991) Architectural analysis of plant root systems 2. Influence of nutrient supply on architecture in contrasting plant species. New Phytol 118:383-389.

Freschet GT & Roumet C. (2017) Sampling roots to capture plant and soil functions. Funct Ecol 31:1506-1518.

Freschet GT, Valverde-Barrantes OJ, Tucker CM, Craine JM, McCormack ML, Violle C, Fort F, Blackwood CB, Urban-Mead KR, & Iversen CM. (2017) Climate soil and plant functional types as drivers of global fine-root trait variation. J Ecol 105:1182-1196.

Garnier E, Shipley B, Roumet C & Laurent G. (2001) A standardized protocol for the determination of specific leaf area and leaf dry matter content. Funct Ecol 15:688-695.

Giehl RF, Gruber BD & von Wirén N. (2013) It's time to make changes: modulation of root system architecture by nutrient signals. J Exp Bot 65:769-778.

Givnish T. (1984) Leaf and canopy adaptations in tropical forests. In E Medina H.A. Mooney C. Vasquez-Yanes (eds.) Physiological Ecology of Plants of the wet Tropics (pp. 51-84. Springer The Netherlands.

Guo D, Xia M, Wei X, Chang W, Liu Y, & Wang Z. (2008) Anatomical traits associated with absorption and mycorrhizal colonization are linked to root branch order in twenty-three Chinese temperate tree species. New Phytol 180:673-683.

Hertel D, Leuschner C & Hölscher D. (2003) Size and strucutre of fine root systems in old-growth and secondary tropical montane forests (Costa Rica). Biotropica 35:143-153.

Holdaway RJ, Richardson SJ, Dickie IA, Peltzer DA & Coomes DA. (2011) Species- and community-level patterns of fine root traits along a 120000-year soil chronosequence in temperate rainforest. J Ecol 99:954-963.

Hodge A, Berta G, Doussan C, Merchan F & Crespi M. (2009) Plant root growth architecture and function. Plant Soil 321:153-187.

Hogan JA, Baraloto C, Valverde-Barrantes O, Xu H, Ding Q (2019) Sapling leaf and root traits from 6.6 km Jianfengling transect. https://doi.org/10.6084/m9.figshare.7996328.v3

Hopkins MS, Redell P, Hewett RK & Graham AW (2996) Comparison of root and mycorrhizal characterstics in primary and secondary forests on a metamorphoic soil in North Queensland, Australia, J of Trop Ecol 12:871-885.

Huang Q, Li Y, Zheng D, Zhang J, Wan L, Jiang Y & Zhao Y. (1995) Study on Tropical Vegetation Series in Jianfengling Hainan Island. In: Q. Zeng G. Zhou L. Yide Z.

Wu & B. Chen (eds.) Researches on Tropical Forest Ecosystems in Jianfengling of China pp. 5-25. China Forestry Publishing House Beijing China.

Iversen CM, McCormack ML, Powell AS, Blackwood CB, Freschet GT, Kattge J, Roumet C, Stover DB, Soudzilovskaia NA & Valverde-Barrantes OJ. (2017) A global Fine-Root Ecology Database to address below-ground challenges in plant ecology. New Phytol 215:15-26.

Jackson R, Canadell J, Ehleringer JR, Mooney H, Sala O & Schulze E. (1996) A global analysis of root distributions for terrestrial biomes. Oecologia 108:389-411.

Jin D, Cao X & Ma K. (2013) Leaf functional traits vary with the adult height of plant species in forest communities. J Plant Ecol 7:68-76.

Keddy P. (1992) A pragmatic approach to functional ecology. Funct Ecol 6:621-626.

Keenan TF & Niinemets Ü. (2017) Global leaf trait estimates biased due to plasticity in the shade. Nat Plants 3:16201.

Kembel SW & Cahill Jr. JF. (2011) Independent evolution of leaf and root triats within and aming temperate grassland plant communities. PloS One 6:e19992.

King DA. (1996) Allometry and life history of tropical trees. J Trop Ecol 12 25-44.

Kong D, Ma C, Zhang Q, Li L, Chen X, Zeng H & Guo D. (2014) Leading dimensions in absorptive root trait variation across 96 subtropical forest species. New Phytol 203:863-872.

Kong D,Wang J, Zeng H, Liu M, Miao Y, Wu H & Kardol P. (2017) The nutrient absorption–transportation hypothesis: optimizing structural traits in absorptive roots. New Phytol 213:1569-1572.

Körner C. (2018) Concepts in empirical plant ecology. Plant Ecol Divers 11: 405-428.

Kramer-Walter KR, Bellingham PJ, Millar TR. Smissen RD, Richardson SJ & Laughlin DC. (2016) Root traits are multidimensional: specific root length is independent from root tissue density and the plant economic spectrum. J Ecol 104:1299-1310.

Laliberté E. (2017) Below-ground frontiers in trait-based plant ecology. New Phytol 213:1597-1603.

Laliberté E, Lambers H, Burgess TI & Wright SJ. (2015) Phosphorus limitation soil-borne pathogens and the coexistence of plant species in hyperdiverse forests and shrublands. New Phytol 206:507-521.

Lambers H, Shane MW, Cramer MD, Pearse SJ, Veneklaas EJ. (2006) Root structure and functioning for efficient acquisition of phosphorus: matching morphological and physiological traits. Ann Bot 98:693-713.

Lambers H, Albornoz F. Kotula L. Laliberté E. Ranathunge K. Teste F. P. & Zemunik G. (2017) How belowground interactions contribute to the coexistence of mycorrhizal and non-mycorrhizal species in severely phosphorus-impoverished hyperdiverse ecosystems. Plant Soil 424:1-23.

Lambers H, Clode PL, Hawkins H, Laliberté E, Oliveira RS, Reddell P, Shane MW, Stitt M, & Weston P. (2018) Metabolic Adaptations of the Non-Mycotrophic Proteaceae to Soils with Low Phosphorus Availability. Annual Plant Reviews online (ed J. A. Roberts) pp. 289-335.

Lenth R. (2018) Emmeans: Estimated marginal means aka least-squares means. R Package Version 1. https://CRAN.R-project.org/package=emmeans.

Li F, Hu H, McCormack ML, Feng DF, Liu X & Bao W. (2018) Community-level economics spectrum of fine roots driven by nutrient limitations in subalpine forests. J Ecol 107:1238-1249.

Liu Y, Dawson W, Prati D, Haeuser E, Feng Y, van Kluenen M. (2016) Does greater specific leaf area plasticity help plants maintain a high performance when shaded? Ann Bot 118:1329-1336.

López-Bucio J, Cruz-Ramırez A & Herrera-Estrella L. (2003) The role of nutrient availability in regulating root architecture. Curr Opin Plant Biol 6:280-287.

Lu M & Hedin LO. (2019) Global plant–symbiont organization and emergence of biogeochemical cycles resolved by evolution-based trait modeling. Nature Ecol Evol 3:239.

Lüdecke D. (2019) sjstats: Statistical function for regression models (version 0.17.3). R packge: https://www.cran.r-project.org/package=sjstats. doi:10.5281/zenodo.1284472.

Lynch J. (2005) Root architecture and nutrient acquisition. In: BassiriRad H. (eds.) Nutrient acquisition by plants (Analysis and Synthesis), vol. 181, pp. 147-183. Springer, Berlin, Heidelbeg.

Ma Z, Guo D, Xu X, Lu M, Bardgett RD, Eissenstat DM, McCormack ML & Hedin LO. (2018) Evolutionary history resolves global organization of root functional traits. Nature 555:94.

Maherali H. (2017) The evolutionary ecology of roots. New Phytol 215:1295-1297.

McCormack ML, Adams TS, Smithwick EA & Eissenstat DM. (2012) Predicting fine root lifespan from plant functional traits in temperate trees. New Phytol 195:823-831.

McCormack ML, Dickie IA, Eissenstat DM, Fahey TJ, Fernandez CW. Guo D, Helmisaari HS, Hobbie EA. Iversen CM & Jackson RB. (2015) Redefining fine roots improves understanding of below-ground contributions to terrestrial biosphere processes. New Phytol 207:505-518.

McCormack ML & Iversem CM. (2019) Physical and functional constraints on viable belowground acquisition strategies. Front Plant Sci 10:1215.

Mommer L & Weemstra M. (2012) The role of roots in the resource economics spectrum. New Phytol 195:725-727.

Niu YF, Chai RS, Jin GL, Wang H, Tang CX & Zhang YS. (2013) Responses of root architecture development to low phosphorus availability: a review. Ann Bot 112:391-408.

Ostonen I, Püttsepp Ü, Biel C, Alberton O, Bakker M, Lõhmus K, Majdi H, Metcalfe D, Olsthoorn A, & Pronk A. (2007) Specific root length as an indicator of environmental change. Plant Biosyst 141:426-442.

Parish JAD & Bazzaz FA. (1976) Underground niche separation in succesional plants. Ecology 57:1281-1288.

Phillips RP, Brzostek E & Midgley MG. (2013) The mycorrhizal-associated nutrient economy: a new framework for predicting carbon–nutrient couplings in temperate forests. New Phytol 199:41-51.

Powers JS and Peréz-Aviles D. (2012) Edaphic factors are a more important control on surface roots than stand age in secondary tropical dry forests. Biotropica 45:1-9.

Qui J. (2008). Relationship between tropical forest canopy structure, understory vegetation and soil organic carbon content in Jianfengling, Hainan Island. Master's Thesis. Chinese Academy of Foresty. doi: 10.7666/d.D602796.

R Core Team. (2018) R: A language and environment for statistical computing. R Foundation for Statistical Computing Vienna Austria.

Reich PB (2014) The world-wide 'fast–slow' plant economics spectrum: a traits manifesto. J Ecol 102:275-301.

Rijkers T, Pons T & Bongers F. (2000) The effect of tree height and light availability on photosynthetic leaf traits of four neotropical species differing in shade tolerance. Funct Ecol 14:77-86.

Rosling A, Midgley MG, Cheeke T, Urbina H, Fransson P & Phillips RP. (2016) Phosphorus cycling in deciduous forest soil differs between stands dominated by ecto-and arbuscular mycorrhizal trees. New Phytol 209 1184-1195.

Schenk HJ & Jackson RB. (2002) Rooting depths lateral root spreads and below-ground/above-ground allometries of plants in water-limited ecosystems. J Ecol 90 480-494.

Shipley B. (1995) Structured interspecific determinants of specific leaf area in 34 species of herbaceous angiosperms. Funct Ecol 312-319.

Shipley B, De Bello F, Cornelissen JHC, Laliberté E, Laughlin DC & Reich PB. (2016) Reinforcing loose foundation stones in trait-based plant ecology. Oecologia 180:923-931.

Turner BL. (2008) Resource partitioning for soil phosphorus: a hypothesis. J Ecol 96 698-702.

Turner BL, Brenes-Arguedas T & Condit R. (2018) Pervasive phosphorus limitation of tree species but not communities in tropical forests. Nature 555 367.

Ushio M, Fujiki Y, Hidaka A & Kitayama K. (2015) Linkage of root physiology and morphology as an adaptation to soil phosphorus impoverishment in tropical montane forests. Funct Ecol 29:1235-1245.

Valverde-Barrantes OJ, Horning AL, Smemo KA & Blackwood CB. (2016) Phylogenetically structured traits in root systems influence arbuscular mycorrhizal colonization in woody angiosperms. Plant Soil 404:1-12.

Valverde-Barrantes OJ & Blackwood CB. (2016) Root traits are multidimensional: specific root length is independent from root tissue density and the plant economic spectrum: Commentary on Kramer-Walter et al. (2016). J Ecol 104:1311-1313.

Valverde-Barrantes OJ, Freschet GT, Roumet C & Blackwood CB (2017) A worldview of root traits: the influence of ancestry growth form climate and mycorrhizal association on the functional trait variation of fine-root tissues in seed plants. New Phytol 215:1562-1573.

Van Kleunen M, Weber E & Fischer M. (2010) A meta-analysis of trait differences between invasive and non-invasive plant species. Ecol Lett 13:235-245.

Wang C, McCormack ML, Guo D & Li J. (2019) Global meta-analysis reveals different patterns of root tip adjustments by angiosperm and gymnosperm trees in response to environmental gradients. J Biogeogr 46:123-133.

Wang R, Wang Q, Zhao N, Yu G & He N. (2017) Complex trait relationships between leaves and absorptive roots: coordiunation in tissue N concentration but divergence in morphology. Ecol Evol 7:2697-2705.

Wang R, Wang Q, Zhao N, Xu Z, Zhu X, Jiao C, Yu G & He N. (2018) Different phylogenetic and environmental controls of first-order root morphological and nutrient traits: Evidence of multidimensional root traits. Funct Ecol 32:29-39.

Warren, JM, Hanson PJ, Iversen CM, Kumar J, Walker AP & Wullschleger, SD. (2015) Root structural and functional dynamics in bioshpere models – evaluation and recommendations. New Phytol 205:59-78.

Weemstra M, Mommer L, Visser EJ, Ruijven J, Kuyper TW, Mohren GM, & Sterck FJ, (2016) Towards a multidimensional root trait framework: a tree root review. New Phytol 211:1159-1169.

Weiher E, Werf A, Thompson K, Roderick M, Garnier E & Eriksson O. (1999) Challenging Theophrastus: a common core list of plant traits for functional ecology. J Veg Sci 10:609-620.

Wenhua L. (2004) Degradation and restoration of forest ecosystems in China. For Ecol Manag 201 33-41.

Werner, P. (1984) Changes in soil properties with wet forest succession in Costa Rica. Biotropica 16:43-50.

Westoby M & Wright IJ. (2006) Land-plant ecology on the basis of functional traits. Trends Ecol Evol 21 261-268.

Wright IJ, Reich PB, Westoby M, Ackerly DD, Baruch Z, Bongers F, Cavender-Bares J, Chapin ST, Cornelissen JH, & Diemer M. (2004) The worldwide leaf economics spectrum. *Nature* 428 821.

Wright IJ, Dong N, Maire V, Prentice IC, Westoby M, Díaz S, Gallagher RV, Jacobs BF, Kooyman R, Law EA, Leishman MR, . Global climatic drivers of leaf size. Science. 2017 Sep 1;357(6354):917-21.

Wright SJ, Kitajima K, Kraft NJ, Reich PB, Wright IJ, Bunker DE, Condit R, Dalling JW, Davies SJ & Diaz S. (2010) Functional traits and the growth-mortality trade-off in tropical trees. Ecology 91:3664-3674.

Wu Z. (1995) An Introduction to the Tropical Forest Soils and Effect of Shifting Cultivation on Soils in Jianfengling Hainan Island. In; Q. Zeng, G. Zhou, L. Yide, Z. Wu & B. Chen (eds) Researches on Tropical Forest Ecosystems in Jianfengling of China pp. 5-25. China Forestry Publishing House Beijing China.

Wurzburg N & Wright SJ. (2015) Fine-root responses to fertilization reveal multiple nutirent limitation in lowland tropical forest. Ecology 96:2137-2146.

Xu H, Li Y, Liu S, Zang R, He F & Spence J. R. (2015) Partial recovery of a tropical rain forest a half-century after clear-cut and selective logging. J App Ecol 52:1044-1052.

Zadworny M, McCormack ML, Mucha J, Reich PB & Oleksyn J. (2016) Scots pine fine roots adjust along a 2000-km latitudinal climatic gradient. New Phytol 212 389-399.

Zangaro W, Alves RA, Lescano LE & Ansanelo AP. (2012) Investment in fine roots and arbuscular mycorrhizal fungi decrease during succession in three Brazilian ecosystems. Biotropica 44: 141-151.

Zemunik G, Turner BL, Lambers H & Laliberté E. (2015) Diversity of plant nutrient-acquisition strategies increases during long-term ecosystem development. Nat Plants 1:15050.

Zeng Q. (1995) Survey of Water-Heat Condition and Vegetation Ecological Series in Jianfengling. In: Q. Zeng G. Zhou, L. Yide, Z. Wu & B. Chen (eds) Researches on Tropical Forest Ecosystems in Jianfengling of China pp. 5-25. China Forestry Publishing House Beijing China.

Zhou G. (1995) Ecological Effects of Human Activities in Jianfenglin Forest Region Hainan Island. In: Q. Zeng, G. Zhou, L. Yide, Z. Wu & B. Chen (eds) Researches on Tropical Forest Ecosystems in Jianfengling of China pp. 38-48. China Forestry Publishing House Beijing China.

Zhu H. (2017) A biogeographical study on the flora of southern China. Ecol Evol 7:10398-10408.

CHAPTER 2: Intraspecific trait variation and species functional turnover in successional tropical forests: assessing gap-filling for community-weighted means

Key message

Most (six of seven) leaf and root functional traits showed negative co-variation between intraspecific trait variation and species successional turnover in tropical forests with range of past logging histories. These patterns were insensitive to a sparse phylogenetic sampling of taxa from only 14 plant families selected to represent key root functional strategies.

Abstract

Accounting for intraspecific trait variation (ITV) is central to plant ecology and crucial for vegetation modeling efforts. ITV can be substantial; however, it remains unclear how ITV influences community-weighted mean (CWM) trait estimates. We use leaf and root trait data from 423 trees of 72 species from 15 Angiosperm families in combination with community data from 164 small plots comprising 582 species to evaluate the contribution of ITV to CWMs, comparing unlogged, primary forest to selectively-logged and clear-cut secondary forest. We examine the effect of gap-filling missing trait values via phylogenetic generalized linear modeling (PhyloPars) on CWMs. For six of seven traits, ITV negatively covaried with species turnover to generate larger CWM differences than observed if ITV was not integrated. For example, plot average CWM specific leaf area was 10.7 and 10.4 m^2 kg^{-1} for primary and secondary forest, not accounting for ITV, but shifted to 9.8 and 11.1 m^2 kg^{-1} after doing so. Specific root length showed a similar trend. Our results from 72-species assemblages were supported by the results from the gap-filled analysis using the entire community, where the contribution of ITV to CWMs ranged from 25 to 75%, with nearly all trait variation due to forest type attributable to ITV. Therefore, CWM trait estimates became more-conservative with forest age, whereas ITV for many traits showed an acquisitive shift, and because of negative covariation between ITV and species turnover, forest age-related CWM differences increased. Differences were unaffected, if not strengthened, by gap-filling incomplete functional trait matrices.

Keywords: plant functional traits, intraspecific trait variability, trait flex ANOVAs, community-weighted, roots, tropical forest, Jianfengling.

Introduction

Plant functional traits broadly scale along a fast-slow axis related to plant life-history variation and demographic rates (Díaz et al. 2016, Reich, 2014, Wright et al. 2010). For example, the most broadly measured plant functional traits distill to two main axes of functional variation – one related to leaf economics (e.g., specific leaf area – SLA, leaf nitrogen) and another related to whole plant size (Díaz et al. 2016). Despite this, there is substantial functional redundancy among plant taxa (i.e., within communities, Pillar et al. 2013) and considerable functional trait variation within taxa (i.e., intraspecific trait variation, hereafter ITV, Siefert et al. 2015) that muddles trends, for example weakening trait-demography relationships (Poorter et al. 2018a, Yang et al. 2018). Additionally, a portion of ITV is due to the environment; thus, properly accounting for ITV across quantified environmental gradients can reveal trait-environment relationships (Bruelheide et al. 2018, Craven et al. 2018) and drivers of variance among them (Hofhansl et al. 2021).

Functional trait variation also has implications for plant fitness and how species partition environmental resources within niche space (Laughlin et al. 2020, Laughlin and Messier 2015, Kunstler et al. 2016). Thus, at the community level, functional traits have popularly been used to infer community shifts in plant resource-acquisition strategies across environmental gradients (e.g., environmental filtering, community assembly, Escudero and Valladares, 2016). For example, in tropical forests, functional diversity accounts for differences in forest productivity more so than taxonomic diversity (van der Sande et al. 2018), richness (Rosenfield and Müller, 2020), or forest dynamics in space and time, especially regarding forest succession (Letcher et al. 2015, Lohbeck et al. 2012, Muscarella et al. 2016a, Hogan et al. 2018). Moreover, it is far easier to infer plant community dynamics or plant-environment relationships from a functional trait perspective than through changes in individual species or community (i.e., multivariate) demographics (Poorter et al. 2018a, Poorter et al. 2018b). This trend is exacerbated with

increasing plant community richness (Baraloto et al. 2010). In hyper diverse tropical forests, where there can be tens or hundreds of species within genera, using a functional trait perspective often uncovers environmental associations between functional plant strategies (e.g., Kraft et al. 2008), trends which would be obscured by a traditional taxonomic approach. Moreover, when functional trait studies in hyper diverse tropical forests couple a functional perspective to phylogenetic data, patterns of inference can be strengthened (Baraloto et al. 2012). However, most of these studies use species-level trait data, ignoring ITV. Hence, there is motivation to understand whether incorporating ITV strengthens our ability to infer plant community-environment relationships (Violle et al. 2012, Siefert et al. 2015). This is of particular importance at the community scale because functional traits are used to inform the plant functional types or benchmark aggregate ecosystem functions in forest demography or ecosystem models, which predict tropical forest responses to global change (Fisher et al. 2018, Powell et al. 2018, Warren et al. 2015, Xu and Trugman, 2021).

Conceptually, ITV arises because of genetic variation among individuals, the environment, and the interaction between the two (Siefert et al. 2015, Bolnick et al. 2011). Accounting for ITV is labor-intensive, requiring extensive trait sampling of individuals; however, ITV is central to the ideological reconciliation of ecological and evolutionary frameworks. On the one hand, ecological frameworks seek to account for ITV in predicting community attributes or ecosystem properties, yet on the other, the evolutionary perspective seeks to better understand how natural selection shapes communities, ecosystems, and their constituent biota (Bolnick et al. 2011, Turcotte and Levine, 2016, Violle et al. 2012). Studies seeking to account for ITV in plant communities have traditionally looked at ITV between populations, communities, and ecosystems (e.g., Albert et al. 2010). Few studies have looked at ITV across successional or environmental gradients in tropical forests; moreover, none have sought to assess how such variation scales up to influence estimates of community-weighted mean (CWM) trait patterns.

The lack of studies aimed at quantifying the contribution of ITV to CWM trait patterns is likely due to the laborious undertaking of measuring the functional traits for

individuals and the community composition across environmental or successional gradients (Paine et al. 2011). This is particularly difficult in tropical forests, where large trees and high levels of diversity complicate trait sampling (Baraloto et al. 2010). Methodological approaches that have looked for ways around this issue by gap-filling or imputing trait values for missing taxa are a potential solution. Still, each imputation approach has its assumptions, and some are more useful than others (reviewed by Swenson 2014). One of the first proposed methods was multiple imputation chained equations (MICE, van Buuren and Groothuis-Oudshoorn 2010); however, this method has since been shown to be flawed for several reasons, perhaps the most-supreme of which, in the context of plant functional traits, is a lack of phylogenetic consideration (Penone et al. 2014). Two of the next most-desirable methods include Bayesian hierarchal probabilistic matrix factorization (BHPMF, Schrodt et al. 2015), which can use a hierarchical taxonomic structure (e.g., genera within families within orders) to infer phylogenetic structure in the imputation of missing trait values, and PhyloPars (Bruggeman et al. 2009, Goolsby et al. 2017), which uses phylogenetic generalized linear models (pGLM) to impute missing trait values, thereby directly accounting for species relatedness via branch lengths. A recent study compared the three methods, concluding that PhyloPars outperforms MICE and BHPMF for trait imputation (Johnson et al. 2021).

Forest communities typically move from acquisitive to conservative functional composition as species composition changes with forest succession (Christensen and Peet 1984, Letcher et al. 2015, Lohbeck et al. 2013, Muscarella et al. 2016a, Swenson et al. 2012, Garnier et al. 2004). Thus, CWM functional trait values shift toward traits associated with species conservativeness (or slow life-history strategy, e.g., SLA and higher wood density – WD), partly because of turnover in community composition alone (Chazdon et al. 2010). The contribution of ITV in a successional context is less well understood; however, contributions can be substantial. For example, ITV of key leaf traits (i.e., leaf area, SLA, leaf nitrogen content, and leaf phosphorus content) accounted for >25% to about 75% of the variation in CWM leaf trait values in a temperate rainforest in Chile (Fajardo and Siefert 2018). Root functional traits are of interest because they are abstruse and ecologically complex (Bardgett et al. 2014, Laliberté, 2017), rarely studied

in the context of ITV, and control ecosystem function via the flow of nutrients and water through trees (Freschet et al. 2020). Thus, understanding how CWM root traits vary in the context of environmental variation and forest age is potentially key to modeling the functioning of tropical forests into the future (Bardgett et al. 2014, McCormack et al. 2017, Warren et al. 2015),

Few studies have examined how CWM patterns in root traits change with forest succession and how they may be different or similar to leaf traits. A recent study from a temperate forest that used BHMPF to gap-fill missing root trait data (Caplan et al. 2019) found that CWMs shifted toward conservative root strategies (thicker diameters, lower specific root length, higher root tissue density, and lower root nitrogen content) with increasing forest age and that acquisitive (e.g., pioneer) species and invasive species with acquisitive root strategies were able to persist in disturbed communities. A different study sampled a strong edaphic chronosequence in temperate rainforest in New Zealand and found that ITV in root traits showed similar patterns to CWM patterns in root functional traits (Holdaway et al. 2011). The differences in these two studies highlight the need for more studies that quantify the degree to which soil environment-structured variation, forest succession-driven variation, and other ITV sources have on influencing CWM estimates of root functional traits. Here we use root and leaf trait data collected in a paired sampling design along a 6.6-km transect in a tropical forest in Hainan, China, to scale up trait measurements to the community level using a complementary network of small vegetation plots (Xu et al. 2015a, Xu et al. 2015b). Specifically, we address two research questions:

1. To what extent do species turnover (i.e., changes in community composition because of forest age and environmental filtering effects), ITV, and their covariation influence community-weighted mean functional trait estimates? W*e expected that changes in plant community composition and species relative abundances (i.e., species turnover) with forest age would influence estimates of community-weighted traits to a greater degree than ITV because the magnitude of interspecific trait variation would be more important if ITV were substantial.*

2. How sensitive are these patterns to phylogenetic trait imputation for missing taxa (i.e., gap-filling of missing trait data)? *The testable null hypothesis is no difference in the relative contributions of species turnover and ITV between using directly measured and imputed functional trait data. Accepting the null hypothesis here would validate trait imputation methods and provide a way forward for future functional trait measurement strategies.*

Materials and Methods

Study site: Jianfengling, Hainan Island, China

The Jianfengling forest reserve (JFL), in Hainan, China (18°23'–18°15'N, 108°36'–109°05'E, Fig. 1) is a 47,200 ha mountainous forest with a history of logging and forest resource extraction that dates back to 1957, where about two-thirds of the area was either clear-cut or selectively-logged, meaning 30-40% of large timber-valuable trees were extracted (Xu et al. 2015b, Zhou 1995). All logging ceased in 1994 under a state-wide (Hainan Island only) logging ban, followed by a Chinese national logging ban in 1998 (Wenhua 2004, Zhou 1995). The reserve encompasses several ecological life zones of vegetation, from tropical semi-deciduous monsoon forest at the lower elevations to mossy high elevation forest, with evergreen-monsoon forest dominated by Podocarpaceae intermixed throughout at elevations < 1000 m (Huang et al. 1995). The most common vegetation life zone is tropical montane rain forest (per the Holdridge life zone classification), which occurs at elevations between 600 and 1100 m. It is characterized by a mix of palms and broadleaf evergreen trees that reach an average canopy height of 18 m (Jin et al. 2013).

JFL has a tropical monsoon climate with seasonal rainfall, where the wet season occurs between May and October (Zeng 1995). Cumulative annual rainfall over the last 30 years at JFL has averaged 2700 mm (Wu 1995). The soils are derived from porphyritic granite and are classified as lateritic and humic yellow soils (Wu 1995). They are infertile, leached tropical soils with an exchangeable base content of 30 mL per kg and some aluminum accumulation. Nutrient supplies in these soils are principally derived from the surface accumulation of organic matter, with rates of mineral and

organic matter cycling in the soils being slower than other tropical soils (e.g., latisols, Wu 1995).

Root and leaf functional trait data

Functional traits were collected from May to July 2017. Saplings (i.e., trees >1m tall, but less than <10 cm diameter at 1.3m) of 72 species from 15 selected Angiosperm families, comprising 423 saplings (roughly 6 per species), were measured for leaf and root functional traits. Trait collection from saplings was done systematically along a 6.6 km transect that spanned primary and secondary forest with logging history (Fig. 1, see Hogan et al. 2020 for further details). Three leaves and five fine root systems (i.e., those containing 3-4 root orders, per McCormack et al. 2015) per sapling were collected, washed, scanned, dried, and weighed following standard trait measurement protocols. Scanned images were analyzed using leaf and root image analysis software (WinFolia 2007b and WinRhizo 2016, Regent Instruments, Quebec, Canada) for morphological traits. For each individual sapling, trait values were averaged across the three leaf and five root samples analyzed.

These individual-level trait data can be condensed to a few axes of key morphological variation among roots and leaves. A principal components analysis (Hogan et al. 2020) showed that three leaf traits – leaf area, specific leaf area (SLA), and leaf thickness, and four root traits – root system average diameter, specific root length (SRL), root tissue density (RTD), and root branching intensity (RBI) accounted for most of the two to three dimensional above and belowground trait variation among individuals. Therefore, we also focus on those seven traits in these analyses.

The network of small plots

We integrate data from a network of small plots previously established in the JFL forest reserve (Xu et al. 2015a, Xu et al. 2015b). Between August 2007 and June 2009, a network of 164 0.0625-ha (25m × 25m) plots were established in the JFL reserve (Xu et al. 2015b, Fig. 1). The plots span the local variability in vegetative life-zones and range in altitude from 259 to 1135 m. Roughly one-third (52 of 164) of the small plots are in old-growth forest, with no record or visible evidence of logging in the last 200 years (Xu et al. 2015b). The remainder of the plots (112) are in forest that was either selectively

logged or clear cut, with human land-use ceasing between 20 and 56 years ago (see Table 1 in Xu et al. 2015b). Selective-logging practices in the area typically result in the removal of 30-40% of the mature stems ≥ 40 cm in diameter of commercially valuable timber species (Xu et al. 2015b, Zhou 1995). In each of the 164 small plots, all free-standing stems ≥ 2.5 cm in diameter at 1.3 m height were mapped, measured, and identified to species.

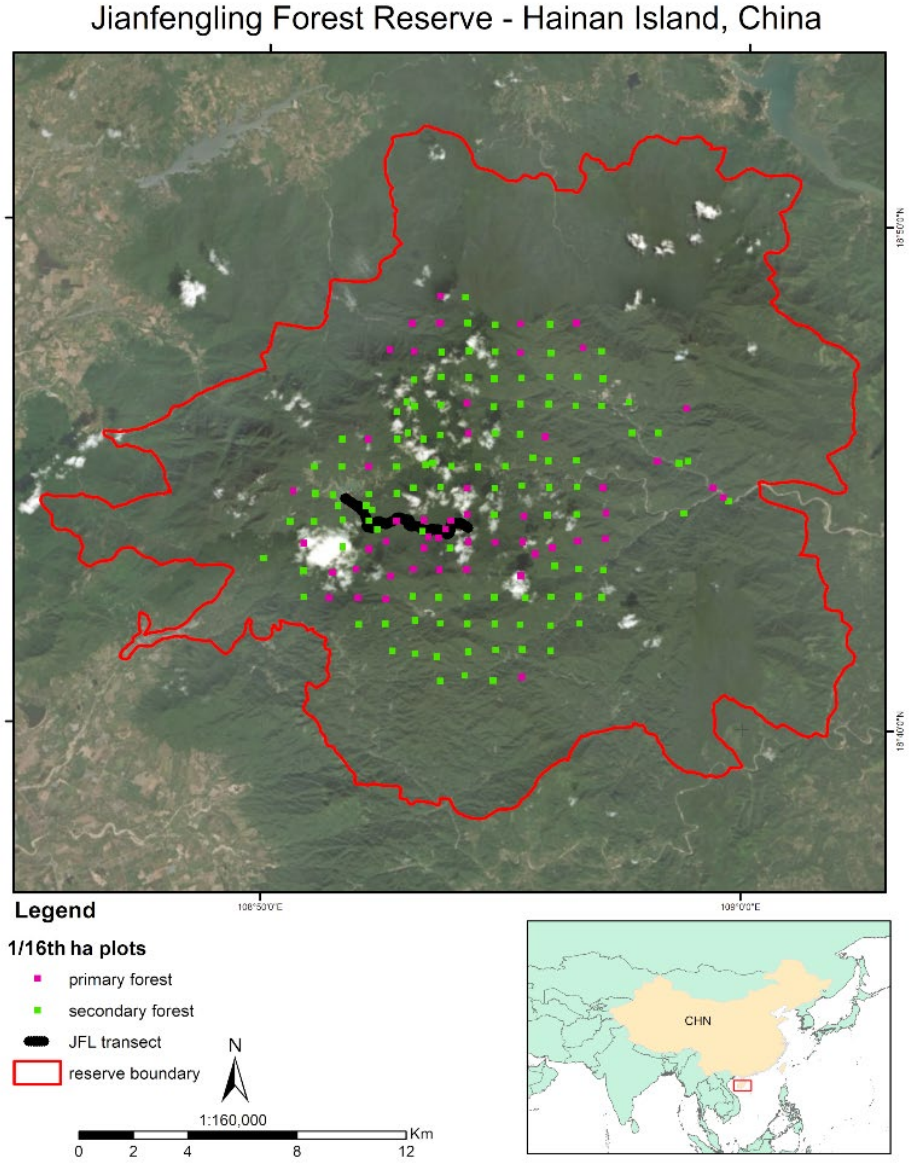

Fig. 1: The study site: the Jianfengling Forest Reserve (JFL) of Hainan Island, China. Hainan Island is a small continental island off China's southeastern coast, shown in the red box of the inset map. The 47,200 ha JFL boundary is shown with red boundary. The

6.6 km transect of where functional traits of saplings were sampled is shown in black. The first half of the transect is in secondary forest with a history of logging, and the second half of the transect is in unlogged, primary forest. Small 0.0625-ha plots (Xu et al. 2015a, Xu et al. 2015b) in unlogged, primary and either clear-cut or logged secondary forest are shown as pink and green points, respectively. Logging and forest disturbance in the secondary plots has happened in the last 20-55 years.

Data analyses: the network of small plots and Lepš' Intraspecific variability effects

In the interest of scaling up our functional trait measurements from individual trees along the gradient to the scope of the JFL forest reserve using tree community data from the network of small plots, we used an assemblage (i.e., partial community) – weighted mean approach, with basal area species weights. We call this an assemblage-weighted mean (AWM) in lieu of the classical community-weighted mean (CWM) because we could not measure traits for all species found in the plant communities. However, we did employ a sampling design that controlled for plant lineage, targeting species from 15 families across the Angiosperm phylogeny. This sampling design targeted families representing the functional variation in root morphologies across the angiosperm phylogeny and sampled many individuals within each species (average of 6) to assess ITV, where ITV was found to be structured across forest types (Hogan et al. 2020). Species for which we sampled functional traits accounted for 12.4% of species (72 of 582) and 37 % of stems (20,673 of 65,144) in the network of small plots. Basal area (measured in August 2007 to June 2009) in the array of small plots ranged from 16.7 to 77.8 m^2 ha^{-1}, averaging 44.2 m^2 ha^{-1}. The basal area of species in those plots for which functional traits were sampled along the 6.6 km gradient was between <1 and 42.3, averaging 18.4 m^2 ha^{-1}. Thus, the proportion of plot basal area for which there was trait coverage ranged from <1 to 82.3%, averaging 43.6%.

For each of the seven traits of interest, using mean trait values from all individuals for each species sampled along the transect (x_i), we calculated AWMs for each plot. We term these the fixed averages (after Lepš et al. 2011), thus:

$$fixed\ average = \sum_{i=1}^{S} p_i x_i,$$

where p_i is the basal area fraction of that species within the plot (i.e., the community weight). For the AWMs, species weights were calculated after removing all species for which trait data were not sampled; this was necessary as weights must sum to one. We

then calculated AWM trait values for each plot using habitat-specific trait values for each species ($x_{i\_habitat}$). For example, for plots in secondary forests, trait values from saplings sampled in secondary forest. We term these the specific averages (again after Lepš et al. 2011), as such:

$$specific\ average = \sum_{i=1}^{S} p_i x_{i\_habitat}.$$

The intraspecific variability effects for the assemblages were calculated as the difference between the fixed and specific averages. Two-way analyses of variance (ANOVAs) assuming homoscedasticity were conducted with respect to each of the seven functional traits chosen. Then using the sum of squares of these tests, the variance in trait values was decomposed into intraspecific and community (i.e., species turnover) portions and their covariation (i.e., interaction). This was done using the 'trait flex ANOVA' function (see supplemental material of Lepš et al. 2011) in R v.3.5.0 (R Core Team, 2018)

Data analyses: gap-filling traits and validation of assemblage-weighted means

To validate the results regarding intraspecific variability effects using AWMs, we employed an approach to gap-fill trait data for unsampled taxa. As we have explained, PhyloPars (Bruggeman et al. 2009) appears to be one of the best tools available for gap filling functional traits (Penone et al. 2014, Johnson et al. 2021). Additionally, due to the high degree of phylogenetic-conservatism in certain root traits (e.g., root diameter), PhyloPars is particularly appropriate. It uses a pGLM that calculates phylogenetic covariance of taxa from a Brownian motion model of trait evolution. Parameter estimates from the phylogenetic and functional trait variance-covariance matrix are then used to estimates missing data values.

A rudimentary phylogeny for all 582 taxa in the network of small plots was obtained from Phylomatic v3 (www.phylodiversity.net/phylomatic, Webb and Donoghue, 2005), using the 'slik2015' base tree, which contains the most comprehensive phylogenetic skeleton for tropical trees to date (Slik et al. 2018). Wood density (WD) was used as an additional trait in the pGLM, in that we wanted to have one trait that was imputed for all taxa. WD is a highly phylogenetically-conserved trait (Kraft et al. 2010, Swenson and Enquist, 2007), which can be used in the pGLM to constrain modeled trait

values for taxa and clades with no trait data. WD values were obtained from the global database of WD values (Chave et al. 2009, Zanne et al. 2009) where available, and the CTFS Forest-GEO WD database (http://ctfs.si.edu/Public/Datasets/CTFSWoodDensity/) via the 'BIOMASS' package ('getWoodDensity' function, Réjou-Méchain et al. 2017). Where species WD values were unavailable, values from a higher taxonomic classification (e.g., genus or family) were used (see Online Resource 3).

WD data was combined with three separate incomplete trait matrices, one using fixed trait values (x_i, i.e., species mean values for all individuals measured along the transect), and two habitat-specific matrices ($x_{i\_habitat}$), with the habitats being secondary and primary forest, as delineated along the sampling transect (see Hogan et al. 2020). pGLMs were fit separately to each incomplete trait matrix and predicted to complete them for all 582 taxa using PhyloPars (http://zeus.few.vu.nl/programs/phylopars, Bruggeman et al. 2009) and the Phylomatic-generated phylogeny. For the model setting in PhyloPars, we allowed for correlated evolution of the different traits, but did not allow for intraspecific variation in the models because, in our case, the separate fitting of the pGLMs accounts for this. We then used the gap-filled trait matrices and basal area species weights (p_i) of species in the small plots to recalculate fixed and specific averages (i.e., weighted means) for each plot. We re-ran the trait flex ANOVAs, comparing the AWM analysis, using only the species for which we measured functional traits (i.e., 72 species), to the CWM analysis, which used the PhyloPars-imputed trait data for all 582 species in the communities of the small plots.

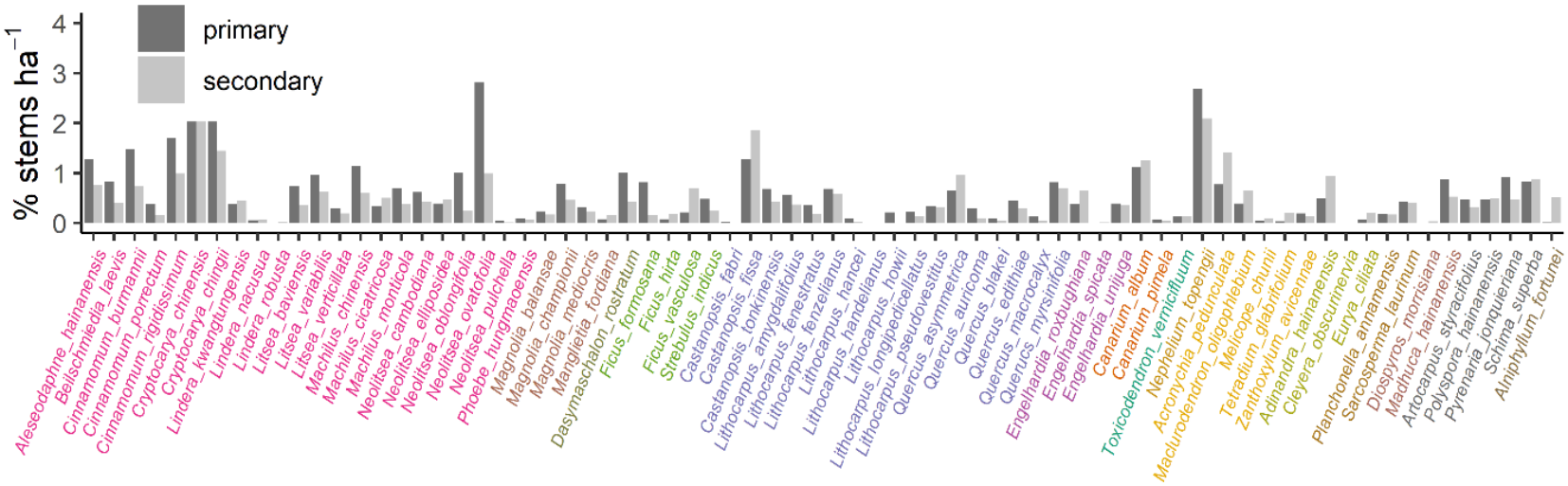

Fig. 2: Relative stem densities (% of stems ha^{-1}) for the 72 species in 164 0.0625-ha plots in Jianfengling, Hainan Island, China (Fig. 1, Xu et al. 2015b), for which trait data were sampled (Hogan et al. 2020). Fifty-two of those plots are in well-conserved, primary forest, while 112 are in secondary forest (i.e., previously logged or clear-cut). Relative stem densities of these 72 species sum to 44% of stems in primary forest plots, and 33% of stems in secondary forest plots. Colors of species names correspond to plant family in order from phylogenetically oldest (i.e., more basal) to youngest (i.e., more derived): Lauraceae, Magnoliaceae, Annonaceae, Moraceae, Fagaceae, Juglandaceae, Burseraceae, Anacardiaceae, Sapindaceae, Rutaceae, Pentaphylacaceae, Sapotaceae, Ebenaceae, Theaceae, Styracaceae.

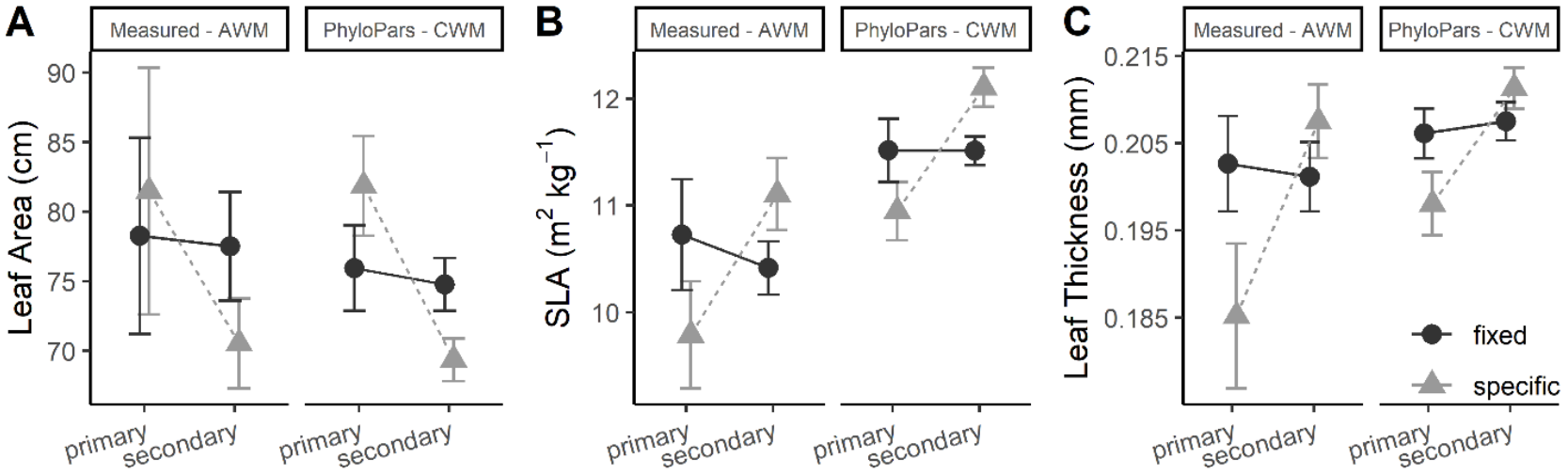

Fig. 3: Community weighted mean (CWM) trait values for leaf area (A), SLA (B) and leaf thickness (C) for 164 0.0625-ha plots in Jianfengling, Hainan, China. Points are mean CWM values (± 95% confidence intervals) for plots by forest type (52 in primary and 112 in secondary). Fixed CWMs (in black) use trait values irrespective of forest type, while specific CWMs (in gray) use trait data from individuals collected within each forest type. The left panel in each figure shows assemblage-weighted mean (AWM) values, which use only measured data from 72 species, while the right panel shows PhyloPars pGLM-imputed CWM functional trait values using the entire community (582 species).

Table 1: Trait flex Analysis of Variance (ANOVA) table for forest type as a factor in assemblage-weighted functional trait variance. Statistics for residual variance not shown (see Online Resource 2). These assemblage-weighted analyses use small plot tree community data and functional trait data for 72 species (i.e., only those for which trait data was directly measured along the 6.6 km transect in JFL). Fixed assemblage-weighted mean values use all functional trait data from individuals sampled along the transect (n = 423), whereas specific assemblage-weighted means match functional trait data from plant individuals to plots with corresponding forest-type classification (n = 198 for primary forest and n = 225 for secondary forest). Intraspecific variability = fixed – specific. Abbreviations are as follows: *df* = degrees of freedom, SS = sum of squares, *F* = F-statistic, *p* = probability of obtaining the F-statistic. Probabilities are denoted as: **p* < .05, ***p* < .01, ****p* < .001. Note that in this case, the mean squared error is equal to the sum of squares because there is 1 degree of freedom; therefore, mean squared errors are not shown. (See Online Resource 2)

Trait	Fixed				Specific				Intraspecific variability			
	df	SS	*F*	*p*	*df*	SS	*F*	*p*	*df*	SS	*F*	*p*
Leaf Area	1	20.00	0.04	0.84	1	4260.00	8.15	**	1	3696.90	47.42	***
SLA	1	3.46	1.50	0.22	1	61.50	19.10	***	1	94.12	112.14	***
Leaf Thickness	1	8.00E-05	0.19	0.67	1	0.02	28.28	***	1	0.02	89.12	***
Root Diameter	1	3.01E-03	0.29	0.59	1	0.04	3.15	0.08	1	0.07	18.42	***
SRL	1	81.30	0.83	0.36	1	4400.80	37.20	***	1	3285.60	88.93	***
RTD	1	8.99E-03	0.73	0.39	1	0.04	6.49	*	1	0.10	86.33	***
RBI	1	1.59E-02	4.92	*	1	5.59	156.76	***	1	5.15	275.00	***

Table 2: Trait flex Analysis of Variance (ANOVA) table for forest type in community-weighted functional trait variance. Statistics on residual variance are not shown. These ANOVAs were done using small plot tree community data and functional trait data for 582 species (i.e., the entire community for which we applied pGLM data imputation to). Fixed values use pGLM-imputed functional trait data for a matrix containing species means irrespective of forest type (i.e., all trait data collected along the 6.6 km transect), whereas specific values use pGLM-imputed functional traits data corresponding to either secondary or primary forest portions of the transect. Intraspecific variability = fixed – specific. Abbreviations are as follows: *df* = degrees of freedom, SS = sum of squares, *F* = F-statistic, *p* = probability of obtaining the F-statistic. Probabilities are denoted as: **p* < .05, ***p* < .01, ****p* < .001. Note that in this case, the mean squared error is equal to the sum of squares because there is 1 degree of freedom; therefore, mean squared errors are not shown.

Trait	Fixed				Specific				Intraspecific variability			
	df	SS	*F*	*p*	*df*	SS	*F*	*p*	*df*	SS	*F*	*p*
Leaf Area	1	48.10	0.44	0.51	1	5548.40	56.97	***	1	4563.30	271.24	***
SLA	1	3.45E-4	5E-4	0.98	1	47.68	50.36	***	1	47.91	317.85	***
Leaf Thickness	1	6.76E-5	0.53	0.47	1	6.24E-3	38.69	***	1	5.02E-3	150.38	***
Root Diameter	1	9.01E-3	2.24	0.14	1	0.09	21.26	***	1	0.16	192.09	***
SRL	1	50.10	1.63	0.20	1	1515.60	51.59	***	1	2116.90	361.98	***
RTD	1	1.91E-3	1.80	0.18	1	0.03	15.42	***	1	0.04	132.44	***
RBI	1	5.68E-3	1.50	0.22	1	4.58	528.60	***	1	4.26	1480.70	***

Results

Linking the transect to the network of small plots – species forest-type preferences and soils comparison

Of the 72 species that were sampled for functional traits along the 6.6 km transect, plot community composition showed that 65% of them (47 species) preferred primary forest. In comparison, the remainder (25 species) favored plots in secondary forest (Fig. 2). The basal area in primary and secondary forest plots was roughly equal, averaging 40.5 (± 0.2, standard error) m^2 ha^{-1} for small plots in primary forest and 42.7 (± 0.2) m^2 ha^{-1} for those in secondary forest. Soils in secondary forest were significantly finer in texture than soils from the primary forest t (% sand: $F_{1,298} = 63.9$, $p < .001$, % silt: $F_{1,298} = 53.8$, $p < .001$, % clay: $F_{1,298} = 38.5$, $p < .001$) and significantly less acidic (average pH of 2.5:1 soil in water of 4.39 vs. 4.27, $F_{1,298} = 14.1$, $p < .001$). Soils in the secondary forest had significantly greater total exchangeable base content ($F_{1,298} = 35.7$, $p < .001$), effective cation exchange capacity ($F_{1,298} = 11.62$, $p < .001$), and base saturation ($F_{(1,298)} = 22.5$, $p < .001$) than the soils in the primary forest. These trends from the soils of the transect mirrored trends in soil properties between small plots in secondary and primary forests (Online Resource 1). Thus, the range of variability in soil conditions between the transect and the network of small plots was similar, making comparisons between functional trait measurements from the transect to the community composition of the network of small plots unbiased relative to the soil environment.

Estimates of assemblage-weighted trait values – fixed vs. specific means

Our analytical approach involved calculating AWM estimates of functional traits using all data irrespective of forest type (i.e., fixed means) and using only data from each forest type (i.e., specific means, see complete analyses in Online Resource 2). Fixed AWM values for leaf functional traits differed drastically from specific AWMs (Table 1, Fig. 3). For example, plot average fixed AWMs for leaf area were 77.5 cm^2 and 78.2 cm^2 (a 0.7 cm^2 difference) for secondary and primary forest, respectively. Those estimates shifted to 70.5 cm^2 and 81.5 cm^2 (a difference of 11 cm^2) for specific AWMs (Fig. 3A). Fixed AWM estimates for SLA were 10.7 and 10.4 m^2 kg^{-1} for small plots in primary and secondary forest, respectively. In contrast, specific AWM estimates for SLA showed a

greater difference between forest types, being 9.3 and 10.8 m^2 kg^{-1} for small plots in primary and secondary forest, respectively, (Fig. 3B). The trend for leaf thickness was similar to those for leaf area and SLA. AWM differences were not significantly different for fixed averages but were for specific averages (Table 1), being about 0.02 mm greater in secondary forest than in primary forest (Fig. 3C).

Similarly, for root functional traits, fixed AWM values were similar and statistically indistinguishable (in all cases) between primary and secondary forest plots. At the same time, specific AWMs showed apparent and often statistically significant differences (Fig. 4). For example, fixed and specific AWMs for average root system diameter (Fig. 4A) showed an opposite trend, with fixed estimates being slightly (<0.01 mm) narrower in primary than secondary forest, but with specific estimates being marginally thicker (0.03 mm) in primary than secondary forest. For both the fixed and specific AWMs for root diameter, these differences were not significant (Table 1). Fixed AWMs for SRL, the belowground analog to SLA, were 4.85 m g^{-1} in primary forest plots and 5.00 m g^{-1} in secondary forest plots, while the specific CWM estimates for SRL were 3.91 m g^{-1} in primary forest plots and 5.11 m g^{-1} in secondary forest plots (Fig. 4B). The difference of specific AWMs for SRL between secondary and primary forest plots was 1.11 m g^{-1} instead of a difference of 0.15 m g^{-1} for fixed AWMs for SRL. These differences went from being statistically non-significant for the fixed AWM comparison by forest type to significant for the specific AWMs (Table 1). The results for RTD were similar to those for average root system diameter (Fig. 4C). Fixed AWMs for RTD showed a decreasing trend from primary to secondary forest, with roots being about 0.02 g cm^{-3} less dense in secondary than primary forest. Specific AWMs for RTD showed the opposing trend, with AWMs for RTD being about 0.3 g cm^{-3} denser in secondary than in primary forest. Differences between fixed AWMs were not statistically different, but the difference between specific AWMs were statistically significant (Table 1). Lastly, AWM RBI showed no significant differences when specific means were compared across forest types, with values averaging about 1.97 root tips cm^{-1} (Figure 4D, Table 1). However, fixed AWM RBI values were statistically different, averaging 1.73 tips cm^{-1} in primary

forest plots and 2.13 tips cm^{-1} in secondary forest plots (Fig. 4D), a weighted-mean difference of 0.4 tips cm^{-1}.

In summary, the only difference in fixed AWM values by forest type for or any of the seven functional traits considered was for RBI (Table 1, Figs. 3 and 4), but statistical differences in specific AWM trait estimates occurred for all traits except for root diameter, which had a marginally significant difference (p = .08, Table 1). Even when differences between specific AWMs between forest types were not statistically significant, they were always greater than differences in fixed AWMs. In some cases, they were also different in sign (i.e., for SLA, leaf thickness, root diameter, and SRL, Figs. 3 and 4).

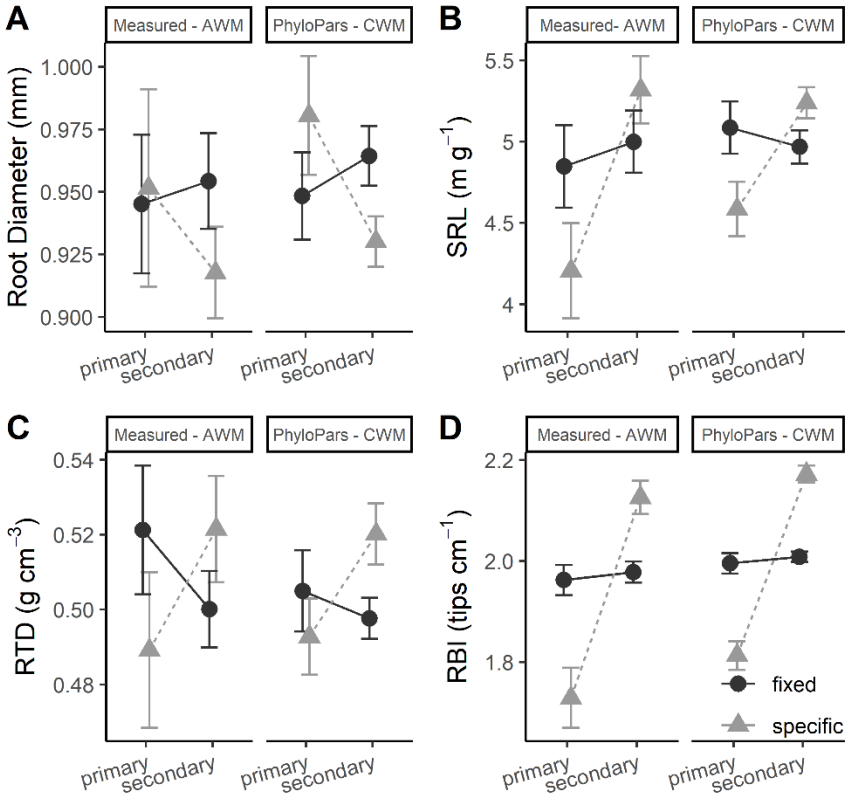

Fig. 4: CWM trait values for fine root system average diameter (A), specific root length (SRL, B), root tissue density (RTD, C), and root branching intensity (RBI, D) for 164 0.0625-ha plots in Jianfengling, Hainan, China. Points are mean CWM values (± 95% confidence intervals) for plots by forest type (52 in primary and 112 in secondary). Fixed CWMs use trait values irrespective of forest type, while specific CWMs use trait data that accounts for ITV between forest types. The left panel in each figure shows assemblage-weighted mean (AWM) values, which use only measured data from 72 species, while the

right panel shows PhyloPars pGLM-imputed CWM functional trait values using the entire community (582 species).

Comparing assemblage-weighted means to community-weighted means – evaluating pGLM-imputed trait values

Trends in CWM means confirmed the results of the AWM analyses. Like the AWM analysis, the pattern of having larger differences in habitat-specific means than for fixed means between forest types was consistent across all leaf (Fig. 3) and root (Fig. 4) CWMs using pGLM-imputed trait matrices. When pGLM-imputed functional trait matrices for the entire community were used, the variability among weighted trait estimates for plots decreased (i.e., 95% confidence interval breadth contracted). This decrease in estimate variability led to more statistically significant differences for specific CWMs relative to specific AWMs (Table 2). For leaf traits (leaf area, SLA, and leaf thickness), no qualitative difference emerged from CWMs using pGLM-imputed trait data for taxa, versus only measured trait data (Fig. 3, Table 2). The only noticeable difference between the AWM and CWM values in Fig. 3 is that pGLM-imputed CWM values for SLA were translated about 1 m^2 kg^{-1} greater across the fixed and specific means for both forest types. Additionally, the difference between fixed CWMs for RBI was not statistically significant (Table 2), where it was for the fixed AWMs for RBI (Table 1). Also, the difference in specific CWMs for root diameter was statistically significant (Table 2), where the difference between AWMs was marginally significant (Table 1).

Comparing AMWs to CWMs for root traits, we see similar patterns. Using AWMs resulted in no differences between fixed and specific estimates for root diameter (Fig 4A). However, when the pGLM-imputed data were used, the specific estimates for root diameter increased slightly for primary forest and decreased for secondary forest, creating a statistically significant difference between forest-types (Table 2). For the three other root traits (SRL, RTD, and RBI), differences were accentuated slightly, as pGLM-imputed functional trait matrices were used (Fig. 4 B, C, D). This discrepancy in forest-type weighted-trait estimates resulted more from ITV with environment than from species turnover among plots (Table 2, Fig. 5). In many cases, for example for SLA, root diameter, SRL, and RTD, ITV and species turnover had negative covariance values

(Table 4, Table S4), meaning that beta diversity in species composition drives weighted-trait values one way (in our case, usually slightly toward the conservative end of the plant economics spectrum, but not always), while ITV with environment causes shifts in the opposite direction (in our case, roots morphologies became more conservative while leaf morphologies were more acquisitive from primary to secondary forest, Hogan et al. 2020).

Interspecific variability effects – the relative effect of ITV and turnover on weighted-mean trait estimates

Results from the interspecific variability effects from AWMs (Table 1) and CWMs (Table 2) can be used to infer the relative contribution of ITV and species turnover by forest type to functional trait variability. They can also be compared to understand the effect of pGLM gap-filling on the relative contribution of ITV and species turnover by forest type to functional trait variability. Between the AWM and CWM analyses, ITV and species turnover had similar contributions to total functional trait variance for the seven traits considered (Fig 5, left panel). The relative contribution of ITV in explaining the trait variation due to forest type increased markedly from the AWMs to CWMs (Fig. 5, middle panel). This decrease came as the contribution of ITV to trait-flex ANOVA error decreased from the AWM analysis to the CWM analysis (Fig. 5, right panel). For example, when using only measured data (i.e., the AWM analysis), the total relative contribution of forest type for leaf area, SLA, and leaf thickness was 5, 11, and 15 percent, respectively (Fig. 5). The relative contribution of forest-type for those three leaf traits increased to 26, 24, and 19 percent, respectively, when pGLM-imputed trait matrices were used in the CWM analysis (Fig. 5). Nearly all this variation was due to ITV and not to species turnover (i.e., β-diversity, relative contributions < 1%) among the small vegetation plots. Moreover, the relative contribution of forest type to functional trait variation in root diameter, SRL, RTD, and RBI was 2, 19, 4, and 49 percent (Table 4), respectively, using only directly-measured functional traits (i.e., AWMs). In contrast, the relative contribution to forest-type increased to 12, 24, 9, and 77 percent, respectively, when using pGLM-imputed data (i.e., CWMs).

Overall, the trait-flex ANOVA model were strikingly similar between the AWM analysis and the CWM analysis (Fig. 5). For each of the seven traits considered, the trait flex ANOVA models had comparable total explanatory power (Fig. 5, left panel). Considering total weighted-mean trait variation, five traits (SRL, SLA, root system diameter, leaf thickness, and leaf area) showed negative covariation for the AWM trait-flex ANOVAs. For the CWM analysis, only three traits (SRL, root system diameter, and leaf area) showed negative covariation in relation to total trait variation. However, the magnitude of their negative covariation increased. For weighted-mean trait variation due to forest type, both the AWM and CWM analysis were mostly attributable to ITV and not to turnover, although the magnitude differed slightly, with small differences in ITV and species turnover covariation (Fig. 5, middle panel). Lastly, trait flex ANOVA model errors were comparable between AWM and CWM analyses. The general pattern is that the error associate with ITV decreased when using data from the entire plant community (i.e., pGLM-imputed complete functional trait matrices as opposed to the 72 species assemblages). The magnitude of error attributable to species turnover and the covariation between ITV and species turnover was similar between AWM and CWM models (Fig. 5, right panel).

Discussion

The utility of functional perspectives to species-rich tropical forests

The application of functional perspectives (Keddy 1992, Westoby and Wright 2006) to understand the ecology of plants in relation to environmental variation is a promising way to reduce complex and subtle changes in species composition and variation in functional composition of communities into ecologically meaningful information. This has been demonstrated regarding patterns of community assembly (Baraloto et al. 2012, Kraft et al. 2008, Laughlin, 2014, Spasojevic and Suding, 2012) and their underlying variability in plant traits (Letcher et al. 2015, Muscarella et al. 2016b). The data used in this study confirm that ITV in tropical tree communities is substantial (Hogan et al. 2020), which has a consequence for CWM trait estimates (Baraloto et al. 2010, Muscarella and Uriarte, 2016). ITV has been shown to account for vital ecological differences among species, such as rates of photosynthesis and growth

(Shipley et al. 2006, Wright et al. 2010), intrinsic rates of population growth (Adler et al. 2014), or variation in ecosystem productivity (Lohbeck et al. 2013, Poorter et al. 2017, van der Sande et al. 2018)

Yet, there has been a burgeoning in examining the role of ITV in functional ecology (i.e., ecologically accounting for species trait variance rather than the mean trait values; Siefert et al. 2015, Violle et al. 2012, Hulshof and Swenson 2010). Undoubtedly, some amount of ITV is related to environmental variation, but difficulty exists in quantifying dimensions of niche space or specific ecosystem properties that systematically relate to this variation (Lavorel and Garnier 2002, Shipley et al. 2016). Furthermore, there is the possibility of genetic variation and genetic × environment interactive effects (Kunstler et al. 2016, Soliveres et al. 2014, Yang et al. 2018). Whether to focus on interspecific or intraspecific trait variation, the two approaches employ drastically different sampling designs (Baraloto et al. 2010). On the one hand, diversity-differences are favored by a focus in among taxa trait variation. On the other, when ITV is the focus, sampling effort is maximized for one to a few species potentially at the expense of diversity-driven differences. In the tropics, the costs of this trade-off are particularly acute, as species diversity and environmental variation are both extensive. A second practical difficulty arises in that species compositional differences are often confounded with environmental variation (i.e., environmental filtering), making it challenging to assess ITV for all taxa, especially less-common ones. Despite this, Lepš et al. (2011) propose a middle-of-the-road solution that appeals, group trait sampling by *a priori* ecological classification (i.e., measure habitat or experimental-treatment specific trait values). This approach proved useful in assessing how fertilization and mowing shape the functional traits of European grasslands (Lepš 1999, Lepš et al. 2011).

We employed a similar approach to assess how environmental variation in resource availability (i.e., soil nutrient content and light availability, see Hogan et al. 2020), roughly summarized by the successional progression of a forest (Odum 1969, Christensen and Peet 1984, Guariguata and Ostertag 2001, Chazdon et al. 2010) leads to functional and compositional community change. In our case, the principal axis of environmental variation, irrespective of compositional differences among forest-types,

was a gradient in soil fertility and texture, with soil texture and fertility decreasing along the transect from more-secondary to primary forest (Online Resource 1, Hogan et al. 2020). ITV along this gradient was consistent and measured 7 cm^2 for leaf area, 0.8 m^2 kg^{-1} for SLA, 0.4 mm for root diameter, 0.35 m g^{-1} for SRL, and 0.3 tips cm^{-1}, on average (Hogan et al. 2020). Additionally, there was considerable interfamilial variation among the taxa, which were preselected to collect a range in root functional strategies. We carefully sampled leaves and roots from individual juvenile trees that spanned environmental variation in soil environment and forest type. These considerations led to the trait data being well suited to scale to the community level using the forest demography data from the network of small plots (Online Resource 1, Xu et al. 2015a, Xu et al. 2015b). Thus, the middle-of-the-road solution proposed by Lepš et al. (2011) of structuring functional trait sampling across known environmental variability is useful when carefully applied to forests, as well.

Consequences of ITV for CWM estimation with tropical forest successional status

On one-hand interpreting, CWM patterns of trait variation can help interpret ecological processes shaping community assembly from regional species pools (i.e., environmental filtering of species or even phenotypes) (Kraft et al. 2008, Muscarella and Uriarte, 2016, Spasojevic et al. 2016). On the other, they are gross generalizations of the aggregate function of species assemblages that may or may not reflect broader forest-level or ecosystem functioning (e.g., total photosynthetic, nutrient uptake, or biomass production capacity of a stand; Warren et al. 2015, Fisher et al. 2018). Their accuracy depends on proper estimates of species traits in relation to the environment, which must account for both among and within species variation (Violle et al. 2012, Shipley et al. 2016, Yang et al. 2018). Measuring the morphology of all the plants within a community may one day be feasible but is currently not possible. Yet, the ability to accurately estimate trait values (e.g., leaf area, or more so even, belowground traits like root-tip abundance) is critical to accurately modeling how vegetation will respond to future changes in the biosphere (Warren et al. 2015, McCormack et al. 2017).

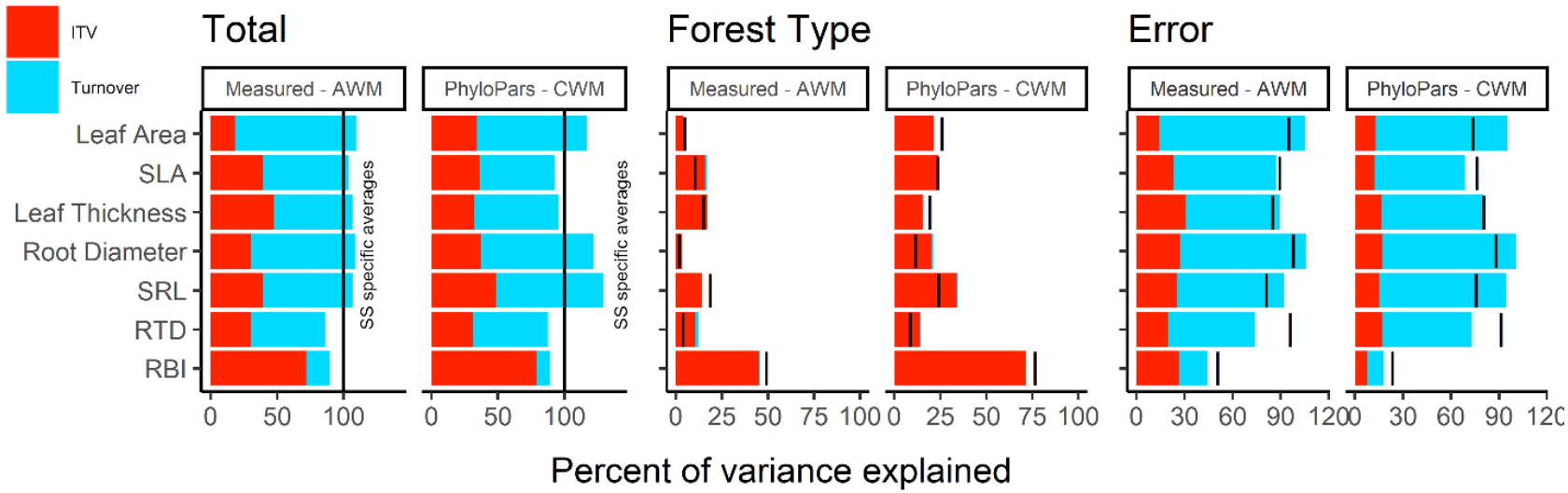

Fig. 5: Decomposition of the total variability in root and leaf traits for the tree communities in 164 0.0625-ha small plots in Jianfengling, Hainan China. The blue portion of the bars corresponds to the percent of variance explained by species turnover, while the red part shows the intraspecific variability effect – or the percent of variance explained by ITV. Black bars denote total variation (i.e., the variation, or total sum or squares – SS, in specific weighted-mean averages). The space between the top part of the column and bar corresponds to ITV and species turnover covariation; if the bar is above the column, the covariation is positive, and if below, the covariation is negative. The values are standardized by the total variation in specific CWM averages. The figure follows Figure 3 in Lepš et al. (2011).

Scaling up trait measurements from along the JFL gradient to the forest using data from a network of small plots revealed that ITV compounded with compositional differences (i.e., species basal area weights) to create discrepancies in community-weighted trait values concerning forest successional status. That is, specific weighted-means were much more different than fixed weighted-means, which was consistent for both the AWM and CWM analyses. These differences would not have been detected had we not sampled functional traits along an environmental gradient consistent with the environmental variation found in the network of small plots (Figs. 3 and 4). This is due to the negative covariation of ITV and compositional turnover for most (six of seven) of the traits examined (for either the AWM or CWM analysis, Fig. 5). For example, along the JFL gradient, we measured a plant lineage-consistent decrease of about 0.35 m g^{-1} in root-system SRL from secondary to primary forest (Hogan et al. 2020). Accounting for such ITV, the specific mean difference in SRL between primary and secondary plots was 1.11 m g^{-1} for the AWMs and about 0.65 m g^{-1} when pGLM-imputed data were used (Fig 4B). Covariation between ITV and species turnover was positive for the assemblage-weighted mean estimate but was negative for the more-complete analysis (Fig. 5). Regardless, like SRL, the difference in CWM trait estimates exceeded the magnitude of ITV measured across the JFL gradient (Hogan et al. 2020). This is because ITV compounds with β-diversity to move CWM trait values toward the conservative end of the plant economics spectrum (Tables 1 and 2, Figs. 3 and 4) as species composition shifts toward more conservative species in older forest (Lohbeck et al. 2013, Letcher et al. 2015, Muscarella and Uriarte, 2016, Spasojevic et al. 2016).

Several studies have reported negative covariation between species turnover and ITV for a variety of functional traits (grass leaf traits in response to mowing and leaf nitrogen in response to fertilization: Lepš et al. 2011, leaf traits: Fajardo and Siefert, 2018, leaf traits: Kichenin et al. 2013, SLA, leaf phosphorus, leaf thickness: Derroire et al. 2018, plant height and leaf traits excepting SLA: Zuo et al. 2017). Negative trait covariances between drivers of trait variability (e.g., ITV because of environment or disturbance, and species turnover in our case) confer resistance in the change of CWM trait values to a single driver because the effect of one driver limits the trait response to

the other driver. This dampening can be understood in the context of the portfolio effect (Schindler et al. 2015), where negative covariance between system components (e.g., drivers of community trait variation) leads to dampened dynamics at higher-order levels (e.g., the community) (Bolnick et al. 2011). On the other hand, positive covariation between species turnover and ITV has been found in some other studies from an equal variety of traits (leaf nitrogen: Kichenin et al. 2013, leaf area, leaf dry matter content, leaf nitrogen: Derroire et al. 2018, SLA: Zuo et al. 2017). The idiosyncrasy of these results points to the context-dependency in the covariation of ITV in decomposing the functional trait variation of plant communities (Kichenin et al. 2013). In the AWM analysis we conducted, we found slight negative covariation for SLA, RTD, root system diameter, leaf thickness, and leaf area (Fig. 5). Extending the analysis to the entire community using pGLM-imputed functional trait matrices created some minor variation in these patterns. The sign of the covariation because of forest type changed for three of the seven traits (leaf area, leaf thickness, and SRL). Thus, although these changes were small, trait covariation seems sensitive to the assemblage of species for which functional traits are measured, potentially pointing to the role of species-specific responses in CWM trait patterns (Muscarella and Uriarte 2016).

With respect to tropical forests, differing patterns in the contribution of ITV versus species turnover and their covariation and may emerge for wet and dry tropical forests (Poorter et al. 2019). We report more negative than positive covariation in ITV and specie turnover in CWM trait estimates. However, positive covariation of ITV and turnover was reported for most leaf traits in the Guanacaste dry forest of Costa Rica (Derroire et al. 2018). Additionally, Zuo et al. (2017) found positive covariation between trait variation because of species turnover and ITV for several leaf traits, excepting SLA, in dune grassland communities in Mongolia.

Patterns of β- diversity among sampled communities in relation to the functional uniqueness of the species contributing to those patterns (i.e., those lost or gained across assemblages) (Spasojevic et al. 2016) drives the covariation of the drivers of trait variability within and across plant communities. In communities with high levels of functional redundancy, such as tropical forests, responses may be muted as individual

species play a less significant role in driving overall patterns (Baraloto et al. 2010, Laughlin, 2014, Umaña et al. 2017).

Conclusions

In response to our first research question on whether species turnover is a more significant contributor to variation CWM trait values than ITV, for six of seven traits (i.e., all traits except RBI), species turnover outweighed the contribution of ITV in explaining functional trait variation. However, trait variation due to forest type was nearly entirely explained by ITV, which was consistent across all root and leaf functional traits. This likely reflects both functional trait variation maximized by the sampling design because of forest type and actual ITV among tropical trees. Concerning our second research question, on the sensitivity of patterns of CWMs to gap-filling via phylogenetic trait imputation, we find support for the PhyloPars method, which is in congruence with some recent work (Johnson et al. 2021). Inference was not unchanged quantitively by trait imputation (i.e., accepting the null hypothesis as outlined in the introduction), however patters were strikingly similar (i.e., changed very little qualitatively). This result speaks to the need to create ecologically relevant designs for the sampling of plant functional traits (Baraloto et al. 2010, Lepš et al. 2011) that capture ITV efficiently relative to measurement labor. The approach we demonstrate here accounts for trait variation across the community using phylogenetic sampling, as well as for ITV across gradients of environmental variation, like soil fertility, texture, and forest age. Its application captured important variability in CWM trait estimates with land-use driven variation in tropical forest tree communities, which would have been overlooked using traditional analyses with single, fixed trait values for species.

References

Adler PB, Salguero-Gómez R, Compagnoni A, Hsu JS, Ray-Mukherjee J, Mbeau-Ache C, Franco M (2014) Functional traits explain variation in plant life history strategies. Proceedings of the National Academy of Sciences, 111:740-745

Albert CH, Thuiller W, Yoccoz NG, Soudant A, Boucher F, Saccone P, Lavorel S (2010) Intraspecific functional variability: extent, structure and sources of variation. Journal of Ecology 98:604-613

Baraloto C, Hardy OJ, Paine CET, Dexter KG, Cruaud C, Dunning LT, Gonzalez MA, Molino JF, Sabatier D, Savolainen V (2012) Using functional traits and phylogenetic trees to examine the assembly of tropical tree communities. Journal of Ecology 100:690-701

Baraloto C, Paine CET, Patiño S, Bonal D, Hérault B, Chave J (2010) Functional trait variation and sampling strategies in species-rich plant communities. Functional Ecology 24:208-216

Bardgett RD, Mommer L, De Vries FT (2014) Going underground: root traits as drivers of ecosystem processes. Trends in Ecology & Evolution 29:692-699

Bolnick D, Amarasekare P, Araújo M, Bürger R, Levine J, Novak M, Rudolf V, Schreiber S, Urban M, Vasseur D (2011) Why intraspecific trait variation matters in community ecology. Trends in Ecology & Evolution 26:183-92

Bruelheide H, Dengler J, Purschke O, Lenoir J, Jiménez-Alfaro B, Hennekens SM, Botta-Dukát Z, Chytrý M, Field R, Jansen F, Kattge J, Pillar VD, Schrodt F, Mahecha MD, Peet RK, Sandel B, van Bodegom P, Altman J, Alvarez-Dávila E, Arfin Khan MAS, Attorre F, Aubin I, Baraloto C, Barroso JG, Bauters M, Bergmeier E, Biurrun I, Bjorkman AD, Blonder B, Čarni A, Cayuela L, Černý T, Cornelissen JHC, Craven D, Dainese M, Derroire G, De Sanctis M, Díaz S, Doležal J, Farfan-Rios W, Feldpausch TR, Fenton NJ, Garnier E, Guerin GR, Gutiérrez AG, Haider S, Hattab T, Henry G, Hérault B, Higuchi P, Hölzel N, Homeier J, Jentsch A, Jürgens N, Kącki Z, Karger DN, Kessler M, Kleyer M, Knollová I, Korolyuk AY, Kühn I, Laughlin DC, Lens F, Loos J, Louault F, Lyubenova MI, Malhi Y, Marcenò C, Mencuccini M, Müller JV, Munzinger J, Myers-Smith IH, Neill DA, Niinemets Ü, Orwin KH, Ozinga WA, Penuelas J, Pérez-Haase A, Petřík P, Phillips OL, Pärtel M, Reich PB, Römermann C, Rodrigues AV, Sabatini FM, Sardans J, Schmidt M, Seidler G, Silva Espejo JE, Silveira M, Smyth A, Sporbert M, Svenning JC, Tang Z, Thomas R, Tsiripidis I, Vassilev K, Violle C, Virtanen R, Weiher, E, et al. (2018) Global trait–environment relationships of plant communities. Nature Ecology & Evolution 2:1906-1917

Bruggeman J, Heringa J, Brandt BW (2009) PhyloPars: estimation of missing parameter values using phylogeny. Nucleic Acids Research 37:W179-W184

Caplan JS, Meiners SJ, Flores-Moreno H, McCormack ML (2019) Fine-root traits are linked to species dynamics in a successional plant community. Ecology 100:e02588

Chave J, Coomes D, Jansen S, Lewis SL, Swenson NG, Zanne AE (2009) Towards a worldwide wood economics spectrum. Ecology Letters 12:351-366

Chazdon RL, Finegan B, Capers RS, Salgado-Negret B, Casanoves F, Boukili V, Norden N (2010) Composition and dynamics of functional groups of trees during tropical forest succession in northeastern Costa Rica. Biotropica 42:31-40

Christensen NL, Peet RK (1984) Convergence during secondary forest succession. Journal of Ecology 72:25-36

Craven D, Eisenhauer N, Pearse WD, Hautier Y, Isbell F, Roscher C, Bahn M, Beierkuhnlein C, Bönisch G, Buchmann N, Byun C, Catford JA, Cerabolini BEL, Cornelissen JHC, Craine JM, De Luca E, Ebeling A, Griffin JN, Hector A, Hines J, Jentsch A, Kattge J, Kreyling, J, Lanta V, Lemoine N, Meyer ST, Minden V, Onipchenko V, Polley HW, Reich PB, van Ruijven J, Schamp B, Smith MD, Soudzilovskaia NA, Tilman D, Weigelt A, Wilsey B, Manning, P (2018) Multiple facets of biodiversity drive the diversity–stability relationship. Nature Ecology & Evolution 2:1579-1587

Derroire G, Powers JS, Hulshof CM, Cárdenas Varela LE, Healey JR (2018) Contrasting patterns of leaf trait variation among and within species during tropical dry forest succession in Costa Rica. Scientific Reports 8:285

Díaz S, Kattge J, Cornelissen JH, Wright IJ, Lavorel S, Dray S, Reu B, Kleyer M, Wirth C, Prentice IC (2016) The global spectrum of plant form and function. Nature 529:167.

Escudero A, Valladares F (2016) Trait-based plant ecology: moving towards a unifying species coexistence theory. Oecologia 180:919-922

Fajardo A, Siefert A (2018) Intraspecific trait variation and the leaf economics spectrum across resource gradients and levels of organization. Ecology 99:1024-1030

Fisher RA, Koven CD, Anderegg WRL, Christoffersen BO, Dietze MC, Farrior CE, Holm JA, Hurtt GC, Knox RG, Lawrence PJ, Lichstein JW, Longo M, Matheny AM, Medvigy D, Muller-Landau HC, Powell TL, Serbin SP, Sato H, Shuman JK, Smith B, Trugman AT, Viskari T, Verbeeck H, Weng E, Xu C, Xu X, Zhang T, Moorcroft PR (2018) Vegetation demographics in Earth System Models: A review of progress and priorities. Global Change Biology 24:35-54

Freschet GT, Roumet C, Comas LH, Weemstra M, Bengough AG, Rewald B, Bardgett RD, De Deyn GB, Johnson D, Klimešová J, Lukac M, McCormack ML, Meier IC, Pagès L, Poorter H, Prieto I, Wurzburger N, Zadworny M, Bagniewska-Zadworna A, Blancaflor EB, Brunner I, Gessler A, Hobbie SE, Iversen CM, Mommer L, Picon-Cochard C, Postma JA, Rose L, Ryser P, Scherer-Lorenzen M, Soudzilovskaia NA, Sun T, Valverde-Barrantes OJ, Weigelt A, York LM, Stokes A (2020) Root traits as drivers of plant and ecosystem functioning: current

understanding, pitfalls and future research needs. New Phytologist, doi:10.1111/nph.17072

Garnier E, Cortez J, Billès G, Navas ML, Roumet C, Debussche M, Laurent G, Blanchard A, Aubry D, Bellmann A (2004) Plant functional markers capture ecosystem properties during secondary succession Ecology 85:2630-2637

Goolsby EW, Bruggeman J, Ané C (2017) Rphylopars: fast multivariate phylogenetic comparative methods for missing data and within-species variation. Methods in Ecology and Evolution 8:22-27

Guariguata MR, Ostertag R (2001) Neotropical secondary forest succession: changes in structural and functional characteristics. Forest Ecology and Management 148:185-206

Hofhansl F, Chacón-Madrigal E, Brännström Å, Dieckmann U, Franklin O (2021) Mechanisms driving plant functional trait variation in a tropical forest. Ecology and Evolution, doi: 10.1002/ece3.7256

Hogan JA, Hérault B, Bachelot B, Gorel A, Jounieaux M, Baraloto C (2018) Understanding the recruitment response of juvenile Neotropical trees to logging intensity using functional traits. Ecological Applications 28:1998-2010

Hogan JA, Valverde-Barrantes OJ, Ding Q, Xu H, Baraloto, C (2020) Morphological variation of fine root systems and leaves in primary and secondary tropical forests of Hainan Island, China. Annals of Forest Science 77:79

Holdaway RJ, Richardson SJ, Dickie IA, Peltzer DA, Coomes DA (2011) Species-and community-level patterns in fine root traits along a 120 000-year soil chronosequence in temperate rain forest. Journal of Ecology 99:954-963

Huang Q, Li Y, Zheng D, Zhang J, Wan L, Jiang Y, Zhao Y (1995) Study on Tropical Vegetation Series in Jianfengling, Hainan Island. In: Zeng Q, Zhou G, Yide L, Wu Z, Chen B (eds) Researches on Tropical Forest Ecosystems in Jianfengling of China. China Forestry Publishing House, Beijing, China, pp 5-25

Hulshof CM, Swenson NG (2010) Variation in leaf functional trait values within and across individuals and species: an example from a Costa Rican dry forest. Functional Ecology 24:217-223

Jin D, Cao X, Ma K (2013) Leaf functional traits vary with the adult height of plant species in forest communities. Journal of Plant Ecology 7:68-76

Johnson TF, Isaac NJB, Paviolo A, González-Suárez M (2021) Handling missing values in trait data. Global Ecology and Biogeography 30:51-62

Keddy P. (1992) A pragmatic approach to functional ecology. Functional Ecology 6:621-626

Kichenin E, Wardle DA, Peltzer DA, Morse CW, Freschet GT (2013) Contrasting effects of plant inter- and intraspecific variation on community-level trait measures along an environmental gradient. Functional Ecology 27:1254-1261

Kraft NJ, Metz MR, Condit RS, Chave J (2010) The relationship between wood density and mortality in a global tropical forest data set. New Phytologist 188:1124-1136

Kraft NJ, Valencia R, Ackerly DD (2008) Functional traits and niche-based tree community assembly in an Amazonian forest. Science 322:580-582

Kunstler G, Falster D, Coomes DA, Hui F, Kooyman RM, Laughlin DC, Poorter L, Vanderwel M, Vieilledent G, Wright SJ, Aiba M, Baraloto C, Caspersen J, Cornelissen JHC, Gourlet-Fleury S, Hanewinkel M, Herault B, Kattge J, Kurokawa H, Onoda Y, Peñuelas J, Poorter H, Uriarte M, Richardson S, Ruiz-Benito P, Sun IF, Ståhl G, Swenson NG, Thompson J, Westerlund B, Wirth C, Zavala MA, Zeng H, Zimmerman JK, Zimmermann NE, Westoby M. (2016) Plant functional traits have globally consistent effects on competition. Nature 529:204-207

Laliberté E (2017) Below-ground frontiers in trait-based plant ecology. New Phytologist 213:1597-1603

Laughlin DC (2014) The intrinsic dimensionality of plant traits and its relevance to community assembly. Journal of Ecology 102:186-193

Laughlin DC, Gremer JR, Adler PB, Mitchell RM, MooreMM (2020) The net effect of functional traits on fitness. Trends in Ecology & Evolution 35:1037-1047

Laughlin DC, Messier J (2015) Fitness of multidimensional phenotypes in dynamic adaptive landscapes. Trends in Ecology & Evolution 30:487-496

Lavorel S, Garnier É (2002) Predicting changes in community composition and ecosystem functioning from plant traits: revisiting the Holy Grail. Functional Ecology16:545-556

Lepš J (1999) Nutrient status, disturbance and competition: an experimental test of relationships in a wet meadow. Journal of Vegetation Science 10:219-230

Lepš J, de Bello F, Šmilauer P, Doležal J (2011) Community trait response to environment: disentangling species turnover vs intraspecific trait variability effects. Ecography 34:856-863

Letcher SG, Lasky JR, Chazdon RL, Norden N, Wright SJ, Meave JA, Pérez-García EA, Muñoz R, Romero-Pérez E, Andrade AJJE (2015) Environmental gradients and the evolution of successional habitat specialization: a test case with 14 Neotropical forest sites. Journal of Ecology 103:1276-1290

Lohbeck M, Poorter L, Lebrija-Trejos E, Martínez-Ramos M, Meave JA, Paz H, Pérez-García EA, Romero-Pérez IE, Tauro A, Bongers F (2013) Successional changes in functional composition contrast for dry and wet tropical forest. Ecology 94:1211-1216

Lohbeck M, Poorter L, Paz H, Pla L, van Breugel M, Martínez-Ramos M, Bongers F. (2012) Functional diversity changes during tropical forest succession. Perspectives in Plant Ecology, Evolution and Systematics 14:89-96

McCormack ML, Dickie IA, Eissenstat DM, Fahey TJ, Fernandez CW, Guo D, Helmisaari HS, Hobbie EA, Iversen CM, Jackson RB (2015) Redefining fine roots improves understanding of below-ground contributions to terrestrial biosphere processes. New Phytologist 207:505-518

McCormack ML, Guo D, Iversen CM, Chen W, Eissenstat DM, Fernandez CW, Li L, Ma C, Ma, Z, Poorter H (2017) Building a better foundation: improving root-trait measurements to understand and model plant and ecosystem processes. New Phytologist 215:27-37

Muscarella R, Uriarte M (2016) Do community-weighted mean functional traits reflect optimal strategies? Proceedings of the Royal Society B: Biological Sciences 283:20152434

Muscarella R, Uriarte M, Aide TM, Erickson DL, Forero-Montaña J, Kress WJ, Swenson NG, Zimmerman JK (2016a) Functional convergence and phylogenetic divergence during secondary succession of subtropical wet forests in Puerto Rico. Journal of Vegetation Science 27:283-294

Muscarella R, Uriarte M, Erickson DL, Swenson NG, Kress WJ, Zimmerman JK (2016b) Variation of tropical forest assembly processes across regional environmental gradients. Perspectives in Plant Ecology, Evolution and Systematics 23:52-62

Odum EP (1969) Strategy of ecosystem development. Science 164:262-270

Paine CET, Baraloto C, Chave J, Hérault B (2011) Functional traits of individual trees reveal ecological constraints on community assembly in tropical rain forests. Oikos 120:720-727

Penone C, Davidson AD, Shoemaker KT, Di Marco M, Rondinini C, Brooks TM, Young BE, Graham CH, Costa GC (2014) Imputation of missing data in life-history trait datasets: which approach performs the best? Methods in Ecology and Evolution 5:961-970

Pillar VD, Blanco CC, Müller SC, Sosinski EE, Joner F, Duarte, LD (2013) Functional redundancy and stability in plant communities. Journal of Vegetation Science 24:963-974

Poorter L, Castilho C, Schietti J, Oliveira R, Costa F (2018a) Can traits predict individual growth performance? A test in a hyperdiverse tropical forest. New Phytologist 219:109-121

Poorter L, Rozendaal DMA, Bongers F, de Almeida-Cortez JS, Almeyda Zambrano AM, Álvarez FS, Andrade JL, Villa LFA, Balvanera P, Becknell JM, Bentos TV, Bhaskar R, Boukili V, Brancalion PHS, Broadbent EN, César RG, Chave J, Chazdon RL, Colletta GD, Craven D, de Jong BHJ, Denslow JS, Dent DH, DeWalt SJ, García ED, Dupuy JM, Durán SM, Espírito Santo MM, Fandiño MC, Fernandez GW, Finegan B, Moser VG, Hall JS, Hernández-Stefanoni JL, Jakovac CC, Junqueira AB, Kennard D, Lebrija-Trejos E, Letcher SG, Lohbeck M, Lopez OR, Marín-Spiotta E, Martínez-Ramos M, Martins SV, Massoca PES, Meave JA, Mesquita R, Mora F, de Souza Moreno V, Müller SC, Muñoz R, Muscarella R, de Oliveira Neto SN, Nunes YRF, Ochoa-Gaona S, Paz H, Peña-Claros M, Piotto D, Ruíz J, Sanaphre-Villanueva L, Sanchez-Azofeifa A, Schwartz NB, Steininger MK, Thomas WW, Toledo M, Uriarte M, Utrera LP, van Breugel M, van der Sande MT, van der Wal H, Veloso MDM, Vester HFM, Vieira ICG, Villa PM, Williamson GB, Wright SJ, Zanini KJ, Zimmerman JK, Westoby M (2019) Wet and dry tropical forests show opposite successional pathways in wood density but converge over time. Nature Ecology & Evolution 3:928-934

Poorter L, van der Sande M, Arets E, Ascarrunz N, Enquist B, Finegan B, Licona J, Martinez-Ramos M, Mazzei L, Meave J, Muñoz R, Nytch C, Oliveira A, Pérez-García E, Prado Júnior J, Rodríguez-Velazques J, Ruschel A, Negret B, Schiavini I, Peña-Claros M (2018b) Biodiversity and climate determine the functioning of Neotropical forests. Global Ecology and Biogeography 27:389-390

Poorter L, van der Sande MT, Arets EJ, Ascarrunz N, Enquist BJ, Finegan B, Licona JC, Martínez-Ramos M, Mazzei L, Meave JA (2017) Biodiversity and climate determine the functioning of Neotropical forests. Global Ecology & Biogeography 26:1423-1434

Powell TL, Koven CD, Johnson DJ, Faybishenko B, Fisher RA, Knox RG, McDowell NG, Condit R, Hubbell SP, Wright SJ, Chambers JQ, Kueppers LM (2018) Variation in hydroclimate sustains tropical forest biomass and promotes functional diversity. New Phytologist 219:932-946

R Core Team (2018) R: a language and environment for statistical computing. R Foundation for Statistical Computing, Vienna, Austria. https://www.R-project.org

Reich PB (2014) The world-wide 'fast–slow' plant economics spectrum: a traits manifesto. Journal of Ecology 102:275-301

Réjou-Méchain M, Tanguy A, Piponiot C, Chave J, Hérault B. (2017) biomass: an R package for estimating above-ground biomass and its uncertainty in tropical forests. Methods in Ecology and Evolution 8:1163-1167

Rosenfield MF, Müller SC (2020) Plant traits rather than species richness explain ecological processes in subtropical forests. Ecosystems 23:52-66

Schindler DE, Armstrong JB, Reed TE (2015) The portfolio concept in ecology and evolution. Frontiers in Ecology and the Environment 13:257-263

Schrodt F, Kattge J, Shan H, Fazayeli F, Joswig J, Banerjee A, Reichstein M, Bönisch G, Díaz S, Dickie J (2015) BHPMF–a hierarchical Bayesian approach to gap-filling and trait prediction for macroecology and functional biogeography. Global Ecology and Biogeography 24:1510-1521

Shipley B, De Bello F, Cornelissen JHC, Laliberté E, Laughlin DC, Reich PB (2016) Reinforcing loose foundation stones in trait-based plant ecology. Oecologia 180:923-931

Siefert, A, Violle, C, Chalmandrier, L, Albert, C. H, Taudiere, A, Fajardo, A, Aarssen, L. W, Baraloto, C, Carlucci, M. B. & Cianciaruso, M. V. (2015) A global meta-analysis of the relative extent of intraspecific trait variation in plant communities. Ecology Letters 18: 1406-1419

Slik JWF, Franklin J, Arroyo-Rodríguez V, Field R, Aguilar S, Aguirre N, Ahumada J, Aiba SI, Alves LF, A K, Avella A, Mora F, Aymard CGA, Báez S, Balvanera P, Bastian ML, Bastin JF, Bellingham PJ, van den Berg E, da Conceição Bispo P, Boeckx P, Boehning-Gaese K, Bongers F, Boyle B, Brambach F, Brearley FQ, Brown S, Chai SL, Chazdon RL, Chen S, Chhang P, Chuyong G, Ewango C, Coronado IM, Cristóbal-Azkarate J, Culmsee H, Damas K, Dattaraja HS, Davidar P, DeWalt SJ, Din H, Drake DR, Duque A, Durigan G, Eichhorn K, Eler ES, Enoki T, Ensslin A, Fandohan AB, Farwig N, Feeley KJ, Fischer M, Forshed O, Garcia QS, Garkoti SC, Gillespie TW, Gillet JF, Gonmadje C, Granzow-de la Cerda I, Griffith DM, Grogan J, Hakeem KR, Harris DJ, Harrison RD, Hector A, Hemp A, Homeier J, Hussain MS, Ibarra-Manríquez G, Hanum IF, Imai N, Jansen PA, Joly CA, Joseph S, Kartawinata K, Kearsley E, Kelly DL, Kessler M, Killeen, TJ, Kooyman RM, Laumonier Y, Laurance SG, Laurance WF, Lawes MJ, Letcher SG, Lindsell J, Lovett J, Lozada J, Lu X, Lykke AM, Mahmud KB,

Mahayani NPD, Mansor A, Marshall AR, Martin EH, Calderado Leal Matos D, Meave JA, Melo FPL, Mendoza ZHA, Metali F, et al. (2018) Phylogenetic classification of the world's tropical forests. Proceedings of the National Academy of Sciences 115:1837-1842

Soliveres S, Maestre FT, Bowker MA, Torices R, Quero JL, García-Gómez M, Cabrera O, Cea AP, Coaguila D, Eldridge DJ (2014) Functional traits determine plant co-occurrence more than environment or evolutionary relatedness in global drylands. Perspectives in Plant Ecology, Evolution and Systematics 16:164-173

Spasojevic MJ, Suding KN (2012) Inferring community assembly mechanisms from functional diversity patterns: the importance of multiple assembly processes. Journal of Ecology 100:652-661

Spasojevic MJ, Turner BL, Myers JA (2016) When does intraspecific trait variation contribute to functional beta-diversity? Journal of Ecology 104:487-496

Swenson NG (2014) Phylogenetic imputation of plant functional trait databases. Ecography 37: 105-110

Swenson NG, Enquist BJ (2007) Ecological and evolutionary determinants of a key plant functional trait: wood density and its community-wide variation across latitude and elevation. American Journal of Botany 94:451-459

Swenson NG, Stegen JC, Davies SJ, Erickson DL, Forero-Montaña J, Hurlbert AH, Kress WJ, Thompson J, Uriarte M, Wright SJ (2012) Temporal turnover in the composition of tropical tree communities: functional determinism and phylogenetic stochasticity. Ecology 9:490-499

Turcotte MM, Levine JM (2016) Phenotypic Plasticity and Species Coexistence. Trends in Ecology & Evolution 31:803-813

Umaña MN, Mi X, Cao M, Enquist BJ, Hao Z, Howe R, Iida Y, Johnson D, Lin L, Liu X, Ma K, Sun IF, Thompson J, Uriarte M, Wang X, Wolf A, Yang J, Zimmerman JK, Swenson NG (2017) The role of functional uniqueness and spatial aggregation in explaining rarity in trees. Global Ecology and Biogeography 26:777-786

van Buuren S, Groothuis-Oudshoorn K (2010) MICE: Multivariate imputation by chained equations in R. Journal of Statistical Software 45:1-68

van der Sande M, Arets E, Peña-Claros M, Hoosbeek M, Cáceres-Siani Y, Van der Hout P, Poorter L (2018) Soil fertility and species traits, but not diversity, drive productivity and biomass stocks in a Guyanese tropical rainforest. Functional Ecology 32:461-474

Violle C, Enquist BJ, McGill BJ, Jiang L, Albert CH, Hulshof C, Jung V, Messier J (2012) The return of the variance: intraspecific variability in community ecology. Trends in Ecology & Evolution 27:244-252

Warren JM, Hanson PJ, Iversen CM, Kumar J, Walker AP, Wullschleger SD (2015) Root structural and functional dynamics in terrestrial biosphere models–evaluation and recommendations. New Phytologist 205:59-78

Webb CO, Donoghue MJ (2005) Phylomatic: tree assembly for applied phylogenetics. Molecular Ecology Notes 5:181-183

Wenhua L. (2004) Degradation and restoration of forest ecosystems in China. Forest Ecology and Management 201:33-41

Westoby M, Wright IJ (2006) Land-plant ecology on the basis of functional traits. Trends in Ecology & Evolution 21:261-268

Wright SJ, Kitajima K, Kraft NJ, Reich PB, Wright IJ, Bunker DE, Condit R, Dalling JW, Davies SJ, Díaz S. (2010) Functional traits and the growth–mortality trade-off in tropical trees. Ecology 91:3664-3674

Wu Z (1995) An Introduction to the Tropical Forest Soils and Effect oif Shifting Cultiviation on Soils in Jianfengling. In: Zeng Q, Zhou G, Yide L, Wu Z, Chen B (eds) Researches on Tropical Forest Ecosystems in Jianfengling of China. China Forestry Publishing House, Beijing, China, pp 5-25

Xu H, Detto M, Fang S, Li Y, Zang R, Liu S (2015a) Habitat hotspots of common and rare tropical species along climatic and edaphic gradients. Journal of Ecology 103:1325-1333.

Xu H, Li Y, Liu S, Zang R, He F, Spence JR (2015b) Partial recovery of a tropical rain forest a half-century after clear-cut and selective logging. Journal of Applied Ecology 52:1044-1052

Xu X, Trugman A (2021) Trait-Based Modeling of Terrestrial Ecosystems: Advances and Challenges Under Global Change. Current Climate Change Reports doi:10.1077/s406541-020-00168-6

Yang J, Cao M, Swenson NG (2018) Why functional traits do not predict tree demographic rates. Trends in Ecology & Evolution 33:326-336

Zanne AE, Lopez-Gonzalez G, Coomes DA, Ilic J, Jansen S, Lewis SL, Miller RB, Swenson NG, Wiemann MC, Chave J (2009) Data from: Towards a worldwide

wood economics spectrum. Dryad Digital Repository. https://doi.org/10.5061/dryad.234

Zeng Q (1995) Survey of Water-Heat Condition and Vegetation Ecological Series in Jianfengling. In: Zeng Q, Zhou G, Yide L, Wu Z, Chen B (eds) Researches on Tropical Forest Ecosystems in Jianfengling of China. China Forestry Publishing House, Beijing, China, pp 5-25

Zhou G (1995) Ecological Effects of Human Activities in Jianfenglin Forest Region, Hainan Island. In: Zeng Q, Zhou G, Yide L, Wu Z, Chen B (eds) Researches on Tropical Forest Ecosystems in Jianfengling of China. China Forestry Publishing House, Beijing, China, pp 38-48

Zuo X, Yue X, Lv P, Yu Q, Chen M, Zhang J, Luo Y, Wang S, Zhang, J (2017) Contrasting effects of plant inter- and intraspecific variation on community trait responses to restoration of a sandy grassland ecosystem. Ecology and Evolution **7**:1125-1134

CHAPTER 3: Evidence of elemental homeostasis in fine root and leaf tissues of saplings across a fertility gradient in tropical montane forest in Hainan, China

This chapter has been published in *Plant & Soil*:

Hogan JA, Valverde-Barrantes OJ, Tang W, Ding Q, Xu H & Baraloto C. Evidence of elemental homeostasis in fine root and leaf tissues across a fertility gradient in tropical montane forest in Hainan, China. *Plant & Soil* 460:625-646. doi: 10.1007/s11104-020-04802-y. It is reproduced, here, with permission from Springer Nature.

Key message

Generally, elemental concentrations in leaf and root tissues vary less than concentration of key soil elements reflecting soil fertility (i.e., nitrogen, phosphorus, or base saturation). When elemental concentrations were high in leaf tissues, they were lower in root tissues and vice versa, leading us to conclude that elemental homeostasis is a key process governing tropical tree nutrient status.

Abstract

For plants, elemental nutrients are important belowground resources that sustain growth and survival. To understand how tropical plant nutrient status responds to environmental variation, we asked whether concentrations of nutrients in root and leaf tissues track gradients in soil nutrient concentrations and if tissue nutrient concentrations respond independently or in concert to soil nutrient concentrations. We measured soil nutrient concentrations of rhizosphere soil and root and leaf tissue elemental concentrations of saplings of 14 Angiosperm families in montane tropical forest of Jianfengling, China. Using mixed-effects models, we modeled the nutrient concentration of plant tissues as a function of soil resources. Of fourteen elements measured, seven — nitrogen, boron, phosphorus, potassium, manganese, copper, and zinc— increased in concentrations in root and leaf tissues with higher soil nutrient availability; two decreased —aluminum and carbon; three were invariant —magnesium, sulfur, and calcium; and two —sodium and iron— showed contrasting patterns between leaves and roots. Eight elements necessary to leaf physiological function, but also used in root functioning —

nitrogen, boron, magnesium phosphorus, sulfur, potassium, calcium, manganese— were more concentrated in leaves than roots. Additionally, most elements showed tradeoffs in concentrations between roots and leaves. Plant lineage (i.e., family) explained very little of the variation about this overall trend. Overall, increases in tissue nutrient concentrations with soil fertility were subtle if present at all. Thus, we conclude that tissue nutrients of juvenile tropical trees have a high degree of elemental homeostasis with local-scale soil nutrient content in Jianfengling.
Keywords: plant nutrient analysis, leaf chemistry, root chemistry, stoichiometry, tropical forest, Jianfengling

Introduction

The study of the mineral nutrition of plants has long been a hallmark of the agricultural sciences (Aulie 1974; Chapin 1980; Marschner 2012); however, understanding how wild plants use and store nutrients is becoming increasingly important as humans continue to alter biogeochemical cycles (Cleland and Harpole 2010; Elser et al. 2007; Hobbie 2015). Plant growth and proper cellular functioning are directly dependent on nutrient uptake from the soil, and nutrient deficiencies can lead to poor plant health and reduced performance (Aerts and Chapin 1999; Chapin 1980; Marschner 2012), which can affect ecosystem processes. Plants respond to changes in soil nutrient fertility, and they regulate their response based upon the flow of energy, water, and nutrients within the plant (Pons et al. 1998). Therefore, from an ecological perspective, quantifying the nutrient status of plant organs can inform about whole plant nutrition and physiology (Chapin 1980; Kramer and Kozlowski 1979; Pons et al. 1998).

Organismal stoichiometry, or the study of the elemental composition of organisms (Elser et al. 2000a, b), examines how the chemical make-up of organisms reflects the function of their biological parts within the environment. Stoichiometric theory contends that organisms generally have fixed nutritional requirements that result in a consistent stoichiometry (i.e. elemental composition). Although the stoichiometry of plant tissues is more flexible and tends to reflect their abiotic environment to a greater degree than in animals (Elser et al. 2000b), some stoichiometric balance between the elemental

concentration and composition in plant tissues and their growth environment is expected, in order to maintain optimal physiological functioning; this balance is termed elemental homeostasis (Sterner and Elser 2009; Sterner and Elser 2002), and the degree to which it operates in wild plants, and varies with environment or plant lineage is not entirely known. As such, elemental homeostasis remains the testable null hypothesis for applied stoichiometric studies (Sterner and Elser 2009, Figure 1).

Fourteen to twenty elements are essential for plant growth (depending on the species of plant and definition used for essentiality) (Table 1). From a plant nutrition perspective, these elements are best understood when divided into four groups based on chemical behavior and function (Mengel and Kirkby 2001; Marschner 2012). Group 1 elements (*carbon*, hydrogen, oxygen, *nitrogen*, and *sulfur*)[1] are taken up as ions from the soil solution or as gases from the atmosphere. They are the principal constituent elements of organic matter assimilated via oxidation-reduction reactions in plant cells. Group 2 elements (*phosphorus*, *boron*, and silicon)[1] are obtained as inorganic anions or acids from the soil solution and are found in similar forms within plant cells (e.g., phosphate). Group 3 elements (*potassium, sodium, calcium, magnesium, manganese.* and chlorine)[1] are taken up from the soil in ionic form and occur in cells as cationic compounds or chelates. Lastly, group 4 elements (*iron, copper, zinc,* and *molybdenum*) are obtained as ions or chelates from the soil solution and are used in the cell as ions that engage in various cellular functions including electron transport. The purpose of nutrients in groups 3 and 4 depends on their oxidation state to create osmotic potentials and ionic gradients, influencing structural changes to enzymes, and mediating cellular redox reactions (Marshner 2012).

Nitrogen (N) is arguably the most studied element in terms of plant function and growth (Enríquez et al. 1993, Güsewell 2004, Elser et al. 2000b, see references in Table 1). Leaf tissues are richer in nitrogen than stems and roots (Pregitzer et al. 1997) because of the many specialized proteins and enzymes required for photosynthesis (Pons et al. 1998; Reich and Oleksyn 2004). Moreover, leaf nitrogen generally is higher in species with fast life-history strategies and high rates of photosynthesis and carboxylation,

[1] Italicized elements are the ones measured in this study.

because they have more of proteins (e.g., thylakoid proteins) and enzymes (e.g., Rubisco) that are nitrogen-rich than species with slower life-history strategies (Field and Mooney 1986; Lambers and Poorter 1992; Reich et al. 1992; Wright et al. 2004).

Variation in root nitrogen concentration appears to be more related to construction costs in roots than acquisition performance (Maire et al. 2009; McCormack and Iversen 2019; Bergmann et al. 2020); but, concentrations tend to reflect inorganic N-availability in the soil and variation in life history and root functional strategies. For example, root nitrogen concentrations are related to rates of root respiration (Makita et al. 2009; Paradiso et al. 2020). Moreover, root tissue N concentration and rates of N-uptake decrease with increasing root length, area, and biomass (Hilbert 1990; Raper Jr et al. 1978; Taub and Wang 2008). Thus, as soil nitrogen becomes more available, generally, whole-plant nitrogen increases, whole-plant and photosynthetic nitrogen-use efficiency decreases, and plants allocate more resources to root production (i.e., root to shoot ratios increase) (Hilbert 1990). Yet, nitrogen pools within the plant (i.e., leaf and root nitrogen) interplay with one another and their respective carbohydrate pools, and therefore root nitrogen, may not precisely track soil nitrogen availability (Chapin et al. 2011; Raper Jr et al. 1978).

Because nitrogen and phosphorus (P) are often limiting macronutrients, examining their ratio and their ratios to carbon (C) can be informative (Elser et al. 2000a; Sterner and Elser 2009). For balanced plant growth in most terrestrial systems, plants absorb ten times as much (mass-based) nitrogen as phosphorus (Aerts and Chapin 1999; Pons et al. 1998). Therefore, the N:P ratios in leaves are a good indicator of which nutrient is limited. In general, mass-based N:P ratios < 14 (molar N:P ratios < 35.4) signify nitrogen limitation, whereas mass-based N:P ratios >16 (molar ratios > 40.0) correspond to phosphorus limitation with colimitation occurring at mass-based ratios between 14 and 16 (molar ratios between 35.4 and 40.0) (Aerts and Chapin 1999; Güsewell 2004). N:P mass-based ratios for terrestrial plants average 12-13 (molar ratios of 26.5-28.7), owing to the ubiquity of nitrogen limitation in plants globally (Güsewell 2004). Interestingly, average foliar phosphorus is greater in temperate than in tropical

trees (averaging 1.4 vs. 0.75 mg g^{-1} using data from 2962 tree leaves in the TRY database Kattge et al. 2020, David Ellsworth, personal communication).

Several other micronutrients, like calcium, magnesium, sulfur and other trace metals are needed in small quantities by plants, but rarely limit their physiological functioning (Aerts and Chapin 1999; Hawkesford et al. 2012) (Table 1). For example, iron is needed for plant growth and photosynthesis, due to its role in facilitating electron transport in light-reactions of leaves (Kramer and Kozlowski 1979). The oxidation state of iron in the soil interacts with decomposing organic matter and soil nutrients to influence soil nutrient availability for uptake through plant roots (Hall and Silver 2013; Silver et al. 2013). The absorption and concentration of the many other trace metals (aluminum, magnesium, manganese, zinc, copper, and molybdenum) in plant tissues behave similarly and interact with one another and the electrochemical conductivity and chemical composition of the soil (Andresen et al. 2018; Kramer and Kozlowski 1979; Marschner 2012; Mengel and Kirkby 2001; Broadley et al. 2012a; Broadley et al. 2012b) (see Table 1). However, an excess of micronutrients can become toxic, and plants use a variety of mechanisms to avoid toxicity, such as exclusion, restriction of transport from the root, re-translocation from the plant to roots or leaves prior to organ senescence, root exudation, excretion from the leaves, or compartmentalization (Marshner 2012).

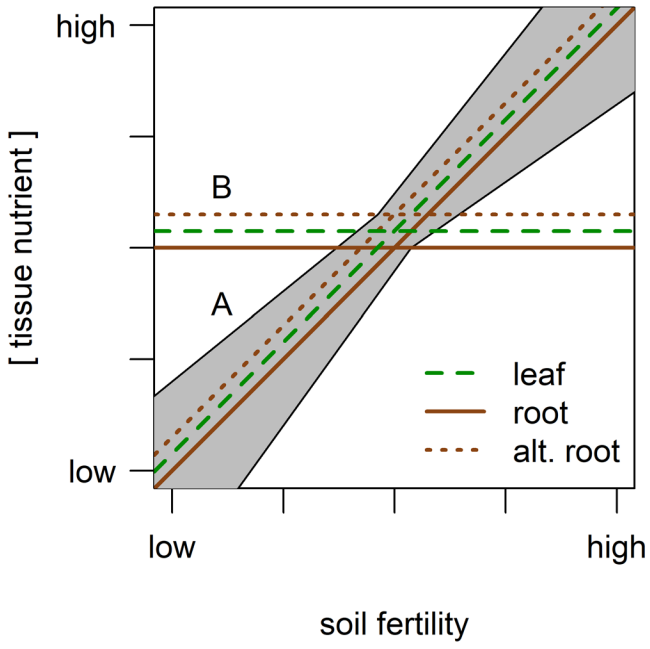

Fig. 1: Competing hypotheses regarding relationships of tissue nutrient concentrations (y-axis) to soil fertility (x-axis). Note that x and y-axes should be logarithmic when analyzing actual data (Sterner and Elser 2002). Hypothesis A: soil nutrients track soil fertility in a linear fashion; for example, leaf and root tissue N concentration increase in direct proportion to soil available N. This is the null hypothesis of ecological stoichiometric theory (i.e., the "you are what you eat" hypothesis) (Sterner and Elser 2002), where plant tissue chemistry changes in lockstep with its chemical availability in the soil resource. Hypothesis B: plants maintain homeostasis in tissue nutrient concentrations, independently of resource availability in the soil (i.e., no change in tissue nutrient concentration). Within that hypothetical framework, root tissue nutrient concentrations may either be less than (solid brown line) or greater than (dotted brown line) the tissue nutrient concentrations of leaves (dashed green line). The gray shaded areas show that the slope of the relationship in hypothesis A may vary, i.e., relationships of leaf and root tissue nutrient concentrations may create intersecting lines.

Much of the knowledge about how tropical tree tissue elemental concentrations vary with the environment has focused on variation in foliar chemistry, with the majority of studies focusing solely on carbon, nitrogen, and phosphorus (Reich and Oleksyn 2004, Wright et al. 2004, Niklas 2006, but see Asner and Martin 2015). Additional macronutrients, such as potassium, magnesium, and calcium, have essential biological roles within plants (Table 1), and their concentrations in plant tissues interact with their availability in the soil environment to influence plant growth and forest development (Bond 2010, Hawkesford et al. 2012). Several studies have found that the elemental composition of wood follows soil fertility in tropical forests (e.g., Heineman et al 2016, Lira-Martens et al 2019); yet the extent to which root and leaf elemental concentrations vary with soil fertility, and whether they coordinate in their response, has received less attention. Here, we employ an organismal stoichiometric perspective to compare the concentration of fourteen elemental nutrients in root and leaf tissues of a diverse sample of Angiosperms across a local gradient in soil fertility. In particular, we ask the following questions:

1. Do concentrations of elements in plant root and leaf tissues increase with increasing soil fertility? *If elemental homeostasis is strong in tropical forest saplings, then tissue nutrient concentrations of both roots and leaves should be invariant to differences in soil nutrient concentrations. However, if the strength of elemental homeostasis varies over a broad range of soil conditions, more fertile*

soils may lead to higher concentrations of tissue nutrient concentrations (Fig. 1). Moreover, since roots are the entry point for nutrients, we hypothesize that they may track soil environmental variation more closely than leaves.

2. How do concentrations of nutrients in roots relate to those in leaves? *Plant strategies may result in a relatively consistent tissue stoichiometry (i.e., homeostasis). However, due to differences in function, tissues may accumulate nutrients at different rates. For instance, nutrients associated with photosynthetic performance (nitrogen, magnesium, phosphorus) should have higher concentrations in leaf than in root tissues, whereas elements with potential toxicity and only secondary physiological function in leaves (zinc, copper, boron) may accumulate at higher concentrations in roots. Based on their elemental function in leaves and root tissues, hypotheses for each element are given in Table 1.*

3. Do plant lineages vary in their leaf and root tissue chemistry-soil environment relationships? *Because of the variation in Angiosperm plant form, especially regarding roots (Valverde-Barrantes et al. 2017), the degree of whole-plant elemental homeostasis may vary with plant lineage. Certain families, like the Fabaceae and Magnoliaceae, have been shown to have higher root N concentrations than others (Valverde-Barrantes et al. 2017; Bergmann et al. 2020). Families with higher concentrations of root N might have higher concentrations of other elements in roots. We did not formulate any specific expectation as to which families might have more homeostatic regulation than others, but instead employed a sampling design that sought to target taxa across a broad range in plant form and ecological life-history strategy (see Table 2) to test the hypothesis that plant identity has little effect on plant tissue elemental concentration- soil nutrient concentration relationships.*

Table 1: Elemental information, known functions within the plant, and hypothesized relationships with gradients of soil fertility for 15 essential plant nutrients, which were analyzed in root and leaf tissue of juvenile trees from Jianfengling, Hainan Island, China. For typical concentrations of elements in plant tissues see Table 3.1 in Fitter and Hay (2012). Much of the general information in this table was drawn from (Kramer and Kozlowski 1979; Marschner 2012; Mengel and Kirkby 2001). Literature-based hypothetical relationships for plant tissue concentrations of each element with an increase in soil fertility are represented with arrows to denote increasing tissue concentrations (↑), decreasing tissue concentrations (↓), or no change (↔). Note that in this table we include Molybdenum, however concentrations were undetectable for the majority of tissue samples that we measured, so it was excluded from our analyses.

Element		Atomic Number	Usual Oxidation State(s)	Iso-topes	common environmental forms	Associated physiological function in leaf tissue	Associated physiological function in root tissue	Associated whole-plant physiological function	Relationship to soil fertility or pH and explanation	Sources
C	carbon	6	-4, -3, -2, -1, +1, +2, +3, +4	^{12}C, ^{13}C	carbonates	Carbohydrates, simple sugars, lignin, and hemicellulose compounds for plant structure (e.g., cell walls), herbivory defense.	Translocation to other plants, mycorrhizae, root nodules, root cell membrane health.	Growth and tissue production, resistance to drought.	↓/↔ Plant tissue carbon is thought to be largely invariant to soil fertility but may decrease in less fertile soils if allocation to roots is increased, or more liable carbon is being exchanged to the rhizosphere for nutrients.	(Dietze et al. 2014; Kozlowski 1992; Ma et al. 2018; Silver and Miya 2001)
N	nitrogen	7	-3, +3, +5	^{14}N, ^{15}N	nitrates, nitrites, ammonium	maximum photosynthetic	Nitrogen uptake by	building block of amino acids	↑	(Evans 1989; Field and

						rate, maximum rate of carboxylation, RuBP content, Rubisco content.	roots, root protein, and enzyme content.	and (soluble) proteins, a major component of DNA.	Whole plant and leaf N increase with soil N. Root N concentrations should reflect soil availability, and root enzyme production and N cycling rates.	Mooney 1986; Fitter and Hay 2012; Jackson et al. 1997; Lambers and Poorter 1992; Silver and Miya 2001; Valverde-Barrantes et al. 2007; Wright et al. 2004)
B	boron	5	+3	^{10}B, ^{11}B	borax, boric acid, kernite, ulexite, colemanites, borates	Helps build sugars following photosynthesis, interacts with K to regulate stomatal guard cell function, involved with nitrogen and metabolism and protein formation.	Adventitious rooting (potentially counteracting the adverse effect of phenolics), and root development.	Unclear, but potentially: sugar transport, cell division, cell wall construction, lignification, carbohydrate, RNA and phenol metabolism, membrane function, and respiration.	↔ Boron deficiency may result when concentrations are low in the soil (i.e., <20 ppm). Boron weakly adsorbs to the soil, but can undergo passive uptake, once in soluble form. It likely never limits plant growth alone. Tissue concentrations should be consistent	(see table 2 in Hull 2002; Kutschera and Niklas 2017; Lewis 2019; Middleton et al. 1978)

									across soil gradients.	
Na	sodium	11	+1	^{23}Na	sodium chloride, sodium carbonate, sodium borate, sodium nitrate, sodium sulfate	Enhances nitrate assimilation, regulation of leaf area and stomatal density, related to leaf chlorophyll content.	Enhances nitrate uptake by roots and nitrate assimilation in leaves. Interacts with K in root ATPase regulation.	Growth stimulation (depending on species sensitivity); can cause physiological stress at high concentrations, phloem mobility, cell expansion, plant water balance, proper tonoplast, and vacuole function.	↑ In the absence of salt stress, sodium concentrations in plant tissues should be low in low fertility soils but may increase as soil fertility increases given sodium's ability to enhance nutrient uptake.	(Garg et al. 1993; Hampe and Marschner 1982; Subbarao et al. 2003)
Mg	magnesium	12	+2	^{24}Mg, ^{25}Mg, ^{26}Mg	magnesium sulfate,	Photosynthetic rates, chloroplast & photosystem function, leaf enzyme regulation, leaf longevity.	Important for cell division and root growth interacts with other nutrients to regulate nutrient transport across membranes, associated with root apoplast function, involved in	Starch synthesis, and maintenance of starch sinks, important for the aggregation of ribosomal subunits and protein synthesis.	↑ Magnesium deficiency in tissues may increase with decreasing soil fertility and increasing soil acidity, due to the presence of competing divalent cations in acidic,	(Mayland 1990; Shaul 2002)

							phosphatase production (e.g., alpha phosphatase).		nutrient-depleted soils (Al, Ca, Na).	
Al	aluminum	13	+3	^{27}Al	aluminum hydroxide, aluminum oxide, aluminum silicates	Limited functionality, but a higher concentration, Al reduces chlorophyll function and photosynthetic electron flow, membrane, and protein through negative effects on the Golgi apparatus.	Interacts primarily with the root cap, at high concentration can reduce root elongation, can aid in reducing the toxicity of other metals (Fe, Mn), can reduce fungal parasitism of roots.	Toxic at high concentrations. In Al toxicity, Al interferes with the uptake and transport of essential cations (Cu, Zn, Ca, Mg, Mn, K, P, and Fe), reduces photosynthesis, respiration, and protein synthesis.	↓ Concentrations of Al in plant tissues should be low but have the potential to increase with decreasing soil fertility and increasing soil acidity.	(Delhaize and Ryan 1995; Kahle 1993; Roy et al. 1988)
P	phosphorus	15	-3, +3, +5	^{31}P	phosphates, organophosphates, phospho mono- and di-esters.	Constrains A_{max}-leaf N relationships, acts as the principal element in ATP, involved in enzyme reactions, used in healthy ribosome function and DNA and RNA transcription/ translation.	Involved in regulation of root architecture (P deficiency leads to root elongation and branching (i.e., increasing acquisitiveness), associated with mycorrhizal colonization of roots and regulation of	Cellular health (phospholipid bilayer), seed production (phosphorylated alcohol), nucleic acids, enzymatic activity, regulation of plant metabolism, cytoplasmic function, involved in root-shoot ratio	↑ Soil P often limits plant growth, so it should increase in plant tissues with availability in the soil. However, species differ drastically in their affinities for P, seeking to maintain inorganic P	(Lambers et al. 2006; Reich et al. 2009a; Schachtman et al. 1998; Shen et al. 2011; Smith 2001; Turner 2008; Turner et al. 2018; White and Hammond 2008)

							rhizosphere microbiome, root enzyme activity (especially phosphatase).	regulation, hormonal signaling.	homeostasis in the cytoplasm. Mechanisms exist to increase or regulate P uptake from the soil, or store P in plant tissue.	
S	sulfur	16	-2, +2, +4, +6	^{32}S, ^{33}S, ^{34}S, ^{36}S	sulfides, sulfates.	Involved in cysteine synthesis in the chloroplast, associated with bundle sheath cell function in C4 plants.	Inorganic sulfate uptake in roots associated with cotransport of proteins (ATPase activity).	Amino acid function (specifically, cysteine and methionine), protein cofactor function and protein synthesis, cystol function, photosynthesis, respiration.	↔ Globally, sulfur deficiency in soils is widespread. Plants can only utilize inorganic sulfur from the soil, which is always in low supply. Therefore, no relationships between tissue concentrations and soil gradients are known.	(Anderson 1990; Balk and Pilon 2011; Lewandowska and Sirko 2008)
K	potassium	19	+1	^{39}K, ^{41}K	potassium chloride,	Ion transport in chloroplasts and mitochondria,	Key to establishing root membrane	Xylem function, enzyme activation,	↑ Potassium uptake in roots in	(Cakmak 2005; Maathuis and

						Glucose synthesis, ATP synthesis, photosynthesis, stomatal behavior via regulation of turgor pressure in guard cells.	potentials for active ion transport into the tonoplast, cation-anion balance, response to physiological stress (e.g., drought, severe nutrient limitation).	protein synthesis (ribosomal function), osmotic function (cystol / vacuole stoichiometry), counter ion for nitrate transport in xylem, key to nucleic acid construction.	biphasic, meaning both passive and active uptake are possible and depend on the difference in concentration of potassium in the rhizosphere and root tissue. Tissue concentrations should, therefore, reflect soil availability, increasing with soil fertility.	Sanders 1996; Mengel 2016)
Ca	calcium	20	+2	^{40}Ca, ^{42}Ca, ^{43}Ca, ^{44}Ca, ^{46}Ca	calcium oxides, calcium silicates, calcium carbonate, calcium chloride, calcium phosphate	Stabilizes cell membranes through interactions with phospholipid head, cell wall formation, cystol signaling, enzymatic activation.	Root signaling in ionic uptake processes, regulation of root ion carries and channels, root elongation.	Regulation of intercellular water flow, transpiration, endoplasmic reticulum function.	↑ Calcium uptake and concentration in plant tissues is highly dependent on soil pH and should decrease with decreasing soil pH and fertility. Calcium	(Epstein 1961; Gilliham et al. 2011; Kahle 1993; Marschner 1991; Marschner 2012; White and Broadley 2003)

									concentrations in the soil affect Na and K uptake.	
Mn	manganese	25	+2, +4, +7	^{55}Mn	pyrolusite, rhodochrosite	Involved in photosynthesis – the manganoproti en of photosystem II is involved in the water-splitting process of photosynthesis, involved in cell wall function and metal transport across cell membranes.	Linked to other divalent cation (Ca, Mg, Fe, Cu, Zn) uptake in roots (via transport proteins).	Functionally similar to magnesium, involved in enzyme synthesis and function, involved in most enzyme-activated cellular reactions, such as phosphorylation, decarboxylation, reduction, and hydrolysis reactions.	↔ Due to its exchangeability for other soil cations, relationships of Manganese are likely invariant to soil fertility. Manganese toxicity may develop with decreasing soil fertility and increasing soil acidity.	(Andresen et al. 2018; Burnell 1988; Edwards and Walker 1983; Marschner 1991; Mukhopadhyay and Sharma 1991)
Fe	iron	26	+2, +3, +6	^{54}Fe, ^{56}Fe, ^{57}Fe, ^{58}Fe	iron oxides, ferrosic hydroxide, siderite, iron chelates	Key to the energy transduction pathway in photosynthesis, a principle reducing agent in mitochondrial and chloroplast activities.	Essential to root phosphatase activity (e.g., purple acid phosphatases), interacts with ion transport of other divalent metals through ion channels.	Toxic at high concentrations, involved in nitrate reductase enzymatic activity, involved in increased tolerance of metals.	↔ In tropical forest soils, Iron is non-limiting; however, most of the iron in tropical soils (Ferric ionic forms, iron oxides. etc.) is inaccessible to plants and	(Andresen et al. 2018; Brown 1978; Jeong and Guerinot 2009; Kahle 1993; Vose 1982)

									must undergo reduction (to Ferrous ion) at the root surface, depending on soil pH. Along soil gradient of the same soil type, tissue concentrations of iron should be consistent.	
Cu	copper	29	+2	^{63}Cu, ^{65}Cu	ionic forms (CU^{2+}), cupric oxide, cuprous oxide, copper sulfate,	Chloroplast function (light reactions), involved in leaf photorespiration (via polyphenol oxidase), enzyme activation (cofactor behavior, interchangeable with Zn).	Associated with nitrogen fixation (i.e., *Rhizobium* root nodule).	Xylem function, associated with proper enzyme function (e.g., ascorbic acid), mitochondrial respiration.	↔ Tissue copper concentrations are suspected to be far higher than needed for physiological functioning; therefore, no relationship with soil fertility is expected.	(Andresen et al. 2018; Kahle 1993; Marston 1952; Yruela 2005)
Zn	zinc	30	+2	^{64}Zn, ^{66}Zn, ^{68}Zn, ^{68}Zn, ^{70}Zn	zinc oxide, zinc chloride, zinc phosphate, zinc sulfide.	Chloroplast and mitochondrial function, involved in thylakoid lumen and	Essential to phosphatase activity and other root enzymatic activity.	Xylem function, cytoplasm function, crucial to the active center of carbonic	↓ Zinc accumulation typically occurs to a higher degree in nutrient-	(Andresen et al. 2018; Broadley et al. 2007; Kahle 1993; Longnecker

						chloroplast stroma activity, associated with increased mesophyll conductance in woody plants.		anhydrase activity, which interconverts CO_2 and carbonate, regulates gene expression (e.g., Zinc finger proteins).	poor soils, accumulation is typically higher in roots than in leaves and should be decrease with soil fertility.	and Robson 1993)
Mo	molybdenum	42	+4, +6	^{92}Mo, ^{94}Mo, ^{95}Mo, ^{96}Mo, ^{97}Mo, ^{98}Mo	molybdenite, molybdenum oxide, wulfenite ($PbMoO_4$), powellite ($Ca(MO, W)O_4$)	Associated with peroxisome function, mitochondrial function, leaf enzyme activity (e.g., aldehyde and xanthine oxidases).	Associated with nitrogen fixation in root nodules (i.e., *Rhizobium* enzyme function – nitrogenase), interacts with iron and sulfur uptake in roots.	Involved with the reduction of nitrate through processes that provide activation energy, associated with the function of the azotase enzyme.	↔ Alkaline conditions favor Molybdenum liberation from soils, but plant uptake increase with soil acidity. Molybdenum accumulation is increased by phosphate and sulfate addition. Therefore, association with soil fertility unclear.	(Andresen et al. 2018; Bittner 2014; Kahle 1993; Marston 1952; Zimmer and Mendel 1999)

Materials and methods

Study site

The Jianfengling forest of Hainan Island, China (18°23' –18° 15'N & 108° 36' – 109° 05'E) is a montane tropical rain forest (600-1100 meters elevation) on lateric and humic yellow soils that are derived from porphyritic granite (Wu 1995). The soils have low fertility and are characterized by slow rates of mineral cycling when compared to other tropical soils, such as Latisols or Ultisols, intermediate levels of mineral leaching, and an exchange base content of about 30 mL kg^{-1} with some accumulation of aluminum. The soils support a vegetation community of broadleaf evergreen trees intermixed with palms and Podocarpaceae that reaches a canopy height of 18 meters. The average annual rainfall at Jianfengling from 1965-1995 was about 2700 mm, and is seasonal, with most of the rainfall occurring between May and October (Zeng 1995).

Tissue collection

Leaf and fine root tissues were collected from juvenile tropical trees with stem diameters of < 10 cm at 1.3m height (hereafter saplings) from May to July of 2017. Three hundred saplings of 50 tropical tree species (6 individuals per species) chosen to broadly represent 13 Angiosperm families (Table 2) were sampled from across a 6.6 km gradient (along a road and trails) spanning an area of secondary and primary tropical forest in the Jianfengling forest reserve (Hogan et al. 2020b). The 13 plant families were chosen to target variation in root morphologies (i.e., from thicker, fleshier roots like those of Magnolids to thinner, more-lignified roots like those in the Fagaceae) (Valverde-Barrantes et al. 2017; Maherali 2017). All selected species were native species to the local flora and are considered a representative sample of the flora across the 13 targeted families (Table 2; Xu et al., 2015). Saplings were sampled in a balanced design along the 6.6 km gradient collecting 3 individuals from each half of the gradient (Hogan et al. 2020b). Three mature, intact leaves in full sun (i.e., those located on the transect edge) and five lateral entire root systems (i.e., those containing the first three root orders of fine-root tissue, McCormack et al. 2015) were harvested from each sapling. The collected root systems ranged from 0.3 to 3.0 mm in diameter and averaged 98 cm in root length (Hogan et al. 2020b). The 6.6 km gradient was representative of

the landscape-scale variation in soil texture and fertility for the greater Jianfengling Forest Reserve (Xu et al. 2015; see Hogan et al. 2020b for further details).

Soil collection & analyses

Following tissue collection, we collected ~1 kg of surface soil (0-10 cm soil depth) from the excavated area. Soils were air-dried for several weeks until completely dry and sieved using a 2mm mesh (#10) sieve. For each sample, we used approximately 300 g of sieved soil for analysis (Guangzhou Xinhua Agricultural Technical Development Limited Company, Guangzhou, Guangdong, China). Soil texture was measured using the international mechanical soil classification standard. Soil pH was measured using a glass electrode in a 2.5:1 water to soil dilution. We measured soil organic matter employing the high temperature, external-heat, potassium dichromate oxidation volumetric method. Total nitrogen content was measured using the Kjeldahl-distillation titration method, and total phosphorus, available potassium (K), and exchangeable sodium, calcium, and magnesium were all measured using an ammonium-acetate extraction, followed by flame atomic absorption spectrophotometry. Sodium-hydroxide melting-flame atomic absorption spectrophotometry was used to measure total soil K. The alkali-solution diffusion method was used to measure available (i.e., alkali-hydrolysable) soil N. Soil available P was measured using by the hydrochloric acid–ammonium fluoride extraction and the molybdenum antimony anti-coloring method, and soil base saturation and cation exchange capacity were measured with the ammonium acetate methods.

Tissue homogenization and elemental analysis

Root tissue samples were washed thoroughly, removing soil, and both surfaces of leaf samples were wiped with a paper towel. Leaf and root tissues were oven-dried at 70°C for at least 48 hours until completely dry. Tissue samples were placed individual into sterile 5mL propylene screwcap vials and finely ground using a Fisher Beadmill 24 multi-sample homogenizer (Fisher Scientific, USA) with 5mm stainless steel beads over multiple 30-second cycles at high speed. Prior to homogenization, stainless steel beads were cleaned and sterilized with ethanol to prevent contamination. This method is commonly used and does not result in systematic bias in tissue trace metal or other

elemental concentrations (Maia and Shaddox 2019). Homogenized leaf and root tissues were microweighed (2-3 µg) into aluminum micro tins on a Mettler Toledo XS3DU microbalance (Metler Toledo, Columbus, OH, USA) and put through continuous flow isotope ratio mass spectrometry and elemental analysis using a Thermo Delta Plus GC-IRMS (Thermo-Fisher, Waltham, MA, USA) for analysis of carbon and nitrogen. Agricultural macronutrient analyses were done using wet-acid digestion (following the methods in Jones Jr 2001) at the Soil Testing and Plant Analysis Lab at Louisiana State University. Briefly, digestion of one-half (0.5) grams of finely-ground plant tissue was done in 2.2 mL of deionized water using 5 mL of concentrated Nitric Acid. The solution was heated for 2.75 hours at 125°C. At the end of the heating, 3 mL hydrogen peroxide was added, and the solution was cooled and filled to a volume of 20 mL with deionized water. Elemental concentrations of aluminum (Al), boron (B), calcium (Ca), copper (Cu), iron (Fe), N, magnesium (Mg), manganese (Mn), molybdenum (Mo), sodium (Na), P, potassium (K), sulfur (S), and zinc (Zn) of homogenized tissue samples were determined using inductively coupled plasma optical emission spectroscopy (Avio 500 ICP-OES, Perkin Elmer, Waltham, MA, USA). Tissue concentrations of molybdenum were mostly below the detectable range, so we did not include them in our analyses.

Statistical analyses

A principal components analysis (PCA) was used to identify variables that represent the main axes of variation in soil nutrients. Data were scaled and centered before the PCA ordination. The PCA showed that the first two axes explained 61.8% of the variance. Three soil variables: base saturation (soil BS), total nitrogen (soil N), and total phosphorus (soil P) mostly characterized the soil differences among plant habitats (Fig. 5). Variation in those three soil parameters encompasses the range of soil variability among habitats, and they were only weakly correlated with one another (Pearson's r values all ≤ 0.38, Fig.6). Therefore, we used these three soil variables as representations of soil fertility.

To address the research question of whether tissue nutrient concentrations track soil fertility (i.e., question 1), we used linear mixed-effects models (LMMs). Tissue nutrient concentration data were $\log_{10}$-transformed to improve the normal distribution of

error. We determined that random intercept terms for both species and family were justifiable given that we had a balanced sampling design of six individuals per species for 50 species and were interested in differences among species and by plant lineage (i.e., family, question 3). LMMs were fit separately for each of the fourteen tissue nutrients using the 'lme4' package (Bates et al. 2015) in R v.3.6.0 (R Core Team 2019). A saturated model was built including random intercepts for species and family and fixed effects for soil N, soil P, and soil BS, and their interactions with organ type (i.e., leaf vs. root): $\log_{10}([Tissue\ Nutrient]) = (\beta soilN + \beta soilP + \beta soilBS) * organ + 1|family + 1|species$. Model selection was then performed using the 'step()' function from the 'lmerTest' package (Kuznetsova et al. 2017) in R v.3.6.0 (R Core Team 2019), which implements backward elimination of random-effect terms where applicable, followed by backward elimination of fixed effects based on model Akaike Information Criterion. Final models were fit using residualized maximum likelihood estimates, which accounts for the number of model parameters when estimating parameter values by applying the likelihood function over the least-squares residuals. Statistical significance was determined using the Wald method.

To analyze if leaf nutrients directly tracked root nutrients (i.e., passive transport of nutrients among plant organs, question 2), we used a paired Wilcoxon signed-rank test (Wilcoxon 1945). It is a nonparametric statistical test that compares whether the population mean ranks differ, where the null hypothesis is that the difference between pairs follows a symmetric distribution around zero. It is often used as a nonparametric alternative to a paired Student's T-test to test if two samples come from populations that have the same distribution because it does conform to the same statistical assumptions of normality as a paired Student's T-test. In the context of our data, a non-statistically significant result means that the ranks of tissue element concentrations between leaves and roots of individual saplings do not differ and can thus be considered equal. On the other hand, if the test statistic is significant at .05 level of statistical significance, we interpret this to mean that concentrations of elements between leaves and roots of individual saplings are not equal.

Results

We first discuss the measured stoichiometry of tissues in context. Then, we present results from the linear mixed-effects models for each of the 14 elements analyzed. Finally, we summarize results related to our three research questions.

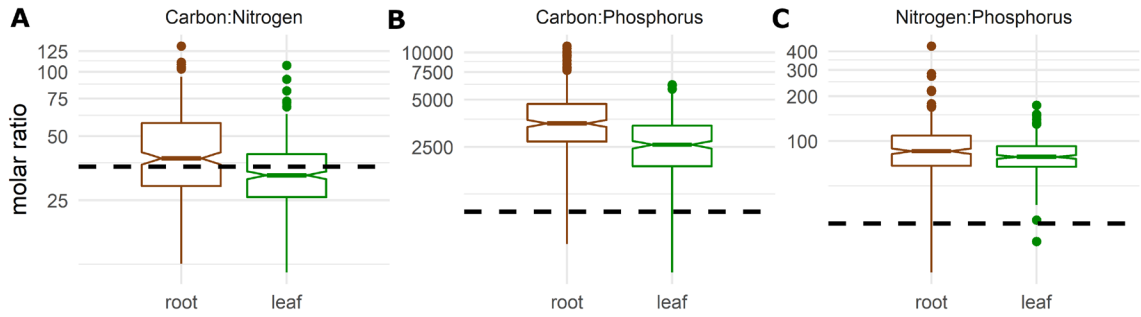

Fig. 2: Box and whisker plots for foliar and root elemental molar ratios for C, N, and P for 300 individuals sampled in the Jianfengling Forest Reserve, China. Vertical axes are log-scale. Boxplots show means (center line), interquartile ranges (boxes), and the smallest and largest values within 1.5 times the interquartile range (whiskers). Points are >1.5 times outside the interquartile ranges. Horizontal dashed lines represent the global average of foliar C:N, C:P, and N:P molar ratios, as reported by Sterner and Elser (2009) (36, 968, and 28, respectively).

Carbon, nitrogen, and phosphorus stoichiometric ratios

Average (± standard error) molar C:N ratios were 44.8 ± 1.1 (range: 13-132) for roots, and 34.7 ±0.8 (range: 11-107) for leaves (Fig. 2A); mass-based C:N ratios averaged 38.5 ± 1.0 (range: 10.8 – 113.2) for roots and 29.7 ± 0.7 (range: 9.8 – 92.0) for leaves. Molar ratios for N:P were 92. 8 ± 2.4 (range: 13-434) for roots and 80.4 ± 1.2 (range:21-174) for leaves (Fig. 2B); mass-based N:P ratios averaged 43.3 ± 1.3 (range: 5.9 – 196.4) for roots and 37.2 ± 0.08 (range: 9.6 – 116.8) for leaves . Lastly, molar ratios for C:P were 3869.4 ± 103.1 (range:600-10972) for roots and 2739.6 ± 64.6 (range: 395-6230) for leaves (Fig. 2C); mass-based C:P ratios averaged 1500.2 ± 39.7 (range: 223.4 – 4254.5) for roots and 1060.3 ± 25.1 (range: 153.1 – 2510.5) for leaves . Horizontal lines in Figure 2 show global nutrient ratio averages as reported by Sterner and Elsner (2009). The high C:P and N:P ratios relative to the global averages for terrestrial plants show that, generally, tissues were phosphorus-poor (Fig. 2).

Tissue nutrients in relation to soil nutrients – results from LMMs

Of the fourteen tissue nutrients analyzed, half showed increasing concentrations with increasing soil fertility; those being nitrogen (Fig 3B), boron (Fig 3C), phosphorous (Fig 3G), potassium (Fig 3I), manganese (Fig. 3K), copper (Fig. 3M), and zinc (Fig. 3N). Concentrations of three of fourteen tissue nutrients: magnesium (Fig. 3E), sulfur (Fig. 3H), and calcium (Fig. 3J) showed no relationship to soil fertility. Tissue concentrations of carbon (Fig 3A) and aluminum (Fig 3F) showed a slightly decreasing trend with soil fertility. Two of fourteen tissue nutrients showed divergent relationships between roots and leaves (i.e. non-parallel slopes or strong interactions of soil fertility and leaf type). With increasing soil P, sodium content in leaf tissues showed a decreasing trend but increased slightly in roots (Fig. 3D). Conversely, with increasing soil P, iron concentrations in roots decreased somewhat, but iron concentrations in leaves were invariant (Fig. 3L).

Tissue carbon concentration responded weakly positively to soil N (β coefficient of 0.01), more-strongly negatively to soil P (β of -0.26), and did not vary with soil BS. Leaf carbon concentrations were statistically lower than root carbon concentrations (Fig. 3A, β of -0.03). There was a minimal degree interfamilial variation in tissue C concentrations among species in the Lauraceae, Sapotaceae, Anacardiaceae, Pentaphylacaceae, Sapindaceae, Juglandaceae, and Fagaceae having slightly higher tissue carbon concentrations than those in the Theaceae, Ebenaceae, Burseraceae, Rutaceae, Moraceae, Annonaceae and Magnoliaceae (Online Resource 1 S1).

Tissue nitrogen concentration did not respond to soil N; that is, the best-fitting LMM for tissue nitrogen did not include soil N as an explanatory variable but included soil P instead. Soil P had a relatively-strong positive effect on tissue N (β of 0.49, Fig. 3B). Leaf tissue N concentrations was higher than root N concentrations (β of 0.05), and there was a weak interaction between organ type and soil BS (β negligible), with increasing soil BS slightly decreasing leaf N. Interfamilial variation in tissue N was greater than that of tissue C. The Rutaceae and Lauraceae families had significantly more N in tissues. The Pentaphylacaceae, and Fagaceae and Theaceae had significant less N in tissue than the remaining 9 Angiosperm families, whose random effect coefficient confidence intervals included zero (Online Resource 1 S2).

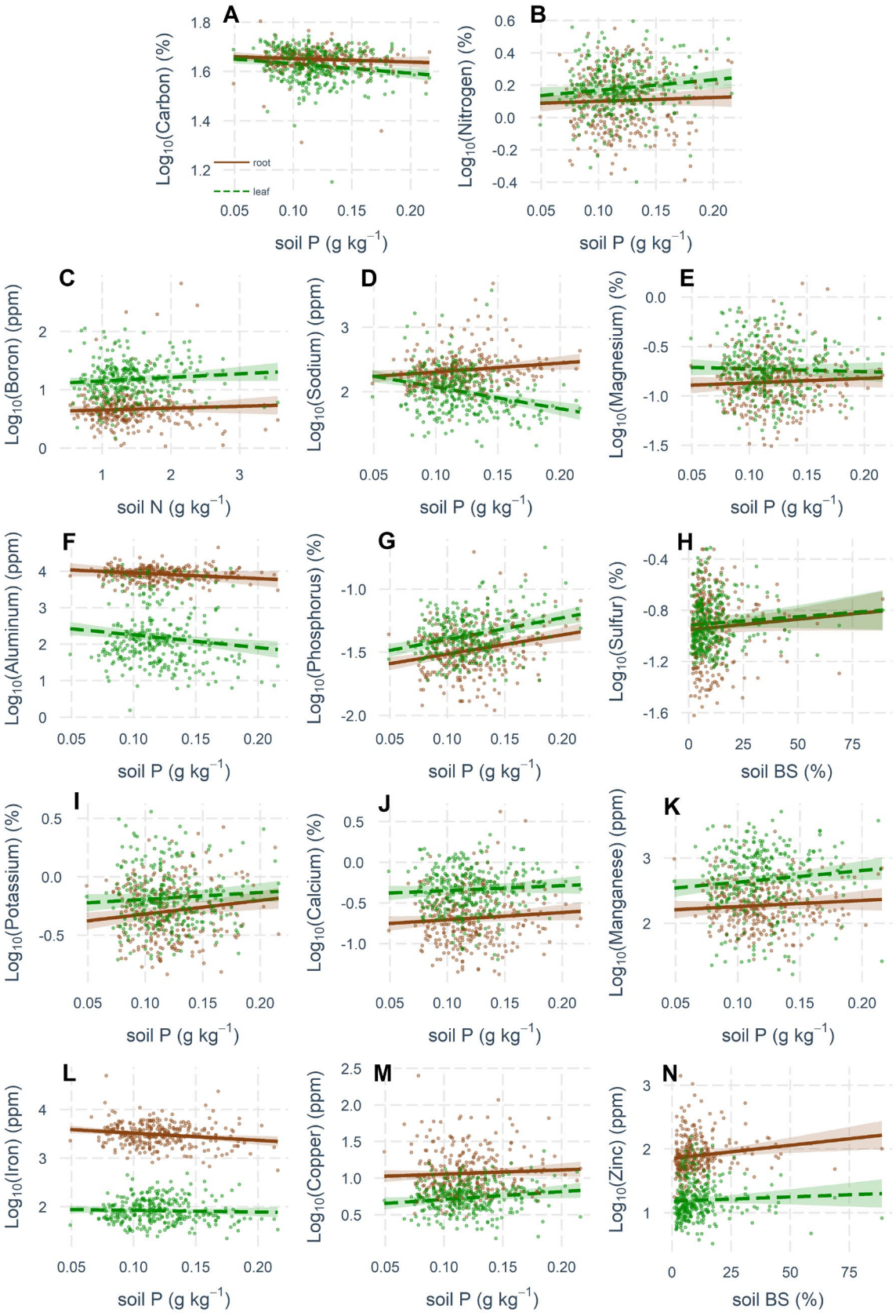
A
Log10(Carbon) (%)
root
leaf
soil P (g kg−1)
B
Log10(Nitrogen) (%)
soil P (g kg−1)
C
Log10(Boron) (ppm)
soil N (g kg−1)
D
Log10(Sodium) (ppm)
soil P (g kg−1)
E
Log10(Magnesium) (%)
soil P (g kg−1)
F
Log10(Aluminum) (ppm)
soil P (g kg−1)
G
Log10(Phosphorus) (%)
soil P (g kg−1)
H
Log10(Sulfur) (%)
soil BS (%)
I
Log10(Potassium) (%)
soil P (g kg−1)
J
Log10(Calcium) (%)
soil P (g kg−1)
K
Log10(Manganese) (ppm)
soil P (g kg−1)
L
Log10(Iron) (ppm)
soil P (g kg−1)
M
Log10(Copper) (ppm)
soil P (g kg−1)
N
Log10(Zinc) (ppm)
soil BS (%)

Fig. 3 (previous page): Plant tissue Carbon (A), Nitrogen (B), Boron (C), Sodium (D), Magnesium (E), Aluminum (F), Phosphorus (G), Sulfur (H), Potassium (I), Calcium (J), Manganese (K), Iron (L), Copper (M) and Zinc (N) in relation soil fertility (i.e., either soil nitrogen – soil N, phosphorus – soil P, or base saturation – soil BS). Measured concentrations of tissue nutrients (roots in brown and leaves in green) and linear mixed model fits (with 95% confidence intervals) are plotted. The soil fertility variable on the x-axis varies based on the best fitting linear mixed-effects models, fitted after backward selection of variables (see methods). For a complete statistical description of linear mixed-effects models, see Online Resource 1.

Soil P had a strong effect on tissue phosphorus (β of 1.71, Fig. 3G), soil N had a minute negative effect on tissue phosphorus (β of -0.07), and soil BS had little effect on tissue phosphorus (β negligible). Tissue phosphorus concentration was greater in leaves than in roots (β of 0.12). Among families, species in Rutaceae had slightly greater tissue phosphorus concentrations, and species in the Fagaceae, Pentaphylacaceae, and Theaceae had slightly less tissue phosphorus than the remaining 11 Angiosperm families, whose random effect coefficient confidence intervals included zero (Online Resource 1 S7).

Boron, potassium, manganese, copper, and zinc concentrations tended to increase in tissues with soil nutrient availability. In the case of Boron (Online Resource 1 S3), soil P was removed as an explanatory variable during model selection. Soil N had a weak, but statistically insignificant, positive effect on tissue boron concentrations (β of 0.03), which were greater in leaves than roots (β of 0.47, Fig. 3C). Species in the Moraceae had greater than average tissue boron concentrations, while Lauraceae species had less than average tissue boron concentration. Tissue potassium concentrations responded positively to soil P (β of 0.95, Fig. 3I), negatively to soil N (β of -0.07), and were unaffected by soil BS (β negligible). Potassium was greater in leaf than in root tissue (β of 0.11, Fig. 3I), with species in the Rutaceae, and Moraceae having significantly greater potassium concentration and species in the Pentaphylacaceae, Theaceae and Fagaceae having significantly less concentration content than the familial average (Online Resource 1, S9). Concerning manganese concentration in tissues, soil P had a relatively-strong positive effect (β of 1.72, Fig. 3K), and soil N had a weak negative effect (β of -0.19). Manganese concentrations were greater in leaves than they were in roots (β of 0.39, Fig. 3K). Considerable intraspecific variation existed in leaf and

root manganese concentrations; however, all families were statistically equal except for the Moraceae which had greater magnesium concentrations than the other 13 plant families (Online Resource 1, S11). Copper concentrations in plant tissues responded positively to increasing soil P (β of 0.90, Fig. 3M), and weakly negatively to soil N (β of -0.09). Soil BS had no strong effect on tissue copper concentration (β of 0) but was included in the best-fitting model. Contrary to many of the other nutrients, copper concentration was greater in root tissues and in that of leaves (β of -0.34 for leaf type). Additionally, copper concentrations were higher in the Rutaceae and Lauraceae, and lower in the Theaceae and Pentaphylacaceae than in the other 10 plant families (Online Resource 1, S13). Lastly, zinc concentration was also greater in roots than in leaves (β of -0.48 for leaf type, Fig. 3N). Increasing soil N concentration led to a decrease in leaf zinc concentration (interaction-term β of -0.13). Lauraceae and Rutaceae had statistically greater than average amounts of tissue zinc, and Theaceae and Fagaceae had statistically less than average amounts of tissue zinc among all plant families (Online Resource 1, S14).

Concentrations of elements in plant tissues with soil fertility

Three nutrients showed no relationships with soil nutrient availability, those being magnesium, sulfur, and calcium. Soil N had a slight positive effect on tissue magnesium concentration (β of 0.06); however, it led to a decrease in leaf magnesium (interaction-term β of -0.07). Amounts of magnesium were found to be higher in leaf than roots tissues (β of 0.23). Species in the Lauraceae, Sapotaceae, and Fagaceae families had significantly lower than, and species in the Moraceae had significantly higher than familial average trends in tissue magnesium concentrations (Online Resource 1, S5). The best-fitting model for sulfur included a fixed effects for soil BS (β negligible) and organ type (β of 0.03 for leaves) and random intercept terms for family and species, thus we can understand plant sulfur concentration to be invariant with changes in soil nutrients (Fig. 3H). Again, species in the Lauraceae and Rutaceae families had greater than average amounts of tissue sulfur, while those from the Fagaceae had less (Online Resource 1 S8). A slight negative effect of soil N (β of -0.06) and negligible positive effect (β of 0.01) of soil BS on tissue calcium emerged from the

LMM fit for calcium (Online Resource 1, S10). However, calcium concentrations of tissue were invariable with environmental variation in soil P (Fig. 3J). Calcium was greater in leaves than in roots (β of 0.40 for leaves). Plants in the Sapotaceae and Fagaceae families had lower than average calcium concentrations.

Finally, two plant nutrients, sodium, and iron exhibited diverging trends among roots and leaves. For sodium, soil N had a positive effect (β of 0.06) and soil P had a non-significant positive effect (β of 1.01, but with confidence interval overlapping zero) on tissue concentrations. Sodium concentrations were higher in leaves than in roots (β of 0.23), and both increases in soil P (interaction term β of -3.89) and soil BS (interaction term β of -0.01) caused decreases in leaf sodium concentration (Fig. 3D, Online Resource 1, S4). Amounts of iron in root tissues decreased with increasing soil P (β of -0.94), and iron was higher in root tissues than in leaf tissue (β of -1.67 for organ type leaf). Soil N interacted to increase leaf iron concentration (β of 0.11), while soil BS had a negative effect (β of -0.01), hence the slight difference in slopes in Fig. 3L (Online Resource 1, S12).

Comparing element concentrations in roots and leaves

We found significant differences in the ranks of tissue nutrient concentrations between plant organs. Wilcoxon probabilities were highly statistically significant (all p values << .001) for carbon (Fig. 4A), nitrogen (Fig. 4B), sodium (Fig. 4D), magnesium (Fig. 4E), phosphorus (Fig. 4G), potassium (Fig. 4I), calcium (Fig. 4J), manganese (Fig. 4K), iron (Fig. 4L), zinc (Fig. 4N). . For those nutrients, ranks of leaf and root nutrient concentrations were not symmetric, in that when the concentration of an element was relatively high in root tissue, it tended to be low in leaf tissue, and vice versa. Ranks of tissue nutrient concentrations were not significantly different for boron (Fig. 4C), aluminum (Fig. 4F), sulfur (Fig. 4H), and Copper (Fig. 4M).

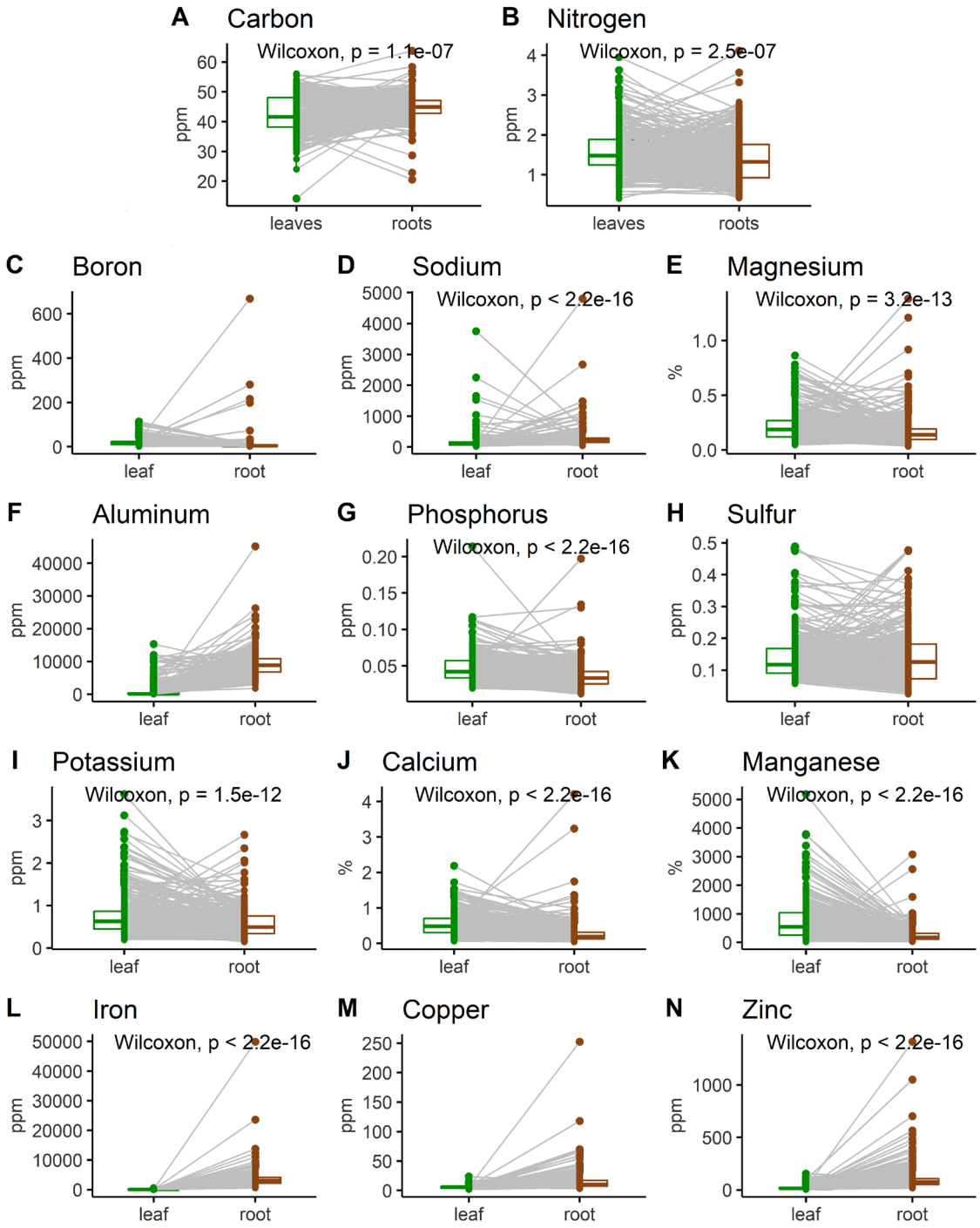

Fig. 4: Comparison of leaf and root concentrations of 14 essential elements. Boxplots show averages and interquartile ranges. Paired samples are connected with grey lines, and statistically significant paired-Wilcoxon signed-rank test probabilities are shown.

Variation in relationships due to plant family and species identity

Random effect variance of fitted LMMs, attributed to family and species identity, was low ranging from < 0.1 for carbon to 0.21 for aluminum, and averaging 0.06 (values are $\log_{10}$-transformed tissue concentration units). Thus, in all LMMs, the random effects of species and family accounted for a small amount of random effect variation about model fits, although in all cases where models included random effects for families and species, the amount variation explained by families was slightly greater than the variation explained by species (i.e., $\tau_{family} > \tau_{species}$). Intraclass correlations (ICC), or the proportion of variation explained by the random effect grouping structure of the model, ranged from 0.10 for iron to 0.52 for Magnesium, averaging 0.34 across all 14 models (Online Resource 1), signifying that tissue nutrient measurements within random effects groupings were not that related (note that ICC values can be interpreted like Pearson correlation coefficients). Yet, in some instances, statistically significant deviations from model averages were observed for plant families, and to a lesser degree, for individual species (see caterpillar plots in Online Resource 1).

On tissue carbon concentration, Ma et al. (2018) report in a global meta-analysis of all plants (>20000 measurements) that leaf C concentration is equal to or greater than root C concentration, measuring 470 ± 40 mg g^{-1} and 460 ± 50 mg g^{-1}, respectively. We found leaf C concentration to measure, on average, over 2% lower than in root C concentration (426 ± 40 mg g^{-1} for leaves and 449 ± 20 mg g^{-1} C for roots). Although these differences are not large, they are statistically significant at individual level (Wilcoxon sign ranked test *p-value* highly significant, Figure 4A), and broadly among organs across all the 50 species we sampled (Online Resource 1, Figure 3A). One explanation for this difference could be plant ontogeny; we were working with saplings, which tend to be photosynthate-limited due to their understory habitats and relatively small total leaf areas, which could create a greater difference in tissue carbon concentration between leaves and roots (i.e., a greater degree of whole-plant carbon limitation). Differences likely exist because of ontogenetic differences in relative amounts of the common C-containing molecules, such as lignin, cellulose, sugars, proteins, lipids, etc., of the leaf and root tissues of saplings relative to adult trees which differ in their C content (Hobbie and Werner 2004). Indeed, Martin et al. (2013) found

that stem wood of tropical saplings in Panama had 21 % less hemicellulose and 36 % more lignin, making them about 2% greater in carbon than conspecific adult tress. Additionally, differences in plant labile carbon allocation vary with tree age, with younger trees allocating relatively more carbon belowground than their established adult, non-light limited counterparts (Chapin et al. 1990; Dietze et al. 2014; Kozlowski 1992; Raich et al. 2014).

Question 1: Do concentrations of elements in plant root, and leaf tissue track increases soil fertility?

Our first research question asked whether root and leaf tissue elemental concentrations increase with increasing soil fertility. Concentrations of N and P in both root and leaf tissue increased with more soil P, but tissue C concentration showed a slight decreasing trend (Fig. 3A). Eight of the other eleven elements we studied showed relationships with soil fertility. The three nutrients that did not display links to soil fertility were boron, aluminum, and sulfur, which have either unclear or substitutable functions within the plant (Table 1) and may be toxic at high levels. The eight nutrients that responded to some degree to variation in soil nutrient concentrations were sodium, magnesium, potassium, calcium, manganese, iron, copper and zinc (Fig. 3), which are all cations with unique, indispensable functions within the plant cell (Table 1).

Literature-based hypotheses for changes in tissue nutrient concentrations to an increase in soil fertility (Table 1) were correct for half (7 of 14) of the elements we studied. For nitrogen, phosphorus, and potassium, hypothesized increases in tissue nutrient concentrations with increasing soil fertility were supported by the data (Fig. 3B, G, I). For carbon and aluminum, the hypotheses of decreasing tissue concentrations with increasing soil fertility were confirmed (Fig. 3A, F), and additionally, for sulfur, iron, and copper we were able to confirm the literature-based invariant relationships in tissue nutrient concentrations to variation in soil nutrients (Table 1). On the other hand, we observed no change in tissue concentrations of magnesium, where the literature predicted an increase (Fig. 3E), and we found a decrease in leaf sodium with increasing soil P in opposition to the hypothesized increase, although concentrations in root tissue did increase (Fig. 3D). We observed a slight increase in tissue zinc concentration with

increasing soil nutrient concentration (Fig 3N), despite the literature supporting the hypothesis that concentrations should decrease. However, this trend was driven by only a few datapoints for plants collected in soils with high soil BS. Similarly, we observed tiny increases in tissue boron and manganese concentrations with soil N and P, respectively (Fig. 3C, 3K), where the literature supported that relationships should be invariant.

Furthermore, responses of tissue nutrients to soil fertility did not vary systematically with Marschner's 4-group nutrient classification (Marschner 2012; Kirby 2012; Mengel and Kirby 2001). Recall that group 1 nutrients are taken up as ions, group 2 nutrients are absorbed as inorganic anions or acids, group 3 nutrients are mostly taken up as catatonic compounds (excepting chlorine which is group 3 anion), and group 4 nutrients are actively taken up in their ionic forms. At least one element from all four groups (N – group 1, B and P – group 2, K and Mn – group 3, and Cu and Zn – group 4) increased in concentration in plant tissues with increasing soil fertility. Carbon (a group 1 nutrient) and aluminum (a group 4 nutrient) were the two that decreased slightly with increasing soil fertility. Those showing no change were magnesium, calcium (both group 3 nutrients) and sulfur (a group 1 nutrient). Sodium (a group 3 nutrient) and iron (a group 4 nutrient) interacted with soil fertility to show diverging trends between root and leaf tissue concentrations with increasing soil fertility.

Tissue phosphorus showed the strongest increasing trend with soil P availability (Fig. 3E). This suggests that plants in Jianfengling are P-limited (Fig. 2, Vitousek 1984; Vitousek and Sanford Jr 1986) and that adding P to the soil would have the greatest effect on plant growth and likely tissue nutrient concentrations. Indeed, Wright (2019) reported a strong effect of P-addition on leaf tissue P concentration (Hedges g effect size of 1.7) in a meta-analysis of nutrient addition experiments in tropical forests. However, responses of tropical tree tissue stoichiometry to increases in P probably varies with species sensitivities (Turner et al. 2018), tree size (Wright et al. 2018), and by plant organ (e.g., roots, stems and leaves). Wurzburger and Wright (2015) reported clear increases in fine root tissue P concentration when adding P in a lowland Panamanian forest, with roots decreasing in morphological traits associated with nutrient

acquisitiveness per the "do it yourself" root functional strategy (sensu Bergmann et al. 2020), that is roots had less total biomass, decreased root length, but increased in specific root length. At Jianfengling, we found similar morphological shifts in the roots of saplings from which tissue nutrients were measured, where the diameter of root systems was narrower, and specific root length (SRL) and root system branching intensity were greater in lower soil fertility areas than in areas with more soil nutrients; increased levels in soil bases and P were significantly related to increased SRL (Hogan et al. 2020b) .

Tissue nitrogen showed a similar pattern to phosphorus, increasing with soil P availability but to a lesser degree (Fig 3). Soil N was not backward selected as a fixed effect in the model selection process, suggesting that saplings are more limited by P than N. However, Wurzburg and Wright (2015) reported no change in root tissue N with nutrient addition in a lowland Panamanian forest. The variety of strategies by which and sources from which plants obtain N, along with the demand for and homeostatic movement of N within the plant, make the interpretability of root N concentration, by itself, difficult, although some progress on conceptualizing root N in relation to root economics is being made (McCormack & Iversen 2019, Bergmann et al 2020). Ultimately N concentrations in leaf and root tissues depends on a suite of abiotic (e.g., diffuse nutrient flows in the soil) and biotic biogeochemical processes (e.g., microbial and fungal nutrient mobilization in the soil), which interact with plant and soil stoichiometry (Aerts and Chapin 1999; Brown 1978; Elser et al. 2000b; Gordon and Jackson 2000; Güsewell 2004; Marschner 2012).

Question 2: How do concentrations of nutrients in roots relate to those in leaves?

We found that concentrations of carbon, sodium, iron, copper, and zinc were greater in roots than leaves (Fig. 3), whereas concentrations of nitrogen, boron, magnesium, phosphorus, sulfur, potassium, calcium and manganese were greater in leaves than in roots. Elements that had higher concentrations in leaves than in roots, excluding magnesium, calcium, and sulfur, tended to increase in concentration in leaves with increasing levels of soil nutrients. This supports the idea that, at least for some elements, there is within-plant homeostatic elemental regulation. The most supportive

evidence we found for homeostatic regulation came from the results of the Wilcoxon sign-ranked test, which was significant for carbon, nitrogen, phosphorus and seven of the eight, above mentioned elements that responded to variation in soil nutrient concentration. The evidence that when element concentrations are high in roots, they tend to be lower in leaves, and vice versa, points to selective plant use, movement and storage of these elements within plant tissue and cells. Copper was the lone case of an element that responded to soil nutrient availability but was not regulated within the plant. Active within-plant elemental regulation may be responsible for these patterns, as we have discussed, however alternative mechanisms could result in similar patterns. First, roots can act as filter for certain elements (e.g., boron, aluminum, iron, copper and zinc), excluding their movement into plants (Marchner 2012), actively uptaking other less toxic cations in their place (i.e. selecting against their uptake, Khale 1993) or though complex alterations of soil biogeochemistry and pH via root exudates (Jones and Darrah 1994). Moreover, certain elements may accumulate in leaves (e.g., calcium, if they are in compounds that phloem-insoluble or too large for phloem transport (Hill 1980).

Question 3: Do plant lineages vary in their leaf and root tissue chemistry-soil environment relationships?

Among all elemental concentrations in tissues, there was considerable variation within families and species. In other words, among plant variation far exceeded any intraspecific or intrafamilial variation (σ^2 for random effects < 0.1, except for aluminum where σ_2 was 0.21, Supplement 1). Yet, for each element, certain families differed statistically from the fitted trend for all families. There was no interfamilial or intraspecific variation (i.e. no statistically significant effects for levels of random family or species intercept terms) in modeled tissue carbon concentration; however, there was for each of the 13 other elements studied (see caterpillar plots in Online Resource 1). For example, plants in the Theaceae had higher tissue Aluminum concentrations than the modeled trend (Online Resource 1, S6) Thus, in certain cases, plant lineage does modulate the relationship strength between leaf and root tissue chemistry and the soil environment, which is already subtle at the local environment and individual plant scales. This is likely due to slight differences in the physiological functioning among

plant lineages, which are the result of their evolved biological differences and variation in life-history strategies. Plant evolutionary history has strongly influenced root morphologies (Valverde-Barrantes et al 2017), which may have direct effects on nutrient uptake physiologies, soil habitat preferences, or mechanisms for dealing with soil element toxicity (Marschner 2012). However, with an incomplete sampling of the Angiosperm phylogeny, it is difficult to thoroughly assess the role of plant lineage, as deeper nodes in the phylogeny may be driving such differences, and thus patterns of nutrient concentration variation among taxa(Kerkhoff, 2006). For example, variation for some nutrients, especially these involved in cell wall structures (carbon, calcium, magnesium) occurs at the level of order, rather than family or species (Broadly et al. 2004). In our case, any slight differences in physiology (e.g., nutrient requirement or use) seem to be overshadowed larger nutrient constraints of the soil environment itself. This result is congruent with previous research that has found a wide range in tropical tree tissue nutrient concentrations (Hattenschwiler et al. 2008, Townsend et al. 2007) and their stoichiometries (Townsend et al. 2008, Elser et al. 2010).

In summary, using data on root and leaf tissues of 300 saplings of 50 species from across a representative range of local habitat variability in soils of a tropical montane forest, we found stable tissue concentrations for half of the 14 elements we considered. Therefore, at least some-degree of elemental homeostasis, that is, the maintenance of constant levels of tissue nutrients despite changes in the nutrient status of the external soil environment, was observed. In cases where plant tissue nutrients either decreased or increased with soil nutrient status, trends tended to be weak, potentially because of nutrient limitation in highly leached tropical forest soil. Thus, plant functioning of saplings in montane tropical forest is stoichiometrically constrained across environmental variation (i.e., has a broad stoichiometric knife-edge, at least with respect to the range of soil environments studied here). However, their stoichiometry does respond to variation in environment and resource quantity with potential for nutrient regulation between plant organs (i.e., roots and leaves), especially for elements that have a critical physiological functions in leaves (e.g., nitrogen, phosphorus, potassium, magnesium, and manganese).

Online Resources
Online Resource 1: Complete model description of best-fitting linear mixed-effects models for 14 elemental concentrations in leaf and root tissues.
link: https://bit.ly/3xls1FM

References

Asner GP, Martion RE (2016) Convergent elevation trends in canopy chemical traits of tropical forests. Global Change Biology 22:2216-2227.

Aerts R, Chapin FS (1999) The mineral nutrition of wild plants revisited: a re-evaluation of processes and patterns. Advances in Ecological Research. Elsevier.

Anderson J (1990) Sulfur metabolism in plants. The Biochemistry of Plants 16:327-381.

Andresen E, Peiter E, Küpper H (2018) Trace metal metabolism in plants. Journal of Experimental Botany 69:909-954.

Aulie RP (1974) The Mineral Theory. Agricultural History 48:369-382.

Balk J, Pilon M (2011) Ancient and essential: the assembly of iron–sulfur clusters in plants. Trends in Plant Science 16:218-226.

Bates D, Mächler M, Bolker B, Walker S (2015) Fitting Linear Mixed-Effects Models Using lme4. Journal of Statistical Software 1. doi:10.18637/jss.v067.i01.

Bergmann J, Weigelt A, van der Plas F, Laughlin DC, Kuyper TW, Guerrero-Ramirez N, Valverde-Barrantes OJ, Bruelheide H, Freschet GT, Iversen CM, Kattge J, McCormack ML, Meier IC, Rillig MC, Roumet C, Semchenko M, Sweeney CJ, van Ruijven J, York LM, Mommer L (2020) The fungal collaboration gradient dominates the root economics space in plants. Science Advances 6:eaba3756.

Bittner F (2014) Molybdenum metabolism in plants and crosstalk to iron. Frontiers in Plant Science 5. doi:10.3389/fpls.2014.00028.

Bond WJ (2010) Do nutrient-poor soils inhibit development of forests? A nutrient stock analysis. Plant and Soil 334:47-60.

Broadley MR, Bowen HC, Cotterill HL, Hammond JP, Meacham MC, Mead A, White PJ (2004) Phylogenetic variation in the shoot mineral concentration of angiosperms. Journal of Experimental Botany 55: 321-336.

Broadley M, Brown P, Cakmak I, Ma JF, Rengel Z, Zhao F (2012a) Beneficial elements In: Marschner P, ed. Marschner's mineral nutrition of higher plants. London, UK: Academic Press, 249-269.

Broadley M, Brown P, Cakmak I, Rengel Z, Zhao F (2012b) Function of nutrients: micronutrients In: Marschner P, ed. Marschner's mineral nutrition of higher plants. London, UK: Academic Press, 191-248.

Broadley MR, White PJ, Hammond JP, Zelko I, Lux A (2007) Zinc in plants. New Phytologist 173:677-702.

Brown JC (1978) Mechanism of iron uptake by plants. Plant, Cell & Environment 1:249-257.

Burnell JN (1988) The biochemistry of manganese in plants. Manganese in soils and plants. Springer.

Cakmak I (2005) The role of potassium in alleviating detrimental effects of abiotic stresses in plants. Journal of Plant Nutrition and Soil Science 168:521-530.

Chapin FS (1980) The mineral nutrition of wild plants. Annual Review of Ecology and Systematics 11:233-260.

Chapin FS, Matson PA, Vitousek P (2011) Principles of Terrestrial Ecosystem Ecology. Springer Science & Business Media.

Chapin FS, Schulze E, Mooney HA (1990) The ecology and economics of storage in plants. Annual Review of Ecology and Systematics 21:423-447.

Cleland EE, Harpole WS (2010) Nitrogen enrichment and plant communities. Annals of the New York Academy of Sciences 1195:46-61.

Delhaize E, Ryan PR (1995) Aluminum Toxicity and Tolerance in Plants. Plant Physiology 107:315-321. doi:10.1104/pp.107.2.315.

Dietze MC, Sala A, Carbone MS, Czimczik CI, Mantooth JA, Richardson AD, Vargas R (2014) Nonstructural carbon in woody plants. Annual Review of Plant Biology 65:667-687.

Edwards G, Walker D (1983) C3, C4: mechanisms, and cellular and environmental regulation, of photosynthesis. Univ of California Press.

Elser J, Fagan W, Kerkhoff A, Swenson N, Enquist B (2010) Biological stoichiometry of plant production: metabolism, scaling and ecological response to global change. New Phytologist 186:593-608.

Elser J, Sterner R, Gorokhova EA, Fagan W, Markow T, Cotner J, Harrison J, Hobbie S, Odell G, Weider L (2000a) Biological stoichiometry from genes to ecosystems. Ecology Letters 3: 540-550.

Elser JJ, Bracken MES, Cleland EE, Gruner DS, Harpole WS, Hillebrand H, Ngai JT, Seabloom EW, Shurin JB, Smith JE (2007) Global analysis of nitrogen and phosphorus limitation of primary producers in freshwater, marine and terrestrial ecosystems. Ecology Letters 10: 1135-1142.

Elser JJ, Fagan WF, Denno RF, Dobberfuhl DR, Folarin A, Huberty A, Interlandi S, Kilham SS, McCauley E, Schulz KL (2000b) Nutritional constraints in terrestrial and freshwater food webs. Nature 408: 578.

Enríquez S, Duarte CM, Sand-Jensen K (1993) Patterns in decomposition rates among photosynthetic organisms: the importance of detritus C:N:P content. Oecologia 94:457-471.

Epstein E (1961) The essential role of calcium in selective cation transport by plant cells. Plant Physiology 36:437.

Evans JR (1989) Photosynthesis and nitrogen relationships in leaves of C3 plants. Oecologia 78:9-19.

Field C, Mooney H (1986) Photosynthesis--nitrogen relationship in wild plants. On the Economy of Plant Form and Function: Proceedings of the Sixth Maria Moors Cabot Symposium, Evolutionary Constraints on Primary Productivity, Adaptive Patterns of Energy Capture in Plants, Harvard Forest, August 1983. Cambridge [Cambridgeshire]: Cambridge University Press, c1986.

Fitter AH, Hay RK (2012) Environmental physiology of plants. Academic Press.

Garg B, Vyas S, Kathju S, Lahiri A, Mali P, Sharma P (1993) Salinity-fertility interaction on growth, mineral composition and nitrogen metabolism of Indian mustard. Journal of Plant Nutrition 16:1637-1650.

Gilliham M, Dayod M, Hocking BJ, Xu B, Conn SJ, Kaiser BN, Leigh RA, Tyerman SD (2011) Calcium delivery and storage in plant leaves: exploring the link with water flow. Journal of Experimental Botany 62:2233-2250.

Gordon WS, Jackson RB (2000) Nutrient concentrations in fine roots. Ecology 81:275-280.

Güsewell S (2004) N: P ratios in terrestrial plants: variation and functional significance. New Phytologist 164:243-266.

Hall SJ, Silver WL (2013) Iron oxidation stimulates organic matter decomposition in humid tropical forest soils. Global Change Biology 19:2804-2813.

Hampe T, Marschner H (1982) Effect of sodium on morphology, water relations and net photosynthesis of sugar beet leaves. Zeitschrift für Pflanzenphysiologie 108:151-162.

Hattenschwiler S, Aeschlimann B, Coteaux MM, Roy J, Bonal D (2008) High variation in foliage and leaf litter chemistry among 45 tree species of a neotropical rainforest community. New Phytologist 179:165-175.

Hawkesford M, Horst W, Kichey T, Lambers H, Schjoerring J, Møller IS, White P (2012) Functions of macronutrients In: Marschner P, ed. Marschner's mineral nutrition of higher plants. London, UK: Academic Press, 135-189.

Heineman KD, Turner BL, Dlling JW (2016) Variation in wood nutrients along a tropical soil fertility gradient. New Phytologist 211:440-454.

Hilbert DW (1990) Optimization of plant root: shoot ratios and internal nitrogen concentration. Annals of Botany 66:91-99.

Hill J (1980) The remobilization of nutrients from leaves. Journal of Plant Nutrition 2:407-444.

Hobbie EA, Werner RA (2004) Intramolecular, compound-specific, and bulk carbon isotope patterns in C3 and C4 plants: a review and synthesis. New Phytologist 161: 371-385. doi:10.1111/j.1469-8137.2004.00970.x.

Hobbie SE (2015) Plant species effects on nutrient cycling: revisiting litter feedbacks. Trends in Ecology & Evolution 30:357-363.

Hogan JA, Baraloto C, Valverde-Barrantes OJ, Xu H, Ding Q (2020a) Sapling leaf and root chemistry from 6.6 km Jianfengling transect. https://doi:10.6084/m9.figshare.8283593.v3

Hogan JA, Valverde-Barrantes OJ, Ding Q, Xu H, Baraloto C (2020b) Morphological variation of fine root systems and leaves in primary and secondary tropical forest Hainan Island, China. Annals of Forest Science. doi:10.1007/s13595-020-00977-7.

Hull RJ (2002) Recent research offers clues to boron's purpose. TurfGrass Trends.

Jackson RB, Mooney H, Schulze E-D (1997) A global budget for fine root biomass, surface area, and nutrient contents. Proceedings of the National Academy of Sciences 94:7362-7366.

Jeong J, Guerinot ML (2009) Homing in on iron homeostasis in plants. Trends in Plant Science 14:280-285.

Jones DL, Darrah PR (1994) Role of root derived acids in the mobilization of nutrients from the rhizosphere Plant and Soil:166:247-257.

Jones Jr JB (2001) Laboratory guide for conducting soil tests and plant analysis. CRC press.

Kattge J, Bönisch G, Díaz S, Lavorel S, Prentice IC, Leadley P, Tautenhahn S, Werner GDA et al. (2020) TRY plant trait database – enhanced coverage and open access. Global Change Biology 26:119-188.

Kahle H (1993) Response of roots of trees to heavy metals. Environmental and Experimental Botany 33:99-119.

Kerkhoff A, Fagan WF, Elser JJ, Enquist BJ (2006) Phylogenetic and growth form variation in the scaling of nitrogen and phosphorus in the seed plants. American Naturalist 168:E103-E122.

Kirkby E (2012) Introduction, definition and classification of nutrients. Marschner's mineral nutrition of higher plants. Elsevier.

Kozlowski TT (1992) Carbohydrate sources and sinks in woody plants. The Botanical Review 58: 107-222.

Kramer PJ, Kozlowski TT (1979) Physiology of Woody Plants. Academic Press, New York, NY.

Kutschera U, Niklas KJ (2017) Boron and the evolutionary development of roots. Plant Signaling & Behavior 12:e1320631.

Kuznetsova A, Brockhoff PB, Christensen RHB (2017) lmerTest package: tests in linear mixed-effects models. Journal of Statistical Software 82.

Lambers H, Poorter H (1992) Inherent variation in growth rate between higher plants: a search for physiological causes and ecological consequences. Advances in Ecological Research. Elsevier.

Lambers H, Shane MW, Cramer MD, Pearse SJ, Veneklaas EJ (2006) Root structure and functioning for efficient acquisition of phosphorus: matching morphological and physiological traits. Annals of Botany 98:693-713.

Lewandowska M, Sirko A (2008) Recent advances in understanding plant response to sulfur-deficiency stress. Acta Biochim Pol 55:457-471.

Lewis DH (2019) Boron: the essential element for vascular plants that never was. New Phytologist 221:1685-1690.

Lira-Martins D, Humpreys-Williams E, Strekopytov S, Ishida FY, Quiesada CA, Lloyd J (2019) Tropical tree branch-leaf nutrient scaling relationships with sampling location. Frontiers in Plant Science 10:877. doi:10.3389/fpls.2019.0087

Longnecker NE, Robson AD (1993) Distribution and transport of zinc in plants. Zinc in soils and plants. Springer.

Ma S, He F, Tian D, Zou D, Yan Z, Yang Y, Zhou T, Huang K, Shen H, Fang J (2018) Variations and determinants of carbon content in plants: A global synthesis. Biogeosciences 15:693-702.

Maathuis FJ, Sanders D (1996) Mechanisms of potassium absorption by higher plant roots. Physiologia Plantarum 96:158-168.

Maia LOR, Shaddox TW (2019) Grinding methods infleunce nutrient analysis of Bahiagrass and St. Augistinegrass. Crop Science 59:787-791.

Maherali, H (2017) The evolutionary ecology of fine roots. New Phytologist 215: 1295-1297.

Maire V, Gross N, Pontes LDS, Picon-Cochard C, Soussana JF (2009) Trade-off between root nitrogen acquisition and shoot nitrogen utilization across 13 co-occurring pasture grass species. Functional Ecology 23:668-679.

Makita N, Hirano Y, Dannoura M, Kominami Y, Mizoguchi T, Ishii H, Kanazawa Y (2009) Fine root morphological traits determine varaition in root respiration of Quercus seratta. Tree Physiology 29:579-585.

Marschner H (1991) Mechanisms of adaptation of plants to acid soils. Plant and Soil 134:1-20.

Marschner P (2012) Marschner's Mineral Nutrition of Higher Plants. Academic Press, Waltham, MA.

Marston HR (1952) Cobalt, Copper and Molybdenum in the Nutrition of Animals and Plants. Physiological Reviews 32:66-121.

Martin AR, Thomas SC, Zhao Y (2013) Size-dependent change in wood chemical traits: a comparison of neotropical saplings and large trees. AOB Plants 5:plt039.

Mayland H (1990) Magnesium in plants: uptake, distribution, function, and utilization by man and animals. Marcel Dekker, Inc New York and Basel, Switzerland.

McCormack ML, Dickie IA, Eissenstat DM, Fahey TJ, Fernandez CW, Guo D, Helmisaari HS, Hobbie EA, Iversen CM, Jackson RB (2015) Redefining fine roots improves understanding of belowground contributions to terrestrial biosphere processes. New Phytologist 207:505-518.

McCormack ML, Iversen CM (2019) Physical and functional constraints on viable belowground acquisition strategies. Frontiers in Plant Science 10:1215.

Mengel K (2016) Potassium. Handbook of plant nutrition. CRC Press.

Mengel K, Kirkby E (2001) Principles of plant nutrition. Kluwer Academic Publishers.

Middleton W, Jarvis B, Booth A (1978) The boron requirement for root development in stem cuttings of Phaseolus Aureus Roxb. New Phytologist 81:287-297.

Mukhopadhyay MJ, Sharma A (1991) Manganese in cell metabolism of higher plants. The Botanical Review 57:117-149.

Niklas KJ (2006) Plant allometry, leaf nitrogen and phosphorus stoichiometry, and interspecific trends in annual growth rates. Annals of Botany 97:155-163.

Paradosio E, Jevon F, Matthes J. Fine root respiratio is more strongly correlated with root traits than species identity. Ecosphere 10:e02944.

Pons T, Lambers H, Chapin FS (1998) Plant physiological ecology. Springer-Verlag, New York.

Pregitzer KS, Kubiske ME, Yu CK, Hendrick RL (1997) Relationships among root branch order, carbon, and nitrogen in four temperate species. Oecologia 111:302-308.

R Core Team (2019) R: A language and environment for statistical computing. R Foundation for Statistical Computing, Vienna, Austria.

Raich JW, Clark DA, Schwendenmann L, Wood TE (2014) Aboveground tree growth varies with belowground carbon allocation in a tropical rainforest environment. PloS One 9:e100275.

Raper Jr CD, Osmond DL, Wann M, Weeks WW (1978) Interdependence of root and shoot activities in determining nitrogen uptake rate of roots. Botanical Gazette 139:289-294.

Reich P, Walters M, Ellsworth D (1992) Leaf life-span in relation to leaf, plant, and stand characteristics among diverse ecosystems. Ecological Monographs 62:365-392.

Reich PB, Oleksyn J (2004) Global patterns of plant leaf N and P in relation to temperature and latitude. Proceedings of the National Academy of Sciences of the United States of America 101:11001-11006.

Reich PB, Oleksyn J, Wright IJ (2009a) Leaf phosphorus influences the photosynthesis–nitrogen relation: a cross-biome analysis of 314 species. Oecologia 160:207-212.

Reich PB, Oleksyn J, Wright IJ, Niklas KJ, Hedin L, Elser JJ (2009b) Evidence of a general 2/3-power law of scaling leaf nitrogen to phosphorus among major plant groups and biomes. Proceedings of the Royal Society B: Biological Sciences 277:877-883.

Roy AK, Sharma A, Talukder G (1988) Some aspects of aluminum toxicity in plants. The Botanical Review 54:145-178.

Schachtman DP, Reid RJ, Ayling SM (1998) Phosphorus uptake by plants: from soil to cell. Plant Physiology 116:447-453.

Shaul O (2002) Magnesium transport and function in plants: the tip of the iceberg. Biometals 15:307-321.

Shen J, Yuan L, Zhang J, Li H, Bai Z, Chen X, Zhang W, Zhang F (2011) Phosphorus dynamics: from soil to plant. Plant Physiology 156:997-1005.

Silver WL, Liptzin D, Almaraz M (2013) Soil redox dynamics and biogeochemistry along a tropical elevation gradient. Pages 195-210 in G González, MR Willig, and RB Waide, editors Ecological gradient analyses in a tropical landscape Ecological Bulletins 54 Wiley-Blackwell, Hoboken, NJ.

Silver WL, Miya RK (2001) Global patterns in root decomposition: comparisons of climate and litter quality effects. Oecologia 129:407-419.

Smith FW (2001) Sulphur and phosphorus transport systems in plants. Plant and Soil 232:109-118.

Sterner R, Elser J (2009) Ecological Stoichiometry. In: SA Levin (ed) The Princeton Guide to Ecology. Princeton University Press, Princeton, NJ.

Sterner RW, Elser JJ (2002) Ecological stoichiometry: the biology of elements from molecules to the biosphere. Princeton University Press, Princeton, NJ.

Subbarao G, Ito O, Berry W, Wheeler R (2003) Sodium—a functional plant nutrient. Critical Reviews in Plant Sciences 22: 391-416.

Taub DR, Wang X (2008) Why are nitrogen concentrations in plant tissues lower under elevated CO_2? A Critical Examination of the Hypotheses. Journal of Integrative Plant Biology 50:1365-1374.

Townsend AR, Asner GP, Cleveland CC (2008). The biogeochemical heterogeneity of tropical forests. Trends in Ecology and Evolution 23:424-431.

Townsend AF, Cleveland CC, Asner GP, Bustamante MMC (2007) Controls over foliar N:P ratios in tropical rain forest. Ecology 88:107-118.

Turner BL (2008) Resource partitioning for soil phosphorus: a hypothesis. Journal of Ecology 96: 698-702.

Turner BL, Brenes-Arguedas T, Condit R (2018) Pervasive phosphorus limitation of tree species but not communities in tropical forests. Nature 555: 367.

Valverde-Barrantes OJ, Raich JW, Russell AE (2007) Fine-root mass, growth and nitrogen content for six tropical tree species. Plant and Soil 290: 357-370.

Valverde-Barrantes OJ, Freschet GT, Roumet C, Blackwood CB (2017) A worldview of root traits: the influence of ancestry, growth form, climate and mycorrhizal association on the functional trait variation of fine-root tissues in seed plants. New Phytologist 215: 1562-1573.

Vitousek PM (1984) Litterfall, nutrient cycling, and nutrient limitation in tropical forests. Ecology 65: 285-298.

Vitousek PM, Sanford Jr RL (1986) Nutrient cycling in moist tropical forest. Annual Review of Ecology and Systematics 17: 137-167.

Vose P (1982) Iron nutrition in plants: a world overview. Journal of Plant Nutrition 5: 233-249.

Wang Z, Yu K, Lv S, Niklas KJ, Mipam TD, Crowther TW, Umaña MN, Zhao Q, Huang H, Reigh PB (2019) The scaling of fine root nitrogen versus phosphorus in terrestrial plants: A global synthesis. Functional Ecology 33:2081-2094.

White PJ, Broadley MR (2003) Calcium in plants. Annals of Botany 92:487-511.

White PJ, Hammond JP (2008) Phosphorus nutrition of terrestrial plants. The Ecophysiology of Plant-Phosphorus Interactions. Springer.

Wilcoxon F (1945) Individual comparisons by ranking methods. Biometrics Bulletin 1: 80-83.

Wright IJ, Reich PB, Westoby M, Ackerly DD, Baruch Z, Bongers F, Cavender-Bares J, Chapin FS, Cornelissen JH, Diemer M (2004) The worldwide leaf economics spectrum. Nature 428:821.

Wright SJ (2019) Plant responses to nutrient addition experiments conducted in tropical forests. Ecological Monographs 84: e01382.

Wright SJ, Turner BL, Yavitt JB, Harms KE, Kaspari M, Tanner EVJ, Bujan J, Griffin EA, Mayor JR, Pasquini SC, Sheldrake M, Garcia MN (2018) Plant responses to fertilization experiments in lowland, species-rich, tropical forests. Ecology 99:1129-1138.

Wu Z (1995) An Introduction to the Tropical Forest Soils and Effect of Shifting Cultivation on Soils in Jianfengling, Hainan Island. In: Q Zeng, G Zhou, L Yide, Z Wu, B Chen (eds) Researches on Tropical Forest Ecosystems in Jianfengling of China. China Forestry Publishing House, Beijing, China.

Wurzburger N, Wright SJ (2015) Fine-root responses to fertilization reveal multiple nutrient limitation in a lowland tropical forest. Ecology 96:2137-2146.

Xu H, Detto M, Fang S, Li Y, Zang R, Liu S (2015) Habitat hotspots of common and rare tropical species along climatic and edaphic gradients. Journal of Ecology 103:1325-1333.

Yruela I (2005) Copper in plants. Brazilian Journal of Plant Physiology 17:145-156.

Zeng Q (1995) Survey of Water-Heat Condition and Vegetation Ecological Series in Jianfengling. In: Q. Zeng G. Zhou, L. Yide, Z. Wu & B. Chen (eds) Researches on Tropical Forest Ecosystems in Jianfengling of China. China Forestry Publishing House Beijing China

Zhang SB, Zhang JL, Slik JF, Cao KF (2012) Leaf element concentrations of terrestrial plants across China are influenced by taxonomy and the environment. Global Ecology and Biogeography 21:809-818.

Zhu B, Gutknecht JL, Herman DJ, Keck DC, Firestone MK, Cheng W (2014) Rhizosphere priming effects on soil carbon and nitrogen mineralization. Soil Biology and Biochemistry 76:183-192.

Zimmer W, Mendel R (1999) Molybdenum metabolism in plants. Plant Biology 1:160-168.

PART 2: Root morphology in relation to the fungal microbiome

CHAPTER 4: Root-associated fungal communities are structured more by environment than plant-host functional traits in a Chinese tropical forest

Key message

The soil environment acts as a first, higher-order filter for root-inhabiting fungal communities in tropical forests. In addition, root architecture and tissue chemistry secondarily relate to root-inhabiting fungal assemblages, further structuring fungal community composition.

Abstract

In forests, soil and root environments are complementary environmental filters that structure the communities of root-associated fungi of host trees. The relative roles of the soil environment, root functional characteristics, and plant host identity in structuring root-associated fungal assemblages are not entirely understood. We examined how root-fungal composition is influenced by variation in soils, root morphology, and tissue elemental concentrations. We collected 450 root systems from 150 host trees of 66 species across three plots of varying soil environment and forest successional status in tropical forests of Xishuangbanna, China. Root functional traits were analyzed from scanned images, and root tissue chemistry was analyzed. Arbuscular and ectomycorrhizal fungal ITS2 was amplified and sequenced via next-generation sequencing, and host-plant identity was verified via Sanger sequencing of plant rbcL. Distance-based redundancy analysis and hierarchical partitioning of predictors were employed to quantify the relative importance of two soil variables (site average total and available phosphorus), four root functional traits (root dry matter content, root tissue density, specific root tip abundance, and the number of root system forks), and three root tissue elemental concentrations (root calcium, nitrogen, and manganese) on root-associated fungal community dissimilarity. The collective soil and root system environment explained 23% of the variation in root-associated fungal Bray-Curtis dissimilarities. Hierarchical variation partitioning showed that soil variables explained 76% of that variation, while root functional traits and root tissue elemental concentrations

collectively explained the remaining 24%. Twenty fungal taxa were instrumental in driving root-associated fungal dissimilarity, with patho-symbiotrophic and strictly symbiotropic guilds associating with roots in secondary forests and sapro-symbiotropic taxa associating with primary forest tree roots. We used multiple regression of distance matrices (MRM) to evaluate the added explanatory power host-species phylogenetic distance, which revealed similar explanatory ability of plant phylogenetic identity as root functional traits, thereby only slightly improving MRM fit. We further explore the non-linear relationships of root-inhabiting fungal communities to the multifaceted soil and root environment. Our results show that soils dominate the environmental structuring of fungal taxa across landscapes. However, root functional traits, principally an architectural tradeoff between dense, highly-branched root systems vs. less-dense, herringbone root systems, and tissue calcium concentrations, are also important determinants of fungal compositional variation among host trees.
Keywords: root-associated fungi, mycorrhizae, root functional traits, root tissue chemistry, ITS2, tropical forest, Xishuangbanna

Introduction

Modern-day relationships of plants and their root-associated fungi span the breadth of known biological interactions among species from parasitic to mutualistic, and all forms in between (e.g., commensiality, etc., Smith & Read, 2010; van der Heijden *et al.*, 2015). One of the significant evolutionary leaps that led to the diversification of land plants was the development of root systems colonizable by fungi (Kenrick & Strullu-Derrien, 2014; Strullu-Derrien *et al.*, 2016). Fungal colonization of root systems occurred concurrently with root system development, and the ability of plants to harbor fungi has been crucial to the terrestrial radiation and dominance of plant life over the last several geological eras (Brundrett, 2002). Nowhere are the consequences of such an intertwined evolutionary dance between plant roots and fungi more visible than in hyperdiverse tropical forests, where high levels of plant and fungal diversity can be found interacting to influence forest community and ecosystem processes (e.g., Lovelock & Ewel, 2005; Peay *et al.*, 2013; Sarmiento *et al.*, 2017; Corrales *et al.*, 2018).

Thus, interactions between fungal function (e.g., nutrient acquisition) and host tree root systems have shaped root form (e.g., root diameter or topology) (Hetrick, 1991; McCormack & Iversen, 2019). For example, a fundamental axis of root functional trait variation, the root system fungal-collaboration gradient, describes a tradeoff between thin diameter, long roots with thin root cortical areas that acquire nutrients primarily by themselves, and thicker, shorter roots, with large root cortical volumes that acquire nutrients via mycorrhizal outsourcing (Chen et al. 2016, Ma *et al.*, 2018; Bergmann *et al.*, 2020). In this light, the entire length of absorptive roots (those < 2mm in diameter, on average), especially root systems tips, can be considered distinct habitats that harbor separate assemblages for root symbionts, much like how individual sites can harbor distinct assemblages of organisms which are subsets of the greater regional species pool in metacommunity theory (Leibold *et al.*, 2004; Leibold & Chase, 2018). Within this framework, and because fungi are largely dispersal-limited to varying degrees (Peay *et al.*, 2010a; Peay *et al.*, 2010b), soils and roots can be viewed as successive environmental filters that structure root-associated fungal assemblages.

Separating the effects that soils have on structuring fungal communities, the environmental filtering of tree species, and the interaction between the two has proven difficult. For example, in the western Amazon, soil type (e.g., terra firme vs. white sands) is a principal driver of fungal community structure (Peay *et al.*, 2013). Soil type also drives environmental filtering of tree communities from the regional species pool (Fine & Kembel, 2011, Baraloto *et al.,* 2021). Furthermore, fungal and tree diversity are correlated across gradients in soil type, pointing to intricate linkages between the soil environment, the composition of the tree community, and plant-fungal interactions (Peay *et al.*, 2013). Many other studies have shown that the soil environment in tropical forests has a strong effect in structuring tree-fungal community associations (Gourmelon *et al.*, 2016; Essene *et al.*, 2017; Weemstra *et al.*, 2020); however, it is not well known how root functional (i.e., morphological, and chemical) traits modulate such interactions. Additionally, many of the studies that evaluate how root morphology and root-associated fungal communities co-vary with variation in soil habitat often do so at a functionally coarse resolution, either classifying taxa generally as ectomycorrhizal (ECM) vs.

arbuscular mycorrhizal (AM) or by using indirect measures of root functional traits (e.g., those from trait databases).

We endeavored to link root functional traits to variation in root-associated fungal communities at the individual tree level in southwest China's tropical forest of the Xishuangbanna region. Measuring root morphology, chemistry, and fungal assemblages of entire root systems and linking them to plot-level measurements of soils, for three forest plots of varying forest age and tree composition, we asked:

1) *How do root functional traits and root tissue chemistry vary among the tree forest plots?*

Root systems of tropical saplings were more acquisitive (i.e., decreased diameter and increased specific root length and branching intensity) in secondary than in primary forest of a tropical forest on Hainan Island, China (Hogan *et al.,* 2020, Chapter 1). They also had tissue chemistry that was variable with the soil environment in primary and secondary forests (e.g., increased root phosphorus content with increasing soil available phosphorus content (Hogan *et al.,* 2021, Chapter 2). Thus, we expected similar trends in root functional traits and tissue chemistry here.

2) *How do root morphology and chemistry vs. soil environment influence fungal richness, diversity, and evenness of root-associated fungi?*

We expected fungal diversity and richness to relate to root morphological complexity positively (e.g., the number of root tips or root branching intensity) (Kong *et al.*, 2019). Moreover, more diverse assemblages of mycorrhizae could decrease the need for plants to forage for nutrients using roots per the 'do it yourself' root strategy (Bergmann *et al.,* 2019) and hence be associated with narrower root system diameters or lower specific root length (SRL).

3) *How do root functional traits, root chemistry, and the soil environment shape the composition of root-associated fungi? What are their relative strengths?*

Recent studies have shown that soils control fungal community composition more than plant hosts (Essene *et al.*, 2017; Weemstra *et al.*, 2020). We, therefore, anticipated strong effects of soil environment, outweighing effects of species and their functional traits. However, we expected distinct assemblages among AM and ECM hosts, which

should relate to functional tradeoff in root morphology (e.g., root tissue density – RTD, or root system topology).

4) *What fungal taxa and functional guilds drive differentiation in root-associated communities across plots and among tree root systems?*

Tree root system associations with arbuscular mycorrhizal and saprophytic fungi dominate tropical forests, especially in older, well-developed stands (Janos, 1980; Muthukumar et al., 2003a; Alexander & Lee, 2005, Soudzilovskaia et al., 2019); however, ectomycorrhizal tree roots present unique fungal niches (Corrales *et al.* 2003). Thus, discriminating taxa among sites should reflect differences in root-host preference for arbuscular vs. ectomycorrhizal taxa.

5) *Does plant lineage, a surrogate for the evolved root-mycorrhizal symbiosis, structure fungal community composition?*

Many of the most important root functional traits to root economical tradeoffs (e.g., RTD, SRL) are highly phylogenetically structured (Valverde-Barrantes *et al.*, 2017). Furthermore, concerning all plant taxa, significant differences in how root traits optimize and compensate for influencing root strategies exist among woody and non-woody plants (Ma *et al.*, 2018), with the deeper nodes in the Angiosperm phylogeny driving variation in root functional traits among woody Angiosperms (Liu *et al.*, 2019). Therefore, we expected traits to be as good as phylogenetic relatedness in explaining root-associated fungal community variation.

Materials and Methods

Study sites

We sampled trees from three plots in the Xishuangbanna tropical forest region of southwestern China. The forest is classified as a lowland tropical seasonal rainforest, with >5000 plant species (Cao *et al.*, 2006). The forest has a complex forest structure, reaching canopy heights of up to 60 m with tree biomass ranging between 170 and 690 Mg ha^{-1}, and is dominated by large *Terminalia myriocarpa*, *Pometia tomentosa*, *Antiaris toxicaria*, *Pouteria grandifolia*, *Canarium album* and *Shorea wangtianshuea* trees (Zhang & Cao, 1995; Zheng *et al.*, 2006). Precipitation averages between 1200 and 2500 mm $year^{-1}$ and is strongly seasonal with a distinct wet season between May and October,

during which 80% of the annual rainfall occurs (Cao et al., 2006). Temperatures range from 15.1 to 21.7 °C and never freeze. The soils of tropical seasonal rainforests in Xishuangbanna are typically latosols (brown and yellow tropical earth soils), derived from siliceous bedrock and with deep solum and humus horizons (Cao et al. 2006). They are characterized by high (56%) clay content, poor permeability, and pH values between 4.5 and 5.

In the Xishuangbanna region, forests are heavily utilized for their ecosystem services. For example, harvesting wild fungi for market sale is common and widespread (McLellan & Brown, 2017). Additionally, there has been a proliferation of monoculture rubber (*Hevea brasiliensis*) plantations throughout the region over the last several decades (Li *et al.*, 2008; Chen *et al.*, 2016). This has led to declines and pervasive fragmentation of natural tropical forest areas in the region. We selected plots of varying forest successional status and past land-use history to capture a broad gradient in environmental conditions at the site. We chose three Chinese Ecological Research Network (CERN) plots near Xishuangbanna Tropical Botanical Garden (XTBG). The first plot (0.5 ha area) was located within the grounds of the XTBG. This was a secondary forest of approximately 60 years of age situated adjacent to and surrounded by a rubber plantation. Two plots were located in a nearby conservation area. One was a secondary forest of approximately 60 years age, also (0.5 ha area); the other (1 ha area) was a primary, old-growth forest with unknown age, but no history of past last use. We refer to the three plots as secondary near rubber plantation, secondary evergreen, and rainforest, respectively.

The sampling of fine root systems

Root systems were collected from previously tagged and identified individual trees within the plots. We targeted trees of known taxonomic identity from the Anacardiaceae, Annonaceae, Burseraceae, Clusiaceae, Ebenaceae, Euphorbiaceae, Fagaceae, Juglandaceae, Lauraceae, Lecythidaceae, Moraceae, Myristicaceae, Myrsinaceae, Pittosporacaeae, Polygalaceae, Rutaceae, Sapindaceae, and Ulmaceae. These families represent the breadth of evolutionary histories across the Angiosperm phylogeny to maximize the range of variation in root functional traits, which are

phylogenetically conserved (Valverde-Barrantes *et al.*, 2017). Lateral roots were traced-out and carefully excavated by hand from target trees to their most delicate first-order root tip. Root material was transported back to the lab in plastic bags and stored in a refrigerator until processed. Finally, root samples were washed and delineated into entire root systems (sensu McCormack *et al.,* 2015) by trimming them at the fourth-order transportive root. Thus, our morphological analyses pertain to the first three orders of the fine root system (diameters ≤ 2mm).

Soil measurements

We characterized the soil environments of each of the three permanent forest plots using data from routine soil sampling that is carried out as part of the CERN program (Pan et al. 2019). A total of 72 soil samples were used to characterize the soil environment of each of the three forest plots. Soil samples were collected during the 2010 and 2015 calendar years (n = 36 per plot per year). In each year, every two months from February to December, six samples were collected randomly within habitats (two per ridge, slope, and valley habitat) of each plot. Each sample was collected using a 100 cm^2 area (Ø 11.3cm) soil auger to a depth of 20 centimeters.

Soil samples were air-dried at room temperature, and the dried soil was passed through a 0.15mm (100 mesh) sieve. Dry soil was analyzed for soil organic carbon, soil total carbon, total nitrogen, soil total phosphorus, soil total potassium, available phosphorus. Soil organic carbon, total carbon and total nitrogen were measured using a VarioMAX organic elemental analyzer (Elementar Analysensysteme GmbH, Germany). Soil available phosphorus was extracted using a 0.03 mol l^{-1} NH_3F and 0.025 mol l^{-1} HCl solution. Total phosphorus and potassium were extracted using soil digestion with $HClO_4$–HF. Available phosphorus, total phosphorus, and total potassium were measured using an inductively coupled plasma atomic emission spectrometer (ICP-AES; Thermo Fisher Scientific USA).

We conducted a principal components analysis (PCA) of soil variables, and we tested for statistical differences in soil variables among plots using one-way analysis of variance with a Tukey HSD posthoc comparison between groups. The principal components analysis showed slight separation among sites, with axis 1 explaining almost

half (47.3%) of variation and being directly related to total soil N. Axis 2 explained 19.3% of the soil data variation and was related to total soil K (Fig. 1). Average soil nutrient concentrations were statistically different among plots for all seven variables considered (Table 1, $F_{(2,213)}$ ranging from 25.87-84.18, all $p < 0.001$). Tukey HSD groups were distinct among all three plots for soil organic matter – which was greatest in the secondary forest plot near the rubber plantation, total N – which was also greatest in the secondary forest plot near the rubber plantation, and available P – which was greatest in the primary rainforest. Tukey HSD groups for soil pH showed that the secondary forest plot near the rubber plantation had slightly more acidic soils than the other two plots. The secondary forest plot near the rubber plantation also had more available and total P than the other two plots (Table 1).

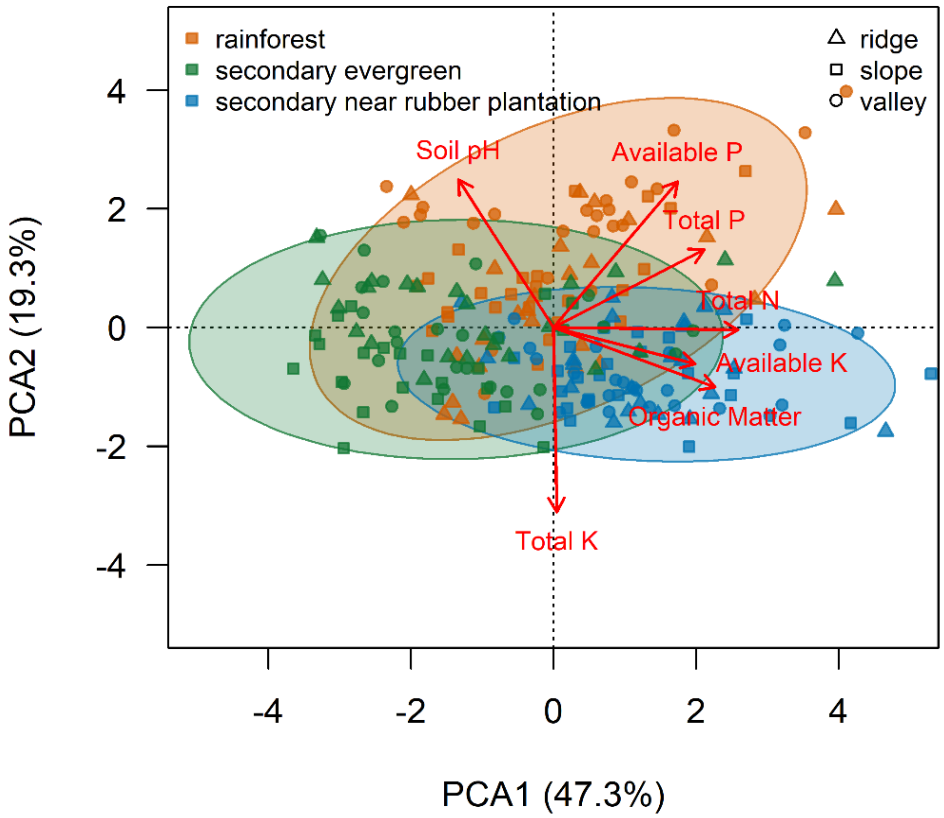

Fig. 1: Principal components biplot of the first two principal components using seven soil variables measured on ridge, slope, and valley habitats on each of the three study plots. Study plots were located near the Xishuangbanna Tropical Botanical Garden in Menglun, Mengla, Yunnan, China. Soil samples (n = 72 per plot) were collected in 2010 and 2015 randomly across plots by habitat (ridge, slope, and valley, see methods). Units for

organic matter, total N, total P, total K are g kg^{-1}, while available K and available P are in mg kg^{-1}. Colors represent each plot, while shapes represent habitats. Ellipses show 95% confidence envelopes.

We used averages of soil nutrients in our analyses (from n = 72 soil measurements per plot) because there were no records of spatial locations of soil samples relative to the coordinates of trees in the plots. Although plot averages obscure variability among habitats within plots, they generally represent landscape-scale variation in soil fertility among the three plots. Thus, the average soil conditions can be viewed as a first, higher-order environmental filter structuring root-inhabiting fungal communities, while the root systems themselves can be treated as individual sites from a metacommunity perspective.

Table 1: Mean (± standard error) soil properties for three small forest dynamics plots near the Xishuangbanna Tropical Botanical Garden in Menglun, Yunnan, China. Analysis of variance statistics given with associated p-values. Letters denote post-hoc Tukey HSD test groupings. P-values are denoted as follows: *ns* non-significant $p > 0.1$, ‡ marginally significant $p < 0.1$, * $p < 0.05$, ** $p < 0.01$, *** $p < 0.001$.

Plot	Soil pH	Organic Matter (g kg^{-1})	Total N (g kg^{-1})	Total P (g kg^{-1})	Total K (g kg^{-1})	Available P (mg kg^{-1})	Available K (mg kg^{-1})
Primary rainforest	4.41 ± 0.02^{b}	30.77 ± 0.76^{a}	1.99 ± 0.04^{b}	0.35 ± 0.01^{b}	8.42 ± 0.01^{a}	3.77 ± 0.17^{c}	66.36 ± 2.32^{a}
Secondary evergreen	4.42 ± 0.02^{b}	34.20 ± 0.97^{b}	1.60 ± 0.04^{a}	0.22 ± 0.01^{a}	8.61 ± 0.02^{a}	1.84 ± 0.12^{a}	62.17 ± 2.58^{a}
Secondary near rubber plantation	4.26 ± 0.02^{a}	41.95 ± 0.92^{c}	2.34 ± 0.04^{c}	0.33 ± 0.01^{b}	9.53 ± 0.01^{b}	2.78 ± 0.11^{b}	87.57 ± 3.07^{b}
F	$F_{(2,213)} = 26.25$	$F_{(2,213)} = 41.83$	$F_{(2,213)} = 76.45$	$F_{(2,213)} = 84.18$	$F_{(2,213)} = 20.27$	$F_{(2,213)} = 51.12$	$F_{(2,213)} = 25.87$
p	***	***	***	***	***	***	***

Root system functional trait measurements

Three entire root systems per tree were selected for subsequent morphological analysis and DNA amplicon sequencing of fungal communities. Root systems were massed (wet mass), then scanned using a double-sided optical scanner (EPSON in black and white at high resolution (600 dpi). Each root system was placed in an acrylic scanning tray, submerged in water, positioned flat, and scanned. Scanned images were

analyzed morphologically using WinRHIZO (2016 version, Regent Instruments, Quebec, Canada). The WinRHIZO software measures root morphology, returning data on average root diameter, root system length, area, and volume, and the number of root tips and forks. From these measurements and the root system dry mass, twenty-five root functional traits can be derived, of which fifteen are of chief importance (root system mass, root system average diameter, root system length, root system area, root system volume, root system length-to-volume ratio, the number of root tips, the number of root forks, RTD, root dry matter content – RDMC, root tip mass fraction – RTMF, SRL, specific root area – SRA, specific root tip abundance – SRTA and root branching intensity – RBI).

All first order root tips were removed from the root system, massed, and preserved in CTAB (cetyl trimethyl ammonium bromide) buffer. The remainder of the root system (root orders 2-4) was placed in an envelope and dried for several days to constant mass at 70°C in a drying oven. Dry root systems were massed (dry mass). The dry mass of the removed root tips was estimated using a regression of root system wet mass to dry mass ($y = 0.2853x$, $p < 0.05$, $R^2 = 0.77$, Fig. S1), and added to the measured root system dry mass to get an estimate of total root system dry mass.

Measurements of root tissue chemistry

For each sample, we used the remainder of the entire root system (containing root orders 2-4, but without the 1st-order root tips), which was dried following the scanning of root systems. Dried root sample replicates (n=3) were pooled by individual, and the finest roots (<2 mm diameter) were placed into sterile 5 mL propylene screwcap vials. Samples were homogenized into a fine powder using a Fisher Beadmill 24 multi-sample homogenizer (Fischer Scientific, USA) using 5mm stainless steel beads over multiple 30-second cycles at high speed. Prior to homogenization, stainless steel beads were sterilized with ethanol to prevent sample contamination.

Homogenized samples were sent to the Plant Analysis Lab at Louisiana State University, where tissue macronutrient concentrations for 15 elements were measured (following the methods in Jones Jr, 2001). Roughly 500 mg of each homogenized tissue sample was digested in 2.2 mL of deionized water using 5 mL concentration Nitric Acid.

The sample solution was heated for 2.75 hours at 125 °C. Following heating, 3 mL hydrogen peroxide was added. The solution was cooled and filled to a volume of 20 mL with deionized water. Elemental concentrations of aluminum (Al), boron (B), calcium (Ca), carbon (C), copper (Cu), iron (Fe), magnesium (Mg), manganese (Mn), molybdenum (Mo), nitrogen (N), sodium (Na), phosphorus (P), potassium (K), sulfur (S) and zinc (Zn) of the solution were measured using inductively-coupled plasma optical emission spectroscopy (Avio 500 ICP-OES , Perkin Elmer, Waltham, MA USA). Tissue concentrations of Mo were mostly below their detectable range, so they were not included in analyses.

Sequencing of root fungal communities

Root tips preserved in CTAB were frozen until processed at the Department of Plant Pathology at the University of Florida (see Fig. S2). To homogenize samples and maximize DNA extraction, we heated samples in a 65°C water bath for 2 hours then bead beat samples at 1500 rpm for 3-5 minutes with 3 sterile stainless-steel ball bearings in each sample vial using a Mini-G 1600 tissue homogenizer (SPEX Sample Prep, Metuchen, NJ). Samples were frozen once more, then prior to DNA extraction, thawed in a 65°C water bath for 1 hour. CTAB from homogenized samples was pooled from root system replicates (n=3) of individual trees in equal proportions (1 mL per replicate), and DNA extraction was done using the glass milk method on 100 µL of the pooled CTAB sample (see Methods S1).

The fungal ITS2 (nuclear ribosomal Internal Transcribed Spacer 2) region was amplified from 1:10 diluted DNA extracts using a primer mix that consisting of equal parts of the fITS7 and fITS7o forward primers (Kohout *et al.*, 2014) and ITS4 reverse primer (Kohout *et al.*, 2014, see Table S1 for primer sequences). This primer combination has been shown to amplify both ectomycorrhizal and arbuscular mycorrhizal fungi (Lekberg *et al.*, 2018). Primers included the Illumina NextGen adapters. Polymerase chain reaction (PCR) was used to amplify fungal ITS sequences. In certain cases, PCR was repeated using different concentrations of DNA extracts and/or pvp (polyvinylpyrrolidone) to reduce PCR inhibition. PCR products were verified with electrophoresis gels. PCR products were cleaned, quantified, and pooled to equimolar

concentrations and Illumina sequencing identifiers were applied in a second PCR reaction. Fungal ITS2 amplicons were sequenced on an Illumina MiSeq (2 × 300 bp reads).

Sequences were processed using the AMPtk bioinformatics pipeline (Palmer *et al.*, 2018). Forward and reverse reads were demultiplexed, merged and quality checked. Poor quality reads were filtered out, sequences were dereplicated and operational taxonomic units (OTUs) were assigned via clustering, using a 97% identity threshold. Then, sequences were chimera-filtered and mapped back to assigned OTUs and an OTU abundance table was created. AMPtk is unique in its ability to look for, identify and correct for index-bleed (Palmer *et al.*, 2018), by using a non-biological synthetic mock community of ITS sequences (SynMock). Thus, index-bleed was identified, and corrected for in a two-step (standardization and substitution filtering) process. Finally, sequences were blasted against all know ITS2 sequences in GenBank, and fungal taxonomy was assigned using GenBank and fungal classification was done using the FunGuild database (Nguyen *et al.*, 2016).

Sequencing of plant DNA

To verify the taxonomic identity of plant roots that were collected and preserved in CTAB, we sequenced the coding region of the rbcL marker of the Chloroplast plastid in all samples for which we sequenced fungal ITS2 (Kress & Erickson, 2007, see Table S1 for primer sequences). We used Sanger sequencing to identify rbcL sequences and blasted them against rbcL sequences for trees from Xishangbanna (Huang *et al.*, 2015, GenBank accession numbers KR528589-KR534171), using a 98% similarity threshold. Considering commonly used genetic markers for plant identification, Huang *et al.* (2015) found that rbcL was most-readily amplified genetic marker, although it only has genus resolution for the tree species in XTBG. Therefore, if the rbcL sequence blasted within the genus of field identification, we considered it a match. Only matched samples were used in further statistical analyses, leaving a dataset with 150 individual trees from 66 plant species comprising 18 plant families (see Fig. S15). Twelve of the 66 species are ectomycorrhizal, from the Fagaceae or Juglandaceae families. The primary rainforest plot and the secondary forest near the rubber plantation each had four ECM individual

trees sampled (7% and 10% of trees sampled, respectively), while the secondary evergreen plot had 18 ECM trees sampled (41% of trees sampled).

Statistical analyses – forward selection of variables

Variable reduction is a first step in analyses that consider relationships with a large number of environmental variables (Legendre & Legendre, 2012). We chose forward selection (Blanchet *et al.*, 2008) to reduce the number of variables to a manageable set. This procedure uses two stopping criteria (an alpha stopping criteria of statistical significance of predictors, and the adjusted model coefficient of [multiple] determination) to choose the best set of unrelated explanatory variables. We applied the forward selection to a Hellinger-transformed site × OTU matrix. The Hellinger transformation gives less weight to lower abundance taxa and is appropriate for dataset with skewed abundances or double absences, both of which pertain to speciose OTU matrices (Legendre & Gallagher, 2001). We considered the seven measured soil variables (soil organic matter, total N, total P, total K, available P, available K, and pH), 15 root functional traits (mass, average diameter, length, area, volume, length-to-volume ratio, tips, forks, RTD, RDMC, RTMF, SRL, SRA, SRTA and RBI), and fourteen root tissue elemental concentrations (Al, B, Ca, C, Cu, Fe, Mg, Mn, N, P, K, Na, S, and Zn) as explanatory environmental variables. The forward was implemented using the 'forward.sel' function in the 'adespatial' R package (Dray *et al.*, 2018) using 49999 permutations. Following forward selection, we compared functional traits and root tissue elemental concentration for selected variables among plots using one-way analysis of variance with a Tukey HSD post-hoc comparison between groups. We also assessed each set of environmental variables separately using principal components to check orthogonality (i.e., independence) of forward selected variables.

The forward section of variables identified nine independent environmental parameters that most related to variation in the Hellinger-transformed site × OTU matrix (Table S2). Those included two soils variables at the plot level – average available and total soil P content, four root functional traits – RDMC, SRTA, the number of root forks, and RTD, and three root tissue elemental concentrations – root N, Ca, and Mn.

Collectively, these variable explained about 18% of compositional differences in root-associated fungal communities (Table S2). Coefficients of determination from forward-selection were 0.07 and 0.05 for soil available P and soil total P, respectively. The four forward selected root functional traits were similar in their strength of selection, having coefficients of determination near 0.01. Root tissue elemental concentrations for N, Ca, and Mn had had coefficients of determination < 0.01 (Table S2).

Statistical analyses –root functional traits, fungal richness, diversity, and evenness in relation to environment

We compared the forward selected root functional traits and tissue chemistry concentrations from 450 root systems of 150 individual trees using single factor (i.e., one-way) analysis of variance, followed by a Tukey HSD post-hoc comparison between plots. For each community of fungi sequenced for each individual tree, we computed species richness, Shannon's diversity (H`) (Shannon, 1948), and Pileou's species evenness (J`) (Pielou, 1966). Analyses of variance, followed by a Tukey HSD post-hoc comparisons, were conducted to compare richness, diversity, and evenness across the three plots. We used ordinary least-squares regressions to analyze relationship between the nine forward selected environmental variables (soil available P, soil total P, RDMC, SRTA, root system forks, RTD, root N, root Ca and root Mn) and H`, richness and J`.

Statistical analyses – distance-based redundancy analyses and hierarchical partitioning of predictor variables, and generalized additive models for environmental variables

To examine the relative influence of root functional traits, root tissue chemistry, and soil nutrient status on root tip fungal composition we used multivariate distance-based redundancy analysis (db-RDA, Legendre & Anderson, 1999). db-RDA is a form or constrained (i.e., canonical) ordination, which evaluates the strength of environmental variables, as linear predictors, on a multivariate distance matrix (e.g., fungal community compositional dissimilarities) (Ter Braak, 1994; Legendre & Anderson, 1999; Legendre & Legendre, 2012). The method takes a site by species distance matrix and extract eigenvector scores from a principal coordinates analysis that are used as multivariate composition models in relation to environmental predictors at the site level. For the db-RDA, we used a Hellinger-transformed fugal ITS2 OTU matrix and the Bray-Curtis

distance measure (Bray & Curtis, 1957). The nine forward-selected environmental variables were z-score transformed (i.e., subtracted by their mean and divided by their standard error), prior to the analysis. The db-RDA was statistically evaluated using analysis of variance, where we tested the significance of the entire model, each of the constrained ordination axes, and the terms of the model, separately. The db-RDA was implemented using the 'capscale' function of the vegan R package (Oksanen *et al.*, 2020).

Next, we used a newly-developed extension of variation partitioning (Peres-Neto *et al.*, 2006; Legendre & Legendre, 2012) called hierarchical partitioning, which allows for the variation partitioning of more than three predictor variables (or sets of predictor variables, Lai *et al.*, 2021). The method extends commonality analysis to evaluate the importance of predictors (and all possible combinations of predictors) in a multivariate multiple regression (i.e., db-RDA) framework (Lai *et al.* 2021). Using variation partitioning, the method calculates the overall importance of each of the environmental predictors based upon the unique contribution of that variable and all possible combinations of shared fractions with other covariates. This is an advancement in variation partitioning, because previously the method was limited to three individual variables or sets of variables. Notably, the number of fractions in a variation partitioning (including shared fractions), increases exponentially with the number of predictors (i.e., is equal to 2^n-1). Thus, although the method is highly useful, there are many shared factions that can have values near zero or even slight negative, which can make their interpretation, by themselves, difficult. Thus, we focus on the overall importance of the nine forward-selected variables, which includes the effects of shared fractions.

One of the limitations of db-RDA is that it can only examine unimodal, linear relationships between the multivariate response matrix (i.e., the Bray-Curtis dissimilarities in root-associated fungal communities) and the environmental predictors, akin to a multivariate multiple linear regression. Oftentimes, environmental variables may have non-linear relationships to community dissimilarities, because of the nature of how species abundances respond to environmental gradients (e.g., via indirect interactions of species) (Clark *et al.*, 2020). One potential solution is to include squared and cubed predictors of environmental predictors in the db-RDA to allow for non-linear

responses (e.g., Legendre *et al.*, 2009), however this is a less than ideal workaround. To directly assess the nature of how each forward-selected environmental variable was related to root-associated fungal-community dissimilarity, we used generalized additive models (GAMs). The method fits a smooth surface of the predictor variable to the constrained ordination (i.e., db-RDA) space using penalized thin plate regression splines (Wood, 2003) via a single parameter GAM. The form of the GAM has one smooth term and one linear term. The flexibility of the smooth is defined by the effective degrees of freedom (edf), with edf equal 1 representing linear relationships, 2 representing quadratic relations, 3 representing a cubic relationship, and so on. We fit GAMs using the 'ordisurf' function in the vegan R package (Oksanen *et al.*, 2020), which calls 'gam' from mcgv package that estimates the smoothness of model terms is estimated as part of fitting (Wood, 2011). The statistical significance of the linear term and smooth terms are tested with a t- and F-test, respectively. To visualize GAM fits, we plotted model surface contours onto the constrained ordination space.

Statistical analyses – similarity percentages for discriminating taxa

To identify which taxa were driving community dissimilarity among the three plots, we calculated the similarity percentages (i.e., SIMPER, Clarke, 1993) among plots. Because site effects greatly outweighed tree species effects in structuring fungal community composition, we used plot as the grouping variable rather than root species identity. The SIMPER procedure calculates the average contribution of each species to the average pairwise dissimilarity among groups (i.e., plots in our case). It then identifies the most important species for each pairwise comparison among groups. These species represent the most abundant or most variable OTUs which account for at least 70% of the compositional difference among groups. We first removed OTUs that contributed to <1% of total reads and used 9999 permutations. To test the statistical significance for abundances of OTUs identified by the SIMPER analysis, we used the non-parametric Kruskal-Wallis rank-sum test for each pairwise comparison. We adjusted p-values from the Kruskal-Wallis test for false discovery rate (Benjamini & Hochberg, 1995).

Statistical analyses – assessing the role of plant lineage; multiple regression of distance matrices and phylogenetic signal analysis of root functional traits and tissue elemental concentrations

To evaluate the effect of tree species relatedness (i.e., phylogenetic lineage) on the fungal community composition of fine root samples we analyzed, we used multiple regression on distance matrices (MRM, Lichstein, 2007). MRM is advantageous because it allows for the unfolding (i.e., collapsing) of matrices into vectors prior to doing multiple linear regression. This allows for the inclusion of a wide variety of multivariate or distance based-predictors (e.g., a phylogenetic distance matrix). A phylogeny for the 66 tree species from which we sampled root systems was generated using the V.PhyloMaker package using the GenBank Open Tree of Life backbone (Smith & Brown, 2018, see Fig. S15). We constructed the same model that was used in the db-RDA analyses, then added the pairwise phylogenetic distances (PD) of the plant species for which the sequenced root samples belonged to as an additional covariate. We compared the strength of each of the predictors, their statistical significance, and their contribution to the overall model fit between the MRM without and with PD.

Lastly, to supplement the MRM and determine the degree of overlap in explanatory ability of root functional traits and tissue element concentrations, we tested for phylogenetic signal in root functional traits and root tissue elemental concentrations. We used average root functional trait values for species across all three plots (n = 450 entire root systems collected from 150 individual trees of 66 species), and compositely ground fine-root elemental concentrations (n = 150 from 66 species) Bloomberg's K (Blomberg *et al.*, 2003) and Pagel's λ (Pagel, 1999) were computed using the 'phylosig' function in the phytools R package (Revell, 2012). Statistical probabilities are derived from randomization and bootstrapping in the case of Bloomberg's K and likelihood ratio tests for Pagel's λ.

All statistical analyses were carried out in R 4.0.5 (R Core Team, 2021).

Results

Root functional trait and tissue chemistry differences among plots

Basic trends in the forward-selected root functional traits and tissue elemental concentrations showed that four of seven traits (RDMC, Forks, STRA, and root Ca) differed significantly among plots, one trait (RTD) was marginally different, and two traits (root N and Mn) were not statistically different (Table 2). RDMC in the secondary forest plot near the rubber plantation was less than RDMC in the other two plots. The number of forks in sampled root systems was greater in the primary forest plot than in the secondary evergreen forest plot, with the secondary forest plot near the rubber plantation being equal to them both. RTD was lower in the secondary evergreen forest than in the other two plots. SRTA was greater in the primary and secondary evergreen forest plots than in the plot near the rubber plantation. Lastly, root Ca was greatest in the primary forest, but root N and Mn showed no statistical difference (Table 2). The four forward-selected root functional traits roughly represented a tradeoff along in root architectural strategy (i.e., along axis 1 of the PCA, Fig. S3), however they had variable contributions to the first three principal components (Table S3). The three forward-selected root tissue elements were arranged at varying angles within the root tissue chemistry ordination space, with root N and Ca roughly being opposed to each other and root Mn arranged somewhat orthogonally. They also had varying contributions along the first three components, with root Ca contributing substantially to PC2 and root N contributing substantially to PC3 (Table S4).

Table 2: Average fine root system functional trait values and tissue elemental concentrations for 450 root systems of 150 individual trees collected across three small forest dynamics plots near the Xishuangbanna Tropical Botanical Garden in Menglun, Mengla, Yunnan, China. Analysis of variance statistics given with associated p-values. Letters denote post-hoc Tukey HSD test groupings. P-value notation follows Table 1.

Plot	N root systems	RDMC (mg g^{-1})	Forks	RTD (g cm^{-3})	SRTA (tips g^{-1})	Root Ca (%)	Root N (%)	Root Mn (mg kg^{-1})
Primary rainforest	186	310.5 ± 4.3[b]	272 ± 33[a]	0.367 ± 0.009[b]	2186 ± 175[a]	0.70 ± 0.05[b]	0.99 ± 0.07[a]	164.03 ± 13.93[a]
Secondary evergreen	138	307.2 ± 4.9[b]	502 ± 38[b]	0.362 ± 0.011[a]	3016 ± 204[a]	0.22 ± 0.06[a]	1.13 ± 0.08[a]	140.29 ± 16.79[a]

Secondary near rubber plantation	126	285.6 ± 5.2[a]	293 ± 40[ab]	0.397 ± 0.012[b]	1659 ± 215[b]	0.35 ± 0.06[a]	1.14 ± 0.08[a]	174.72 ± 16.14[a]
F		$F_{(2,447)}$ = 8.11	$F_{(2,447)}$ = 11.70	$F_{(2,447)}$ = 2.69	$F_{(2,447)}$ = 10.88	$F_{(2,147)}$ = 18.93	$F_{(2,147)}$ = 1.37	$F_{(2,147)}$ = 1.14
p		***	***	‡	***	***	*ns*	ns

Root-associated fungal richness, diversity, and evenness

We sequenced a total of 5771 fungal OTUs from 102 fungal families on the roots of 150 trees from the three plots in Xishuangbanna. Based on the FUNGuild classification of ITS2 sequences, the most five most specious fungal families that emerged from sequencing were Glomeraceae (230 OTUs), Herpotrichiellaceae (104 OTUs), Mortierellaceae (89 OTUs) Clavariaceae (52 OTUs) and Agaricaceae (44 OTUs). One third (34) of the families included in root-associated fungal communities contained five or more OTUs. Shannon's diversity of root-associated fungi was different among plots ($F_{(2,147)} = 3.089$, $p < 0.05$), being greater in the primary rainforest plot than the secondary evergreen plot with the secondary forest near the rubber plantation being equal to them both (Fig. 2). Root-associated fungal species richness was greater in the two secondary forests than in the primary rainforest ($F_{(2,147)} = 6.028$, $p < 0.01$), however species evenness showed the inverse trend ($F_{(2,147)} = 13.440$, $p < 0.05$, Fig. 2).

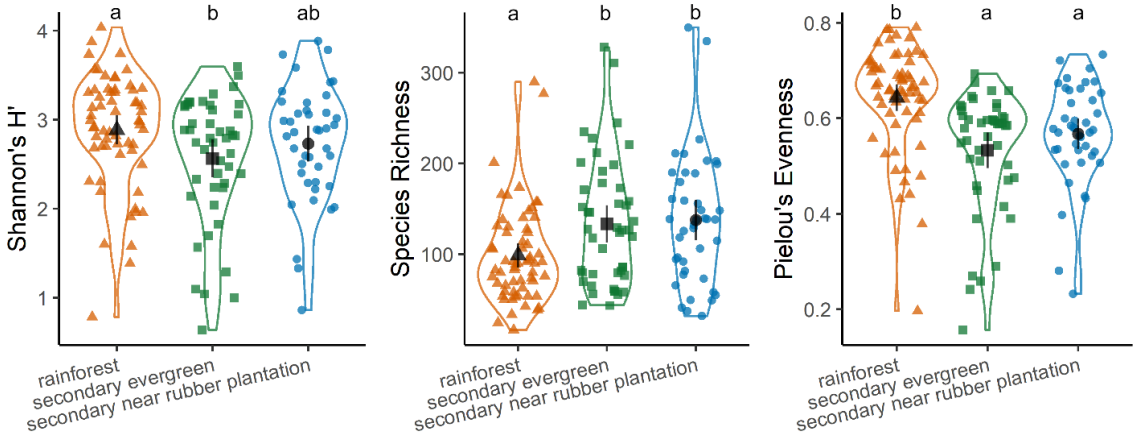

Fig. 2: Diversity (Shannon's H`), species richness, and evenness of Fungal ITS2 sequences from fine (1st order) root tips of 150 tropical Angiosperm trees of 66 species from three plots of varying successional status in Xishuangbanna, China. Diversity metrics for root-associated fungal communities for each tree are shown as points with

outlines showing violin (i.e., mirrored) densities. Black points and bars are means with 95% confidence intervals. Letters denote statistical grouping from Tukey HSD post-hoc tests.

Relationships fungal richness, diversity and evenness with the root and soil environment

Shannon's diversity of root-associated fungi increased with total and available soil P, decreased with RDMC, SRTA, the number of root system forks and RTD, and was unrelated to root tissue N, Ca, or Mn (Fig. S4, Table S5). Root-associated fungal species richness decreased with soil total and available soil P , RDMC, SRTA, the number of root system forks, RTD and root Ca (Fig. S5, Table S5). Fungal assemblage evenness showed the strongest linear relationships of the three diversity measures with any of the forward-selected variables. Evenness increased with total and available soil P and RTD, decreased with the number of root system forks, but was unrelated to the remaining five variables (RDMC, SRTA, and root N, Ca or Mn; Fig. S6, Table S5).

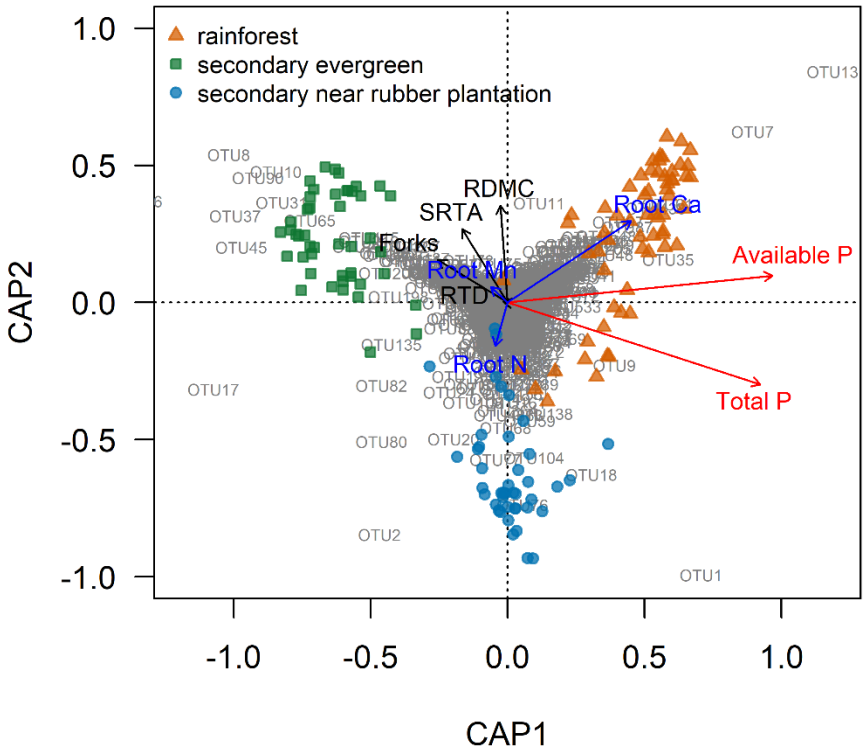

Fig. 3: Constrained ordination of fungal ITS2 read counts based on distance-based redundancy analysis (db-RDA) in relation to two soil variables (available and total soil phosphorus, P, shown in red), four root functional traits (number of root forks, root dry matter content – RDMC, root tissue density – RTD, and specific root tip abundance –

SRTA, shown in black), and three root tissue elemental concentrations (calcium – Ca, nitrogen – N, and manganese – Mn, shown in blue). Points are individual root systems of 150 trees, colored by collection plot. Species (i.e., OTU) scores in the multivariate space are plotted in gray. The scaling of the plot is symmetrical, meaning that both species and site eigenvalues are scaled to their square root. This preserves many of the features of the biplot (i.e., distance interpretation among sites and vector interpretation of environmental variables), without overemphasizing either site or species scores.

Soil and root environmental relationships with root-associated fungal composition

To understand how root-associated fungal compositional dissimilarity related to the soil and root environments, we used a db-RDA constrained ordination (Fig. 3). The db-RDA was statistically significant ($F_{(9,140)} = 4.57$, $p < 0.001$) and the constrained ordination axes explained 23% of the variation in root fungal community composition ($I_{total} = 62.07$, $I_{constrained} = 14.09$, $I_{unconstrained} = 47.79$). The first four constrained ordination axes were statistically significant (axis 1: $F_{(1,140)} = 19.30$, $p < 0.001$, axis 2: $F_{(1,140)} = 11.17$, $p < 0.001$, axis 3: $F_{(1,140)} = 2.77$, $p < 0.001$, axis 4: $F_{(1,140)} = 1.89$, $p < 0.005$), with the first two axes explaining three-quarters of the variation explained by the db-RDA (Fig. S7). Composition of individual tree root-associated fungal community clearly clustered by forest plot in the db-RDA, illustrating strong-site level differences (Fig. 3). All terms in the db-RDA were either statistically significant (soil available P: $F_{(1,140)} = 19.04$, $p < 0.001$; soil total P: $F_{(1,140)} = 10.67$, $p < 0.001$; RDMC: $F_{(1,140)} = 2.03$, $p < 0.001$; Forks: $F_{(1,140)} = 1.97$, $p < 0.01$; RTD: $F_{(1,140)} = 1.56$, $p < 0.05$, root Ca: $F_{(1,140)} = 1.72$, $p < 0.05$) or marginally significant (SRTA: $F_{(1,140)} = 1.37$, $p = 0.059$; root N: $F_{(1,140)} = 1.39$, $p = 0.054$; root Mn: $F_{(1,140)} = 1.36$, $p = 0.060$).

Accordingly, hierarchical partitioning of the environmental variables from the db-RDA revealed that average total and available soil P were the most significant contributors to constraining root-associated fungal community composition (Fig. 4). Plot averages for soil total and available P contributed 76% of the explanatory power of the environmental variables in the constrained ordination (Fig. 4). Of the forward-selected root functional traits and root tissue elemental concentrations, root Ca was the strongest predictor, explaining 8% of constrained inertia (i.e., db-RDA R^2), followed by the four root functional traits – RDMC, Forks, RTD, and SRTA, which each explained between 3

and 4 % of constrained inertia. Root N and Mn each contributed about 1% to explanatory power of forward selected variables in the db-RDA.

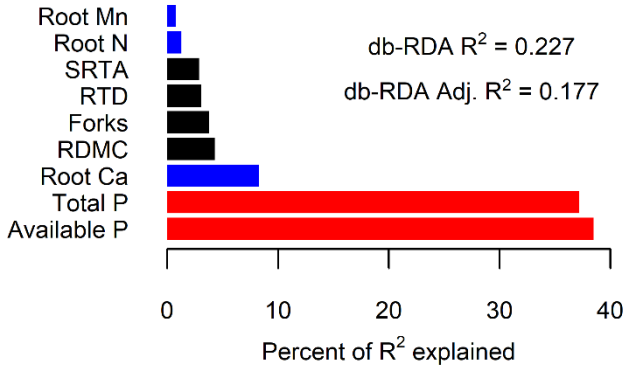

Fig. 4: (previous page) The relative contribution of soil variables, root functional traits and root chemistry to fungal ITS2 dissimilarity, based on hierarchical variation partitioning of variables included in db-RDA. Soil variables are shown in red, root functional traits are colored black, and root tissue elemental concentrations are colored blue.

We further investigated how environmental predictors were related to root associated fungal community dissimilarities using GAMs and by plotting the fitted surfaces of the variables over the constrained ordination space (Fig. 5). The linear terms of the GAMs were statistically significant for all nine forward-selected variables, and the smooth terms were significant for all terms except for root tissue N and Mn (Table 3). The intercept for the linear term gives the average value for the environmental co-variate across root associated-fungal assemblages for all 3 plots. Fitted surfaces for the environmental variables were close to linear (edf near 1) for SRTA and the number or root system forks (Fig. 5D, E, Table 3), meaning roughly monotonic increases in these root functional trait measures across the fungal assemblages of roots in the three plots. Root tissue N and Mn concentrations had smooth terms with edf less than 1, signifying slightly logarithmic relationships with fungal community dissimilarity among root samples in the three plots (Table 3). Accordingly, the fitted surfaces to the constrained ordination space were convex (Fig. 5G,I). The remaining environmental variables (average total soil P, average available soil P, root tissue Ca, RDMC, and RTD) had edf greater than 1, meaning exponential relationships to root associated fungal community dissimilarity (Table 3). Therefore, their fitted surfaces to the compositional variation

across the ordination space were roughly concave, with varying complexity (Fig. 5A-C,F,H).

Table 3: Generalized additive model (GAM) summaries for forward selected variables. For each forward-selected variable, a GAM was fit containing a linear and smooth term to the two-dimensional constrained ordination (db-RDA) plane. The smooth term of the model was fit using penalized regression splines. For smooth terms, edf stand for effective degrees of freedom, which controls the flexibility of the term. P-value notation follows Table 1. The percent of model deviance explained and adjusted coefficients of determination R^2_{adj} values are given for each GAM.

variable	N	Linear term			Smooth term			Deviance explained (%)	$\boldsymbol{R^2_{adj}}$
		Int	*t*	*p*	edf	$F_{(edf,9)}$	*p*		
Soil Total P (g kg^{-1})	150	0.31	475.00	***	8.81	837.60	***	98.2	0.98
Soil Available P (mg kg^{-1})	150	2.90	241.80	***	8.73	496.60	***	97.0	0.97
Root Ca (%)	150	0.45	14.86	***	6.46	8.48	***	36.7	0.34
RDMC (mg g^{-1})	150	302.3	93.46	***	7.07	5.19	***	27.5	0.24
Forks	150	348	11.49	***	3.30	1.67	***	11.2	0.09
RTD (g cm^{-3})	150	0.37	47.14	***	6.99	3.24	***	20.3	0.16
SRTA (tips g^{-1})	150	2299	14.33	***	1.75	1.45	***	9.1	0.08
Root N (%)	150	1.08	25.41	***	1.15	0.21	*ns*	2.0	0.01
Root Mn (‰)	150	160.7	8.92	***	0.01	0	*ns*	<0.1	<0.01

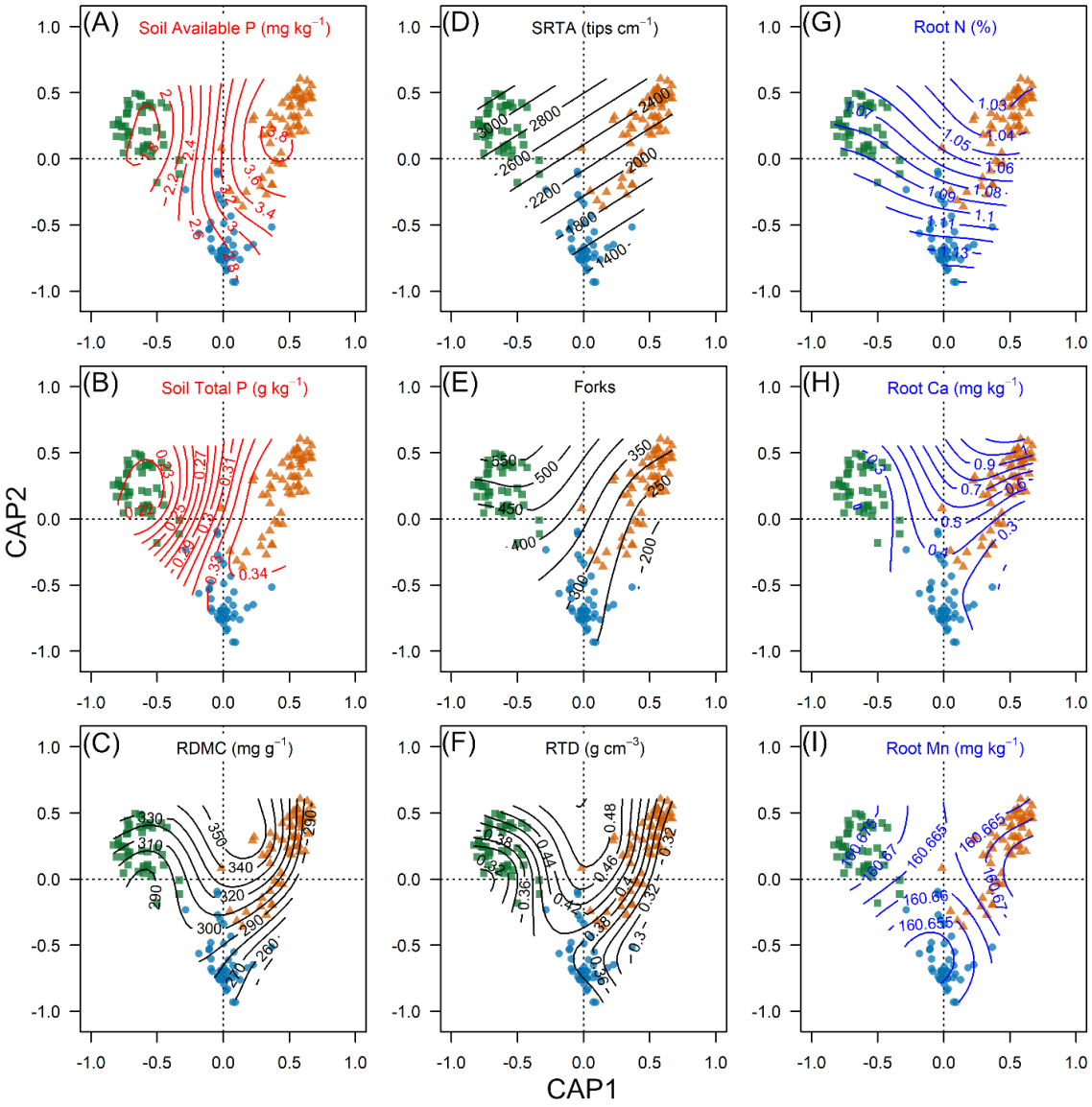

Fig. 5: Constrained ordination (db-RDA) contour plots of fitted GAM model surfaces for forward-selected predictor variables (A: soil available phosphorus, B: soil total phosphorus, C: root dry matter content, D: specific root tip abundance, E: number of root system forks, F: root tissue density, G: root tissue nitrogen concentration, H: root tissue calcium concentration, and I: root system manganese concentration). Points in the ordination space are the db-RDA site (i.e., individual root system) scores, as appearing in Figure 3. Fitted GAM surfaces are overlaid as contour plots in the units of each variable, illustrating how they correspond to root-associated fungal composition in the constrained ordination space.

Fitted GAMs varied in their goodness of fit to the constrained ordination plane. When fitted as single-variable GAMs, soil total and available P were explained >95% of the variation in root-fungi compositional differences among sites. Root functional traits

(RDMC, forks, RTD and SRTA) each explained between 9 and 28% of the variation, while root Ca explained 37% of the variation, but root N and root Mn alone explained very little (2% or less) or the variation in root associated fungal community dissimilarities (Table 3). These results were consistent with those from hierarchical variation partitioning (Fig. 4). Fitted GAMs for the entire set of environmental variables (i.e., those not forward-selected) were constructed and plotted (see Tables S6-S8, and Figs. S8-S10). Soils variables were strongly related to db-RDA site scores, each explaining between 87-94% of the dissimilarities in root-associated fungal compositing (Fig. S8, Table S6). Non-forward selected root functional traits explained between 0 and 23% of the variation in root-associated fungal community composition (Fig. S9, Table S7), and similarly, the additional root tissue elemental concentrations explained between 2 and 23% of the variation root-associated fungal community composition (Fig. S10, Table S8).

Discriminating fungal taxa and guilds among forest plots

The SIMPER analysis identified 20 fungal OTUs that contributed substantially (i.e., at least to 70%) to the compositional differences in root-associated fungi among plots. SIMPER values ranged from 0.0103 to 0.0439, which represent contribution of individual species to overall (i.e., sum of all species) Bray-Curtis dissimilarities among root-associated fungal assemblages. These raw values can be difficult to interpret beyond comparison to one another, to understand the relative contribution of individual species, and are small because of the number of fungal OTUs in the community dataset (>5000). Thus, for each identified OTU, we visually plotted the relative abundance of these taxa (Fig. S11) and compared abundances using a Kruskal-Wallis tests (Table 4). These 20 fungal OTUs ordinated on the outskirts of the species space in the db-RDA (Fig. 2), illustrating their influence on root fungal community differences among the three plots. The growth forms of the 20 taxa were comprised of seven microfungi, four agaracoid fungi, two claravoid fungi, a tremelloid, an endophyte, and five unidentified growth morphologies (Table 4). The trophic modes of these 20 taxa were five symbionts, four saprotrophs, four sapro-symbiotrophs, two pathotrophic-sybiotrophs, one pathotroph, one patho-sapro-symbiotroph, and three unidentified modes. Sixteen of the taxa had OTU

read counts which statistically differed among two of the pairwise comparisons between plots, one taxa (OTU17, an agaracoid fungus from the Tricholomataceae family) differed among all three plots and three taxa differed among a single pair of plots (see Table 4, Fig. S11).

The classification of all taxa by FUNGuild trophic mode and growth form revealed differences in the relative abundance of root associated fungal types among the three study plots. Relative abundances of fungal trophic modes and growth forms in the secondary forest plot near the rubber plantation more-closely resembled primary rainforest plot than the secondary evergreen plot (Figs. S12 and S13). For example, the secondary forest plot had a much larger relative abundance of symbiotrophic fungi than the primary or secondary forest plot near the rubber plantation. There were relatively fewer pathotrophic-symbiotrophic fungi in the primary forest plot than the other two plots, but more pathotrophic, patotroph-sapropthic, and saprotroph-symbiotrophic fungi (Fig. S12). Similarly, there was a greater proportion of agaricoid fungi, but a decreased relative abundance of microfungi found on roots of trees growing in the secondary evergreen forest plot relative to the other two plots (Fig. S13).

Table 4: Similarity percentages and FUNGuild taxonomy for fungal OTUs which statistically contributed to Bray-Curtis dissimilarities among root-inhabiting fungal communities within 3 forest plots in Xishuangbanna. SIMPER statistics are given for each pairwise comparison between plots. False-discovery rate corrected probabilities for Kruskal-Wallis test follow the notation described in Table 1.

OTU	Fungal Trophic mode	Fungal Guild	Fungal growth morphology	Fungal Family	Species	Comparison		
						Secondary near rubber – secondary evergreen	Secondary evergreen – rainforest	Secondary near rubber – rainforest
OTU1	—	—	—	—	—	0.0405 **	0.0176*	—
OTU2	Pathotroph-Saprotroph-Symbiotroph	Fungal Parasite-Undefined Saprotroph	Tremelloid-Yeast	Trimorphomycetaceae	*Saitozyma podzolica*	—	0.0237 ***	0.0247 ***
OTU3	Saprotroph-Symbiotroph	Endophyte-Litter Saprotroph-Soil Saprotroph-Undefined Saprotroph	Microfungus	Mortierellaceae	*Mortierella elongata*	—	0.0313 ***	0.0311 ***
OTU6	Symbiotroph	Endophyte	—	Vibrisseaceae	*Phialocephala fluminis*	0.0405 ***	—	0.0370 ***
OTU7	Saprotroph	Undefined Saprotroph	Microfungus	Nectriaceae	*Dactylonectria* sp.	—	0.0119 ***	0.0119 ***
OTU8	Symbiotroph	Ectomycorrhizal	Agaricoid	Russulaceae	*Lactarius laccarioides*	0.0439 **	0.0424 ***	—
OTU10	Symbiotroph	Ectomycorrhizal	Agaricoid	Russulaceae	*Lactarius* sp.	0.0277 **	0.0266 ***	—

OTU13	Saprotroph-Symbiotroph	Endophyte-Litter Saprotroph-Soil Saprotroph-Undefined Saprotroph	Microfungus	Mortierellaceae	*Mortierella amoeboidea*	—	0.0165 ***	0.0163 ***
OTU15	Saprotroph	Plant Saprotroph-Wood Saprotroph	Microfungus	Hyaloscyphaceae	Glutinomyces sp.	0.0190 ***	0.0183 ***	—
OTU17	Pathotroph-Symbiotroph	Ectomycorrhizal-Fungal Parasite	Agaricoid	Tricholomataceae	—	0.0381 *	0.0233 ***	0.0175 ***
OTU18	Pathotroph	Plant Pathogen	Microfungus	Valsaceae	*Phomopsis asparagi*	—	—	0.0108 ***
OTU23	Saprotroph	Plant Saprotroph-Wood Saprotroph	Microfungus	Hyaloscyphaceae	—	0.0164 ***	—	0.0136 ***
OTU24	Saprotroph-Symbiotroph	Ectomycorrhizal-Undefined Saprotroph	Clavarioid	Thelephoraceae	—	—	—	0.0189 ***
OTU26	—	—	—	Class: Sordariomycetes	—	0.0197 ***	—	0.0196 ***
OTU28	Symbiotroph	Ectomycorrhizal	Clavarioid	Clavulinaceae	*Clavulina* sp.	0.0109 ***	0.0103 ***	—
OTU32	Saprotroph-Symbiotroph	Endophyte-Litter Saprotroph-Soil Saprotroph-	Microfungus	Mortierellaceae	*Mortierella* sp.	—	0.0311 ***	0.0313 ***

		Undefined Saprotroph						
OTU36	Saprotroph	Undefined Saprotroph	—	Tricholomataceae	*Hydropus* sp.	0.0288 ***	0.0278 ***	—
OTU37	Symbiotroph	Ectomycorrhizal	Agaricoid	Cortinariaceae	—	0.0252 **	0.0225 ***	—
OTU45	Pathotroph-Symbiotroph	Ericoid Mycorrhizal	Dark Septate Endophyte	Myxotrichaceae	*Oidiodendron* sp.	0.0156 ***	0.0130 ***	—
OTU80	—	—	—	Order: Trechisporales	—	—	—	0.0169 **

To visualize these compositional tradeoffs in fungal trophic mode and growth form in relation to the soil and root environment, we re-ran the db-RDA using community matrices that grouped fungal taxa accordingly. Results confirmed the trends of the SIMPER analysis. However, the environmental relationships changed slightly, because of changes in the community matrix and hence Bray-Curtis dissimilarities among sites (i.e., roots). In the FUNGuild trophic mode db-RDA, we were principally interested in the species space of ordination, which revealed sapro-sybiotrophic taxa to be related to the rainforest plot and higher levels of soil total P, soil available P, and root Ca (i.e., positively to CAP axes 1 and 2, Fig. 6). Symbiotrophic fungi were positively related to increased RDMC, RTD, SRTA and the number of root system forks and associated to the secondary evergreen plot (i.e., positively to CAP axis 2 and negatively to CAP axis 1, Fig. 6). Lastly, patho-symbiotrophic fungi were positively related to root Mn and associated with the secondary forest plot near the rubber plantation (i.e., ordinated on the negative side of both CAP axes, Fig. 6). The fungal growth form constrained ordination did not show as clear species patterning as the trophic mode ordination, because there were nine trophic classes but 33 growth morph classes. Plot-based separation among fungal communities was also less clear (Fig. S14). Still, fungi classified as endophytic, clavarioid, gasteroid, agaracoid and microfungi were associated most-strongly with the two secondary forest plots (i.e., ordinated on the negative side of both CAP axes, Fig. S14). These taxa were also associated with environments that has less total and available soil phosphorus (Fig. S14).

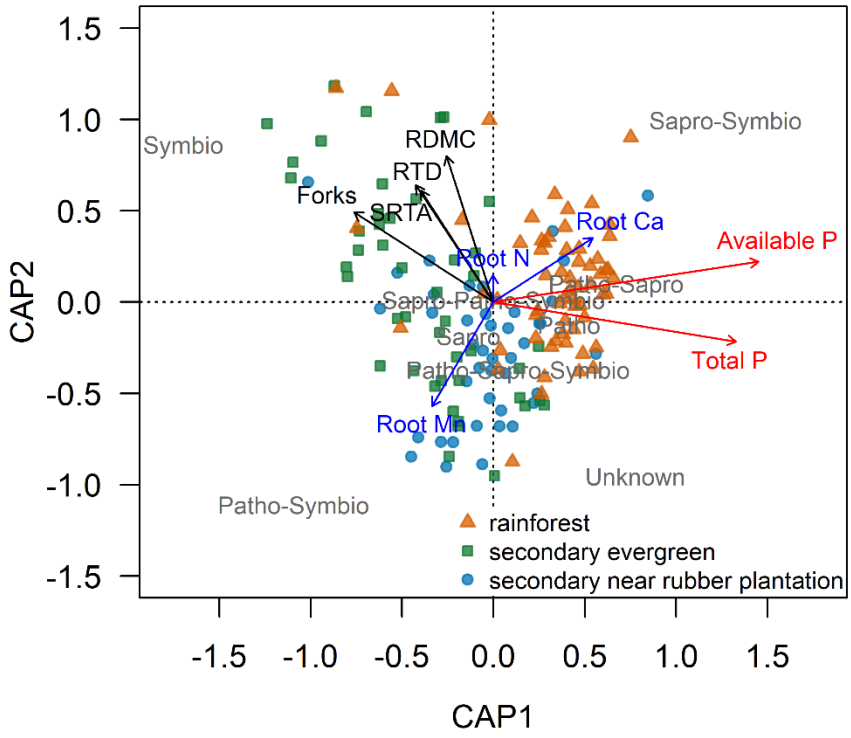

Fig. 6: Distance-based redundancy analysis by FUNGuild trophic mode. This db-RDA is statistically significant ($F_{(9,140)} = 4.19$, $p < 0.001$) and the constrained ordination axes explain 21% of the variation in root FUNGuild composition ($I_{total} = 12.22$, $I_{constrained} = 2.60$, $I_{unconstrained} = 9.63$). Only the first two constrained ordination axes are statistically-significant (axis 1: $F_{(1,140)} = 23.90$, $p < 0.001$, axis 2: $F_{(1,140)} = 8.17$, $p < 0.001$). Soil available P ($F_{(1,140)} = 119.82$, $p < 0.001$), soil total P ($F_{(1,140)} = 4.16$, $p < 0.001$), RDMC ($F_{(1,140)} = 2.62$, $p < 0.01$), Forks ($F_{(1,140)} = 2.81$, $p < 0.01$), RTD ($F_{(1,140)} = 2.56$, $p < 0.05$), and root Mn ($F_{(1,140)} = 2.27$, $p < 0.05$) are the statistically-significant terms in this db-RDA. SRTA, root Ca and root N are statistically non-significant terms.

Assessing the effect of host-plant plant lineage on root-associated fungal communities

To directly include the effect of plant lineage (i.e., phylogenetic distance – PD) in a model similar to that of the db-RDA constrained ordination, we used two MRMs (Table 5). The first MRM was an identical model to the db-RDA, although in the form of a linear regression of multivariate distances on root-associated fungal community dissimilarities. That model was statistically significant ($F_{(9,11165)} = 922.32$, $p < 0.001$), and explained about 43% of variation in root system fungal community dissimilarities ($R^2 = 0.426$). Linear regression coefficients for soil available P, root Ca, RDMC, number of root system forks, and RTD were all significant ($p < 0.05$), while soil total P, STRA, root

N, and root Mn had non-significant regression coefficients (Table 5). Adding PD for host-plant identity to the MRM model only slightly improved model fit, explaining an additional 1% of variation in root system fungal community dissimilarities ($R^2 = 0.435$). The model was still statistically significant ($F_{(10,11164)} = 858.04$, $p < 0.001$) and the statistical significance of model parameters was unchanged, except for RTD which went from being statistically significant, to marginally significant ($0.05 < p < 0.1$, Table 5). The effect of PD in that model was positive and similar in magnitude to that of the number of root forks and RDMC (table 5). Thus, PD and root functional traits (e.g., RTD) fought for explanatory power in the MRM which contained PD as a predictor.

Additionally, to better understand the degree to which plant species identity (i.e., phylogeny) constrains root functional traits for the 66 species in our dataset, we assessed phylogenetic signal of root functional traits and tissue elemental concentrations using Pagel's λ and Bloomberg's K statistics. Both or the statistics generally showed agreement, demonstrating phylogenetic conservatism for all 15 root functional traits of interest (Table S9). SRL, SRA, SRTA, RTD, and the number of root system forks and tips showed highest degrees of phylogenetic conservatism. Among root tissue elemental concentrations, root tissue carbon and iron concentrations were the only elements that were not phylogenetically conserved (Table S10). However, for root tissue manganese, sodium, and phosphorus concentrations, Pagel's λ did not agree with Bloomberg's K in registering phylogenetic conservatism (Table S10). Root tissue aluminum and copper concentrations were some of the most-highly constrained traits, possibly evidencing evolutionary variation in the exclusion and processing of heavy metals in root tissues.

Table 5: Model coefficients and associated probabilities for the Multiple Regression of Distance Matrices (MRM). MRM models were constructed in an identical fashion to the db-RDA, using the nine forward selected variables, however one model contained phylogenetic distances (PD) of for host-tree species. Summary statistics for the model without PD: $R^2 = 0.426$, $F = 922.32$, $p < 0.001$. Summary statistics for the model with PD: $R^2 = 0.435$, $F = 858.04$, $p < 0.001$.

Term	Model without PD		Model with PD	
	Coefficient	*p* value	Coefficient	*p* value
Intercept	0.8244	***	0.8152	***
Available P	0.0679	***	0.0678	***
Total P	-0.0102	*ns*	-0.154	*ns*
Root Ca	0.0162	***	0.0171	***

RDMC	0.0154 E-2	***	0.0150 E-2	***
Forks	0.0191 E-3	***	0.0178 E-3	***
RTD	0.0420	*	0.0381	‡
SRTA	0.0140 E-5	*ns*	-0.0210 E-5	*ns*
Root N	-0.0157 E-1	*ns*	-0.0214 E-1	*ns*
Root Mn	-0.0123 E-3	*ns*	-0.0117 E-3	*ns*
PD	—	—	0.0693 E-3	***

Discussion

We found differences in root morphologies among the three forest plots sampled (Table 2). Notably the root systems sampled in the primary forest had less branched root systems than the two secondary forest plots, meaning they generally had a more conservative functional strategy (Hogan *et al.*, 2020, Chapter 1, Bergmann *et al.*, 2020). Although this confirmed our hypothesis (research question 1), we were unable to control for plant host identity, so this difference in root morphology is mainly attributable to interspecific differences, although some intraspecific trait variation may have contributed. Root tissue calcium was significantly greater in the primary forest plot relative to the two secondary forest plots, illustrating how variation in root tissue chemistry accompanies root morphological differences (Hogan *et al.*, 2020, Chapter 1, Hogan et al 2021, Chapter2), although there was no difference in root tissue nitrogen.

Contrary to our hypothesis for research question 2, fungal diversity, richness and evenness had decreasing trends with root morphological complexity (i.e., STRA, and root forks). This illustrates that fungal symbiont identity is more important than species richness in root-associated fungal interactions. These interactions have been shown to be highly species specific (Smith and Read 2010), and the presence of other fungal species (e.g,, saprotrophic or pathogenic fungi) likely reduces the benefit of species-specific symbiosis.

The role of the soil environment in structuring plant root-fungi interactions in tropical forest

The principal motivation of this study was to determine the relative strength of the soil environments versus root system habitat in structuring root-associated fungal communities (research question 3). We narrowed the set of environmental variables that represented both the soil and root environments to a manageable set using forward

selection (Table S2). Still, the soil environment overpowered the effects of the root environment. Average total and available soil P accounted for three quarters of the explained variation in root associated-fungal community dissimilarities, with four independent root traits and three tissue elemental concentrations explaining the remaining quarter (Fig. 4). Phosphorus is the main limiting nutrient in tropical forests (Walker & Syers, 1976; Vitousek & Sanford Jr, 1986; Turner et al., 2007; Reed et al., 2011) and thus drives a trade of in the acquisition of soil nutrients per the 'do-it-yourself' vs outsourcing tradeoff (Bergmann *et al.,* 2020; Lugli *et al.*, 2020; Cabaugo *et al.*, 2021), which has consequence for variation root morphology (Hogan *et al.* 2020, Chapter 1). Individual soils variables explained three- to four-fold the variance explained by either root functional traits or tissue elemental concentration in the GAM fitted surfaces to db-RDA site scores (Fig. 5, Table 3, also see Fig. S8 vs Figs. S9 & S10 and Table S6 vs. Tables S8 & S9). The relationships of the soil environment to root-associated fungal community composition were non-linear (Fig. 5 & S8), suggesting a complexity in how fungal species richness increases and varies with decreasing soil fertility, expense of species evenness (e.g., unequal β-diversity turnover among fungal species; Figs. S5 & S6).

We found clear separation in Bray-Curtis dissimilarities among the three forest plots where we sampled roots (Fig. 3). The increased relative abundances of ECM trees (i.e. Fagaceae) relative to AM trees (i.e., Lauraceae and other families) in the secondary evergreen plot led to a higher proportion of strictly symbiotic fungi, whereas the trees sampled in primary rainforest were mostly associated to saprotrophic-symbiotic fungi and trees in the secondary forest near the rubber plantation were associated with patho-symbiotic fungi (i.e., a higher prevalence of yeast-type and other saprotrophic fungi). Other studies have confirmed the association of saprotrophs in secondary forests that are dominated by pioneer and early successional tree species with fast life histories, especially following forest agricultural land-use in tropical forest (Liu *et al.*, 2019; Ma *et al.*, 2019). Such land-use effects are a result of changes in the soil environment (i.e., pH, and the form and availability of nutrients), which are mediated by alterations to the tree community via plant-soil feedbacks (Bahram *et al.*, 2020).

In the case of the Xishuangbanna region, rubber (*Hevea brasiliensis*) cultivation alters soil fungal assemblages, decreasing the relative abundance of Basidiomycota and EMC fungi and community beta-diversity, without changing soil fungal richness (Song *et al.*, 2019). Our results largely confirm this finding clear differences in fungal guilds among secondary evergreen ECM-dominated plot and the other two plots (Fig.S12). Therefore, such changes to soil fungal species pools likely occurs primarily through the removal of ECM-host trees and secondarily through the subsequent effects on soil biogeochemical properties (e.g., altered litterfall composition and differing plant-soil feedbacks). A similar study to this one that sequenced ECM (primarily Fagaceae) and AM trees in a mixed secondary forest in Japan found non-typical (i.e., novel) assemblages of root-associated fungi, concluding that ECM fungi from Fagaceous trees can invade nearby AM hosts, influencing AM host- AM fungal interactions (Toju *et al.*, 2014). Therefore, ECM-hosts, which likely have more temperate evolutionary origins (Tedersoo *et al.*, 2012; but see Tedersoo & Smith, 2013; Lu & Hedin, 2019), appear to have a distinct contribution to the soil environment in mixed subtropical and tropical forests (Liang *et al.*, 2020; Segnitz *et al.*, 2020). In tropical and subtropical forests, it likely that ECM taxa have higher host-specificity than AM taxa (Klironomos, 2000; Smith & Read, 2010), although due to the dominance of AM species in these forests, ECM host-fungal community assemblages are context dependent (Tedersoo *et al.*, 2010; Smith *et al.*, 2011), reflecting landscape scale β-diversity patterns in host plants and fungi, which are further successively filtered by the soil environment.

The secondary role of the root system environment in structuring plant root-fungi interactions in tropical forest

In congruence with our hypothesis, the root environment was secondary to the soil environment in shaping root-associated fungal community composition. The four forward-selected root traits roughly represent a tradeoff in root construction strategy for tropical woody Angiosperms with RTD and RDMC interacting with STRA and the number of root forks. On one end of the tradeoff are dense, often lignified roots (e.g., those of Fagaceae); on the other are highly-branched roots with many first-order tips per unit length (i.e., a herringbone topology like those of species in the Lauraceae and

Myristicaceae, and to a lesser degree the Annonaceae and Euphorbiaceae). The roots of the Fagaceae are ECM associated, while Lauraceous roots are AM associated. Both families co-dominate forests at Xishuangbanna (Zhang & Cao, 1995; Cao *et al.*, 2006), however, as in other Fagaceae-Lauraceae forests of the region, they roughly partition the soil profile (although to varying degrees depending on the forest), with Fagaceae roots forming dense mats within and under the soil organic layer and roots of Lauraceous trees growing several centimeters below in the mineral soil of soil A horizon (Luo *et al.*, 2021). Root architecture (i.e., topology) is a main axis of functional differentiation between these two groups of trees, with the number of root forks (i.e., a highly branched morphology) distinguishing Fagaceae from herringbone (i.e., a many single order roots emanating from a transportive root) architecture characteristic of Lauraceae roots. Thus, root branching is a key trait that relates to both above- and belowground resource acquisition strategies (Liese *et al.*, 2017), and which acts as a functional filter for the composition of root-inhabiting fungi, especially AM taxa.

Three root tissue elemental concentrations were identified in our analyses. Root calcium was highly significant in structuring assemblages of root-associated fungi. Calcium increase (termed "spiking") in root tissues is a molecular hallmark of the symbiotic signaling pathway in fine root tissues that facilitates arbuscular mycorrhizal establishment (Kosuta *et al.*, 2008; Bonfante & Genre, 2010; Luginbuehl & Oldroyd, 2016). Calcium spiking occurs within the nucleus of root cortical cells via increased calcium channel activity, which alters root gene expression, and stimulates AM hyphal penetration and arbuscule development. In the case of our analyses, root Ca is likely a key trait that functionally differentiates roots of AM and ECM host trees, thus clearly structuring the assemblages of their root-associated fungi. In Xishuangbanna, root AM colonization rates range from 6 to 91%, which vary among species, but not by forest type; on average 35% of roots are colonized by AM fungi in both primary and secondary forests, however, AM fungal spore densities in bulk soil of secondary forests are more than double the density in bulk soil of primary forest (Muthukumar *et al.*, 2003b). Thus, AM roots are highly-selective to fungal taxa and likely maintain similar rates of colonization in similar soil environments, despite potential differences in species

composition of AM fungi, or morphological variability (Johnson 2010, Lugli *et al.*, 2020). Analysis of the root-associated fungal community composition by FUNGuild trophic mode showed the primary rainforest plot to be associated with sapro-symbiotic fungi (i.e., AM functional class), which was strongly correlated to root Ca. This plot was dominated by Lauraceae, Myristicaceae, and other AM trees, although there were ECM taxa intermixed. The importance of root Ca in this plot likely reflects differences in AM-host fungi specificity and variation in the Ca signaling strength among taxa, illustrating a key symbiotic control of root tissue chemistry despite similarities in root morphology (Johnson 2010).

The effects of root nitrogen were less apparent. Recent research on the interplay of root economics has shown that root N is independent of root functional traits and most other root elemental concentrations and does not always reflect root strategy, especially for AM species, because tissue N concentration does not differentiate N source, and can be highly interdependent on other pools of N within the plant (i.e., N demand for photosynthesis; Valverde-Barrantes *et al.* 2015, Averill *et al.*, 2019; McCormack & Iversen, 2019). Lastly, root Mn concentrations were identified in the forward selection of variables and the db-RDA analysis as having a minor influence on root inhabiting fungal assemblages. Certain AM fungi (e.g., *Glomus* and *Paraglomus sp.*) increase Mn concentrations in root tissues by aiding in Mn uptake (Wu *et al.*, 2011; Bagheri *et al.*, 2018). Mn is a key element to plant functioning, especially for the light reactions of photosynthesis, which must be actively taken up by roots.

Root functional traits mediate evolutionary controls on root-fungal community composition

Our last research objective questioned the role of plant-host identity (represented as relatedness via phylogenetic distance– PD) in further structuring root-associated fungal communities, beyond the effects of the soil and root environments. Results from the MRM analyses showed that plant PD explained a similar amount of variation in root-inhabiting fungal dissimilarity as any single root functional trait. Additionally, when PD was included the strength of MRM coefficients for several root traits decreased (Table 5), evidencing the co-variation of certain root traits (e.g., RTD) with plant lineage. Plant

root functional traits are highly-phylogenetically constrained (Valverde-Barrantes *et al.*, 2017), and the root functional traits measured in this study are no exception (Tables S9 & S10). Therefore, we conclude that root functional traits are putative surrogates for evolved root function among topical woody angiosperms, and advocate for their direct use, over phylogeny, when measuring them is feasible.

Conclusion

Multivariate community analyses applied to root-associated fungal communities of 150 host trees sampled across a range of tropical forest habitats showed an overwhelming relative contribution of the soil environment in structuring tropical tree root-associated fungal communities. At least in regard to woody angiosperm root functional strategies in Chinese Fagaceae-Lauraceae seasonal tropical forests, a secondary environmental filter by root-systems exists, which further structures root fungal assemblages. For ECM taxa, primarily, this is a root system morphological filter driven by architectural complexity (i.e., SRTA, the number of root system, forks) and root tissue density. For AM angiosperms, which dominate these forests, root tissue Ca Mn, and N concentrations are key root elements that are most related to variation in fungal assemblages, all of which have confirmed physiological function in tree-mycorrhizal symbiosis. Accordingly, clear difference in type of functional associations between fungal communities varied among the forest types sampled, with trees in primary forest most strongly associating with sapro-symbiotrophic fungi, those in ECM-dominated secondary forest most strongly associating with symbiotrophic fungi, and trees in AM-dominated secondary forest with rubber land-use legacy most strongly associating with patho-saprotrophic fungi. Future research might further investigate the functional ecosystem consequences of such tropical -host fungal community interactions, potentially exploring how plant-soil and fungal-soil interactions shape environmental filtering of tree species and fungi, and how these affect ecosystem and soil biogeochemical cycles.

References

Alexander IJ, Lee S. 2005. Mycorrhizas and ecosystem processes in tropical rain forest: implications for diversity. *Biotic interactions in the tropics: Their role in the maintenance of species diversity*: 165-203.

Averill C, Bhatnagar JM, Dietze MC, Pearse WD, Kivlin SN. 2019. Global imprint of mycorrhizal fungi on whole-plant nutrient economics. *Proceedings of the National Academy of Sciences* **116**(46): 23163-23168.

Bagheri V, Shamshiri M, Shirani H, Roosta H. 2018. Nutrient uptake and distribution in mycorrhizal pistachio seedlings under drought stress.

Bahram M, Netherway T, Hildebrand F, Pritsch K, Drenkhan R, Loit K, Anslan S, Bork P, Tedersoo L. 2020. Plant nutrient-acquisition strategies drive topsoil microbiome structure and function. *New Phytologist* **227**(4): 1189-1199.

Benjamini Y, Hochberg Y. 1995. Controlling the False Discovery Rate: A Practical and Powerful Approach to Multiple Testing. *Journal of the Royal Statistical Society. Series B (Methodological)* **57**(1): 289-300.

Bergmann J, Weigelt A, van der Plas F, Laughlin DC, Kuyper TW, Guerrero-Ramirez N, Valverde-Barrantes OJ, Bruelheide H, Freschet GT, Iversen CM, et al. 2020. The fungal collaboration gradient dominates the root economics space in plants. *Science Advances* **6**(27): eaba3756.

Blanchet FG, Legendre P, Borcard D. 2008. Forward selection of explanatory Vvariables. *Ecology* **89**(9): 2623-2632.

Blomberg SP, Garland Jr T, Ives AR. 2003. Testing for phylogenetic signal in comparative data: behavioral traits are more labile. *Evolution* **57**(4): 717-745.

Bonfante P, Genre A. 2010. Mechanisms underlying beneficial plant–fungus interactions in mycorrhizal symbiosis. *Nature Communications* **1**(1): 48.

Bray JR, Curtis JT. 1957. An Ordination of the Upland Forest Communities of Southern Wisconsin. *Ecological Monographs* **27**(4): 325-349.

Brundrett MC. 2002. Coevolution of roots and mycorrhizas of land plants. *New Phytologist* **154**(2): 275-304.

Cao M, Zou X, Warren M, Zhu H. 2006. Tropical Forests of Xishuangbanna, China. *Biotropica* **38**: 306-309.

Cabugao KG, Yaffar D, Stenson N, Childs J, Phillips J, Mayes MA, Yang X, Weston DJ, Norby RJ. 2021. Bringing function to structure: Root–soil interactions shaping phosphatase activity throughout a soil profile in Puerto Rico. *Ecology and Evolution* **11**(3): 1150-1164.

Chen H, Yi Z-F, Schmidt-Vogt D, Ahrends A, Beckschäfer P, Kleinn C, Ranjitkar S, Xu J. 2016. Pushing the Limits: The Pattern and Dynamics of Rubber Monoculture Expansion in Xishuangbanna, SW China. *PLoS one* **11**(2): e0150062.

Chen W, Koide RT, Adams TS, DeForest JL, Cheng L, Eissenstat DM. 2016. Root morphology and mycorrhizal symbioses together shape nutrient foraging strategies of temperate trees. *Proceedings of the National Academy of Sciences* 113(31): 8741-8746.

Clark JS, Scher CL, Swift M. 2020. The emergent interactions that govern biodiversity change. *Proceedings of the National Academy of Sciences of the United States of America* **117**(29): 17074-17083.

Clarke KR. 1993. Non-parametric multivariate analyses of changes in community structure. *Australian Journal of Ecology* **18**(1): 117-143.

Corrales A, Henkel TW, Smith ME. 2018. Ectomycorrhizal associations in the tropics – biogeography, diversity patterns and ecosystem roles. *New Phytologist* **220**(4): 1076-1091.

Dray S, Bauman D, Blanchet G, Borcard D, Clappe S, Guenard G, Jombart T, Larocque G, Legendre P, Madi N. 2018. Package 'adespatial', version 0.3-14. *R Package version* **2**(6).

Essene AL, Shek KL, Lewis JD, Peay KG, McGuire KL. 2017. Soil Type Has a Stronger Role than Dipterocarp Host Species in Shaping the Ectomycorrhizal Fungal Community in a Bornean Lowland Tropical Rain Forest. *Frontiers in Plant Science* **8**(1828).

Fine PVA, Kembel SW. 2011. Phylogenetic community structure and phylogenetic turnover across space and edaphic gradients in western Amazonian tree communities. *Ecography* **34**(4): 552-565.

Gourmelon V, Maggia L, Powell JR, Gigante S, Hortal S, Gueunier C, Letellier K, Carriconde F. 2016. Environmental and Geographical Factors Structure Soil Microbial Diversity in New Caledonian Ultramafic Substrates: A Metagenomic Approach. *PLoS one* **11**(12): e0167405.

Hetrick BAD. 1991. Mycorrhizas and root architecture. *Experientia* **47**(4): 355-362.

Huang X-c, Ci X-q, Conran JG, Li J. 2015. Application of DNA Barcodes in Asian Tropical Trees – A Case Study from Xishuangbanna Nature Reserve, Southwest China. *PLoS one* **10**(6): e0129295.

Hogan JA, Valverde-Barrantes OJ, Ding Q, Xu H, Baraloto C. 2020. Morphological variation of fine root systems and leaves in primary and secondary tropical forests of Hainan Island, China. *Annals of Forest Science* **77**(3): 79.

Hogan JA, Valverde-Barrantes OJ, Tang W, Ding Q, Xu H, Baraloto C. 2021. Evidence of elemental homeostasis in fine root and leaf tissues of saplings across a fertility gradient in tropical montane forest in Hainan, China. *Plant and Soil* **460**(1): 625-646.

Janos DP. 1980. Mycorrhizae Influence Tropical Succession. *Biotropica* **12**(2): 56-64.

Johnson NC. 2010. Resource stoichiometry elucidates the structure and function of arbuscular mycorrhizas across scales. *New Phytologist* **185**(3): 631-647.

Jones Jr B. 2001. *Laboratory guide for conducting soil tests and plant analysis*: CRC press.

Kenrick P, Strullu-Derrien C. 2014. The origin and early evolution of roots. *Plant physiology* **166**(2): 570-580.

Klironomos JN. 2000. Host-Specificity and Functional Diversity among Arbuscular Mycorrhizal Fungi. In: Bell CR, Brylinski M, Johnson-Green P eds. *Microbial Biosystems: New Frontiers. Proceedings of the 8th International Symposium on Microbial Ecology*. Halifax: Atlantic Canada Society from Microbial Ecology, 845-851.

Kohout P, Sudová R, Janoušková M, Čtvrtlíková M, Hejda M, Pánková H, Slavíková R, Štajerová K, Vosátka M, Sýkorová Z. 2014. Comparison of commonly used primer sets for evaluating arbuscular mycorrhizal fungal communities: is there a universal solution? *Soil Biology and Biochemistry* **68**: 482-493.

Kong D, Wang J, Wu H, Valverde-Barrantes OJ, Wang R, Zeng H, Kardol P, Zhang H, Feng Y. 2019. Nonlinearity of root trait relationships and the root economics spectrum. *Nature Communications* **10**(1): 2203.

Kosuta S, Hazledine S, Sun J, Miwa H, Morris RJ, Downie JA, Oldroyd GE. 2008. Differential and chaotic calcium signatures in the symbiosis signaling pathway of legumes. *Proceedings of the National Academy of Sciences* **105**(28): 9823-9828.

Kress WJ, Erickson DL. 2007. A two-locus global DNA barcode for land plants: the coding rbcL gene complements the non-coding trnH-psbA spacer region. *PLoS one* **2**(6): e508.

Lai J, Zou Y, Zhang J, Peres-Neto P. 2021. rdacca.hp: an R package for generalizing hierarchical and variation partitioning in multiple regression and canonical analysis. *bioRxiv*: 2021.2003.2009.434308.

Legendre P, Anderson MJ. 1999. Distance-based redundancy analysis: testing multispecies responses in multifactorial ecological experiments. *Ecological Monographs* **69**(1): 1-24.

Legendre P, Gallagher ED. 2001. Ecologically meaningful transformations for ordination of species data. *Oecologia* **129**(2): 271-280.

Legendre P, Legendre L. 2012. *Numerical ecology*: Elsevier.

Legendre P, Mi X, Ren H, Ma K, Yu M, Sun I-F, He F. 2009. Partitioning beta diversity in a subtropical broad-leaved forest of China. *Ecology* **90**(3): 663-674.

Leibold MA, Chase JM. 2018. *Metacommunity Ecology, Volume 59*: Princeton University Press.

Leibold MA, Holyoak M, Mouquet N, Amarasekare P, Chase JM, Hoopes MF, Holt RD, Shurin JB, Law R, Tilman D, et al. 2004. The metacommunity concept: a framework for multi-scale community ecology. *Ecology Letters* **7**(7): 601-613.

Lekberg Y, Vasar M, Bullington LS, Sepp SK, Antunes PM, Bunn R, Larkin BG, Öpik M. 2018. More bang for the buck? Can arbuscular mycorrhizal fungal communities be characterized adequately alongside other fungi using general fungal primers? *New Phytologist* **220**(4): 971-976.

Li H, Ma Y, Aide TM, Liu W. 2008. Past, present and future land-use in Xishuangbanna, China and the implications for carbon dynamics. *Forest Ecology and Management* **255**(1): 16-24.

Liang M, Johnson D, Burslem DFRP, Yu S, Fang M, Taylor JD, Taylor AFS, Helgason T, Liu X. 2020. Soil fungal networks maintain local dominance of ectomycorrhizal trees. *Nature Communications* **11**(1): 2636.

Lichstein JW. 2007. Multiple regression on distance matrices: a multivariate spatial analysis tool. *Plant Ecology* **188**(2): 117-131.

Liese R, Alings K, Meier IC. 2017. Root Branching Is a Leading Root Trait of the Plant Economics Spectrum in Temperate Trees. *Frontiers in Plant Science* **8**(315).

Liu C, Xiang W, Zou L, Lei P, Zeng Y, Shuai O, Deng X, Fang X, Liu Z, Peng C. 2019. Variation in the functional traits of fine roots is linked to phylogenetics in the common tree species of Chinese subtropical forests. *Plant and Soil* **436**: 1-18.

Lovelock CE, Ewel JJ. 2005. Links between tree species, symbiotic fungal diversity and ecosystem functioning in simplified tropical ecosystems. *New Phytologist* **167**(1): 219-228.

Lu M, Hedin L. 2019. Global plant–symbiont organization and emergence of biogeochemical cycles resolved by evolution-based trait modelling. *Nature Ecology & Evolution* **3**.

Luginbuehl L, Oldroyd GE 2016. Calcium signaling and transcriptional regulation in arbuscular mycorrhizal symbiosis. In: Martin FM ed. *Molecular Mycorrhizal Symbiosis*. Hoboken, New Jersey: John Wiley & Sons, 125-140.

Lugli LF, Andersen KM, Aragão LE, Cordeiro AL, Cunha HF, Fuchslueger L, Meir P, Mercado LM, Oblitas E, Quesada CA. 2020. Multiple phosphorus acquisition strategies adopted by fine roots in low-fertility soils in Central Amazonia. *Plant and Soil* **450**(1): 49-63

Luo W, Ni M, Wang Y, Lan R, Eissenstat DM, Cahill JF, Li B, Chu C. 2021. Limited evidence of vertical fine-root segregation in a subtropical forest. *New Phytologist* **231**(6): 2308-2318.

Ma H, Zou W, Yang J, Hogan JA, Xu H, Chen J. 2019. Dominant Tree Species Shape Soil Microbial Community via Regulating Assembly Processes in Planted Subtropical Forests. *Forests* **10**(11): 978.

Ma Z, Guo D, Xu X, Lu M, Bardgett RD, Eissenstat DM, McCormack ML, Hedin LO. 2018. Evolutionary history resolves global organization of root functional traits. *Nature* **555**(7694): 94-97.

McCormack ML, Dickie IA, Eissenstat DM, Fahey TJ, Fernandez CW, Guo D, Helmisaari HS, Hobbie EA, Iversen CM, Jackson RB. 2015. Redefining fine roots improves understanding of below-ground contributions to terrestrial biosphere processes. *New Phytologist* **207**(3): 505-518.

McCormack ML, Iversen CM. 2019. Physical and Functional Constraints on Viable Belowground Acquisition Strategies. *Frontiers in Plant Science* **10**(1215).

McLellan T, Brown M. 2017. Mushrooms and cash crops can coexist in mountain livelihoods: Wild mushrooms as economic and recreational resources in the Greater Mekong. *Mountain Research and Development* **37**(1): 108-120.

Muthukumar T, Sha L, Yang X, Cao M, Tang J, Zheng Z. 2003a. Distribution of roots and arbuscular mycorrhizal associations in tropical forest types of Xishuangbanna, southwest China. *Applied Soil Ecology* **22**(3): 241-253.

Muthukumar T, Sha L, Yang X, Cao M, Tang J, Zheng Z. 2003b. Mycorrhiza of plants in different vegetation types in tropical ecosystems of Xishuangbanna, southwest China. *Mycorrhiza* **13**(6): 289-297.

Nguyen NH, Song Z, Bates ST, Branco S, Tedersoo L, Menke J, Schilling JS, Kennedy PG. 2016. FUNGuild: An open annotation tool for parsing fungal community datasets by ecological guild. *Fungal Ecology* **20**: 241-248.

Oksanen J, Blanchet F, Friendly M, Kindt R, Legendre P, McGlinn D, Minchin PR, O'Hara RB, L. SG, Stevens HH, et al. 2020. vegan: community ecology package. R package version 2.5-7.

Pan, XZ, Guo ZY, Pan K. 2019. Protocols for stand soil observation and measurement in terrestrial ecosystems. China Environmental Publishing House, Beijing, China.

Pagel M. 1999. Inferring the historical patterns of biological evolution. *Nature* **401**(6756): 877-884.

Palmer JM, Jusino MA, Banik MT, Lindner DL. 2018. Non-biological synthetic spike-in controls and the AMPtk software pipeline improve mycobiome data. *PeerJ* **6**: e4925.

Peay KG, Baraloto C, Fine PVA. 2013. Strong coupling of plant and fungal community structure across western Amazonian rainforests. *The ISME Journal* **7**(9): 1852-1861.

Peay KG, Bidartondo MI, Elizabeth Arnold A. 2010a. Not every fungus is everywhere: scaling to the biogeography of fungal–plant interactions across roots, shoots and ecosystems. *New Phytologist* **185**(4): 878-882.

Peay KG, Garbelotto M, Bruns TD. 2010b. Evidence of dispersal limitation in soil microorganisms: Isolation reduces species richness on mycorrhizal tree islands. *Ecology* **91**(12): 3631-3640.

Peres-Neto PR, Legendre P, Dray S, Borcard D. 2006. Variation partitioning of species data matrices: estimation and comparison of fractions. *Ecology* **87**(10): 2614-2625.

Pielou EC. 1966. The measurement of diversity in different types of biological collections. *Journal of theoretical biology* **13**: 131-144.

R Core Team 2021. R: A language and environment for statistical computing v. 4.0.5. Vienna, Austria: R Foundation for Statistical Computing. https://cran.r-project.org/.

Reed SC, Townsend AR, Taylor PG, Cleveland CC 2011. Phosphorus cycling in tropical forests growing on highly weathered soils. *Phosphorus in action*: Springer, 339-369.

Revell LJ. 2012. phytools: an R package for phylogenetic comparative biology (and other things). *Methods in ecology and evolution* **3**(2): 217-223.

Sarmiento C, Zalamea P-C, Dalling JW, Davis AS, Stump SM, U'Ren JM, Arnold AE. 2017. Soilborne fungi have host affinity and host-specific effects on seed germination and survival in a lowland tropical forest. *Proceedings of the National Academy of Sciences* **114**(43): 11458-11463.

Segnitz RM, Russo SE, Davies SJ, Peay KG. 2020. Ectomycorrhizal fungi drive positive phylogenetic plant–soil feedbacks in a regionally dominant tropical plant family. *Ecology* **101**(8): e03083.

Shannon CE. 1948. A mathematical theory of communication. *The Bell system technical journal* **27**(3): 379-423.

Smith ME, Henkel TW, Catherine Aime M, Fremier AK, Vilgalys R. 2011. Ectomycorrhizal fungal diversity and community structure on three co-occurring leguminous canopy tree species in a Neotropical rainforest. *New Phytologist* **192**(3): 699-712.

Smith SA, Brown JW. 2018. Constructing a broadly inclusive seed plant phylogeny. *American Journal of Botany* **105**(3): 302-314.

Smith SE, Read DJ. 2010. *Mycorrhizal symbiosis*: Academic press.

Song H, Singh D, Tomlinson KW, Yang X, Ogwu MC, Slik JWF, Adams JM. 2019. Tropical forest conversion to rubber plantation in southwest China results in lower fungal beta diversity and reduced network complexity. *FEMS Microbiology Ecology* **95**(7).

Soudzilovskaia NA, van Bodegom PM, Terrer C, Zelfde Mvt, McCallum I, Luke McCormack M, Fisher JB, Brundrett MC, de Sá NC, Tedersoo L. 2019. Global mycorrhizal plant distribution linked to terrestrial carbon stocks. *Nature Communications* **10**(1): 5077.

Strullu-Derrien C, Kenrick P, Selosse MA 2016. Origins of the mycorrhizal symbioses. In: Martin FM ed. *Molecular Mycorrhizal Symbiosis*. Hoboken, New Jersey: Wiley-Blackwell, 1-20.

Tedersoo L, Bahram M, Toots M, Diedhiou AG, Henkel TW, Kjøller R, Morris MH, Nara K, Nouhra E, Peay KG. 2012. Towards global patterns in the diversity and community structure of ectomycorrhizal fungi. *Molecular Ecology* **21**(17): 4160-4170.

Tedersoo L, Sadam A, Zambrano M, Valencia R, Bahram M. 2010. Low diversity and high host preference of ectomycorrhizal fungi in Western Amazonia, a neotropical biodiversity hotspot. *The ISME Journal* **4**(4): 465-471.

Tedersoo L, Smith ME. 2013. Lineages of ectomycorrhizal fungi revisited: Foraging strategies and novel lineages revealed by sequences from belowground. *Fungal Biology Reviews* **27**(3): 83-99.

Ter Braak CJ. 1994. Canonical community ordination. Part I: Basic theory and linear methods. *Ecoscience* **1**(2): 127-140.

Toju H, Sato H, Tanabe AS. 2014. Diversity and spatial structure of belowground plant-fungal symbiosis in a mixed subtropical forest of ectomycorrhizal and arbuscular mycorrhizal plants. *PLoS one* **9**(1): e86566-e86566.

Turner BL, Condron LM, Richardson SJ, Peltzer DA, Allison VJ. 2007. Soil organic phosphorus transformations during pedogenesis. *Ecosystems* **10**(7): 1166-1181.

Valverde-Barrantes OJ, Smemo KA, Blackwood CB. 2015. Fine root morphology is phylogenetically structured, but nitrogen is related to the plant economics spectrum in temperate trees. Functional Ecology 29(6): 796-807.

Valverde-Barrantes OJ, Freschet GT, Roumet C, Blackwood CB. 2017. A worldview of root traits: the influence of ancestry, growth form, climate and mycorrhizal association on the functional trait variation of fine-root tissues in seed plants. *New Phytologist* **215**(4): 1562-1573.

van der Heijden MGA, Martin FM, Selosse M-A, Sanders IR. 2015. Mycorrhizal ecology and evolution: the past, the present, and the future. *New Phytologist* **205**(4): 1406-1423.

Vitousek PM, Sanford Jr RL. 1986. Nutrient cycling in moist tropical forest. *Annual review of Ecology and Systematics* **17**(1): 137-167.

Walker T, Syers JK. 1976. The fate of phosphorus during pedogenesis. *Geoderma* **15**(1): 1-19.

Weemstra M, Peay KG, Davies SJ, Mohamad M, Itoh A, Tan S, Russo SE. 2020. Lithological constraints on resource economies shape the mycorrhizal composition of a Bornean rain forest. *New Phytologist* **228**(1): 253-268.

Wood SN. 2003. Thin plate regression splines. *Journal of the Royal Statistical Society: Series B (Statistical Methodology)* **65**(1): 95-114.

Wood SN. 2011. Fast stable restricted maximum likelihood and marginal likelihood estimation of semiparametric generalized linear models. *Journal of the Royal Statistical Society: Series B (Statistical Methodology)* **73**(1): 3-36.

Wu Q-S, Li GH, Ying-Ning Z. 2011. Roles of arbuscular mycorrhizal fungi on growth and nutrient acquisition of peach (Prunus persica L. Batsch) seedlings. *Journal of Animal and Plant Sciences* **21**.

Zhang J, Cao M. 1995. Tropical forest vegetation of Xishuangbanna, SW China and its secondary changes, with special reference to some problems in local nature conservation. *Biological Conservation* **73**(3): 229-238.

Zheng Z, Feng Z, Cao M, Li Z, Zhang J. 2006. Forest Structure and Biomass of a Tropical Seasonal Rain Forest in Xishuangbanna, Southwest China 1. *Biotropica: The Journal of Biology and Conservation* **38**(3): 318-327.

PART 3: Root respiration, thermal acclimation, and the contribution of root respiration to soil respiration

CHAPTER 5: Functional variability in specific root respiration translates to slight differences in belowground CO_2 efflux in a temperate deciduous forest in Oak Ridge, Tennessee

Key message

Root system-specific respiration rates (R_r) are related to root functional traits. R_r relates positively to N_{root} and inversely to root tissue density. A new method to measure CO_2 efflux of root systems and surrounding soil is used (R_s), finding that autotrophic R_s was positively related to specific root length, root tip abundance, and root tissue density.

Abstract

CO_2 release from forest soils (R_s) is a prominent flux in the global carbon cycle. R_s is derived from root (R_a) and microbial respiration and is highly dynamic, as it depends on edaphic and environmental conditions, as well as root functional traits and microbial community composition. It is unclear how root functional traits affect root and microbial respiration rates; however, incorporating them may help parse out how the relative contributions of root and microbial respiration affect R_s. *In-situ* root trays housing entire root systems of 3-4 functional root orders and their surrounding soil were installed in a paired experimental design on eight temperate tree species that varied in their root functional strategies and mycorrhizal affinity. R_s was measured bi-weekly to monthly for nearly one year using a custom chamber attached to a gas exchange system, with concurrent soil moisture and temperature measurements. R_s rates varied over time, ranging from 0.3 to 12 μmol m^{-2} s^{-1}. Rates of specific root respiration from excised root systems ranged from 2.5 to 9.0 nmol g^{-1} s^{-1} and were negatively correlated with root tissue density and positively related to root tissue nitrogen concentration. We estimate that Ra accounts for <10%, on average, 2-3% of R_s at the entire root system-level *in situ*. The contribution of R_a peaked in the fall (September and October), coinciding with leaf senescence of the forest canopy. Experimental treatments reduced bacterial biomass in half of the trays; however, no reduction in R_s was observed because of the compensation

of heterotrophic respiration between soil fungi and bacteria. The R_a to R_s ratio increased with acquisitive root strategies, as represented by root functional trait space axes related to high specific root length, high root tip abundance, and low root tissue density. The ratio of R_a to R_s also increased with warmer soil temperatures and decreased slightly with increasing soil moisture. We discuss how incorporating root functional traits as modulators of the autotrophic contribution to R_s could be considered when modeling total soil CO_2 efflux from forests.
Keywords: soil respiration, root traits, root respiration, microbial respiration, ZeroTol, Tennessee, temperate forest.

Introduction

Soil carbon dioxide (CO_2) efflux, or belowground respiration (R_s), is a dominant process in the carbon cycling of forests (Janssens et al., 2001; Raich and Nadelhoffer, 1989; Xu and Shang, 2016). Globally, R_s represents the second-largest flux in the global carbon cycle behind only gross primary production (~130 pG per year, Madani et al., 2020), accounting for 85-110 pG per year (Bond-Lamberty and Thomson, 2010a; Bond-Lamberty and Thomson, 2010b; Raich et al., 2002). R_s is strongly influenced by soil temperature and moisture, but these are inherently linked both to climate and to vegetation type (e.g., conifer vs. broadleaf evergreen forests). Climate was found to account for nearly half of the variation in R_s in three coniferous forest types in Oregon but stand age and disturbance history were also significant sources of variation (Campbell and Law, 2005). Comparisons of R_s within forests located in the same climatic zone have reported R_s rates in broadleaf forests to be greater than those in coniferous forests (Raich and Tufekciogul, 2000; Wang et al., 2006). Differences in R_s between forest types and under different tree species may result from their influence on soil temperature and moisture, variation in litter quantity and chemistry, differences in root density and distribution, variation in root structure and function, and interactions between plant roots and microbial communities.

R_s has distinct autotrophic and heterotrophic components (Hanson et al., 2000; Kuzyakov, 2006; Ryan and Law, 2005). The heterotrophic component (R_h) arises

primarily from microbial respiration in the soil, mycorrhizae, and soil fauna, whereas the autotrophic component (R_a) mainly comes from plant root respiration. Although species differ in their specific-root (i.e., mass-based tissue) respiration rates (R_r), surface fine root biomass is the driver of variation in R_s in forest ecosystems (Pregitzer et al., 2008; Wang et al., 2017). Spatial variation in the amount and metabolic activity of root tissues makes the contribution of root respiration (R_a) to R_s highly variable. For example, Wang et al. (2009) found that R_a made up 53% (range 33-72%) of belowground respiration in a temperate grassland. Similarly, in a boreal forest, (Högberg et al., 2001) found R_a to contribute up to 56% of R_s. In forest ecosystems, R_a comprises about 46%, on average, of the R_s, but is normally distributed about a broad range from <10% to >90% (Hanson et al., 2000). One reason for the wide range in estimates is because of the wide range of methods used for measuring R_s and quantifying R_a (Bond-Lamberty et al., 2011; Hanson et al., 2000; Ryan and Law, 2005) and the influence of site and forest characteristics, but additional variation in the contribution of heterotrophic and autotrophic sources of respiration contributes, as well.

The functional linkages of R_a to R_s have proved difficult because of the manifold controls on R_s and the methodological difficulties of understanding how the components of R_s work together. For example, decomposition can greatly influence R_s (Singh and Gupta, 1977; Ryan and Law, 2005) because decomposition-derived labile C tightly controls R_s magnitude (Hanson et al., 2003). Additionally, R_a and R_s are tightly interconnected via the labile carbon transfer between roots and soil microbes (Bouma et al., 1997; Cleveland et al., 2007; Hill et al., 2015; Lavigne et al., 2003; Pausch and Kuzyakov, 2018; Teodosio et al., 2017). For example, Warren et al. (2011) showed how isotopically-labeled R_s was related to previous-day total sap flow in young Loblolly Pines. Thus, plant carbon dynamics (e.g., photosynthesis, labile C movement to the soil, and R_r) are intertwined with R_s through their effect on R_h (i.e., soil priming effects). Because of the interlinking of plant root carbon dynamics and soil respiration, which is not often considered empirically in models, even the most sophisticated models of R_s (see model summaries by Blagodatsky and Smith, 2012; *e.g.*, Fang and Moncrieff, 1999) can

improve of how plant roots contribute to R_s (either indirectly or directly) and other C fluxes between roots and soils (Reichstein and Beer, 2008).

Regarding R_a, root functional traits provide the potential to understand and constrain variance in R_a, if differences in specific respiration rates can be linked to variation in R_s in a meaningful way (Bergmann et al., 2020; Freschet et al., 2020; Warren et al., 2011). Variation in R_r scales along the root nitrogen (N_{root}) - root tissue density (RTD) axis of the root functional trait space (Burton et al., 2002; Paradiso et al., 2019; Reich et al., 2008). RTD and N_{root} are typically aligned oppositely in root functional trait space and represent a physiological tradeoff between acquisitive capacities and lifespan (Bergmann et al., 2020; McCormack and Iversen, 2019). Thus, species with faster life-history strategies typically have higher N_{root} and R_r (Comas et al., 2002; Makita et al., 2012). However, it is unclear if such differences lead to detectable differences in R_a, R_h or how they interact to influence R_s. An additional and orthogonal axis of root functional variation to the RTD-N_{root} tradeoff is the degree of mycorrhizal association, commonly represented by mycorrhizal type (i.e., arbuscular mycorrhizal: AM vs. ectomycorrhizal: ECM association) (Bergmann et al., 2020; McCormack and Iversen, 2019). Several studies have shown that R_s is greater under AM trees than ECM trees (Lang et al., 2020; Taylor et al., 2016; Wurzburger and Brookshire, 2017). At least some of this increase in R_s for AM trees relative to ECM trees is related to the respiratory cost of mycorrhizal association, which is estimated at 2-17%, via an increase in R_h (Bryla and Eissenstat, 2005). Additionally, AM trees tend to produce more labile tissues, which exert distinct effects on soil C pools, contributing up to twice as much root-derived C to soils (Keller et al., 2021) and doubling rates of soil C decomposition and cycling potentially via increased soil microbial enzyme activity (Liming et al., 2021).

Moreover, the link between the variation in R_s due to altered soil microbiomes by tree mycorrhizal type and variation in R_r and how each contributes to variation in R_s over time and with changes in soil moisture and temperature is not entirely understood, especially at the physiological scale of functional root systems (i.e., entire root units containing 3-4 orders of the most-physiologically active fine roots). ECM vs. AM species can create differences in ecosystem functioning at the ecosystem level, including

variation in tree species competition, recruitment dynamics, and stand biomass (Bennett et al., 2017; Johnson et al., 2018; Soudzilovskaia et al., 2019). Therefore, it is expected that variation in R_s could be related to R_r or at least how R_r relates to mycorrhizal status and labile carbon movement between plants and rhizosphere soil (Keller et al., 2021, Liming et al., 2021). Indeed, this is the central tenet of the MANE (mycorrhizal absorption nutrient economies) hypothesis (Phillips et al., 2013): that AM and ECM trees differ in their C-cycling and nutrient-use linkages because of differences in their soil microbiomes. Thus, one might expect R_a to be greater for AM than ECM species, leading to a greater contribution of R_a to R_s in AM than ECM species. However, ECM fungi may have higher rates of respiration and more fungal biomass per unit soil surface area than AM fungi, increasing the contribution of R_h (and hence decreasing the relative contribution of R_a) to R_s.

Using a novel methodology that measured R_s of entire root systems and their surrounding soil *in situ*, we empirically sought to understand the linkage of R_a to R_s. Using eight study species from a North American deciduous forest, we asked:

1) How do rates of root respiration relate to interspecific differences in root functional strategy? and,

2) Does the contribution of autotrophic (i.e., root) respiration to total belowground CO_2 efflux (R_a / R_s) vary with species and root functional strategy?

Regarding our first research question, if thicker root diameters are a conservative functional strategy (Bergmann et al., 2020; Eissenstat et al., 2015), we expected species with narrower root diameters to have higher rates of root tissue respiration than species with thicker roots. Tree species with thick roots (e.g., basal Angiosperms) are usually AM hosts (Valverde-Barrantes et al., 2017), which have different root functional trait – R_r relationships than ECM species (Burton et al., 2002; Gao et al., 2021). Additionally, high N_{root} is considered an acquisitive root functional trait, which can vary considerably among species and thus, we expected that R_a should be positively related to N_{root} (Burton et al., 2002; Paradiso et al., 2019; Reich et al., 2008). For the second question, we hypothesized that R_r might lead to a difference in R_a / R_s and that species with higher measured R_r should have greater R_a / R_s. Concerning mycorrhizal type, we expected that

ectomycorrhizal species should have more significant heterotrophic components (R_h) of R_s than arbuscular associated species, thus decreasing R_a / R_s, when R_r is equal.

Methods

In-situ root trays and custom respiration chamber

Eighty-six *in-situ* root system housings (hereafter trays) were constructed from 4-gallon square buckets (part number S-13650W, ULINE, Pleasant Prairie, WI). Buckets were sliced into about 2"-high square strips using a table saw; buckets tapered slightly from bottom (8 1/2" square) to top (9 7/8" square), which permitted nesting of strips inside one another. Two strips were nested within each other with a 2 mm fine aluminum wire mesh stretched over the bottom of the tray and secured between the two square strips with contractor staples. A notch was cut in the side of the tray to accommodate the placement of the root system within the tray. Trays were constructed to permit the repeated measurement of soil gas flux at the level of entire root systems and the surrounding soil.

Next, a custom respiration chamber was constructed for use with the Li-6800 portable gas exchange system (Li-COR Inc. Lincoln, NE), following their theory and recommendation (https://www.licor.com/env/support/LI-6800/topics/chamber-custom-note.html). The chamber measured 12" × 12" × 4 1/4" with an open front design and was constructed out of 1/2" acrylic sheeting by solvent bonding all pieces together. An 8mm 12V computer fan was installed to the top inside of the chamber to mix the chamber air volume. Holes were drilled in the back of the chamber to accommodate the Li-6800 custom chamber adaptor, which allowed it to interface with the gas exchange system; the chamber was secured to the gas exchange system with rubber washers and machine bolts, which minimized leaking. The front of the chamber was constructed out of the same 1/2" acrylic sheeting with a 2" by 1/2" notch to accommodate the root systems. The front of the chamber was fitted with 1" heavy-duty rubber weather stripping to seal its connection to the root box, and toggle clamps were installed to allow the chamber to be opened and closed as needed.

Study site

The study was carried out at the University of Tennessee Forest Resources Education Center and Arboretum in Oak Ridge, Tennessee (35.9935°N, 84.2201°W). The study area was located on the Chestnut Ridge research area to the northwest of the Arboretum grounds (Fig. S1). The site's soils are classified as Fullerton cherty silt loam (Typic Paleudult, clayey, kaolinitic, and thermic) with a bulk density of about 1.3 g cm^{-3}. These soils have a moderately fine granular texture, comprised about 15% gravel, and are hence, well-drained. They are dark greyish brown, mottled with yellowish-red in color, moderately acidic, and highly fertile (Luxmoore, 1982). From January 2019 to August 2020 (i.e., during the period of this study), cumulative monthly precipitation averaged 145 ± 13.1 (standard error) mm, and average maximum and minimum daily temperatures averaged 21.2 ± 0.3 °C and 10.4 ± 0.3 °C, respectively (meteorological station: Oak Ridge Museum, Data from Menne et al., 2012)

Forty study trees of eight species (five per species) were selected to target a range of root functional strategies (i.e., sample a variety of root morphologies), as root diameter roughly scales with plant evolutionary history (Valverde-Barrantes et al., 2017). The eight study species from evolutionarily oldest to youngest were: *Pinus taeda* L. (Pinaceae), *Liriodendron tulipifera* L. (Magnoliaceae), *Liquidambar styraciflua* L. (Altingiaceae), *Cercis canadensis* L. (Fabaceae), *Fagus grandifolia* L. (Fagaceae), *Acer rubrum* L. (Sapindaceae), *Nyssa sylvatica* Marshall (Nyssaceae), and *Oxydendrum arboreum* L. (DC.) (Ericaceae). Two of the eight species are ectomycorrhizal (*Pinus taeda*, *Fagus grandifolia*,), *Oxydendrum arboreum* is ericoid mycorrhizal, while the remaining five are arbuscular mycorrhizal. The *P. taeda* and *L. styraciflua* trees were found in a planted loblolly stand at the west end of the research area (see Fig. S1). The *L. tulipifera* and the *C. canadensis* trees were in an area at the east of the research area, which had been clear cut with a BioBaler (Anderson Group Inc, Chesterville, Quebec, Canada) about 15 years earlier. Trees of the remaining four species were found in a mature hardwood stand between the two areas, dominated by an Eastern deciduous oak-hickory forest community (Delcourt and Delcourt, 2000). Selected trees were 5 to 20 cm in diameter at 1.3m height, appeared healthy, and were far enough apart that root systems

were unlikely to overlap. Tree heights were measured using a telescoping measuring pole at the end of the experiment, and species averages ranged from 7.2m for Cercis canadensis to 14.6m for *Nyssa sylvatica* and *Oxydendrum arboreum*.

Experimental design and treatments

Complete fine root systems, comprising at least three root orders (McCormack et al., 2015), were traced out from target trees and gently excavated to the first-order roots. Root systems were placed in the *in-situ* root trays, with the transportive portion of the root system exiting a notch in the tray and still being connected to the tree. Two root systems per study tree were excavated and placed into the root trays in a paired design. Trays were filled with soil loosened during the excavation process and recessed in the ground to be even with the soil surface. After initial placement into root trays, all trays were well watered. Over time, separate experimental treatments were applied to tray pairs, as described below. If a root system was damaged or broken at some point during the experiment, a new root system was established into the root tray using the same soil; this occurred for 14 of 80 root systems. Three sets of trays not containing root systems were used as soil-only controls, where we measured respiration rates of soils for comparison to the measurements from trays containing roots. One was located at the edge of the hardwood stand and the pine plantation, a second was located within the hardwood stand, and a third was located near the *C. canadensis* and *L. tulipifera* stand.

For each pair of trays per study tree, one of two root trays was treated with ZeroTol (BioSafe Systems, Hartford, CT USA), a low-level, broad-spectrum algaecide, bactericide, fungicide, which uses peroxyacetic acid (2%), and hydrogen peroxide (17%) as the active ingredients, to reduce the abundance of soil microbes and fungi in the root microbiome. The ZeroTol was applied every two weeks for the duration of the experiment, with each dose consisting of approximately 350 mL of a 1% solution, which was enough to saturate the soil. The second tray of each pair was treated with about 350 mL of water to reduce any soil moisture effects of the ZeroTol application. Leaf litter was removed for each application of the ZeroTol and water and was replaced over the trays after.

Measurements of specific root respiration (R_r) and root system functional traits

On three dates, during the spring and summer of 2020 (March 26, May 20, and June 24), we measured specific respiration rates of excised entire root systems (R_r) for all study species. Root material was traced out and excavated from five trees of each species, being careful to keep each root system intact to their finest, first-order roots. Trees from which root systems were harvest were not those with the *in-situ* root trays but were in the same vicinity. Root material was thoroughly washed, removing all dirt. In some instances (e.g., *Fagus*, *Oxydendrum*, and *Pinus* roots), ectomycorrhizal hyphae were left attached to roots if removing them would damage the root system. Root material was delineated into entire root systems, containing at least three root orders including the finest first-order roots (as described in McCormack et al., 2015) by cutting root systems off at the fourth-order transportive root. Root systems were placed in a Walz WK-G1 respiration chamber, which was set to a temperature of 25°C. The Walz respiration chamber was attached to the Li-6800, which fed air into the chamber and recorded the gas exchange measurements. Stability criteria for these measurements were ΔCO_2, slope <0.25, and standard deviation <0.1 μmol mol^{-1} and ΔH_2O slope <0.25, and standard deviation <0.1 μmol mol^{-1}, assessed over a 20 s interval.

Following R_r measurements, root systems were scanned using a double-sided optical scanner (Epson Perfection V800, Epson America Inc.) at high resolution (1400 dpi) in black and white. Roots were then dried in paper bags at 60°C for several days and then weighed. Scanned root images were analyzed using WinRHIZO (2016 version, Regent Instruments, Quebec, Canada). WinRHIZO measures root length, area, average diameter volume, and architectural parameters of root systems. Specific root length (SRL) and specific root area (SRA) were calculated by dividing root length and area by root system dry mass, respectively. RTD was calculated as the ratio of the root system volume to its dry mass. Root samples were ground to a fine powder using 15-mL sterile plastic vials and 1mm stainless steel beads using the SPEX miniG 1600 (SPEX Sample Prep, Metuchen, NJ, USA). C and nitrogen (N) concentrations of root tissues (C_{root} and N_{root}, respectively) were determined using a CE Flash 1112 Elemental Analyzer (Thermo

Fisher, Waltham, MA USA) using standard carbon-nitrogen sample protocols at the Blue Carbon Analysis Lab at Florida International University in Miami, Florida.

Field Measurements of R_s

From June 2019 to May 2020, we measured gas exchange of the root trays using the Li-6800 portable photosynthesis system (Li-COR Inc., Lincoln, NE USA). Measurements were taken bi-weekly from June until November 2019, wherein measurements were done monthly for the winter months until March 2020. For each of the eighty root trays and the six soil-only controls, leaf litter was removed, and the tray was placed in the custom gas exchange chamber attached to the Li-6800. The chamber was closed and sealed around the root system at the transportive root, which was still attached to the tree, using plumber's putty (Oatey, Cleveland, OH USA). The air pump of the Li-6800 was set to high, resulting in a flow rate of between 1400 and 1500 μmols s^{-1}. Accounting for the volume of the chamber, the time constant (τ) of the gas exchange system, or the chamber volume to flow rate ratio, was about 260 seconds, meaning that the air in the chamber could completely turn over in that time. Therefore, we set the following stability criteria to be evaluated over a 60-second window: relative humidity of the chamber, slope <0.5% and standard deviation < 1%, and respiration rate, slope, and standard deviation both <1 μmol m^{-2} s^{-1}. Once stability was reached, the data point was logged.

During each root tray measurement, soil moisture and temperature of the top 5 cm of soil were measured. Soil moisture was measured with the SM150T soil moisture sensor with 5.1 cm measurement rods (from Delta T Devices Ltd. Cambridge, UK), and soil temperature was measured with a digital thermometer (accuracy 0.3°C, Fisherbrand Traceable Flipstick thermometer, Thermo Fisher, Waltham, MA). While root trays were in the gas exchange chamber, three measurements were taken in each of the three cardinal directions opposite the origin of the plant root and averaged. Root trays were collected on May 28, 2020, by cutting root systems from trees. Trays containing root systems and soil were allowed to dry for one week. This allowed for the soil in the trays to be dried and separated easily from root systems. Root systems were removed from the trays, washed, and assessed for root system health. Root systems from the *in-situ* root

trays were scanned in the same manner as roots used for R_r measurements, using a double-sided optical scanner (Epson Perfection V800, Epson America Inc.) at high resolution (1400 dpi) in black and white, and dried at 60°C for several days then weighed. The root system scans were analyzed using WinRHIZO (2016 version, Regent Instruments, Quebec, Canada) as described above. The total soil dry mass was weighed for each tray, and soils were sieved using sterile 1 mm mesh before laboratory analyses.

Laboratory Analyses of Soils – soil chloroform fumigation

Soil carbon pools reflect the amount of recalcitrant vs. labile carbon, which are a function of decomposition and activity of plant-root microbial associations (Trumbore, 2006, Condrol et al. 2010, Rossi et al. 2020), and soil nitrogen pools indicate soil microbial abundance and metabolic activity (Brookes et al., 1985, Insam 2001). To determine the effect of the ZeroTol treatment on soil microbial biomass (i.e., abundance), we used soil chloroform extraction. For each of the eighty root trays and the six soil-only controls, soil total organic carbon (TC), dissolved organic carbon (DOC), microbial carbon (MBC), total nitrogen (TN), dissolved nitrogen (DN), and microbial nitrogen (MBN) were determined using the chloroform fumigation technique (Brookes et al., 1985) on the dried, sieved soil samples. All analyses were performed using a Shimadzu TOC-L CSH/CSN analyzer (Shimadzu Scientific Instruments Inc. USA, Columbia, MD). TC and TN were measured by sample combustion catalytic oxidation and gas analysis per standard analysis protocols for the instrument. DOC and MBC were determined using the K_2SO_4 extraction and chloroform fumigation-extraction method. Briefly, 7 g soil was combined with 35 mL of 0.5M K_2SO_4, placed on a shaker for 1 hour, and then filtered through Whatman #1 filters. A second set of soil samples were placed in a desiccator with 20 mL chloroform under a vacuum of 11 atmospheres and fumigated for 48 hours prior to extraction with K_2SO_4 (as described above). Filtrate C content was determined with the combustion catalytic oxidation method on a Shimadzu TOC-L analyzer at Oak Ridge National Laboratory in Tennessee. Unfumigated samples represent DOC, and MBC is calculated as the difference between fumigated and unfumigated samples.

Laboratory analyses of soils – sequencing of microbial communities

Soil DNA extraction was performed with the DNEASY Powersoil HTP 96 Kit (Qiagen, Hilden, Germany) according to the manufacturer's instructions with DNA eluted in 100 µL water. Extractions were quantified with the Qubit dsDNA BR Assay kit and diluted to a concentration of 10 ng μL^{-1}. A two-step PCR (polymerase chain reaction) amplification approach was used with barcode tagged templates and primers targeting the V4 region of the 16S rRNA gene for archaea & bacteria and the ITS2 region for fungi using pooled primer sets to increase coverage of archaeal, bacterial, and fungal taxa (see Table S1). PCR amplification of target regions was performed using the following thermal cycler conditions: 95°C for 3 minutes, 25 cycles of 95°C for 30 seconds, 78°C for 30 seconds, 55°C for 30 seconds and 72°C for 30 seconds, and a final extension of 72°C for 5 minutes. The second step of PCR indexed reads using the conditions: 95°C for 3 minutes, eight cycles of 95°C for 30 seconds, 55°C for 30 seconds and 72°C for 30 seconds, and a final extension of 72°C for 5 minutes. After PCR amplification and indexing, all samples were pooled equimolar and purified with Agencourt AMPure XP beads (0.7:1 bead to DNA ratio; Beckman Coulter Inc., Pasadena, CA, USA). Paired-end sequencing (2 x 251) was completed on pooled prepared libraries on an Illumina MiSeq instrument (San Diego, CA) at Oak Ridge National Laboratory using V2 chemistry, which included a 15% PhiX sequencing control library.

Microbial sequences were processed with QIIME 2 v 2020.2 platform (Bolyen et al., 2019). Paired sequences were demultiplexed with the plugin demux and quality filtered (denoised, dereplicated, chimera filtered, and pair-end merged) and processed in Sequence Variants (SVs) with the dada2 plugin (Estaki et al., 2020). Taxonomy was assigned using a pre-trained Naive Bayes classifier based on the Silva trimmed to the 515F/806R primer pair (16S) or the Unite (ITS) databases. Unassigned sequences, mitochondrial, and chloroplast sequences were removed. Sequence variant-based richness and Shannon diversity were calculated with the QIIME package. Beta diversity (Bray-Curtis) was calculated with the phyloseq package (McMurdie and Holmes, 2013).

Statistical analyses – Functional differences among species

We tested for statistical differences in root functional traits, including tissue elemental concentrations, using single-factor analysis of variance (ANOVA). One-way ANOVAs were calculated to test for statistical differences among species for SRL, $C_{root,}$ and N_{root}. For each response, Tukey's post hoc test for honest significant differences (HSD) was used to determine which species were distinct from one another.

Statistical analyses – analyzing soil nutrient pools & microbial biomass, richness, and diversity

Analysis of variance was used to examine differences in soil carbon (TC, DOC, MNC) and nitrogen pools (TN, DN, MBN) from the soil chloroform extractions and differences in bacterial 16s and fungal ITS richness and Shannon diversity. ANOVA models were fitted considering effects by species, treatment, collection area (as explained above in the study area description, see Fig. S1), and any possible interactions between those three factors. Model selection was performed to determine the best fitting ANOVA models for each response variable. Concerning the soil carbon and nitrogen pool data, models were indistinguishable for TN, DN, and MBC and microbial carbon (MBC). For TC, the ANOVA with just an effect for species was the best-fitting model, and for DOC, that same model (i.e., with just an effect of species) was marginally better-fitting ($p = .076$). The best-fitting model for MBN included effects for species, treatment, and their interaction. Regarding bacterial 16S richness and Shannon diversity, all ANOVAs were equivalent; however, for fungal ITS richness and Shannon diversity, the best-fitting ANOVA models had terms for species, treatment, collection area, and an interaction term for treatment with collection area.

Statistical analyses – root functional trait space and R_r

For each of the three measurements (March, May, and July) and their average, we tested for differences between R_r among species using single factor ANOVAs, followed by a post hoc Tukey HSD test. A principal components analysis (PCA) was used to characterize the root functional trait space for the eight study species. Ten root functional traits were used: root system average diameter, length, surface area, and tip abundance, SRL, SRA, specific root tip abundance (SRTA), RTD, and root tissue C and N

concentrations. Species mean root functional trait values from 15 entire root systems each were scaled and centered and then used for PCA. The first two axes of the PCA explained >80% of the trait variation among species. To examine relationships between the root functional trait space and specific respiration rates (i.e., research question 1), average R_r rates (measured from the same 15 entire root systems per species over three separate sampling periods, Table 2) were regressed (ordinary least squares regression) against the first two PC axes.

Statistical analyses – modeling root respiration for the in-situ root trays

To relate rates of root tissue respiration measured from excised entire root systems to the in-situ root trays, we used the Q_{10}-temperature relationship of Palta & Noble (1989, Atkin et al., 2000, Fig. S2). Average R_r measured at 25°C (Table 2) was used in combination with the Q_{10}-temperature function of Palta and Noble (1989) via Atkin et al. (2000) to create R_r-temperature response curves for each species. In other words, the R_r measurements from excised root systems determined the elevation of the R_r-temperature relationship, and we use the assumption of Q_{10}-temperature variation on R_r to construct the shape of the R_r-temperature curve which is identical for all species (Fig. S2).

Then, for each tray, rates of *in situ* root system respiration (R_a) at soil temperature were calculated from the R_r-T relationship by species, accounting for fine root system biomass, as measured at the end of the experiment. We found it best to model R_s trends and examine the contribution R_a to R_s using mass-based fluxes because this allowed us to work with raw fluxes of CO_2 after accounting for variation in root biomass and soil dry mass between trays. We completed our analyses also with area-based fluxes, and our results were qualitatively similar, but area-based R_s created difficulty interpreting results because root material was measured on a per-mass basis. It is unclear if the shallow depth of the root tray (2 inches) affected area-based inferences. Thus, R_r at the soil measurement T (in nmol g^{-1} s^{-1}) was multiplied by the amount of root biomass per tray. R_s (the sum of R_a and R_h, as the emergent measurement taken with the respiration chamber) was calculated as a mass-based flux using formulae for mass-based CO_2 fluxes developed by Li-Cor and dry mass of soil for each tray.

A separate PCA was done using root morphological measurements from the root systems housed in the root trays. The PCA used eight functional traits: root system average diameter, length, surface area, and tip abundance, SRL, SRA, SRTA, RTD (i.e., the same as those used for the PCA of the root systems where R_r was measured except for root C and N content). Using trait data from the individual root systems accounted for trait variation among root systems and species.

We modeled the ratio of root respiration to total CO_2 efflux from root-soil tray system (R_a / R_s) using a linear mixed-effects model (i.e., gaussian error with identity link function). R_a / R_s values were log-transformed to improve their normality. We explored including fixed effects for measurement date, root functional trait principal components 1 and 2 (from the PCA using root morphological data from root systems housed in the root trays), treatment (i.e., control vs. ZeroTol trays), soil moisture, soil temperature, mycorrhizal type (i.e., and species identity and random intercept terms for species, root tray, and root tray nested within species. The 'step' function was used to find the best fitting mixed-effects models, which uses backward model section on the random and fixed parts of the model (in that order) based on AIC. The best-fitting model included fixed effects for each sampling date. Model coefficients from the best-fitting model were estimates using restricted maximum likelihoods. Analyses were done using R v.4.0.3 (R Core Team, 2020) and made use of the lme4 (Bates et al., 2015), lmerTest (Kuznetsova et al., 2017), and sjPlot (Lüdecke, 2018) packages.

Results

Functional variation among study species

Root functional traits varied considerably among species, demonstrating that the eight species studied represented a wide range in root functional strategies. SRL varied about 6 m g^{-1} among the eight study species, ranging from about 3 m g^{-1} for *Liquidambar styraciflua* to about 9 m g^{-1} for *Cercis canadensis* (Table 1). Root C concentrations varied little among species ranging from about 41 to 43 mg g^{-1}; while the *F*-statistic was statistically significant, the Tukey HSD groupings were not different. N_{root} varied up to 0.85 mg g^{-1} and was greater for *Cercis canadensis* and *Liriodendron tulipifera* than the

other tree species studied (except for *Liriodendron tulipifera* compared to *Oxydendrum arboreum*).

Table 1: Root functional trait values for eight temperate tree species in the study. Specific root length (SRL) and root tissue elemental concentrations are averages for each species from 15 root systems excavated during the spring and summer of 2020. Asterix notation for statistical significance of F-statistics (ANOVA) is as follows: $*p < .05$, $**p < .01$, $***p < .001$, otherwise non-significant. Post-hoc Tukey HSD pairwise comparison groupings are denoted with letters.

Species	SRL ($m\ g^{-1}$)	C_{root} ($mg\ g^{-1}$)	N_{root} ($mg\ g^{-1}$)
Acer rubrum L.	8.22 ± 1.27^{CD}	41.85 ± 1.64^{A}	0.79 ± 0.07^{A}
Cercis canadensis L.	9.06 ± 0.67^{D}	42.24 ± 1.18^{A}	1.64 ± 0.11^{C}
Fagus grandifolia L.	5.17 ± 0.32^{ABC}	41.51 ± 1.03^{A}	0.80 ± 0.05^{A}
Liriodendron tulipifera L.	4.38 ± 0.36^{AB}	40.85 ± 0.60^{A}	1.41 ± 0.07^{B}
Liquidambar styraciflua L.	3.20 ± 0.31^{A}	41.52 ± 0.91^{A}	0.79 ± 0.07^{A}
Nyssa sylvatica Marshall	7.06 ± 0.97^{BCD}	43.25 ± 0.56^{A}	0.92 ± 0.04^{A}
Oxydendrum arboreum (L.) DC.	5.88 ± 0.48^{ABC}	41.73 ± 0.47^{A}	1.11 ± 0.14^{AB}
Pinus taeda L.	4.18 ± 0.55^{AB}	42.87 ± 0.98^{A}	0.95 ± 0.11^{A}
$F_{species}$	$F_{(7, 113)} =$ 8.534***	$F_{(7, 43)} =$ 0.665*	$F_{(7, 43)} =$ 16.11***

The differences in the multivariate root functional trait space among a greater suite of root traits were summarized in a PCA (Fig. 1A), which used species average functional trait values (from 15 excised entire root systems) for ten root functional traits (root system average diameter, N_{root}, SRA, root system area, SRL, root system length, SRTA, tip abundance, RTD, and root C content). The first two axes of the PCA explained 83.2% of the variation in root functional variation among the eight study species. Principal component 1 (PC1, the x-axis in Fig. 1A) depicts root length and diameter tradeoff. In contrast, component 2 (PC2, the y-axis) is directly related to high N_{root} and SRA, with root C content and RTD trading off with these two traits, although not directly (i.e., not being complete opposite in the PCA; Fig. 4). Thus, the PCA adequately characterized functional variation in root morphologies among species, justifying regression with R_r rates.

Specific root respiration rates – variation among species and with root functional traits

Specific root respiration (R_r) rates were variable over time and among species (Table 2). There was a considerable variation in R_r over the spring to summer months

when excised root systems were collected and measured (Table 2). Variation in measured R_r over this time was not systematic in that some species showed an increase in R_r from spring to summer (e.g., *Acer rubrum*), while others showed a decrease (e.g., *Pinus taeda*). Despite this, statistical differences in R_r among species emerged for each measurement, with patterns among species being qualitatively consistent (see Table 2 for *F*-statistics and Tukey HSD grouping by measurement). Thus, the average R_r rates over the three measurements are likely the best representation of variation in R_r among the eight study species. *Liriodendron tulipifera* had the greatest average R_r, being at least double that of the remaining seven species ($F_{(7,113)} = 13.95$, $p < .001$; Table 2), with average R_r rates of the remaining seven species were all contained in the same Tukey HSD grouping (Table 2).

Table 2: Average (± standard error) specific root respiration rates for eight temperate tree species. Respiration was measured at 25°C for excised entire root systems (with ≥ three root orders) using a Li-6800 portable gas exchange system attached to a Walz 3010-GWK1 chamber. Three replicates of five root systems per species were measured during each measurement date in the spring and summer of 2020. Averages are given in the rightmost column, which were used to estimate tissue respiration rates for *in-situ* root trays using the temperature-response curves constructed via the Q_{10}-temperature function from Palta & Noble (1989, see methods and Fig. S2).

Species	Measurement 1 3/26/2020 (n=5) nmol g^{-1} s^{-1}	Measurement 2 5/20/2020 (n=5) nmol g^{-1} s^{-1}	Measurement 3, 7/24/2020 (n=5) nmol g^{-1} s^{-1}	Average (n=15) nmol g^{-1} s^{-1}
Acer rubrum L.	2.18 ± 0.18^{A}	3.58 ± 0.66^{A}	4.45 ± 0.80^{A}	3.41 ± 0.41^{A}
Cercis canadensis L.	4.51 ± 0.72^{AB}	5.42 ± 1.15^{AB}	2.50 ± 0.28^{A}	4.14 ± 0.54^{A}
Fagus grandifolia L.	3.02 ± 0.28^{A}	2.64 ± 0.60^{A}	1.81 ± 0.31^{A}	2.49 ± 0.26^{A}
Liriodendron tulipifera L.	10.02 ± 2.66^{B}	7.17 ± 0.68^{B}	9.94 ± 1.68^{B}	9.04 ± 1.05^{B}
Liquidambar styraciflua L.	2.03 ± 0.64^{A}	4.33 ± 0.92^{AB}	2.51 ± 0.29^{A}	2.96 ± 0.45^{A}
Nyssa sylvatica Marshall	5.66 ± 0.95^{AB}	3.18 ± 0.58^{A}	1.79 ± 0.17^{A}	3.54 ± 0.55^{A}
Oxydendrum arboreum (L.) DC.	3.74 ± 1.54^{A}	3.00 ± 0.36^{A}	1.94 ± 0.12^{A}	2.89 ± 0.53^{A}
Pinus taeda L.	5.57 ± 0.74^{AB}	4.34 ± 0.96^{AB}	3.75 ± 0.16^{A}	4.56 ± 0.33^{A}
	$F_{(7,32)} = 4.509^{**}$	$F_{(7,32)} = 4.375^{**}$	$F_{(7,32)} = 15.84^{***}$	$F_{(7,113)} = 13.95^{***}$

The regression of R_r rates on PC1 (i.e., the tradeoff in root length and diameter) was not statistically significant, yet a slight trend was evident (Fig. 4=1B; slope $p = .20$). However, the regression of R_r rates on PC2 (i.e., the Nroot – RTD axis of root functional variation) was statistically significant (Fig. 4C, slope $p = .02$). Thus, species with higher N_{root} typically had higher R_r rates. Because N_{root} was aligned almost perfectly to the negative side of PC2, we can interpret the slope of the regression in terms of N_{root}, meaning that for the eight temperate trees species in this study, respiration rates roughly decline 1 nmol g^{-1} s^{-1} per mg g^{-1} decrease in N_{root} (Fig. 1C).

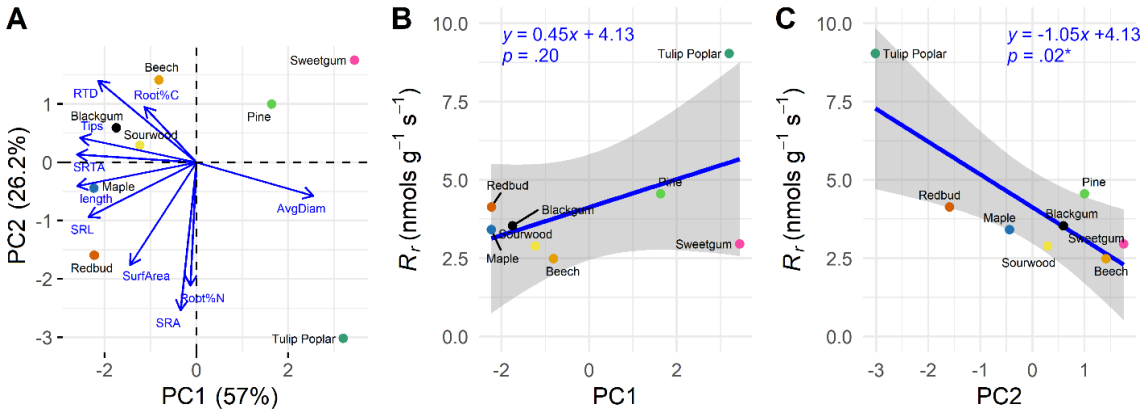

Fig. 1: A) Principal components analysis of root functional traits for eight temperate tree species (Maple: *Acer Rubrum* L., Redbud: *Cercis canadensis* L., Beech: *Fagus grandifolia* L. Tulip Poplar: *Liriodendron tulipifera* L. Sweetgum: *Liquidambar styraciflua* L., Blackgum: *Nyssa sylvatica* Marshall, Sourwood: *Oxydendrum arboreum* (L.) DC., Pine: *Pinus taeda* L., where point color matches the Latin binomials in Fig. 3). The PCA uses species mean root functional trait values from 15 entire root systems collected during the spring and summer of 2020. Functional traits considered included morphological traits derived from WinRHIZO (2016b version, Regent Instruments, Ontario, Canada) and root tissue elemental analysis for root C and N concentrations. B and C) linear regressions of specific root respiration rates (R_r) and principal component axes. PC1 represents a tradeoff in root diameter and root tip abundance, while PC2 represents the N_{root} - RTD tradeoff. Regression equations and p-values for regressions slopes are shown.

Soil bacterial and fungal communities – the effect of the ZeroTol treatments on in-situ root trays

Overall, the effect of the ZeroTol on microbial communities was weak in that it did not completely sterilize the soils as intended. While, application of the low-level algaecide-bactericide-fungicide, ZeroTol, led to a decrease in microbial (i.e., bacterial)

biomass in the root trays as evidenced by a decrease in MBN concentrations ($F_{(1,75)}$ = 31.660, p < .001; Fig. 1F, Table S2), it had no effect on bacterial 16S community composition (Fig. 2A), species richness, or Shannon diversity (Table S3). This was confirmed with the ANOVA analysis, which found that the ZeroTol treatment did not significantly affect 16S alpha richness ($F_{(1,82)}$ = 2.612, p = .11). Including effects for species or collection area or their interactions with treatment did not improve the ANOVA or lead to an increase in the ZeroTol treatment effect. Similarly, the effect of the ZeroTol on 16S Shannon Diversity was non-significant ($F_{(1,82)}$ = 1.763, p = .19), and all ANOVAs (i.e., those examining the effect of species, treatment, collection area, and all possible interactions) were statistically equivalent.

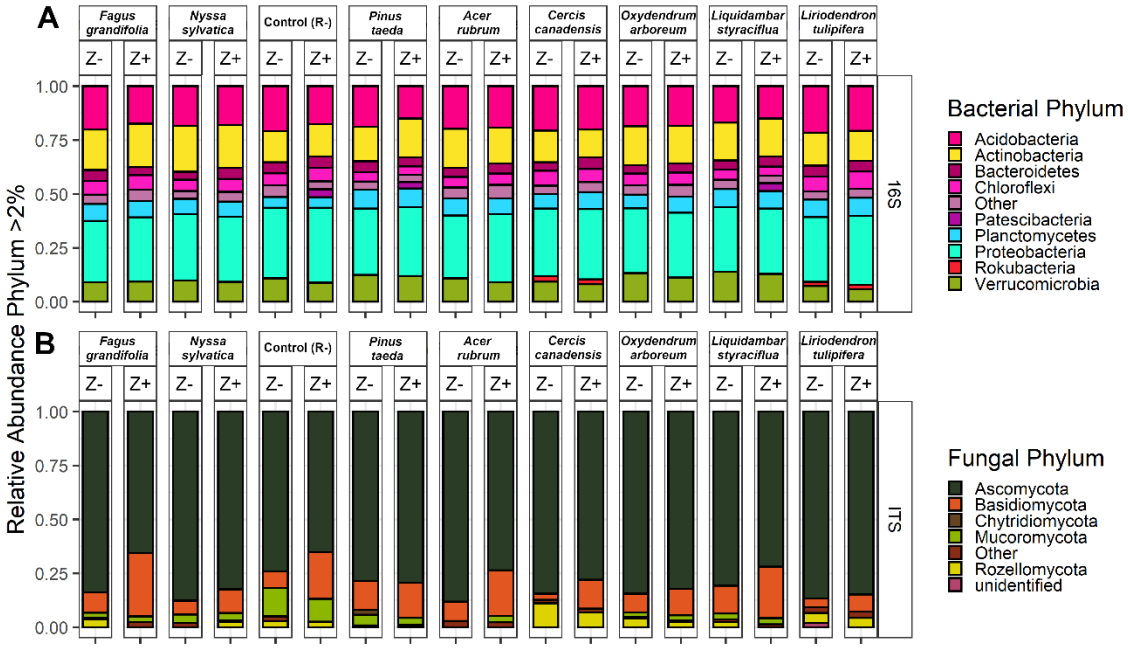

Fig. 2: Phylum level relative abundance in 16S bacterial (A) and fungal ITS (B) gene sequences from the soil of 80 *in situ* root trays for eight temperate tree species. Phyla comprising <2% of sequence reads are not included. ZeroTol treatments (Z+) and controls (Z-) trays for each species (n = 5 trays per treatment per species) and soil-only controls lacking roots (R-, n = 3 per treatment) are shown.

Fungal ITS richness and diversity were similarly unaffected by the ZeroTol treatment, although in the trays of some species, there was an increase in the relative abundance of Basidiomycota at the expense of Ascomycota (Fig. 2B, Table S3). In the ANOVAs for ITS richness and Shannon Diversity, which included effects for collection

area, species, treatment, and an interaction between treatment and collection area, the effect of treatment was not significant (richness: $F_{(1,71)} = 0.37$, $p = .54$, Shannon diversity: $F_{(1,71)} = 0.12$, $p = .50$). Differences in ITS fungal richness were observed between collection areas ($F_{(3,71)} = 6.45$, $p < .001$) and among tree species : ($F_{(5,71)} = 3.73$, $p < .01$), however. Similarly, fungal ITS Shannon Diversity was statistically different between collection areas ($F_{(3,71)} = 4.07$, $p < .01$) and among tree species : ($F_{(5,71)} = 2.46$, $p < .05$).

Except for the difference in MBN among treatments, differences in soil carbon and nitrogen pools were found among species, but not between treatments (Fig. 3, see Table S2 for *F*-statistics). For example, total and dissolved organic carbon differed statistically among species based on the ANOVA (TC: $F_{(9,75)} = 3.05$, $p < .01$; DOC: $F_{(9,75)} = 2.618$, $p < .05$) although Tukey HSD groupings show no difference among species. The same trend was evident in soil total and dissolved nitrogen (TN: $F_{(9,75)} = 2.08$, $p < .05$; DN: $F_{(9,75)} = 2.618$, $p < .10$; Table S2).

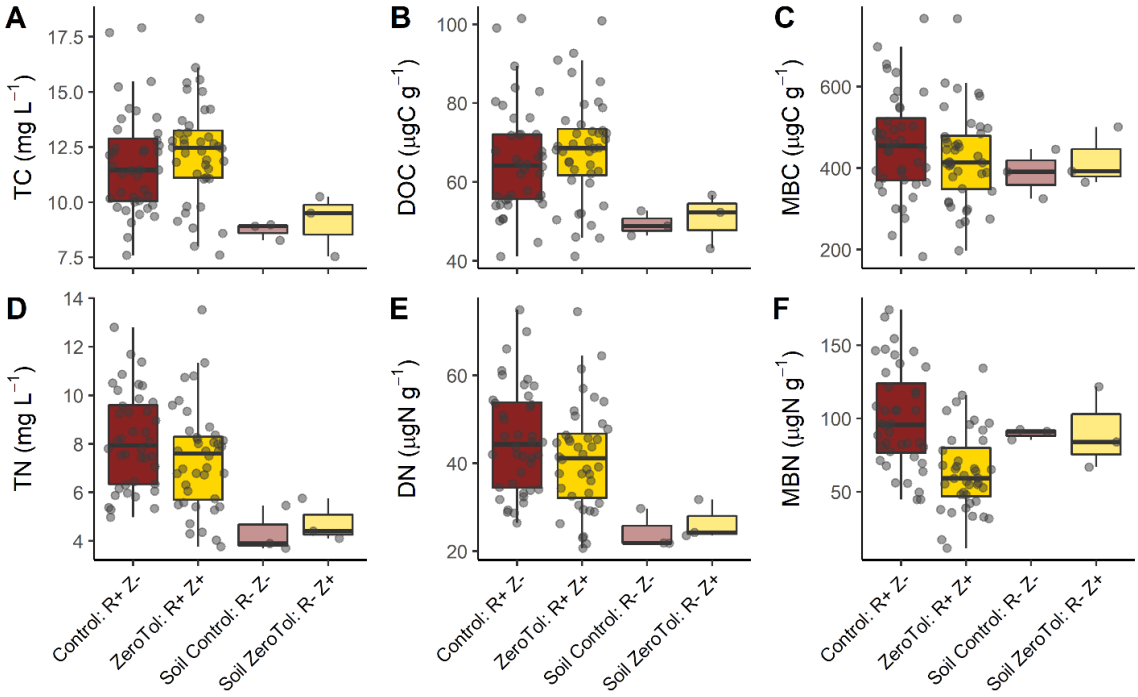

Fig. 3: Soil carbon and nitrogen pools from 80 in-situ root trays and soil only controls – results from soil chloroform fumigation-extraction analyses. Measurements (points) for total soil carbon (TC, A), dissolved organic carbon (DOC, B), microbial carbon (MBC, C), total nitrogen (TN, D), dissolved nitrogen (DN, E), and microbial nitrogen (MBN, F) by treatment are shown, where n = 40 for the control and ZeroTol treatments on the in-situ root trays (R+) and n = 3 for those respective treatments on soil only controls (R-).

MBN (B) is an indicator of soil bacterial abundances because it measures the cytoplasmic component of soil microbial biomass (Brookes et al., 1984). The box and whisker plots show the mean and interquartile ranges.

The NMS of root tray soil bacterial and fungal communities showed that soil microorganismal composition was primarily structured by collection area (Fig. 4), despite differences in the ANOVA analysis for collection area only being detectable for fungal ITS sequences and not 16S bacterial sequences. Indeed, the clustering of fungal ITS communities by collection in Fig. 3 is more distinct than the clustering of the bacterial communities; however, in both the fungal and bacterial composition, we see three distinct assemblages of species, where communities are similar for species in the planted Loblolly stand at the west end of the study area (*Pinus taeda* and *Liquidambar styraciflua),* for the species in the eastern end of the study area in the area that was clear-cut in the last decade (*Liriodendron tulipifera* and *Cercis canadensis*) and among the four species sampled in the forested area in between (*Nyssa sylvatica*, *Acer rubrum*, *Fagus grandifolia*, and *Oxydendrum arboreum*, see Fig. S1).

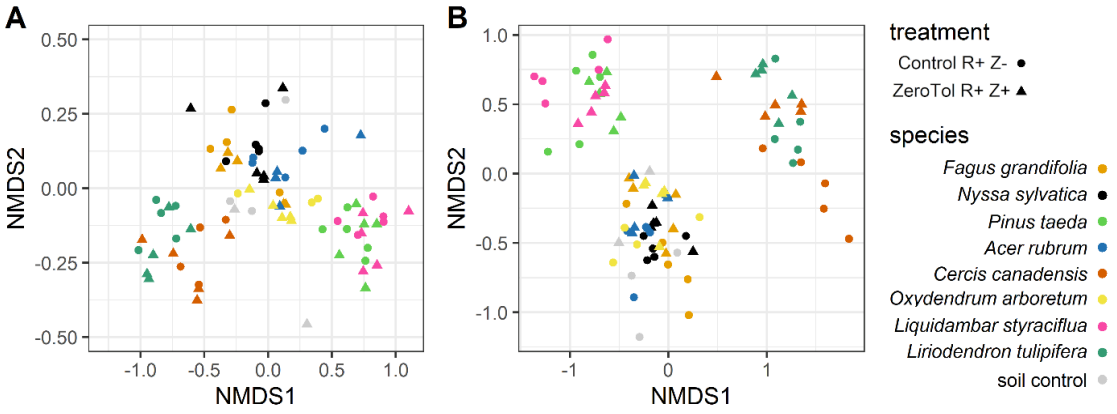

Fig. 4: Non-metric multidimensional scaling of 16S bacterial (A) and fungal ITS (B) gene sequences from the soil of the *in-situ* root trays by tree species and treatment. Symbols show root tray treatments, with triangles corresponding to treatment with the broad-spectrum algaecide/ fungicide/ bactericide ZeroTol (1% hydrogen peroxide & peroxyacetic acid), and circles corresponding to untreated soil. Colors show studied tree species with grey symbols showing the soil-only controls (i.e., lacking roots).

Estimating the contribution of R_r to R_s for the in-situ root trays

Total soil surface CO_2 efflux from the *in-situ* root trays (R_s) ranged from 0.30 to 11.99 µmol m^{-2} s^{-1} (11.74 to 475.42 nmol kg^{-1} s^{-1}) and averaged 2.21 ± 0.04 µmol m^{-2} s^{-1}

(82.47 ± 1.51 nmol kg^{-1} s^{-1}) over the 11-month study period (Fig. S3). For the soil only control trays (i.e., those lacking roots, R-), total soil surface CO_2 efflux ranged from 0.48 to 7.13 μmol m^{-2} s^{-1} (19.78 to 314.49 nmol kg^{-1} s^{-1}), averaging 1.73 ± 0.11 μmol m^{-2} s^{-1} (67.85 ± 4.61 nmol kg^{-1} s^{-1}). Accounting for variation in the amount of soil among trays, the total raw CO_2 flux from trays ranged from 14.43 to 583.66 nmol s^{-1}, with a mean value of 107.46 ± 2.00 nmol s^{-1} and with 95% of observations measuring between 26.09 and 317.94 nmol s^{-1} (Fig. S4A).

Using some assumptions about how R_r varies with temperature via the Q_{10}-temperature function of Palta & Noble (1989; Fig. S2; Atkin et al., 2002), we separated the R_s measurements from the *in-situ* root trays into R_a and R_h components. The partitioning of R_s was best done using mass-based measurements of soil CO_2 efflux because R_a was calculated on a per root system mass basis using R_r for the entire root systems housed in the in-situ root trays. R_a varied from 0.15 to 18.04 nmol s^{-1}, averaging 2.18 ± 0.06 nmol s^{-1} (Fig. S4B) and with 95 % of measurements being between 0.28 and 7.57 nmol s^{-1} (Fig. S4B). Thus, the R_a : R_s ratio, or the contribution of autotrophic root respiration to total belowground CO2 efflux for the in-situ root trays, was between 0.52e-3 and 0.65 with 95% of observations measuring between 2.72e-3 and 0.13 (Fig. S4C). Accordingly, the 95% confidence interval for the contribution of root respiration to the total CO_2 efflux from root-soil tray system (R_a / R_s) was 0.27% to 12.86%.

Effects of root morphology on R_a / R_s

Our second research question inquired if differences in root functional traits could explain variation in belowground CO_2 efflux. Moreover, given the differences in R_r among species (Table 2, Fig. 1), we could ask which axis of the root functional trait space best relates to species-driven variation in R_a / R_s? Root morphological differences were determined by a second PCA using root trait data from the root systems housed in the trays. This second PCA was similar to the first PCA, in that STA roughly trades off with RTD on axis 2, being organized orthogonally to SRL. The first two principal components of that functional trait space accounted for the vast majority (nearly 83%) of the functional trait variation among the root system housed in the in-situ root trays. SRL and the root tip abundance were the largest contributors to principal component 1 (PC1),

each explaining about 17% of the variation in the first axis (although axis 1 was also associated with total root length, root system surface area, SRA, SRTA, and root system average diameter). In contrast, RTD was the largest contributor to principal component 2 (PC2), explaining about 54% of the variation in the second axis (Fig. 5A). The best-fitting linear mixed-effects model included fixed effects for both components, with coefficients being negative (β for PC1 = -0.24, $p < .001$, β for PC2 = -0.24, $p < .001$, Fig. S6, Table S4). Thus, root systems that had higher SRL, root tip abundance, and separately, higher RTD had greater R_a / R_s fractions, and the contribution of R_a to R_s decreased as root system SRL, tip abundance, and RTD decreased (Fig. 5B).

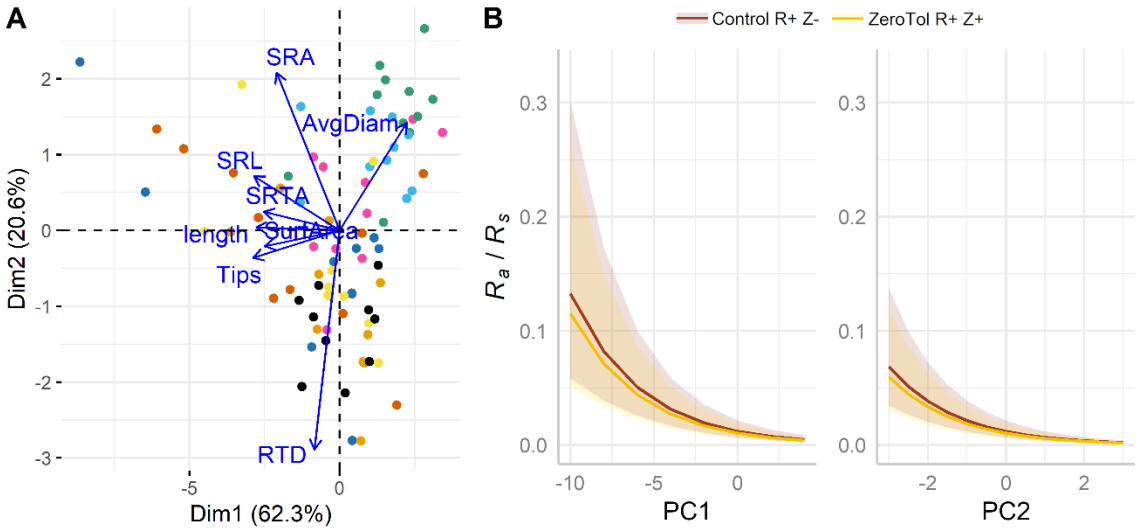

Fig. 5: A) Principal components analysis for root morphological traits of 80 entire root systems placed in *in-situ* root trays. Arrows show root trait variable loadings within the trait space, while individual points show locations of each root system within the root functional trait space. Points are colored by species in correspondence with the Latin binomials in Fig. 3. Abbreviations are: SRL – specific root length, SRA – specific root area, SRTA – specific root tip abundance, and RTD – root tissue density. SRL and root tip abundance (Tips) are loaded heaviest on PC1, and RTD is loaded heaviest on PC2. B) predicted average marginal effects of PC1 and PC2 on the ratio of autotrophic root respiration to soil respiration (R_a / R_s) from the linear mixed-effects model. R_a / R_s from the *in-situ* root trays is positively related to SRL, number or root tips (left panel in B), and RTD (right panel) and decreases as SRL, tip abundance, and RTD decrease.

Variation in R_a / R_s – treatment, seasonal, soil moisture, and soil temperature effects

Differences in area-based soil CO_2 efflux rates between the control and ZeroTol-treated trays of a sampled tree ranged from 8.31 μmol m^{-2} s^{-1} greater to 4.65 μmol m^{-2} s^{-1}

smaller in the ZeroTol trays relative to control trays, with 95% of observations being between 2.61 μmol m^{-2} s^{-1} greater and 1.42 μmol m^{-2} s^{-1} smaller, respectively (Fig. S3). There was a tendency for area-based soil CO_2 efflux rates to be greater in ZeroTol than in Control trays, especially for *Fagus sylvatica*, *Pinus taeda*, and *Liriodendron tulipifera* (Fig. S3). However, when soil and root system masses were incorporated, differences in mass-based R_s between treatments were subtle (Fig. S4). Differences in R_s and R_a were similarly minor among the ZeroTol and control root trays. Because of the slight difference in root system biomass with the trays of each treatment, average R_s was 13.45 nmol s^{-1} greater in the ZeroTol root trays than in the controls, and average R_a was 0.21 nmol s^{-1} greater in the ZeroTol root trays than in the control root trays (Fig. S4).

Differences in root biomass among trays of different treatments were particularly evident for root systems of *Pinus taeda*, which had slightly more root system biomass in ZeroTol than in control trays ($F_{(1,8)} = 3.05$, $p = .12$). These differences in root system biomass led to greater estimated R_a in the ZeroTol than the control trays for Pinus taeda, creating differences in R_a / R_s. For all species, there were no differences among treatments in root system biomass ($F_{(1,64)} = 0.01$, $p = 0.98$), however there were differences among species ($F_{(7,64)} = 2.56$, $p = .02$), and the interaction between treatment and species was non-significant ($F_{(7,64)} = 1.51$, $p = .18$). Accordingly, the model selection procedure used to determine the best-fitting linear-mixed effects model did not initially include an effect for treatment; however, we opted to include an effect for treatment to aid in inference and because including the effect did not significantly improve or decrease model fit. Including the effect of treatment allows for estimating the effects of other factors after accounting for the effect of the ZeroTol on CO_2 efflux rates. Additionally, linear mixed-effects models including non-significant effects are statistically equivalent to those that omit their inclusion. However, the overall effect of the ZeroTol on R_a / R_s was slightly negative, meaning that the contribution of root respiration to total belowground CO_2 efflux decreased in the ZeroTol trays.

The mixed-effects model (Table S4, Fig. S8) showed that temporal fluctuations in R_a / R_s dominated the variability in the dataset. There was a clear and significant increase in R_s just before leaf senescence and shed in the fall months (i.e., September and early

October) (Fig. S3). The mixed-effects models showed that at least some of the increase in R_s during this time was related to R_a, as the R_a / R_s fraction increased (Fig. 6A). The mixed-effects models showed that the average marginal effect of date (i.e., the effect of sampling date alone on R_a / R_s, holding all other variables in the fixed effects constant) was greatest for measurements taken on these dates (September 13, 25 and October 10, 2019, β values all near 1, see Fig. S6). Additionally, the best-fitting mixed-effects model included terms for soil moisture and temperature, which also varied over time. Mean soil moisture ranged from about 11% to about 30% and tended to be higher in the winter and spring months relative to the fall (Table S5). Average soil temperatures fluctuated between 6 and 26°C and were lowest from November until the beginning of March (Table S5). The effect of soil moisture on R_a / R_s alone (i.e., the average marginal effect) was negative (β of -0.04, $p < 0.05$, TableS4, Fig. 6B). However, the effect of soil temperature alone on R_a / R_s was positive (β of 0.41, $p < 0.001$, TableS4, Fig. 6C).

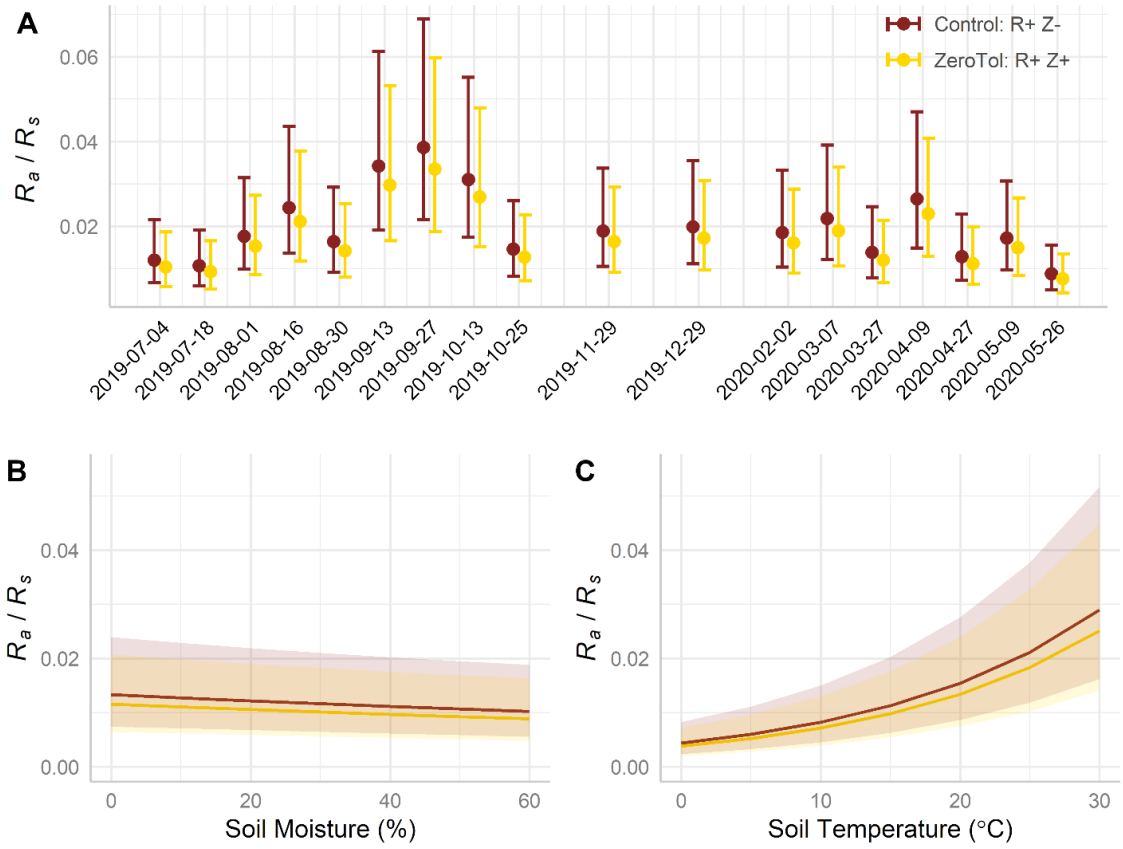

Fig. 6: Predicted mean marginal effects for time, soil moisture and soil on R_a / R_s. A) Predicted average marginal mean (±95 % confidence interval) contribution of root

respiration to total soil CO_2 efflux (R_a / R_s) over time. Estimates are for entire root systems (i.e., root systems of 3-4 root orders or physiologically active root tissue, ranging between about 1 and 3 g dry mass) within 1-2 kg of soil. Control root trays (treated with water only) are colored brown, and ZeroTol-treated trays (sprayed with peracetic acid, hydrogen peroxide) are colored yellow. B) Generalized linear-mixed model-predicted mean changes in the contribution of root respiration to total soil CO_2 efflux with soil temperature and soil moisture (C) by treatment. Shaded regions are 95% confidence intervals.

Additional effects of tree species on R_a / R_s

A random intercept term for species was included in the best-fitting linear mixed-effects model. This random effect accounted for variation in R_a / R_s because of species identity not otherwise accounted for in variation among root systems, as represented in the PCA axes. Notably, we did not measure N_{root} for the root systems placed within the in-situ root trays, so the random intercept term for species may represent some functional variation among species and their root functional strategies. The empirical best linear unbiased predictors (BLUPs) are shown in Fig. S6. Four species (*Oxydendrum arboreum*, *Cercis canadensis*, *Acer rubrum,* and *Fagus grandifolia* had negative BLUPs with 95% confidence intervals, not including 0. Two species (*Liriodendron tulipifera* and *Pinus taeda*) had positive BLUPs with 95% confidence intervals, not including 0, and the remaining two species (*Liquidambar styraciflua* and *Nyssa sylvatica*) had BLUPs with 95% confidence intervals including 0, and thus were not different from the intercept of the mixed-effects model. These results illustrate that even after accounting for morphological difference among root systems of the tree species, *Pinus taeda* and *Liriodendron tulipifera* had greater contributions of R_a to R_s than *Oxydendrum arboreum*, *Cercis canadensis*, *Acer rubrum,* and *Fagus grandifolia*, with *Liquidambar styraciflua* and *Nyssa sylvatica* being statistically equal to these two species groupings (Fig. S6, Table S4). These results were robust to random variance due to individual root trays with variance three times more structured among species than among trays (see Table S4).

Indeed, *Liriodendron tulipifera* and *Pinus taeda* showed the greatest modeled increase of R_a / R_s concerning root system variation in SRL and root tip abundance (PC1) and RTD (PC2, Fig. 7). Similarly, these two species showed strong variation over time and with soil moisture and temperature (Fig. 6). Conversely, the four species with

negative BLUPs, *Oxydendrum arboreum*, *Cercis canadensis*, *Acer rubrum,* and *Fagus grandifolia,* had little increase in the contribution of R_a to R_s over time, with root system functional variation, or with variation in soil moisture and temperature (Fig. 7). Lastly, the mode of fungal association among tree species did not contribute significantly to explaining variation in R_a / R_s. Tree species mycorrhizal type was the only term dropped from the backward model selection procedure, signifying that after time, soil moisture, soil temperature, root system morphology (as represented by PC1 and PC2), and the random intercept terms for species and root tray, there was no remaining variance in R_a / R_s to be explained by mycorrhizal type. This came despite a mean difference in R_s and R_a being 19.89 nmol s^{-1} and 0.82 nmol s^{-1} greater for AM than ECM species, respectively, resulting in R_a / R_s being greater by 0.007%, on average, for AM than ECM species (Fig. S5).

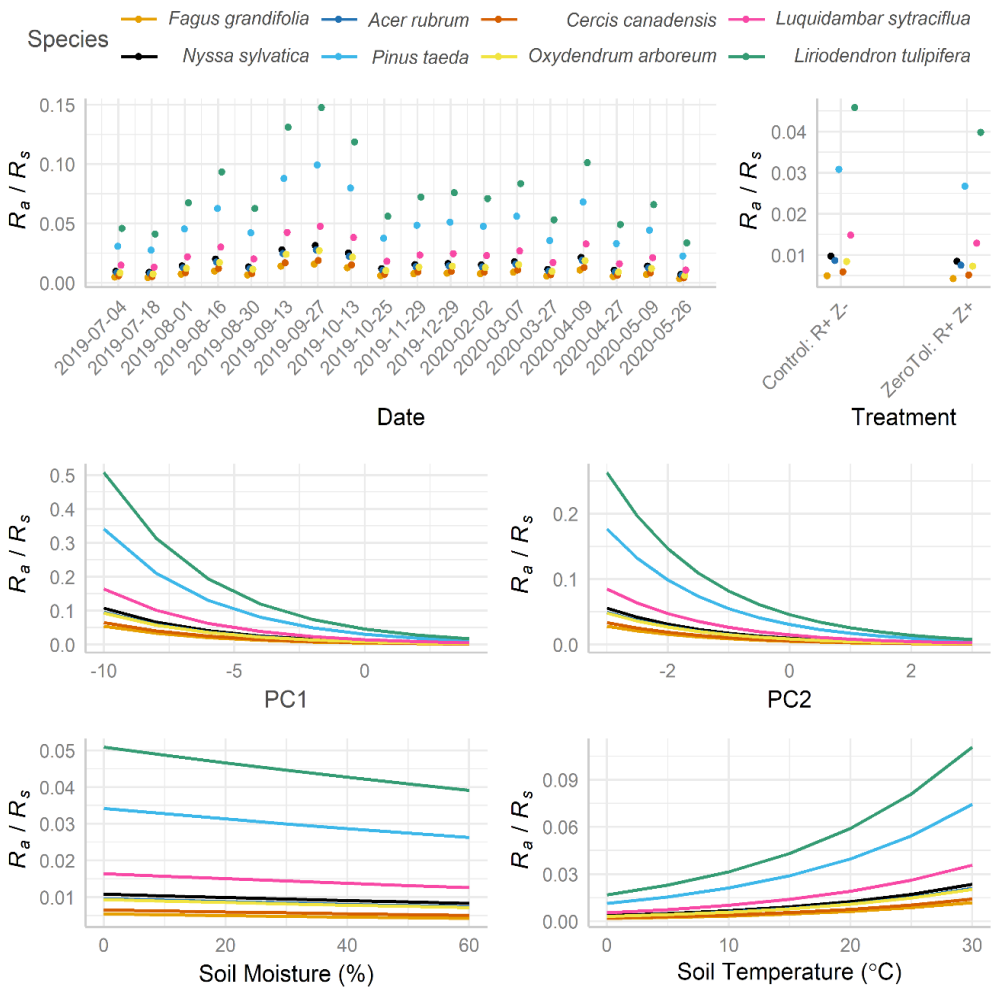

Fig. 7: (previous page) Mean marginal effects for date, treatment, root functional trait space PC1, PC2, soil moisture, and soil temperature on R_a / R_s for each of the eight study species**.** These plots are the same as the mean marginal effects plotted in Figs. 5 and 6 of the main text; however, they are conditioned on the empirical best linear unbiased predictors of species (shown in Fig. S6 bottom left panel).

Discussion

Interpreting R_r results concerning tree species functional strategy

Specific root tissue respiration rates (R_r) have been demonstrated to scale with the RTD – N_{root} content axis of functional trait variation in root strategy (Burton et al., 2002; Ceccon et al., 2016; Gao et al., 2021; Jia et al., 2013; Makita et al., 2015; Paradiso et al., 2019; Reich et al., 2008). N_{root} reflects variation in species ability to acquire for soil N, which is a function of soil N availability and the myriad metabolic processes by which roots uptake and assimilate N. Variation in species abilities to acquire and assimilate N informed our hypothesis about how root strategy, as indicated by root functional traits would relate to R_r; specifically, we questioned whether species with thicker root diameters, as a proxy for the conservative root strategy, had higher R_r. Root functional trait data from the eight temperate tree species studied here, condensed nicely into two axes of variation, with a N_{root} falling directly onto axis 2, which was clearly related to R_r and inversely related to RTD, and root system diameter trading off with root system tip abundance on axis 1. Thus, we confirm previous findings that R_r scales with the RTD – N_{root} tradeoff in root functional strategy. We found marginal support for the hypothesis that R_r is positively related to root system diameter; however, this was driven by the high R_r for the thick-rooted *Liriodendron tulipifera*. The root systems of *L. tulipifera*, *Liquidambar styraciflua*, and *Pinus taeda* have relatively few root tips per root system compared to the other five species in the study, and our results indicate that high root tip abundance likely leads to lower R_r. These results need to be tested and verified across more species.

Root functional strategy and its effect on Ra / R_s

Our second research question addressed whether variation in R_r as a function of root morphology would translate to differences in the contribution of root respiration to total belowground CO_2 efflux from the in-situ root trays (i.e., R_a / R_s). The hypothesis

was that species with higher R_r would contribute a more significant proportion of R_a to R_s and that the magnitude of the contribution might be modulated by mycorrhizal type (i.e., with AM species contributing on average more than ECM species because of differences in labile carbon allocation to within root metabolic processes vs. fungal symbionts). The contribution of R_a to R_s was positively related to root system acquisitiveness, as represented by the principal components of root system variation, with axis 1 most-strongly representing variation SRL and root tip abundance and axis 2 representing RTD variability. Thus, the contribution of *Ra* to R_s decreased with decreasing SRL, root system tip abundance, and RTD.

The minimal effect of the ZeroTol treatment on R_s

The ZeroTol treatments lysed bacteria, which primed soil fungi in cases (i.e., accelerated the proliferation of fungi because of available nutrients related to dead bacteria), yet overall, the net effect on bacterial richness or diversity was slight and non-significant. Microbial N dropped as a result of repeated bi-weekly ZeroTol application to the soil surface, illustrating that bacterial loads were affected slightly, as intended. Despite that, rates of CO_2 efflux from ZeroTol trays were not different from control trays (i.e., those treated with water only, Fig. S3 & Fig. S4A), providing evidence for a compensatory dynamic between the contribution of bacterial and fungal R_h to R_s. Although the linear mixed-effects model, which included an effect for treatment, was statistically the same as the model, which did not include an effect for treatment, opting to include the effect helped estimate the effect of the ZeroTol alone on R_a / R_s. The effect was negative, meaning that the ratio (or the contribution of R_a to R_s) decreased slightly. This decrease in the R_a / R_s ratio was primarily driven by a slightly greater R_s in the ZeroTol trays (Fig. S3) via an increased abundance of certain fungal groups (e.g., the Basidiomycota, Fig. 2). The effect was particularly evident for the four species that were studied in the native forest area (*Nyssa sylvatica*, *Oxydendrum arboreum*, *Fagus grandifolia*, and *Acer rubrum*), as well as the soil-only controls.

Future studies that seek to sterilize soils should rely on more reliable methods (e.g., gaseous chemical application, as opposed to liquid), which often use more potent and hazardous chemicals (e.g., methyl bromide, chloroform, mercuric chloride, etc.).

Despite the efficacy of many potent agents in sterilizing soils, there are often side effects on soil fertility (Trevors, 1996), which we wanted to avoid because of the effects that changes in soil nutrient availability can have on root growth and morphology. As sterilizing the soil was a secondary objective to our research questions related to root morphology Rr and the contribution of Ra to RS, we opted to use a low-potency, organic chemical liquid (i.e., the ZeroTol).

Comparing measured R_s fluxes with other studies – interpreting temporal variation in R_a / R_s over time

In a similar *Fagus sylvatica* forest in northeastern France, Epron et al. (1999) found that root respiration accounted for 60% of the soil CO_2 efflux; total soil CO_2 efflux measured 1.74 μmol m^{-2} s^{-1}, of which the root-associated portion was estimated to be about 1.06 μmol m^{-2} s^{-1}. In the present study, we measured total CO_2 efflux to be around 2.17 (± 0.04 standard error, n= 1537) μmol m^{-2} s^{-1}; however, because we were working at the level of the individual entire root system (which contains three or more root orders), the amount of root biomass per unit soil area or volume was a great deal less than what would occur in normal conditions. Hence, we estimated root respiration in the trays to be, on average, 2.9 (± 0.01 standard error) %. There was considerable temporal variation, and the contribution of root respiration to total soil CO_2 efflux peaked in the fall of 2019 (i.e., August to September), contributing between 5.5 and 7.5% of total soil CO_2 efflux (Fig. 6). Thus, our measurements are roughly comparable to those in the literature for similar forests.

In temperate deciduous forests of the Northern hemisphere, temporal variability in the direct (via R_a) autotrophic contribution to R_s peaks in the late fall (Edwards and Sollins, 1973; Yang and Wang, 2006). Additionally, the increased litterfall during this time can lead to an increase in R_s (Metcalfe et al., 2011; Raich and Tufekciogul, 2000). Our results provide support to the understanding that at least some of the increase in R_s during the fall is related to increases in R_r. Empirically, across a variety of forest types, the autotrophic and heterotrophic components of R_s have been shown to correlate to one another (Bond-Lamberty et al., 2004), as they are linked via labile C allocation and partitioning among the plant-soil system, which varies over time as trees modulate their

aboveground to belowground carbon allocation (Chen et al., 2011; Chen et al., 2014; Metcalfe et al., 2011).

Many studies support our findings of the positive effects soil temperature on R_a / R_s (Chen et al., 2011; Edwards and Sollins, 1973; Reichstein and Beer, 2008). R_r is highly temperature dependent, increasing on average about 2 nmol g^{-1} per 10°C increase in soil temperature (Atkin et al. 2000). Soil temperature varied consistently with season in the temperate deciduous forest studied, here, and plant metabolic activity slowed considerable in the winter months when trees were leafless, which also likely indirectly affected R_r and thus R_a *in situ*. The positive relationship between the contribution of R_a to R_s and increasing soil temperatures could also be a result of temperature-dependent metabolic process within soils and how roots interact with soil microhabitats to modulate the flow or air and water and other resources through the soil matrix to facilitate microbial activity (i.e., R_h) (Davidson and Janssens, 2006; Metcalfe et al., 2011). However, such relationships with soil temperature may equal in magnitude as the effect of variation carbon allocation on R_a / R_s (Bond-Lamberty et al., 2004; Chen et al., 2014)

Implication for ecosystem models: root traits matter

Most ecosystem or terrestrial biosphere models include R_s (belowground carbon flux) as a major component of system carbon loss (see summary table in Warren et al., 2015). It is often modeled as a fraction of total gross primary productivity, which sometimes varies with the root biomass stock or root age, and within some models, R_s magnitudes vary as it competes with other carbon sinks for photosynthate allocation. To our knowledge, such models have never included root functional traits such as SRL, RTD, or mycorrhizal type as potential modulators of R_s. In addition to temporal dynamics, our results show that species with acquisitive morphologies such as higher SRL and greater root tip abundance contribute a more significant percentage of R_a to R_s. However, RTD, a trait associated with a conservative root functional strategy, also positively affects R_a / R_s. These seemingly contrasting results provide evidence for the multidimensionality of root trait-physiological relationships, where orthogonal root functional traits from competing root functional (i.e., acquisitive vs. conservative) strategies can have similar

effects on a physiological response or ecosystem process (Bardgett et al., 2014; Bergmann et al., 2020; Freschet et al., 2020; Laliberté, 2017; Weemstra et al., 2016)

Physical models of R_s within the soil seldom include root properties (Blagodatsky and Smith, 2012; Reichstein and Beer, 2008). However, a compelling case for including aggregate (i.e., community level) root system traits within the soil A horizon (first half-meter or so) can be made. The physical (i.e., length and density), chemical (e.g., tissue properties and exudates), and physiological traits (e.g., mycorrhizal affinities) modulate the physical soil environment through their feedbacks on the flow of water, gasses, and solutes through the root-soil system. For example, using state-of-the-art rhizotron technology in a mixed temperate forest, total daily R_s was found to be correlated with variation in variation in total fine root length, which was not related to short-term changes in soil volumetric water content (Vargas and Allen, 2008). Thus, the physical presence of roots and variation in their morphological traits likely influence R_s magnitude.

Root traits are also related to the biological components of the root-soil system. A recent study showed that the ratio of root-inhabiting fungi to bacteria decreased with increasing SRL and microbial community composition (i.e., the ratio of gram-positive to gram-negative bacteria) was related to RTD (Wan et al., 2021). Such effects of root functional traits on soil microbial communities and hence soil functioning superseded effects of leaf litter or individual tree effects, illustrating the need to incorporate root functional traits into our understanding and modeling of soil biogeochemical dynamics. A second recent study showed that the finest (i.e., 1st and 2nd order) roots modulate (i.e., environmentally filter) bacterial community composition to the most significant degree and that microbial loads are largest on the most physiologically active fine roots (King et al., 2021). This process occurred for bacterial communities, which were already distinct among the roots of the six temperate tree species examined. Linking similar biological variation in microbial associations of tree roots at the root system (or even root order) levels and linking them to soil biogeochemical processes via root physiology and functional traits holds excellent promise in deepening our understanding of root-level controls R_s and its contribution to R_s.

Assumptions of the method and the analytical approach

Determining the R_a contribution to R_s for each in-situ root tray relies on several assumptions. First, we assumed that the biomass of the root systems is not changing over time and that measurements of root system biomass at the end of the experiment represent the entire experimental period; and second, we assumed that root morphology is consistent over time. We imaged root systems before their installation in the *in-situ* root trays, and visual comparison of these images with the root system scans showed that generally, root systems were similar in morphological form and extent at the end of the experiment to that at the beginning. In some cases, roots decreased in health or increased slightly in root tip abundance. However, there were no clear trends observed across the 80 root systems studied. Moreover, the method places some stress on the transportive base of the root system, which remains attached to the tree and is repeatedly excavated and sealed to take measurements using the custom chamber. Several (14 in total) root systems broke (i.e., became detached) from the tree during measurement, but new root systems were promptly re-established in the trays. Tree species differ in their transportive root strength and toughness, and the *Liriodendron* roots were the most fragile, which is consistent with observations from other studies (Eissenstat et al., 2015).

Additionally, we assume a universal temperature sensitivity of R_r to model R_a, which was derived from the Q_{10}-temperature relationship for *Agave deserti* roots by Palta & Noble (1989, see Atkin et al. 2000). Ideally, we could have measured the R_r – temperature response curves; however, doing so would have significantly increased the time it takes to measure a single root system (i.e., from minutes to hours per root system). As root systems need to be measured immediately after excision, this dramatically decreases the number of root systems one can measure over a given period of time. We opted for a sampling strategy that examined variation in R_r at 25 °C in relation to root morphology, as was dictated by the first research objective. However, the assumption that the Q_{10} values of R_r do not vary much across species is supported by empirical evidence. For example, a recent study by Noh et al. (2020) found no difference in the Q_{10} values of R_r for temperate versus tropical seedlings (using eight species, four temperate and four tropical) grown between 16 and 32 °C. Q_{10} values ranged from 1.77 to 2.46 and

averaged 2.15, which mirrors that range of Q_{10} values we used to model R_a (root system respiration at soil temperature for roots housed in the in-situ root trays) from R_r (root tissue-specific respiration rates, see Fig. S2). Additionally, the temperature sensitivity of temperate tree R_r (at least for Sugar Maple and Red Pine) has been shown to be consistent (i.e., not statistically different) among seasons, further supporting the use of a consistent Q_{10}-temperature relationship in R_a models (Burton and Pregitzer, 2003). Therefore, any temporal variance should be evenly distributed among the eight study species).

Using a novel method, we repeatedly measured the belowground CO_2 efflux of 80 entire root systems for a year. This new approach has the advantage of isolating individual entire root systems of 3-4 root orders of the most physiologically active root tissues, which facilitated linking root physiology to morphology at the root system level. However, this comes at a cost because it artificially creates a scenario where a single root system is isolated and housed within about 1 kg (2434 cm^3) of soil. Having a single root system within this area of soil is unrealistic considering that for the forest type that the study was conducted in, 74 % of fine roots can be found in the top 30 cm of soil with a fine root density of about 600 g m^{-2} (Joslin and Wolfe, 1999). Therefore, fine root systems of many individuals are typically present in 1 kg of surface soil under typical environmental conditions. Despite the artificially low representation of root to soil biomass in the in-situ root trays, we were still able to partition total autotrophic root respiration (R_a) from heterotopic respiration, illustrating that the method worked as envisioned.

Conclusion

Repeated measurements of R_s for entire root systems and their surrounding soil *in situ* and some applied assumptions enabled our estimate that the contribution of R_a to R_s for functional entire root systems of 3 to 4 root orders ranges from 0 to 10 %, averaging 2-3%. The R_a / R_s fraction increased with root acquisitiveness, as represented by root system functional trait space, with SRL and root tip abundance increasing R_a / R_s, but also increased with RTD, a conservative root functional trait. Specific respiration rates of excised root systems showed similar patterns concerning root functional strategy, being most strongly related to variation in Nroot, which was arranged roughly opposite RTD in

the root functional trait space and being more weakly related tradeoff in root diameter vs. root tip abundance. Such variation in R_r with root functional strategy translated to the variation in R_a / R_s, although not perfectly, pointing to interactions between R_a and R_h which contribute to R_s.

The ZeroTol experimental treatment modified the soil microbiome on root trays where it was applied, although not strongly. Microbial loads decreased; however, bacterial richness and diversity were unaffected. Opportunistic fungi were able to take advantage of increased available soil N, increasing in abundances with changes in fungal community composition occurring in some of the in-situ root trays. Increases in soil fungi presence where bacteria had died because of ZeroTol led to a slight but negligible increase in R_s. More importantly, fungal increases demonstrate a compensatory dynamic between bacteria and fungi to create resistance in the magnitude of R_s to disturbance. Moreover, these results show that declines in R_s are invariant to some degree to reduction in microbial abundances are to a certain degree without significantly reducing affecting.

Temporal and environmental variation were also essential modulators of R_a / R_s. The ratio peaked at the beginning of fall, which coincided with forest canopy leaf senescence, likely as allocation of labile C to roots increased. Higher soil moisture slightly negatively affected the ratio, likely as soil waterlogging decreases R_a, potentially shifting metabolic activity away from C allocation and transfer dynamics toward prioritizing water uptake. Warmer soil temperatures increased the ratio, probably through temperature effects on enzymatic kinetics of root physiological processes and via increases in soil metabolic processes. Thus, root systems are physiologically dynamic within the soil microbiome, especially at the rhizosphere, yet extending into the larger soil environment. The respiratory signal of functional root systems in R_s is subtle yet evident.

References

Atkin, O.K., Edwards, E.J., Loveys, B.R., 2000. Response of root respiration to changes in temperature and its relevance to global warming. New Phytologist 147(1), 141-154.

Bardgett, R.D., Mommer, L., De Vries, F.T., 2014. Going underground: root traits as drivers of ecosystem processes. Trends in Ecology & Evolution 29(12), 692-699.

Bates, D., Mächler, M., Bolker, B., Walker, S., 2015. Fitting Linear Mixed-Effects Models Using lme4. Journal of Statistical Software 67(1), 1-48.

Bennett, J.A., Maherali, H., Reinhart, K.O., Lekberg, Y., Hart, M.M., Klironomos, J., 2017. Plant-soil feedbacks and mycorrhizal type influence temperate forest population dynamics. Science 355(6321), 181-184.

Bergmann, J., Weigelt, A., van der Plas, F., Laughlin, D.C., Kuyper, T.W., Guerrero-Ramirez, N., Valverde-Barrantes, O.J., Bruelheide, H., Freschet, G.T., Iversen, C.M., Kattge, J., McCormack, M.L., Meier, I.C., Rillig, M.C., Roumet, C., Semchenko, M., Sweeney, C.J., van Ruijven, J., York, L.M., Mommer, L., 2020. The fungal collaboration gradient dominates the root economics space in plants. Science Advances 6(27), eaba3756.

Blagodatsky, S., Smith, P., 2012. Soil physics meets soil biology: Towards better mechanistic prediction of greenhouse gas emissions from soil. Soil Biology and Biochemistry 47, 78-92.

Bolyen, E., Rideout, J.R., Dillon, M.R., Bokulich, N.A., Abnet, C.C., Al-Ghalith, G.A., Alexander, H., Alm, E.J., Arumugam, M., Asnicar, F., 2019. Reproducible, interactive, scalable and extensible microbiome data science using QIIME 2. Nature Biotechnology 37(8), 852-857.

Bond-Lamberty, B., Bronson, D., Bladyka, E., Gower, S.T., 2011. A comparison of trenched plot techniques for partitioning soil respiration. Soil Biology and Biochemistry 43(10), 2108-2114.

Bond-Lamberty, B., Thomson, A., 2010a. A global database of soil respiration data. Biogeosciences 7(6), 1915-1926.

Bond-Lamberty, B., Thomson, A., 2010b. Temperature-associated increases in the global soil respiration record. Nature 464(7288), 579-582.

Bond-Lamberty, B., Wang, C., Gower, S.T., 2004. A global relationship between the heterotrophic and autotrophic components of soil respiration? Global Change Biology 10(10), 1756-1766.

Bouma, T.J., Nielsen, K.L., Eissenstat, D.M., Lynch, J.P., 1997. Estimating respiration of roots in soil: Interactions with soil CO2, soil temperature and soil water content. Plant and Soil 195(2), 221-232.

Brookes, P., Landman, A., Pruden, G., Jenkinson, D., 1985. Chloroform fumigation and the release of soil nitrogen: a rapid direct extraction method to measure microbial biomass nitrogen in soil. Soil Biology and Biochemistry 17(6), 837-842.

Bryla, D.R., Eissenstat, D.M., 2005. Respiratory Costs of Mycorrhizal Associations. In: H. Lambers, M. Ribas-Carbo (Eds.), Plant Respiration: From Cell to Ecosystem. Springer Netherlands, Dordrecht, pp. 207-224.

Burton, A., Pregitzer, K., Ruess, R., Hendrick, R., Allen, M., 2002. Root respiration in North American forests: effects of nitrogen concentration and temperature across biomes. Oecologia 131(4), 559-568.

Burton, A.J., Pregitzer, K.S., 2003. Field measurements of root respiration indicate little to no seasonal temperature acclimation for sugar maple and red pine. Tree Physiology 23(4), 273-280.

Campbell, J. L., Law, B. E. (2005). Forest soil respiration across three climatically distinct chronosequences in Oregon. Biogeochemistry, 73(1), 109-125.

Ceccon, C., Tagliavini, M., Schmitt, A.O., Eissenstat, D.M., 2016. Untangling the effects of root age and tissue nitrogen on root respiration in Populus tremuloides at different nitrogen supply. Tree Physiology 36(5), 618-627.

Chen, G.-s., Yang, Y.-s., Guo, J.-f., Xie, J.-s., Yang, Z.-j., 2011. Relationships between carbon allocation and partitioning of soil respiration across world mature forests. Plant Ecology 212(2), 195-206.

Chen, G., Yang, Y., Robinson, D., 2014. Allometric constraints on, and tradeoffs in, belowground carbon allocation and their control of soil respiration across global forest ecosystems. Global Change Biology 20(5), 1674-1684.

Cleveland, C., Nemergut, D., Schmidt, S., Townsend, A., 2007. Increases in soil respiration following labile carbon additions linked to rapid shifts in soil microbial community composition. Biogeochemistry 82(3), 229-240.

Comas, L., Bouma, T., Eissenstat, D., 2002. Linking root traits to potential growth rate in six temperate tree species. Oecologia 132(1), 34-43.

Condron, L., Stark, C., O'Callaghan, M., Clinton, P., Huang, Z., 2010. The role of microbial communities in the formation and decomposition of soil organic matter, Soil microbiology and sustainable crop production. Springer, pp. 81-118.

Davidson, E.A., Janssens, I.A., 2006. Temperature sensitivity of soil carbon decomposition and feedbacks to climate change. Nature 440(7081), 165-173.

Delcourt, H., Delcourt, P., 2000. Eastern Deciduous Forests of Eastern North America. In: M. Barbour, W. Billings (Eds.), North American terrestrial vegetation. Cambridge University Press, Cambridge, UK, pp. 357-395.

Edwards, N.T., Sollins, P., 1973. Continuous measurement of carbon dioxide evolution from partitioned forest floor components. Ecology 54(2), 406-412.

Eissenstat, D.M., Kucharski, J.M., Zadworny, M., Adams, T.S., Koide, R.T., 2015. Linking root traits to nutrient foraging in arbuscular mycorrhizal trees in a temperate forest. New Phytologist 208(1), 114-124.

Epron, D., Farque, L., Lucot, E., Badot, P.-M., 1999. Soil CO2 efflux in a beech forest: the contribution of root respiration. Annals of Forest Science 56(4), 289-295.

Estaki, M., Jiang, L., Bokulich, N., McDonald, D., González, A., Kosciolek, T., Martino, C., Zhu, Q., Birmingham, A., Vázquez-Baeza, Y., Dillon, M., Bolyen, E., Caporaso, J., Knight, R., 2020. QIIME 2 Enables Comprehensive End-to-End Analysis of Diverse Microbiome Data and Comparative Studies with Publicly Available Data. Current Protocols in Bioinformatics 70(1), e100.

Fang, C., Moncrieff, J.B., 1999. A model for soil CO2 production and transport 1: Model development. Agricultural and Forest Meteorology 95(4), 225-236.

Freschet, G.T., Roumet, C., Comas, L.H., Weemstra, M., Bengough, A.G., Rewald, B., Bardgett, R.D., De Deyn, G.B., Johnson, D., Klimešová, J., 2020. Root traits as drivers of plant and ecosystem functioning: current understanding, pitfalls and future research needs. New Phytologist. doi: 10.1111/nph.17072

Gao, J., Zhou, M., Shao, J., Zhou, G., Liu, R., Zhou, L., Liu, H., He, Y., Chen, Y., Zhou, X., 2021. Fine root trait-function relationships affected by mycorrhizal type and climate. Geoderma 394, 115011.

Hanson, P.J., Edwards, N.T., Garten, C.T., Andrews, J.A., 2000. Separating root and soil microbial contributions to soil respiration: A review of methods and observations. Biogeochemistry 48(1), 115-146.

Hanson, P.J., O'Neill, E.G., Chambers, M.L.S., Riggs, J.S., Joslin, J.D., Wolfe, M.H., 2003. Soil Respiration and Litter Decomposition. In: P.J. Hanson, S.D. Wullschleger (Eds.), North American Temperate Deciduous Forest Responses to Changing Precipitation Regimes. Springer New York, New York, NY, pp. 163-189.

Hill, P.W., Garnett, M.H., Farrar, J., Iqbal, Z., Khalid, M., Soleman, N., Jones, D.L., 2015. Living roots magnify the response of soil organic carbon decomposition to temperature in temperate grassland. Global Change Biology 21(3), 1368-1375.

Högberg, P., Nordgren, A., Buchmann, N., Taylor, A.F.S., Ekblad, A., Högberg, M.N., Nyberg, G., Ottosson-Löfvenius, M., Read, D.J., 2001. Large-scale forest girdling

shows that current photosynthesis drives soil respiration. Nature 411(6839), 789-792.

Insam, H., 2001. Developments in soil microbiology since the mid-1960s. Geoderma 100(3-4), 389-402.

Janssens, I., Lankreijer, H., Matteucci, G., Kowalski, A., Buchmann, N., Epron, D., Pilegaard, K., Kutsch, W., Longdoz, B., Grünwald, T., 2001. Productivity overshadows temperature in determining soil and ecosystem respiration across European forests. Global Change Biology 7(3), 269-278.

Jia, S., McLaughlin, N.B., Gu, J., Li, X., Wang, Z., 2013. Relationships between root respiration rate and root morphology, chemistry and anatomy in Larix gmelinii and Fraxinus mandshurica. Tree Physiology 33(6), 579-589.

Johnson, D.J., Clay, K., Phillips, R.P., 2018. Mycorrhizal associations and the spatial structure of an old-growth forest community. Oecologia 186(1), 195-204.

Joslin, J.D., Wolfe, M.H., 1999. Disturbances during minirhizotron installation can affect root observation data. Soil Science Society of America Journal 63(1), 218-221.

Katabuchi, M., 2015. LeafArea: an R package for rapid digital image analysis of leaf area. Ecological Research 30(6), 1073-1077.

Keller, A.B., Brzostek E.B., Craig M.E., Fisher J.B., Phillips R.P., 2021. Root -derived inputs are major contributors to soil carbon in temperate forests, but vary by mycorrhizal type. Ecology Letters 24(4), 626-635.

King, W.L., Yates, C.F., Guo, J., Fleishman, S.M., Trexler, R.V., Centinari, M., Bell, T.H., Eissenstat, D.M., 2021. The hierarchy of root branching order determines bacterial composition, microbial carrying capacity and microbial filtering. Communications Biology 4(1), 1-9.

Kuznetsova, A., Brockhoff, P.B., Christensen, R.H.B., 2017. lmerTest Package: Tests in Linear Mixed Effects Models. 2017 Journal of Statistical Software 82(13), 26.

Kuzyakov, Y., 2006. Sources of CO2 efflux from soil and review of partitioning methods. Soil Biology and Biochemistry 38(3), 425-448.

Laliberté, E., 2017. Below-ground frontiers in trait-based plant ecology. New Phytologist 213(4), 1597-1603.

Lang, A.K., Jevon, F.V., Ayres, M.P., Matthes, J.H., 2020. Higher soil respiration rate beneath arbuscular mycorrhizal trees in a northern hardwood forest is driven by associated soil properties. Ecosystems 23(6), 1243-1253.

Lavigne, M.B., Roster, R.J., Goodine, G., Bernier, P.Y., Robitaille, G., 2003. Soil respiration responses are controlled more by roots than by decomposition in balsam fir ecosystems. Canadian Journal of Forest Research 33(9), 1744-1753.

Liming, Y., Dijkstra, F.E., Phillips, R.E., Zhu, B., Wang, P., Chen, W., 2021. Arbuscular mycorrhizal trees cause a higher carbon to nitrogen ratio of soil organic matter decomposition via rhizosphere priming than ectomycorrhizal trees. Soil Biology and Biochemistry 157, 108246.

Lüdecke, D., 2018. sjPlot: Data visualization for statistics in social science. R package version 2(1).

Luxmoore, R.J., 1982. Physical characteristics of soils of the southern region: Fullerton and Sequoia series. ORNL-5868, Oak Ridge National Lab., TN (USA).

Madani, N., Parazoo, N.C., Kimball, J.S., Ballantyne, A.P., Reichle, R.H., Maneta, M., Saatchi, S., Palmer, P., Liu, Z., Tagesson, T., 2020. Recent amplified global gross primary productivity due to temperature increase is offset by reducted productivity due to water contsrtians. AGU Advances 1, e2020AV000180.

Makita, N., Hirano, Y., Sugimoto, T., Tanikawa, T., Ishii, H., 2015. Intraspecific variation in fine root respiration and morphology in response to in situ soil nitrogen fertility in a 100-year-old *Chamaecyparis obtusa* forest. Oecologia 179(4), 959-967.

Makita, N., Kosugi, Y., Dannoura, M., Takanashi, S., Niiyama, K., Kassim, A.R., Nik, A.R., 2012. Patterns of root respiration rates and morphological traits in 13 tree species in a tropical forest. Tree Physiology 32(3), 303-312.

McCormack, M.L., Dickie, I.A., Eissenstat, D.M., Fahey, T.J., Fernandez, C.W., Guo, D., Helmisaari, H.S., Hobbie, E.A., Iversen, C.M., Jackson, R.B., 2015. Redefining fine roots improves understanding of below-ground contributions to terrestrial biosphere processes. New Phytologist 207(3), 505-518.

McCormack, M.L., Iversen, C.M., 2019. Physical and Functional Constraints on Viable Belowground Acquisition Strategies. Frontiers in Plant Science 10(1215).

McMurdie, P.J., Holmes, S., 2013. phyloseq: An R Package for Reproducible Interactive Analysis and Graphics of Microbiome Census Data. PLOS ONE 8(4), e61217.

Menne, M.J., Durre, I., Vose, R.S., Gleason, B.E., Houston, T.G., 2012. An overview of the global historical climatology network-daily database. Journal of Atmospheric and Oceanic Technology 29(7), 897-910.

Metcalfe, D.B., Fisher, R., Wardle, D.A., 2011. Plant communities as drivers of soil respiration: pathways, mechanisms, and significance for global change. Biogeosciences 8(8), 2047-2061.

Noh, N.J., Crous, K.Y., Li, J., Choury, Z., Barton, C.V., Arndt, S.K., Reich, P.B., Tjoelker, M.G., Pendall, E., 2020. Does root respiration in Australian rainforest tree seedlings acclimate to experimental warming? Tree Physiology 40(9), 1192-1204.

Palta, J.A., Nobel, P.S., 1989 Root respiration for *Agave deserti*: Influence of temperature, water status and root age on daily patterns. Journal of Experimental Botany 40(2), 181-186.

Paradiso, E., Jevon, F., Matthes, J., 2019. Fine root respiration is more strongly correlated with root traits than tree species identity. Ecosphere 10:e02944.

Pausch, J., Kuzyakov, Y., 2018. Carbon input by roots into the soil: Quantification of rhizodeposition from root to ecosystem scale. Global Change Biology 24(1), 1-12.

Phillips, R.P., Brzostek, E., Midgley, M.G., 2013. The mycorrhizal-associated nutrient economy: a new framework for predicting carbon–nutrient couplings in temperate forests. New Phytologist 199(1), 41-51.

Pregitzer, K.S., Burton, A.J., King, J.S., Zak, D.R., 2008. Soil respiration, root biomass, and root turnover following long-term exposure of northern forests to elevated atmospheric CO2 and tropospheric O3. New Phytologist 180(1), 153-161.

R Core Team, 2020. R: A language and environment for statistical computing (4.0. 3)[Computer software]. R Foundation for Statistical Computing. Retrieved from http://www.R-project.org.

Raich, J.W., Nadelhoffer, K.J., 1989. Belowground carbon allocation in forest ecosystems: global trends. Ecology 70(5), 1346-1354.

Raich, J.W., Potter, C.S., Bhagawati, D., 2002. Interannual variability in global soil respiration, 1980–94. Global Change Biology 8(8), 800-812.

Raich, J.W., Tufekciogul, A., 2000. Vegetation and soil respiration: correlations and controls. Biogeochemistry 48(1), 71-90.

Reich, P.B., Tjoelker, M.G., Pregitzer, K.S., Wright, I.J., Oleksyn, J., Machado, J.L., 2008. Scaling of respiration to nitrogen in leaves, stems and roots of higher land plants. Ecology Letters 11(8), 793-801.

Reichstein, M., Beer, C., 2008. Soil respiration across scales: The importance of a model–data integration framework for data interpretation. Journal of Plant Nutrition and Soil Science 171(3), 344-354.

Rossi, L.M., Mao, Z., Merino-Martin, L., Roumet, C., Fort, F., Taugourdeau, O., Boukcim, H., Fourtier, S., Del Rey-Granado, M., Chevallier, T., 2020. Pathways to persistence: plant root traits alter carbon accumulation in different soil carbon pools. Plant and Soil 452(1), 457-478.

Ryan, M.G., Law, B.E., 2005. Interpreting, measuring, and modeling soil respiration. Biogeochemistry 73(1), 3-27.

Singh, J.S., Gupta, S.R., 1977. Plant Decomposition and Soil Respiration in Terrestrial Ecosystems. Botanical Review 43(4), 449-528.

Soudzilovskaia, N.A., van Bodegom, P.M., Terrer, C., Zelfde, M.v.t., McCallum, I., Luke McCormack, M., Fisher, J.B., Brundrett, M.C., de Sá, N.C., Tedersoo, L., 2019. Global mycorrhizal plant distribution linked to terrestrial carbon stocks. Nature Communications 10(1), 5077.

Taylor, M.K., Lankau, R.A., Wurzburger, N., 2016. Mycorrhizal associations of trees have different indirect effects on organic matter decomposition. Journal of Ecology 104(6), 1576-1584.

Teodosio, B., Pauwels, V.R.N., Loheide II, S.P., Daly, E., 2017. Relationship between root water uptake and soil respiration: A modeling perspective. Journal of Geophysical Research: Biogeosciences 122(8), 1954-1968.

Trevors, J., 1996. Sterilization and inhibition of microbial activity in soil. Journal of Microbiological Methods 26(1-2), 53-59.

Trumbore, S., 2006. Carbon respired by terrestrial ecosystems–recent progress and challenges. Global Change Biology 12(2), 141-153.

Valverde-Barrantes, O.J., Freschet, G.T., Roumet, C., Blackwood, C.B., 2017. A worldview of root traits: the influence of ancestry, growth form, climate and mycorrhizal association on the functional trait variation of fine-root tissues in seed plants. New Phytologist 215(4), 1562-1573.

Vargas, R., Allen, M.F., 2008. Dynamics of fine root, fungal rhizomorphs, and soil respiration in a mixed temperate forest: integrating sensors and observations. Vadose Zone Journal 7(3), 1055-1064.

Vargas, R., Baldocchi, D.D., Querejeta, J., Xe, I, Curtis, P.S., Hasselquist, N.J., Janssens, I.A., Allen, M.F., Montagnani, L., 2010. Ecosystem CO_2 Fluxes of Arbuscular

and Ectomycorrhizal Dominated Vegetation Types Are Differentially Influenced by Precipitation and Temperature. New Phytologist 185(1), 226-236.

Wan, X., Chen, X., Huang, Z., 2021. Contribution of root traits to variations in soil microbial biomass and community composition. Plant and Soil 460, 482-495.

Wang, C., Ma, Y., Trogisch, S., Huang, Y., Geng, Y., Scherer-Lorenzen, M., He, J.-S., 2017. Soil respiration is driven by fine root biomass along a forest chronosequence in subtropical China. Journal of Plant Ecology 10(1), 36-46.

Wang, C., Yang, J., & Zhang, Q. (2006). Soil respiration in six temperate forests in China. Global Change Biology, *12*(11), 2103-2114.

Wang, W., Feng, J., Oikawa, T., 2009. Contribution of root and microbial respiration to soil CO_2 efflux and their environmental controls in a humid temperate grassland of Japan, Pedosphere 19(1), 31-39.

Warren, J.M., Hanson, P.J., Iversen, C.M., Kumar, J., Walker, A.P., Wullschleger, S.D., 2015. Root structural and functional dynamics in terrestrial biosphere models – evaluation and recommendations. New Phytologist 205(1), 59-78.

Warren, J.M., Iversen, C.M., Garten, C.T., Jr, Norby, R.J., Childs, J., Brice, D., Evans, R.M., Gu, L., Thornton, P., Weston, D.J., 2011. Timing and magnitude of C partitioning through a young loblolly pine (*Pinus taeda* L.) stand using ^{13}C labeling and shade treatments. Tree Physiology 32(6), 799-813.

Weemstra, M., Mommer, L., Visser, E.J., Ruijven, J., Kuyper, T.W., Mohren, G.M., Sterck, F.J., 2016. Towards a multidimensional root trait framework: a tree root review. New Phytologist 211(4), 1159-1169.

Wurzburger, N., Brookshire, E.N.J., 2017. Experimental evidence that mycorrhizal nitrogen strategies affect soil carbon. Ecology 98(6), 1491-1497.

Xu, M., Shang, H., 2016. Contribution of soil respiration to the global carbon equation. Journal of Plant Physiology 203, 16-28.

Yang, J., Wang, C., 2006. Partitioning soil respiration of temperate forest ecosystems in northeastern China. Acta Ecologica Sinica 26(6), 1640-1646.

CHAPTER 6: The physiological acclimation and growth response of *Populus trichocarpa* to warming

This chapter has been published in *Physiologia Plantarum* :

Hogan JA, Baraloto C, Ficken C, Clark MD, Weston DJ & Warren JM. The physiological acclimation and growth response of Populus trichocarpa to warming. *Physiologia Plantarum* 77:79. doi: 10.1111/ppl.13498.

Key message

The maximum physiological acclimation of western black cottonwood (*Populus trichocarpa*) is between 4°C and 8°C. Root and soil respiration declined with warming. Acclimation of root respiration with warming was less than leaf photosynthetic or respiratory acclimation and was mediated by soil nitrogen availability.

Abstract

Plant metabolic acclimation to thermal stress remains underrepresented in current global climate models. Gaps exist in our understanding of how metabolic processes (i.e., photosynthesis, respiration) acclimate over time and how aboveground versus belowground acclimation differs. We measured the thermal acclimation of *Populus trichocarpa*, comparing aboveground vs. belowground physiology over time. Ninety genetically identical ramets were propagated in mesocosms that separated root and microbial components. After establishment at 25°C for six weeks, sixty clones were warmed +4°C or +8°C and monitored for ten weeks, measuring photosynthesis (A), leaf respiration (R), soil respiration (R_s), root plus soil respiration (R_{s+r}), and root respiration (R_r). We observed thermal acclimation in both A and R, with rates initially increasing, then declining as the thermal photosynthetic optimum (T_{opt}) and the temperature-sensitivity (Q_{10}) of respiration adjusted to warmer conditions. Photosynthetic acclimation was constructive, based on an increase in both T_{opt} and peak A. Belowground, R_{s+r} decreased linearly with warming, while R_s rates declined abruptly, then remained constant with additional warming. Plant biomass was greatest at +4°C, with 30%

allocated belowground. Rates of mass-based R_r were similar among treatments, however, root nitrogen declined at +8°C leading to less mass-Nitrogen based Rr in that treatment. The Q_{10}-temperature relationship of R_r was affected by warming, leading to differing values among treatments. Aboveground acclimation exceeded belowground acclimation, and plant nitrogen-use mediated the acclimatory response. Results suggest that moderate climate warming (+4°C) may lead to acclimation and increased plant biomass production but increases in production could be limited with severe warming (+8°C).
Keywords: thermal acclimation, photosynthesis, respiration, temperature, root respiration, poplar

Abbreviations: *A,* net photosynthetic rate; A_{max}, the maximum rate of light-saturated photosynthesis; $A_{net,29}$, the net photosynthetic rate at 29°C, A_{opt}, the rate of net photosynthesis at the thermal optimum of photosynthesis; C, carbon; CO_2, carbon dioxide; ETR_{PSII}, electron transport rate of photosystem II; g_{sw}, stomatal conductance to water vapor; IRGA, infrared laser gas analyzer; J_{max}, the maximum rate or electron transport; N, nitrogen; Φ, the apparent quantum yield of photosynthesis; Φ_{CO_2}, the quantum yield of CO_2 assimilation corrected for dark respiration; Φ_{PSII}, the quantum efficiency of photosystem II; PPFD, photosynthetic photon flux density; R_{BG}, belowground (i.e., soil and soil + root) respiration (see methods); R_{root}, root respiration; R_s, rate of soil CO_2 efflux; R_{s+r}, rate of soil plus plant root CO_2 efflux, $R_{s+r} - R_s$, the difference between the rate of soil only CO_2 efflux and the rate of soil plus plant root CO_2 efflux; T_{leaf}, leaf temperature; $T_{opt,}$ thermal optimum of photosynthesis; T_{opt} R_r, the thermal optimum of root respiration; Q_{10}, the temperature sensitivity of leaf respiration; Q_{10} R_{root}, temperature sensitivity of root respiration; Q_{10} $R_{r,29}$, the temperature sensitivity of mass-based root respiration at 29°C; Root R_{opt}, Mass-based respiration at temperature optima; RuBP, ribulose bisphosphate; V_{cmax}, the maximum rate of carboxylation; VPD, vapor pressure deficit.

Picture 1: Morning sun graces the greenhouse where *P. trichocarpa* clones are established for warming treatments. The experimental set up used AKRO grid containers separated into two compartments with a 1-micron mesh and PVC soil respiration collars. The picture was taken on day 44 of the experiment prior to the introduction of clones into temperature treatments. Picture by Chrissi Schnell (DOE ORNL).

Introduction

Surface temperatures of the Earth system continue to rise as anthropogenic climate change intensifies (Hansen *et al.* 2010). By 2100, global surface temperatures are predicted to be between 0.3 and 4.8°C higher than in 1850-1900, depending on the emissions scenario (IPCC 2014), with even greater increases at higher latitudes. Such widespread warming of the earth's terrestrial ecosystems, including natural forests and agricultural forest plantations, will undoubtedly affect tree physiology, growth, and survival (Aitken *et al.* 2008, Allen *et al.* 2015). Although evidence for changes in tree growth rates and biomass production is mixed (Canham *et al.* 2018, McMahon *et al.* 2010, Peñuelas *et al.* 2011), some effects of increasing temperatures on tree physiology are already being observed. These include geographic range shifts (Monleon and Lintz 2015, Walther 2003), an increase in tree water use efficiency (Adams *et al.* 2020, Mathias and Thomas 2021), and changes in rates of photosynthesis and respiration (Dusenge *et al.* 2019, Kamarathunge *et al.* 2019). The degree of physiological plasticity to climate change within dominant tree genera, such as *Populus* is not well known, yet will affect carbon (C) and water fluxes at the ecosystem and global levels (King *et al.* 2006, Lombardozzi *et al.* 2015, Smith and Dukes 2013) and the provisioning of essential ecosystem services (e.g., net ecosystem exchange, tree plantation biomass production) in the future. Forest ecosystems and their dominant tree genera will have to either physiologically acclimate to warming or adapt in some way to increased temperatures; otherwise, they will face decline (Feeley *et al.* 2012).

Net C storage in the plant-soil system is the balance of aboveground plant metabolism (i.e., photosynthesis and respiration) and belowground plant and soil microbial respiration (i.e., C fixation vs. release) (Luo 2007). Plant and soil metabolic processes have varying temperature-sensitivities. Warming has been shown to affect soil respiration rates (Bond-Lamberty and Thomson 2010), and both hetero- and autotrophic respiration are predicted to increase as the planet continues to warm (Atkin *et al.* 2005, Atkin and Tjoelker 2003, Bond-Lamberty and Thomson 2010). Photosynthesis, on the other hand, can acclimate (i.e., adjust to maintain or improve physiological functioning) to increasing temperature (Berry and Björkman 1980, Sage and Kubien 2007,

Kamarathunge *et al.* 2018); but, there is little evidence that increases in photosynthetic rates with increasing temperature will keep pace with increases in respiration rates (Smith *et al.* 2020), especially if plants reach critical thermal thresholds. This mismatch could lead to an abrupt decline in C uptake and storage (Jump and Peñuelas 2005). To infer how continued warming will affect the ecosystem C balance of natural and agricultural systems, changes in whole plant physiology and their interaction with plant-soil feedbacks require greater understanding (Chapin III *et al.* 2009, García-Carreras *et al.* 2018).

Plant metabolism is the net sum of photosynthesis and respiration. Photosynthesis and respiration are complex biochemical processes that are highly enzyme-catalyzed, and thus temperature is a crucial factor that controls process rates (Bernacchi *et al.* 2003, Farquhar *et al.* 1980, Von Caemmerer 2000, Moore et al. 2021). Photosynthesis and respiration can both acclimate to increased temperature to some degree (Slot and Kitajima 2015, Slot and Winter 2016, Way and Yamori 2014), although the capacity for thermal acclimation has not been precisely quantified for many species. Photosynthetic acclimation is defined as any adjustments in leaf C assimilation that improve the plant's performance at higher temperatures (Slot and Winter 2016, Way and Yamori 2014). A *constructive* acclimatory response to increased temperature (*sensu* Way and Yamori 2014) increases both the temperature optimum of photosynthesis (T_{opt}) and the rate of photosynthesis at the growth temperature. Such a response demonstrates that leaf physiological adjustments (e.g., enzyme kinetics of dark photosynthetic reactions) make the plant equally or better suited for carbon gain at the increased temperature. The increase in the rate of photosynthesis at the warmer temperature helps offset increases in respiration rates, which allows the plant to maintain a positive C balance. Internal leaf photosynthetic processes acclimate to temperature changes within days to weeks of temperature change (Berry and Björkman 1980, Yamori *et al.* 2014). The consensus for temperate trees is that T_{opt} can shift by one-third to half of the magnitude of change in mean daily air temperatures (i.e., there is an increase in T_{opt} of 0.4°C per degree change in air temperature) (Kumarathunge *et al.* 2019, Sage and Kubien 2007, Yamori *et al.* 2014). However, the physiological cost of photosynthetic and respiratory acclimation on whole

plant carbon balance (e.g., biomass production, rates of root respiration) or whole plant metabolism (e.g., nutrient use patterns) is less well understood.

Photosynthetic thermal acclimation is governed mainly by the temperature adjustment of three critical biochemical processes in the leaf: 1) the capacity of ribulose-1,5-bisphosphate carboxylase/oxygenase (Rubisco) to process (i.e., carboxylize) ribulose bisphosphate (RuBP), 2) the rate at which the Calvin cycle and light reactions can regenerate RuBP (i.e., RuBP regeneration), and 3) the capacity to regenerate organic phosphates for phosphorylation (i.e., triosephosphate use efficiency) (Sage and Kubien 2007, Von Caemmerer 2000). Thus, RuBP carboxylation and regeneration are two of the three main biochemical processes that govern how photosynthetic rates acclimate to increased temperature (Berry and Björkman 1980, Von Caemmerer 2000). These processes are thought to dominate the biochemical adjustments that underlie acclimation under saturated light conditions and at ambient CO_2 levels (Sage and Kubien 2007). Also according to Sharkey (2019), we may be misassigning the biochemical limitation of photosynthesis concerning RuBP carboxylation and regeneration and how these processes interact with triose phosphate limitation, which may or may not affect the up or down-regulation of CO_2 and RuBP limitation on assimilation (Rogers et al. 2020). At moderate temperature increases, RuBP-carboxylation limitation of photosynthesis is common, whereas RuBP regeneration becomes limiting at higher temperatures (Berry and Björkman 1980). Changes in the rates of RuBP carboxylation and regeneration, improved heat stability of Rubisco activase (Hikosaka *et al.* 2005, Sage and Kubien 2007, Yamori *et al.* 2006), and the regulation of the amount of RuBP and Rubisco in C_3 plant leaves are the main biochemical changes that drive acclimation of C_3 photosynthesis to increased temperatures (Scafaro *et al.* 2017). Because RuBP and Rubisco are nitrogen (N) rich, leaf N content serves as a good proxy for RuBP- and Rubisco-driven acclimation of photosynthesis to warming (Hikosaka 1997, Reich *et al.* 1998, Scafaro *et al.* 2017). Additionally, part of the acclimation of C_3 photosynthesis to increased temperatures is attributable to an increase in electron transport rates and temperature-related changes in the light reactions of photosynthesis (e.g., changes in J_{max} rates or

chlorophyll fluorescence, Yamasaki *et al.* 2002) if the heat stress is moderate and does not damage photosystems (Song *et al.* 2014).

Unlike photosynthesis, which occurs primarily in plant leaves, respiration occurs throughout the plant. Key metabolic processes, including cell growth, biomass maintenance, and ATP production, rely on cellular respiration. We know less about root respiration than that of leaves or stems. It is not entirely clear if acclimation of root metabolic processes coincides with the acclimation of photosynthesis. Root respiration, which generates the C compounds used for uptake in the roots (e.g., sugars – fructose, galactose; enzymes - amylase, phosphatase; and organic, phenolic or amino acids), represents a significant component of CO_2 loss in plants, with 8-52% of photosynthate being respired back through the roots (Lambers *et al.* 1996, Pregitzer *et al.* 1998). Over short time periods, root respiration has been shown to increase significantly in response to warming (Bryla *et al.* 2001, Wang et al. 2021). Rates of root respiration do acclimate to rising temperatures; however, it is predicted that roots have a lower capacity for physiological acclimation to increased temperatures than do leaves, either due to a lower degree of temperature sensitivity in cellular biochemical processes or to the temperature buffering capacity of the soil (Atkin *et al.* 2000, Eissenstat *et al.* 2013, Pregitzer *et al.* 2000). Studies that have measured respiratory acclimation of roots to increased temperature have not linked it to plant physiological or soil metabolic acclimation, thus the consequences of thermal acclimation in root respiration to plant-soil system functioning are not entirely understood.

The temperature sensitivity of root respiration has been shown to vary with root age, root order, and soil moisture (Palta and Nobel 1989, Atkin *et al.* 2000, Ceccon et al. 2014), with younger, more-hydrated roots having higher rates of respiration, which reflects greater metabolic activity (i.e., active nutrient uptake and root enzyme production). Additionally, if root respiration rates are related to root lifespan, warming could decrease root lifespan as respiration rates increase (Eissenstat *et al.* 2013). Using data from eight commonly-studied taxa, Smith *et al.* (2019) reported that respiration rates of leaves and photosynthetic stems increased to a greater extent than roots following temperature increase, indicating that leaves and stems have greater thermal acclimation

capacity than roots. A second recent study on the respiration rates of tropical seedlings of eight species (Noh *et al.* 2020) found no clear trend in root respiration in response to warming but reported that respiration rates were correlated with root N content, and that the temperature sensitivity of root respiration (Q_{10} R_r) was positively related to root tissue density. Many other studies have confirmed the relationship between root respiration and root tissue N content (Burton *et al.* 2002, Pregitzer *et al.* 2000, Pregitzer *et al.* 1998, Reich *et al.* 2008, Roumet *et al.* 2016). Few studies have compared the degree of acclimation of photosynthesis and respiration across plant organs and in relation to the plant-soil system over time, and few studies have related acclimatory differences to variation in plant biomass production with temperature.

To address the magnitude and time course of above versus belowground responses to thermal stress, we investigated the physiological acclimation of *Populus trichocarpa* Torr. & A.Gray ex Hook. (Salicaceae) to increased temperatures in a whole-plant warming experiment. Our experiment used a novel mesocosm methodology able to link plant acclimation to belowground carbon dioxide (CO_2) efflux. We used several routines for high-frequency leaf gas exchange measurements and belowground CO_2 efflux to compare aboveground vs belowground physiological acclimation of *P. trichocarpa*. poplar trees have been shown to be able to acclimate to increased temperatures (Silim *et al.* 2010), with relatively consistent responses across genotypes (i.e., populations from differing geographic origins) (Gornall and Guy 2007, Silim *et al.* 2010). Experiments that have investigated the thermal acclimation of poplar often rely on two measurements, pre, and post-warming. We sought to understand the time course of acclimation responses and how they compare among the different organs and thermal acclimation parameters because of the dynamic nature of temperature changes and the potential for source-sink imbalances above and belowground. We asked:

1. *In* P. trichocarpa*, do rates of belowground (root and root plus soil) respiration acclimate to warming?*
2. *What is the time course of aboveground physiological acclimation to warming, and does belowground acclimation track aboveground acclimation?*

We expected to find some degree of acclimation to warming in root respiration rates and root plus soil CO_2 efflux. Still, we hypothesized that root respiration would show less acclimation than leaf physiological acclimation (i.e., photosynthetic, and respiratory acclimation of leaves). Additionally, we hypothesized that that rate (i.e., time course) of aboveground acclimation would be faster with more warming and that belowground acclimation (i.e., root plus soil CO_2 efflux) should track aboveground acclimation.

Methods

Experimental Design – P. trichocarpa clones & mesocosm growth boxes

Western black cottonwood (*Populus trichocarpa*) ramets of the Nisqually-1 genotype were obtained from the Joint Genome Institute (Walnut Creek Campus) in October 2018. Ramets were planted into leach tubes containing growth medium and allowed to establish for ten weeks. The growth medium used throughout the experiment was a well-draining potting mix (pH 5.5 - 6.5), consisting of peat moss, vermiculite, perlite, and processed pine bark (Farfad 52 mix, SunGro Horticulture, Agawam, MA), mixed with time-release Osmocote Plus Fertilizer (0.7 g kg^{-1} 15-9-12, NPK). Ninety established clones with an average height of 14.4 cm (range: 8.1–24.8 cm) and average basal stem diameter of 4.5 mm (range:2.9–6.5 mm) were transplanted from leach tubes into mesocosm growth boxes on 29 July 2019. Stems were trimmed at the 7^{th} leaf node, and any roots extending beyond the bottom of the leach tube were cut off to standardize clone size prior to transplanting.

Mesocosm growth boxes (38 × 23.5 × 18 cm L× W × H, 15.14 L capacity) were constructed from AkroGrid containers (model 33168, Akro-Mils, Akron, OH), using a modified methodology of Ficken and Warren (2019). Three small holes were drilled on either side of the boxes, near the bottom, to allow for water drainage. Each box was filled with 3.5 kg. of potting mix (as described above; hereafter, soil) and had a 1-micron mesh partition installed to separate one-third of the box volume. The mesh barrier was designed to exclude plant roots but permit the movement of microbes and water between mesocosm portions, effectively creating a soil control for each mesocosm. *P. trichocarpa* clones were positioned in the middle of the larger compartment (one plant per container). Each compartment was equipped with a PVC soil CO_2-efflux collar.

Collars were made from schedule 40 PVC (5 cm diameter and 10 cm in length), with twelve 3.7 cm-diameter holes drilled into the collar portion that sat below the soil surface. Mesocosm boxes were encased in CoolShield thermal bubble wrap (ULINE, Pleasant Prairie, WI) to mimic natural temperature differences between the soil and air.

Experimental design – Growth conditions & temperature treatments

The duration of the experiment was 16 weeks. For an initial 6-week establishment period, all ninety of the plants were grown together in a climate-controlled greenhouse to allow them to establish root biomass in the mesocosms. During the initial establishment period, the plants were drip irrigated, receiving about 1 liter of water day^{-1}. At weeks two and four, plants received two doses of soluble fertilizer (about 1.4 g fertilizer $dose^{-1}$ delivered in approximately 1.5 liters of water, Southern Ag Nitrate Special 20-10-20, NPK). When the plants were 44 days old, sixty of the plants were transferred to two walk-in growth chambers (30 per chamber, CONVIRON, Ontario, Canada). Following this, plants were grown at experimental temperatures for ten weeks. Throughout the experiment, axillary sprouts were pinched off by hand before development to constrict plant growth to the main stem.

The control environment for the experiment (i.e., ambient treatment) remained the greenhouse, and two separate growth chambers were used for the warming treatments. Growth chambers were set to 70% relative humidity, and at 29°C (i.e., a +4°C treatment) and 33°C (i.e., a +8°C treatment), respectively, each with a 4°C degree nighttime temperature drop (Table 1). Growth chamber conditions were matched to the environmental conditions of the greenhouse during the initial establishment period, where temperatures peaked at 25°C with at most a 4°C nighttime decrease. A climate station with two air thermometers, two relative humidity sensors, two quantum sensors, and 12 soil temperature sensors was used throughout the experiment and rotated among the three treatments at 2-week intervals to monitor environmental conditions.

The plants grew vigorously during the initial establishment period, on average >2 cm day^{-1} in height, were 1.5 to 2 m in height when transferred to the growth chambers and reached the ceiling in the growth chambers about three weeks into warming treatments. Therefore, at week 10 (day 71) of the experiment, corresponding to the

midpoint of the treatment portion of the experiment, all plants were cut to 1.5 m height. Trimmed biomass and leaf areas were measured and accounted for in the final biomass calculations. Additionally, at that time, the experimental treatments were swapped between growth chambers to spread any latent effects of each specific growth chamber equally over both treatments. During the last week of the experiment, mesocosm box water loss (i.e., due to evapotranspiration) was quantified by entirely watering each replicate, recording its weight at that time and again 24 hours later.

Aboveground acclimation to warming – measurements of leaf gas exchange & fitting of response curves

poplars have indeterminate growth, meaning stems continuously elongate; moreover, they have leaf orthostichies (i.e., where 8 leaves form a single growth unit and can share photosynthate) (Larson and Isebrands 1971), so photosynthesis measurements were always conducted on a recently mature leaf located at the 8^{th}-most terminal position (i.e., standardized by leaf plastochron index). All measurements were made using the Li-6800 portable photosynthesis system (Li-COR Inc., Lincoln, NE). Criteria for assessing leaf stability in the photosynthesis system leaf chamber and logging data points was consistent throughout the experiment and across all measurements (see supplemental information, Table S1). To assess aboveground acclimation, we measured leaf photosynthesis over time using several measurement routines – survey measurements were done weekly at experimental conditions, and leaf gas exchange responses to temperature, CO_2 and light were done every two weeks.

First, survey measurements of coupled leaf gas exchange and chlorophyll fluorescence were done weekly on every plant in the experiment at treatment temperature. Chlorophyll fluorescence can help identify thermal stress responses of leaves, and classify light (i.e., photochemistry) vs. dark (i.e., biochemical) photosynthetic acclimation. Fluorometer parameters were consistent, throughout and we utilized a pulse-modulated flash, followed by a dark pulse (see List S1 for Li-6800 fluorometer settings). For survey measurements, instrument settings were 1000 µmol m^{-2} s^{-1} light, 400 µmol mol^{-1} CO_2, 600 µmol s^{-1} flow rate, and the leaf chamber humidity was controlled to maintain leaf vapor pressure deficit (VPD) at 1.25 kPa. Controlling leaf

chamber humidity to maintain leaf VPD at 1.25 kPa resulted in little to no change in leaf environmental conditions when taking gas exchange measurements (see Table 1 for environmental VPD).

Second, three types of leaf gas exchange response curves were measured – leaf photosynthesis and dark respiration responses to temperature, leaf photosynthesis-CO_2 responses and leaf photosynthesis-light responses. Response curves were conducted every two weeks on the same leaf for at least six plants per treatment. All response curve models were fitted separately for each leaf.

Leaf photosynthesis- and respiration-temperature response curves were measured across a temperature range of ± 10 °C from growth environment concurrently on the same leaf, one after another. While holding constant all other Li-6800 leaf chamber parameters (i.e., leaf VPD at 1.25 kPa), the air temperature was increased in 2°C increments (ranges: 18-42°C for the ambient treatment, 20-44°C for the +4°C treatment, and 24-48°C for the +8°C), with light at 1000 μmol m^{-2} s^{-1}. Maintaining VPD constant (rather than RH) reduces the confounding impact of VPD on measurements and helps isolate the response of photosynthesis to temperature alone. After completion of the photosynthetic temperature-response curve, we turned the actinic light off and waited for stability of leaf dark respiration. The dark respiration temperature response curve was initiated at this point to take advantage of the leaf already being acclimated to the high temperature. Once stable, we developed the response curve by progressively decreasing the leaf chamber temperature in 2°C increments, each time waiting for stability prior to recording the rate of leaf dark respiration. Each leaf gas exchange measurement (i.e., photosynthesis and respiration) was carefully observed and logged, and contingent on machine stability. Photosynthesis-temperature response curves were fit using a standard quadratic equation that modeled leaf photosynthesis (A) as a function of leaf temperature (T_{leaf}) (as measured by the Li-COR thermocouple): $A = aT_{leaf} + bT_{leaf}^{2} + c$. Quadratic model fits were exemplary with R^2 values always greater than 0.9 (and usually greater than 0.95), negating the need to use a more sophisticated model (i.e., that of Cunningham and Read (2002)). The temperature optimum of net photosynthesis (T_{opt}) and the rate of net photosynthesis at T_{opt} (A_{opt}) were determined via the T_{leaf} and A values

at the maximum of the fitted curve, respectively. Leaf dark respiration-temperature response curves were fit using an exponential linear model: $\log R_d = aT_{leaf}$. Models were fit using the range of the measured data, roughly ± 10 °C from growth environment temperature (see measurement temperature intervals by treatment above), and predicted from 16 to 47°C. Our leaf dark respiration-temperature data followed a typical Arrhenius-style exponential increase within our measurement range, and since we saw no evidence of a decline in leaf dark respiration at higher temperatures, we fit the simple exponential linear model instead of a more complex model (e.g., that of Heskel *et al.* 2016). The Q_{10} value of leaf dark respiration, or the magnitude of increase in leaf dark respiration for a 10°C increase in temperature, was calculated using the exponential function of the fitted model coefficient (i.e., slope parameter, α) times 10.

Leaf photosynthesis-CO_2 response curves were conducted at treatment temperatures using the traditional method, where all leaf chamber parameters were held constant, but the concentration of extracellular CO_2 was varied between 50 and 2000 μmol mol^{-1} in 13 steps. We explored the applicability of the RACiR technique (Stinziano *et al.* 2017) but decided to use the traditional method. The Farquhar-Berry-von Caemmerer model (Farquhar *et al.* 1980) was fit to the CO_2 response data using the 'plantecophys' package (Duursma 2015) in R v.3.6.1 (R Core Team 2019), which derives temperature-standardized estimates (at 25°C) of the maximum velocity of carboxylation ($V_{cmax,25}$) and the maximum rate of electron transport ($J_{max,25}$) from the fitted curves.

In order to confirm that light sensitivity was not a confounding factor in our experiment, we measured light response curves throughout the experiment at the same interval and on the same leaves as the temperature- and CO_2 -response curves. Light curves were assembled at treatment temperatures from high to low light intensity, decreasing light from 2000 to 0 μmol m^{-2} s^{-1} in 15 steps. Light response curve parameters were estimated using non-linear regression of a non-rectangular parabola (Marshall and Biscoe 1980) in the form of: $A_{net} = \frac{\Phi PPFD + \sqrt{(\Phi PPFD + A_{max})^2 - 4\theta\Phi PPFD + A_{max}}}{2\theta} - R_{d,}$, where A_{net} and A_{max} are net and maximum (area-based) rates of photosynthesis, respectively, $PPFD$ is light intensity, Φ is the apparent quantum yield, $R_{d,}$ is leaf dark respiration, and θ is the dimensionless

curvature parameter. From fitted light-response curves, estimates of the light compensation point (I_{comp}), and the light saturation point at 75% of A_{max} ($I_{sat(75)}$) were computed. Code was used from Heberling and Fridley (2013).

Measurement of leaf functional traits

Leaf morphology and tissue nutrient concentration were also always measured on the 8th most terminal leaf. Leaf areas where the Li-6800 was attached were sampled immediate after photosynthetic responses were measured. Specific leaf area (SLA) and leaf N content were assessed using the leaf punch method, where six circular leaf discs (Ø 18.5 mm) were punched out from the leaf tissue area where the Li-6800 was clamped to measure photosynthetic responses (to CO_2, light, and temperature). SLA was averaged across all six discs, and discs were homogenized into one sample for elemental analysis. Leaf C and N content were measured using a Carlo Erba NA 1500 Elemental Analyzer (Thermo Scientific, Waltham, MA USA) at the Duke Environmental Stable Isotope Laboratory in Durham, North Carolina.

Belowground acclimation to warming – measurements of belowground CO_2 flux, root respiration, and their temperature sensitivities

Measurements of belowground soil CO_2 efflux (R_{BG}) were conducted weekly and separately for both (i.e., soil and soil with plant root) compartments of each mesocosm using an Li-6252 infrared gas analyzer (IRGA, Li-COR Inc., Lincoln, NE) set up to detect small volume CO_2 gas injections. PVC collars were capped with PVC caps fitted with 20mm butyl septa. When capping collars, a needle was used to vent the collar headspace (volume of 196 cm^3) to avoid changes in air pressure. Headspace air was mixed by pumping 3 × 50 mL syringe. The needle was removed from the septum, and a 1-mL air sample was drawn from the headspace and immediately injected into the IRGA setup. An N_2 carrier gas at 0.1 liters min^{-1} flowrate carried the air sample to the IRGA, where IRGA integration values (maximum and total integrated area) were recorded over a 15-second interval from the time of injection. PVC collars were left capped to incubate for at least 1 hour and resampled. To minimize diel variation in soil respiration and to standardize soil moisture effects, we sampled mesocosms and their respiration chambers at roughly the same time of day and in the same order for all dates. For each sampling

run, we used four CO_2 gas standards (100, 500, 1000, and 1600 ppm) to create a standard curve using least-squares regression, with which we calculated headspace sample CO_2 concentrations using their IRGA integration values. Differences in CO_2 concentrations over incubations time were converted to R_{BG} rates using chamber volume and area.

To measure the temperature sensitivity of belowground CO_2 flux, we conducted whole-plant temperature responses using the growth chambers. Five plants from each treatment were selected, placed in the growth chamber, and allowed to acclimate overnight to 15°C. Over the period of one day, the temperature of the growth chamber was varied from 15 to 35°C at a rate of 5°C increase every 2 hours. Plants were allowed about 45 minutes to acclimate as temperatures increased, and then measurements of rates of belowground CO_2 flux (for both soil and soil + root mesocosm compartments, as described above) were conducted, incubating the chambers for at least an hour. The climate station was used throughout to monitor air and soil temperatures. Ordinary least-squares linear regressions were fitted to the soil and soil + root measurements by treatment (n = 25 for each compartment per treatment). The temperature sensitivity of belowground CO_2 flux was determined using the following equation, based on the linear regression fits: $Q_{10} = \left(\frac{R_2}{R_1}\right)^{10℃/(T_2-T_1)}$.

At the end of the experiment (on day 86 and 101, which was 42 and 57 days after warming began), root respiration (R_r)-temperature response curves were conducted on six plants per treatment. About 60 g (range 40–79 g) of fresh fine root biomass was placed in a Walz 3010-GWK1 gas exchange chamber (Heinz Walz GmbH, Effeltrich, Germany), fitted to a Li-6800 IRGA (Li-COR Inc. Lincoln, NE) and rates of R_r were measured from 15 to 50°C in 2.5° increments. The Walz 3010-GWK1 gas exchange chamber permits precise temperature control using the GFS-Win software. Following gas-exchange measurements, root biomass was dried and weighed, and root respiration measurements were standardized by the amount of dry root biomass present in the chamber (range: 4–10 g). The temperature response of R_r was modeled using non-linear least-squares regression in the form of: $R_T = R_0(c - bT)^{T/10}$, where R_T is R_r at a given temperature, T, R_0 is the root respiration rate at 0°C, and b and c are constants that describe the slope and intercept of the Q_{10} versus T relationship of R_r (Atkin *et al.* 2005,

Atkin *et al.* 2000, Palta and Nobel 1989). The root respiration-temperature relationship is not constant with increasing temperature (i.e., the slope of the Q_{10}-T relationship varies with T, Atkin *et al.* 2000). The Q_{10} value for R_r at each temperature can be calculated via the slope of (i.e., differentiating) the R_r-T relationship. Accordingly, a third-order polynomial linear regression was fitted to log-transformed R_r data in relation to T, and the derivative of the fitted curve was taken at each measurement T (Q_{10} R_r). We also differentiated the models at 29°C (an intermediate temperature) to compare Q_{10} R_r at a standard temperature. Lastly, the R_r Q_{10}-T relationship was modeled using a quadratic curve.

Quantifying plant growth and biomass production

Repeated stem basal diameter and plant height measurements were made using a digital Vernier caliper (0.1 mm precision) and tape measure (to the nearest 0.1 cm), respectively. Stem basal diameter and plant height measurements were conducted when clones were planted in the mesocosms, when plants were moved to the warming treatments (day 44), just after plants were trimmed (day 72), and when the experiment concluded (day 118). Plants were harvested at various intervals, on average, every three weeks to quantify whole plant biomass over time, compare among treatments and collect leaf and root tissue samples, however we only use growth and biomass from plants that grew to the end of the experiment for statistical analyses (n = 51, 17 plants per treatment in a balanced design). Upon harvesting, whole-plant leaf area was estimated by scanning all plant leaves through a Li-3100 Area Meter (Li-Cor, Lincoln, NE USA). For plant biomass measurements plant material was dried at 70°C in an oven for several days, until constant mass, then weighed. The height and biomass of plants that was removed because of trimming was quantified and incorporated into all calculations.

Statistical Analyses

Environmental conditions of the treatments were statistically compared using a one-way Analysis of Variance (ANOVA), where treatment was the dependent variable, followed by the post-hoc Tukey test for honest significant differences (HSD).

For measured leaf gas exchange rates or related model-derived parameters from photosynthetic or respiratory response curves, we used a two-way ANOVA in the form of

y ~ treatment × time. This statistically tests for differences in the physiological acclimation to temperature among treatments, and time, including the interaction between treatment and time. We examined if a repeated-measure error term greatly affected ANOVA inference, and in all cases the statistics changed little, indicating weak or only partial correlation between samples within each treatment over time. Potentially, randomly selecting plants helped limit the correlation. However, for most (i.e., 4 of 7) of the parameters, the interaction of treatment and time was significant. Therefore, we elected to fit ANOVA models (in the form of y ~ treatment) separately for each time period. ANOVA statistics were Bonferroni corrected to account for multiple comparisons over time. Similarly, within each time period, Tukey HSD post-hoc tests were applied to determine which treatments were statistically different from one another. This same procedure was applied to the leaf functional trait measurements that accompanied the photosynthetic or respiratory response curves.

For the chamber-based measurements of R_{BG}, we used a linear mixed-effects model (LMM). The data were verified to adhere to normality, and the model was fit using data from the 10-weeks of experimental warming (excluding measurements during the initial phase, where plants were establishing root biomass in the mesocosms). Based on the design, a random intercept term was justifiable for each mesocosm containing a single plant with two chambers (root + soil and soil only). Fixed effects for time, chamber, and treatment, including all interactions were considered. The best fitting LMM was selected based on AIC using model backward selection via the step function in the 'LmerTest' package (Bates *et al.* 2015, Kuznetsova *et al.* 2017), which backward selects random effects then fixed effects. Model diagnostic were verified, effects were estimated using restricted maximum likelihood, and the model was visualized and interpreted with tools from the 'sjPlot' package. The temperature sensitivity of belowground respiration (i.e., Q_{10} of R_{BG}) was compared with a two-way ANOVA (treatment × time) followed by Tukey HDS post-hoc test for treatment.

For R_r measurements (both mass-based and mass N-based rates) and their temperature sensitivity, we grouped all measurements together and compared treatments using a one-way ANOVA, where treatment was the dependent variable. Similarly, plant

growth and biomass data for plant grown from the start to the end of the experiment, were analyzed using a one-way ANOVA which tested for treatment differences. Treatments were compared using Tukey post-hoc HSD tests. All analyses were done in R v.3.6.1 (R Core Team 2019), and all the ANOVAs were conducted using the 'aov' function in the base package in R. All statistical analyses are shown in Appendix S2 (https://rpubs.com/hogieskier/PoplarPhys_StatsCheck) Throughout the results, mean values ± standard errors are presented (unless otherwise specified).

Results

Using two walk-in growth chambers to raise temperatures +4°C and +8°C and a greenhouse for the ambient treatment (i.e., control), the implemented temperature treatments created consistent differences in air and soil temperatures among growth environments (Table 1). Although closer to 25°C at the start of the experiment, the temperature dropped slightly to around 21°C in the ambient treatment as the experiment progressed. Small differences in growing environment vapor pressure deficit (VPD) were recorded; however environmental VPD was always between 1 and 1.3 kPa, even for the warmest treatment. All of the environmental variables in Table 1 (i.e., daytime air temperature, nighttime air temperature, air relative humidity, daytime photosynthetically active radiation, daytime soil temperature, nighttime soil temperature, and VPD) differed across treatments. Water losses due to evaporation and transpiration from mesocosms (measured on the last day of the experiment) were 1.29 ± 0.01 L day^{-1} in the ambient treatment, 1.81 ± 0.02 L day^{-1} in the +4°C treatment, and 2.23 ± 0.02 L day^{-1} in the +8°C treatment. Therefore, mesocosms in +4°C and +8°C treatments lost 41% and 73% more water, respectively, than mesocosms at ambient conditions ($F_{(2,48)} = 43.99$, $p < .001$).

Table 1: Environmental conditions (light conditions, daytime and nighttime air and soil temperatures, relative humidity, and vapor pressure deficit) of the experimental treatments (mean values ± standard errors). Data are from a meteorological station comprised of 2 air temperature, relative humidity, and light quantum sensors, and 12 soil temperature sensors. Data were collected at hourly intervals, and after experimental-warming initiated, the station was rotated throughout the treatment at roughly two-week intervals. *F*-statistics are for Analyses of Variance in the form of: ~ Treatment. *F* probabilities are all statistically significant: ***$p < .001$. Letters denote statistical groupings from Tukey HSD post-hoc tests.

Treatment	Daytime air temperature (°C)	Nighttime air temperature (°C)	Relative humidity (%)	Daytime PAR (μmol m^{-2} s^{-1})	Daytime soil temperature (°C)	Nighttime soil temperature (°C)	Vapor Pressure Deficit (kPa)
Initial	23.95 ± 0.11^{B}	25.38 ± 0.23^{B}	69.90 ± 3.00^{B}	311.07 ± 16.87^{B}	24.61 ± 0.13^{B}	25.64 ± 0.32^{B}	1.024 ± 0.007^{A}
Ambient	21.55 ± 0.28^{A}	19.75 ± 0.38^{A}	58.28 ± 2.23^{A}	99.71 ± 15.39^{A}	20.81 ± 0.38^{A}	20.26 ± 0.81^{A}	1.081 ± 0.035^{A}
+4 °C	29.33 ± 0.07^{C}	25.53 ± 0.27^{B}	72.53 ± 1.03^{B}	139.81 ± 9.21^{A}	26.69 ± 0.07^{C}	26.62 ± 0.13^{B}	1.102 ± 0.027^{A}
+8 °C	32.91 ± 0.19^{D}	29.01 ± 0.07^{C}	67.45 ± 1.85^{B}	107.15 ± 9.04^{A}	29.94 ± 0.10^{D}	29.41 ± 0.18^{C}	1.303 ± 0.048^{B}
Treatment $F_{(3,103)}$	730.90***	269.60***	14.91***	54.62***	293.70***	107.60***	15.23***

Leaf photosynthetic acclimation

During the initial establishment period, rates of A and g_{sw} averaged 20.2 (± 0.1) μmol m^{-2} s^{-1} and 0.47 (±0.01) mol m^{-2} s^{-1}, respectively (Fig. 1A, B). Following their introduction to the warming treatments, survey measurements of A (at treatment air temperatures) diverged among treatments, increasing slightly in the warming treatments but continuing to decline slightly in the ambient treatment (Fig. 1A). A was statistically different among treatments ($F_{(2,636)} = 79.212$, $p << .001$) and over time (see Appendix 2 for complete ANOVA result). Treatment differences in A persisted for first seven weeks of warming, then became statistically similar (Appendix 2). After 10 weeks of warming, A averaged 13.9 (± 0.9) μmol m^{-2} s^{-1} for ambient treatment and 13.8 (± 0.6) and 12.5 (± 0.7) μmol m^{-2} s^{-1} for plants in the +4°C and +8°C treatments, respectively (Fig. 1A). Rates of g_{sw} initially decreased in the warmed treatments relative to the ambient treatment during the first week of warming but then roughly mirrored patterns in A (Fig. 1B). Over the entire experiment, g_{sw} differed significantly among treatments ($F_{(2,636)} = 111.41$, $p << .001$) with g_{sw} in the ambient treatment (0.461 ± 0.01 mol m^{-2} s^{-1}) being significantly lower the warming treatments (0.561 ± 0.01 mol m^{-2} s^{-1} for the +4°C treatment and 0.572 ± 0.01 mol m^{-2} s^{-1} for the +8°C treatment), which were statistically equivalent. After 10 weeks of warming, g_{sw} averaged 0.313 (± 0.04) mol m^{-2} s^{-1} for the ambient treatment and 0.262 (± 0.03) and 0.160 (± 0.02) mol m^{-2} s^{-1} for the +4°C and +8°C treatments, respectively (Fig. 1B). At this time, differences in g_{sw} were still statistically significant ($F_{(2,48)} = 7.03$, $p < .01$), being about 0.1 mol m^{-2} s^{-1} and 0.15 mol m^{-2} s^{-1} lower in the 8°C treatment, relative to the +4°C and ambient treatment, respectively (Fig. 1B).

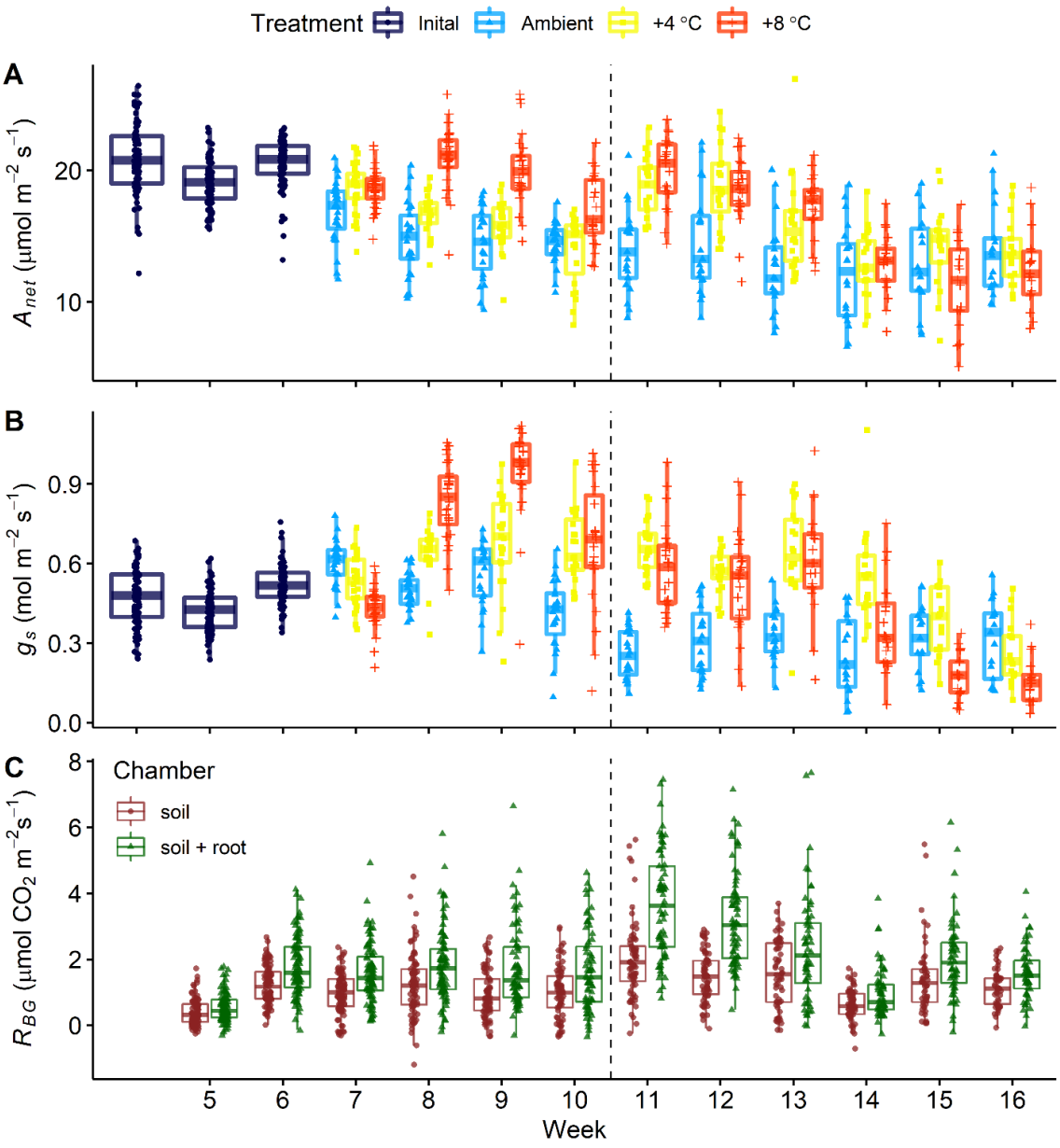

Fig. 1: A) Measurements of maximum leaf net photosynthetic rates (A_{net}, in micromoles CO_2 per square meter leaf area per second), B) stomatal conductance to water vapor (g_{sw}, in moles per square meter leaf area per second) and C) belowground respiration (R_{BG}, for respiration collars containing soil only and soil with roots in micromoles CO_2 per square meter soil area per second) for experimentally-warmed *P. trichocarpa* clones. Temperature treatments were applied starting on week 7. The vertical line denotes when plants were trimmed at day 71.

Chlorophyll fluorescence measurements tracked the acclimation of the photosynthetic light reactions to increased temperature. The Chlorophyll fluorescence

ratio (F_v'/F_m') averaged 0.657 ± 0.006 in week 6 in the initial greenhouse conditions, increased slightly as plants matured to maximize at 0.670 ± 0.005 at week 9 (three weeks after warming initiated), then decreased over time (average F_v'/F_m' at week 16 was 0.538 ± 0.01 across all treatments, Fig. S1A). F_v'/F_m' was statistically different over time ($F_{(9,636)} = 23.838$, $p < .001$) and among treatments ($F_{(2,636)} = 4.862$, $p < .01$), with a significant interaction between treatment and time (Appendix S2). The other notable differences in leaf chlorophyll fluorescence among treatments were in the quantum efficiency of photosystem II (Φ_{PSII}, Fig. S1B), the quantum yield of CO_2 assimilation corrected for dark respiration (Φ_{CO_2}, Fig. S1C), the quantum yield of non-photochemical quenching (Φ_{NPQ}, Fig. S1D), and fluorometer-estimated electron transport rate of photosystem II (ETR_{PSII}, Fig. S1E). Φ_{PSII} showed immediate and stark differences among treatments ($F_{(2,636)} = 113.44$, $p << .001$) which were sustained for nearly two months after the onset of warming, but then balanced out toward the end the experiment (i.e., weeks 8 and 10 of warming were not different, see Appendix S2; differences over time: $F_{(9,636)} = 11.06$, $p < .001$). Φ_{CO_2} showed a similar trend being initially between 0.020 and 0.035 during the initial pre-treatment growth phase, but then measuring mostly between 0.010 and 0.025 by the end of the experimental warming phase (differences were significant over time: $F_{(9,636)} = 43.69$, $p << .001$ and among treatments: $F_{(2,636)} = 36.19$, $p << .001$). Differences in Φ_{CO_2} among treatments persisted until week 7 of warming, then diminished (Appendix 2). Φ_{NPQ} was not different among treatments ($F_{(2,636)} = 1.431$, $p = .24$) exhibited an increasing trend over time ($F_{(9,636)} = 186.43$, $p << .001$), ranging from 0.09 ± 0.02 during pretreatment to 0.33 ± <0.01 at the end of the experiment. The interaction of treatment and time was significant ($F_{(18,636)} = 7.624$, $p << .001$), leading to difference among treatments for the first 5 weeks of warming, then subsided, with treatments being similar at weeks 6, 8 and 9 of warming (Appendix 2). ETR_{PSII} measured 153.52 ± 1.56 μmol m^{-2} s^{-1} under pretreatment conditions, showed maximum differences between treatments of roughly 75.76 μmol m^{-2} s^{-1} at week 9 to 11 (3 to 5 weeks after the onset of warming), with differences among temperature treatments equilibrating to around 112.97 ± 3.57 μmol m^{-2} s^{-1} thereafter (Appendix 2, weeks 8 and

10 of warming were not different). Again, differences were significant over time ($F_{(9,636)}$ = 11.96, $p < .001$) and among treatments ($F_{(2,636)}$ = 137.92, $p << .001$).

Before experimental warming, T_{opt} was between 29 and 30°C, and A_{opt} rates were >20 μmol m^{-2} s^{-1}. Temperature optima for photosynthesis increased immediately (i.e., within 12 days of warming) and stabilized, with T_{opt} in both warming treatments settling around 33°C, and T_{opt} for the ambient treatment staying closer to 29°C (Fig. 2, Table 2, Fig. S8). Increases in T_{opt} and A_{opt} occurred faster in the +8°C treatment than in the +4°C treatment (Fig. 2, Table 2, Fig. S8), with A_{opt} peaking at 28 days of warming in the +8°C treatment (measuring 22.03 ± 0.62 μmol m^{-2} s^{-1}), but peaking at 41 days of warming for the +4°C treatment (measuring 20.44 ± 0.97 μmol m^{-2} s^{-1}, see Table 3 for F statistics). Over time, rates of A_{opt} displayed a similar divergent trend as rates of net photosynthesis from survey measurements (shown in Fig. 1A), separating out by treatment with the greatest differences coming two to four weeks after the initiation of the temperature treatments and then steadily declining (Fig. 2, Fig. S8). At that time differences in A_{opt} were largest, and T_{opt} measured about 3°C greater in the two warming treatments than in the ambient treatment (Table 2). At the end of the warming experiment, T_{opt} was similar (i.e., within 0.6 °C) for the two warming treatments, which were greater than the ambient treatment ($F_{(2,22)}$ = 42.28, $p << .001$, Table 2, Table 3, Fig. S8). The net photosynthetic rate at 29°C ($A_{net,29}$, from photosynthetic-temperature response curves) between the ambient and +8°C treatment became statistically different at 28 days after warming began ($F_{(2,21)}$ = 4.83, p = .02, Table 3). Differences in $A_{net,29}$ among also emerged 55 days after warming began ($F_{(2,22)}$ = 3.70, p = .04, Table 3). A_{opt} and $A_{net,29}$ showed a similar pattern, with no difference in rates at 41 days after the start of warming Table 3). However, differences between treatments emerged once more by 99 days because of a decrease in A_{opt} and $A_{net,29}$ in the ambient treatment (Table 2, Table 3, Fig. S8).

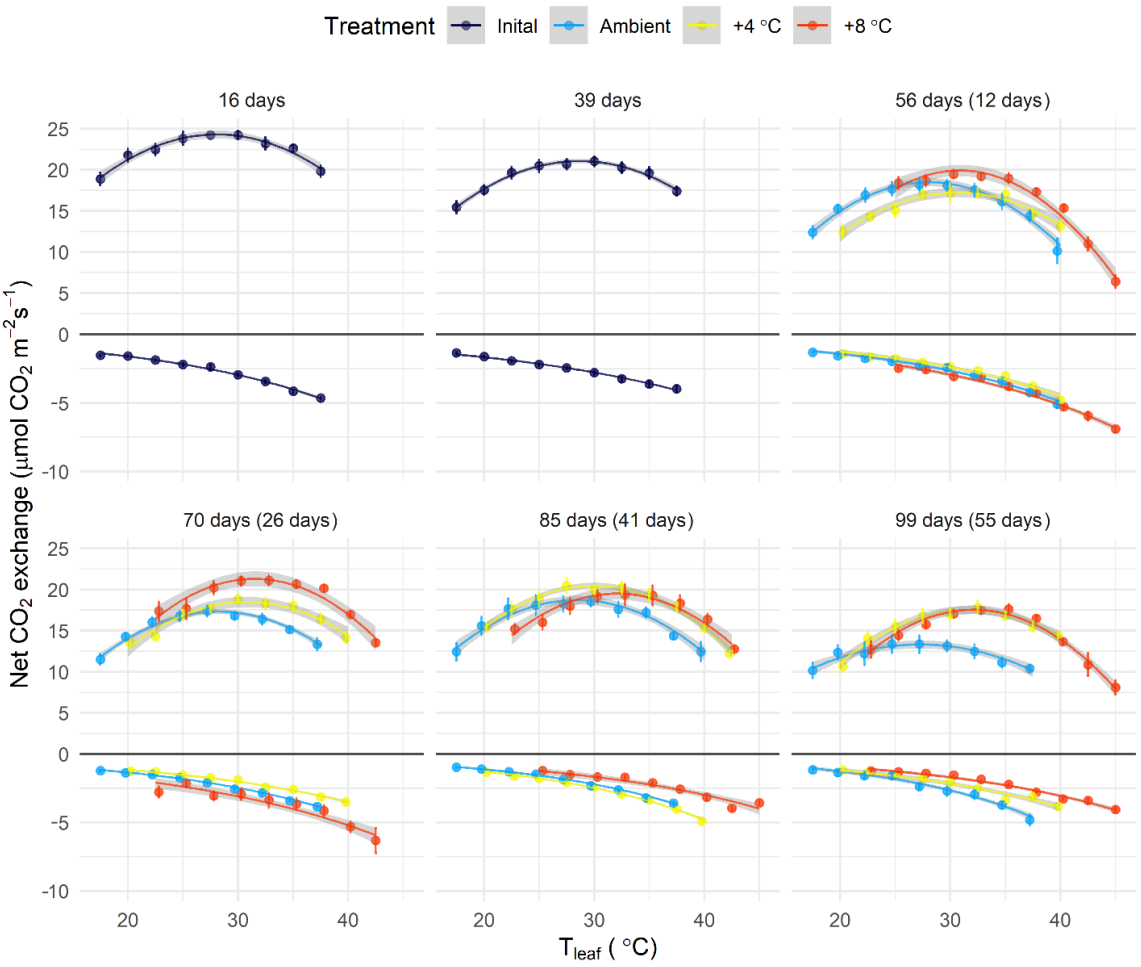

Fig. 2: Temperature responses of leaf net CO_2 exchange over time for experimentally warmed *P. trichocarpa* clones. Values >0 are from photosynthesis-temperature response curves, while values <0 are from leaf dark respiration-temperature response curves. Points are means for at least six response curves, with bars showing standard errors. Lines are quadradic model fits for values >0 and exponential fits for values <0. Shading around lines shows 95% confidence intervals. Note the differences in the y-axis scale about zero. Photosynthesis and respiration temperature responses were measured on the same leaves (see methods). For fitted curves for each individual leaf see Fig. S6 and S7. Note the differences in y-axis scale about zero. The number of days in parentheses indicates the number of warmed days at the time of measurement.

Table 2: Leaf photosynthetic parameters over time. Mean values (± standard errors) for the temperature optimum of net photosynthesis (T_{opt}), the rate of net photosynthesis at T_{opt} (A_{opt}), the rate of dark respiration at 29°C (*Leaf* $R_{d,29}$), the temperature sensitivity of leaf dark respiration (Q_{10} R_d), the net rate of photosynthesis at 29°C ($A_{net,29}$), and Farquhar- Von Caemmerer-Berry model-derived estimates of the maximum carboxylation velocity at 25°C ($V_{cmax,25}$), and the maximum rate of electron transport at 25°C ($J_{max,25}$) by treatment, over time for *P. trichocarpa* clones. N denotes the number of physiological response curves used for parameter estimates. Numbers in parentheses in the Time column are the number of warmed days at the time of measurement. See Table 3 for ANOVA statistics. Letters denote statistical groupings from Tukey HSD post-hoc tests; Tukey tests were done within each measurement time to account for repeated measures; thus, letters can only be compared among treatments within each time. For a visual representation of these data over time, see Fig. S8.

Treatment	Time	N	T_{opt} (°C)	A_{opt} (µmol m^{-2} s^{-1})	*Leaf* $R_{d,29}$ (µmol m^{-2} s^{-1})	Q_{10} R_d	$A_{net.29}$ (µmol m^{-2} s^{-1})	$V_{cmax,25}$ (µmol m^{-2} s^{-1})	$J_{max,25}$ (µmol m^{-2} s^{-1})
Initial	16 days	13	29.5 ± 0.2	24.38 ± 0.71	2.61 ± 0.09	1.82 ± 0.07	24.34 ± 0.71	97.21 ± 3.36	153.62 ± 4.66
Initial	39 days	7	29.7 ± 0.3	21.74 ± 0.97	2.52 ± 0.06	1.69 ± 0.07	20.50 ± 0.92	75.32 ± 1.88	114.07 ± 3.45
Ambient	56 days (12 days)	6	29.2 ± 0.3^{A}	18.51 ± 0.88^{A}	2.37 ± 0.13^{A}	1.79 ± 0.03^{A}	18.50 ± 1.00^{A}	71.87 ± 0.90^{A}	109.93 ± 2.43^{A}
+4°C		7	32.0 ± 0.3^{B}	17.55 ± 1.02^{A}	2.12 ± 0.15^{A}	1.80 ± 0.05^{A}	17.06 ± 1.00^{A}	71.46 ± 4.95^{A}	100.07 ± 5.09^{A}
+8°C		6	32.5 ± 0.3^{B}	20.13 ± 0.74^{A}	2.71 ± 0.21^{A}	1.71 ± 0.03^{A}	19.27 ± 1.00^{A}	89.26 ± 2.76^{B}	149.97 ± 6.72^{B}
Ambient	70 days (28 days)	9	29.2 ± 0.3^{A}	17.29 ± 0.76^{A}	2.18 ± 0.07^{A}	1.85 ± 0.09^{A}	17.26 ± 0.82^{A}	61.40 ± 3.19^{A}	84.86 ± 5.22^{A}
+4°C		8	32.1 ± 0.3^{B}	18.80 ± 0.74^{A}	1.76 ± 0.18^{A}	1.83 ± 0.17^{A}	18.22 ± 0.87^{AB}	63.78 ± 3.29^{A}	87.07 ± 5.03^{A}
+8°C		7	32.9 ± 0.7^{B}	22.03 ± 0.62^{B}	2.56 ± 0.40^{A}	1.61 ± 0.06^{A}	20.49 ± 0.87^{B}	77.59 ± 3.22^{B}	113.88 ± 6.37^{B}

Ambient	85 days (41 days)	6	30.4 ± 0.5^{A}	18.65 ± 1.07^{A}	1.89 ± 0.09^{AB}	1.97 ± 0.03^{A}	18.54 ± 1.00^{A}	61.41 ± 2.29^{A}	91.11 ± 4.24^{A}
+4°C		6	31.5 ± 0.2^{A}	20.44 ± 0.97^{A}	2.17 ± 0.17^{B}	1.90 ± 0.03^{A}	20.11 ± 1.00^{A}	66.88 ± 6.31^{A}	101.61 ± 12.55^{A}
+8°C		6	33.5 ± 0.3^{B}	19.67 ± 1.30^{A}	1.45 ± 0.08^{A}	1.85 ± 0.05^{A}	18.42 ± 1.00^{A}	71.81 ± 5.27^{A}	102.39 ± 7.84^{A}
Ambient	99 days (55 days)	6	28.1 ± 0.6^{A}	13.62 ± 1.14^{A}	2.31 ± 0.30^{B}	2.11 ± 0.09^{A}	13.52 ± 0.82^{A}	64.08 ± 7.35^{A}	90.28 ± 9.95^{A}
+4°C		8	33.2 ± 0.5^{B}	17.66 ± 0.94^{B}	1.90 ± 0.15^{AB}	1.90 ± 0.07^{A}	16.82 ± 0.93^{A}	54.16 ± 3.63^{A}	78.02 ± 6.10^{A}
+8°C		8	33.8 ± 0.2^{B}	17.88 ± 0.51^{B}	1.43 ± 0.06^{A}	1.97 ± 0.11^{A}	16.43 ± 0.82^{A}	69.93 ± 4.33^{A}	102.59 ± 5.29^{A}

Table 3: Analysis of Variances (ANOVA) table for leaf photosynthetic parameters over time. Parameters are the same as those included in Table 2. Abbreviations are as follows: DFn, degrees of freedom in the numerator of the *F*-statistic, DFd, degrees of freedom in the denominator of the *F*-statistic, η^2, eta-squared effect size estimator. η^2 values can be interpreted as the proportion of variation in the parameter due to treatment. ANOVAs were done separately for each time, and probabilities were Bonferroni corrected (adjusted *p*). Asterisks denote a statistically-significant ANOVA prior to Bonferroni correction. Statistically significant results after Bonferroni correction are bolded. See Table 2 for parameter means and standard errors and Tukey HSD pairwise comparisons. $^{\$}$adjusted *p*-value is marginally significant, Tukey HSD groups statistically distinct in Table 2.

Parameter	Time	DFn	DFd	*F*	*p*	*p* < .05	η^2	adjusted *p*
T_{opt}	56 days (12 days)	2	15	33.144	3.13E-6	*	0.815	1.25E-5
	70 days (28 days)	2	21	21.291	8.88E-6	*	0.670	3.55E-5
	85 days (41 days)	2	15	18.424	9.12E-5	*	0.711	3.65E-4
	99 days (55 days)	2	22	46.281	1.31E-8	*	0.808	5.24E-8
A_{opt}	56 days (12 days)	2	15	2.158	0.15		0.223	0.60
	70 days (28 days)	2	21	10.773	6.03E-4	*	0.506	2.41E-3
	85 days (41 days)	2	15	0.642	0.54		0.079	1.00
	99 days (55 days)	2	22	6.911	5.00E-3	*	0.386	0.02
Leaf $R_{d,29}$	56 days (12 days)	2	15	3.240	0.07		0.302	0.27

	70 days (28 days)	2	22	2.556	0.10		0.189	0.40
	85 days (41 days)	2	15	8.754	3.00E-3	*	0.539	0.01
	99 days (55 days)	2	22	4.821	0.02	*	0.302	0.07[$]
Q_{10} R_d	56 days (12 days)	2	15	1.858	0.19		0.199	0.76
	70 days (28 days)	2	21	3.396	0.05		0.244	0.21
	85 days (41 days)	2	15	2.785	0.09		0.271	0.38
	99 days (55 days)	2	22	1.296	0.29		0.105	1.00
$A_{net,29}$	56 days (12 days)	2	15	1.429	0.27		0.160	1.00
	70 days (28 days)	2	22	4.829	0.02	*	0.305	0.07[$]
	85 days (41 days)	2	15	0.765	0.48		0.093	1.00
	99 days (55 days)	2	22	3.702	0.04	*	0.252	0.64
$V_{cmax,25}$	56 days (12 days)	2	15	7.340	6.00E-3	*	0.495	0.02
	70 days (28 days)	2	21	6.807	5.00E-3	*	0.393	0.02
	85 days (41 days)	2	15	0.353	0.35		0.130	1.00
	99 days (55 days)	2	22	0.124	0.12		0.173	0.50
$J_{max,25}$	56 days (12 days)	2	15	24.429	1.91E-5	*	0.765	7.64E-5
	70 days (28 days)	2	21	8.057	3.00E-3	*	0.434	1.20E-2
	85 days (41 days)	2	15	0.503	0.62		0.063	1.00
	99 days (55 days)	2	21	2.524	0.10		0.187	0.41

CO_2-response curves showed that there was a slight increase in the CO_2 compensation point of photosynthesis with increasing temperature, and that rates of CO_2 assimilation at the compensation point increased (i.e., A-C_i curves shifted higher in the warmed treatments relative to the ambient treatment, Table 2, Fig. S2). This change was most evident in the first 12 to 26 days following warming, wherein differences among treatments lessened as biochemical acclimation of photosynthesis to the increased temperatures occurred (Table 3). The result was that maximum rates of carboxylation ($V_{cmax,25}$) and electron transport ($J_{max,25}$) at 25°C decreased as plants matured during the initial establishment phase of the experiment, increased with warming, and then stabilized as leaf physiology acclimated to increased temperatures (Table 2, Fig. S8). For example, at 12 days after the start of the warming treatment, $J_{max,25}$ was greatest at 149.97 ± 6.72 μmol m^{-2} s^{-1} in the warmest treatment, being statistically greater than $J_{max,25}$ in the ambient and +4°C treatments, which measured 109.93 ± 2.43 and 100.07 ± 5.09 μmol m^{-2} s^{-1}, respectively ($F_{(2,15)} = 24.43$, $p < .001$, Table 2). These differences in $J_{max,25}$ were statistically significant and remained so for about a month after warming began (28 days), then they equalized (Table 3, Fig. S8). $V_{cmax,25}$ increased and became more variable with increasing with temperature. Throughout the experiment $V_{cmax,25}$ was 10-20 μmol m^{-2} s^{-1} greater in the warming treatment relative to the ambient treatment; however, these differences were no longer statistically significant after one month of warming (see table 3 for F-statistics and Table 2 for Tukey HSD groupings).

Photosynthetic light response curves (Fig. S4) showed a similar pattern in acclimation to the CO_2 response curves. Maximum rates of light-saturated photosynthesis (A_{max}) were different between at least two treatments for up to 28 days of warming (Table S2, see Table S3 or Appendix S2 for F-statistics). Differences in A_{max} among treatments reemerged at the end of the experiment, but only because A_{max} dropped substantially in the ambient treatment (Table S2, Fig. S8). The quantum yield of photosynthesis (Φ) exhibited an increasing then decreasing trend over time (which was statistically significant: $F_{(3,72)} = 31.683$, $p << .001$). Differences in Φ over time interacted with differences by treatment ($F_{(6,72)} = 2.728$, $p < .05$), which were greatest at 41 days after the start of the warming treatments, with Φ being lower in the warmest (+8°C)

treatment relative to the ambient treatment ($F_{(2,72)} = 7.173$, $p < .001$), wherein differences in light curves among treatments equalized (Table S2, Fig. S4). Light compensation (I_{comp}) and light saturation ($I_{sat(75\%)}$) points were variable over time but were generally tracked other trends in photosynthetic acclimation across treatments (F-statistics were all significant, except for the interaction between treatment and time for $I_{sat(75\%)}$, see Appendix S2, Table S2, Table S3, and Fig. S8).

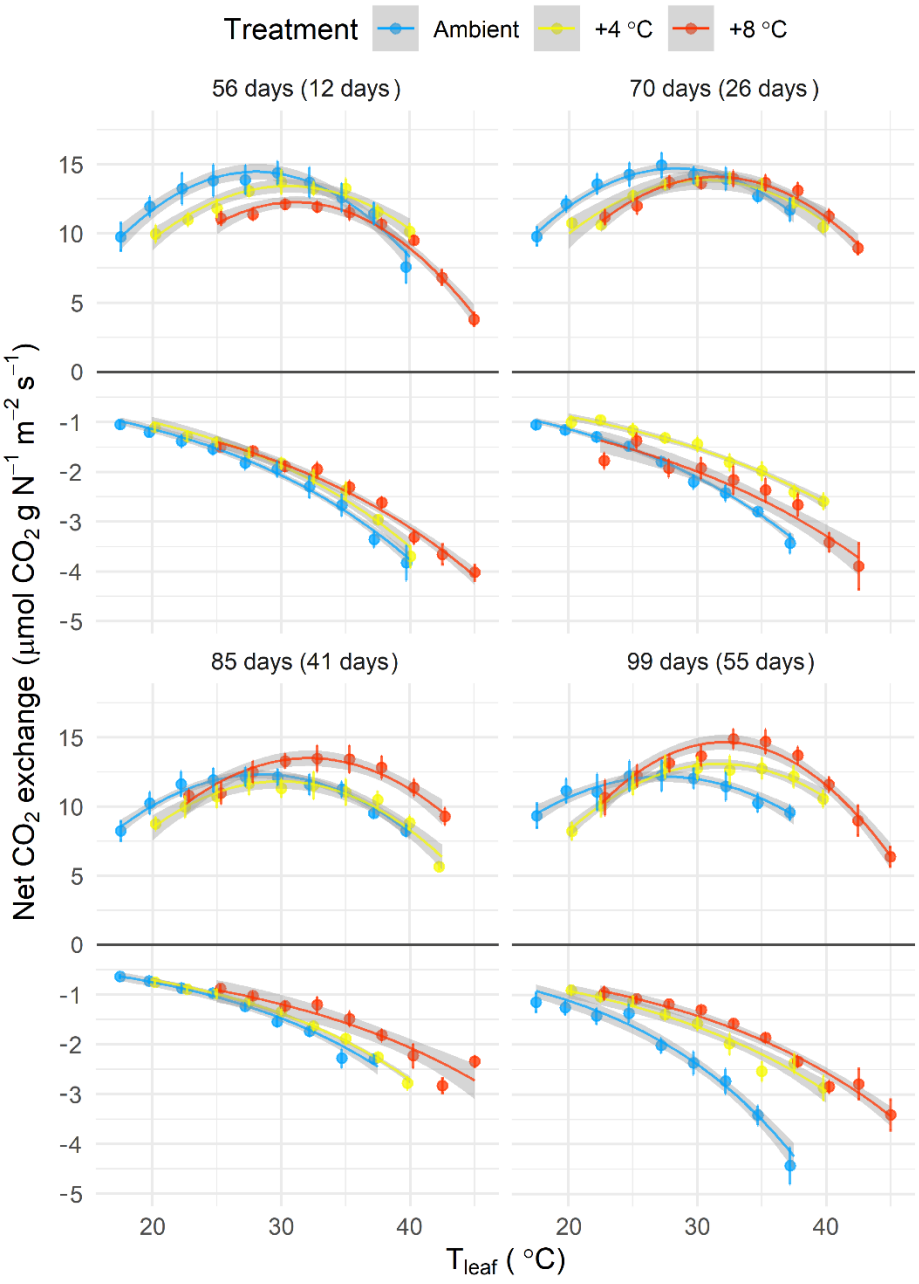

Fig. 3: (previous page) Temperature responses of N-based leaf net CO_2 exchange over time for *P. trichocarpa* clones. Curves are shown after plants were introduced to experimentally warmed conditions. These are the same data as Fig. 2, except standardized by leaf N_{area} (in g cm^{-2}). Points are means for many response curves, with bars showing standard errors. Lines are quadradic model fits for values >0 and exponential fits for values <0. Shading around lines shows 95% confidence intervals. Note the differences in the y-axis scale about zero. The number of days in parentheses indicates the number of warmed days at the time of measurement.

Acclimation of leaf dark respiration (R_d)

During the establishment period, leaf R_d rates at 29°C ($R_{d,29}$, from respiration-temperature response curves) were around 2.5 μmol m^{-2} s^{-1} and declined slightly as plants matured (Table 2, Table 3). $R_{d,29}$ was not statistically different among treatment ($F_{(2,74)}$ = 1.480, p = .24), but was different over time ($F_{(3,74)}$ = 4.418, p = .007), with a significant interaction between treatment and time ($F_{(6,74)}$ = 4.216, p = .001). This led to differences in $R_{d,29}$ between treatments at 41 and 55 days after warming began (Table 2, Table 3, Fig. S8). Additionally, during the establishment period, the temperature sensitivity of R_d (Q_{10} R_d) was about 1.7 (Table 2, Fig. 2). Leaf R_d acclimation lagged behind photosynthetic acclimation and seemed to be affected by the trimming of the plants, in that leaf $R_{d,29}$ rates were not different for the first month of warming (Table 3) but were depressed in the +8°C treatment after (Fig. 2, Table 2, Table 3, Fig. S8). For instance, differences in $R_{d,29}$ were largest at 85 days (12 days after the start of the warming treatments), with depressed rates in the +8°C relative to the +4°C treatment (see Table 2 for Tukey HSD groupings). A decrease in $R_{d,29}$ of nearly 1 μmol m^{-2} s^{-1} occurred after trimming of the plant (Table 2, Fig. S8). Patterns in leaf R_d at treatment temperature (as measured during light response curves at 0 μmol m^{-2} s^{-1} light) showed a similar acclimation pattern to $R_{d,29}$, albeit less variable (Table S2, Fig. S8). R_d showed significant differences among treatments ($F_{(2,72)}$ = 11.52, p < .001), and over time ($F_{(3,72)}$ = 13.07, p < .001), with the interaction being significant (Table S2, Table S3, Appendix S2) .Rates of leaf R_d always averaged <2 μmol m^{-2} s^{-1}, except for 12 days of warming in the +8°C treatment, and they were sometimes higher in warmed treatments than they were in the ambient treatment (Fig. S8 see Table S2 for Tukey HSD groupings over time). Acclimation of R_d and $R_{d,29}$ reached homeostasis by 41 days of warming (day 85 of the experiment) in the +8°C

treatment. In contrast, it continued to 55 days of warming (day 99) in the +4°C treatment (Fig. 2, Table 2, Table S2, see Fig. S7 for individual leaf R_d-T response curves over time by treatment). Toward the end of the experiment (i.e., 55 days of warming), rates of $R_{d,29}$ were lowest in the +8°C treatment and highest in the ambient treatment (Table 2). ANOVA results for the temperature sensitivity of leaf dark respiration (Q_{10} R_d) showed differences among treatments ($F_{(2,73)} = 4.364$, $p = .02$) and over time ($F_{(3,743)} = 7.776$, $p < .001$), however these difference became marginally significant when the repeated measures error structure was incorporate into the ANOVA models (treatment: $F_{(2,10)} = 3.697$, $p = .06$, time: $F_{(3,15)} = 3.106$, $p = .06$, Appendix S2) . Differences in Q_{10} R_d among treatment were greatest at 28 to 41 days after the start of the temperature treatments, with the differences being marginally significant ($p = .05$ and .09, respectively, Table 3, Appendix S2). By the end of the experiment at 55 days after warming began, Q_{10} R_d was roughly 0.1-0.2 greater in the ambient treatment than in either of the warmed treatments (Table 2, Fig. S8)

Variation in leaf morphology and nitrogen concentrations over time

Prior to pruning at week 10 (day 71) of the experiment, leaf morphologies were similar, with specific leaf area (SLA) values between 200 and 300 g cm^{-2} and leaf tissue N content between 3 and 4%. After plants were trimmed, leaf N content significantly decreased, dropping to below 3%, on average, in all treatments (Table S5 and Fig. S8, also see Tukey HSD groupings and *F*-statistics in Table S6). Leaf N content did not differ among treatments ($F_{(2,74)} = 0.517$, $p > .05$), but differed significantly over time ($F_{(3,74)} = 97.446$, $p < .001$), with the interaction of treatment and time being non-significant ($F_{(6,74)} = 1.435$, $p > .05$). These results were invariable to accounting for repeated measures error structure in the ANOVA (Appendix S2). There was a decrease in leaf C following plant trimming (time: $F_{(3,74)} = 45.948$, $p < .001$), in that prior to trimming, leaf C content was greater than 45%, whereas after plants were trimmed, leaf C content dropped to between 43 and 45% (Table S3). Leaf C content was also different among treatments $F_{(2,74)} = 4.558$, $p < .05$, with the differences being greatest just before trimming at 28 days after the beginning of the temperature treatments (Table S4, Table S5, Fig. S8). Similarly, SLA decreased significantly followed trimming (Table S5, Fig.

S8, despite differences among treatments throughout the experiment, Table S4), as plants were forced to produce new stem and leaf biomass. Accordingly, the amount of leaf N per area (N_{area}) increased slightly, if not remaining the same (i.e., Tukey HSD groupings increased in certain cases after trimming like for the +4 °C treatment, but did not in others, see Table S4). At the end of the experiment, whole plant SLA, the ratio of the entire plant's leaf area to its leaf dry mass at the time of harvest, was statistically lower in the +4°C treatment than the ambient treatment ($F_{(2,48)} = 3.531$, $p < 0.05$), but was not different between the +4°C and +8°C, or ambient and +8°C treatments (Table 6).

To evaluate if standardizing photosynthesis and respiration measurements by leaf N was necessary, we analyzed the relationships of leaf photosynthetic parameters (i.e., assimilation rates at 400 ppm from *A*-C_i curve fits, respiration rates at 0 μmol m^{-2} s^{-1} from light curves) to leaf N. Linear regressions showed that differences in leaf N content affected leaf gas exchange variably treatments (i.e., the slopes of the relationships of the leaf photosynthetic parameters to leaf N were statistically different, $p < .05$) (see Fig. S3). Therefore, we standardized leaf temperature response curves by leaf N_{area}, and subtle differences emerged compared to the non-normalized temperature response curves (Fig. 3). Leaf mass-N-based assimilation rates initially decreased in the warmer treatments, relative to the ambient treatments, before shifting their T_{opt} to warmer temperature and increasing rates of photosynthesis at T_{opt} (Fig. 3). For example, at 56 days (12 days after warming began), standardizing *A* by leaf N_{area} showed decreasing rates in the +8 °C treatment relative to the other two treatments (Fig. 3), whereas not accounting for leaf N_{area} showed that *A* increased in the +8 °C treatment relative to the other two treatments (Fig. 2). Similarly, at 70 days, standardizing *A* by leaf N_{area} decreased differences among the warmed treatments in *A* and R_d, and then after plant trimming, standardizing *A* by leaf N_{area} revealed greater differences in *A* and R_d between treatments than for non-N standardized measurements (Fig. 2 vs. Fig. 3).

Table 4: The temperature sensitivity (Q_{10}) of belowground CO_2 efflux (R_{BG}). Q_{10} values are based on whole-plant temperature responses using the growth chambers (see methods). F statistics are for Analyses of Variance in the form of: ~ Treatment × Chamber. *F* probabilities are all non-significant. Letters denote statistical groupings from Tukey HSD post-hoc tests.

Treatment	Chamber	Q_{10}
Ambient	soil	0.539 ± 0.497^{A}
	soil + root	0.649 ± 0.758^{A}
+4 °C	soil	0.582 ± 0.792^{A}
	soil + root	0.666 ± 0.923^{A}
+8 °C	soil	0.493 ± 0.416^{A}
	soil + root	0.285 ± 0.458^{A}
Treatment		$F_{(2,6)} = 0.224$
Chamber		$F_{(1,6)} = 0.393$
Treatment: Chamber		$F_{(2,6)} = 0.720$

Table 5: Root respiration (R_r)- temperature response parameters. Means ± standard errors for the temperature optimum of root reparation (T_{opt} R_r), the root respiration rate at T_{opt} ($R_{r,\,opt}$), the root respiration rate at 29°C ($R_{r,\,29}$), and the temperature sensitivity of root respiration at 29°C (Q_{10} $R_{r,29}$). Mass-based and mass N-base values are given (in µmol and mmol CO_2, respectively). *F*-statistics for Analyses of Variance in the form of: ~Treatment. *F* probabilities are denoted as follows: $^{**}p < .01$. Letters denote statistical groupings from Tukey HSD post-hoc tests. Note that the Q_{10} $R_{r,\,29}$ values for mass-based R_r and mass-N based R_r are equivalent, because the mass-N based measurements, the tissue CO_2 flux is divided by constant – the root tissue N concentration.

Treatment	T_{opt} R_r (°C)	Mass-based R_r		Mass N-based R_r		Q_{10} $R_{r,\,29}$
		$R_{r,\,opt}$ (µmol g^{-1} s^{-1})	$R_{r,\,29}$ (µmol g^{-1} s^{-1})	$R_{r,\,opt}$ (mmol g N^{-1} s^{-1})	$R_{r,\,29}$ (mmol g N^{-1} s^{-1})	
Ambient	45.40 ± 0.50^{A}	223.3 ± 18.6^{A}	145.5 ± 7.9^{A}	20.5 ± 2.2^{A}	12.8 ± 0.9^{A}	1.133 ± 0.004^{A}
+4 °C	45.51 ± 0.22^{A}	241.5 ± 19.3^{A}	132.8 ± 11.1^{A}	19.5 ± 1.0^{A}	10.7 ± 0.6^{A}	1.143 ± 0.003^{AB}
+8 °C	45.04 ± 0.26^{A}	229.1 ± 22.1^{A}	131.3 ± 14.3^{A}	15.6 ± 1.3^{A}	8.8 ± 0.7^{A}	1.153 ± 0.003^{B}
Treatment $F_{(2,15)}$	0.509	0.215	0.101	$2.889^{\$}$	2.134	9.906**

Table 6: Growth parameters (growth rates, biomass increments, allocation ratios, and whole plant SLA – total plant leaf area divided by its dry weight) for *P. trichocarpa* plants grown in experimental conditions for the 16-week duration of the experiment (n = 51, with 17 per treatment, because some plants were harvested at various intervals during the experiment). The belowground–aboveground allocation ratio is the quotient of fresh root biomass to fresh leaf plus shoot biomass. Means ± 95% confidence intervals are presented, with letters denoting Tukey HSD statistical groupings of analysis of variance. *F*-statistics for Analyses of Variance in the form of ~Treatment. *F* probabilities are denoted as follows: **p* < .05, ***p* < .01, and ****p* < .001.

Treatment	Plant height growth (cm day^{-1})	Basal diameter growth rate (mm day^{-1})	Leaf Biomass increment (g day^{-1})	Stem Biomass increment (g day^{-1})	Root Biomass increment (g day^{-1})	Total Biomass increment (g day^{-1})	Leaf area increment (cm^2 day^{-1})	Belowground–Aboveground allocation Ratio	Whole Plant SLA (cm^2 g^{-1})
Ambient	2.30 ± 0.10^{A}	0.086 ± 0.005^{A}	0.46 ± 0.04^{A}	0.63 ± 0.06^{A}	0.23 ± 0.04^{A}	1.30 ± 0.13^{A}	83.0 ± 7.8^{A}	0.21 ± 0.01^{A}	182.4 ± 9.1^{B}
+4°C	2.83 ± 0.11^{B}	0.094 ± 0.004^{B}	0.77 ± 0.04^{B}	0.86 ± 0.07^{B}	0.43 ± 0.07^{B}	2.01 ± 0.12^{B}	125.5 ± 7.0^{B}	0.26 ± 0.01^{B}	163.2 ± 10.0^{A}
+8°C	2.89 ± 0.09^{B}	0.084 ± 0.004^{A}	0.55 ± 0.10^{A}	0.67 ± 0.08^{A}	0.22 ± 0.05^{A}	1.40 ± 0.18^{A}	90.9 ± 16.3^{A}	0.18 ± 0.01^{A}	176.6 ± 13.6^{AB}
Treatment $F_{(2,48)}$	30.83***	5.88**	26.29***	14.43**	23.59***	31.39***	18.39***	9.39***	3.531*

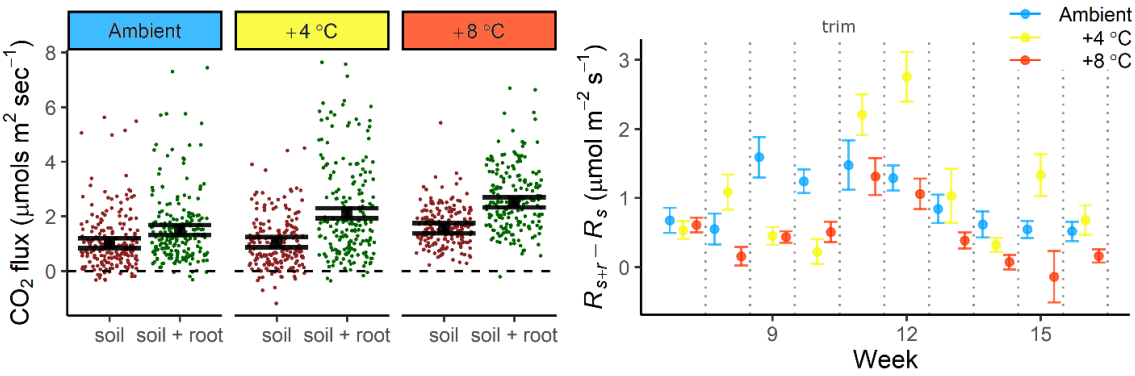

Fig. 4: Belowground CO_2 flux (in µmol CO_2 per square meter soil area per second) from respiration collars within mesocosm growth boxes. Each box was divided into two portions (soil, R_s, and soil +root, R_{s+r}, see Fig. 1C) using a 1-micron mesh barrier that prevented root growth into one-third of the mesocosm volume (see methods). Left: average (±95 % confidence intervals) for model predicted rates of belowground CO_2 flux for the 10-week warming period, where measurements were taken weekly. See table 4 for belowground CO_2 flux Q_{10} values. Right: mean (± standard error) rates of root-associated belowground CO_2 flux, or the difference in soil plus root and soil only CO_2 release ($R_{s+r} - R_s$) for the ten weeks of experimental warming. Note that plants were trimmed between weeks 10 and 11 (on day 71) of the experiment.

Belowground soil CO_2 efflux

Rates of belowground CO_2 efflux (*RBG*) were different by chamber, with chambers that had roots emitting about 1 µmol m^{-2} s^{-1} CO_2 on average than chambers with soil only (β of 0.95 for the soil + roots, $p < .001$, Fig. 1C, Fig. 4, Fig., S9). During the initial establishment period, rates of soil CO_2 efflux (R_s) averaged 0.81 (± 0.05) µmol m^{-2} s^{-1} and rates of soil plus plant root CO_2 efflux (R_{s+r}) were 1.17 (± 0.07) µmol m^{-2} s^{-1}. The difference between R_{s+r} and R_s tended to increase as the plants established root biomass in the mesocosms (Fig. 1C). Notably, R_{s+r} peaked after trimming the plants in week 11of the experiment, then declined over following several weeks (Fig. 1C). The effect of time alone was only marginally significant in the LMM (β = -0.03, $p = 0.17$), however the interaction of time with treatment was significant form both warmed treatments (both β = 0.06, $p < .05$), being slightly stronger for the +4°C than +8°C treatment, because of a greater difference in R_s and R_{s+r} in that treatment. During the 10-week warming period, rates of R_s were higher in the ambient than in the two warmed treatments , averaging 1.58 (±0.05) µmol m^{-2} s^{-1} in the ambient treatment and 1.07 (±0.06) and 1.04 (±0.07) µmol m^{-2} s^{-1} in the +4°C and +8°C treatments, respectively (Fig.

4). The LMM showed R_s to be significantly depressed in the two warmed treatments relative to the ambient treatment (β of -1.13, and -1.23 for the +4°C, and +8 °C treatments, respectively $p < .001$, Fig. S9, Table S7). Rates of R_{s+r}, however, were depressed with increasing temperature, measuring 2.53 (±0.08), 2.14 (±0.11) and 1.52 (±0.08) μmol m^{-2} s^{-1} from the ambient to the +8°C treatment (Fig. 4, Fig. S9). The LMM showed that this was due to a significant negative interaction between treatment and chamber in the warmest +8°C treatment (β = -0.47, $p = .002$). The interaction between chamber and treatment was positive for the +4°C treatment (although non-significant, β = 0.12, $p = .44$, Fig. S9, Table S7)

Differences in R_s and R_{s+r} ($R_{s+r} - R_s$), or the net rates of belowground root-associated respiration, were higher on average and less variable in the ambient than in the two warming treatments (Fig. 4). Two weeks into warming (i.e., at week 8 of the experiment), $R_{s+r} - R_s$ rates were higher in the +4°C treatment but lower in the +8°C treatment, relative to the ambient treatment (Fig. 4). By the third week of warming, $R_{s+r} - R_s$ rates were similar in the two warming treatments, and to about half that of the rates measured in the ambient treatment. The trimming of plants at week 10, led to considerable increases in $R_{s+r} - R_s$ rates, with increases being greatest in the 4°C treatment (Fig. 1C, Fig. 4). In the weeks following the trim, $R_{s+r} - R_s$ rates declined in all treatments and then began to rebound around week 15 (Fig. 4). $R_{s+r} - R_s$ rates were lowest in the +8°C treatment at the end of the experiment, with rates in the +4°C treatment being comparable to the ambient treatment. Net rates of belowground root-associated respiration during the 10-week warming period ($R_{s+r} - R_s$) were statistically different by treatment ($F_{(2,642)} = 20.074$, $p << .001$), and different over time ($F_{(9,642)} = 14.130$, $p << .001$), with a significant interaction between treatment and time ($F_{(18,642)} = 4.243$, $p < .001$, Fig. 4 ,Fig. 1C, Appendix S2). We measured the Q_{10} of R_{BG} using whole-plant temperature responses using the growth chambers, recording Q_{10} ranging from -0.34 to 2.74. Means were not different by chamber or treatment (see Table 4 for means and *F*-statistics).

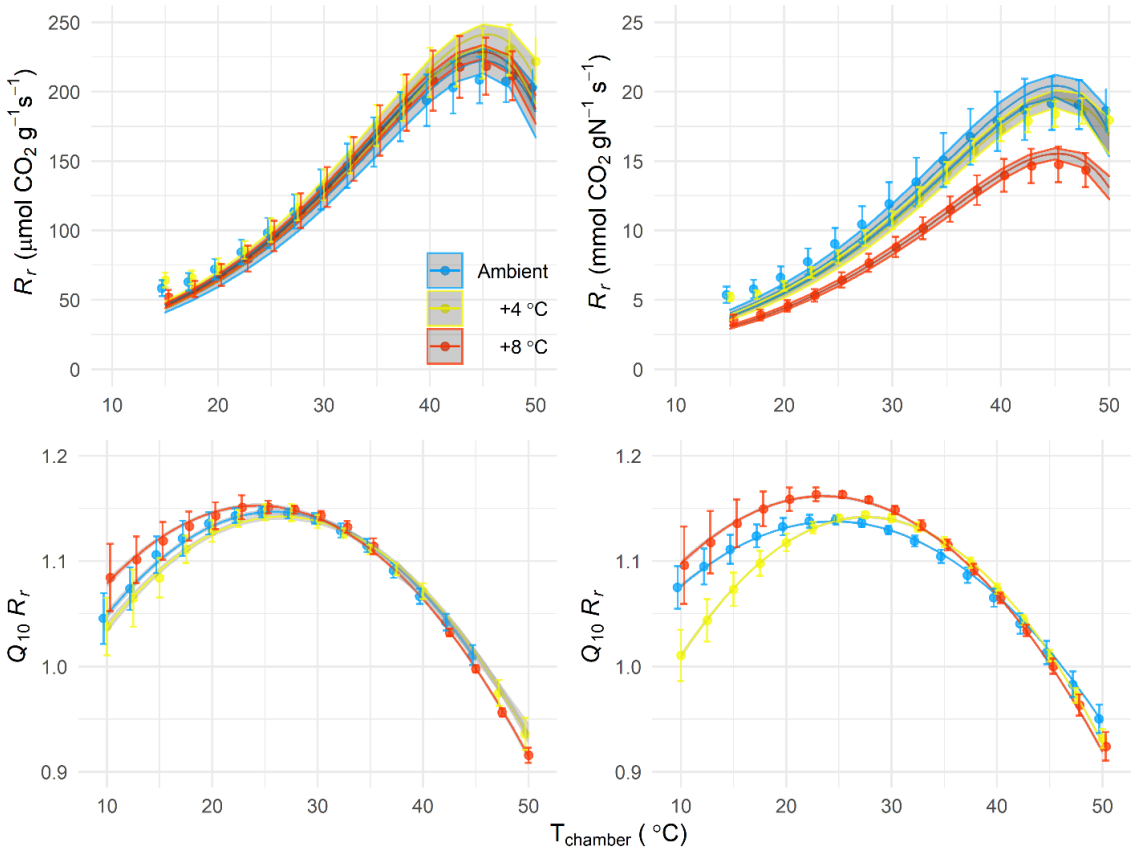

Fig. 5: Root respiration rates (R_r, top panels) and their temperature sensitivities (bottom panels). Mass-based (left panel) and mass-N-based (right panel) root respiration-temperature response curves by treatment for experimentally warmed *P. trichocarpa* clones. $R_r - T$ response curves were measured at the end of the experiment (at 94 and 109 days) on 6 root systems per treatment (see Fig.s S11 and S12 for curves by individual root tissue samples). Points are means (± standard errors), and shaded areas show 95% confidence intervals for model fits. The $R_r - T$ curves were fit using an exponential model. Because R_r Q_{10} varies with T (Palta and Noble 1989), R_r Q_{10} was calculated at each T by differentiating a fitting third-order polynomial curve to log-transformed R_r data (see Atkin et al. 2000). Finally, a quadradic model was fit to the R_r $Q_{10} - T$ curves (shown in bottom panels).

Root tissue respiration

At the end of the experiment, root material was harvested from 6 plants per treatment to measure R_r-temperature responses. The temperature optima of R_r (T_{opt} R_r) were not statistically different among treatments ($F_{(2, 15)} = 0.509$, $p > .05$), and all optima were between 45 and 46°C (Table 5). Mass-based respiration rates at temperature optima ($R_{r, opt}$) were about 10-20 µmol g^{-1} greater in the +4°C treatment than in either the +8°C

or ambient treatments, and mass-based respiration rates 29°C ($R_{r,\,29}$) were about 10 µmol g^{-1} greater for the ambient treatment than for the warmed treatments; however, these, differences was not statistically significant ($F_{(2,\,15)} = 0.215$, $p > .05$, Table 5). When R_r-temperature responses were standardized by root N content, $R_{r,\,opt}$ decreased with increasing temperature measuring 21, 20, and 16 mmol gN^{-1} s^{-1} from the ambient and two warming treatments, respectively. In this case, differences were marginally significant ($F_{(2,\,15)} = 2.889$, $p < .1$). The temperature sensitivity of root respiration at 29°C (Q_{10} $R_{r,29}$), measured 1.113 ± 0.004 in the ambient treatment, 1.143 ± 0.003 in the +4°C treatment, and 1.153 ± 0.003 in the +8°C treatments. These differences were significant ($F_{(2,\,15)} = 9.906$, $p < .01$), with the +8°C treatment being distinct from the ambient, but with the +4°C treatment being similar to them both (Table 5).

Plant growth & biomass production

Statistical differences in plant growth and biomass occurred because of the experimental warming treatments. Plants grew taller in the two warmed treatments than in the ambient treatment (Table 6, $F_{(2,48)} = 31.09$, $p < .001$). Basal diameter stem growth rates were greater in the +4°C treatment than in either the ambient or +8°C treatment (Table 6, $F_{(2,48)} = 5.88$, $p < .01$). Similarly, leaf ($F_{(2,48)} = 26.29$, $p < .001$), stem ($F_{(2,48)} = 14.43$, $p < .001$), root ($F_{(2,48)} = 23.59$, $p < .001$), and total biomass ($F_{(2,48)} = 31.39$, $p < .001$) increments were all greater in the intermediated warming +4°C treatment than in the two other experimental treatments (Table 6, Fig. S5). Plants produced more leaf area ($F_{(2,48)} = 18.39$, $p < .001$), and had greater belowground–aboveground (i.e. root to leaf plus shoot) allocation ratios ($F_{(2,48)} = 9.39$, $p < .01$), in the +4°C treatment than in the two other treatments (Table 6). Allocation to roots was 20.50 ± 0.01% and 17.6 ± 0.01% in the ambient and +8°C treatments, respectively, which was statistically different from the 26.20 ± 0.01% of biomass allocated to roots in the +4°C treatment (Table 6).

Discussion

We discuss our findings in three sections regarding the 1) aboveground acclimation (i.e., leaf photosynthesis and respiration), 2) belowground acclimation (i.e., root tissue respiration and soil respiration), and 3) growth response of *P. trichocarpa* to increased temperature over time.

Aboveground acclimation of P. trichocarpa *to warming*

Acclimatory responses were similar in the two warmed treatments but occurred faster in the +8°C than in the +4°C treatment. This illustrates that there is a limit in the thermal acclimation capacity in *P. trichocarpa*. Photosynthetic acclimation to increased temperature showed an initial constructive adjustment (*sensu* Way and Yamori 2014) in that both A_{opt} and T_{opt} increased in the first two to four weeks of warming, but then A_{opt} decreased slightly, as T_{opt} continued to increase in the +4 and +8 °C treatments (Fig. 2, Fig. S8). Based on comparing the differences in our leaf gas exchange measurements among treatments (Table 2, Table 3, Table S2, Table S3, Fig. S8), we can roughly characterize the acclimation of leaf gas exchange into two periods: the first month of warming (up to day 35 of warming – day 77 of the experiment) where acclimation was accelerating, and the second month or warming (from day 77 until the end of the experiment), where acclimation was stabilizing. Photosynthetic and respiratory acclimation to increased temperature was variable across individuals (Fig. S6 and Fig. S7), likely because of small differences in environmental (e.g., light) conditions and inherent differences in the photosynthetic capacities of leaves. Yet, we found T_{opt} to be able to increase to near 34°C despite an air temperature increase of 8°C in our warmest treatment (Fig. 2, Fig. S8). This finding is similar to results from Weston *et al.* (2011), who reported that the temperature optimum of A_{max} for *P. trichocarpa* clones grown at 22°C was 32.6 ± 0.57 °C, beyond which rates of photosynthesis decreased sharply.

Responses of T_{opt} and the A_{opt} were similar in both the +4 and +8 °C treatments (Fig. 2, Table 2, Fig. S8), leading us to conclude that there is a limitation on the ability of *P. trichocarpa* to physiologically acclimate to increased temperature. In theory, if there is no limit on photosynthetic acclimation, T_{opt} would increase twice as much in the +8°C treatment than the +4°C treatment, thus linearly reflecting increases in air temperature. Similarly, lacking limitation on photosynthetic acclimation to warming, constructive adjustments A_{opt} would be twice as large in the +8°C treatment than the +4 °C treatment. We observed maximum increases in T_{opt} of about 4 °C, with similar responses in both warmed treatments despite a 4°C difference in temperature increase, supporting the existence of a limitation. Constructive adjustments in A_{opt} showed less limitation, in that

the immediate constructive adjustment in A_{opt} (at 12 days after warming began) in the +8°C treatment was more than double that of the +4°C treatment. These differences attenuated over time with A_{opt} rates stabling near 18 μmol m^{-2} s^{-1} in both warming treatments by the end of the experiment (Fig. 2 Fig. S8), which is near the optimal photosynthetic rate of the species (Bassman & Zwier 1991).

Despite any limitation in the magnitude of photosynthetic acclimation, acclimation occurred more rapidly in the +8°C treatment relative to the +4°C treatment. Not only did increases in T_{opt} lag increases in air temperature, but the greater the increase in air temperature, the more T_{opt} lagged, suggesting that the increase in T_{opt} with increasing air temperatures might take the form of a saturating curve. Considering our results and the similarity in responses between the +4 and +8°C treatment, we suggest that increase T_{opt} likely saturates near 29°C (i.e., +4°C ambient air temperature in our experiment). We do show, however, that P. *trichocarpa* can increase the thermal optimum of photosynthesis about two degrees but may be physiologically limited to acclimate further. Indeed, a shift in T_{opt} of two degrees is consistent with the consensus in the literature that it can shift by one-third to half of the magnitude of change in air temperatures (Kumarathunge *et al.* 2019, Sage and Kubien 2007). A 33% increase in T_{opt} in our case would be 1.3°C and 2°C for the +4 and +8°C treatments, respectively; Similarly, a 50% increase in T_{opt} would be 2.7°C and 4°C. Net average increases in T_{opt} over 55 days of warming maximized at 4.3°C, being similar among both warming treatments at about 4°C (Table 2) and demonstrating limitation to increase beyond 4°C.

Warming also led to a significant increase in stomatal conductance ($g_{sw,}$ Fig.1B). Increases in g_{sw} reflected increased photosynthetic rates at growth temperatures, which is a principal criterion for acclimation (Way and Yamori 2014). Maintaining similar A with a decline in g_{sw} with warming suggests a combination of adjusting both leaf water loss and inherit photosynthetic capacity to maintain leaf carbon balance at a higher temperature (Berry and Björkman 1980, Sage and Kubien 2007). We measured g_{sw} near 1 mol m^{-2} s^{-1} in our warmest treatment during the first month of acclimation (Fig. 1B). Similarly, Bassman and Zwier (1991) reported rates of g_{sw} of up to 1 μmol m^{-2} s^{-1}, with some variation across poplar varieties because of susceptibility to water stress. In

contrast, Zhang et al. (1999) reported g_{sw} values that averaged 0.271 (±0.013) mol m^{-2} s^{-1}, accounting for seasonal and diurnal variation from mature *P. trichocarpa* trees growing in the floodplain of the Thames River in southeastern England. Thus, the high rates of stomatal conductance we measured are likely because plants were young and leaves were in a developmental stage, optimizing carbon gain over water loss. Additionally, high rates of stomatal conductance help reduce leaf temperature via transpirative cooling, thus increasing *gsw* is likely a strategy poplar leaves use to cope with high temperatures. Stomatal conductance initially decreased during the first week of warming, increased sharply in the following weeks, and then decreased to become similar across treatments (Fig. 1B). Although temperature effects on g_{sw} are considered indirect (i.e., they are mediated by vapor pressure deficit or evapotranspiration) (Urban *et al.* 2017) and vary widely across leaves and individual trees, an initial, short-term reduction of g_{sw} in response to temperature stress has been documented in other te,perate C_3 trees, like red maple (Weston and Bauerle 2007).

Increased rates of photosynthesis were driven, in part, by adjustments in the light-capturing reactions and biochemical mechanics of photosynthesis (Table 2, Fig. S1, Table S2, Table S3, Fig. S4, Fig. S8). This is consistent with previous research in that both the kinetics of electron transport in photosystems (i.e., light reactions) and the enzyme-catalyzed biochemical (i.e., dark) reactions of the Calvin cycle in C_3 photosynthesis have been shown to increase with temperature and then adjust their rates of reaction (i.e., acclimate) with time (Bernacchi *et al.* 2003, Berry and Björkman 1980, Von Caemmerer 2000, Yamasaki *et al.* 2002). We observed more rapid and slightly greater increases in chlorophyll fluorescence parameters (Fig. S1) and in estimates of $J_{max,25}$ and $V_{cmax,25}$ in the +8°C treatment than in the +4°C treatment (Fig. S8). Additionally, we observed an increase in leaf N_{area} with increasing temperature (Table S4, Table S5, Fig. S8). This increase was affected by (i.e., did not persist after) trimming of the plants. Increased leaf Narea could be related to upregulation of photosynthetic enzyme (e.g. Rubisco) production and use, increased soil N availability in the soil due to higher rates mineralization at higher temperatures resulting in increased plant uptake, and/or a increased demand for N to maintain growth, respiration and photosynthesis at higher

temperatures (i.e., as T_{opt} shifts toward greater T and A-C_i and leaf R_d curves shift upward).

These findings together show that both the light and dark reactions of photosynthesis adjusted to increased temperatures (Table 2, Fig. S2, Fig. S8, Table S2). The increase in chlorophyll fluorescence signifies greater light stress, in that either the downstream (i.e., dark) photosynthetic reactions are limiting the use of captured light energy, or there was a decrease in the quantum efficiency of photosystem photochemistry (Briantais *et al.* 1996). However, after acclimation occurred during the second month of warming, the magnitude of change in $J_{max,25}$, $V_{cmax,25}$, $T_{opt,}$ and A_{opt}, was similar in both the +4°C and +8°C treatments (Table 2), potentially signifying a physiological limitation on the degree of thermal acclimation of photosynthesis in the poplar plants studied. We base this conclusion on the observation that despite double the magnitude of thermal stress in the warmest treatment relative the intermediate warming treatment, adjustments in most photosynthetic parameters were of similar magnitude across both warming treatments. Differences in photosynthetic rates among treatments were greatest at 12 to 26 days post warming, and then photosynthetic rates became more similar, demonstrating that thermal acclimation of photosynthesis can occur in poplar in days to weeks (Table 2, Table 3, Fig. 3, Fig. S4).

Acclimation of leaf respiration occurred in concert with the acclimation of photosynthesis to warming. By 41 to 55 days of warming, the acclimation of R_d was stabilizing, with $R_{d,29}$ rates increasing in warmed treatments during the first month of warming to measure >2 μmol m^{-2} s^{-1}, and then dropping down below 2 μmol m^{-2} s^{-1} in the second month of warming (Fig. 3, Table 2, Fig. S7, Fig. S8). The thermal sensitivity of leaf respiration, Q_{10} R_d, showed little variability among treatments (i.e., differences were never significant among treatments at any single time point), ranging between 1.6 and 2.1 μmol m^{-2} s^{-1}, indicating that the shape of leaf R_d – temperature relationships were largely unaffected because of acclimation of R_d rates to higher temperatures (Table 2, Table 3, Fig. 2, Fig. S7, Fig. S8). When Q_{10} R_d is unaffected in the acclimation of respiration, it suggests that the acclimation is being driven by a change in the elevation and not the

slope of the temperature-respiration relationship. This is consistent with type II acclimation of R_d (Atkin *et al.* 2005, *sensu* Atkin and Tjoelker 2003).

Acclimation of soil CO_2 efflux and belowground acclimation of poplar to warming

Belowground physiological acclimation to warming is much more difficult to measure repeatedly over time than aboveground acclimation. We found only minimal differences in root respiration, R_r, at the end of the experiment, which were moderated by root N content. Among treatments, warming led to a decrease in soil respiration, R_s, of roughly one-third (Table 4, Fig. 4). All belowground respiration Q_{10} values were less than one (Table 4), indicating that heterotrophic R_s decreased with increasing temperature. In a meta-analysis on the temperature sensitivity of belowground respiration, R_{BG}, Li *et al.* (2020) found that root tissues increase the Q_{10} values of R_{BG} (i.e., increase the temperature sensitivity of soil CO_2 efflux), likely because heterotrophic R_s decreases but R_r increases with increasing temperature. Qualitatively consistent with those findings, our results from the whole-chamber temperature response showed that when roots were present in soil, we measured slightly greater Q_{10} values of belowground respiration in the ambient and +4°C treatments than when roots were absent (i.e., growth medium alone, Table 3). These differences were not significant, however, likely because of low levels of replication (n=12, two per each respiration chamber per treatment), relative to the magnitude of respiratory change in the plant-soil experimental system. We completed the whole-plant temperature responses using the growth chambers twice and replicating more would have decreased the variability in our R_{BG} Q_{10} estimates. Yet, for the +8°C treatment, the Q_{10} value for R_{s+r} was about half that of R_s, providing some observational evidence that in the warmest treatment, R_{s+r} had a greater reduction in respiration rate than R_s alone (Table 3). R_{s+r} was 16% lower in the +4°C treatment versus ambient, and 28% lower in the +8°C treatment versus +4°C treatment, and this variation is likely due to differences in heterotrophic (i.e., microbial) and not autotrophic (i.e., root-related) R_{BG}. Indeed, R_r did not vary systematically across treatments (Table 5, Fig. 5), but R_s was statistically distinct in the two warmed treatments relative to the ambient treatment (Table 3, Fig. 4, Fig. S9). Jarvi and Burton (2013) reported an increase in R_{BG} with *in situ* experimental warming of *Acer saccharum* dominated soils, with R_r showing

partial, soil moisture-mediated acclimation, and *Rs* increasing in warmed plots due to increased N-mineralization rates. The difference we observed between R_{s+r} and R_s was largest in the +4°C treatment, potentially illustrating a belowground temperature optimum for the plant–soil system, where heterotrophic metabolism of plant-derived liable C is greatest (Fig. 5). We observed large increases in R_{s+r} (i.e., plant-associated R_{BG}) after trimming the plants (Fig. 4), and these increases were largest in the +4°C treatment, potentially showing how the poplar plants in that treatment allocated the greatest amount of liable C to belowground to mine N for new leaf and stem tissue production (Melillo et al. 2011). The greater ability of plants to access N in the +4°C treatment than the other two treatments likely led to the differences observed in plant growth and biomass production.

Regarding root tissue respiration, R_r averaged between 130 and 150 μmol g^{-1} s^{-1} at 29 °C for *P. trichocarpa*, with substantial variation among the root systems of individual plants (Fig. S10). $R_{r,29}$ values were slightly but not-significantly lower and more variable in the warmed treatments than in the ambient treatment; however, those differences were accentuated (becoming marginally significant) when we standardized by root N content (Table 5, Fig. 5). In agreement with several studies (Ceccon *et al.* 2016, Noh *et al.* 2020, Reich *et al.* 2008), standardizing R_r rates by tissue N content helped constrain variation among individuals (Fig.s S11 and S12) because root tissue N is an important indicator of root metabolic activity due to its involvement with ion uptake and root protein and enzyme function. Although N-based $R_{r,29}$ was not different among treatments (Table 5), N-based R_r at higher temperatures was depressed in the +8 °C treatment relative to the two other treatments (Fig. 5), pointing to the important role that tissue N content has in relation to R_r. Thus, we found clear differences in the temperature sensitivity of root respiration at 29°C (Q_{10} $R_{r,29}$, table 5), with the warmest +8 °C treatment having a greater sensitivity than the ambient treatment. Due to the lower tissue N content of the plants grown in +8°C treatment relative to the two other treatments, the mass-N-based R_r–temperature relationship was shifted lower. The Q_{10} of N-mediated R_r was depressed at lower temperatures (i.e., between 10 and 20°C) in the ambient treatment relative to the two warmed treatments, potentially illustrating the effect of thermal acclimation on

increasing rates of R_r at lower temperatures (i.e., a broadening of the R_r Q_{10}-temperature relationship, Fig. 5).

Severe temperature stress likely requires higher plant N utilization, which can result in an N-dilution effect (Jawrell and Beverly 1981). For example, warming has been shown to decrease the N content and increase lipid content in algal tissues (Converti et al. 2009). However, the dilution effect of temperature on tissue N contents depends on the relative temperature sensitivity of active and passive N uptake, soil N metabolism, diffusion, and mass flow, and microbial and plant N enzyme kinetics in the soil (Jawrell and Beverly 1981, Jarvi and Burton 2013). These processes can all potentially increase with warming as well. For example, warming-induced soil carbon losses were compensated by plant carbon (i.e., root biomass) gains, which were driven by increased N-availability in an ecosystem warming experiment at Harvard Forest, Massachusetts (Melillo *et al.* 2011). Thus, increased N availability and utilization by plants with warming can affects plant-soil carbon dynamics through the production of new roots. Generally, the relative contribution of respiration in roots to ion uptake and root growth decreases with root system age while the relative contribution of respiration to the maintenance of root biomass increases (Bouma 2005, van der Werf *et al.* 1988). For example, *Rr* was substantially different for established root systems (5 weeks and 2 years old) versus rain-produced roots (1 week and six weeks old) in *Agave desertii* (Palta & Noble 1989). Similar results have been reported for poplar, with rates of root respiration decreasing by about 50% in the by 3 weeks of age (Ceccon *et al.* 2016). Root system age-related changes in metabolic activity, and hence R_r, might explain some of the temporal variation in R_{s+r} and $R_{s+r} - R_s$ (Fig. 1C, Fig. 4). Nevertheless, because the root tissues used for the root respiration-temperature response curves were all about the same age (94 to 109 days old), tissue age likely had little effect on the R_r-temperature response curves. Based on the assumption that roots were established, being roughly 3 months old but still being metabolically active, we can infer that the majority (i.e., at least half) of root tissue respiration stemmed from biomass maintenance, with the other half being partitioned between root ion uptake and growth (Ceccon *et al.* 2016). Additionally, we can assume that differences in root N content were a function of N retranslation to

aboveground biomass production, leading to more of a dilution effect in the +4 treatment where more stem and leaf biomass was produced after trimming, however being variable among plants (Table S6, Fig. S5).

The growth response of poplar to warming

Striking differences in plant biomass production resulted because of growth temperature with production being elevated at the intermediate temperature treatment, evidencing a thermal optimum in growth temperature for the species near 29°C. Considering the widespread distribution and cultivation of poplars throughout North America (Kutsokon *et al.* 2015, Wullschleger *et al.* 2002), perhaps the starkest results of this experiment were the differences in plant biomass production (Table 6). Plant biomass production was greatest at intermediate warming (i.e., 29°C daytime temperature and 25°C nighttime temperature), with total biomass increment being nearly 50% greater, root biomass increment having doubled, stem biomass being one-third greater, and leaf biomass being 40-67% greater at intermediate warming than at the other two temperatures (Table 6, Fig. S5). The native range for *P. trichocarpa* is primarily from northern California to southeastern Alaska, experiencing a variable climate (DeBell 1990). The *Nisqually-1* clone used in this project was initially collected in riparian temperate forest of western Washington state. Using plantation yield data from 23 countries, Kutsokon *et al.* (2015) found that poplar plantation productivity was positively correlated with yearly temperature and the number of hot days during the growing season, albeit weakly and with some variation due to the cultivation method and poplar variety. Our results demonstrate that although there is some benefit to increased temperatures for biomass production, that benefit is limited, especially at higher temperatures where the physiological cost of acclimation (in both C and N economics) outweighs any increase in carbon gain via photosynthesis. Although leaf respiration did acclimate, warming led to its increase initially (Fig. 2, Fig. 3, Table 2, Fig. S10, Table S2). R_{s+r} rates were depressed in the warmest +8 °C treatment (Fig. 4), as was N-based R_r. (Fig. 5). The initial increase in leaf and whole plant respiration results in a C cost, which coupled with the N cost of photosynthetic adjustment likely drives decreased C and N economic margins at the whole plant-scale. Collectively, this results in decreased

allocation to roots, labile C release belowground and depressed R_{BG}, which could have further ecosystem feedbacks in a natural system.

The native range of *P. trichocarpa* has been warming and will continue to warm as anthropogenic climate change persists and intensifies (Hansen *et al.* 2010). Like many of the trees in the Salicaceae, *P. trichocarpa* requires large amounts of water to thrive (Théroux Rancourt *et al.* 2015), and there have even been efforts to improve the water use efficiency of the species to conserve water use in agricultural settings (Kalluri *et al.* 2020). A single, small poplar tree of about 5 cm stem diameter and 6 m height can transpire over 25 liters of water in a given day, taking a significant portion (between 10 and 60%) of its water from the groundwater table (Zhang *et al.* 1999). We found that evaporation plus transpiration was 41% and 73% greater at +4 and +8°C, respectively than for mesocosms at ambient conditions. Although the plants in our experiment were not water-limited, temperature stress and subsequent acclimation *in situ* rarely occur in this context. Therefore, photosynthetic, and respiratory acclimation to increased temperatures will likely be dependent on water availability for wild or plantation-grown poplar trees (Broeckx et al. 2014). The increase in g_{sw} associated with thermal acclimation results in increased water loss, which is an important consideration to take into account because the effects of global climate change often couple warming with increased variability in precipitation and increasing drought frequency (Allen *et al.* 2015, McDowell *et al.* 2020).

Conclusion

All else being equal (i.e., given adequate water and nutrients), *P. trichocarpa* can physiologically acclimate to increased temperatures, although we find that the aboveground acclimatory response was restricted to a shift in the photosynthetic temperature optimum (T_{opt}) of 2-3 °C. Both C and N economies potentially limit physiological acclimation with consequences for reduced plant growth, especially when thermal stress is severe. Whole plant N-economics plays a fundamental role in the acclimatory response, as changes in the reaction kinetics of key proteins (e.g., RuBP, Rubisco) involved in photosynthesis underpin leaf acclimation and drive the physiological cost of acclimation. Concerning leaf C-economics, constructive

adjustments in photosynthesis were underpinned by higher rates of electron transport (J_{max}) and carboxylation (V_{cmax}), which persisted for up to about one month after the start of warming, then stabilized to background levels. We found that generally, belowground CO_2 release reflected patterns in aboveground CO_2 assimilation, illustrating a linkage in plant C economics through the plant-soil system as acclimation occurred.

Belowground, we found that rates of root respiration showed some minor differences among temperature treatments (e.g., in their thermal sensitivities of respiration and in respiration rates at the extremes of the temperature range), indicating the ability to acclimate to thermal stress. Notably, there were clear plant biomass production differences among treatments, with aboveground biomass having been stimulated in both warmed treatments, but root biomass reaching its maximum at +4°C warming, with at least 5 % more biomass allocated to roots. Thus, there appears to be some limitation in the magnitude of physiological acclimation in *P. trichocarpa*, with moderate warming (i.e., a few to several degrees C) resulting in increased productivity up to a point, whereafter productivity declines. Our results show that photosynthetic acclimation can occur within a month, whereas belowground acclimation and the consequences of the cost of the acclimation at the plant and ecosystem-scale likely take longer to develop. Environmental warming occurs in concert with other stressors, such as pathogens or drought, so although our results point to the ability of *P. trichocarpa* to acclimate to, or even benefit from, predicted future temperature conditions. Nevertheless, field studies of forest and plantation trees are needed to corroborate our experimental findings and to determine if the results presented here indicate responses of wild or plantation-grown trees of *P. trichocarpa* or other poplar species.

References

Adams MA, Buckley TN, Turnbull TL (2020) Diminishing CO2-driven gains in water-use efficiency of global forests. Nat Clim Change 10: 466-471.

Aitken SN, Yeaman S, Holliday JA, Wang T, Curtis-McLane S (2008) Adaptation, migration or extirpation: climate change outcomes for tree populations. Evol Appl 1: 95-111.

Allen CD, Breshears DD, McDowell NG (2015) On underestimation of global vulnerability to tree mortality and forest die-off from hotter drought in the Anthropocene. Ecosphere 6: 1-55.

Atkin OK, Tjoelker MG (2003) Thermal acclimation and the dynamic response of plant respiration to temperature. Trends Plant Sci 8: 343-351.

Atkin OK, Edwards EJ, Loveys BR (2000) Response of root respiration to changes in temperature and its relevance to global warming. New Phytol 147: 141-154.

Atkin OK, Bruhn D, Tjoelker MG (2005) Response of plant respiration to changes in temperature: mechanisms and consequences of variations in Q_{10} values and acclimation. In: Lambers H, Ribas-Carbo M (eds) Plant respiration: from cell to ecosystem. Springer, Dordrecht, Netherlands, pp 95-135.

Bassman JH, Zwier JC (1991) Gas exchange characteristics of Populus trichocarpa, Populus deltoides and Populus trichocarpa× P. deltoides clones. Tree Physiol 8: 145-159.

Bates D, Mächler M, Bolker B, Walker S (2015) Fitting linear mixed effects models using lme4. J Stat Softw 67,1: 1-48.

Bernacchi C, Pimentel C, Long SP (2003) In vivo temperature response functions of parameters required to model RuBP-limited photosynthesis. Plant Cell Environ 26: 1419-1430.

Berry J, Björkman O (1980) Photosynthetic response and adaptation to temperature in higher plants. Annual Review Plant Physiol 31: 491-543.

Bond-Lamberty B, Thomson A (2010) Temperature-associated increases in the global soil respiration record. Nature 464: 579-582.

Bouma TJ (2005) Understanding plant respiration: Separating respiratory components versus a process-based approach. In: Lambers H, Ribas-Carbo M (eds) Plant respiration: from cell to ecosystem. Springer, Dordrecht, Netherlands, pp 177-194.

Briantais J-M, Dacosta J, Goulas Y, Ducruet J-M, Moya I (1996) Heat stress induces in leaves an increase of the minimum level of chlorophyll fluorescence, Fo: a time-resolved analysis. Photosyn Res 48: 189-196.

Broeckx LS, Verlinden MS, Ceulemans R (2014) Seasonal variations in photosynthesis, intrinsic water-use efficiency and stable isotope composition of poplar leaves in a short-rotation plantation. Tree Physiol 34:701-715.

Bryla D, Bouma T, Hartmond U, Eissenstat D (2001) Influence of temperature and soil drying on respiration of individual roots in citrus: integrating greenhouse observations into a predictive model for the field. Plant Cell Environ 24: 781-790.

Burton A, Pregitzer K, Ruess R, Hendrick R, Allen M (2002) Root respiration in North American forests: effects of nitrogen concentration and temperature across biomes. Oecologia 131(4): 559-568.

Canham CD, Murphy L, Riemann R, McCullough R, Burrill E (2018) Local differentiation in tree growth responses to climate. Ecosphere 9: e02368.

Ceccon C, Tagliavini M, Schmitt AO, Eissenstat DM (2016) Untangling the effects of root age and tissue nitrogen on root respiration in Populus tremuloides at different nitrogen supply. Tree Physiol 36: 618-627.

Chapin III FS, McFarland J, McGuire AD, Euskirchen ES, Ruess RW, Kielland K (2009) The changing global carbon cycle: linking plant-soil carbon dynamics to global consequences. J Ecol 97: 840-850.

Crous, K.Y., Drake, J.E., Aspinwall, M.J., Sharwood, R.E., Tjoelker, M.G. & Ghannoum, O. (2018) Photosynthetic capacity and leaf nitrogen decline along a controlled climate gradient in provenances of two widely distribued eucalyptus species. Global Change Biol, 24, 4626– 4644.

Converti A, Casazza AA, Ortiz EY, Perego P, Del Borghi M (2009) Effect of temperature and nitrogen concentration on the growth and lipid content of Nannochloropsis oculata and Chlorella vulgaris for biodiesel production. Chem Eng Process 48: 1146-1151.

Cunningham S, Read J (2002) Comparison of temperate and tropical rainforest tree species: photosynthetic responses to growth temperature. Oecologia 133: 112-119

DeBell DS (1990) Populus trichocarpa Torr. & Gray. Black Cottonwood. In: Burms RM Honkala BH Silvics of North America, vol 2, Hardwoods, United States Department of Agriculture (USDA) Forest Service, Agriculture Handbook 654. pp. 570-576.

Dusenge ME, Duarte AG, Way DA (2019) Plant carbon metabolism and climate change: elevated CO 2 and temperature impacts on photosynthesis, photorespiration and respiration. New Phytol 221: 32-49.

Duursma RA (2015) Plantecophys-an R package for analysing and modelling leaf gas exchange data. PloS One 10: e0143346.

Eissenstat D, McCormack ML, Du Q (2013) Global change and root lifespan. In: Eschel A, Waisel Y (eds.) Plant Roots: The Hidden Half, Fourth Edition. CRC Press, pp 399-412.

Farquhar GD, von Caemmerer Sv, Berry JA (1980) A biochemical model of photosynthetic CO_2 assimilation in leaves of C 3 species. Planta 149: 78-90.

Feeley KJ, Rehm EM, Machovina B (2012) Perspective: the responses of tropical forest species to global climate change: acclimate, adapt, migrate, or go extinct? Front Biogeogr 4: 69-82.

Ficken CD, Warren JM (2019) The carbon economy of drought: comparing respiration responses of roots, mycorrhizal fungi, and free-living microbes to an extreme dry-rewet cycle. Plant Soil 435: 407-422.

García-Carreras B, Sal S, Padfield D, Kontopoulos D-G, Bestion E, Schaum C-E, Yvon-Durocher G, Pawar S (2018) Role of carbon allocation efficiency in the temperature dependence of autotroph growth rates. P Natl Acad Sci USA 115: E7361-E7368.

Gornall JL, Guy RD (2007) Geographic variation in ecophysiological traits of black cottonwood (Populus trichocarpa). Botany 85: 1202-1213.

Hansen J, Ruedy R, Sato M, Lo K (2010) Global surface temperature change. Rev Geoophys 48: RGR4004.

Heberling JM, Fridley JD (2013) Resource-use strategies of native and invasive plants in Eastern North American forests. New Phytol 200: 523-533.

Heskel MA, O'Sullivan, Reich PB, Tjoelker MG, Weerasinghe LK, Penilland A, Egerton JJG, Creek D, Bloomfield KJ, Xiang J, Sinca F, Stagl ZR, Martinez-de la Torre M, Griffin KL, Huntingford C, Hurry V, Meir P, Turnbill MH, Atkin OK (2016) Convergence in the temperature response of leaf respiration across biomes and plant functional types P Natl Acad Sci USA 3832-3837.

Hikosaka K (1997) Modelling optimal temperature acclimation of the photosynthetic apparatus in C 3 plants with respect to nitrogen use. Ann Bot - London 80: 721-730.

Hikosaka K, Ishikawa K, Borjigidai A, Muller O, Onoda Y (2005) Temperature acclimation of photosynthesis: mechanisms involved in the changes in temperature dependence of photosynthetic rate. J Exp Bot 57: 291-302.

Hogan JA, Baraloto C, Ficken CD, Clark MD, Weston DM, Warren JM (2020) Physiological Responses of *Populus trichocarpa* to Warming. Oak Ridge

National Laboratory, TES SFA, U.S. Department of Energy, Oak Ridge, Tennessee, U.S.A. doi:10.25581/ornlsfa.018/1617459.

IPCC (2014) Climate change 2014 Synthesis Report-Summary for Policymakers. Intergovernmental Panel on Climate Change (IPCC), [Core Writing Team, R.K. Pachauri and L.A. Meyer (eds.)]. IPCC, Geneva, Switzerland, 151 pp.

Jawrell WM, Bevely RB (1981) The dilution effect in plant nutrition studies. In: Brandy NC, vol 34, Advances in Agronronomy. pp.197-224.

Jarvi, M.P. & Burton, A.J. (2013) Acclimation and soil moisture constrain sugar maple root respiration in experimentally warmed soil. Tree Physiol, 33, 949-959.

Jarvi, M.P. & Burton, A.J. (2018) Adenylate control contributes to thermal acclimation of sugar maple fine-root respiration in experimentally warmed soil. Plant, Cell Enviro, 41, 504-51

Jump AS, Peñuelas J (2005) Running to stand still: adaptation and the response of plants to rapid climate change. Ecol Lett 8: 1010-1020.

Kalluri UC, Yang X, Wullschleger SD (2020) Plant Biosystems Design for a Carbon-Neutral Bioeconomy. Biodes Res 2020: 7914051.

King AW, Gunderson CA, Post WM, Weston DJ, Wullschleger SD (2006) Plant respiration in a warmer world. Science 312: 536-537.

Kumarathunge DP, Medlyn BE, Drake JE, Tjoelker MG, Aspinwall MJ, Battaglia M, Cano FJ, Carter KR, Cavaleri MA, Cernusak LA (2019) Acclimation and adaptation components of the temperature dependence of plant photosynthesis at the global scale. New Phytol 222: 768-784.

Kutsokon N, Jose S, Holzmueller E (2015) A Global Analysis of Temperature Effects on Populus Plantation Production Potential. Am J Plant Sci 6: 23-33.

Kuznetsova A, Brockhoff PR, Christensen RHB (2017) LmerTest Package: Tests in Linear Mixed Effects Models. J Stat Sofw 82,13: 1-26.

Lambers H, Atkin OK, Millenaar FF (1996) Respiratory patterns in roots in relation to their functioning. In: Eschel A, Waisel Y (eds.) Plant roots: The hidden half 3: pp. 521-552.

Larson PR, Isebrands J (1971) The plastochron index as applied to developmental studies of cottonwood. Can J Forest Res 1: 1-11.

Li J, Pendall E, Dijkstra FA, Nie M (2020) Root effects on the temperature sensitivity of soil respiration depend on climatic condition and ecosystem type. Soil Tillage Res 199: 104574.

Lombardozzi DL, Bonan GB, Smith NG, Dukes JS, Fisher RA (2015) Temperature acclimation of photosynthesis and respiration: A key uncertainty in the carbon cycle-climate feedback. Geophys Res Lett 42: 8624-8631.

Luo Y (2007) Terrestrial carbon–cycle feedback to climate warming. Annu Rev Ecol Evol Syst 38: 683-712.

Marshall B, Biscoe P (1980) A model for C3 leaves describing the dependence of net photosynthesis on irradiance. J Exp Bot 31: 29-39.

Mathias JM, Thomas RB (2021) Global tree water use efficiency is enhanced by increased atmospheric CO_2 and modulated by climate and plant functional types. P Natl Acad Sci USA 118:e2014286118.

McDowell NG, Allen CD, Anderson-Teixeira K, Aukema BH, Bond-Lamberty B, Chini L, Clark JS, Dietze M, Grossiord C, Hanbury-Brown A, Hurtt GC, Jackson RB, Johnson DJ, Kueppers L, Lichstein JW, Ogle K, Poulter B, Pugh TAM, Seidl R, Turner MG, Uriarte M, Walker AP, Xu C (2020) Pervasive shifts in forest dynamics in a changing world. Science 368: eaaz9463.

McMahon SM, Parker GG, Miller DR (2010) Evidence for a recent increase in forest growth. P Natl Acad Sci USA 107: 3611-3615.

Melillo, J.M., Butler, S., Johnson, J., Mohan, J., Steudler, P., Lux, H. et al. (2011) Soil warming, carbon-nitrogen interactions, and forest carbon budgets. P Natl Acad Sci USA, 108, 9508–9512.

Monleon VJ, Lintz HE (2015) Evidence of Tree Species' Range Shifts in a Complex Landscape. PloS One 10: e0118069.

Moore CE, Meacham-Hensold K, Lemonnier P, Slattery RA, Benjamin C, Bernacchi CJ, Lawson T, Cavanagh AP (2021) The effect of increasing temperature on crop photosynthesis from enzymes to ecosystems. J Exp Bot: earab090.

Noh NJ, Kristine C, Jinquan L, Zineb C, Craig B, Stefan A, Peter R, Mark T, Elise P (2020) Does root respiration in Australian rainforest tree seedlings acclimate to experimental warming? Tree Physiol 40:1192-1204.

Palta JA, Nobel PS (1989) Root respiration for Agave deserti: influence of temperature, water status and root age on daily patterns. J Exp Bot 40: 181-186.

Peñuelas J, Canadell JG, Ogaya R (2011) Increased water-use efficiency during the 20th century did not translate into enhanced tree growth. Global Ecol Biogeogr 20: 597-608.

Pregitzer KS, King JS, Burton AJ, Brown SE (2000) Responses of tree fine roots to temperature. New Phytol 147: 105-115.

Pregitzer KS, Laskowski MJ, Burton AJ, Lessard VC, Zak DR (1998) Variation in sugar maple root respiration with root diameter and soil depth. Tree Physiol 18: 665-670.

R Core Team (2019) R: a language and environment for statistical computing. R Foundation for statistical computing, Vienna, Austria.

Reich PB, Walters M, Tjoelker M, Vanderklein D, Buschena C (1998) Photosynthesis and respiration rates depend on leaf and root morphology and nitrogen concentration in nine boreal tree species differing in relative growth rate. Funct Ecol 12: 395-405.

Reich PB, Tjoelker MG, Pregitzer KS, Wright IJ, Oleksyn J, Machado JL (2008) Scaling of respiration to nitrogen in leaves, stems and roots of higher land plants. Ecol Lett 11: 793-801.

Rogers A, Kumarathunge DP, Lombardozzi DL, Medlyn BD, Serbin SP, Walker AP. Triose phosphate utilization limitation: an unnecessary complexity in terrestial biosphere model representation of photosynthesis. New Pytol 230:17-22.

Roumet C, Birouste M, Picon-Cochard C, Ghestem M, Osman N, Vrignon-Brenas S, Cao K-F, Stokes A (2016) Root structure-function relationships in 74 species: evidence of a root economics spectrum related to carbon economy. New Phytol 210: 815-826.

Sage RF, Kubien DS (2007) The temperature response of C3 and C4 photosynthesis. Plant Cell Environ 30: 1086-1106.

Scafaro AP, Xiang S, Long BM, Bahar NHA, Weerasinghe LK, Creek D, Evans JR, Reich PB, Atkin OK (2017) Strong thermal acclimation of photosynthesis in tropical and temperate wet-forest tree species: the importance of altered Rubisco content. Glob Change Biol 23: 2783-2800.

Sharkey TD (2019) Is triose phosphate utilization important for understanding photosynthesis? J Exp Bot 70: 5521-5525.

Silim SN, Ryan N, Kubien DS (2010) Temperature responses of photosynthesis and respiration in *Populus balsamifera* L.: acclimation versus adaptation. Photosyn Res 104: 19-30.

Slot M, Kitajima K (2015) General patterns of acclimation of leaf respiration to elevated temperatures across biomes and plant types. Oecologia 177(3): 885-900.

Slot M, Winter K (2016) The effects of rising temperature on the ecophysiology of tropical forest trees. In: Santiago LS, Goldstein G (eds.) Tropical Tree Physiology. Springer, pp 385-412.

Smith NG, Dukes JS (2013) Plant respiration and photosynthesis in global-scale models: incorporating acclimation to temperature and CO_2. Glob Change Biol 19: 45-63.

Smith NG, Li G, Dukes JS (2019) Short-term thermal acclimation of dark respiration is greater in non-photosynthetic than in photosynthetic tissues. AoB Plants 11: plz064.

Smith NG, McNellis R, Dukes JS (2020) No acclimation: instantaneous responses to temperature maintain homeostatic photosynthetic rates under experimental warming across a precipitation gradient in Ulmus americana. AoB Plants 12: plaa017.

Song Y, Chen Q, Ci D, Shao X, Zhang D (2014) Effects of high temperature on photosynthesis and related gene expression in poplar. BMC Plant Biol 14: 111-111.

Stinziano JR, Morgan PB, Lynch DJ, Saathoff AJ, McDermitt DK, Hanson DT (2017) The rapid A–Ci response: photosynthesis in the phenomic era. Plant Cell Environ 40: 1256-1262.

Théroux Rancourt G, Éthier G, Pepin S (2015) Greater efficiency of water use in poplar clones having a delayed response of mesophyll conductance to drought. Tree Physiol 35: 172-184.

Urban J, Ingwers M, McGuire MA, Teskey RO (2017) Stomatal conductance increases with rising temperature. Plant Signal Behav 12: e1356534.

van der Werf A, Kooijman A, Welschen R, Lambers H (1988) Respiratory energy costs for the maintenance of biomass, for growth and for ion uptake in roots of Carex diandra and Carex acutiformis. Physiol Plantarum 72: 483-491.

Von Caemmerer S (2000) Biochemical models of leaf photosynthesis. Csiro Publishing, Victoria, Australia.

Walther G-R (2003) Plants in a warmer world. Perspect Plant Ecol 6: 169-185.

Wang J, Dufrenne C, McCormack ML, Yang L, Tian D, Luo Y, Huo E, Yan T, Li Z, Bu W, Chen Y, Niu S (2021) Fine-root functional trait response to experimental warming: a global meta-analysis. New Phytol doi:10.111/nph.17279.

Way DA, Yamori W (2014) Thermal acclimation of photosynthesis: on the importance of adjusting our definitions and accounting for thermal acclimation of respiration. Photosyn Res 119: 89-100.

Weston DJ, Bauerle WL (2007) Inhibition and acclimation of C3 photosynthesis to moderate heat: a perspective from thermally contrasting genotypes of Acer rubrum (red maple). Tree Physiol 27: 1083-1092.

Weston DJ, Karve AA, Gunter LE, Jawdy SS, Yang X, Allen SM, Wullschleger SD (2011) Comparative physiology and transcriptional networks underlying the heat shock response in Populus trichocarpa, Arabidopsis thaliana and Glycine max. Plant Cell Environ 34: 1488-1506.

Wullschleger SD, Jansson S, Taylor G (2002) Genomics and forest biology: Populus emerges as the perennial favorite. Plant Cell 14: 2651-2655.

Yamasaki T, Yamakawa T, Yamane Y, Koike H, Satoh K, Katoh S (2002) Temperature Acclimation of Photosynthesis and Related Changes in Photosystem II Electron Transport in Winter Wheat. Plant Physiol 128: 1087-1097.

Yamori W, Hikosaka K, Way DA (2014) Temperature response of photosynthesis in C 3, C 4, and CAM plants: temperature acclimation and temperature adaptation. Photosynth Res 119: 101-117.

Yamori W, Suzuki K, Noguchi K, Nakai M, Terashima I (2006) Effects of Rubisco kinetics and Rubisco activation state on the temperature dependence of the photosynthetic rate in spinach leaves from contrasting growth temperatures. Plant Cell Environ 29: 1659-1670.

Zhang H, Morison JI, Simmonds LP (1999) Transpiration and water relations of poplar trees growing close to the water table. Tree Physiol 19: 563-573.

Appendix S2: poplarPhys_StatsCheck.html. Literate statistical output showing all statistical analyses done in this paper. See: http://rpubs.com/hogieskier/PoplarPhys_StatsCheck.

CONCLUDING REMARKS

The present dissertation examines three aspects of tree root functional ecology – root morphological and tissue elemental variation, root-inhabiting fungal communities, and root metabolic function (i.e., respiration) in relation to the environment. The role of the environment is key to inferring plant physiological function and its consequences (performance, fitness) i*n situ*. A comparative approach is taken throughout, sometimes manipulating experimental variables, examining root morphology, fungal relationships, and physiology across soil gradients. Here, I briefly summarize the findings for each section and chapter, discussing implications, and then I make a few recommendations for future studies of similar interest.

PART 1: morphological variation within and among species in relation to the environment

CHAPTER 1: Morphological variation of fine root systems and leaves in primary and secondary tropical forest of Hainan Island, China

Chapter one demonstrates how root systems vary in morphology with the soil environment. I compared variation in tree root morphology within and among taxa using a 6.6-km transect that spanned a secondary, historically-logged tropical forest area to a primary tropical forest area with no logging history. Data were analyzed by forest type (primary and secondary) to help generalize the findings to other tropical forests and with respect to soil nutrient content (collected from where root systems were excavated) to identify drivers of root morphological difference. Root systems in the primary forest showed slightly greater average diameter (0.4 mm) than root systems in the secondary forest; however, root systems in the secondary forest had greater specific root length (0.35 m g^{-1}) and branching intensity (0.3 more tips cm^{-1}). These subtle shifts in root morphology were consistent within species and illustrate a tradeoff in plant carbon investment in root form, with increases in root diameter coming at the expense of topological complexity and vice versa (Fitter 1991, Kong et al. 2014, Kramer-Walter et al. 2016, Weemstra et al. 2016, Guerrero-Ramírez et al. 2021).

Additionally, understanding changes in root morphology within and among species concerning soil nutrients showed that soil phosphorus (P) and soil base saturation were important drivers, with soil P affecting root morphologies more in primary than secondary forest. Soil P is the limiting nutrient in tropical forest ecosystems (Vitousek and Sanford Jr 1986, Turner et al. 2018), which strongly controls root biomass production (Huaraca Huasco et al. 2021) and affects root system SRL (Addo-Danso et al. 2019). Soil P is insoluble, being bound within soils, based on soil pH and the oxidation states of many soil elements. Thus the saturation of available bases in soils (BS) and the availability of soil P interact to determine the amount available to plant roots. Tropical tree roots show some plasticity in being able to respond to these changes morphologically. There are likely biological differences in root functioning rhizosphere-effects that accompany morphological adjustment (e.g., root enzyme activity, bacterial and fungal association) (Lugli et al. 2020, Cabugao et al. 2021), which could be the focus of future work. Lastly, the gradient studied in this chapter is not a steep environmental gradient, and although I found consistent trends among lineages, there may be potential for generalist tropical species to have more varied root morphology than was found here.

CHAPTER 2: Intraspecific trait variation and species functional turnover in successional tropical forests: assessing gap filling for community-weighted means

Quantifying the sources and amount of intraspecific trait variation (ITV) in plants represents an essential theme in ecology that can help infer community assembly mechanisms along environmental gradients (McGill et al. 2006, Paine et al. 2011, Baraloto et al. 2012, Shipley et al. 2016). The second chapter leverages data from an existing network of small (0.0625-ha) forest inventory plots located within the same forest landscape as the 6.6-km transect (Xu et al. 2015a, Xu et al. 2015b). I sought to extend the findings on ITV in roots (and leaves, not discussed above) from chapter one. Measuring ITV in highly diverse tropical tree communities is incredibly laborious and time-consuming, if not impossible (Baraloto et al. 2010). To be done perfectly, it requires measuring numerous traits for all individuals within forest inventory plots. For example, the dataset used in chapter two contains over 65,000 individual trees of 582

species spread out across a 47,000-ha forest reserve, with many of the plots located in remote, hard-to-reach reach areas. Chapter one yielded estimates of ITV in root and leaf traits for 72 of those species from 423 trees. I matched estimates of ITV by forest type (primary vs. secondary) to the land-use history of the forest plots, decomposing the sources of ITV for the assemblage of 72 species for which I directly measured traits. I found that for six of seven traits (including all three root traits – specific root length, root tissue density and root branching intensity), trait variation negatively co-varied with species turnover between primary and secondary forest plots. The negative co-variation created more significant differences in community-weighted mean (CWM) trait values than if ITV by forest type were not accounted for. This is one of the first studies to estimate CWM trait values for root traits in tropical forests (however, see Caplan et al. (2019) for a similar study in a temperate forest).

The trait measurement approach was designed to measure species traits from 15 plant families across the breadth of the Angiosperm phylogeny. I examined the robustness of the trend of negative co-variation of ITV with species turnover to missing taxa (i.e., the assemblage of 72 species vs. the whole community) using phylogenetic trait imputation. Analyses using phylogenetic trait imputation revealed consistent patterns. Thus, ITV between secondary and primary tropical forest type (as described in chapter 1), resulting from slightly more fertile soils in secondary forest and slightly more acidic and coarser soils in primary forest, is one crucial trait variation. Structuring trait sampling campaigns to target a range of taxonomic and functional groups across *a priori* habitat classifications followed by phylogenetic trait imputation is one way to sample traits in species-rich tropical forests, which reconciles designs that only sample traits among or within species.

CHAPTER 3: Evidence of elemental homeostasis in fine root and leaf tissue of saplings across a fertility gradient in tropical montane forest in Hainan, China

Utilizing the same tropical forest gradient studied in chapters one and two, I asked how root and leaf tissue elemental concentrations and stoichiometry vary with the soil environment. I tested the idea that tropical tree roots act as biological filters for soil nutrients, preferentially acquiring elements that are of chief physiological importance to

leaf and whole-plant physiological function (e.g., nitrogen (N), magnesium, P), while excluding uptake of elements that can be potentially toxic if acquired within plants at high concentrations (e.g., aluminum, copper, and other metals). I evaluated this idea with respect to soil fertility along the gradient and among plant families. Stoichiometrically, both root and leaf tissues were phosphorus-poor, confirming soil P limitation compared to global averages. Slight increases in seven of fourteen elements were observed as soil N, P or BS increased. Increases were most significant for P and manganese but still evident for N, potassium, sodium, and boron. Plants tissue carbon and elemental metal contents were invariable to variation in soil N, P, or BS.

Comparing root and leaf tissue concentrations showed the concentrations of these elements (i.e., metals and other elements lacking clear physiological function within plants) were higher in root than leaf tissues. The inverse relationships between concentrations of leaf and root tissues provided support for the hypothesis that roots preferentially uptake some essential nutrients over others (Aerts and Chapin III 1999, Marschner 2012) and work inversely to coordinate tissue elemental concentrations. Evaluating these trends regarding tree species and family explained additional variance in modeled relationships of leaf and root tissue nutrient responses in relation to the soil environment; this taxonomic effect varied depending on the element. These findings illustrate that tropical trees display a wide range of tolerance to soil environments, varying in their stoichiometry, but work to maintain elemental homeostasis - or similar tissue nutrient concentrations despite variability in the soil environment. Further research might investigate the mechanisms tropical trees employ to achieve this (i.e., the role of nutrient re-translocation or root exudation) and biological symbionts (e.g., fungi or rhizosphere bacteria) play in tree elemental homeostasis.

PART 2: the biotic dimension: root-fungal community interactions with environment

CHAPTER 4: Root-associated fungal communities are structured more by environment than plant-host functional traits in a Chinese tropical forest

When considering root systems, their association with their fungal symbionts cannot be overlooked. Fungi represent a vital axis of variation in root functional strategy

through the transfer of water and nutrients to host plants in exchange for carbon with host plants. Exchange occurs through various physical interactions and mechanisms and to varying degrees (Bonfante and Genre 2010, Kariman et al. 2018). From a root functional strategy perspective, the interaction of roots systems with fungi has been described as 'nutrient acquisition outsourcing' (Bergmann et al. 2020). Although displaying the opposite pattern to the latitudinal gradient in plant species richness (Větrovský et al. 2019), the high diversity of tropical trees potentially leads to novel and complex interactions between root-associated fungi tree-hosts and the environment.

Chapter four examines the relative roles to which the soil and root system environments structure root-inhabiting fungal community dissimilarity in three tropical forest plots of varying successional status in Xishuangbanna, China. Constrained ordination showed that the soil environment, principally differences in soil P, acts as a first-order filter for root-associated fungal community composition. Root system architecture and chemistry play a secondary role, with a structural tradeoff between dense, highly-branched root systems that cater to ectomycorrhiza, and less-dense, herringbone topologies that are adapted to arbuscular mycorrhizal (AM) associations (Berntson 1997, Guo et al. 2008, Eissenstat et al. 2015). Root calcium was necessary for explaining the difference in root fungal community dissimilarity, potentially because of the role of calcium spiking in root tissues concerning AM symbiosis (Bonfante and Genre 2010). Thus, in tropical forests, root-associated fungi are environmentally sorted first by soil type, then by root form according to tree host preferences. Relationships affect root functioning within the environment through control on functional strategy (i.e., the do-it-yourself vs. outsourcing dimension of nutrient acquisition) (Bergmann et al. 2020) and expression of root functional traits.

PART 3: root respiration – the physiological dimension of tree fine-root functional strategies

CHAPTER 5: Functional variability in specific root respiration translates to slight differences in belowground CO_2 efflux in a temperature deciduous forest in Oak Ridge, Tennessee

Root respiration represents a key endpoint of plant carbon metabolism through structural carbon allocation to root production and liable carbon release to the soil rhizosphere (Noguchi 2005, Roumet et al. 2016). It, therefore, reflects the sum of root metabolic activity (i.e., enzyme activity, active nutrient uptake) and is a crucial dimension of root functional strategy (Gao et al. 2021, Han and Zhu 2021). Root respiration rates of root systems, alone, typically relate strongly to root nitrogen content and specific root length and inversely to root tissue density(Burton et al. 2002, Reich et al. 2008, Paradiso et al. 2019). However, it is less well known how functional variation in root respiration (or other aspects of root-soil carbon interactions) affects magnitudes of root respiration (Freschet et al. 2021), as separating root respiration from heterotrophic soil respiration is difficult (Hanson et al. 2000).

I developed a novel methodology that allows repeated respiration measurements of tree root systems and their surrounding soil *in situ*. This method was tested in a temperate hardwood forest in Tennessee using root systems of eight species growing in three different forest types. Temperate forest trees were used *instead* of tropical trees because of travel constraints and funding. First, measurements were taken on the tree species' entire fine root systems, which confirmed that root respiration is positively related to root nitrogen content and specific root length and negatively related to root tissue density. Then, these data were used in conjunction with a modeled, generalized root respiration response to temperature to estimate the fraction of root respiration to soil respiration at the root system level (accounting for the difference in the root system and soil mass among the *in-situ* root respiration trays). The main finding concerning root functional strategy is that larger diameter, lower wood density, and lower specific root length root systems contributed to greater percentages of root to soil respiration. Thus, root functional differences can affect soil respiration rates and therefore have consequences for ecosystem responses, for example, ecosystem carbon balance or the temperature sensitivity of belowground respiration (Epron et al. 1999, Freschet et al. 2020). Although the effects were minor at the individual root system level, they are potentially consequential for soil and ecosystem carbon balance when considering the amount of biomass present in the topsoil of temperature forests, which is substantial.

CHAPTER 6: The physiological acclimation and growth response of Populus trichocarpa *to warming*

The climate of the Earth is rapidly warming, which is affecting plant physiology, including forest net primary productivity and biomass yields from timber plantations (Saxe et al. 2001). Understanding the physiological limits and the environmental controls on the physiological acclimation to warming of timber trees is necessary to understand and mitigate the adverse effects of warming on timber plantation trees (Keenan 2015). Additionally, the degree to which aboveground (i.e., leaf) vs. belowground (i.e., root) metabolic processes acclimate to warming and interact could have potential consequences for plat carbon balance (Atkin et al. 2000, Atkin et al. 2005).

In chapter six, I conducted a highly-controlled experiment that increased the growing temperature for small *Populus trichocarpa* clones (Nisqually-1 genotype) using growth chambers. The warming experiment was initially envisioned to use *Tectona grandis* (Teak, a tropical timber species); however, difficulties were encountered germinating and growing Teak. Therefore, I used poplar, a famous timber plantation tree, and a model tree species, being the first tree to have its complete genome sequenced (Tuskan et al. 2006). I measured carbon uptake (i.e., photosynthesis) rates in the leaves and rates of carbon loss (i.e., respiration) from leaves, roots, and soil. I found that photosynthetic rates acclimated at monthly time scales and that warming increased leaf, root, and soil respiration rates. Plant biomass was over half a gram per day greater at intermediate warming (+4°C) than for unwarmed or severely warmed (+8°C) trees, with 30% of structural carbon allocated to root production. Plant nitrogen status mediated physiological acclimation responses, especially in roots in the warmest (+8°C) treatment, suggesting that plant-soil interactions vary with temperature and play a key role in the ability of trees to acclimate to warming (Pugnaire et al. 2019). These results demonstrate that poplar can acclimate to moderate warming alone, increasing biomass yields at warming of +4°C, but that biomass gains diminish with further warming, which is consistent with other temperature studies with poplar (Cerasoli et al. 2014).

Synthesis

This dissertation demonstrates three main themes by integrating root functional morphologies with environmental effects shaping soil and rhizosphere biodiversity and ecosystem functioning. First, root functional morphologies are evolutionarily constrained among taxa, having been selected (i.e., optimized) to meet the varying belowground requirements among taxa(Valverde-Barrantes et al. 2017, Ma et al. 2018, Liu et al. 2019). The range of evolutionarily-constrained root morphologies has been dictated by the few to several strategies by which trees have managed to do this (Maherali 2017, Lu and Hedin 2019, Bergmann et al. 2020). Constraints on the morphological and architectural form of roots systems are paramount with slight adjustments occurring with soil environmental conditions (Chapters 1, 4).

Secondly, additional flexibility in root functional strategy of trees about the environment must occur either at the plant and root system scale through a biological change in root physiology or via changes in the biotic dimension of root functioning (i.e., interactions with bacterial and fungi in the rhizosphere) (Hodge et al. 2009). Moreover, the interaction between changes in root biology and the subsequent feedback to changes in the biotic dimension of root functioning (and vice versa) are intricately interlinked and have a stochastic element (Bardgett et al. 2014, Laliberté 2017). For example, in chapter six, soil and root respiration tracked leaf carbon uptake, but root respiration acclimation to temperature was nitrogen-limited, presumably because of temperature-driven changes in soil microbial metabolism. On the other hand, in chapter 5, we treated soil with a low-level algaecide, bactericide, which slightly changed bacterial community composition, but significantly reduced bacterial abundances. The increased bacterial necromass led to an increase in soil fungi and a slight increase in soil respiration, but little change in the contribution of root respiration to total soil respiration.

Lastly, the soil environment is a superior first-order control on both the abiotic dimension of tree root functional strategies (i.e., root morphology and its variability) and the biotic interactions between root and the soil rhizosphere microbiome. Soil habitats, both filter tree and microorganismal species with positive and negative density dependent effects, dispersal limitation, and niche partitioning play a role in structuring their interaction (Chen et al. 2019, van Breugel et al. 2019). Habitat filtering and niche

partitioning leads to specialized interactions between palnts and fungi with feedbacks between root morphology, the microbiome to affect function within the environment.

Recommendation & future work

For those interested in trait-based ecology, especially belowground, I encourage you to pursue your interests. The links between root form and physiology are only beginning to be explored, especially in an environmental context for wild plants. Future work could explore many dimensions, including measuring rates for nutrient and water uptake vary with root functional strategy and with or without mycorrhizal colonization, linking root respiration to non-structural root carbon dynamics (e.g., exudation, mycorrhizal demand, or soil priming effects), and many others. An important consideration is making comparable measurements across samples and time. Therefore, I advocate for working at the whole root system level (as described by McCormack et al. (2015). This limits study to the physiologically active portion of the root system, with diameters <2 mm.

Additionally, decomposing root-system-based measurements by root order can help standardize approaches and reveal meaningful functional differences among or within species. For example, a recent study showed how the bacterial composition of fine root tips varies substantially with root order, with the finest first-order root tips being distinct from the rest of the root system (King et al. 2021). A second consideration is to make careful observations. Much can be seen with the naked eye or a low-magnification stereoscope or hand lens. Such observations help inform hypotheses and create real-world, experiential linkages to the literature that can then be explored using more powerful scientific techniques, given the proper instrumentation (e.g., physiological measurements or sequencing work). Third, archive your data and contribute to large-scale open-science data initiatives, such as the Fine Root Ecological Database (FRED) (Iversen et al. 2017). Making data usable in broad global contexts will facilitate future discoveries in the field of root functional ecology. Lastly, do not be afraid to get dirty and dig roots! You may be amazed at what you will find.

References

Addo-Danso, S. D., C. E. Defrenne, M. L. McCormack, I. Ostonen, A. Addo-Danso, E. G. Foli, K. A. Borden, M. E. Isaac, and C. E. Prescott. 2020. Fine-root morphological trait variation in tropical forest ecosystems: an evidence synthesis. Plant Ecology 221:1-13

Aerts, R., and F. S. Chapin III. 1999. The mineral nutrition of wild plants revisited: a re-evaluation of processes and patterns. Pages 1-67 Advances in Ecological Research. Elsevier.

Atkin, O. K., D. Bruhn, and M. G. Tjoelker. 2005. Response of plant respiration to changes in temperature: mechanisms and consequences of variations in Q_{10} values and acclimation. Pages 95-135 Plant Respiration. Springer.

Atkin, O. K., E. J. Edwards, and B. R. Loveys. 2000. Response of root respiration to changes in temperature and its relevance to global warming. New Phytologist **147**:141-154.

Baraloto, C., O. J. Hardy, C. T. Paine, K. G. Dexter, C. Cruaud, L. T. Dunning, M. A. Gonzalez, J. F. Molino, D. Sabatier, and V. Savolainen. 2012. Using functional traits and phylogenetic trees to examine the assembly of tropical tree communities. Journal of Ecology **100**:690-701.

Baraloto, C., C. Timothy Paine, S. Patino, D. Bonal, B. Hérault, and J. Chave. 2010. Functional trait variation and sampling strategies in species-rich plant communities. Functional Ecology **24**:208-216.

Bardgett, R. D., L. Mommer, and F. T. De Vries. 2014. Going underground: root traits as drivers of ecosystem processes. Trends in Ecology & Evolution **29**:692-699.

Bergmann, J., A. Weigelt, F. van der Plas, D. C. Laughlin, T. W. Kuyper, N. Guerrero-Ramirez, O. J. Valverde-Barrantes, H. Bruelheide, G. T. Freschet, C. M. Iversen, J. Kattge, M. L. McCormack, I. C. Meier, M. C. Rillig, C. Roumet, M. Semchenko, C. J. Sweeney, J. van Ruijven, L. M. York, and L. Mommer. 2020. The fungal collaboration gradient dominates the root economics space in plants. Science Advances **6**:eaba3756.

Berntson, G. M. 1997. Topological scaling and plant root system architecture: developmental and functional hierarchies. The New Phytologist **135**:621-634.

Bonfante, P., and A. Genre. 2010. Mechanisms underlying beneficial plant–fungus interactions in mycorrhizal symbiosis. Nature Communications **1**:48.

Burton, A., K. Pregitzer, R. Ruess, R. Hendrick, and M. Allen. 2002. Root respiration in North American forests: effects of nitrogen concentration and temperature across biomes. Oecologia **131**:559-568.

Cabugao, K. G., D. Yaffar, N. Stenson, J. Childs, J. Phillips, M. A. Mayes, X. Yang, D. J. Weston, and R. J. Norby. 2021. Bringing function to structure: Root–soil interactions shaping phosphatase activity throughout a soil profile in Puerto Rico. Ecology and Evolution **11**:1150-1164.

Caplan, J. S., S. J. Meiners, H. Flores-Moreno, and M. L. McCormack. 2019. Fine-root traits are linked to species dynamics in a successional plant community. Ecology **100**:e02588.

Cerasoli, S., T. Wertin, M. A. McGuire, A. Rodrigues, D. P. Aubrey, J. S. Pereira, and R. O. Teskey. 2014. Poplar saplings exposed to recurring temperature shifts of different amplitude exhibit differences in leaf gas exchange and growth despite equal mean temperature. AoB PLANTS **6**.

Chen, L., N. G. Swenson, N. Ji, X. Mi, H. Ren, L. Guo, and K. Ma. 2019. Differential soil fungus accumulation and density dependence of trees in a subtropical forest. Science **366**:124-128.

Eissenstat, D. M., J. M. Kucharski, M. Zadworny, T. S. Adams, and R. T. Koide. 2015. Linking root traits to nutrient foraging in arbuscular mycorrhizal trees in a temperate forest. New Phytologist **208**:114-124.

Epron, D., L. Farque, E. Lucot, and P.-M. Badot. 1999. Soil CO2 efflux in a beech forest: the contribution of root respiration. Annals of Forest Science **56**:289-295.

Fitter, A. 1991. Characteristics and functions of root systems. Plant roots: the hidden half **2**:1-29.

Freschet, G. T., C. Roumet, L. H. Comas, M. Weemstra, A. G. Bengough, B. Rewald, R. D. Bardgett, G. B. De Deyn, D. Johnson, J. Klimešová, M. Lukac, M. L. McCormack, I. C. Meier, L. Pagès, H. Poorter, I. Prieto, N. Wurzburger, M. Zadworny, A. Bagniewska-Zadworna, E. B. Blancaflor, I. Brunner, A. Gessler, S. E. Hobbie, C. M. Iversen, L. Mommer, C. Picon-Cochard, J. A. Postma, L. Rose, P. Ryser, M. Scherer-Lorenzen, N. A. Soudzilovskaia, T. Sun, O. J. Valverde-Barrantes, A. Weigelt, L. M. York, and A. Stokes. 2021. Root traits as drivers of plant and ecosystem functioning: current understanding, pitfalls and future research needs. New Phytologist doi: 10.1111/nph.17072.

Gao, J., M. Zhou, J. Shao, G. Zhou, R. Liu, L. Zhou, H. Liu, Y. He, Y. Chen, and X. Zhou. 2021. Fine root trait-function relationships affected by mycorrhizal type and climate. Geoderma **394**:115011.

Guerrero-Ramírez, N. R., L. Mommer, G. T. Freschet, C. M. Iversen, M. L. McCormack, J. Kattge, H. Poorter, F. van der Plas, J. Bergmann, T. W. Kuyper, L. M. York, H. Bruelheide, D. C. Laughlin, I. C. Meier, C. Roumet, M. Semchenko, C. J. Sweeney, J. van Ruijven, O. J. Valverde-Barrantes, I. Aubin, J. A. Catford, P. Manning, A. Martin, R. Milla, V. Minden, J. G. Pausas, S. W. Smith, N. A. Soudzilovskaia, C. Ammer, B. Butterfield, J. Craine, J. H. C. Cornelissen, F. T. de Vries, M. E. Isaac, K. Kramer, C. König, E. G. Lamb, V. G. Onipchenko, J. Peñuelas, P. B. Reich, M. C. Rillig, L. Sack, B. Shipley, L. Tedersoo, F. Valladares, P. van Bodegom, P. Weigelt, J. P. Wright, and A. Weigelt. 2021. Global root traits (GRooT) database. Global Ecology and Biogeography **30**:25-37.

Guo, D., M. Xia, X. Wei, W. Chang, Y. Liu, and Z. Wang. 2008. Anatomical traits associated with absorption and mycorrhizal colonization are linked to root branch order in twenty-three Chinese temperate tree species. New Phytologist **180**:673-683.

Han, M., and B. Zhu. 2021. Linking root respiration to chemistry and morphology across species. Global Change Biology **27**:190-201.

Hanson, P. J., N. T. Edwards, C. T. Garten, and J. A. Andrews. 2000. Separating root and soil microbial contributions to soil respiration: A review of methods and observations. Biogeochemistry **48**:115-146.

Hodge, A., G. Berta, C. Doussan, F. Merchan, and M. Crespi. 2009. Plant root growth, architecture and function. Plant and Soil **321**:153-187.

Huaraca Huasco, W., T. Riutta, C. A. J. Girardin, F. Hancco Pacha, B. L. Puma Vilca, S. Moore, S. W. Rifai, J. del Aguila-Pasquel, A. Araujo Murakami, R. Freitag, A. C. Morel, S. Demissie, C. E. Doughty, I. Oliveras, D. F. Galiano Cabrera, L. Durand Baca, F. Farfán Amézquita, J. E. Silva Espejo, A. C. L. da Costa, E. Oblitas Mendoza, C. A. Quesada, F. Evouna Ondo, J. Edzang Ndong, K. J. Jeffery, V. Mihindou, L. J. T. White, N. N'ssi Bengone, F. Ibrahim, S. D. Addo-Danso, A. Duah-Gyamfi, G. Djaney Djagbletey, K. Owusu-Afriyie, L. Amissah, A. T. Mbou, T. R. Marthews, D. B. Metcalfe, L. E. O. Aragão, B. H. Marimon-Junior, B. S. Marimon, N. Majalap, S. Adu-Bredu, K. A. Abernethy, M. Silman, R. M. Ewers, P. Meir, and Y. Malhi. 2021. Fine root dynamics across pantropical rainforest ecosystems. Global Change Biology **27**:3657-3680.

Iversen, C. M., M. L. McCormack, A. S. Powell, C. B. Blackwood, G. T. Freschet, J. Kattge, C. Roumet, D. B. Stover, N. A. Soudzilovskaia, and O. J. Valverde-Barrantes. 2017. A global Fine-Root Ecology Database to address below-ground challenges in plant ecology. New Phytologist **215**:15-26.

Kariman, K., S. J. Barker, and M. Tibbett. 2018. Structural plasticity in root-fungal symbioses: diverse interactions lead to improved plant fitness. PeerJ **6**:e6030-e6030.

Keenan, R. J. 2015. Climate change impacts and adaptation in forest management: a review. Annals of Forest Science **72**:145-167.

King, W. L., C. F. Yates, J. Guo, S. M. Fleishman, R. V. Trexler, M. Centinari, T. H. Bell, and D. M. Eissenstat. 2021. The hierarchy of root branching order determines bacterial composition, microbial carrying capacity and microbial filtering. Communications Biology **4**:1-9.

Kong, D., C. Ma, Q. Zhang, L. Li, X. Chen, H. Zeng, and D. Guo. 2014. Leading dimensions in absorptive root trait variation across 96 subtropical forest species. New Phytologist **203**:863-872.

Kramer-Walter, K. R., P. J. Bellingham, T. R. Millar, R. D. Smissen, S. J. Richardson, and D. C. Laughlin. 2016. Root traits are multidimensional: specific root length is independent from root tissue density and the plant economic spectrum. Journal of Ecology **104**:1299-1310.

Laliberté, E. 2017. Below-ground frontiers in trait-based plant ecology. New Phytologist **213**:1597-1603.

Liu, C., W. Xiang, L. Zou, P. Lei, Y. Zeng, O. Shuai, X. Deng, X. Fang, Z. Liu, and C. Peng. 2019. Variation in the functional traits of fine roots is linked to phylogenetics in the common tree species of Chinese subtropical forests. Plant and Soil **436**:1-18.

Lu, M., and L. O. Hedin. 2019. Global plant–symbiont organization and emergence of biogeochemical cycles resolved by evolution-based trait modelling. Nature Ecology & Evolution **3**:239-250.

Lugli, L. F., K. M. Andersen, L. E. Aragão, A. L. Cordeiro, H. F. Cunha, L. Fuchslueger, P. Meir, L. M. Mercado, E. Oblitas, and C. A. Quesada. 2020. Multiple phosphorus acquisition strategies adopted by fine roots in low-fertility soils in Central Amazonia. Plant and Soil **450**:49-63.

Ma, Z., D. Guo, X. Xu, M. Lu, R. D. Bardgett, D. M. Eissenstat, M. L. McCormack, and L. O. Hedin. 2018. Evolutionary history resolves global organization of root functional traits. Nature **555**:94-97.

Maherali, H. 2017. The evolutionary ecology of roots. New Phytologist **215**:1295-1297.

Marschner, P. 2012. Marschner's Mineral Nutrition of Higher Plants. Third Edition edition. Academic Press, Waltham, MA.

McCormack, M. L., I. A. Dickie, D. M. Eissenstat, T. J. Fahey, C. W. Fernandez, D. Guo, H. S. Helmisaari, E. A. Hobbie, C. M. Iversen, and R. B. Jackson. 2015. Redefining fine roots improves understanding of below-ground contributions to terrestrial biosphere processes. New Phytologist **207**:505-518.

McGill, B. J., B. J. Enquist, E. Weiher, and M. Westoby. 2006. Rebuilding community ecology from functional traits. Trends in ecology & evolution **21**:178-185.

Noguchi, K. 2005. Effects of light intensity and carbohydrate status on leaf and root respiration. Pages 63-83 *in* H. Lambers, editor. Plant Respiration: From Cell to Ecosystem. Springer, Dordrecht, Nethterlands.

Paine, C. T., C. Baraloto, J. Chave, and B. Hérault. 2011. Functional traits of individual trees reveal ecological constraints on community assembly in tropical rain forests. Oikos **120**:720-727.

Paradiso, E., F. Jevon, and J. Matthes. 2019. Fine root respiration is more strongly correlated with root traits than tree species identity. Ecosphere **10**.

Pugnaire, F. I., J. A. Morillo, J. Peñuelas, P. B. Reich, R. D. Bardgett, A. Gaxiola, D. A. Wardle, and W. H. v. d. Putten. 2019. Climate change effects on plant-soil feedbacks and consequences for biodiversity and functioning of terrestrial ecosystems. Science Advances **5**:eaaz1834.

Reich, P. B., M. G. Tjoelker, K. S. Pregitzer, I. J. Wright, J. Oleksyn, and J. L. Machado. 2008. Scaling of respiration to nitrogen in leaves, stems and roots of higher land plants. Ecology letters **11**:793-801.

Roumet, C., M. Birouste, C. Picon-Cochard, M. Ghestem, N. Osman, S. Vrignon-Brenas, K. f. Cao, and A. Stokes. 2016. Root structure–function relationships in 74 species: evidence of a root economics spectrum related to carbon economy. New Phytologist **210**:815-826.

Saxe, H., M. G. R. Cannell, Ø. Johnsen, M. G. Ryan, and G. Vourlitis. 2001. Tree and forest functioning in response to global warming. New Phytologist **149**:369-399.

Shipley, B., F. De Bello, J. H. C. Cornelissen, E. Laliberté, D. C. Laughlin, and P. B. Reich. 2016. Reinforcing loose foundation stones in trait-based plant ecology. Oecologia **180**:923-931.

Turner, B. L., T. Brenes-Arguedas, and R. Condit. 2018. Pervasive phosphorus limitation of tree species but not communities in tropical forests. Nature **555**:367.

Tuskan, G. A., S. DiFazio, S. Jansson, J. Bohlmann, I. Grigoriev, U. Hellsten, N. Putnam, S. Ralph, S. Rombauts, A. Salamov, J. Schein, L. Sterck, A. Aerts, R. R. Bhalerao, R. P. Bhalerao, D. Blaudez, W. Boerjan, A. Brun, A. Brunner, V. Busov, M. Campbell, J. Carlson, M. Chalot, J. Chapman, G.-L. Chen, D. Cooper, P. M. Coutinho, J. Couturier, S. Covert, Q. Cronk, R. Cunningham, J. Davis, S. Degroeve, A. Déjardin, C. dePamphilis, J. Detter, B. Dirks, I. Dubchak, S. Duplessis, J. Ehlting, B. Ellis, K. Gendler, D. Goodstein, M. Gribskov, J. Grimwood, A. Groover, L. Gunter, B. Hamberger, B. Heinze, Y. Helariutta, B. Henrissat, D. Holligan, R. Holt, W. Huang, N. Islam-Faridi, S. Jones, M. Jones-Rhoades, R. Jorgensen, C. Joshi, J. Kangasjärvi, J. Karlsson, C. Kelleher, R. Kirkpatrick, M. Kirst, A. Kohler, U. Kalluri, F. Larimer, J. Leebens-Mack, J.-C. Leplé, P. Locascio, Y. Lou, S. Lucas, F. Martin, B. Montanini, C. Napoli, D. R. Nelson, C. Nelson, K. Nieminen, O. Nilsson, V. Pereda, G. Peter, R. Philippe, G. Pilate, A. Poliakov, J. Razumovskaya, P. Richardson, C. Rinaldi, K. Ritland, P. Rouzé, D. Ryaboy, J. Schmutz, J. Schrader, B. Segerman, H. Shin, A. Siddiqui, F. Sterky, A. Terry, C.-J. Tsai, E. Uberbacher, P. Unneberg, J. Vahala, K. Wall, S. Wessler, G. Yang, T. Yin, C. Douglas, M. Marra, G. Sandberg, Y. V. d. Peer, and D. Rokhsar. 2006. The Genome of Black Cottonwood, *Populus trichocarpa* (Torr. & Gray). Science **313**:1596-1604.

Valverde-Barrantes, O. J., G. T. Freschet, C. Roumet, and C. B. Blackwood. 2017. A worldview of root traits: the influence of ancestry, growth form, climate and mycorrhizal association on the functional trait variation of fine-root tissues in seed plants. New Phytologist **215**:1562-1573.

van Breugel, M., D. Craven, H. R. Lai, M. Baillon, B. L. Turner, and J. S. Hall. 2019. Soil nutrients and dispersal limitation shape compositional variation in secondary tropical forests across multiple scales. Journal of Ecology **107**:566-581.

Větrovský, T., P. Kohout, M. Kopecký, A. Machac, M. Man, B. D. Bahnmann, V. Brabcová, J. Choi, L. Meszárošová, Z. R. Human, C. Lepinay, S. Lladó, R. López-Mondéjar, T. Martinović, T. Mašínová, D. Morais, D. Navrátilová, I. Odriozola, M. Štursová, K. Švec, V. Tláskal, M. Urbanová, J. Wan, L. Žifčáková, A. Howe, J. Ladau, K. G. Peay, D. Storch, J. Wild, and P. Baldrian. 2019. A meta-analysis of global fungal distribution reveals climate-driven patterns. Nature Communications **10**:5142.

Vitousek, P. M., and R. L. Sanford Jr. 1986. Nutrient cycling in moist tropical forest. Annual review of Ecology and Systematics **17**:137-167.

Weemstra, M., L. Mommer, E. J. Visser, J. Ruijven, T. W. Kuyper, G. M. Mohren, and F. J. Sterck. 2016. Towards a multidimensional root trait framework: a tree root review. New Phytologist **211**:1159-1169.

Xu, H., M. Detto, S. Fang, Y. Li, R. Zang, and S. Liu. 2015a. Habitat hotspots of common and rare tropical species along climatic and edaphic gradients. Journal of Ecology **103**:1325-1333.

Xu, H., Y. Li, S. Liu, R. Zang, F. He, and J. R. Spence. 2015b. Partial recovery of a tropical rain forest a half-century after clear-cut and selective logging. Journal of Applied Ecology **52**:1044-1052.

Appendix to Chapter 1: Morphological variation of fine root systems and leaves in primary and secondary tropical forest of Hainan Island, China.

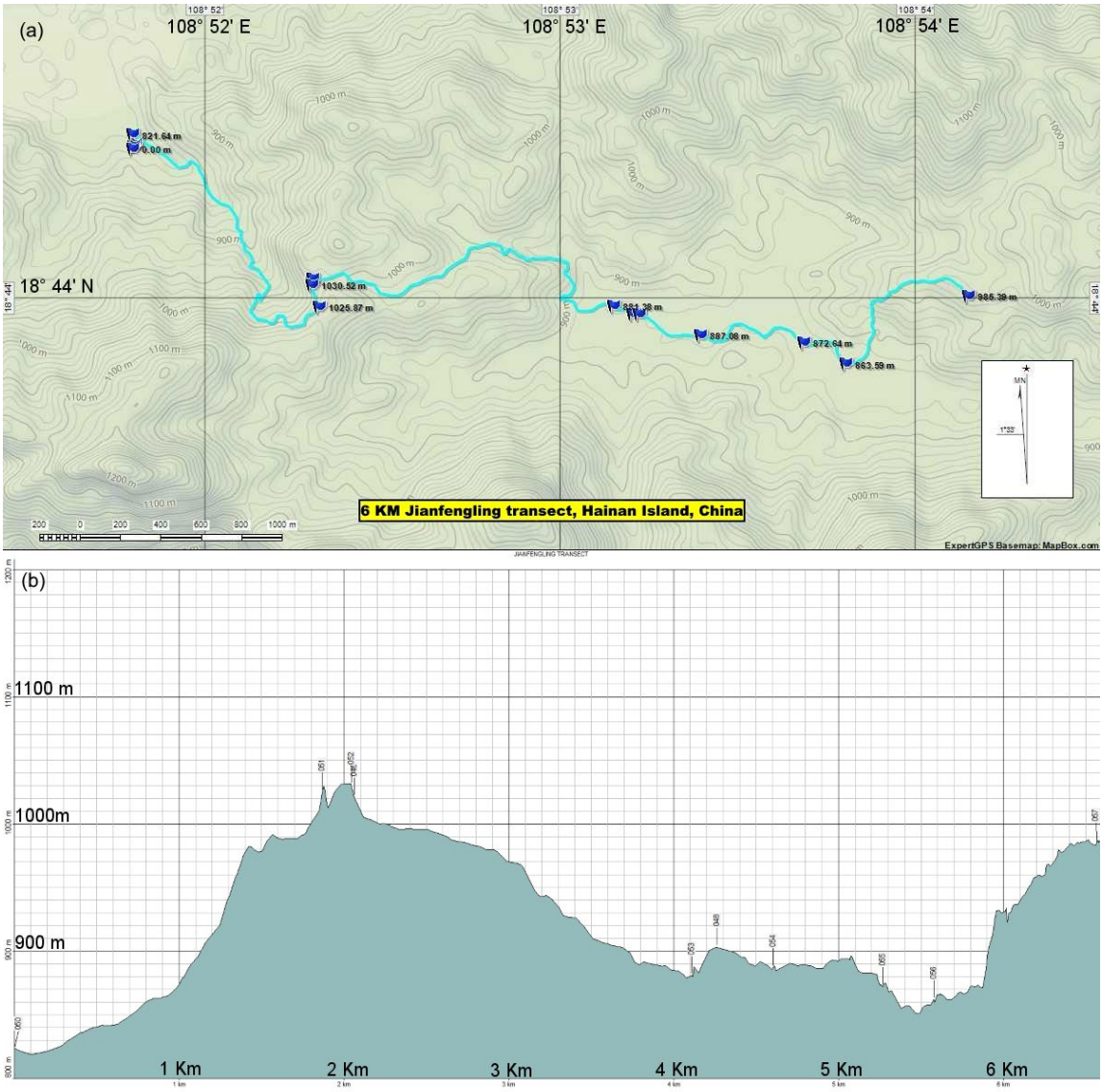

Fig. 6: Detailed topographic map (a) and topographic profile (b) of the 6.6 km transect in the Jianfengling Forest Reserve, Hainan Island, China, where functional traits of saplings were sampled. The transect started near the Jianfengling field house, at the entrance of the forest reserve. It progressed over one mountain, and over a stream (at km 4 of the transect) which delineated the secondary and primary areas of forest. At roughly km 5.5 of the transect, the transect entered the 60-Ha CTFS-ForestGEO permanent forest dynamics plot.

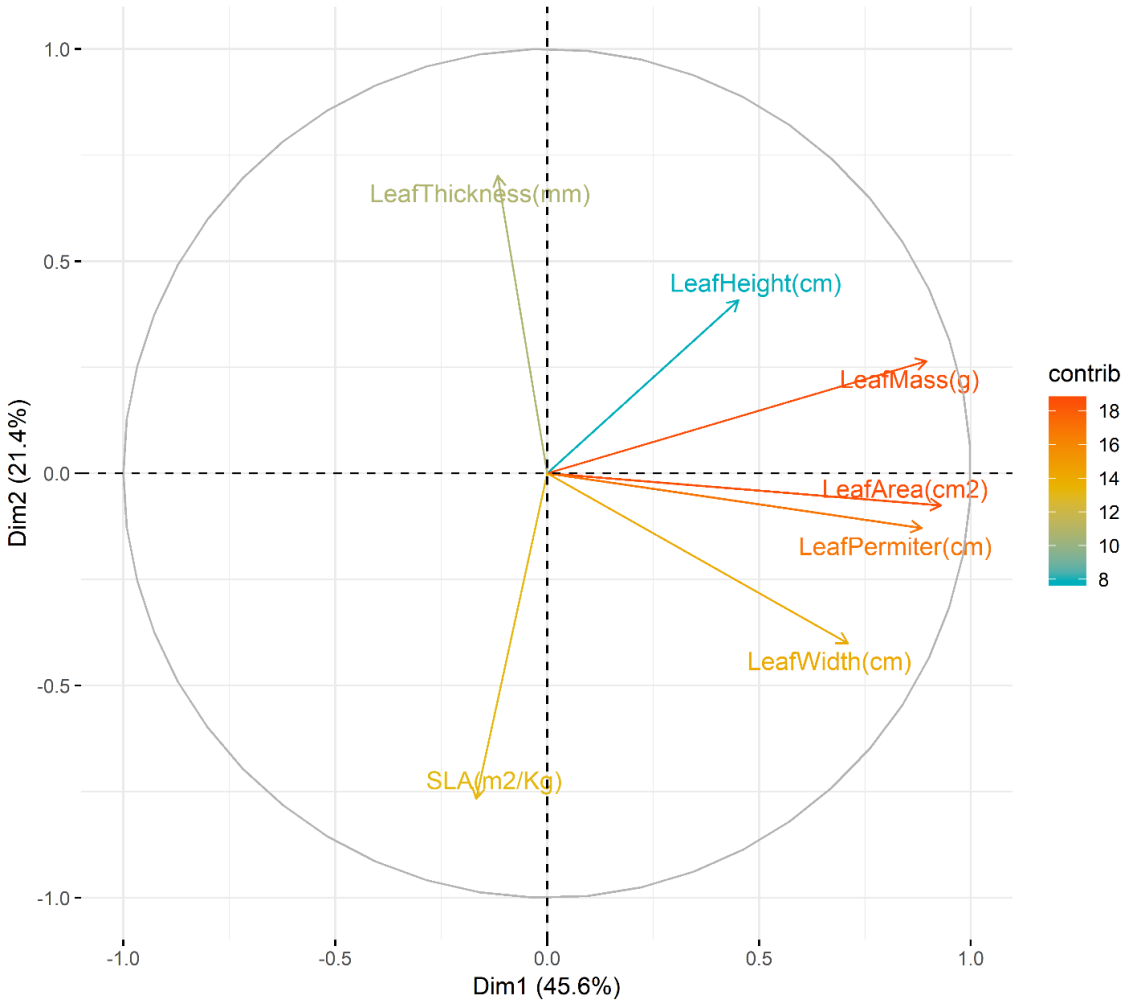

Fig. 7: Principal components analysis (variable scores plotted) of 7 leaf traits measured on 423 saplings of 72 species. Raw trait measurements were first scaled and centered.

Table 4: PCA loadings for the first three principal components for 7 leaf traits. Traits used in analysis of variance models are bolded.

Variable	PC1	PC2	PC3
LeafArea(cm^2)	0.520	-0.062	0.058
LeafPermiter(cm)	0.494	-0.105	0.057
LeafWidth(cm)	0.379	-0.327	-0.491
LeafHeight(cm)	0.253	0.333	0.738
LeafMass(g)	0.501	0.216	-0.076
SLA(m^2/kg)	-0.094	0.336	0.336
LeafThickness(mm)	-0.065	0.573	-0.297

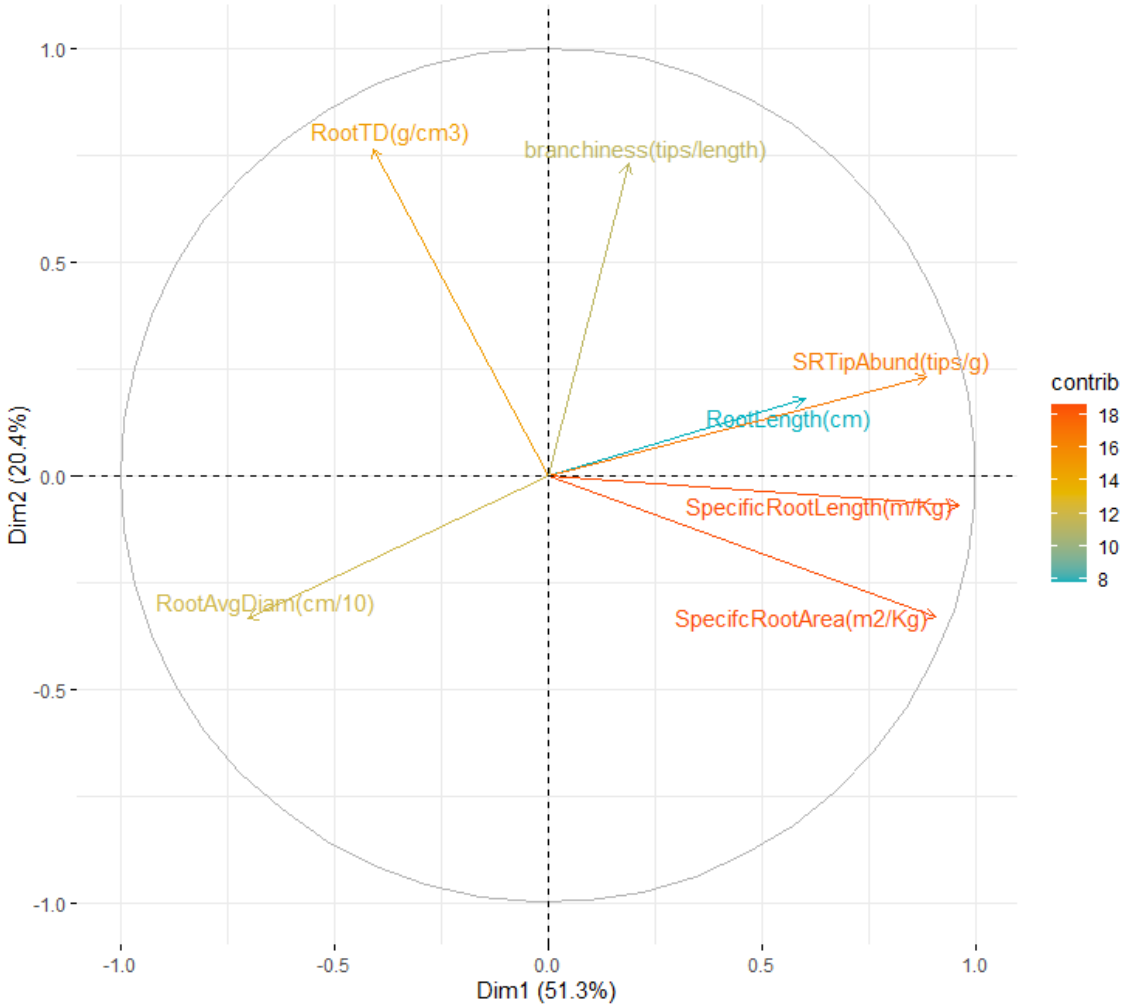

Fig. 8: Principal components analysis (variable scores plotted) of 7 key root traits measured on 423 saplings of 72 species. Raw trait measurements were first scaled and centered.

Table 5: PCA loadings for the first three principal components for 7 root traits. Traits used in analysis of variance models are bolded.

Variable	PC1	PC2	PC3
RootLength(cm)	0.317	0.149	0.532
SpecificRootLength (m/kg)	0.508	-0.060	-0.012
SpecifcRootArea (m^2/kg)	0.479	-0.278	-0.086
RootAvgDiam (cm/10)	-0.369	-0.281	-0.372
RootTD (g/cm^3)	-0.216	0.639	0.345
Branchiness (tips/cm)	0.099	0.610	-0.620
SRTipAbund (tips/g)	0.468	0.193	-0.263

Table 6: Individual collection counts of species along the 6-km JFL transect (Figs. 1 & 6) by forest type. For each individual sapling three to five fine root systems and three leaves were collected. Bolded species denote those where soil samples were analyzed (from three individuals in each primary and secondary forest, totaling 300 individuals of 50 species. Data from those 300 individuals are used in Fig. 5 and Table 3).

Species	Family	No. individuals	
		secondary	primary
Acronychia pedunculata (L.) Miq.	Rutaceae	3	4
Adinandra hainanensis Hayata	Pentaphylacaceae	4	6
Alniphyllum fortunei (Hemsl.) Makino	Styracaceae	1	3
Alseodaphne hainanensis Merr.	Lauraceae	3	3
Artocarpus styracifolius Pierre	Moraceae	3	3
Beilschmiedia laevis C.K.Allen	Lauraceae	3	3
Canarium album (Lour.) DC.	Burseraceae	5	3
Canarium pimela K.D.Koenig	Burseraceae	0	2
Castanopsis faberi Hance	Fagaceae	0	2
Castanopsis fissa (Champ. ex Benth.) Rehder & E.H.Wilson	Fagaceae	3	3
Castanopsis tonkinensis Seemen	Fagaceae	4	3
Cinnamomum burmanni (Nees & T.Nees) Blume	Lauraceae	3	3
Cinnamomum porrectum (Roxb.) Meisn.	Lauraceae	4	4
Cinnamomum rigidissimum H.T.Chang	Lauraceae	4	3
Cleyera obscurinervia (Merr. & Chung) H.T.Chang	Pentaphylacaceae	3	6
Cryptocarya chinensis Hance (Hemsl.)	Lauraceae	5	3
Cryptocarya chingii W.C. Cheng	Lauraceae	3	4
Dasymaschalon rostratum Merr & Chun.	Annonaceae	4	3
Diospyros morrisiana Hance	Ebenaceae	0	2
Eurya ciliata Merr.	Pentaphylacaceae	3	5
Engelhardia roxbughiana Wall.	Juglandaceae	3	3
Engelhardia spicata var. *colebrookeana* (Lindl. ex Wall.) Koord. & Valeton	Juglandaceae	0	1
Engelhardia unijuga (Lindl. ex Wall.) Iljinsk.	Juglandaceae	0	3
Ficus formosana Maxim.	Moraceae	3	3
Ficus hirta Vahl	Moraceae	3	3
Ficus vasculosa Wall. ex Miq.	Moraceae	3	4
Lindera kwangtungensis (H. Liu) C.K. Allen	Lauraceae	3	3
Lindera nacusua (D. Don) Merr.	Lauraceae	0	3
Lindera robusta (C.K. Allen) H.B. Cui	Lauraceae	4	3
Magnolia championii Benth.	Magnoliaceae	3	3
Lithocarpus amygdalifolius (Skan) Hayata	Fagaceae	6	3

Lithocarpus fenestratus (Roxb.) Rehder	Fagaceae	3	2
Lithocarpus fenzelianus A.Camus	Fagaceae	3	3
Lithocarpus hancei (Benth.) Rehder	Fagaceae	0	1
Lithocarpus handelianus A.Camus	Fagaceae	0	1
Lithocarpus howii Chun	Fagaceae	0	2
Lithocarpus longipedicellatus (Hickel & A.Camus) A.Camus	Fagaceae	3	3
Lithocarpus pseudovestitus A.Camus	Fagaceae	4	4
Litsea baviensis Lecomte	Lauraceae	4	3
Litsea variabilis Hemsl.	Lauraceae	3	3
Litsea verticillata Hance	Lauraceae	4	3
Machilus chinensis (Benth.) Hemsl.	Lauraceae	2	5
Machilus cicatricosa S.K. Lee	Lauraceae	5	4
Machilus monticola S.K. Lee	Lauraceae	3	3
Maclurodendron oligophlebium (Merr.) T.G. Hartley	Rutaceae	4	3
Madhuca hainanensis Chun & F.C.How	Sapotaceae	4	3
Manglietia fordiana var. *hainanensis* (Dandy) Noot.	Magnoliaceae	3	3
Melicope chunii T.G. Hartley	Rutaceae	3	3
Magnolia balansae A.DC.	Magnoliaceae	3	3
Michelia mediocris (Dandy) Figlar	Magnoliaceae	5	3
Neolitsea cambodianai Lecomte	Lauraceae	5	4
Neolitsea ellipsoidea C.K. Allen	Lauraceae	3	3
Neolitsea oblongifolia Merr. & Chun.	Lauraceae	3	3
Neolitsea ovatifolia Yen. C. Yang & P.H. Huang	Lauraceae	3	4
Neolitsea pulchella (Meisn.) Merr.	Lauraceae	3	3
Nephelium topengii (Merr.) H.S. Lo	Sapindaceae	4	4
Phoebe hungmoensis S.K. Lee	Lauraceae	0	4
Polyspora hainanensis (Hung T. Chang) C.X. Ye ex B.M. Barthol. & T.L. Ming	Theaceae	3	3
Planchonella annamensis Pierre ex Dubard	Sapotaceae	0	2
Pyrenaria jonquieriana subsp. *multisepala* (Merr. & Chun) S.X. Yang	Theaceae	3	3
Litsea baviensis Lecomte	Lauraceae	3	3
Litsea variabilis Hemsl.	Lauraceae	3	3
Litsea verticillata Hance	Lauraceae	3	3
Quercus auricoma A.Camus	Fagaceae	2	3
Quercus myrsinifolia Blume.	Fagaceae	3	3
Quercus asymmetrica Hickel & A.Camus	Fagaceae	3	3
Sarcosperma laurinum (Benth.) Hook.f.	Sapotaceae	3	3
Schima superba Gardner & Champ.	Theaceae	4	5
Streblus indicus (Bureau) Corner	Moraceae	0	3

Tetradium glabrifolium (Champ. ex Benth) T.G. Hartley	Rutaceae	0	3
Toxicodendron vernicifluum (Stokes) F.A. Barkley	Anacardiaceae	4	3
Zanthoxylum avicennae (Lam.) DC.	Rutaceae	3	3

Appendix to Chapter 2: Evidence of elemental homeostasis in fine root and leaf tissue of saplings across a fertility gradient in tropical montane forest in Hainan, China

Table 2: List of species with taxonomic authorities by Family for which root and leaf tissues were sample and nutrient concentrations were measured. Six juvenile trees were sampled for each of the 50 species listed, where leaf and root tissues were collected, dried, homogenized and chemically analyzed.

Family	Species
Anacardiaceae	*Toxicodendron vernicifluum (Stokes) F.A. Barkley*
Annonaceae	*Dasymaschalon rostratum Merr & Chun.*
Burseraceae	*Canarium album (Lour.) DC.*
Ebenaceae	*Diospyros morrisiana Hance*
Fagaceae	*Castanopsis fissa (Champ. ex Benth.) Rehder & E.H.Wilson*
	Castanopsis tonkinensis Seemen
	Lithocarpus amygdalifolius (Skan) Hayata
	Lithocarpus fenestratus (Roxb.) Rehder
	Lithocarpus fenzelianus A.Camus
	Lithocarpus longipedicellatus (Hickel & A.Camus) A.Camus
	Lithocarpus pseudovestitus A.Camus
	Quercus myrsinifolia Blume.
Juglandaceae	*Engelhardia roxbughiana* Wall.
Lauraceae	*Alseodaphne hainanensis* Merr.
	Beilschmiedia laevis C.K.Allen
	Cinnamomum burmanni (Nees & T.Nees) Blume
	Cinnamomum porrectum (Roxb.) Meisn.
	Cinnamomum rigidissimum H.T.Chang
	Cryptocarya chinensis Hance (Hemsl.)
	Cryptocarya chingii W.C. Cheng
	Lindera kwangtungensis (H. Liu) C.K. Allen
	Lindera robusta (C.K. Allen) H.B. Cui
	Litsea baviensis Lecomte
	Litsea baviensis Lecomte
	Litsea variabilis Hemsl.
	Litsea variabilis Hemsl.
	Litsea verticillata Hance
	Litsea verticillata Hance
	Machilus cicatricosa S.K. Lee
	Neolitsea cambodianai Lecomte
	Neolitsea ellipsoidea C.K. Allen
	Neolitsea oblongifolia Merr. & Chun.
	Neolitsea ovatifolia Yen. C. Yang & P.H. Huang
	Neolitsea pulchella (Meisn.) Merr.

Magnoliaceae	*Michelia mediocris* (Dandy) Figlar
Moraceae	*Artocarpus styracifolius* Pierre
	Ficus formosana Maxim.
	Ficus hirta Vahl
	Ficus vasculosa Wall. ex Miq.
Pentaphylacaceae	*Adinandra hainanensis* Hayata
	Cleyera obscurinervia (Merr. & Chung) H.T.Chang
	Eurya ciliata Merr.
Rutaceae	*Acronychia pedunculata* (L.) Miq.
	Maclurodendron oligophlebium (Merr.) T.G. Hartley
	Melicope chunii T.G. Hartley
	Zanthoxylum avicennae (Lam.) DC.
Sapindaceae	*Nephelium topengii* (Merr.) H.S. Lo
Sapotaceae	*Madhuca hainanensis* Chun & F.C.How
	Sarcosperma laurinum (Benth.) Hook.f.
Theaceae	*Polyspora hainanensis* (Hung T. Chang) C.X. Ye ex B.M. Barthol. & T.L. Ming
	Pyrenaria jonquieriana subsp. *multisepala* (Merr. & Chun) S.X. Yang
	Schima superba Gardner & Champ.

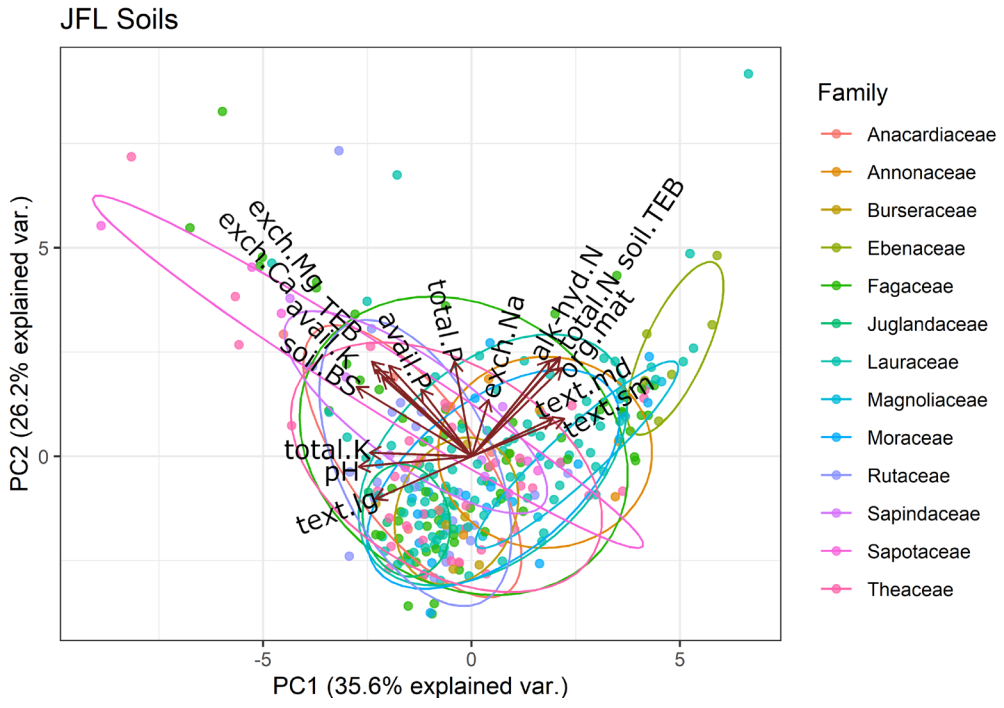

Fig. 5: Principal component ordination for rhizosphere soil samples collected following root system collection for 300 individual saplings in the Jianfengling forest reserve, Hainan Island. Elipses correspond to plant families, which are shown in the color-coded

legend. Variable abbreviations are (in clockwise order from left to right): text.lg – soil texture large (% sand, i.e. soil particles 0.5-2.0 mm), pH – soil pH, total.K – total soil potassium concentration (g kg^{-1}), soil.BS – soil base saturation (%), avail.K – soil available potassium concentration (cmol kg^{-1}), exch. Ca – soil exchangeable calcium content (cmol kg^{-1}), exch.Mg – soil exchangeable magnesium concentration (cmol kg^{-1}), TEB – total exchangeable bases (cmol kg^{-1}), avail.P – soil available phosphorus concentration (mg kg^{-1}), total.P – soil total phosphorus concentration (g kg^{-1}), exch.NA – soil exchangeable sodium concentration (cmol kg^{-1}), alk-hyd.N – available (i.e., alkali-hydrolyzable) soil nitrogen (mg kg^{-1}), total.N – total soil nitrogen concentration (g kg^{-1}), soil.TEB – soil total exchangeable bases (cmol kg^{-1}), org.mat – soil organic matter (g kg^{-1}), text.md – soil texture medium (% silt, i.e., soil particles 0.002-0.5 mm), text.sm – soil texture small (% clay, i.e., soil particles <0.002 mm).

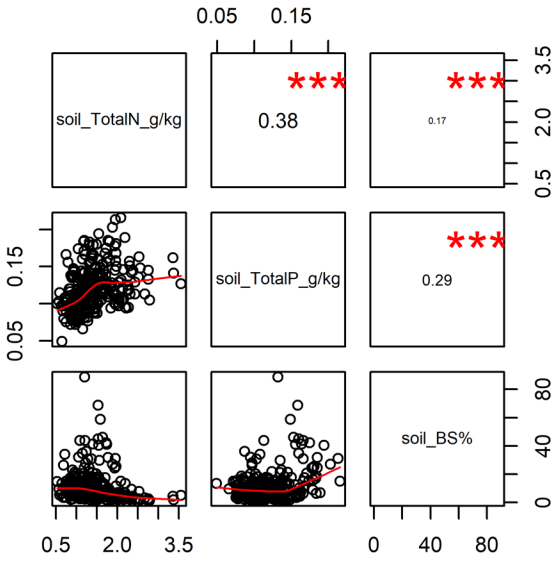

Fig. 6: Pairs plot for the three soil variables used in the linear mixed-effects models. Point plots are shown below the diagonal, where red lines are loess smoothers. Correlation coefficients are shown above the diagonal and are scaled to signify the strength of the relationship. All correlations are statistically significant at $\alpha = 0.05$.

In addition to the above appendix to Chapter 2, one supplementary resource exists online at the given link:

Chaper 2, Online Resource 1: Complete model description of best-fitting linear mixed-effects models for 14 elemental concentrations in leaf and root tissues: https://bit.ly/3xls1FM

Note: There is no appendix to Chapter 3: Intraspecific trait variation and species functional turnover in successional tropical forests: assessing gap filling for community-weighted mean

However, three online resources exist for Chapter 3 – see the Supplementary files section of https://www.researchsquare.com/article/rs-404661/v1

1. S1.pdf: Analysis the soils from 300 individuals from along the gradient to the soils of the 164 1/16th-hectare small plots (data from Xu, Detto et al. 2015).

2. S2.pdf: Literate statistical document implementing the Trait Flex ANOVAS for the assemblage-weight mean analysis, which uses the truncated community of 72 species for which root and leaf functional traits were directly measured.

3. S3.pdf: Literate statistical document describing the gap-filling of functional traits and re-implementing the Trait Flex ANOVAS with pGLM gap-filled trait matrices (using PhyloPars) for complete CWM analysis, which uses the entire plant community (582 species) for the small plots at JFL.

Appendix to Chapter 4: Root-associated fungal communities are structured more by soil environment than by plant-host functional traits in a Chinese tropical forest.

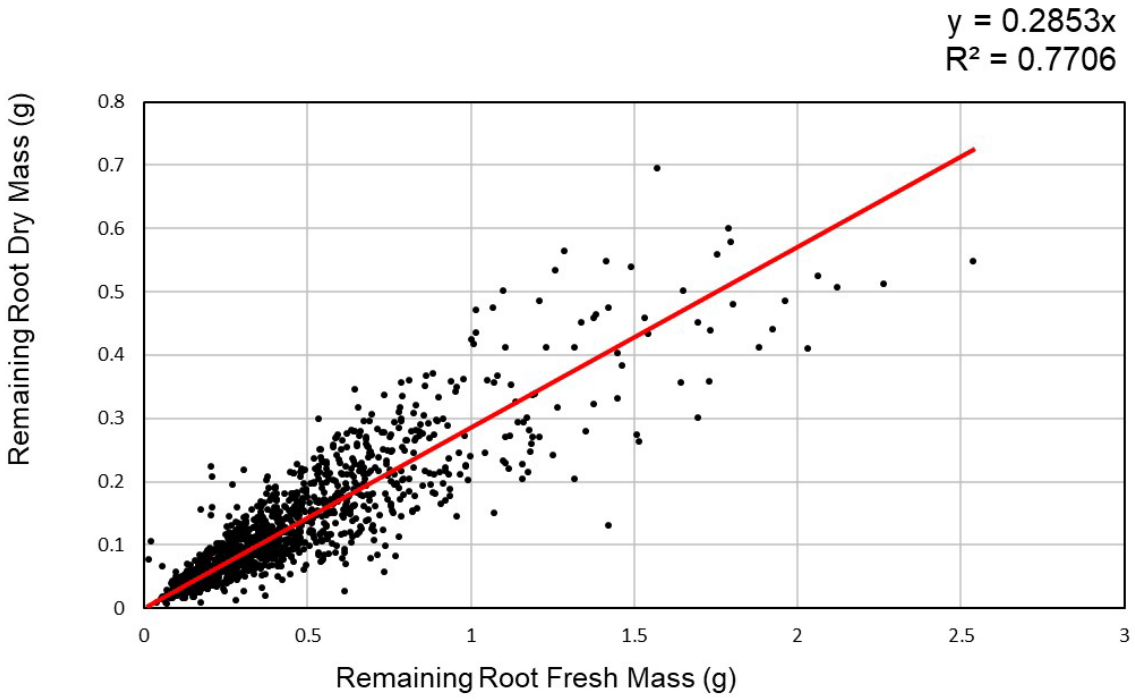

Fig. S1: Relationship between remaining root system (after first order root tips were removed) dry mass and fresh mass. This regression (y = 0.2853x) was used to estimate the dry mass of first order root tips from their wet mass. The estimated dry mass of the root tips was added to the dry mass of the remaining root system to calculate the dry mass of the entire root system (which was used in the quantification of root functional traits, e.g., SRL).

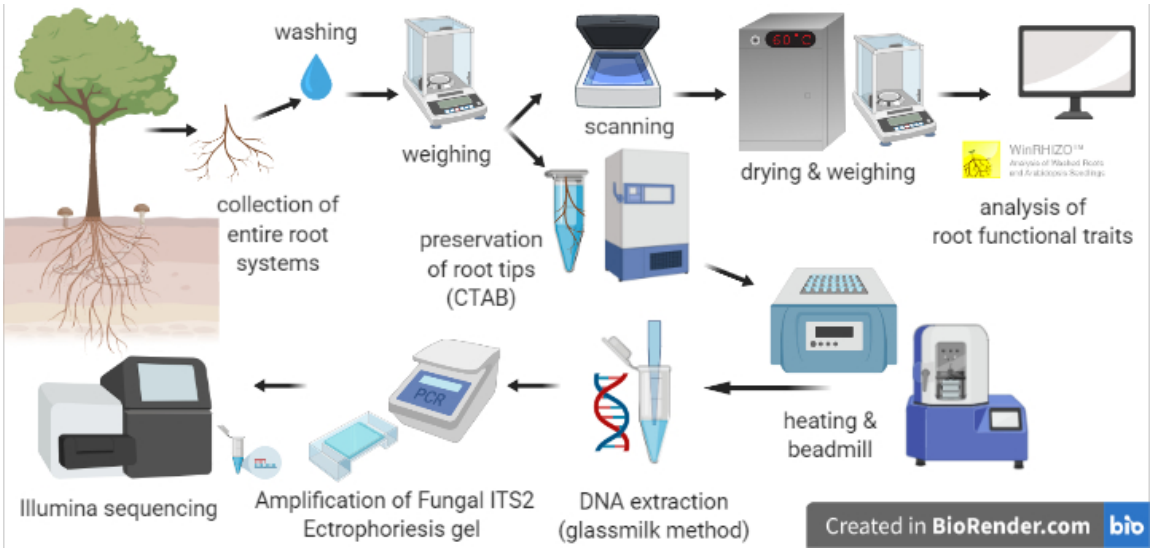

Fig. S2: (previous page) Graphical depiction of root processing methods. Root systems were collected from an identified tree. They were transported back to the lab where they were washed and cleaned. They were delineated into entire root systems, weighed and scanned. The first-order fine root tips were removed, weighed, and preserved in CTAB for sequencing, while the remainder or the root system was dried, then weighed. CTAB-preserved root tip samples were then heated, and bead milled to facilitate DNA extraction. DNA extraction was done with the glass milk method, and we amplified fungal ITS2 sequences via PCR. Sequencing was done on an illumine Mi-Seq.

Table S1 Primer sequences used in DNA amplification

Organism	Primer	F/R	Sequence 5'-3'	Reference
Fungi	fITS7	F	GTG ART CAT CGA ATG TTT G	Ihrmark *et al.* (2012)
Fungi	fITS7o	F	GTG AAT CAT CRA ATY TTT G	Lekberg *et al.* (2018)
Fungi	ITS4	R	TC CTC CGC TTA TTG ATA TGC	Kohout *et al.* (2014)
Plant	rbcLa-F	F	ATG TCA CCA CAA ACA GAG ACT AAA GC	Fay *et al.* (1997)
Plant	rbcLa-R	R	GTA AAA TCA AGT CCA CCR CG	Levin *et al.* (2003)
Plant	Rbcl724R	R	TCG CAT GTA CCT GCA GTA GC	Kress *et al.* (2009)

Table S2: Forward selection of variables on Hellinger-transformed fungal OTU read count matrix 150 root systems sampled across 3 plots in Xishuangbanna, China. Thirty-six variables were considered (7 soil variables, 15 root functional traits and 14 tissue elemental concentrations). Eight variables were selected – two soils variables, four root functional traits, and two root tissue elemental concentrations. The alpha stopping criteria for forward selection was invoked for variable 10 – root tissue magnesium (Mg) concentration, in that the *p*-value was 0.0502 ($p > 0.05$). Forward selection was done using the 'forward.sel' function in the 'adespatial' package (with 49999 permutations), which follows variable selection as outline by Blanchet *et al.* (2008)

Variable	$\boldsymbol{R^2}$	$\boldsymbol{R^2_{cum}}$	$\boldsymbol{Adj.\ R^2_{cum}}$	F	p
Available P (mg kg^{-1})	0.0726	0.0710	0.0663	11.59	<0.001
Total P (mg kg^{-1})	0.0465	0.1175	0.1055	7.48	<0.001
RDMC (mg g^{-1})	0.0115	0.1290	0.1111	1.93	<0.001
SRTA (tips cm^{-1})	0.0096	0.1386	0.1148	1.61	<0.001
Forks	0.0092	0.1478	0.1182	1.55	0.001
RTD (g cm^{-3})	0.0086	0.1563	0.1209	1.45	0.002

Root N (%)	0.0084	0.1647	0.1235	1.43	0.003
Root Ca (%)	0.0084	0.1731	0.1262	1.43	0.004
Root Mn (‰)	0.0072	0.1803	0.1276	1.23	0.047

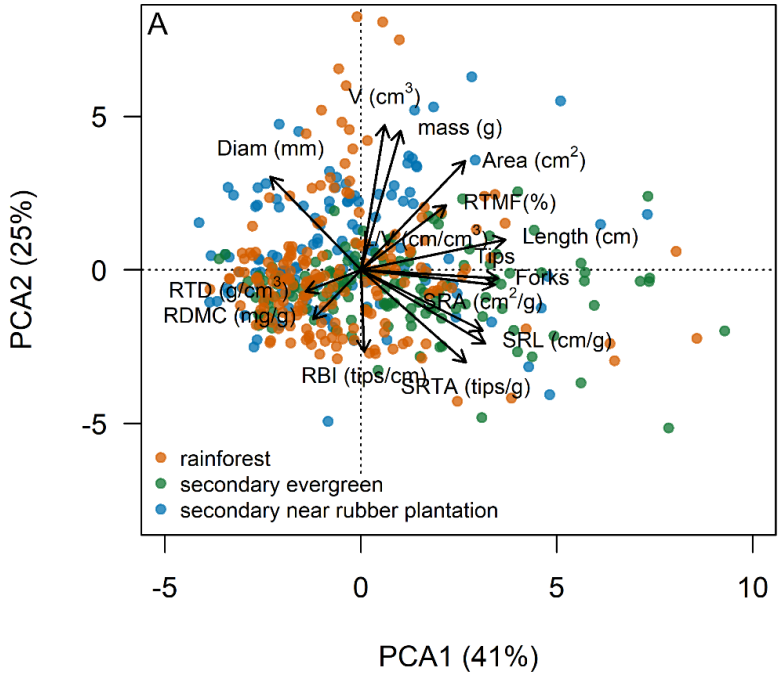

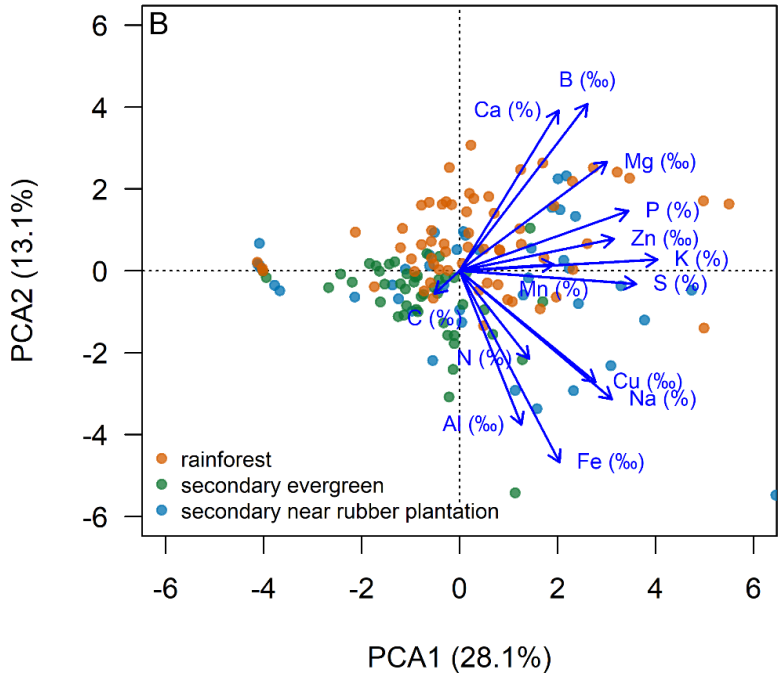

Fig. S3: Principal components analyses for A) 15 root functional traits and B) 14 elemental tissue concentrations from root systems from 150 tropical trees. Data from 450 entire root systems (n = 3 per individual tree) appear in panel A, while composite data from those homogenized tissues appear as 150 points in panel B. Root system functional traits were measured/ analyzed from scanned root system images using WinRHIZO, and tissue elemental concentrations were measured using ICP-MS (see methods).

Table S3: Contributions of root functional traits to the first three Principal Components axes of the root functional trait space (Fig. S3A). Abbreviations are as follows and correspond to the vector labels in Fig. S3A: RTMF – root tip mass fraction, RDMC – root dry matter content, SRL – specific root length, SRA – specific root area, Diam – root system average diameter, RTD – root tissue density, RBI – root branching intensity, SRTA – specific root tip abundance. Bolded traits are those that were forward selected (see Table S2).

Trait	PC1	PC2	PC3
Mass(g)	0.02	22.25	1.89
RTMF (%)	4.20	1.84	15.02
RDMC (mg g^{-1})	1.30	0.64	25.13
Length (cm)	13.18	2.93	2.25
SRL (cm g^{-1})	11.00	5.22	0.71
Area (cm^2)	4.52	7.61	0.09
SRA (cm^2 g^{-1})	17.42	0.02	5.03
Diam (mm)	8.52	10.71	3.04
Length/Volume (cm cm^{-3})	13.18	2.93	2.25
Volume (cm^3)	0.09	22.17	1.42
RTD (g cm^{-3})	1.93	0.06	29.86
Tips	11.86	0.16	5.91
RBI (tips cm^{-1})	0.05	5.82	2.82
SRTA (tips g^{-1})	8.13	7.95	0.02
Forks	12.44	0.35	4.55

Table S4: Contributions of root elemental concentrations to the first three Principal Components axes of the root functional trait space (Fig. S3B). Elements are denoted by their symbols in the period table of elements, which correspond to vector labels in Fig. S3B. Bolded elements are those that were forward selected (see Table S2).

Element	PC1	PC2	PC3
Al (‰)	1.59	14.10	8.76
B (‰)	6.79	16.60	2.72
Ca (%)	4.06	15.33	4.32
C (%)	0.27	0.31	0.58
Cu (‰)	7.69	15.41	6.78
Fe (‰)	4.17	21.86	4.31
K (%)	16.29	0.08	3.37
Mg (%)	9.05	7.10	27.25
Mn (‰)	3.69	0.02	1.24
Na (‰)	9.66	9.81	10.94

N (%)	2.01	4.59	19.16
P (%)	11.85	2.13	7.21
S (%)	12.96	0.10	0.24
Zn (‰)	9.93	0.61	3.13

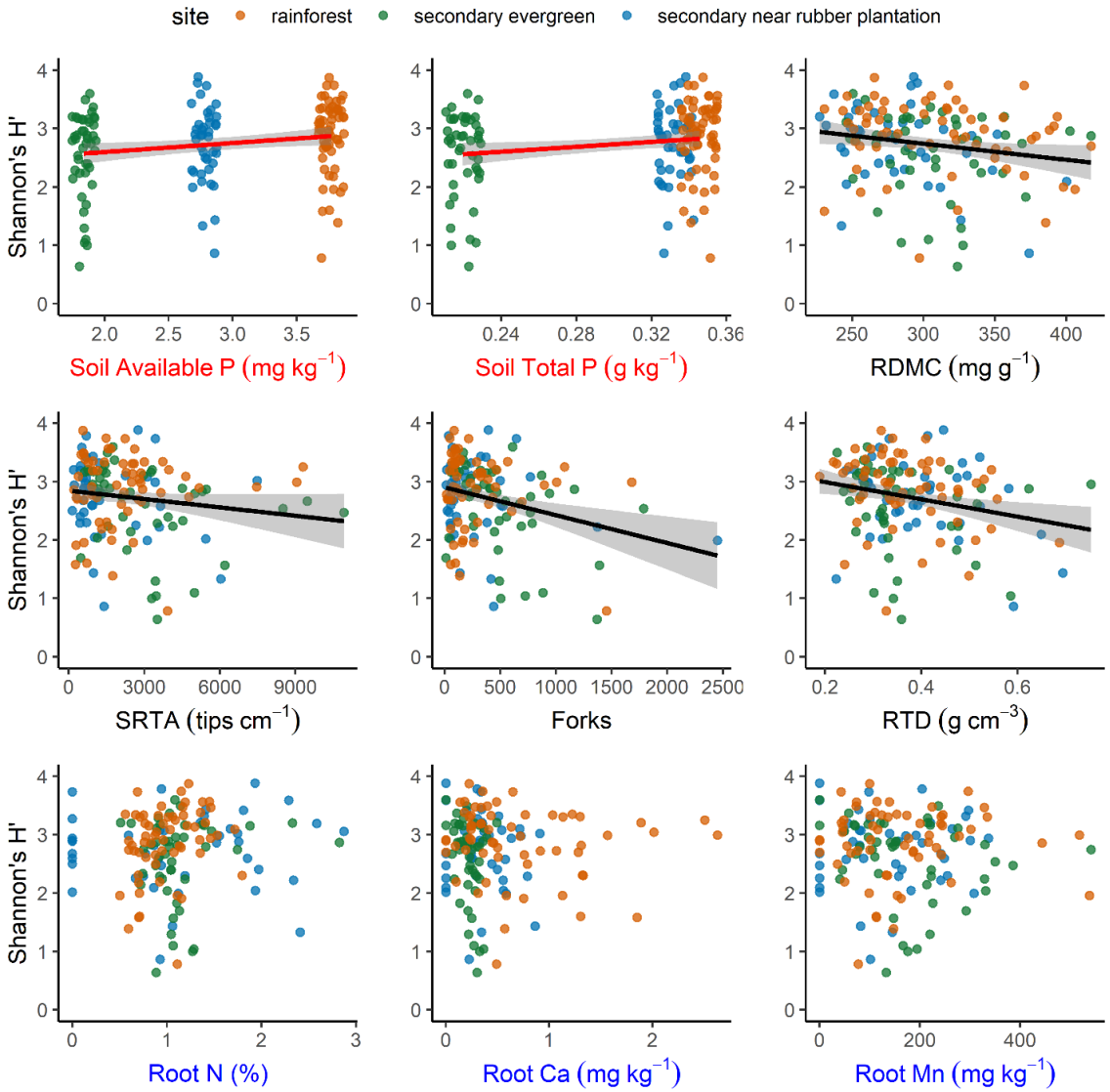

Fig. S4: Fungal Shannon's diversity (H') and it relationship with forward-selected environmental variables (two soils variables (colored in red): soil available and total phosphorus – P, four root functional traits (colored black): root dry matter content – RDMC, specific root tip abundance – SRTA, the number of root system forks – Forks, root tissue density – RTD, and three root elemental concentrations (colored blue): root tissue N – nitrogen, Ca – calcium, and Mn – manganese concentration). Lines show statistically significant regressions (i.e., slopes with $p < 0.05$), and shaded areas are 95% confidence intervals.

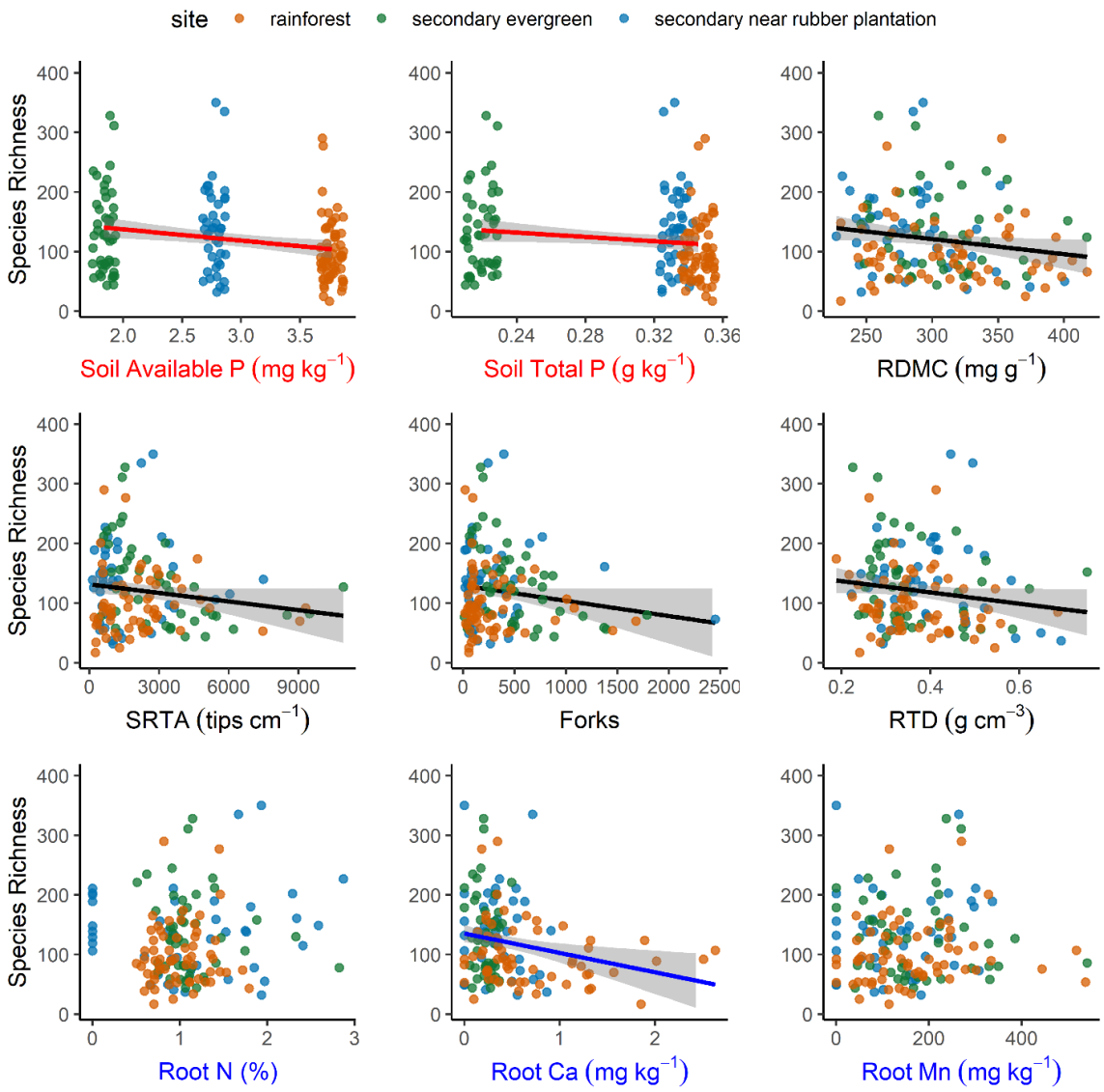

Fig. S5: Fungal species richness in relation to forward-selected environmental variables (two soils variables (colored in red): soil available and total phosphorus – P, four root functional traits (colored black): root dry matter content – RDMC, specific root tip abundance – SRTA, the number of root system forks – Forks, root tissue density – RTD, and three root elemental concentrations (colored blue): root tissue N – nitrogen, Ca – calcium, and Mn – manganese concentration). Lines show statistically significant regressions (i.e., slopes with $p < 0.05$), and shaded areas are 95% confidence intervals.

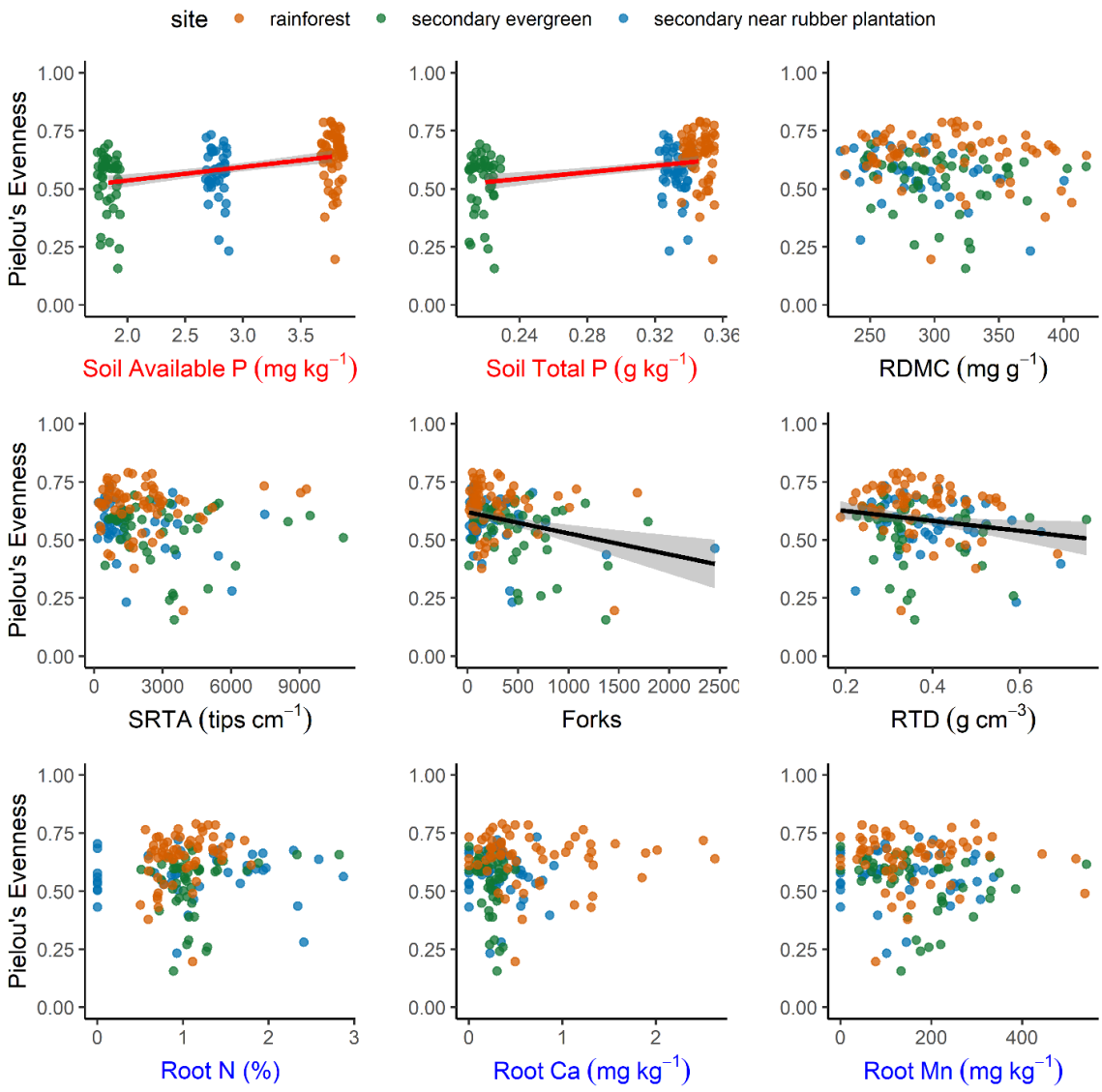

Fig. S6: Linear regression of root-associated fungal community evenness and forward-selected environmental variables (two soils variables (colored in red): soil available and total phosphorus – P, four root functional traits (colored black): root dry matter content – RDMC, specific root tip abundance – SRTA, the number of root system forks – Forks, root tissue density – RTD, and three root elemental concentrations (colored blue): root tissue N – nitrogen, Ca – calcium, and Mn – manganese concentration). Lines show statistically significant regressions (i.e., slopes with $p < 0.05$), and shaded areas are 95% confidence intervals.

Table S5: Linear (ordinary least squares) regression summaries for the relationships of forward-selected environmental variables and species richness, Shannon's Diversity (H′) and evenness of root-associate fungal community. Intercept terms for the simple one-term linear regressions are not shown. Regressions are plotted above in Figs. S4 (species richness), S5 (richness), and S6 (evenness J′). Regression probabilities (of the slope, β) are denoted as follows: ‡ marginally significant p-value ($0.05 < p < 0.1$), * $p < 0.05$, ** $p < 0.01$, *** $p < 0.001$. RMSE stands for root mean squared error.

Variable	Shannon's H′				Richness				Evenness J′			
	β	*p*	R^2	RMSE	β	*p*	R^2	RMSE	β	*p*	R^2	RMSE
Soil available P	0.17	*	0.04	0.66	-18.91	**	0.06	63.64	0.06	***	0.15	0.11
Soil Total P	2.22	*	0.03	0.66	-181.58	‡	0.02	64.69	0.71	***	0.10	0.11
RDMC	-0.25E-2	*	0.03	0.66	-0.25	*	0.03	64.47	-0.30E-3	*ns*	—	—
SRTA	-0.51E-4	‡	0.02	0.66	-0.48E-2	‡	0.02	64.75	-0.77E-7	*ns*	—	—
Forks	-0.49E-3	***	0.08	0.64	-0.03	‡	0.02	64.73	-0.91E-5	***	0.08	0.12
RTD	-1.44	**	0.05	0.65	-94.65	‡	0.02	64.71	-0.21	*	0.03	0.12
Root N	-0.10	*ns*	—	—	8.31	*ns*	—	—	0.02	*ns*	—	—
Root Ca	-0.04	*ns*	—	—	-32.51	**	0.05	63.76	0.03	*ns*	—	—
Root Mn	-0.23E-3	*ns*	—	—	0.02	*ns*	—	—	-0.78E-6	*ns*	—	—

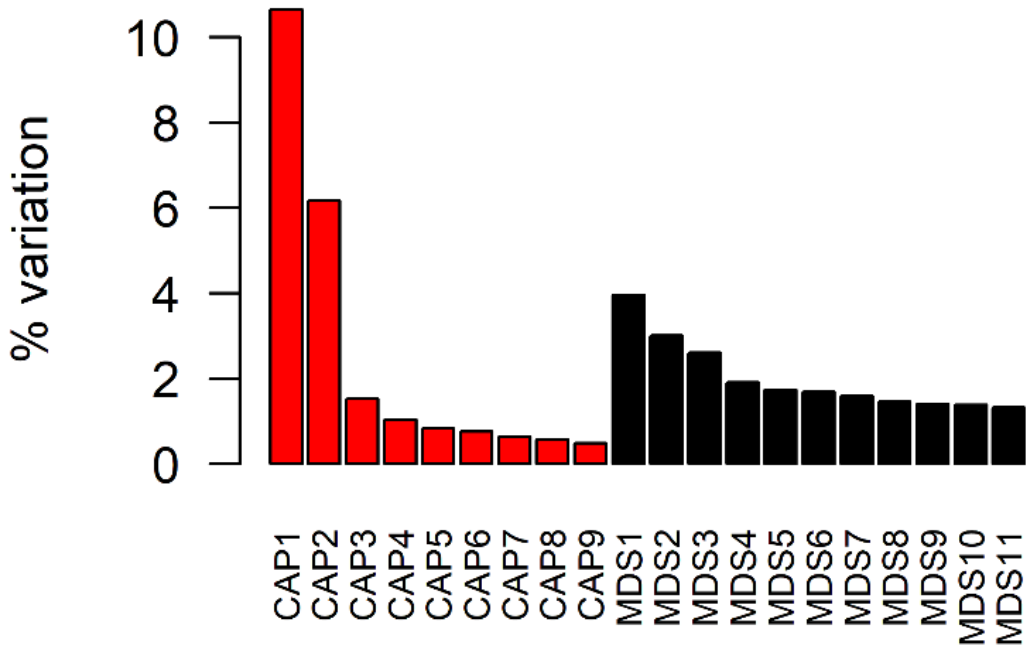

Fig. S7: Percent of variation explained by constrained (red) and unconstrained (black) db-RDA axes. CAP stands for "constrained analysis of principal coordinates", which are the db-RDA axes using Bray-Curtis dissimilarities on Hellinger-transformed OUT reads. NMDS axes are the related unconstrained ordination. The first two dimensions of the db-RDA dominate the variation in eigenvalues, comprising 17% of the total (unconstrained or constrained) variation in the multivariate ordination space.

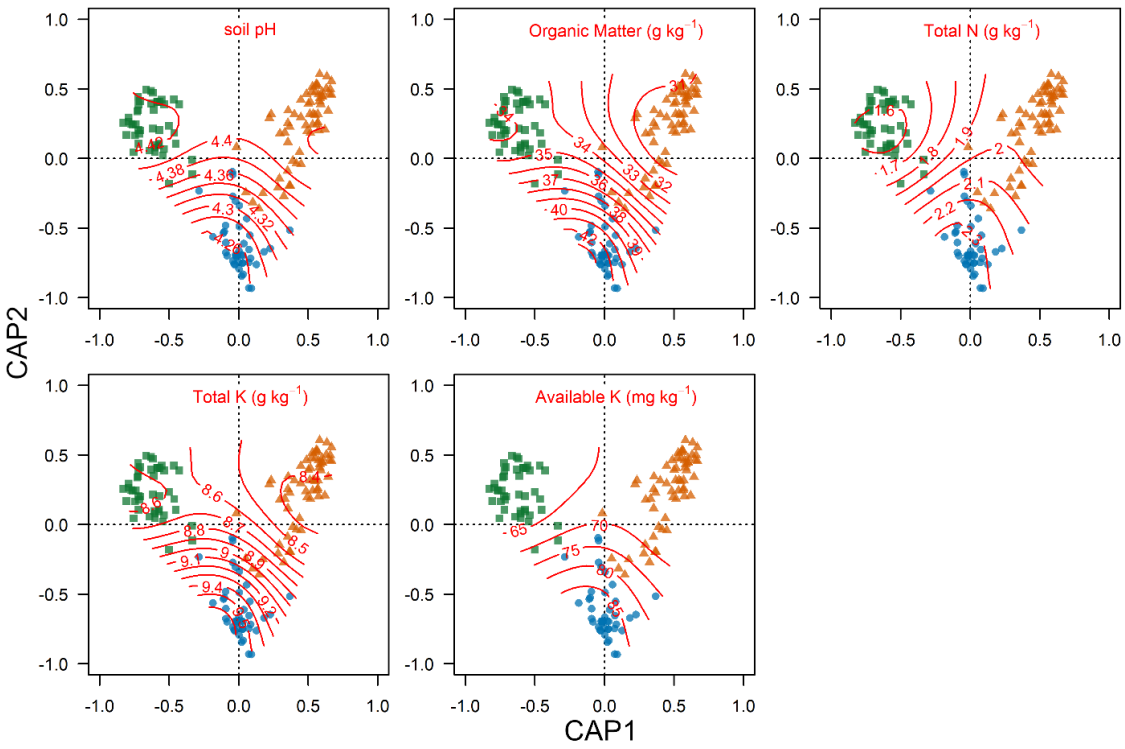

Fig. S8: Constrained ordination (db-RDA) contour plots of fitted GAM model surfaces for non-forward-selected soil variables (soil pH, organic matter, total N, total K, and available K).

Table S6: Model parameter from generalized additive models (GAMs) fitting non-forward selected soils variables to the first two axes of the db-RDA. Smooth surfaces for soil variables were fit via GAMs using the 'ordisurf' function in the vegan R package (Oksanen *et al.*, 2020). Effective degrees of freedom (edf) represent the complexity of the smooth (i.e., 1 is a linear relation, 2 is a quadradic, etc.). P-values are denoted as follows: ‡ marginally significant *p*-value ($0.05 < p < 0.1$), * $p < 0.05$, ** $p < 0.01$, *** $p < 0.001$. RMSE stands for root mean squared error. The percent of model deviance explained and adjusted coefficients of determination R^2_{adj} values are given for each GAM.

Soil variable	N	Linear term			Smooth term			Deviance explained (%)	R^2_{adj}
		Int	*t*	*p*	edf	$F_{(edf,9)}$	*p*		
pH	150	4.37	2122.00	***	8.16	118.60	***	88.4	0.877
Organic Matter (g kg^{-1})	150	34.95	254.90	***	8.10	108.20	***	87.4	0.867
Total N (g kg^{-1})	150	1.97	329.30	***	8.40	232.20	***	93.7	0.933
Total K (g kg^{-1})	150	8.78	629.00	***	8.11	108.60	***	87.5	0.868

Available K(mg kg^{-1})	150	71.01	245.50	***	8.20	129.10	***	89.3	0.886

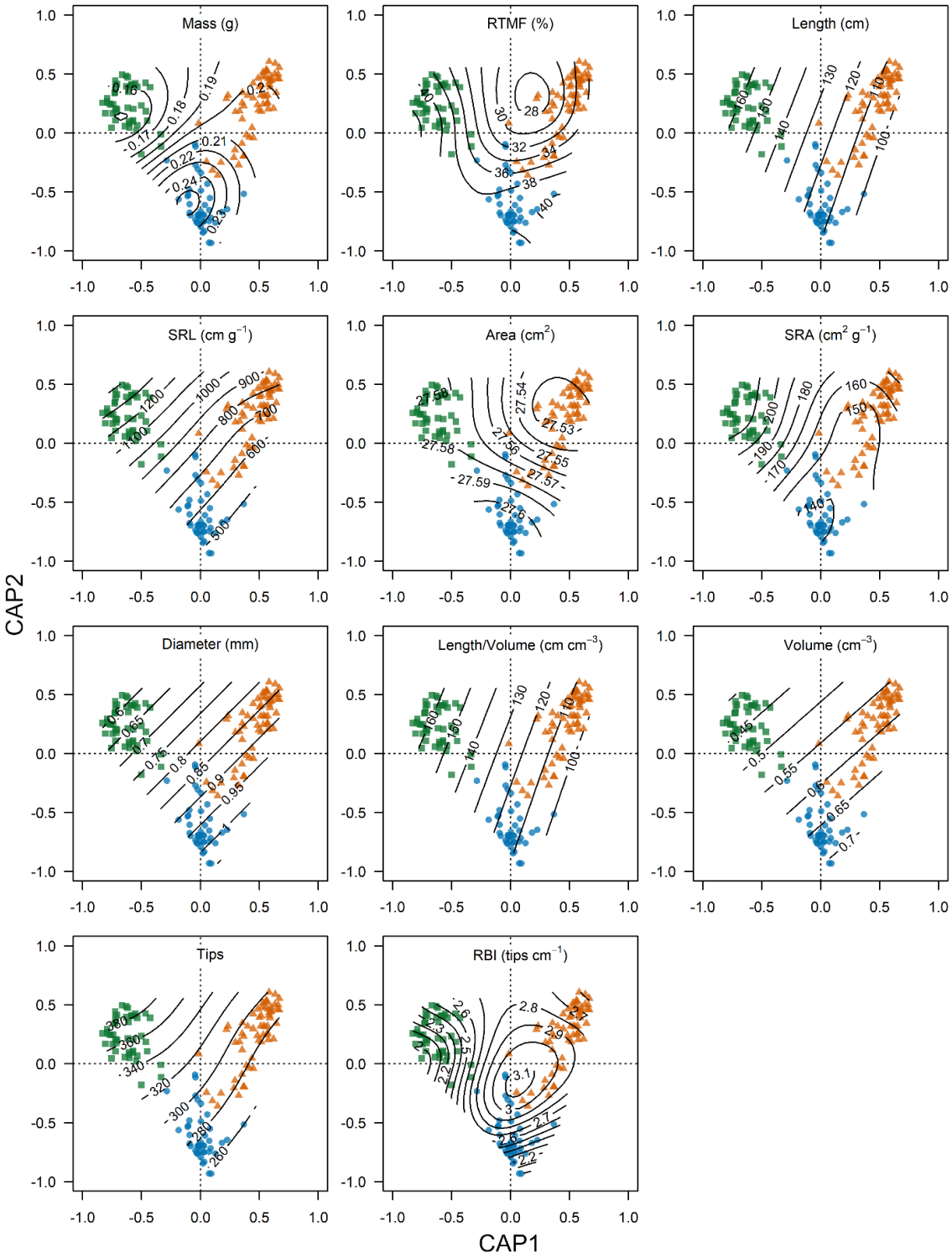

Fig. S9: (previous page) Constrained ordination (db-RDA) contour plots of fitted GAM model surfaces for non-forward-selected root functional traits (root system dry mass, root tip mass fraction – RTMF, root system length, specific root length – SRL, root system area, specific root area – SRA, root system average diameter, root system length-to-volume ratio, root system volume, number of root tips and root branching intensity – RBI).

Table S7: Model parameter from generalized additive models (GAMs) fitting non-forward selected root functional traits to the first two axes of the db-RDA. Smooth surfaces for soil variables were fit via GAMs using the 'ordisurf' function in the vegan R package (Oksanen *et al.*, 2020). Effective degrees of freedom (edf) represent the complexity of the smooth (i.e., 1 is a linear relation, 2 is a quadradic, etc.). P-values are denoted as follows: ‡ marginally significant *p*-value ($0.05 < p < 0.1$), * $p < 0.05$, ** $p < 0.01$, *** $p < 0.001$. RMSE stands for root mean squared error. The percent of model deviance explained and adjusted coefficients of determination R^2_{adj} values are given for each GAM.

Trait	N	Linear term			Smooth term			Deviance explained (%)	$\boldsymbol{R^2_{adj}}$
		Int	*t*	*p*	edf	$F_{(edf,9)}$	*p*		
Mass (g)	150	0.20	21.25	***	3.45	1.72	***	11.5	0.094
RTMF (%)	150	35.96	32.13	***	4.03	1.74	**	11.9	0.095
Length (cm)	150	124.78	6.20	***	1.86	1.64	***	10.1	0.090
SRL (cm g^{-1})	150	846.52	18.50	***	2.94	4.46	***	22.8	0.212
Area (cm^2)	150	27.57	24.98	***	0.05	<0.01	*ns*	<0.1	<0.001
SRA (cm^2 g^{-1})	150	167.75	31.26	***	4.27	3.76	***	20.8	0.185
Diam (mm)	150	0.82	35.10	***	1.90	3.85	***	19.9	0.189
Length/Volume (cm cm^{-3})	150	124.78	6.20	***	1.86	1.64	***	10.1	0.090
Volume (cm^3)	150	0.56	17.73	***	1.65	0.98	**	6.63	0.056
Tips	150	309.12	16.01	***	2.02	0.71	*	5.4	0.041
RBI (tips cm^{-1})	150	2.58	30.09	***	5.07	2.08	**	14.2	0.111

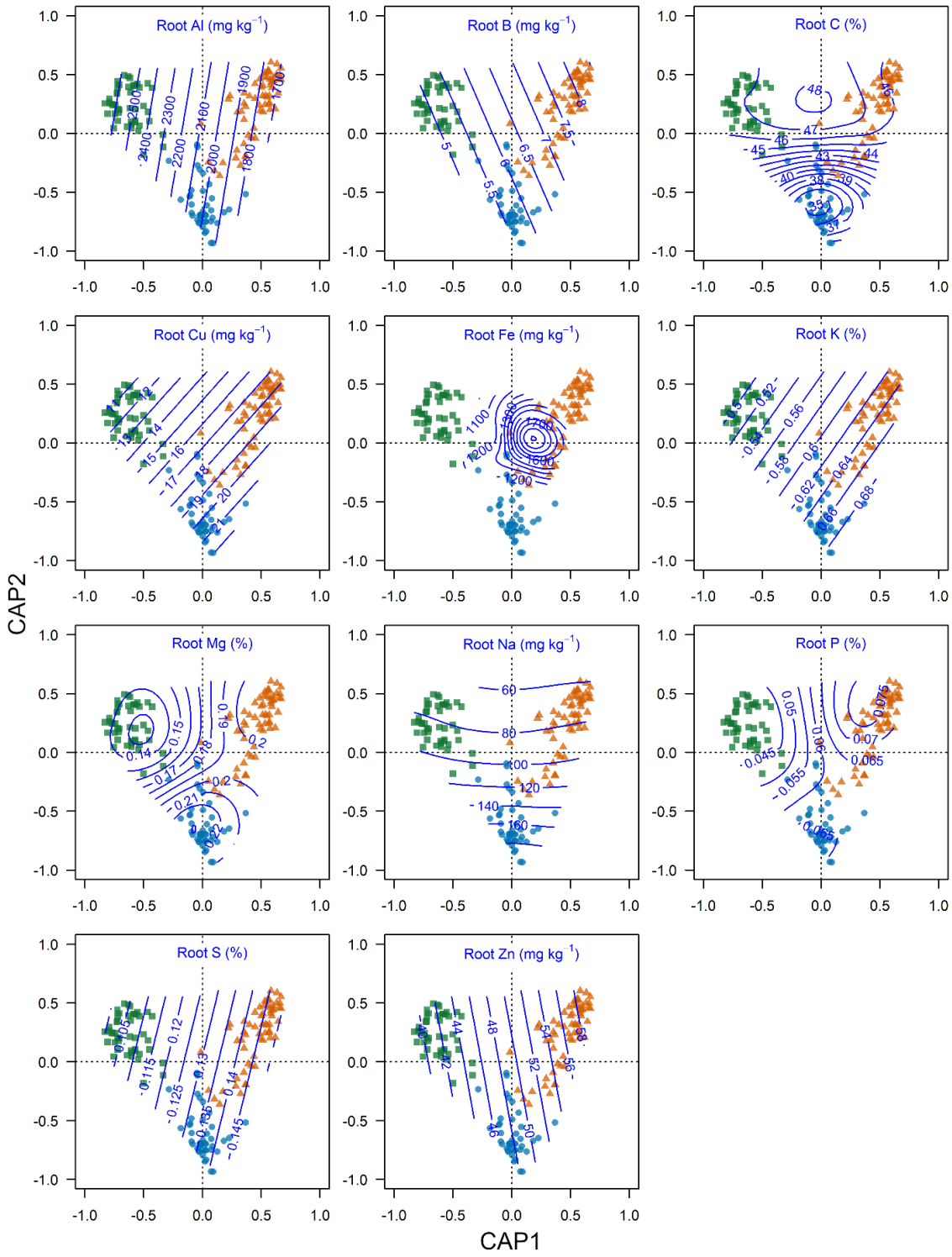

Fig. S10: Constrained ordination (db-RDA) contour plots of fitted GAM model surfaces for non-forward-selected root tissue elemental concentrations (aluminum – Al, boron – B, carbon – C, copper – Cu, iron – Fe, postassium – K, magnesium – Mg, sodium – Na, phosphorus – P, Sulfur – S, and zinc – Zn.).

Table S8: Model parameter from generalized additive models (GAMs) fitting non-forward selected root tissue elemental concentrations to the first two axes of the db-RDA. Smooth surfaces for soil variables were fit via GAMs using the 'ordisurf' function in the vegan R package (Oksanen *et al.*, 2020). Effective degrees of freedom (edf) represent the complexity of the smooth (i.e., 1 is a linear relation, 2 is a quadradic, etc.). P-values are denoted as follows: ‡ marginally significant *p*-value ($0.05 < p < 0.1$), * $p < 0.05$, ** $p < 0.01$, *** $p < 0.001$. RMSE stands for root mean squared error. The percent of model deviance explained and adjusted coefficients of determination R^2_{adj} values are given for each GAM.

Ele-ment	N	Linear term			Smooth term			Deviance explained (%)	$\boldsymbol{R^2_{adj}}$
		Int	*t*	p	edf	$F_{(edf,9)}$	*p*		
Al (‰)	150	2080.50	13.49	***	1.49	0.642	*	4.7	0.037
B (‰)	150	6.38	17.27	***	1.71	1.351	**	8.61	0.076
C (%)	150	43.52	52.83	***	4.54	3.907	***	21.6	0.191
Cu (‰)	150	16.81	8.72	***	1.39	0.49	*	3.8	0.029
Fe (‰)	150	1497.80	15.67	***	3.66	1.724	***	11.7	0.094
K (%)	150	0.60	19.51	***	1.47	0.599	*	4.4	0.035
Mg (%)	150	0.19	12.33	***	2.66	0.896	*	6.8	0.051
Na (‰)	150	103.80	15.72	***	3.19	4.33	***	22.7	0.207
P (%)	150	0.06	21.92	***	3.97	2.877	***	17.1	0.148
S (%)	150	0.13	18.27	***	1.56	0.767	*	5.4	0.044
Zn (‰)	150	49.46	8.13	***	1.04	0.241	*ns*	2.1	0.014

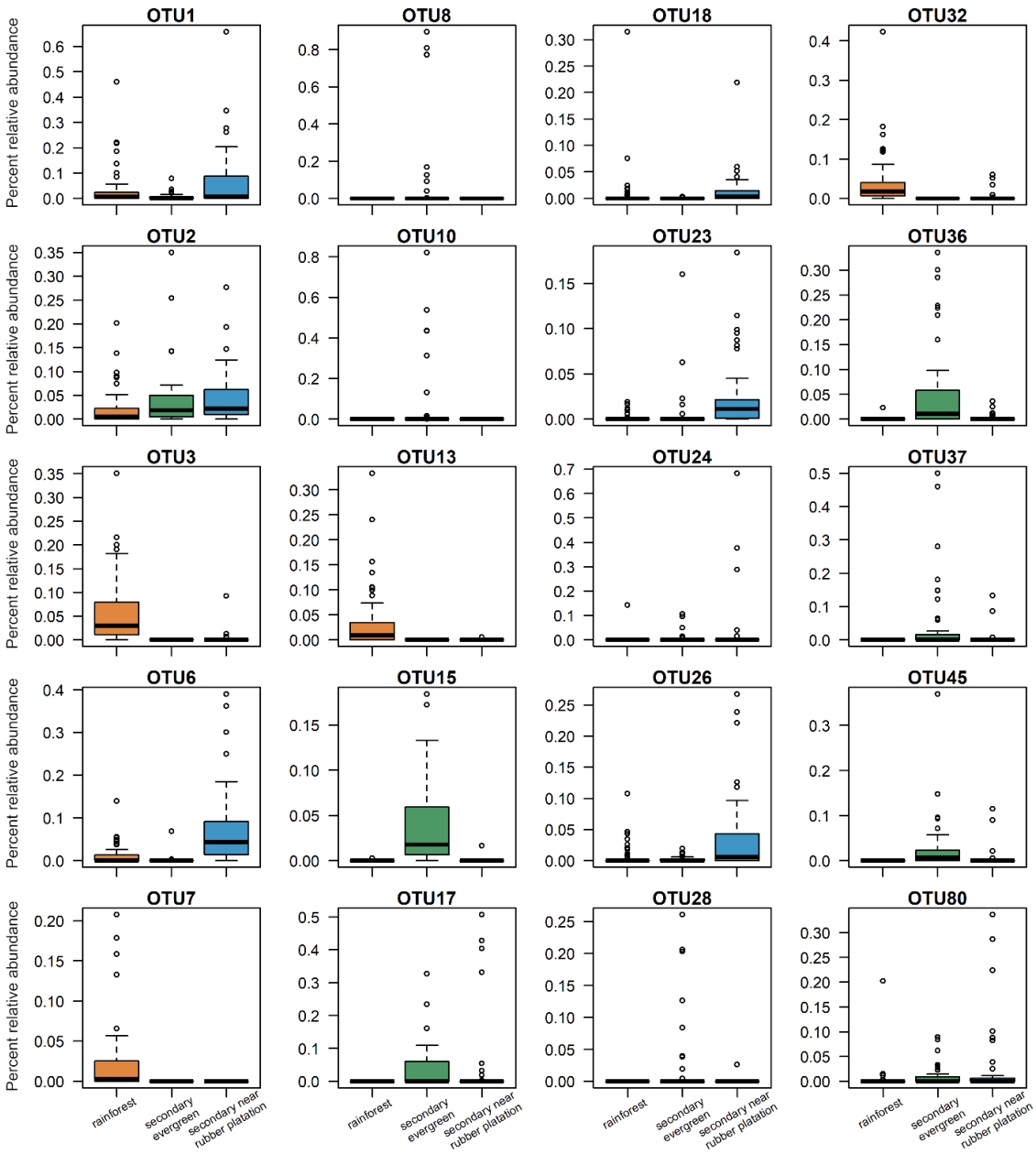

Fig. S11: Percent of relative abundance (ITS2 OTU read counts) for 20 fungi species that drove Bray-Curtis dissimilarity among root-associated fungal communities of 150 trees across 3 plots in Xishuangbanna, China. These 20 species are the discriminating species of root associated fungi among the 3 plots (identified from the SIMPER analysis). See table 4 of the main text for species taxonomic information, and pairwise comparisons of similarity percentages and associated probabilities among plots.

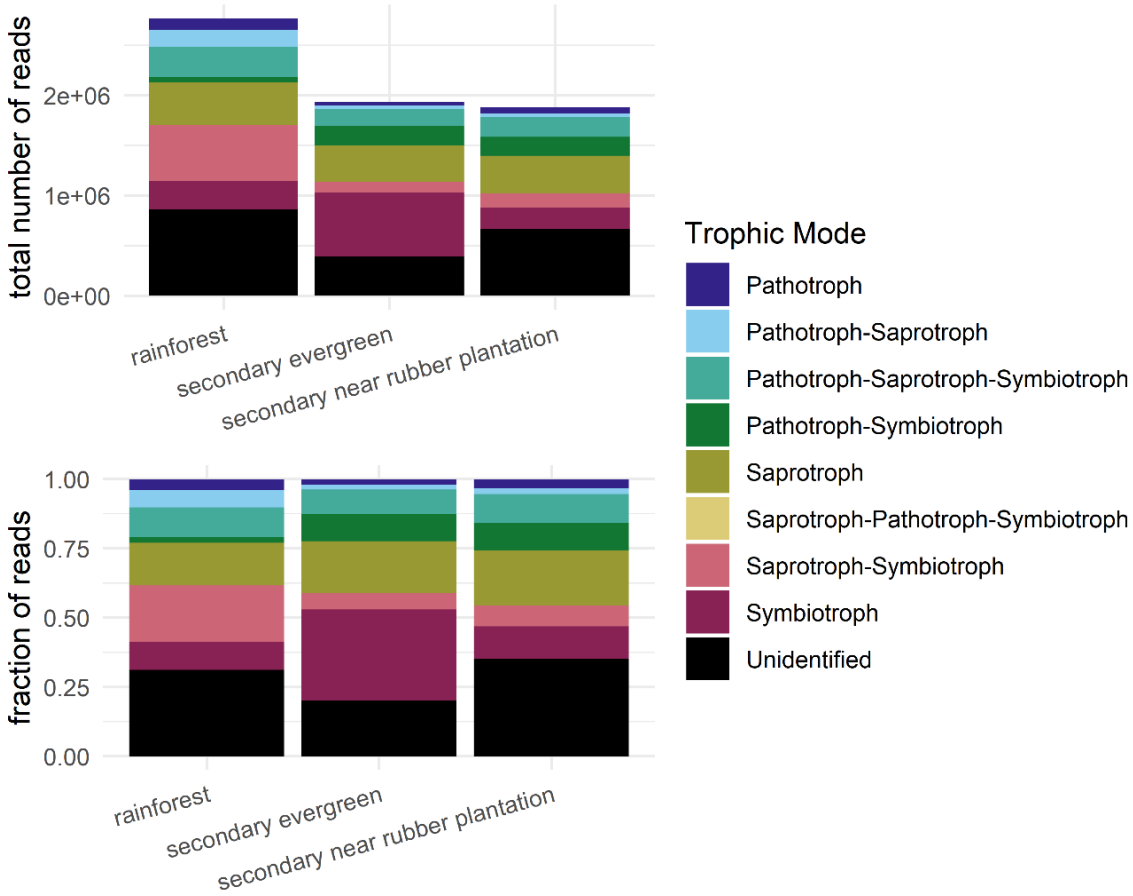

Fig. S12: Absolute (top) and relative abundance (bottom) of ITS2 sequence reads per FunGuild (Nguyen *et al.*, 2016) trophic mode classification for 150 root systems collected in 3 plots in Xishuanbanna, Yunnan, China.

Fig. S13: (next page) Absolute (top) and relative abundance (bottom) of ITS2 sequence reads per FunGuild (Nguyen *et al.*, 2016) growth morphology classification for 150 root systems collected in 3 plots in Xishuanbanna, Yunnan, China.

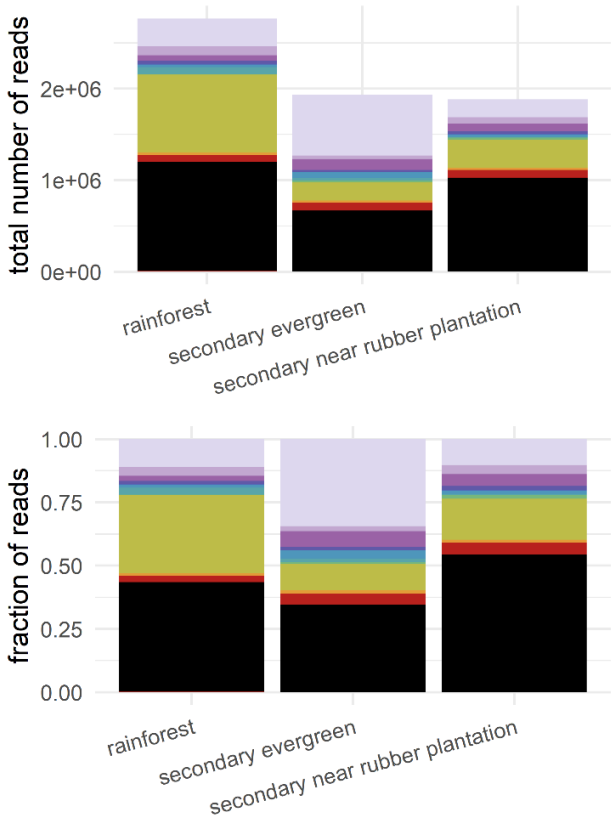

Growth Morphology

- Agaricoid
- Agaricoid-Corticioid-Gasteroid-Secotioid
- Agaricoid-Gasteroid-Microfungus-Secotioid-Yeast
- Agaricoid-Gasteroid-Secotioid
- Boletoid
- Clavarioid
- Coralloid
- Cordyceptoid
- Corticioid
- Corticioid-Gasteroid
- Corticioid-Microfungus
- Corticioid-Polyporoid
- Dark Septate Endophyte
- Facultative Yeast
- Facultative Yeast-Microfungus
- Facultative Yeast-Microfungus-Tremelloid
- Facultative Yeast-Smut
- Gasteroid
- Gasteroid-Pezizoid
- Micofungus
- Microfungus
- Microfungus-Thallus
- Microfungus-Yeast
- Microfungus; Dark Septate Microfungus
- Pezizoid
- Phalloid
- Polyporoid
- Thallus
- Tremelloid
- Tremelloid-Yeast
- Unknown
- Xylarioid
- Yeast

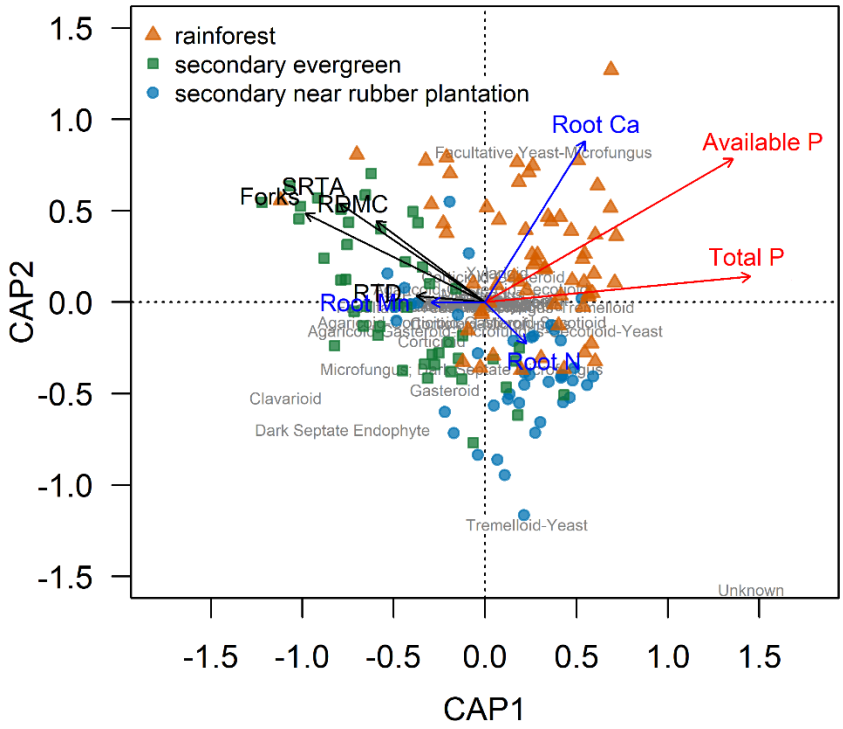

Fig. S14: Distance-base redundancy analysis by FUNGuild trophic mode. This db-RDA is statistically significant ($F_{(9,140)} = 4.94$, $p < 0.001$) and the constrained ordination axes explained 24% of the variation in root fungal community composition ($I_{total} = 16.49$, $I_{constrained} = 3.98$, $I_{unconstrained} = 12.52$). Only the first two constrained ordination axes are statistically significant (axis 1: $F_{(1,140)} = 28.03$, $p < 0.001$, axis 2: $F_{(1,140)} = 8.14$, $p < 0.001$). Additionally, only soil available P ($F_{(1,140)} = 18.94$, $p < 0.001$), soil total P ($F_{(1,140)} = 8.19$, $p < 0.001$), RDMC ($F_{(1,140)} = 5.30$, $p < 0.001$), Forks ($F_{(1,140)} = 5.32$, $p < 0.001$), and root N ($F_{(1,140)} = 2.01$, $p < 0.05$) are statistically-significant terms in this db-RDA.

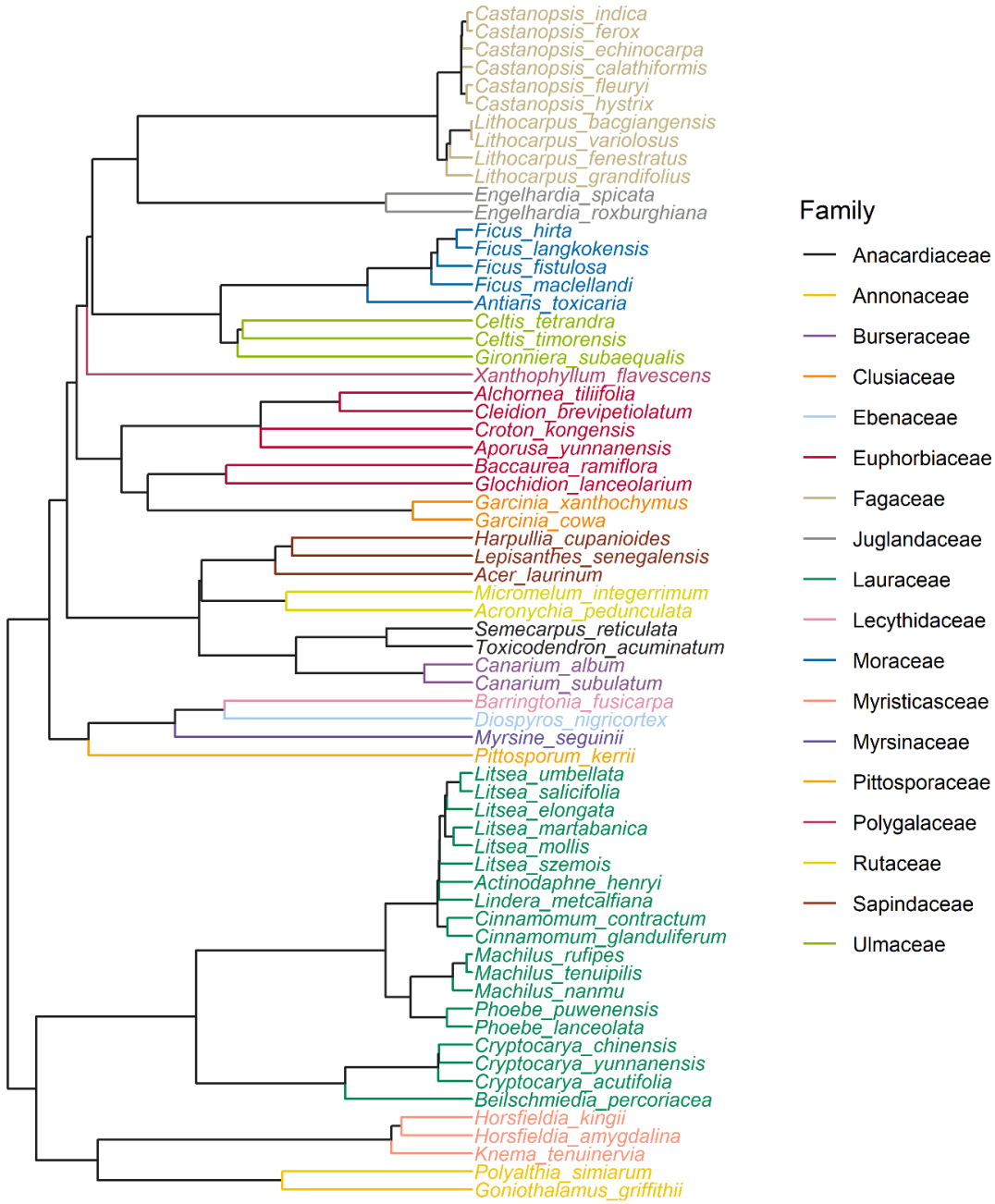

Fig. S15: Phylogenetic tree for the species sampled in this study. 150 trees from these 66 species from 18 tropical Angiosperm families were included in the analyses. This phylogeny was generated using the V.PhyloMaker R package

Table S9: Phylogenetic signal analyses of 15 root functional traits. Root trait data were average trait values by species (n = 66) from 449 entire root systems collected from 150 individual trees. Bloomberg's K and Pagel's λ were computed using the 'phytools' R package (Revell, 2012). Statistical probabilities (*p*) derived from randomization in the case of Bloomberg's K, and likelihood ratio test for Pagels λ; probabilities are denoted as follows: ‡ marginally significant p-value ($0.05 < p < 0.1$), * $p < 0.05$, ** $p < 0.01$, *** $p < 0.001$. Bolded traits are those that were forward-selected (see Table S2).

Trait	K	*p*	λ	*p*
Mass (g)	0.611	***	0.139	***
RTMF (%)	0.143	ns	0.270	**
RDMC (mg g^{-1})	0.091	‡	0.356	***
Length (cm)	0.244	**	0.498	***
SRL (cm g^{-1})	0.469	***	0.667	***
Area (cm^2)	0.295	*	0.426	**
SRA (cm^2 g^{-1})	0.509	***	0.604	***
Diam (mm)	0.244	***	0.674	***
Length/Volume (cm cm^{-3})	0.244	**	0.497	***
Volume (cm^3)	0.729	***	0.194	***
RTD (g cm^{-3})	0.677	***	0.575	***
Tips	0.305	***	0.466	***
RBI (tips $length^{-1}$)	0.250	**	0.025	*ns*
SRTA (tips g^{-1})	0.678	**	0.736	***
Forks	0.648	***	0.906	***

Table S10: Phylogenetic signal analyses of root tissue elemental concentrations Elemental concentrations were measured on compositely-ground fine root tissues for 150 individuals (see methods). Bloomberg's K and Pagel's λ were computed using the 'phytools' R package (Revell, 2012). Statistical probabilities (*p*) derived from randomization in the case of Bloomberg's K, and likelihood ratio test for Pagel's λ; probabilities are denoted as follows: ‡ marginally significant p-value ($0.05 < p < 0.1$), * $p < 0.05$, ** $p < 0.01$, *** $p < 0.001$. Bolded elements are those that were forward-selected (see Table S2).

Element	K	*p*	λ	*p*
Al (‰)	0.416	**	0.790	**
B (‰)	0.346	***	0.445	***
Ca (%)	0.368	***	0.397	**
C (%)	0.045	*ns*	<0.001	*ns*
Cu (‰)	1.034	***	0.301	***
Fe (‰)	0.230	*ns*	0.042	*ns*
K (%)	0.346	**	0.382	***
Mg (%)	0.398	***	0.353	***
Mn (‰)	0.494	***	<0.001	*ns*
Na (‰)	0.501	***	0.404	*ns*
N (%)	0.286	*	0.617	***
P (%)	0.214	‡	0.014	*ns*

S (%)	0.244	‡	0.735	***
Zn (‰)	0.174	*	0.513	***

Methods S1 Protocol for DNA Isolation using the glass milk method

DNA Isolation using glass milk (In Strip Tubes or 600 µL tubes)

Protocol written by: Michelle Jusino

Preparation:

1. Thaw samples to be processed at room temperature. Ensure that tubes are labeled appropriately, with labels that will not come off in the water bath. If need be, assign a temporary labeling system to the tops of the tubes. Ensure all tubes have CTAB in them, for those that do not, add 100 µL of CTAB and place those tubes back in the freezer for the next extraction. Proceed to step 1 below.
2. Place tubes with samples in 65 C water bath for 2 hours. Ensure that your tubes are floating appropriately, if not, remove immediately and find a better float. Once tubes containing samples have been cooked, they may sit at room temperature or be placed back into the freezer if there is not time to proceed with the extraction on the same day.

Extraction:

1. Working in a PCR hood, set-up up to 6 rows of strip tubes (this would be for 47 samples and one negative), or one 600 µL tube for each sample. Label your tubes or strip tubes, and if using strip tubes be sure to pay attention to orientation and be sure to label each strip tube for orientation and row number.
2. Spin all samples for 1 minute at 10000 rcf.
3. Using a filtered pipette tip (for every pipetting step), pipette 100 µL of supernatant and transfer to a new well of a strip tube, or a new 600 µL tube. Avoid any debris present in the buffer. (**If samples are to be combined do so at this time by removing an equal amount of supernatant from each sample and placing them in the same strip tube. Total combined volume should be 100 µL). The remainder of the CTAB (and the sample) can be re-frozen and used for a future extraction.
4. Add 150 µL of ice-cold isopropanol (stored in freezer) to each sample and gently invert several times to mix.
5. Place samples in -80 °C freezer for 5-7 min.
6. Centrifuge at 0 °C and 10000 rcf for 20 min in a refrigerated centrifuge. Be sure to pay attention to tube orientation. Increase centrifuge temperature to 20°C when done.
7. Gently remove and discard supernatant, taking care not to disturb the pellet at the bottom of the tube. Note that the pellet may not be visible.
8. Add 175 µL 70% EtOH to tube to wash pellet.
9. Centrifuge at RT (room temperature) for 5 min at maximum speed. Be sure to use the same tube orientation as before.
10. Gently remove and discard supernatant, air dry pellet for at least 15 min.

11. Add 45 µL of molecular grade (MG) sterile DNA-free water.
12. Add 135 µL of NaI solution**.
13. Add 2.5 µL of glass milk**. Be sure to vortex the stock glass milk tube frequently because it settles out rapidly. If using the multichannel pipette tip mix prior to withdrawing each aliquot.
14. Close tubes and vortex quickly, then immediately place the tubes upside down in a microtiter plate. Sandwich plate with strips using another strip tube rack and rubber band together. Place tube sandwich rack on Vortex and vortex the tubes upside down for 5 min.
15. Centrifuge at RT and maximum speed for 8 sec.
16. Remove and discard supernatant.
17. Add 175 µL of New Wash** and tip mix to disperse pellet.
18. Vortex for 5 min as per step 14.
19. Centrifuge as per step 15.
20. Remove New Wash and discard.
21. Air dry pellet for at least 30 min.
22. Add 50 µL of sterile water and tip mix to disperse pellet.
23. Vortex to resuspend pellet.
24. Centrifuge at RT and maximum speed for 35 sec.
25. Remove supernatant containing clean DNA, and transfer the supernatant to a plate or new strip tubes for storage at -20°C.

*CTAB lysis buffer
1.4 M NaCl
0.1 M Tris-HCl
20 mM EDTA
2% CTAB
pH adjusted to 7.0

**From GeneClean III kits (cat 1001-600) by Qbiogene (www.qbiogene.com)

References

Blanchet FG, Legendre P, Borcard D. 2008. Forward Selection of Explantory Variables. *Ecology* 89(9): 2623-2632.

Fay MF, Swensen SM, Chase MW. 1997. Taxonomic affinities of Medusagyne oppositifolia (Medusagynaceae). *Kew Bulletin*: 111-120.

Ihrmark K, Bödeker I, Cruz-Martinez K, Friberg H, Kubartova A, Schenck J, Strid Y, Stenlid J, Brandström-Durling M, Clemmensen KE. 2012. New primers to amplify the fungal ITS2 region–evaluation by 454-sequencing of artificial and natural communities. *FEMS microbiology ecology* 82(3): 666-677.

Kohout P, Sudová R, Janoušková M, Čtvrtlíková M, Hejda M, Pánková H, Slavíková R, Štajerová K, Vosátka M, Sýkorová Z. 2014. Comparison of commonly used primer sets for evaluating arbuscular mycorrhizal fungal communities: is there a universal solution? *Soil Biology and Biochemistry* 68: 482-493.

Kress WJ, Erickson DL, Jones FA, Swenson NG, Perez R, Sanjur O, Bermingham E. 2009. Plant DNA barcodes and a community phylogeny of a tropical forest dynamics plot in Panama. *Proceedings of the National Academy of Sciences* 106(44): 18621-18626.

Lekberg Y, Vasar M, Bullington LS, Sepp SK, Antunes PM, Bunn R, Larkin BG, Öpik M. 2018. More bang for the buck? Can arbuscular mycorrhizal fungal communities be characterized adequately alongside other fungi using general fungal primers? *New Phytologist* 220(4): 971-976.

Levin RA, Wagner WL, Hoch PC, Nepokroeff M, Pires JC, Zimmer EA, Sytsma KJ. 2003. Family-level relationships of Onagraceae based on chloroplast rbcL and ndhF data. *American Journal of Botany* 90(1): 107-115. (modified from Soltis P *et al.* (1992) *Proceedings of National Academy of Sciences USA,* 89: 449-451).

Nguyen NH, Song Z, Bates ST, Branco S, Tedersoo L, Menke J, Schilling JS, Kennedy PG. 2016. FUNGuild: An open annotation tool for parsing fungal community datasets by ecological guild. *Fungal Ecology* 20: 241-248.

Oksanen J, Blanchet F, Friendly M, Kindt R, Legendre P, McGlinn D, Minchin PR, O'Hara RB, L. SG, Stevens HH, et al. 2020. vegan: community ecology package. R package version 2.5-7.

Revell LJ. 2012. phytools: an R package for phylogenetic comparative biology (and other things). *Methods in ecology and evolution* 3(2): 217-223.

Appendix to Chapter 5: The physiological acclimation and growth response of *Populus trichocarpa* to warming

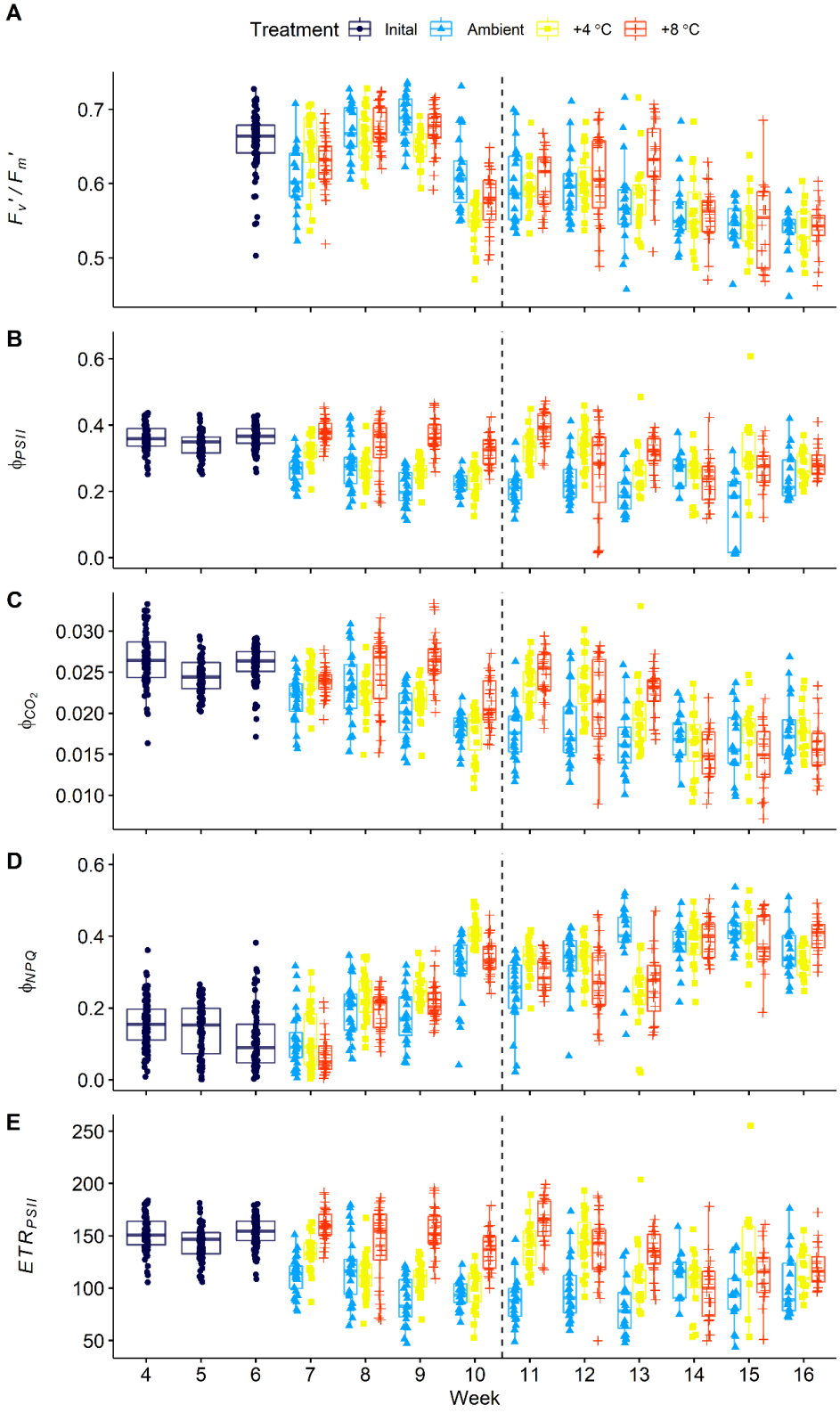

Fig. S1 (previous page): Key Chlorophyll (Chl) florescence parameters over time and by treatment for experimentally warmed *P. trichocarpa* clones. A) Chl florescence ratio (F_v'/F_m'), where F_v' is light-adapted variable Chl fluorescence and $F_m'$is maximal, light-adapted Chl fluorescence B) the quantum efficiency of photosystem II (Φ_{PSII}), calculated as $\frac{(F_m'-F_s)}{F_m'}$, where F_m' is as before and F_s is steady-state Chl fluorescence C) the quantum yield of CO_2 assimilation corrected for dark respiration (Φ_{CO_2}), calculated as $\frac{(A-R_d)}{Q_{abs}}$, where A is photosynthetic rate, R_d is leaf dark respiration rate, and Q_{abs} is the leaf absorption of photosynthetically active radiation, and D) the quantum yield of non-photochemical quenching (Φ_{NPQ}), calculated as $\left(\frac{(F_m-F_m')}{F_m}\right) \times \left(\frac{F_s}{F_m'}\right)$, where F_s and F_m' are as before and F_m is dark-adapted maximum Chl fluorescence, and E) C (ETR_{PSII}) in µmol m^{-2} s^{-1}, calculated as $\Phi PSII \times i \times \alpha \times f_{II}$, where i, is incident light intensity, α is leaf absorbance, and f_{II} is the fraction of light partitioned to *PSII* versus *PSI*. Note: the dotted line shows when plants were trimmed to 1.5m height.

List S1: Pulse-modulated flash fluorometer settings used throughout the experiment for the Li-COR Li-6800:

- Measuring beam: Dark mod rate = 5KHz, Light mod rate = 50 KHz, flash mod rate = 500 KHz, averaging = 15s,
- Multiphase flash: red target = 10000 µmol m^{-2} s^{-1}, phase 1, 2 & 3 = 300 ms, ramp = 40%, output rate = 500 Hz, margin = 5,
- Dark pulse: far red target = 25 µmol m^{-2} s^{-1}, duration = 5s, before & after = 1s, margin = 5.

Parameter (units) - explanation	Stable if:
ΔH_2O (mmol mol^{-1}) – measures the difference in [H_2O] between the reference and sample IRGA.	Slope < 0.5
ΔCO_2 (µmol mol^{-1}) – measures the difference in [CO_2] between the reference and sample IRGA.	Slope < 1 Standard deviation < 0.75
g_{sw} (mol m^{-2} s^{-1}) – calculated rate of leaf stomatal conductance to water vapor	Slope < 0.1
A (µmol m^{-2} s^{-1}) – calculated rate of leaf CO_2 assimilation.	Slope < 0.5 Standard deviation < 0.5

Table S1: Stability criteria for all photosynthesis measurements (i.e. both survey measurements and photosynthetic response curves) taken using the Li-6800 portable photosynthesis system (Li-COR Inc., Lincoln, NE). Stability assessed for all criteria over a 15 second window.

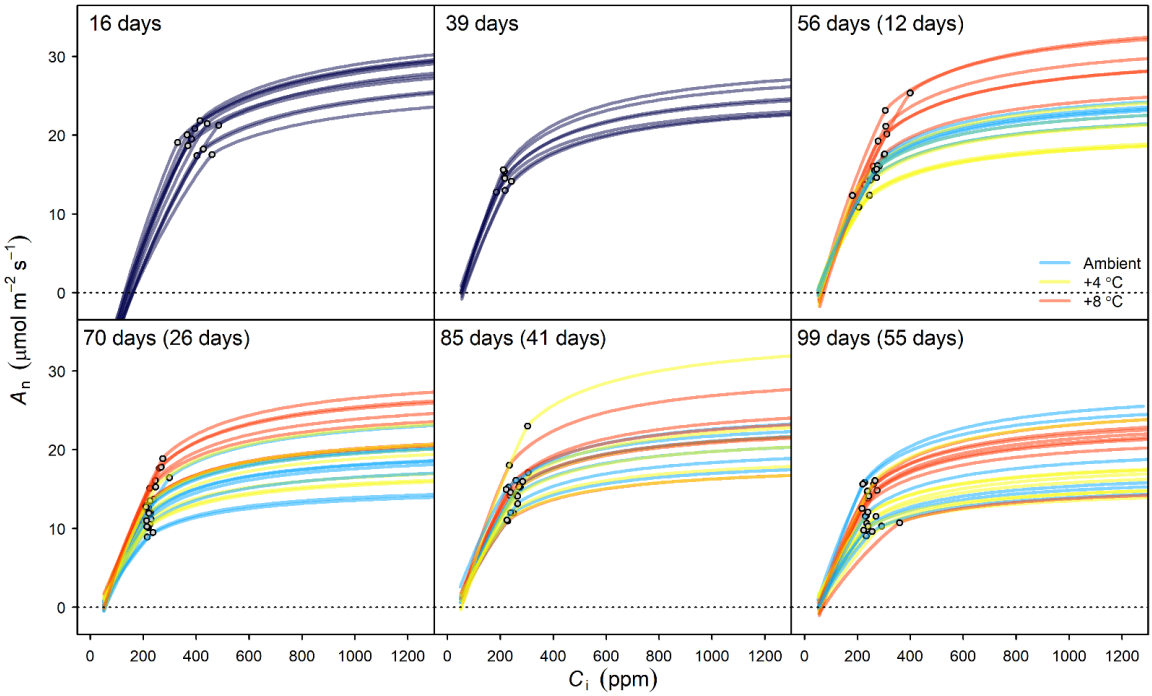

Fig. S2: Fitted photosynthetic CO_2 response curves over time and by treatment for experimentally warmed *P. trichocarpa* clones. Open circles show the c_i transition point for each CO_2 response curve (i.e., the c_i value at which photosynthesis shifts from V_{cmax}-limited: $c_i < c_i$ transition to Jmax limited: $c_i > c_i$ transition). Curves fitted with the 'plantecophys' R package (Duursma, 2015). See table 3 for key parameters from CO_2 response curve fits. The number of days since planting and since the beginning or warming (in parentheses) is given in the upper left corner of the graph panels.

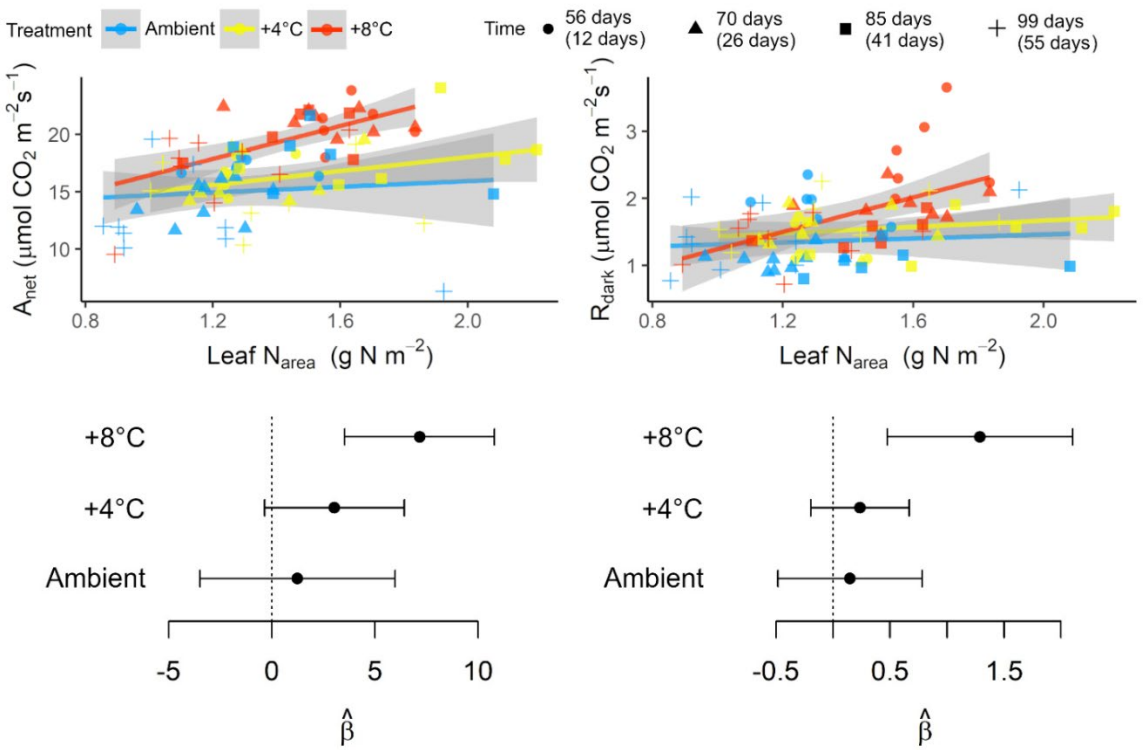

Fig. S3: (top left) Linear relationships of the net photosynthetic rate at 400 µmol mol^{-1} CO_2 (A_{net}) and leaf nitrogen per area (Leaf N_{area}) by treatment over time. (top right). Linear relationships of leaf dark respiration (R_{dark}) and leaf nitrogen per area (Leaf N_{area}) by treatment over time. Points represent the measurements in time (given in days, with the number of days since warming in parentheses), and colors represent the warming treatments. (bottom) slope parameters with 95% confidence intervals for the linear relationships, showing that there are relationship of leaf photosynthesis and dark respiration with leaf nitrogen per areas is statistically different in the +8°C treatment than in the two others. The A_{net} measurement was taken as the first point measured on the A-C_i curve routine (i.e., at 400 ppm CO_2), and R_{dark} was taken from the light curve routine at 0 µmol m^{-2} s^{-1} light intensity. We explored the relationships using assimilation and respiration rates at 29°C from temperature response curves, assimilation rates at T_{opt} from photosynthesis-temperature response curves, and estimated R_d rates from A-C_i curve fits, and they were only slightly different (not shown), with all relationships justifying standardizing leaf gas exchange measurements by leaf nitrogen content, in order to help reduce variability among treatments attributable to leaf N.

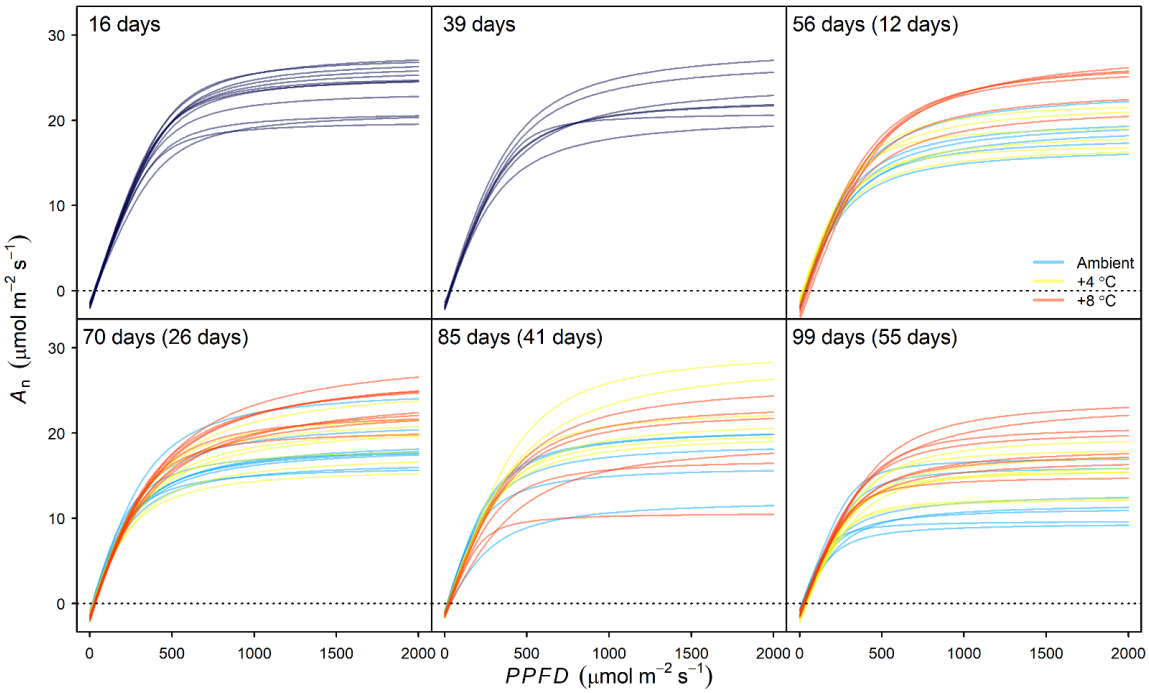

Fig. S4: Fitted light response curves over time and by treatment for experimentally warmed *P. trichocarpa* clones, with light (photosynthetic photon flux density, *PPFD*) on the x-axis and net rates of CO_2 assimilation (A_n) on the y-axis. Curves fitted using code from Heberling & Fridley (2013). See Table 4 for parameters describing light curve fits. The number of days since planting and since the beginning or warming (in parentheses) is given in the upper corner of the graph panels.

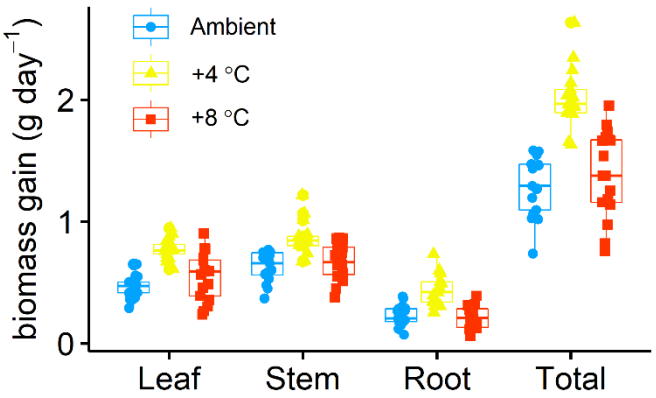

Fig. S5: Plotted rates of leaf, root, stem and total biomass gain (in grams per day) by treatment for experimentally warmed *P. trichocarpa* clones. See table 2 for means ± 95% confidence intervals and statistical grouping of ANOVAs with Tukey HSD tests. For leaf, stem, root and total biomass gain, the +4°C treatment was statistically greater than the other two treatments.2

Table S2: Analysis of Variances (ANOVA) table for leaf photosynthetic parameters over time. Parameters are the same as those included in Table 2. Abbreviations are as follows: DFn, degrees of freedom in the numerator of the *F*-statistic, DFd, degrees of freedom in the denominator of the *F*-statistic, η^2, eta-squared effect size estimator. η^2 values can be interpreted as the proportion of variation in the parameter due to treatment. ANOVAs were done separately for each time, and probabilities were Bonferroni corrected (adjusted *p*). Asterisks denote a statistically-significant ANOVA prior to Bonferroni correction. Statistically significant results after Bonferroni correction are bolded. See Table 2 for parameter means and standard errors and Tukey HSD pairwise comparisons. [$]adjusted *p*-value is marginally significant, Tukey HSD groups statistically distinct in Table 2.

Parameter	Time	DFn	DFd	*F*	*p*	$p < .05$	η^2	adjusted *p*
T_{opt}	56 days (12 days)	2	15	33.144	3.13E-6	*	0.815	1.25E-5
	70 days (28 days)	2	21	21.291	8.88E-6	*	0.670	3.55E-5
	85 days (41 days)	2	15	18.424	9.12E-5	*	0.711	3.65E-4
	99 days (55 days)	2	22	46.281	1.31E-8	*	0.808	5.24E-8
A_{opt}	56 days (12 days)	2	15	2.158	0.15		0.223	0.60
	70 days (28 days)	2	21	10.773	6.03E-4	*	0.506	2.41E-3
	85 days (41 days)	2	15	0.642	0.54		0.079	1.00
	99 days (55 days)	2	22	6.911	5.00E-3	*	0.386	0.02
Leaf $R_{d,29}$	56 days (12 days)	2	15	3.240	0.07		0.302	0.27
	70 days (28 days)	2	22	2.556	0.10		0.189	0.40
	85 days (41 days)	2	15	8.754	3.00E-3	*	0.539	0.01
	99 days (55 days)	2	22	4.821	0.02	*	0.302	0.07[$]
Q_{10} R_d	56 days (12 days)	2	15	1.858	0.19		0.199	0.76
	70 days (28 days)	2	21	3.396	0.05		0.244	0.21
	85 days (41 days)	2	15	2.785	0.09		0.271	0.38
	99 days (55 days)	2	22	1.296	0.29		0.105	1.00
$A_{net,29}$	56 days (12 days)	2	15	1.429	0.27		0.160	1.00
	70 days (28 days)	2	22	4.829	0.02	*	0.305	0.07[$]
	85 days (41 days)	2	15	0.765	0.48		0.093	1.00
	99 days (55 days)	2	22	3.702	0.04	*	0.252	0.64
$V_{cmax,25}$	56 days (12 days)	2	15	7.340	6.00E-3	*	0.495	0.02
	70 days (28 days)	2	21	6.807	5.00E-3	*	0.393	0.02
	85 days (41 days)	2	15	0.353	0.35		0.130	1.00

	99 days (55 days)	2	22	0.124	0.12		0.173	0.50
$J_{max,25}$	56 days (12 days)	2	15	24.429	1.91E-5	*	0.765	7.64E-5
	70 days (28 days)	2	21	8.057	3.00E-3	*	0.434	1.20E-2
	85 days (41 days)	2	15	0.503	0.62		0.063	1.00
	99 days (55 days)	2	21	2.524	0.10		0.187	0.41

Table S3: Mean ± se for the maximum rate of light saturated photosynthesis (A_{max}), apparent quantum yield (Φ), dark respiration rate – measured from light response curves (R_d), light response convexity (θ), light compensation point (I_{comp}), and light saturation point ($I_{sat(75\%)}$) by treatment and over time. Parameter estimates derived from fitted photosynthetic light-response curves for each leaf (see Fig. S3). Parameter estimates are at treatment temperature (see table 1). Numbers in parentheses in the Time column are the number of warmed days at the time of measurement. See Table S3 for repeated measures ANOVA statistics. Letters denote statistical groupings from Tukey HSD post-hoc tests; Tukey tests were done within each measurement time to account for repeated measures; thus, letters can only be compared among treatments within each time. See Fig. S8 for plots of these parameters over time by treatment.

Treatment	Time	N	A_{max} (µmol m^{-2} s^{-1})	Φ (mol CO_2 mol $photons^{-1}$)	R_d (µmol m^{-2} s^{-1})	Θ	I_{comp} (µmol m^{-2} s^{-1})	$I_{sat(75\%)}$ (µmol m^{-2} s^{-1})
Initial	16 days	12	26.57 ± 0.85	0.057 ± 0.004	1.75 ± 0.07	0.89 ± 0.01	30.8 ± 0.9	478.5 ± 12.3
Initial	39 days	7	25.92 ± 1.22	0.060 ± 0.002	1.89 ± 0.11	0.79 ± 0.03	32.0 ± 1.5	559.4 ± 36.7
Ambient	56 days (12 days)	6	21.83 ± 0.94^{A}	0.062 ± 0.001^{B}	1.90 ± 0.12^{AB}	0.68 ± 0.02^{A}	31.5 ± 2.3^{AB}	559.8 ± 19.8^{B}
+4°C		6	20.91 ± 0.95^{A}	0.059 ± 0.001^{AB}	1.30 ± 0.12^{A}	0.77 ± 0.03^{A}	22.4 ± 2.1^{A}	470.6 ± 24.3^{A}
+8°C		6	28.58 ± 1.13^{B}	0.058 ± 0.001^{A}	2.50 ± 0.27^{B}	0.77 ± 0.02^{A}	43.8 ± 5.2^{B}	671.3 ± 27.3^{C}
Ambient		9	20.46 ± 0.93^{A}	0.066 ± 0.001^{B}	1.10 ± 0.04^{A}	0.68 ± 0.02^{A}	17.0 ± 0.7^{A}	477.7 ± 23.4^{A}

+4°C	70 days (28 days)	8	22.19 ± 1.16^{A}	0.061 ± 0.001^{A}	1.43 ± 0.11^{B}	0.69 ± 0.03^{A}	23.9 ± 1.6^{B}	561.3 ± 38.5^{A}
+8°C		9	27.03 ± 1.04^{B}	0.061 ± 0.001^{A}	1.73 ± 0.08^{C}	0.68 ± 0.04^{A}	29.1 ± 1.3^{C}	702.6 ± 48.7^{B}
Ambient	85 days (41 days)	5	20.46 ± 0.93^{A}	0.061 ± 0.005^{A}	1.03 ± 0.08^{A}	0.74 ± 0.02^{A}	18.5 ± 3.8^{A}	437.4 ± 30.7^{A}
+4°C		6	25.52 ± 1.94^{A}	0.059 ± 0.001^{A}	1.43 ± 0.13^{B}	0.77 ± 0.03^{A}	24.4 ± 2.2^{A}	573.9 ± 55.3^{A}
+8°C		6	21.36 ± 2.25^{A}	0.051 ± 0.002^{A}	1.33 ± 0.09^{AB}	0.79 ± 0.03^{A}	26.8 ± 2.4^{A}	552.7 ± 76.5^{A}
Ambient	99 days (55 days)	7	13.82 ± 1.19^{A}	0.053 ± 0.002^{A}	1.17 ± 0.15^{A}	0.81 ± 0.04^{A}	22.8 ± 3.1^{A}	329.3 ± 25.2^{A}
+4°C		8	17.87 ± 1.02^{AB}	0.049 ± 0.001^{A}	1.38 ± 0.12^{B}	0.87 ± 0.01^{A}	34.5 ± 2.5^{B}	408.5 ± 24.7^{AB}
+8°C		8	21.12 ± 1.23^{B}	0.052 ± 0.001^{A}	1.32 ± 0.10^{AB}	0.81 ± 0.03^{A}	25.6 ± 1.9^{A}	501.3 ± 37.1^{B}

Table S4: Analysis of Variances (ANOVA) table for leaf photosynthesis light curve parameters over time. Parameters are the same as those included in Table S2. Abbreviations are as follows: DFn, degrees of freedom in the numerator of the *F*-statistic, DFd, degrees of freedom in the denominator of the *F*-statistic, η^2, eta-squared effect size estimator. η^2 values can be interpreted as the proportion of variation in the parameter due to treatment. ANOVAs were done separately for each time, and probabilities were Bonferroni corrected (adjusted *p*). Asterisks denote a statistically-significant ANOVA prior to Bonferroni correction. Statistically significant results after Bonferroni correction are bolded. See Table S2 for parameter means and standard errors and Tukey HSD pairwise comparisons. $^{\$}$adjusted *p*-value is marginally significant, with Tukey HSD groups statistically distinct in Table S2.

Parameter	Time	DFn	DFd	*F*	*p*	$p < .05$	η^2	adjusted *p*
A_{max}	56 days (12 days)	2	15	17.099	1.35E-4	*	0.695	5.40E-4
	70 days (28 days)	2	23	11.097	4.23E-4	*	0.491	1.69E-3
	85 days (41 days)	2	14	2.878	0.09		0.291	0.36
	99 days (55 days)	2	20	9.769	1.00E-3	*	0.494	4.00E-3

Φ	56 days (12 days)	2	15	4.250	3.40E-2	*	0.362	0.14[$]
	70 days (28 days)	2	23	9.964	7.64E-4	*	0.464	3.06E-3
	85 days (41 days)	2	14	3.215	0.07		0.315	0.24
	99 days (55 days)	2	20	2.452	0.11		0.197	0.45
R_d	56 days (12 days)	2	15	10.535	1.00E-3	*	0.584	4.00E-2
	70 days (28 days)	2	23	16.178	4.11E-5	*	0.585	1.64E-4
	85 days (41 days)	2	14	3.649	5.30E-2		0.343	0.21
	99 days (55 days)	2	20	4.072	3.30E-2	*	0.289	0.13[$]
θ	56 days (12 days)	2	15	3.947	0.04	*	0.345	0.17[$]
	70 days (28 days)	2	23	0.053	0.95		0.005	1.00
	85 days (41 days)	2	14	0.687	0.52		0.089	1.00
	99 days (55 days)	2	20	1.734	0.20		0.148	0.81
I_{comp}	56 days (12 days)	2	15	9.517	2.00E-3	*	0.559	8.00E-3
	70 days (28 days)	2	23	25.223	1.59E-6	*	0.687	6.36E-6
	85 days (41 days)	2	14	2.325	0.13		0.249	0.54
	99 days (55 days)	2	20	6.083	9.00E-3	*	0.378	3.60E-2
$I_{sat(75\%)}$	56 days (12 days)	2	15	17.554	1.185E-4	*	0.701	4.74E-4
	70 days (28 days)	2	23	9.114	1.00E-3	*	0.442	4.00E-3
	85 days (41 days)	2	14	1.403	0.28		0.167	1.00
	99 days (55 days)	2	20	8.082	3.00E-3	*	0.447	1.20E-2

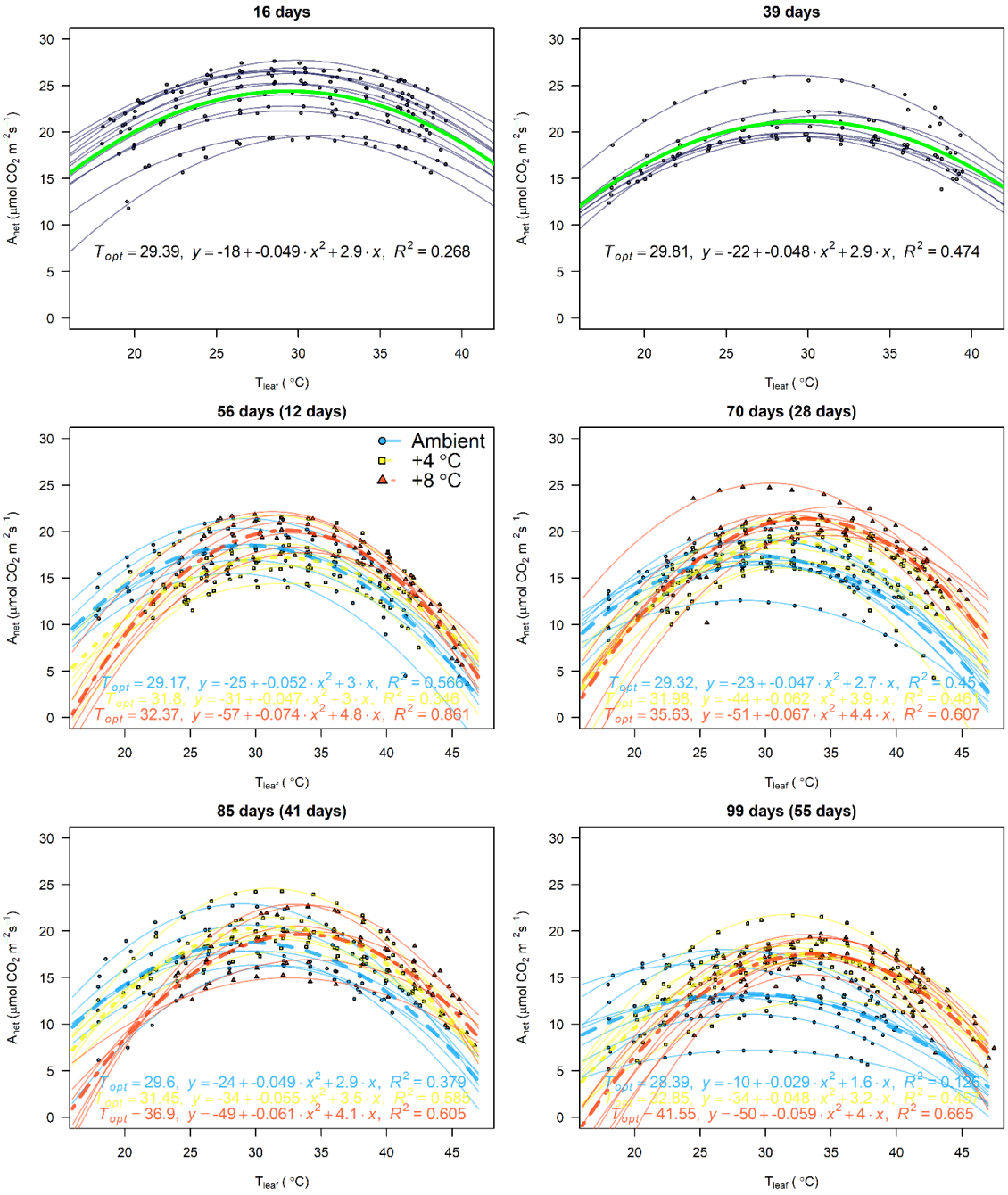

Fig. S6: Photosynthetic-temperature response curves over time. These plots accompany Fig. 2 to show model fits for each leaf for which a response curve was done. Model equations are shown for quadradic models fit to all data per treatment (i.e., thicker lines). T_{opt} was calculated via the maximum of the quadradic model fit. The top two panels were done prior to experimental warming when all plants were in greenhouse conditions. The number of days since planting and since the beginning or warming (in parentheses) is given in on top of each graph panel.

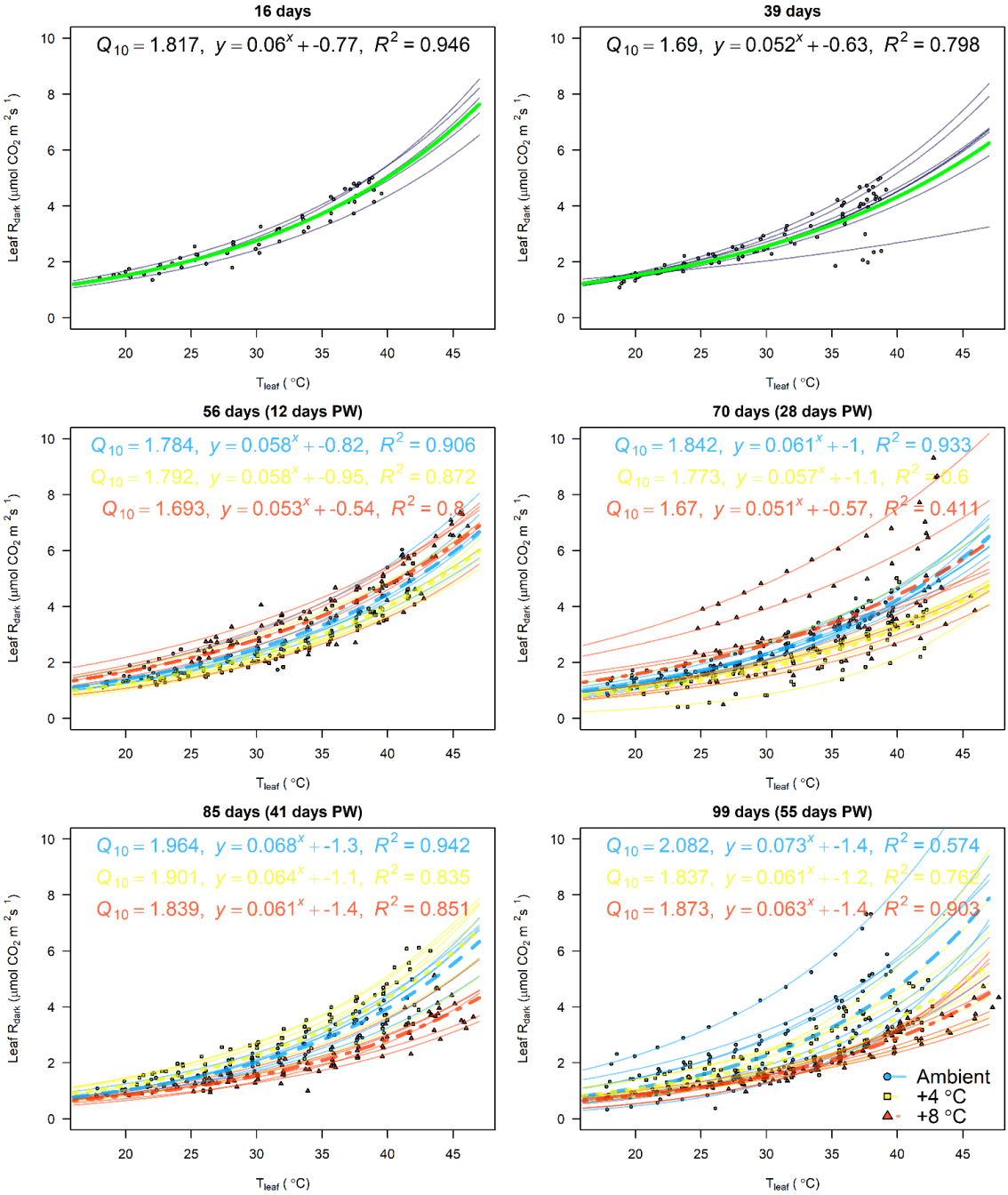

Fig. S7: Dark respiration-temperature response curves over time. These plots accompany Fig. 2 to show fits for each leaf for which a response curve was done. Model equations are shown for exponential models fit to all data per treatment (i.e. thicker lines). Q_{10} values were calculated using the value of the exponent from the model fits (see methods). The top two panels were done prior to experimental warming when all plants were in greenhouse conditions. The number of days since planting and since the beginning or post warming (in parentheses) is given on top of each graph panel.

Treatment	Time	N	SLA ($cm^2\ g^{-1}$)	LDMC ($mg\ g^{-1}$)	Leaf N (%)	Leaf C (%)	Leaf N_{area} ($g\ N\ m^{-2}$)
Ambient	56 days (12 days)	6	251.1 ± 15.1^{B}	282.1 ± 11.5^{A}	3.22 ± 0.09^{A}	45.14 ± 0.30^{A}	1.30 ± 0.06^{A}
+4°C		7	260.1 ± 10.6^{B}	331.6 ± 11.5^{A}	3.33 ± 0.07^{A}	45.62 ± 0.30^{A}	1.28 ± 0.04^{A}
+8°C		6	204.0 ± 5.1^{A}	412.6 ± 30.5^{B}	3.33 ± 0.06^{A}	45.71 ± 0.30^{A}	1.64 ± 0.05^{B}
Ambient	70 days (28 days)	9	291.9 ± 8.4^{B}	238.7 ± 8.4^{A}	3.47 ± 0.14^{A}	45.93 ± 0.24^{B}	1.19 ± 0.04^{A}
+4°C		8	281.9 ± 12.2^{AB}	250.3 ± 6.9^{AB}	3.74 ± 0.15^{A}	45.59 ± 0.26^{AB}	1.34 ± 0.07^{A}
+8°C		7	245.3 ± 15.8^{A}	275.5 ± 12.3^{B}	3.77 ± 0.13^{A}	45.01 ± 0.26^{A}	1.56 ± 0.06^{B}
Ambient	85 days (41 days)	6	155.0 ± 8.1^{B}	353.8 ± 10.8^{A}	2.35 ± 0.09^{B}	43.61 ± 0.30^{A}	1.54 ± 0.12^{A}
+4°C		6	122.4 ± 12.0^{A}	554.7 ± 82.6^{B}	1.96 ± 0.13^{A}	43.84 ± 0.30^{A}	1.81 ± 0.14^{A}
+8°C		6	159.3 ± 5.3^{B}	334.7 ± 4.5^{A}	2.30 ± 0.08^{AB}	42.87 ± 0.29^{A}	1.46 ± 0.08^{A}
Ambient	99 days (55 days)	6	202.4 ± 12.0^{B}	334.8 ± 30.4^{A}	2.27 ± 0.22^{A}	43.78 ± 0.24^{A}	1.13 ± 0.11^{A}
+4°C		8	151.8 ± 18.3^{A}	500.8 ± 88.8^{A}	2.02 ± 0.17^{A}	44.32 ± 0.28^{A}	1.37 ± 0.12^{A}
+8°C		8	177.8 ± 9.9^{AB}	388.0 ± 33.4^{A}	2.09 ± 0.05^{A}	43.52 ± 0.24^{A}	1.20 ± 0.07^{A}

Table S5: Leaf morphological traits and tissue chemistry (mean ± se) over time and by experimental treatment for *P. trichocarpa* clones. Abbreviations are: SLA (specific leaf area), leaf dry matter content (LDMC), nitrogen (N), carbon (C). Numbers in parentheses in the Time column are number of warmed days at the time of measurement. See Table S5 for repeated measures ANOVA statistics. Letters denote statistical groupings from Tukey HSD post-hoc tests; Tukey tests were done within each measurement time to account for repeated measures; thus letters can only be compared among treatments within each time. For a visual representation of these data, see Fig. S8 .

Trait	Time	DFn	DFd	F	p	$p < .05$	η^2	adjusted p
SLA	56 days (12 days)	2	15	7.444	6.00E-3	*	0.498	0.02
	70 days (28 days)	2	22	3.991	3.30E-2	*	0.266	0.13[$]
	85 days (41 days)	2	15	8.459	3.00E-3	*	0.530	0.01
	99 days (55 days)	2	22	3.523	4.70E-2	*	0.243	0.19[$]
LDMC	56 days (12 days)	2	15	10.890	0.001	*	0.592	4.00E-3
	70 days (28 days)	2	22	4.022	0.032	*	0.268	0.13
	85 days (41 days)	2	15	6.081	0.012	*	0.448	4.80E-2
	99 days (55 days)	2	22	2.521	0.103		0.186	0.41
Leaf N	56 days (12 days)	2	15	0.722	0.50		0.088	1.00
	70 days (28 days)	2	22	0.276	0.28		0.111	1.00
	85 days (41 days)	2	15	0.032	0.03	*	0.369	0.13[$]
	99 days (55 days)	2	22	0.562	0.56		0.051	1.00
Leaf C	56 days (12 days)	2	15	1.756	0.21		0.190	0.82
	70 days (28 days)	2	22	7.710	3.00E-3	*	0.412	0.01
	85 days (41 days)	2	15	2.517	0.11		0.251	0.46
	99 days (55 days)	2	22	1.413	0.27		0.114	1.00
Leaf N_{area}	56 days (12 days)	2	15	18.045	1.02E-4	*	0.706	4.08E-4
	70 days (28 days)	2	22	10.418	6.56E-4	*	0.486	2.62E-3
	85 days (41 days)	2	15	2.546	0.11		0.253	0.45
	99 days (55 days)	2	22	1.456	0.26		0.117	1.00

Table S6: Analysis of Variances (ANOVA) table for leaf functional traits over time. Parameters are the same as those included in Table S4. Abbreviations are as follows: DFn, degrees of freedom in the numerator of the F-statistic, DFd, degrees of freedom in the denominator of the F-statistic, η^2, eta-squared effect size estimator. η^2 values can be interpreted as the proportion of variation in the parameter due to treatment. ANOVAs were done separately for each time, and probabilities were Bonferroni corrected (adjusted p). Asterisks denote a statistically-significant ANOVA prior to Bonferroni correction. Statistically significant results after Bonferroni correction are bolded. See Table S4 for parameter means and standard errors and Tukey HSD pairwise comparisons. [$]adjusted p-value is marginally significant, Tukey HSD groups statistically distinct in Table S4.

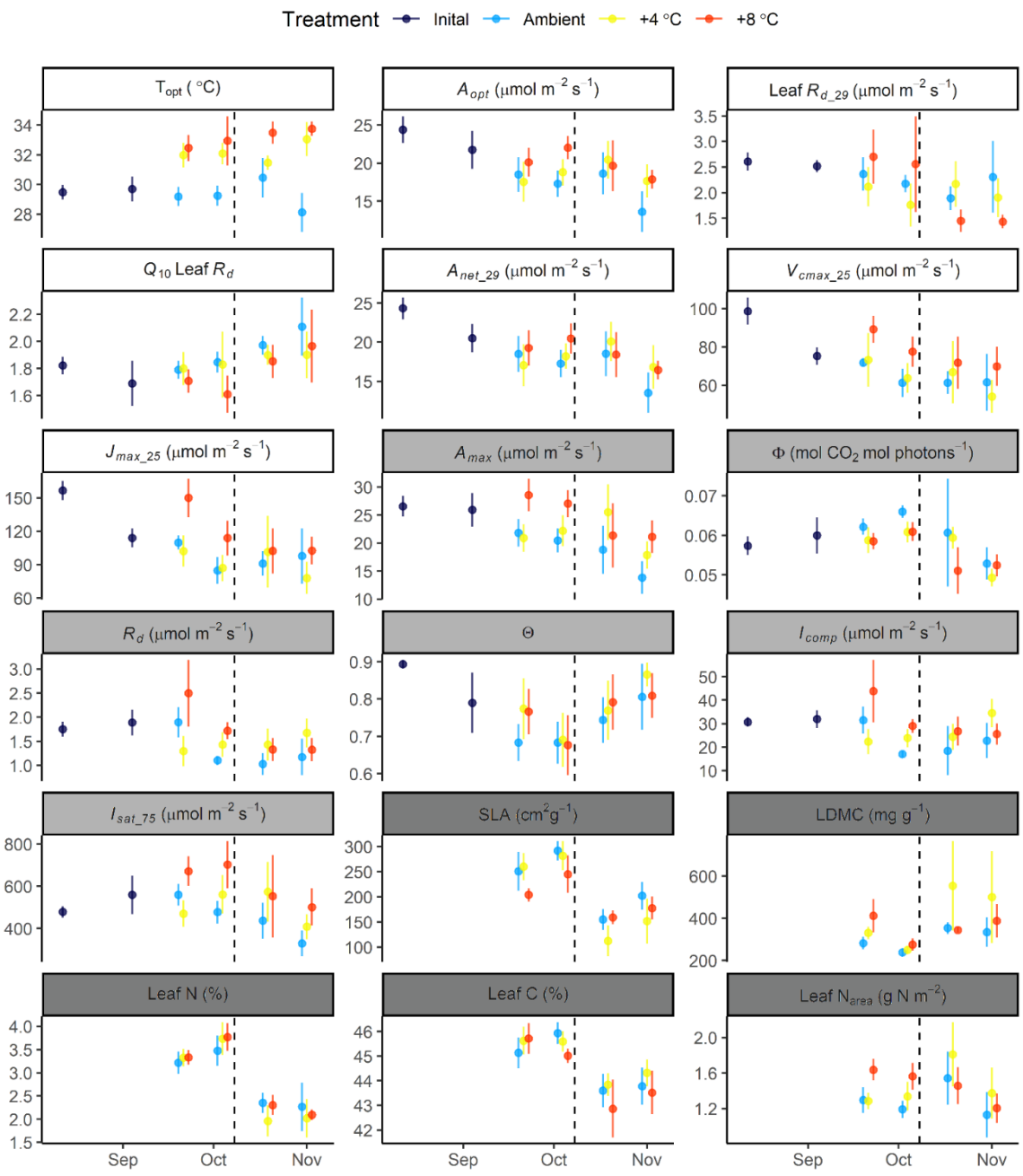

Fig.S8: Temporal changes (means ± 95% CIs) in leaf photosynthetic parameters and functional traits. Background shading of parameter labels corresponds to which table they appear in Table 2 (main text) – photosynthetic parameters from main text: white, Table S2 – light curve parameters: light gray, Table S4 – leaf functional traits: dark gray. The dashed vertical line shows when plants were trimmed on October 7, 2019.

Treatment	Time	N	Root N (%)	Root C (%)
Ambient	94 days (42 days)	3	1.15 ± 0.04^{AB}	46.31 ± 0.26^{A}
+4°C		3	1.69 ± 0.22^{ABC}	47.18 ± 0.60^{A}
+8°C		3	1.27 ± 0.11^{ABC}	46.89 ± 0.54^{A}
Ambient	109 days (57 days)	3	$1.05 \pm 0.06A^{B}$	46.80 ± 0.55^{A}
+4°C		3	0.99 ± 0.07^{A}	46.17 ± 0.80^{A}
+8°C		3	1.74 ± 0.14^{C}	46.15 ± 0.37^{A}
Treatment $F_{(2,16)}$		—	5.181**	0.102
Time $F_{(2,16)}$		—	8.030*	0.459
Treatment: Time $F_{(2,16)}$		—	9.383**	1.220

Table S7: Mean ± se for root tissue nitrogen (N) and carbon (C) content from tissue samples that were used in root respiration temperature response curves. Numbers in parentheses in the Time column are number of warmed days at the time of measurement. *F*-statistics for Analyses of Variance in the form of trait ~ Treatment × Time are given, with numbers following mean values denoting Tukey HSD post-hoc test groupings. *F* probabilities are denoted as follows: **p* < .05, ***p* < .01, *****p* < .001, otherwise *p* > .05.

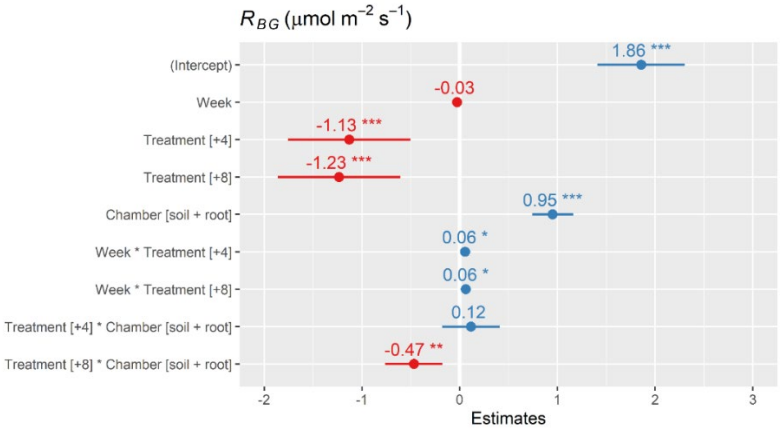

Fig. S9: Caterpillar plot for generalized linear mixed model in the form of: $R_{BG} \sim Week + Treatment + Chamber + (1 \mid Plant) + Week*Treatment + Treatment*Chamber$ (see Table S7 below). Data for the model are from the belowground respiration collars for the 10-week warming period (weeks 7-16, Fig. 1C). Points are linear mixed-effects model estimates (±95% confidence intervals), colored blue for positive estimates and red for negative estimates. Asterix notation for estimate probabilities is: *$p < .05$, **$p < .01$, and ***$p < .001$. Model estimates were calculated using restricted maximum likelihood (REML).

Fixed Effects		R_{BG} (µmols m^{-2} s^{-1})		
Predictors	*Estimates*	*std. Error*	*CI*	*p*
(Intercept)	1.86	0.23	1.41 – 2.30	<0.001
Week	-0.03	0.02	-0.06 – 0.01	0.168
Treatment [+4°C]	-1.13	0.32	-1.76 – -0.50	<0.001
Treatment [+8°C]	-1.23	0.32	-1.86 – 0.61	<0.001
Chamber [soil + root]	0.95	0.11	0.74 – 1.16	<0.001
Week × Treatment [+4°C]	0.06	0.03	0.00 – 0.11	<0.001
Week × Treatment [+8°C]	0.06	0.03	0.01 – 0.12	0.036
Treatment [+4°C] × Chamber [soil + root]	0.12	0.15	-0.18 – 0.41	0.441
Treatment [+8°C] × Chamber [soil + root]	-0.47	0.15	-0.76 – -0.18	0.002
Random Effects				
σ^2	1.24			
$\tau_{00\ Plant}$	0.09			
ICC	0.06			
N_{Plant}	87			
Observations	1344			
Marginal R^2 / Conditional R^2	0.183 / 0.236			
Deviance	4158.394			
AIC	4227.290			

Table S8: Complete model summary in tabular form, where the intercept corresponds to the ambient treatment level and the soil only chamber.

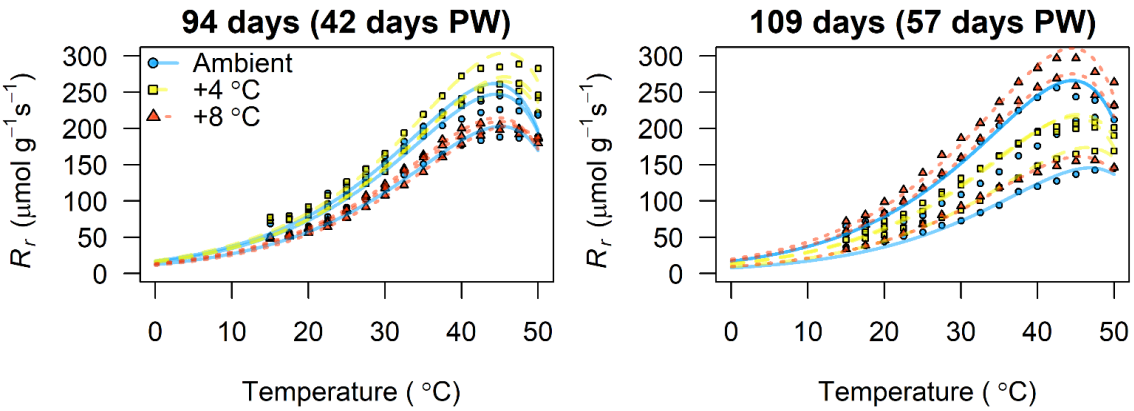

Fig. S10: Mass-based individual root respiration-temperature response curves done toward the end of the experiment (at 94 and 109 days, 3 plant root samples per treatment). These plots accompany Fig.s 5 and S9, which shows curves fit to all data by treatment. The number of days since planting and since the beginning or warming (in parentheses) is given on top of each graph panel.

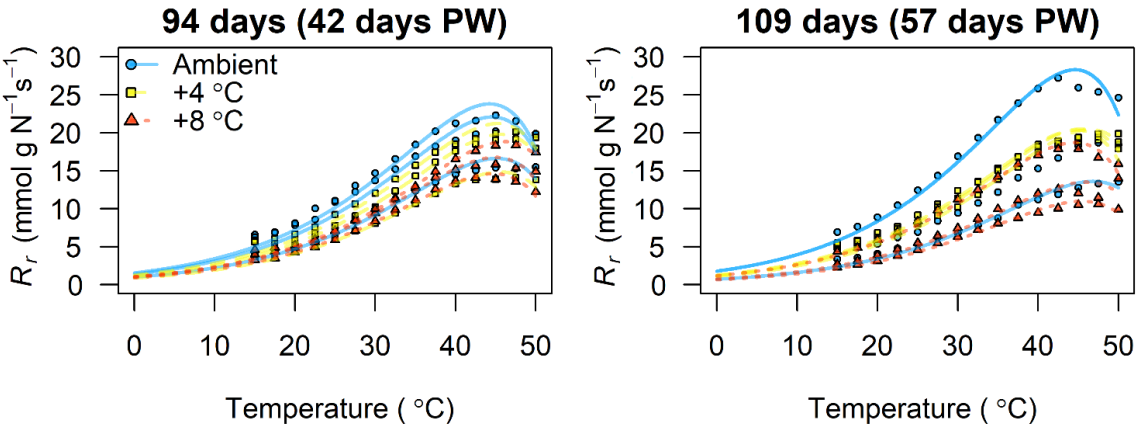

Fig. S11: Mass Nitrogen-based individual root respiration-temperature response curves, showing the same data as Fig. S7 standardized by root tissue nitrogen contents. The number of days since planting and since the beginning or post warming (in parentheses) is given on top of each graph panel.

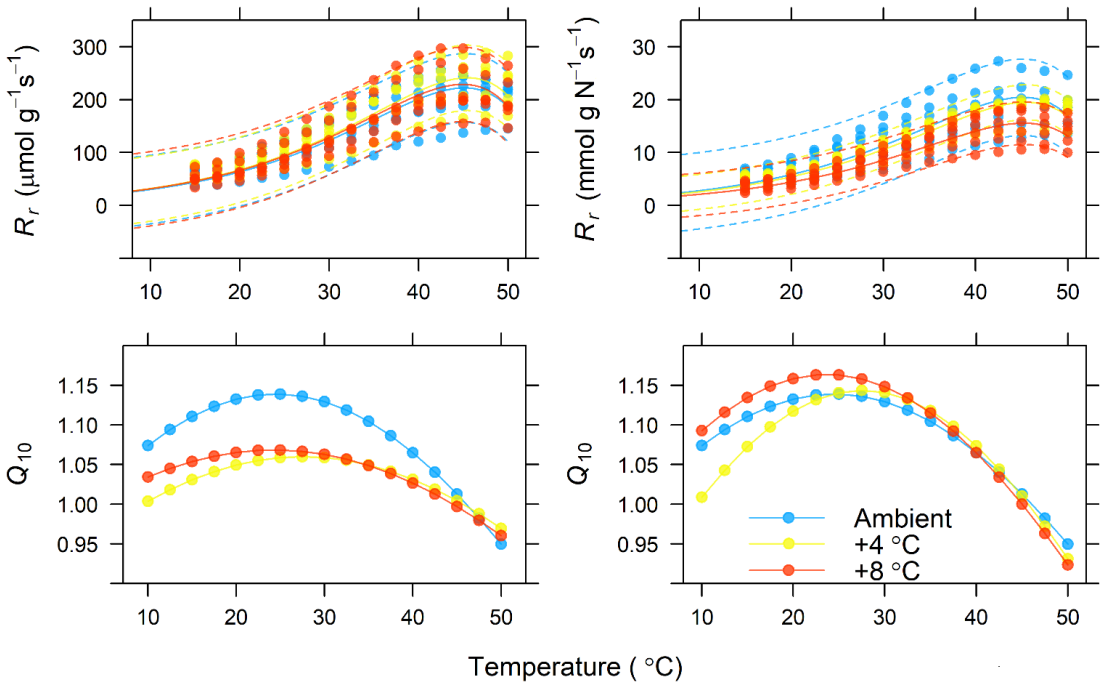

Fig. S12: Mass-based (left panels, in µmol g^{-1} s^{-1}) and nitrogen mass-based (right panels, in mmol gN^{-1} s^{-1}) root respiration (R_{root})-temperature responses. The top panels show measured data, with exponential models fit to all data by treatment. Dashed lines show 95% confidence interval limits. The bottom panels show the Q_{10}-temperature response of R_{root} by treatment for mass-based R_{root} (left) and mass-N based R_{root} (right). To calculate Q_{10} values at each temperature, we followed the procedure outlined by Atkin et al. (2000, *New Phytologist* 147:141-154), where R_{root} data were $\log_{10}$-transformed and plotted against temperature (not shown). A third order polynomial linear model was fitted to the $\log_{10}R_{root}$ versus temperature relationship. Then, the third order polynomial linear model was differentiated at all temperatures (i.e., from 10-50°C in 2.5°C increments) to obtain the slope of the model fit at those temperatures; these slopes were used to calculate the Q_{10} values at each temperature. Note that the R_{root} values in the top-left panel are in µmol, while the R_{root} values in the top right panel are in mmol.

Appendix to Chapter 6: Functional variability in specific root respiration translates to slight differences in belowground CO_2 efflux in a temperate deciduous fores in Oak Ridge, Tennessee

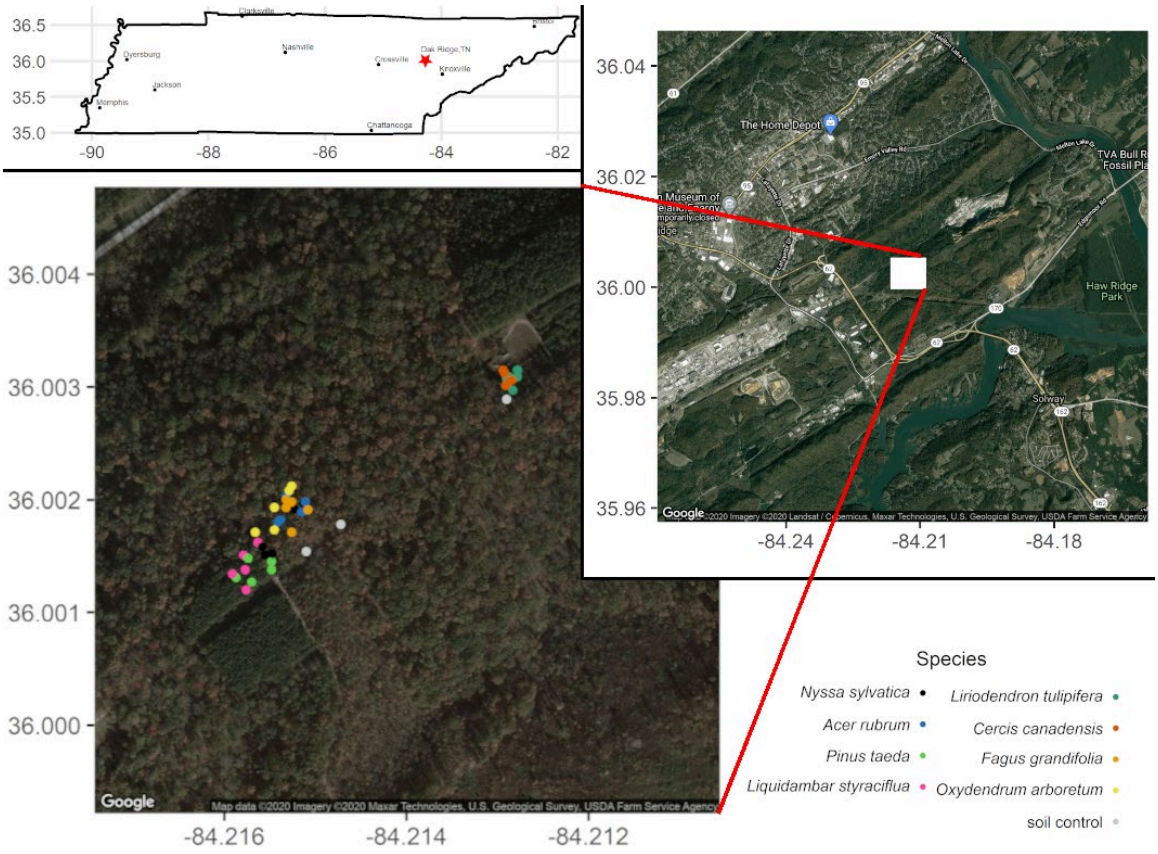

Fig. S1: Map of the study area. top: the location of Oak Ridge, TN, within the state of Tennessee. right: an aerial view of the University of Tennessee Forest Resources AgResearch & Education Center. left: the location of the study area within the Forest Resources AgResearch & Education Center. From the aerial photo, the planted loblolly stand containing the *Pinus* and *Liquidambar* trees is visible at the west end of the study area. At the eastern end of the study area is an area that was clear-cut in the last decade. This is where the *Liriodendron* and *Cercis* were located. The remaining four species were found in the native Oak, Beech, Hickory forest that typifies the forested areas of East Tennessee.

Table S1: List of primer sequences used for polymerase chain reaction (PCR) amplification of fungal and bacterial DNA sequences.

PRIMER NAME	SEQUENCE	DIRECTION	TARGET	REFERENCE
ITS3NGS1	TCGTCGGCAGCGTCAGATGTGTATAAGAGACAGCATCGATGAAGAACGCAG	Forward	Fungi	White et al. (1990)
ITS3NGS2	TCGTCGGCAGCGTCAGATGTGTATAAGAGACAGCAACGATGAAGAACGCAG	Forward	Chytridiomycota	Tedersoo et al. (2014)
ITS3NGS3	TCGTCGGCAGCGTCAGATGTGTATAAGAGACAGCACCGATGAAGAACGCAG	Forward	Sebacinales	Tedersoo et al. (2014)
ITS3NGS4	TCGTCGGCAGCGTCAGATGTGTATAAGAGACAGCATCGATGAAGAACGTAG	Forward	Glomeromycota	Tedersoo et al. (2014)
ITS3NGS5	TCGTCGGCAGCGTCAGATGTGTATAAGAGACAGCATCGATGAAGAACGTGG	Forward	Sordariales	Tedersoo et al. (2014)
ITS3NGS10	TCGTCGGCAGCGTCAGATGTGTATAAGAGACAGCATCGATGAAGAACGCTG	Forward	Stramenopila	Tedersoo et al. (2014)
ITS4NGR	GTCTCGTGGGCTCGGAGATGTGTATAAGAGACAGTCCTSCGCTTATTGATATGC	Reverse	Fungi	White et al. (1990)
ARCH-ITS4	GTCTCGTGGGCTCGGAGATGTGTATAAGAGACAGTCCTCGCCTTATTGATATGC	Reverse	Archaearhizomycetes	Cregger et al. (2018)
515F	TCGTCGGCAGCGTCAGATGTGTATAAGAGACAGGGTGCCAGCMGCCGCGGTAA	Forward	Bacteria/Archaea	Lane et al. (1985)
515F_f1C	TCGTCGGCAGCGTCAGATGTGTATAAGAGACAGGGTGCCAGCMGCWGCGGTAA	Forward	Cloroflexi	Shakya et al. (2013)
515F_f1TM7	TCGTCGGCAGCGTCAGATGTGTATAAGAGACAGGGTGCCAGCMGCCGCGGTCA	Forward	TM7	Shakya et al. (2013)
515F_f4Arc	TCGTCGGCAGCGTCAGATGTGTATAAGAGACAGGGTGKCAGCMGCCGCGGTAA	Forward	Archaea	Shakya et al. (2013)
806R	GTCTCGTGGGCTCGGAGATGTGTATAAGAGACAGGGACTACHVGGGTWTCTAAT	Reverse	Bacteria/Archaea	Lane et al. (1985)

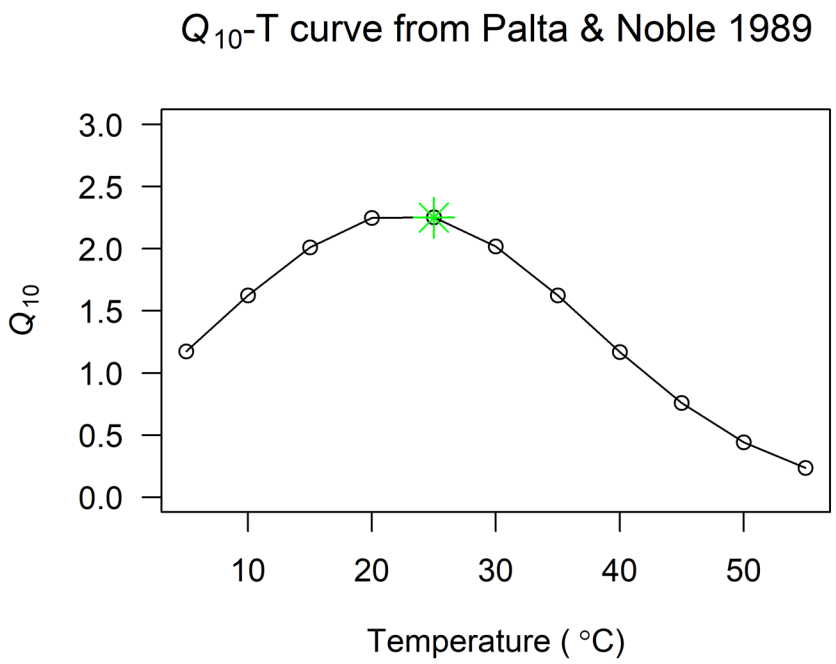

Fig. S2: The Q_{10} – Temperature (T) response of *Agave deserti* root tissue respiration from Palta and Nobel (1989). This curve is characteristic of the T-sensitivity of plant root tissue respiration, where the Q_{10} value changes as a function of T (Atkin et al., 2000). This is different from the general leaf respiration Q_{10} – T response curve, where the Q_{10} value of leaf respiration decreases linearly with T (Atkin and Tjoelker, 2003; Tjoelker et al., 2001). It was derived by differentiating the $\log_{10}$-transforming *Agave deserti* R_r-T response function (a third-order polynomial) to determine the slope of the R_r-T function at each measurement T (i.e., in 5°C increments). The green star denotes the Q_{10} value at 25°C, which is the T we measured specific-root respiration rates on excised root systems (see methods). Notably, from 20-25°C, the Q_{10} value is stable (at its maximum value of 2.25). Using the average root tissue respiration rates for each species (from n = 15 measurements), we constructed species-specific R_{root} – T response curves (see supplement 1). These curves were used with soil T measurements and the amount of root tissue in each root tray (assumed to constant) to estimate R_{root} over time for each in-situ root tray.

Table S2: Mean (± standard error) soil carbon and nitrogen pool values for each tree species (n = 5 per treatment) and soil controls (n=3). Soil total organic carbon (TC), dissolved organic carbon (DOC) and microbial carbon (MBC), and soil total nitrogen (TN), dissolved nitrogen (DN) and microbial nitrogen (MBN) were determined via the chloroform extraction technique. Analyses of Variance in the form of: soil variable ~ Species + Treatment (i.e., with no interaction term. Including an interaction term did not improve ANOVA models). Asterix notation for statistical significance of F-statistics (ANOVA) is as follows: $^{\$}$ $p < .10$, $*p < .05$, $**p < .01$, $***p < .001$, otherwise non-significant. Post-hoc Tukey HSD pairwise comparison groupings are denoted with letters.

Species	Treatment	TC (mg L^{-1})	DOC (µg g^{-1})	MBC (µg g^{-1})	TN (mg L^{-1})	DN (µg g^{-1})	MBN (µg g^{-1})
Acer rubrum L.	Control: R+ Z-	11.79 ± 0.99^{A}	65.81 ± 6.68^{A}	427.45 ± 78.32^{A}	8.49 ± 1.32^{A}	47.42 ± 8.23^{A}	91.34 ± 16.00^{ABC}
	ZeroTol: R+ Z+	12.95 ± 0.86^{A}	72.25 ± 6.24^{A}	350.98 ± 37.67^{A}	6.72 ± 0.54^{A}	37.26 ± 2.88^{A}	41.24 ± 8.69^{BC}
Cercis canadensis L.	Control: R+ Z-	10.47 ± 1.11^{A}	59.04 ± 6.48^{A}	517.13 ± 92.15^{A}	7.85 ± 0.65^{A}	44.19 ± 4.05^{A}	124.50 ± 13.81^{A}
	ZeroTol: R+ Z+	10.57 ± 1.54^{A}	59.48 ± 8.86^{A}	430.26 ± 48.55^{A}	8.49 ± 0.75^{A}	47.75 ± 4.44^{A}	79.54 ± 13.81^{ABC}
Fagus grandifolia L.	Control: R+ Z-	12.95 ± 1.00^{A}	72.96 ± 6.28^{A}	490.28 ± 96.55^{A}	8.60 ± 1.28^{A}	48.93 ± 8.27^{A}	105.97 ± 25.18^{AB}
	ZeroTol: R+ Z+	12.18 ± 0.83^{A}	68.26 ± 5.36^{A}	456.45 ± 47.92^{A}	7.58 ± 1.17^{A}	42.54 ± 6.92^{A}	78.32 ± 11.25^{ABC}
Liriodendron tulipifera L.	Control: R+ Z-	11.90 ± 1.52^{A}	66.02 ± 8.67^{A}	440.55 ± 23.16^{A}	7.59 ± 0.89^{A}	42.19 ± 5.11^{A}	100.77 ± 9.87^{ABC}
	ZeroTol: R+ Z+	12.09 ± 0.73^{A}	66.86 ± 4.24^{A}	434 .49 ± 46.10^{A}	7.28 ± 0.84^{A}	40.33 ± 4.87^{A}	71.42 ± 10.89^{ABC}
Liquidambar styraciflua L.	Control: R+ Z-	11.62 ± 0.81^{A}	64.29 ± 4.76^{A}	425.96 ± 50.59^{A}	8.45 ± 0.95^{A}	46.96 ± 5.73^{A}	89.55 ± 13.53^{ABC}
	ZeroTol: R+ Z+	13.18 ± 0.33^{A}	72.80 ± 2.05^{A}	375.92 ± 55.75^{A}	7.86 ± 1.58^{A}	43.67 ± 8.23^{A}	38.73 ± 6.59^{C}

Nyssa sylvatica Marshall	Control: R+ Z-	13.53 ± 1.22^{A}	75.03 ± 7.27^{A}	480.80 ± 43.12^{A}	8.11 ± 0.72^{A}	44.99 ± 4.23^{A}	107.21 ± 9.09^{AB}
	ZeroTol: R+ Z+	13.84 ± 1.58^{A}	76.81 ± 8.98^{A}	490.86 ± 78.61^{A}	6.90 ± 0.96^{A}	38.24 ± 5.51^{A}	78.12 ± 14.63^{ABC}
Oxydendrum arboreum (L.) DC.	Control: R+ Z-	10.76 ± 0.50^{A}	59.21 ± 2.62^{A}	416.84 ± 74.29^{A}	7.59 ± 0.99^{A}	41.94 ± 5.83^{A}	89.55 ± 13.53^{ABC}
	ZeroTol: R+ Z+	10.81 ± 0.72^{A}	59.32 ± 4.19^{A}	408.01 ± 53.44^{A}	5.93 ± 0.85^{A}	32.63 ± 4.92^{A}	38.73 ± 6.59^{ABC}
Pinus taeda L.	Control: R+ Z-	11.20 ± 0.74^{A}	61.63 ± 4.59^{A}	445.86 ± 40.39^{A}	8.48 ± 0.66^{A}	46.64 ± 3.95^{A}	80.33 ± 10.64^{ABC}
	ZeroTol: R+ Z+	12.51 ± 0.70^{A}	68.84 ± 3.07^{A}	456.31 ± 24.03^{A}	8.34 ± 0.61^{A}	45.89 ± 2.91^{A}	55.37 ± 4.87^{BC}
Soil Only controls	Control: R- Z-	8.73 ± 0.39^{A}	49.29 ± 1.84^{A}	387.50 ± 35.17^{A}	4.35 ± 0.56^{A}	24.45 ± 2.62^{A}	89.61 ± 2.16^{ABC}
	ZeroTol: R- Z+	9.10 ± 1.40^{A}	50.71 ± 4.00^{A}	419.66 ± 41.49^{A}	4.76 ± 0.88^{A}	26.51 ± 2.62^{A}	90.88 ± 16.24^{ABC}
$F_{\text{species (9,75)}}$	—	3.053**	2.618*	0.817	2.083*	1.885$^{\$}$	1.903$^{\$}$
$F_{\text{treatment (1,75)}}$	—	1.044	0.826	1.307	2.753	2.631	31.660***

Table S3: Average (± 95 % Confidence Interval) OTU richness and Shannon Diversity (*H*) for the soils of the *in-situ* root trays placed on roots of 8 temperate tree species. N = 5 for each species treatment combination and N=3 for each of the soil only controls for each treatment.

Species	Treatment	Bacterial 16s		Fungal ITS	
		Richness	*H*	Richness	*H*
Acer rubrum L.	Control: Z-	1074 ± 139	6.55 ± 0.19	290 ± 65	4.68 ± 1.01
	ZeroTol Z+	988 ± 550	6.36 ± 0.98	256 ± 15	4.60 ± 0.19
Cercis canadensis L.	Control: Z-	922 ± 523	6.29 ± 1.05	211 ± 169	4.03 ± 1.49
	ZeroTol Z+	988 ± 550	6.70 ± 0.03	304 ± 87	4.88 ± 0.76
Fagus grandifolia L.	Control: Z-	1083 ± 121	6.62 ± 0.15	258 ± 108	4.79 ± 0.50
	ZeroTol Z+	1118 ± 96	6.64 ± 0.10	237 ± 61	4.28 ± 0.68
Liriodendron tulipifera L.	Control: Z-	1059 ± 111	6.65 ± 0.14	343 ± 30	5.11 ± 0.17
	ZeroTol Z+	1127 ± 47	6.73 ± 0.05	340 ± 43	5.02 ± 0.24
Liquidambar styraciflua L.	Control: Z-	1047 ± 64	6.52 ± 0.06	257 ± 31	4.05 ± 0.76
	ZeroTol Z+	1072 ± 224	6.49 ± 0.29	275 ± 29	4.66 ± 0.30
Nyssa sylvatica Marshall	Control: Z-	1052 ± 139	6.54 ± 0.16	333 ± 31	5.06 ± 0.33
	ZeroTol Z+	1087 ± 254	6.62 ± 0.29	294 ± 56	4.88 ± 0.50
Oxydendrum arboretm (L.) DC.	Control: Z-	812 ± 671	6.06 ± 1.36	252 ± 183	4.82 ± 0.83
	ZeroTol Z+	1139 ± 136	6.65 ± 0.14	313 ± 32	5.01 ± 0.14
Pinus taeda L.	Control: Z-	1091 ± 68	6.58 ± 0.08	227 ± 65	4.53 ± 0.26
	ZeroTol Z+	1109 ± 112	6.59 ± 0.13	197 ± 60	4.40 ± 0.27
soil only controls (R-)	Control: Z-	977 ± 216	6.46 ± 0.23	163 ± 193	4.15 ± 0.44
	ZeroTol Z+	987 ± 597	6.49 ± 0.29	224 ± 515	4.13 ± 5.7

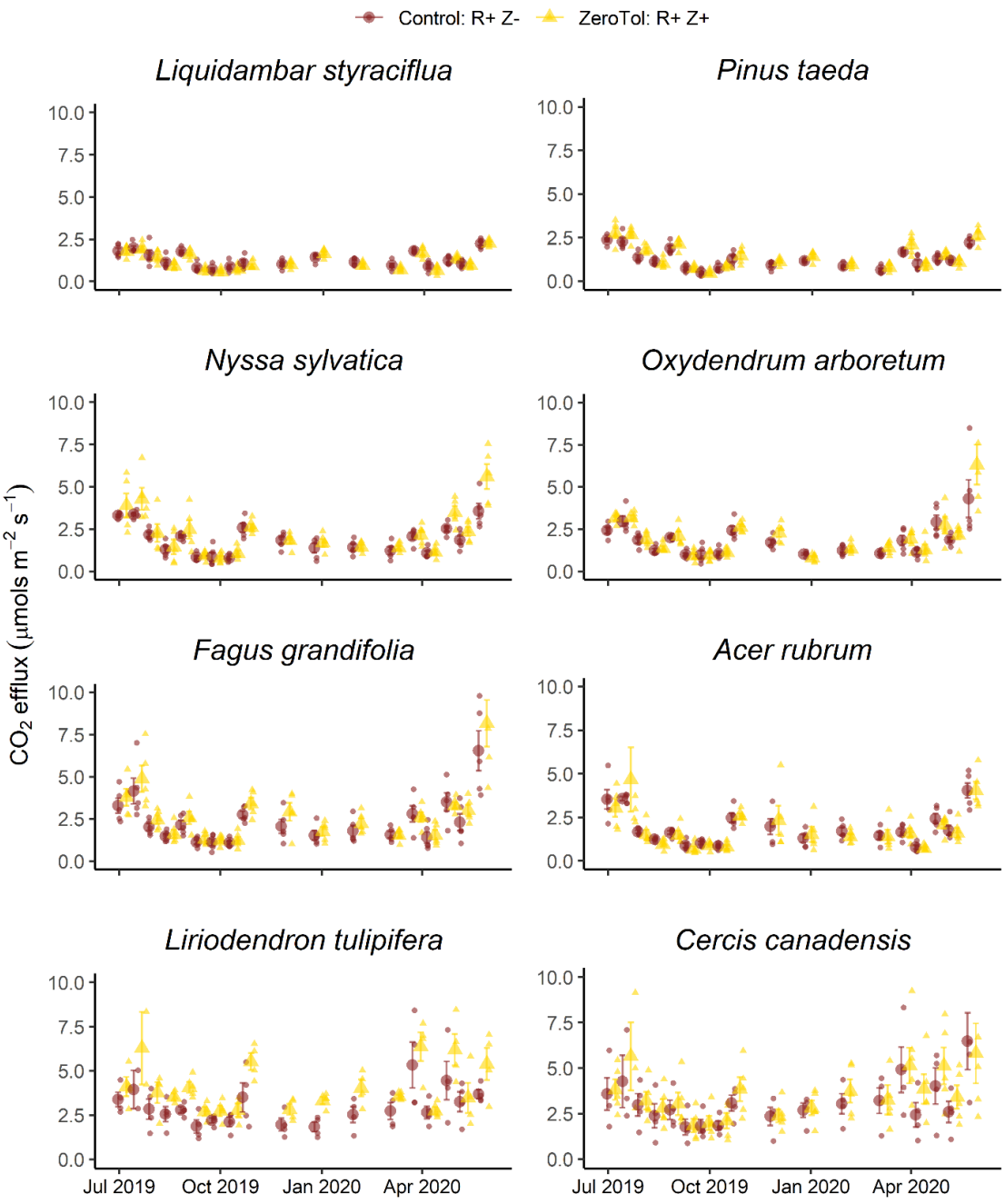

Fig. S3: Rates of belowground CO_2 efflux (area-base measurments) for *in-situ* root trays for eight temperate tree species from July 4, 2019, to May 26, 2020, by tree species. Colors correspond to treatments, with yellow for the ZeroTol-treated trays and brown for controls. Large points represent mean rates per treatment per species (n = 5), with whiskers showing standard errors, while smaller symbols show the measurements for each tray. Panels are organized by collection area with the top two panels, the middle four panels, and the bottom two panels being collected in the same areas are each other (see Fig. S1).

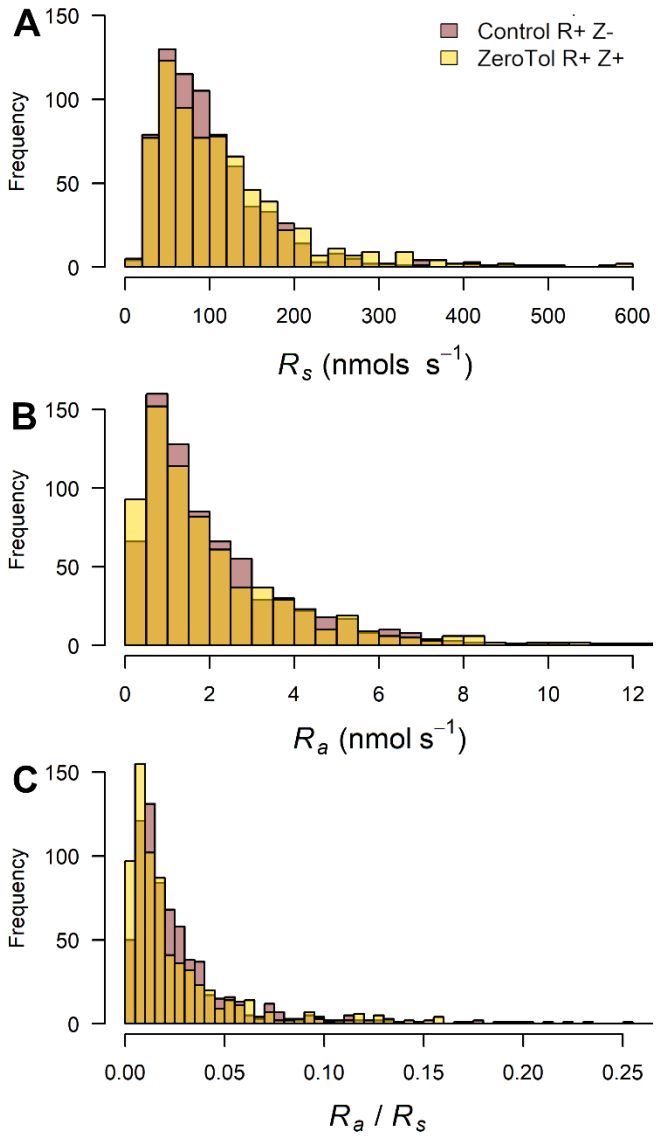

Fig. S4: (left) Histograms of the sources of belowground CO_2 efflux measurements (n = 1526) by treatment. **A**, total belowground CO_2 efflux (R_s) from 80 *in-situ* root trays (tray area is equal to 487 cm^2), **B**, root respiration from entire root systems of housed in the *in-situ* root trays (R_a), and **C**, the contribution of root-based CO_2 efflux to total belowground CO_2 efflux (R_a / R_s) from 80 *in-situ* root trays, which included entire fine root systems and surrounding soil. For A and B, raw CO_2 efflux rates per tray in nmol per second are shown (accounting for soil mass and root biomass). Bars a colored by treatments (brown for control and yellow for the ZeroTol-treated root trays, n = 40 each).

Fig. S5 (next page): (top row) Area-based soil CO_2 efflux rates (in µmol m^{-2} s^{-1}) for arbuscular mycorrhizal species (A, *Liriodendron tulipifera*, *Liquidambar styraciflua*, *Cercis canadensis*, *Acer rubrum,* and *Nyssa sylvatica*) and ectomycorrhizal (B, *Pinus taeda*, *Fagus grandifolia,* and *Oxydendrum arboretum*) in the University of Tennessee Arboretum in Oak Ridge, TN over time from July 4, 2019, to May 26, 2020. Points show means, and whiskers show standard errors. (second row) Rates of fine root system respiration (R_a), (third row) total *in situ* root tray respiration (R_s), and (bottom row) the ratio of fine root system to total *in situ* root tray respiration (R_a / R_s). For the bottom three rows, rates are raw CO_2 flux rates in nmol per second (*i.e.*, have been calculated on a per mass basis accounting for variation in root system biomass and soil dry mass among trays). Colors show treatments with the ZeroTol treated trays shown in yellow and the control trays shown in brown.

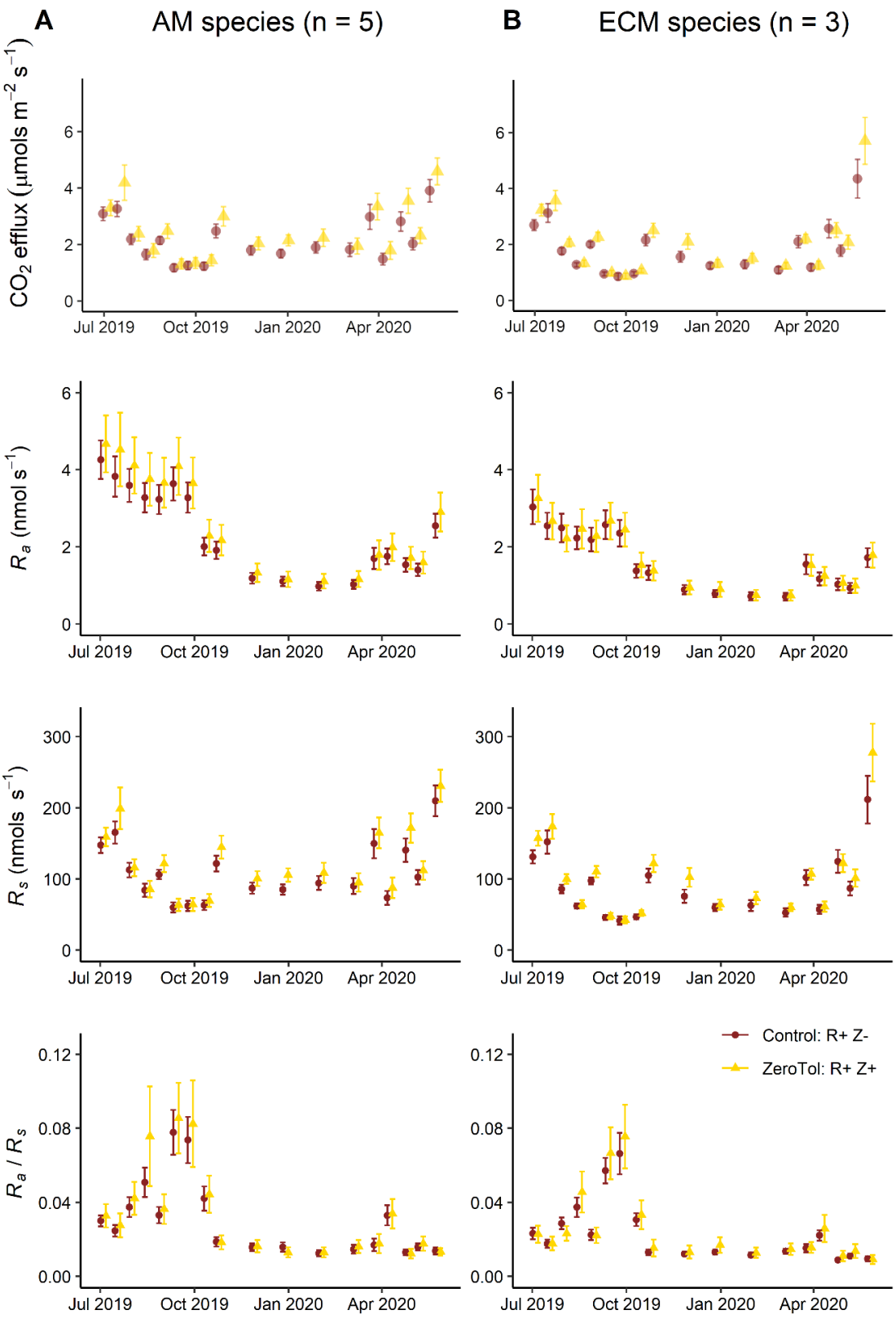
A
AM species (n = 5)
B
ECM species (n = 3)
CO2 efflux (µmols m−2 s−1)
Ra (nmol s−1)
Rs (nmols s−1)
Ra / Rs
Jul 2019
Oct 2019
Jan 2020
Apr 2020
Control: R+ Z-
ZeroTol: R+ Z+

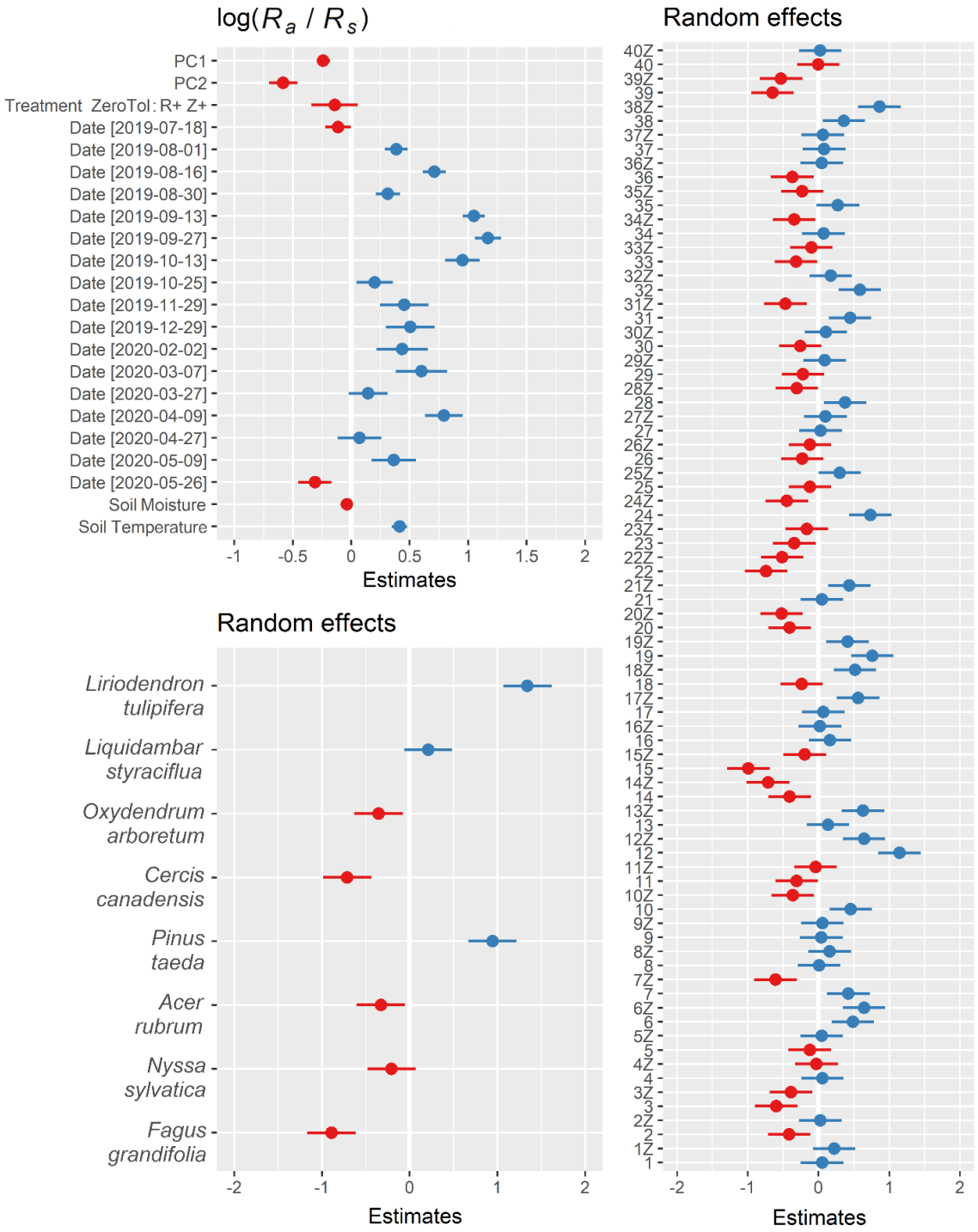

Fig. S6: Caterpillar plots for the best fitting linear mixed-effects model in the form of log(R_a / R_s) ~ Treatment + Date + Soil Moisture + Soil Temperature + (1| Species/Tray). Points are effect estimates, and whiskers are 95% Wald confidence intervals. The top left panel shows the fixed effect estimates. The bottom left panel shows random intercept effects (BLUPs) for the eight study species, and the right panel shows the nested random intercept term for each tray.

Table S4: Model summary table for the best fitting linear mixed-effects model in the form of log(R_a / R_s) ~ Treatment + PC1 + PC2 + Date + Soil Moisture + Soil Temperature + (1| Species) + (1|Tray). For fixed effects, predictor estimates, their standard errors (*std. error*), Wald confidence intervals (*CI*), and associated probabilities (*p*) are given. For random parts, total variance (σ^2), random intercept variances (τ), and interclass correlations (ICC) are given. The table also includes model marginal (including only fixed effects) and conditional (including fixed and random effects) coefficients of determination (R^2), Akaike Information Criterion (AIC), and log-Likelihood (estimated using residualized maximum likelihood: REML).

	log(R_a / R_s)			
Predictors	*Estimates*	*std. error*	*CI*	*p*
(Intercept)	-4.43	0.30	-5.01 – -3.84	<0.001
Treatment: ZeroTol : R+ Z+	-0.14	0.10	-0.34 – 0.06	0.160
PC1	-0.24	0.03	-0.30 – -0.18	<0.001
PC2	-0.58	0.06	-0.70 – -0.46	<0.001
Date2019-07-18	-0.11	0.06	-0.22 – -0.00	0.044
Date2019-08-01	0.39	0.05	0.29 – 0.48	<0.001
Date2019-08-16	0.71	0.05	0.61 – 0.81	<0.001
Date2019-08-30	0.31	0.05	0.21 – 0.42	<0.001
Date2019-09-13	1.05	0.05	0.95 – 1.14	<0.001
Date2019-09-27	1.17	0.06	1.06 – 1.28	<0.001
Date2019-10-13	0.95	0.08	0.80 – 1.10	<0.001
Date2019-10-25	0.20	0.08	0.04 – 0.36	0.012
Date2019-11-29	0.45	0.11	0.24 – 0.66	<0.001
Date2019-12-29	0.51	0.11	0.30 – 0.71	<0.001
Date2020-02-02	0.44	0.11	0.21 – 0.66	<0.001
Date2020-03-07	0.60	0.11	0.38 – 0.82	<0.001
Date2020-03-27	0.14	0.09	-0.02 – 0.31	0.092
Date2020-04-09	0.79	0.08	0.63 – 0.95	<0.001
Date2020-04-27	0.07	0.09	-0.12 – 0.26	0.460
Date2020-05-09	0.36	0.10	0.17 – 0.55	<0.001
Date2020-05-26	-0.31	0.07	-0.45 – -0.17	<0.001
Soil Moisture	-0.04	0.02	-0.07 – -0.01	0.021
Soil Temperature	0.41	0.03	0.35 – 0.48	<0.001
Random Effects				
σ^2	0.09			
$\tau_{00\ Tray}$	0.20			
$\tau_{00\ Species}$	0.64			
ICC	0.91			
$N_{\ Species}$	8			
$N_{\ Tray}$	80			
Observations	1425			
Marginal R^2 / Conditional R^2	0.564 / 0.959			
Deviance	866.350			
AIC	1024.130			

log-Likelihood	-486.065

Table S5: Soil moisture and soil temperature over time (averages ± standard errors) by sampling date from summer 2019 through spring 2020 for in-situ root trays at the University of Tennessee Arboretum in Oak Ridge, TN. For each tray at each measurement, three soil moisture and temperature readings were taken on each of the three cardinal directions opposite the tree root. Measurements were averaged, and averages (by sampling date) of those averages are presented here.

Date	Soil Moisture (%)	Soil Temperature (°C)
2019-07-04	11.94 ± 0.52	25.84 ± 0.22
2019-07-18	26.68 ± 0.93	23.71 ± 0.13
2019-08-01	17.38 ± 0.79	23.25 ± 0.13
2019-08-16	11.10 ± 0.61	21.95 ± 0.14
2019-08-30	18.56 ± 0.55	21.82 ± 0.14
2019-09-13	13.91 ± 0.62	23.56 ± 0.11
2019-09-27	24.78 ± 0.80	21.98 ± 0.12
2019-10-13	25.46 ± 0.81	15.39 ± 0.16
2019-10-25	26.08 ± 0.42	14.64 ± 0.08
2019-11-29	32.46 ± 0.44	8.87 ± 0.11
2019-12-29	24.81 ± 0.70	7.87 ± 0.20
2019-02-02	22.67 ± 0.80	6.41 ± 0.09
2019-03-07	26.79 ± 0.50	6.73 ± 0.12
2019-03-27	28.63 ± 0.39	13.27 ± 0.48
2019-04-09	24.21 ± 0.49	13.40 ± 0.19
2019-04-27	30.87 ± 0.52	11.46 ± 0.14
2019-05-09	28.83 ± 0.50	10.50 ± 0.07
2019-05-26	31.89 ± 0.39	18.08 ± 0.09

References

Atkin, O.K., Edwards, E.J., Loveys, B.R., 2000. Response of root respiration to changes in temperature and its relevance to global warming. New Phytologist 147(1), 141-154.

Atkin, O.K., Tjoelker, M.G., 2003. Thermal acclimation and the dynamic response of plant respiration to temperature. Trends in Plant Science 8(7), 343-351.

Cregger, M., Veach, A., Yang, Z., Crouch, M., Vilgalys, R., Tuskan, G., Schadt, C., 2018. The Populus holobiont: dissecting the effects of plant niches and genotype on the microbiome. Microbiome 6(1), 1-14.

Lane, D.J., Pace, B., Olsen, G.J., Stahl, D.A., Sogin, M.L., Pace, N.R., 1985. Rapid determination of 16S ribosomal RNA sequences for phylogenetic analyses. Proceedings of the National Academy of Sciences 82(20), 6955-6959.

Palta, J.A., Nobel, P.S., 1989. Root respiration for Agave deserti: influence of temperature, water status and root age on daily patterns. Journal of Experimental Botany 40(2), 181-186.

Shakya, M., Gottel, N., Castro, H., Yang, Z.K., Gunter, L., Labbé, J., Muchero, W., Bonito, G., Vilgalys, R., Tuskan, G., 2013. A multifactor analysis of fungal and bacterial community structure in the root microbiome of mature *Populus deltoides* trees. PloS One 8(10), e76382.

Tedersoo, L., Bahram, M., Põlme, S., Kõljalg, U., Yorou, N.S., Wijesundera, R., Ruiz, L.V., Vasco-Palacios, A.M., Thu, P.Q., Suija, A., 2014. Global diversity and geography of soil fungi. Science 346(6213).

Tjoelker, M.G., Oleksyn, J., Reich, P.B., 2001. Modelling respiration of vegetation: evidence for a general temperature-dependent Q_{10}. Global Change Biology 7(2), 223-230.

White, T.J., Bruns, T., Lee, S., Taylor, J., 1990. in: Innis, M.A., D.H. Gelfand, J.J. Sninsky, and T.J. White (Eds.),PCR Protocols: A Guide to Methods and Applications. Academic Press, Inc., New York, pp. 315-322.

VITA

J. AARON HOGAN
www.jamesaaronhogan.com

1988	Born, Vail, Colorado
2006-2011	B.S., Ecology & Biodiversity University of Denver Denver, CO
2011-2012	El Verde Field Station, El Verde, Puerto Rico
2012-2015	M.S., Ciencias Ambientales Universidad de Puerto Rico – Río Piedras, San Juan, Puerto Rico
2016	Auxiliar de Investigaciones II Departamento de Ciencias Ambientales Universidad de Puerto Rico – Río Piedras, San Juan, Puerto Rico
2016-2018 2019	Teaching Assistant Doctoral Candidate Florida International University Miami, Florida
2019 -2020	US Department of Energy Office of Science Graduate Student Research (SCGSR) Fellow Oak Ridge National Laboratory Oak Ridge, Tennessee
2021	Ph.D., Biological Sciences Florida International University Miami, Florida

PUBLICATIONS

Hogan, J. A., Castañeda-Moya, E., Lamb-Wotton, L., Troxler, T., Baraloto, C. (2021) Water levels primarily drive variation in photosynthesis and nutrient use of scrub Red Mangroves in the southeastern Florida Everglades. *Tree Physiology,* tpab151.

Hogan, J. A., Feagin, R. A., Starr, G., Ross, M., Lin, T. C., O'connell, C., Huff, T. P., Stauffer, B. A., Robinson K. L., Chapela-Lara, M., Xue, J., Kiel Reese, B., Geist, S. J.,

Whitman, E. R., Douglas, S., Congdon, V.M., Reustle, J. W., Smith, R. S., Lagomasino, D., Strickland, B. A., Wilson, S. A., Profitt, C. E., Hogan, D. J., Branoff, B. L., Armitage, A. R., Rush, S. A., Santos, R. O., Campos-Cerquiera, M., Montagna, P. A., Erisman, B., Walker, L., Silver. W. L., Crowl, T. A., Wetz, M., Hall, N., Zou, X., Pennings, S. C., Wang, L. J., Change, C. T., Leon, M., McDowell, W. H., Kominoski, J. S., and Patrick, C. J. (2020). A research framework to integrate cross-ecosystem responses to tropical cyclones. *BioScience*, 70(6), 477-489.

Hogan, J. A., Nytch, C. J., Bithorn, J. E., and Zimmerman, J. K. (2019). Proposing the solar-wind energy flux hypothesis as a driver of inter-annual variation in tropical tree reproductive effort. *American Journal of Botany*, 106(11), 1519-1525.

Hogan, J. A., McMahon, S. M., Buzzard, V., Michaletz, S. T., Enquist, B. J., Thompson, J., Swenson N. G., and Zimmerman, J. K. (2019). Drought and the interannual variability of stem growth in an aseasonal, everwet forest. *Biotropica*, 51(2), 139-154.

Hogan, J. A., Hérault, B., Bachelot, B., Gorel, A., Jounieaux, M., and Baraloto, C. (2018). Understanding the recruitment response of juvenile Neotropical trees to logging intensity using functional traits. *Ecological Applications*, 28(8), 1998-2010.

Hogan, J. A., Zimmerman, J. K., Thompson, J., Uriarte, M., Swenson, N. G., Condit, R., Hubbell, S., Johnson D. J., Sun I. F., Chang-Yang, C.H., Su, H.S., Ong, P., Rodriguez, L., Monoy, C., Yap, S., and Davies, S. J. (2018). The frequency of cyclonic windstorms shapes tropical forest dynamism and functional trait dispersion. *Forests,* 9(7), 404.

Hogan, J. A., Mayorquin, S., Rice, K., Thompson, J., Zimmerman, J. K., and Brokaw, N. (2017). Liana dynamics reflect land-use history and hurricane response in a Puerto Rican forest. *Journal of Tropical Ecology*, 33(2), 155.

Hogan, J. A., Zimmerman, J. K., Uriarte, M., Turner, B. L., and Thompson, J. (2016). Land-use history augments environment–plant community relationship strength in a Puerto Rican wet forest. *Journal of Ecology*, 104 (5), 1466-1477.

Hogan, J. A., Zimmerman, J. K., Thompson, J., Nytch, C. J., and Uriarte, M. (2016). The interaction of land-use legacies and hurricane disturbance in subtropical wet forest: twenty-one years of change. *Ecosphere*, 7 (8), e01405.